UNIVERSIDAD DE SALAMANCA
FACULTAD DE MEDICINA

PROGRAMA DE DOCTORADO EN CIRUGÍA Y ODONTOESTOMATOLOGÍA

TESIS DOCTORAL

INFLUENCIA DE LOS FACTORES RELACIONADOS CON LA FATIGA CÍCLICA DE LAS LIMAS ENDODÓNTICAS DE NiTi

Autor

Dr. D. Álvaro Zubizarreta Macho

Directores

Dr. D. Alberto Francisco Albaladejo Martínez

Dr. D. Luis Óscar Alonso Ezpeleta

Salamanca, 2022

AGRADECIMIENTOS

Al Profesor Alberto Francisco Albaladejo, por la supervisión y apoyo recibido durante la realización de esta Tesis Doctoral.

Al Profesor Luis Óscar Alonso Ezpeleta. por su dedicación y por la ayuda proporcionada para avanzar en la investigación, guiándome y aportando sus conocimientos a lo largo de todo este proyecto.

A mis compañeros y amigos.

A mis padres.

A Belén.

A Pablo y Martín.

FACULTAD DE MEDICINA
DEPARTAMENTO DE CIRUGÍA

Alfonso X El Sabio, s/n.
Campus "Miguel de Unamuno"
37007 Salamanca

Tel.: (34) 923 29 45 00 EXT 1895
Fax: (34) 923 29 45 58

E-mail: cirugia@usal.es

D. Francisco Santiago Lozano Sánchez, Director del Departamento de Cirugía de la Universidad de Salamanca

CERTIFICA:

Que el Trabajo Doctoral titulado "Influencia de los factores relacionados con la fatiga cíclica de las limas endodónticas de NiTi" del que es autor D Álvaro Zubizarreta Macho, reúne los requisitos necesarios para su presentación y defensa ante el Tribunal Calificador para optar al **Grado de Doctor por la Universidad de Salamanca**

Y para que así conste a los efectos oportunos, firman el presente Certificado en Salamanca a 20 de junio de dos mil veintidós.

Fdo.: Prof. Fco. S. Lozano Sánchez

INFORME DE LOS DIRECTORES DE LA TESIS DOCTORAL

Dr. D. Alberto Francisco Albaladejo Martínez. Doctor en Odontología. Catedrático de Ortodoncia de la Universidad de Salamanca y Dr. D. Luis Óscar Alonso Ezpeleta. Doctor en Odontología. Profesor Contratado Doctor de la Universidad de Zaragoza.

Hacen constar que el trabajo de investigación realizado por Dr. D. Álvaro Zubizarreta Macho, que lleva por título "**INFLUENCIA DE LOS FACTORES RELACIONADOS CON LA FATIGA CÍCLICA DE LAS LIMAS ENDODÓNTICAS DE NiTi**", ha sido realizado bajo su dirección, siguiendo una rigurosa metodología, presentando unos resultados de interés y unas conclusiones derivadas de los anteriores, que hacen que dicho trabajo de investigación pueda ser defendido para optar al Grado de Doctor en Odontología.

Salamanca, Junio de 2022.

Dr. D. Alberto Francisco Albaladejo Martínez

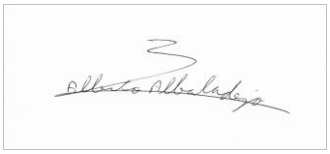

Dr. D. Luis Óscar Alonso Ezpeleta

ÍNDICE DE CONTENIDOS

Anexo 6: Comunicación tipo Póster en 10th Congreso CONSEURO de la European Federation of Conservative Dentistry: “Do Cross Section and Pitch Affect the Mechanical Behavior of Endodontic Rotary Files?”.

Anexo 7: Comunicación tipo Póster en 10th Congreso CONSEURO de la European Federation of Conservative Dentistry: “Comparative Analysis of Stress Distribution of Experimentally Designed Endodontic Rotary Files.

Anexo 8: Finalista en el 38º Congreso Nacional de la Asociación Española de Endodoncia con la Conunicación Oral de Investigación: “FileBreaker. Un nuevo dispositivo de análisis de fatiga cíclica”:

La presente Tesis Doctoral ha sido realizada por compendio de artículos, con un total de 13 artículos JCR posicionadas en primer y segundo cuartil, que se muestran en el apartado “Material, Métodos y Resultados”:

1. Faus-Llácer, V.; Kharrat, N.H.; Ruiz-Sánchez, C.; Faus-Matoses, I.; Zubizarreta-Macho, Á.; Faus-Matoses, V. The Effect of Taper and Apical Diameter on the Cyclic Fatigue Resistance of Rotary Endodontic Files Using an Experimental Electronic Device. Appl. Sci. 2021, 11, 863. https://doi.org/10.3390/app11020863

2. Roda-Casanova V, Pérez-González A, Zubizarreta-Macho A, Faus-Matoses V. Influence of Cross-Section and Pitch on the Mechanical Response of NiTi Endodontic Files under Bending and Torsional Conditions-A Finite Element Analysis. J Clin Med. 2022 May 8;11(9):2642. doi: 10.3390/jcm11092642.

3. Faus-Llácer V, Hamoud-Kharrat N, Marhuenda Ramos MT, Faus-Matoses I, Zubizarreta-Macho Á, Ruiz Sánchez C, Faus-Matoses V. Influence of the Geometrical Cross-Section Design on the Dynamic Cyclic Fatigue Resistance of NiTi Endodontic Rotary Files-An In Vitro Study. J Clin Med. 2021 Oct 14;10(20):4713. doi: 10.3390/jcm10204713.

4. Ruiz-Sánchez C, Faus-Llácer V, Faus-Matoses I, Zubizarreta-Macho Á, Sauro S, Faus-Matoses V. The Influence of NiTi Alloy on the Cyclic Fatigue Resistance of Endodontic Files. J Clin Med. 2020 Nov 21;9(11):3755. doi: 10.3390/jcm9113755.

5. Zubizarreta-Macho Á, Mena Álvarez J, Albaladejo Martínez A, Segura-Egea JJ, Caviedes Brucheli J, Agustín-Panadero R, López Píriz R, Alonso-Ezpeleta Ó. Influence of the Pecking Motion Frequency on the Cyclic Fatigue Resistance of Endodontic Rotary Files. J Clin Med. 2019 Dec 24;9(1):45. doi: 10.3390/jcm9010045.

6. Faus-Matoses V, Faus-Llácer V, Ruiz-Sánchez C, Jaramillo-Vásconez S, Faus-Matoses I, Martín-Biedma B, Zubizarreta-Macho Á. Effect of Rotational Speed on the Resistance of NiTi Alloy Endodontic Rotary Files to Cyclic Fatigue-An In Vitro Study. J Clin Med. 2022 May 31;11(11):3143. doi: 10.3390/jcm11113143.

7. Zubizarreta-Macho Á, Albaladejo Martínez A, Falcão Costa C, Quispe-López N, Agustín-Panadero R, Mena-Álvarez J. Influence of the type of reciprocating motion on the cyclic fatigue resistance of reciprocating files in a dynamic model. BMC Oral Health. 2021 Apr 7;21(1):179. doi: 10.1186/s12903-021-01538-8.

8. Zubizarreta-Macho, Á.; Alonso-Ezpeleta, Ó.; Albaladejo Martínez, A.; Faus Matoses, V.; Caviedes Brucheli, J.; Agustín-Panadero, R.; Mena Álvarez, J.; Vizmanos Martínez-Berganza, F. Novel Electronic Device to Quantify the Cyclic Fatigue Resistance of Endodontic Reciprocating Files after Using and Sterilization. Appl. Sci. 2020, 10, 4962. https://doi.org/10.3390/app10144962

9. Faus-Matoses V, Pérez García R, Faus-Llácer V, Faus-Matoses I, Alonso Ezpeleta Ó, Albaladejo Martínez A, Zubizarreta-Macho Á. Comparative Study of the SEM Evaluation, EDX Assessment, Morphometric Analysis, and Cyclic Fatigue Resistance of Three Novel Brands of NiTi Alloy Endodontic Files. Int J Environ Res Public Health. 2022 Apr 6;19(7):4414. doi: 10.3390/ijerph19074414. PMID: 35410096;

10. Roda-Casanova, V.; Zubizarreta-Macho, Á.; Sanchez-Marin, F.; Alonso Ezpeleta, Ó.; Albaladejo Martínez, A.; Galparsoro Catalán, A. Computerized Generation and Finite Element Stress Analysis of Endodontic Rotary Files. Appl. Sci. 2021, 11, 4329. https://doi.org/10.3390/app11104329

11. Roda-Casanova V, Pérez-González A, Zubizarreta-Macho Á, Faus-Matoses V. Fatigue Analysis of NiTi Rotary Endodontic Files through Finite

Element Simulation: Effect of Root Canal Geometry on Fatigue Life. J Clin Med. 2021 Dec 3;10(23):5692. doi: 10.3390/jcm10235692.

12. Faus-Matoses V, Faus-Llácer V, Aldeguer Muñoz Á, Alonso Pérez-Barquero J, Faus-Matoses I, Ruiz-Sánchez C, Zubizarreta-Macho Á. A Novel Digital Technique to Analyze the Wear of CM-Wire NiTi Alloy Endodontic Reciprocating Files: An In Vitro Study. Int J Environ Res Public Health. 2022 Mar 9;19(6):3203. doi: 10.3390/ijerph19063203.

13. Faus-Matoses V, Burgos Ibáñez E, Faus-Llácer V, Ruiz-Sánchez C, Zubizarreta-Macho Á, Faus-Matoses I. Comparative Analysis of Ease of Removal of Fractured NiTi Endodontic Rotary Files from the Root Canal System-An In Vitro Study. Int J Environ Res Public Health. 2022 Jan 10;19(2):718. doi: 10.3390/ijerph19020718.

La mayoría de ellos han sido realizados con un prototipo registrado como Modelo de Utilidad ES1219520, que se muestra en el apartado “Anexos”.

Así mismo, los resultados han sido divulgados en Congresos de índole nacional e internacional, que se muestra en el apartado “Anexos”:

1. Comunicación tipo Póster de Investigación en el XXIV Congreso Nacional y XI Internacional de la Sociedad Española de Odontología Conservadora y Estética: “Influencia de la velocidad en la fatiga cíclica de las limas NiTi”.

2. Comunicación tipo Póster de Investigación en el XXIV Congreso Nacional y XI Internacional de la Sociedad Española de Odontología Conservadora y Estética: “Estudio comparativo: resistencia a la fatiga cíclica de limas rotatorias endodónticas de NiTi”.

3. Comunicación de Investigación en las Jornadas de Investigación de la Asociación Española de Endodoncia: “Influencia de la sección

transversal en la resistencia a la fatiga cíclica de las limas endodónticas rotatorias de NiTi".

4. Comunicación de Investigación en las Jornadas de Investigación de la Asociación Española de Endodoncia: "¿Influye la sección transversal y el pitch en el comportamiento mecánico de las limas endodónticas rotatorias?".

5. Comunicación tipo Póster en 10th Congreso CONSEURO de la European Federation of Conservative Dentistry: "Do Cross Section and Pitch Affect the Mechanical Behavior of Endodontic Rotary Files?".

6. Comunicación tipo Póster en 10th Congreso CONSEURO de la European Federation of Conservative Dentistry: "Comparative Analysis of Stress Distribution of Experimentally Designed Endodontic Rotary Files.

7. Finalista en el 38º Congreso Nacional de la Asociación Española de Endodoncia con la Conunicación Oral de Investigación: "FileBreaker. Un nuevo dispositivo de análisis de fatiga cíclica":

Además, se ha realizado una estancia internacional en la Universidad Fernando Pessoa de 4 meses, que se muestra en el apartado "Anexos".

ABSTRACT

The endodontic rotary and reciprocating files of NiTi has reported to exhibit unexpected fractures inside the root canal system during the root canal treatment; which can affect the prognosis of the endodontic therapy. Therefore, it is important to assess the variables related to this intraoperative complication.

Aim: To analyze the influence of the variables related to cyclic fatigue on the fracture resistance of NiTi endodontic instruments.

To analyze the influence of the apical diameter and taper of NiTi rotary endodontic instruments on their resistance to cyclic fatigue.

To analyze the influence of cross-sectional design and pitch on the mechanical behavior of NiTi endodontic instruments under bending and torsional conditions.

To analyze the influence of the cross-sectional design of NiTi rotary endodontic instruments on the resistance to cyclic fatigue.

To analyze the influence of the NiTi alloy of endodontic rotary instruments on the resistance to cyclic fatigue.

To analyze the influence of the pecking motion frequency of NiTi rotary endodontic instruments on their resistance to cyclic fatigue.

To analyze the influence of the movement of NiTi rotary and reciprocating endodontic instruments on their resistance to cyclic fatigue.

To analyze the influence of reciprocating movements of NiTi alloy endodontic reciprocating instruments on their resistance to cyclic fatigue.

To analyze the influence of the number of uses and sterilization cycles of NiTi alloy endodontic reciprocating instruments on their resistance to cyclic fatigue.

To analyze the resistance to cyclic fatigue of new NiTi endodontic systems.

To analyze the influence of the radius and angle of curvature of the root canal system on the mechanical behavior of NiTi endodontic instruments.

To analyze the volumetric wear of NiTi endodontic reciprocating instruments subjected to cyclic fatigue.

To analyze the removal capacity of separated NiTi alloy endodontic rotary instruments within the root canal system and the wear of root dentin.

Materials and Methods: In vitro and finite element methods were performed for analyzing the variables related to the cyclic fatigue.

Results: Statistical analisys were performed in order to assess the statistical significant differences among the parameters of each variable.

Conclusions: The variables analized influences on the resistance of the NiTi alloy endodontic instruments to cyclic fatigue.

The increased apical diameter and taper of NiTi endodontic rotary files decreased their resistance to cyclic fatigue.

The use of files with a triangular-shaped cross-section and a small pitch are recommended in order to minimize ledging and maximize fatigue life.

The double S-shaped cross-section of NiTi alloy endodontic files shows higher cyclic fatigue resistance than the rectangular cross-section, the convex triangular cross-section, and the triangular cross-section of NiTi alloy endodontic files.

The NiTi CM-Gold wire alloy of the ProTaper Gold endodontic rotary files resulted in greater resistance to cyclic fatigue than ProFile Vortex Blue, ProTaper Next, and ProTaper Universal endodontic rotary files

A low frequency of pecking motion is recommended to reduce the risk of failure of endodontic rotary files associated with cyclic fatigue.

NiTi alloy endodontic rotary files using reciprocating movement at 350 rpm with 120° counterclockwise and 30° clockwise motion exhibit greater resistance to dynamic cyclic fatigue than files used with a reciprocating movement at 400 rpm with 120° counterclockwise and 30° clockwise motion, continuous rotational speed at 200 rpm, continuous rotational speed at 350 rpm, or continuous rotational speed at 500 rpm; it is therefore advisable to use reciprocating movements at a low speed.

The ReFlex Smart reciprocating movement increased the cyclic fatigue resistance of endodontic reciprocating files compared with traditional reciprocating movement.

The time of use of NiTi endodontic reciprocating files negatively afects dynamic cyclic fatigue resistance; however, dynamic cyclic resistance is not afected by the number of sterilization cycles.

Smarttrack NiTi alloy endodontic reciprocating files display greater resistance to cyclic fatigue than Endogal and Path Max Pro NiTi alloy endodontic rotary files, due to the reciprocating movement and metallurgical composition.

Significant influence of the root canal geometry on the fatigue life of the NiTi rotary files and reveal the higher importance of the radius of curvature with respect to the angle of curvature of the root canal.

The CM-wire NiTi alloy endodontic reciprocating files exhibit a volumen wear after clinical use.

Ultrasonic tips enable greater ease of removal of NiTi endodontic rotary files from the root canal system, with similar amounts of dentin removal between the two methods.

KEY WORDS: Alloy; Cyclic fatigue; Endodontics; Fracture resistance; Nitinol.

INTRODUCCIÓN

ANTECEDENTES HISTÓRICOS DEL INSTRUMENTAL ENDODÓNTICO

Según la Asociación Dental Americana, se estima que en el año 2013 se realizaron más de 20 millones de tratamientos de conductos en Estados Unidos (1). La etiología del fracaso de la terapia endodóntica está relacionada con infecciones endodónticas secundarias o persistentes, lo que implica la necesidad de realizar un retratamiento de conductos; lo cual disminuye el porcentaje de éxito hasta el 70% (2), e incluso una microcirugía endodóntica; que presenta una tasa de cicatrización del 78.3% y una tasa de supervivencia del 95.2% entre 5-9 años de evolución (3).

En los últimos años, la caracterización molecular de la microbiota oral ha permitido detectar 700 especies bacterianas o biotipos bacterianos con capacidad para colonizar los tejidos de la cavidad bucal: superficie epitelial gingival, tejido conectivo subyacente, mucosa yugal, lengua, y dientes (4). Sin embargo, solo un limitado número de especies bacterianas tienen la capacidad para colonizar y proliferar en el sistema de conductos radiculares (5,6,7), a consecuencia de las características inherentes al sistema de conductos radiculares (7).

La infección bacteriana constituye un papel esencial en la etiología, instauración y desarrollo de la patología pulpar en el sistema de conductos radiculares y la formación de lesiones en los tejidos periapicales (8).

Los objetivos del tratamiento de conductos radiculares implican la limpieza y conformación del sistema de conductos radiculares (9). La caracterización molecular de la microbiota endodóntica ha permitido identificar las especies bacterianas más prevalentes y patógenas de los dientes afectados por infecciones endodónticas primarias; las cuales están constituidas por una microbiota mixta en la que predominan (10).

La mayoría de los biotipos bacterianos que infectan el sistema de conductos radiculares son patógenos oportunistas anaerobios con capacidad para colonizar el sistema de conductos radiculares; formando biofilms mixtos, complejos y resistentes a (11). Algunas especies bacterianas tienen incluso la capacidad para colonizar los túbulos dentinarios hasta una profundidad de 266.5±92.63 µm y adherirse al colágeno; permitiendo colonizar conductos accesorios, anastomosis, istmos y espacios de difícil acceso para el instrumental endodóntico y los agentes irrigantes; los cuales solo tienen capacidad para penetrar 130 µm en el interior de los túbulos dentinarios (12).

La remoción completa de los microorganismos presentes en el sistema de conductos radiculares durante la terapia endodóntica o al menos una reducción significativa que permitir la reparación de los tejidos periapicales, se considera un factor determinante en el pronóstico del tratamiento de conductos (13).

El pronóstico de la terapia endodóntica está íntimamente asociado a la carga bacteriana preoperatoria, así como a la microbiota endodóntica remanente tras realizar el tratamiento de conductos. Los cultivos microbiológicos negativos obtenidos tras realizar el tratamiento de conductos se relacionan con tasas de éxito cercanas al 94%; sin embargo, el porcentaje de éxito de la terapia endodóntica se reduce al 68% en cultivos microbiológicos positivos (14).

Sin embargo, los avances en radiodiagnóstico, sistemas de magnificación, agentes de desinfección del sistema de conductos radiculares y el desarrollo de sistemas de activación de los agentes irrigantes, han permitido aumentar la tasa de éxito del tratamiento de conductos (6). Además, el diseño geométrico de los instrumentos rotatorios de NiTi ha permitido una mayor desinfección del sistema de conductos radiculares; especialmente el aumento del diámetro apical (15) y la conicidad, que ha permitido que los agentes irrigantes puedan penetrar hasta el tercio apical del sistema de conductos (16).

SITUACIÓN ACTUAL DEL INSTRUMENTAL ENDODÓNTICO

El instrumental endodóntico ha experimentado notables cambios desde su aparición, inspirados en el diseño geométrico y aleación metalúrgica. Inicialmente, los instrumentos endodónticos se fabricaban en acero inoxidable con una sección cuadrada; posteriormente, Buehler & Wang introdujeron la aleación de Niquel-Titanio (NiTi) durante sus investigaciones en ingeniería naval (17). Posteriormente, Walia et al utilizaron por primera vez la aleación de NiTi en endodoncia, tras utilizar un alambre ortodóncico de NiTi para fabricar limas K manuales de 150 µm de diámetro apical, las cuales mostraban entre 2 y 3 veces mayor flexibilidad y resistencia a la fractura torsional en comparación con instrumentos similares de acero inoxidable (18).

Las propiedades físico-mecánicas proporcionadas por la aleación de NiTi a las limas K manuales mejoró el comportamiento del instrumental endodóntico durante la instrumentación del sistema de conductos radiculares, lo que extendió su uso hasta la actualidad.

Concretamente, las propiedades de superelasticidad y memoria de forma proporcionadas por la aleación de NiTi permitieron reducir el transporte apical accidental de los instrumentos manuales y realizar una instrumentación más conservadora con una adaptación más centrada en el sistema de conductos radiculares (19,20,21,22) en base a la mayor flexibilidad proporcionada por su menor módulo de elasticidad (18).

Posteriormente, la aparición de los sistemas de instrumentación rotatorios accionados por micromotores de endodoncia permitió reducir el tiempo de conformación y alisado radicular de la terapia endodóntico, gracias a su movimiento continuo de rotación y su mayor capacidad de corte; reduciendo a su vez el riesgo de complicaciones intraoperatorias (23).

Así mismo, las modificaciones realizadas en el diseño geométrico del instrumental rotatorio; en especial el aumento de la conicidad permitió aumentar la resistencia a la fractura de estos instrumentos, en comparación con las limas K manuales de acero inoxidable (24).

COMPOSICIÓN QUÍMICA DEL INSTRUMENTAL ENDODÓNTICO DE NI-TI

En sus inicios, la composición química de los instrumentos de NiTi estaba compuesta exclusivamente por átomos de níquel y titanio dispuestos en una proporción equiatómica (relación 1:1) y un peso atómico heterogéneo de níquel (56%) y titanio (44%), que se corresponde con la aleación SE-Wire o NiTiNOL-55 o NiTiNOL SE508 (25,26).

ESTRUCTURA QUÍMICA DEL INSTRUMENTAL ENDODÓNTICO DE NI-TI

La aleación de NiTi puede alterar la distribución de los elementos atómicos de níquel y titanio adquiriendo diferentes geometrías espaciales termo-dependientes. Estas formas reciben el nombre de fases “microestructurales” o “cristalográficas” de la aleación de NiTi y son las responsables de alterar las propiedades y por ende el comportamiento físico-mecánico de los instrumentos endodónticos de NiTi (27,28).

Tradicionalmente, se han descrito dos fases microestructurales de la aleación de NiTi llamadas “martensita” y “austenita”. Posteriormente, se ha descrito una tercera fase denominada como fase “R”, “premartensítica” o de “transformación premartensítica”, que surge durante la transición de la fase martensítica a la fase austenítica y viceversa, tras someter a la aleación a cambios térmicos y/o tensionales (29,30).

FASE MICROESTRUCTURAL AUSTENÍTICA

Esta fase cristalográfica de la aleación de NiTi se caracteriza por presentar una estructura estable, descrita como fase “madre” o de “alta temperatura”.

Presenta una geometría cúbica (B2) con los átomos de titanio localizados en los extremos y los átomos de níquel en el centro. Esta fase microestructural proporciona dureza al instrumental endodóntico de NiTi (31), pero mantiene la capacidad elástica de recuperar la forma original tras cesar la tensión que provoca la deformación del material (19).

FASE MICROESTRUCTURAL MARTENSÍTICA

Esta fase cristalográfica de la aleación de NiTi se caracteriza por presentar una estructura monoclínica (B19´) compleja e inestable, descrita como fase "hija" o de "baja temperatura". Esta fase microestructural proporciona ductilidad al instrumental endodóntico de NiTi que le dota de mayor plasticidad, pero impide la capacidad elástica de recuperar la forma original tras cesar la tensión que provoca la deformación del material (31). Por último, la martensita muestra un módulo de elasticidad más bajo (30-40 GPa) que la austenita (80-90 GPa) (32), y el módulo de elasticidad de la fase R es incluso más bajo que el de la martensita (30), por lo que la austenita se define como un material más rígido.

FASE MICROESTRUCTURAL R O PREMARTENSÍTICA

Esta fase cristalográfica de la aleación de NiTi se caracteriza por presentar una geometría romboidal. Esta fase microestructural precede a la transformación martensítica en un rango térmico estrecho entre la fase cristalográfica austenítica y martensítica (33), pero presenta propiedades termoelásticas que le permiten recuperar la fase microestructural austenítica al incrementar la temperatura (34). Así mismo, la fase R o romboédricamente distorsionada puede aparecer antes de la transformación a martensita, bajo ciertas condiciones, como incrementar la temperatura de la aleación de NiTi hasta los 400°C para provocar la precipitación de la fase Ti_3Ni_4, incorporar un tercer elemento aleante (aluminio, carbono, oxígeno) o aplicar un tratamiento térmico tras la fabricación en frío para crear estructuras de dislocación reorganizadas. (35). Esta transformación en fase R se establece como una transformación

martensítica propiamente dicha que compite con la transformación martensítica posterior (36).

TRANSFORMACIÓN DE FASE MICROESTRUCTURAL

La aleación de NiTi tiene la capacidad de transformar su fase cristalográfica sometida a alteraciones térmicas, así como estrés mecánico durante su funcionamiento en el interior del sistema de conductos radiculares (37).

PROPIEDADES FÍSICO-MECÁNICAS DEL INSTRUMENTAL ENDODÓNTICO DE NITI

La aleación de NiTi ofrece propiedades físico-mecánicas superiores a las aleaciones de acero inoxidable que influyen sobre su superelasticidad y memoria de forma, permitiendo realizar tratamientos más seguros con menor incidencia de complicaciones intraoperatorias. La microestructura cristalina de la aleación de NiTi permite adquirir diferentes propiedades físico-mecánicas al instrumental endodóntico.

SUPERELASTICIDAD INDUCIDA POR TENSIÓN

La superelasticidad inducida por tensión de la microestructura cristalina de la aleación de NiTi permite al instrumental endodóntico experimentar deformaciones elásticas superiores a las del acero, sin entrar en deformación plástica (19).

La microestructura cristalina en fase austenítica sometida a tensión experimenta una transformación a fase martensítica reversible si cesa la tensión (37,30).

A pesar de que la microestructura cristalina martensítica se considera una fase inestable, se ha mostrado estable bajo tensión, lo que resulta clínicamente relevante durante la instrumentación del sistema de conductos radiculares (38). En caso de exponer al instrumental endodóntico de NiTi a curvaturas severas o conductos obliterados por metamorfosis cálcicas, la microestructura cristalográfica a alta temperatura (austenítica) de la aleación de NiTi adapta su geometría espacial adquiriendo una estructura monoclínica (martensítica), con mayor capacidad para absorber las tensiones generadas controlando la deformación. Concretamente, la superelasticidad de los instrumentos de aleación NiTi en fase martensítica pueden deformarse elásticamente hasta un 8% sin detrimento de recuperar su forma original; sin embargo, los instrumentos de acero inoxidable permiten una deformación elástica del 1% antes de comenzar a deformarse irreversiblemente (19,20).

Adicionalmente, se ha descrito también el concepto “pseudoelasticidad”, como la transformación entre austenita estable y fase de martensita inducida por tensión (39).

MEMORIA DE FORMA INDUCIDA TÉRMICAMENTE

La microestructura de la aleación de NiTi experimenta cambios en su microestructura cristalina inducidos térmicamente, que influyen sobre las propiedades físico-mecánicas del instrumental endodóntico. La microestructura cristalina de la aleación de NiTi se mantiene estable a altas temperaturas, con sus átomos dispuestos en geometría cúbica (fase austenítica). Sin embargo, el enfriamiento de la aleación produce un cambio en la disposición espacial de los átomos de NiTi, que adquieren una geometría monoclínica inestable (fase de baja temperatura). La temperatura en la que los átomos de NiTi comienzan a modificar su geometría adquiriendo una forma monoclínica inestable recibe el nombre de “inicio de transformación martensítica” (Ms). Sin embargo, La temperatura en la que los átomos de NiTi finalizan la transformación de fase martensítica recibe el nombre de “temperatura final de transformación martensítica” (Mf).

La transformación de fase martensítica es reversible, pudiendo volver a una fase de alta temperatura (“fase austenítica”) si se aumenta gradualmente la temperatura de la aleación. La temperatura en la que los átomos de NiTi comienzan a modificar su geometría adquiriendo una forma cúbica estable recibe el nombre de “inicio de transformación austenítica” (As). Sin embargo, La temperatura en la que los átomos de NiTi finalizan la transformación de fase austenítica recibe el nombre de “temperatura final de transformación austenítica” (Af) (19,20).

Las temperaturas de inicio y finalización relativas a la transformación de fases pueden variar al enfriar o calentar la aleación de NiTi (40).

El rango de las temperaturas de transición de la fase cristalina de alta temperatura (austenítica) a la fase cristalina de baja temperatura (martensítica), recibe el nombre de “rango de temperaturas de transición”. El rango de las temperaturas de transición de la fase cristalina de baja temperatura (martensítica) a la fase cristalina de alta temperatura (austenítica), recibe el nombre de “rango de temperaturas de transición reverso” (41). La fase microestructural premartensítica (fase R) se localiza en una franja estrecha de este rango de temperaturas de transición (40).

La transformación de fase martensítica deformada estable inducida térmicamente proporciona la capacidad de recuperar la forma original del instrumental endodóntico de NiTi al aumentar la temperatura de la aleación (42) por encima de los 125° (19).

Si la temperatura ambiente está por encima de la

FACTORES RELACIONADOS CON LAS TEMPERATURAS DE TRANSICIÓN

Sin embargo, factores como la composición metalúrgica, elementos aleantes, impurezas o el tratamiento térmico inherente al proceso de manufactura

pueden influir sobre las temperaturas de transformación de las microestructuras cristalográficas y, por ende, sobre el comportamiento físico-mecánico del instrumental endodóntico de NiTi (43,44,45).

COMPOSICIÓN DE LA ALEACIÓN DE NiTi

Originalmente, la composición química de los instrumentos endodónticos de NiTi fabricados en base a la aleación SE-Wire, NiTiNOL-55 o NiTiNOL SE508 estaban compuesta por níquel y titanio; sin embargo, modificaciones en el peso atómico de estos elementos aleantes pueden variar las propiedades físico-mecánicas de los instrumentos endodónticos de NiTi (41).

La aleación de NiTi es especialmente sensible a las variaciones en el peso atómico del níquel y a las modificaciones realizadas en el rango de temperaturas de transición. Los instrumentos endodónticos de NiTi cuyas aleaciones presentan un 60% de peso atómico de níquel (NiTiNOL-60) en su composición, muestran una menor capacidad para recuperar su forma original; sin embargo, son más susceptibles a recibir tratamientos térmicos durante el proceso de fabricación. Además, el incremento del peso atómico del níquel o la incorporación de otros elementos aleantes como el cobalto, pueden reducir la temperatura de transición (19).

ELEMENTOS ALEANTES DE LA ALEACIÓN DE NiTi

Por otra parte, la existencia de dos microestructuras cristalinas diferentes y la correspondiente transformación alotrópica influyen notablemente sobre las propiedades físico-mecánicas del titanio y sus aleaciones. El titanio es un metal alotrópico y puede estar constituido por dos microestructuras cristalográficas:

- Hexagonal compacta o HCP, que se identifica como α.
- Cúbica centrada en el cuerpo o BCC que se identifica como β.

Dependiendo del efecto estabilizador sobre las fases α y β, los elementos de aleación del titanio se clasifican en:

- Elementos neutros.
- Elementos betágenos o estabilizadores de la fase α.
- Elementos alfágenos o estabilizadores de la fase β.

La estabilización de las fases implica el aumento o disminución de la temperatura de transición β. Pues bien, los elementos alfágenos incrementan la temperatura de transición β. Entre los elementos alfágenos el aluminio es con diferencia el elemento de aleación más importante, aunque también se puede emplear el oxígeno estos dos elementos químicos se utilizan comercialmente en las aleaciones de titanio, pero el carbono y el nitrógeno también se pueden emplear, aunque no comercialmente o industrialmente.

IMPUREZAS

Los procesos de manufactura del instrumental endodóntico de NiTi no están exentos de irregularidades. Así mismo, las tensiones o deformaciones generadas durante el proceso de fabricación pueden influir sobre la orientación de la microestructura cristalina y por ende sobre la superelasticidad de la aleación de NiTi. Los sistemas de instrumentación rotatoria de NiTi fabricados por torsión (Twisted File) son especialmente sensibles a este concepto. Por otra parte, los sistemas de instrumentación rotatoria de NiTi fabricados por mecanizado y/o sometidos a tratamientos térmicos pueden incorporar imperfecciones que pueden influir sobre las temperaturas de transformación de fases cristalográficas (30).

TRATAMIENTOS TÉRMICOS DE LA ALEACIÓN DE NiTi

Brantley et al demostraron que los instrumentos endodónticos de NiTi fabricados por mecanizado o sometidos a tratamiento térmico durante su manufactura presentan una temperatura final de transformación austenítica inferior o similar a la temperatura corporal lo que dota al instrumental endodóntico de propiedades superelásticas durante el uso clínico del instrumental (46).

La fabricación del instrumental endodóntico se realiza en frío en hornos de aire o de atmósfera inerte que permiten que la aleación adquiera propiedades de superelasticidad y memoria de forma. El trabajo en frío aumenta significativamente la incidencia de defectos de la microestructura cristalina de la aleación de NiTi y da como resultado una microestructura que contiene martensita residual en una matriz austenítica (45). Actualmente, disponemos de sistemas de instrumentación endodóntica de NiTi cuyas aleaciones tratadas térmicamente difieren en el rango de transformación térmica de las microestructuras cristalinas; específicamente en la temperatura final de transformación austenítica. El tratamiento térmico de la aleación de NiTi fresada en frío en un rango térmico entre 450–550°C genera tensiones internas en la microestructura cristalina y reduce los defectos de la red cristalina al proporcionar a los átomos suficiente energía térmica para reorganizarse (45). Además, las aleaciones de NiTi tratadas térmicamente aumentan significativamente la resistencia a la fatiga cíclica, así como las temperaturas de transformación que la aleación de NiTi no tratada térmicamente, obteniendo mayor concentración de microestructura cristalina en fase martensítica (45). Por otra parte, las propiedades superelásticas de la aleación de NiTi se pueden potenciar sometiendo a la aleación a ciclos térmicos bajo estrés mecánico (baño frío entre 0–10°C y baño caliente entre 100–180°C bajo restricción de elongación entre 1-4%) (47). Cabe destacar que las propiedades físico-mecánicas del instrumental endodóntico de NiTi, las temperaturas de transformación y las composiciones de fase de la aleación de NiTi están influenciadas principalmente por el tratamiento termomecánico más que por la composición química elemental (37). Una composición mixta de las diferentes fases cristalográficas de la microestructura de NiTi debido a cambios en las temperaturas de transformación constituye la principal diferencia entre la aleación de NiTi tratada termomecánicamente y la aleación de NiTi convencional. Mientras que la aleación de NiTi convencional contiene austenita (19), la aleación de NiTi tratada termomecánicamente contiene cantidades variables de fase R y martensita (26,48).

ALEACIÓN NiTi EN FASE AUSTENÍTICA

Zhou et al confirman que la microestructura cristalina de los instrumentos endodónticos de NiTi deben estar constituida principalmente en fase de alta temperatura para presentar propiedades superelásticas (49), así mismo, la aleación de NiTi en fase austenítica puede experimentar una transformación de fase cristalina a martensita inducida por tensión (en sistemas de conductos radiculares obliterados o radios y/o ángulos de curvatura pronunciados) denominada "martensita inducida por tensión" (*stress-induced martensite* (SIM)). La microestructura cristalina en fase martensítica inducida por tensión no es estable a temperatura ambiente o corporal, por lo que se revierte la microestructura cristalina a la fase austenítica original.

Aleación NiTi convencional

La aleación de NiTi convencional presenta una microestructura cristalina en fase austenítica, ya que la temperatura final de transformación de fase austenítica está por debajo de los 37°C (46), lo que le proporciona propiedades superelásticas. El proceso de fabricación de estos instrumentos debe realizarse por mecanizado en vez de torsionado (19), lo que puede conducir la aparición de defectos superficiales que pueden condicionar el comportamiento del instrumental endodóntico de NiTi, reduciendo su resistencia a la fractura, eficacia de corte y resistencia a la corrosión (19).

Algunos sistemas de instrumentación fabricados con una aleación de NiTi formulada en fase austenítica son: Mtwo, OneShape, ProFile, ProTaper Universal.

Electropulido

Se describe como un proceso de remoción superficial de instrumentos de metal que permite una eliminación electroquímica controlada de la superficie del material que conduce a una superficie más suave con mayor brillo (50,51,52). Durante la fabricación del instrumental endodóntico de NiTi se utiliza para

eliminar las irregularidades superficiales y la tensión residual causada por el proceso de pulido anterior. Se supone que esto mejora la resistencia a la fractura, la eficiencia de corte y la resistencia a la corrosión (30), con respecto a instrumentos endodónticos de NiTi no electropulidos (53,54,55).

Algunos sistemas de instrumentación fabricados mediante electropulido son: RaCe, BioRaCe, iRace, F360, F6 Skytaper.

Aleación NiTi M-Wire

La aleación M-Wire (denominada así por Gambarini et al (56) introducida en 2007 por Sportswire LLC (Langley, OK, USA), constituye una aleación de NiTi procesada térmicamente y estable a temperatura corporal a base de 55.8 ± 1.5 (% en peso) de níquel, 44,2 ± 1,5 (% en peso) de titanio y menos de 1% en peso de otros elementos. Fue desarrollada mediante procesamiento termomecánico y contiene tres fases cristalinas a temperatura corporal: martensita, fase R y austenita. Esta aleación finaliza la transformación austenítica entre los 43-50°C (57,58); sin embargo, las aleaciones Gold Wire no experimentan una transformación austenítica hasta los 50°C (59,60), por lo que se encuentran en fase martensítica a temperatura corporal, pudiendo transformarse a una mezcla de fase R y austenita durante su uso clínico, manteniendo un estado superelástico (61).

Las aleaciones M-Wire han demostrado mayor flexibilidad que las aleaciones de NiTi convencional (62). Así mismo, las estructuras cristalinas en fase martensítica y fase R han demostrado menor módulo elástico que las estructuras cristalinas en fase austenítica. Por este motivo se considera que la mayor flexibilidad de la aleación M-Wire puede atribuirse a la presencia de las fases R y martensítica.

Algunos sistemas de instrumentación fabricados con una aleación de NiTi formulada en M-Wire son: ProFile Vortex, ProFile GT Series X, ProTaper Next, Reciproc, WaveOne

Aleación NiTi en fase R

En 2008 se desarrolló un sistema de instrumentación endodóntico de aleación NiTi llamado Twisted File (SybronEndo, Orange, CA, USA), cuyo proceso de fabricación incluía tres avances: tratamiento térmico en una nueva fase microestructural (fase R), fabricación por torsión, en vez de mecanizado y un acondicionamiento superficial (63). La temperatura final de transformación austenítica se encuentra entre 18-25°C, lo que indica que estos instrumentos se mantienen en fase austenítica a temperatura ambiente, conservando las propiedades superelásticas (64). La incorporación del nuevo tratamiento térmico permitió la fabricación por torsión, ya que el módulo de cizallamiento y la deformación por transformación de fase es menos de un 10% de la experimentada por la transformación de fase martensítica (65), por lo que se requiere menos tensión para causar la deformación plástica que de lugar a la torsión. Tras el proceso de torsión, la microestructura cristalina vuelve a transformarse en austenita mediante procedimientos térmicos (64).

Algunos sistemas de instrumentación fabricados mediante electropulido con una aleación de NiTi formulada en fase R son: X3XF, Twisted File y Twisted File Adaptive.

ALEACIÓN NiTi EN FASE MARTENSÍTICA

La microestructura cristalina en fase martensítica ha demostrado ser más suave y dúctil que la austenita, se puede deformar con facilidad y conserva el efecto de memoria de forma al aumentar la temperatura. Para fabricar instrumentos endodónticos de NiTi cuya microestructura cristalina esté principalmente constituida por una fase martensítica es imprescindible elevar la temperatura final de transformación a fase austenítica mediante tratamiento termomecánico.

Aleación NiTi CM-Wire

La aleación CM-Wire De Vasconcelos et al demostraron que la composición química de la aleación "*Control-memory*" (CM)-Wire se caracteriza por un menor peso atómico de níquel, lo que aumenta la temperatura final de transformación austenítica. Esta aleación introducida en 2010 se define como la primera aleación de aplicación endodóntica tratada termomecánicamente que no posee propiedades superelásticas ni a temperatura ambiente ni a temperatura corporal (66). Debido a una composición de fase modificada, los instrumentos CM-Wire pueden deformarse debido a la reorientación de las variantes de martensita (20), por lo que no tienden a recuperar su forma original durante la instrumentación de conductos curvos (control de memoria de forma), evitando le deformación de la anatomía original del sistema de conductos radiculares.

La temperatura final de transformación a la microestructura austenítica de la aleación CM-Wire se encuentra entre los 47 y 55°C (26); sin embargo, esta temperatura puede verse alterada por el uso del instrumental endodóntico, ya la temperatura final de transformación austenítica de los instrumentos con aleación CM.Wire sin usar se encuentra entre los 32-37°C, y aumenta tras su uso hasta los 54–61°C (67). Los instrumentos endodónticos de NiTi formulados en aleación CM-Wire han evidenciado una mayor flexibilidad que los instrumentos endodónticos de NiTi con microestructura cristalina en fase de alta temperatura (68,69), manteniendo la capacidad de corte (70). Además, instrumentos endodónticos de NiTi formulados en aleación CM-Wire han mostrado una mayor resistencia a la fatiga cíclica comparado con los instrumentos endodónticos de NiTi con microestructura cristalina en fase de alta temperatura, debido principalmente a su microestructura cristalina en fase martensítica (71,72,73).

Algunos sistemas de instrumentación fabricados con una aleación de NiTi formulada en CM-Wire son: Hyflex CM, THYPOON Infinite Flex, V-Taper 2H y Hyflex EDM.

Aleación NiTi Electrical Discharge Machining (EDM)

La empresa Coltène/Whaledent introdujo en el mercado un nuevo sistema de instrumentación endodóntico de NiTi cuya microestructura cristalina se basa en una aleación CM-Wire, pero con un proceso de mecanizado fundamentado en la electroerosión, lo que proporciona a la aleación CM-Wire de mayor resistencia a la fractura y una mayor capacidad de corte. Este proceso de fabricación permite mecanizar geométricamente el instrumento a través de descargas eléctricas pulsadas (74), lo que evita el contacto con el instrumento y reduce el estrés mecánico asociado al proceso de fabricación (75). Además, Uslu et al observaron la orografía superficial de los instrumentos endodónticos de NiTi con aleación EDM antes y después de su uso clínico e informaron a que la perfilometría aumentaba, pero la rugosidad de los instrumentos endodónticos de aleación NiTi EDM era inferior a los de CM-Wire (76). La principal diferencia entre estas aleaciones radica en que la temperatura inicial de transformación de austenita y martensita y la temperatura de transformación final de austenita es más elevada en la aleación EDM, debido a que está constituida esencialmente por martensita y fase R (77); sin embargo, la microestructura cristalina de la aleación de CM-Wire está compuesta principalmente por martensita y austenita (67). Concretamente, la temperatura inicial de transformación a fase de alta temperatura de la aleación EDM es de 42°C; sin embargo, la temperatura inicial de transformación a fase de alta temperatura de la aleación CM-Wire es de 21°C a temperatura ambiente o corporal (67).

Estas condiciones han proporcionados a los instrumentos endodónticos de NiTi una mayor resistencia a la fractura que los instrumentos endodónticos de NiTi con microestructura cristalina formulada en aleación CM-Wire (78). Además, proporcionan una instrumentación más centrada en el conducto radicular, respetando la anatomía original del conducto (79,80).

Algunos sistemas de instrumentación fabricados con una aleación de NiTi formulada en CM-Wire son: Hyflex EDM.

Aleación NiTi Gold and Blue-Wire

Actualmente, existen nuevas aleaciones térmicamente tratadas que aportan un color distintivo al instrumental endodóntico de NiTi. El sistema de instrumentación endodóntico de NiTi ProFile Vortex Blue, fue el primer instrumento fabricado con tratamiento térmico por la empresa Dentsply Tulsa Dental (Tulsa, OK, USA) en 2011. Hu et al evidenció que el color azul distintivo de los instrumentos. de NiTi ProFile Vortex Blue se debe a una capa de óxido de titanio presente en la superficie de los instrumentos (81). Posteriormente, se han desarrollado otros sistemas de instrumentación endodóntica de NiTi térmicamente tratadas como ProTaper Gold (Dentsply Sirona Endodontics, Baillagues, Switzerland), Reciproc Blue, (VDW, Baillagues, Switzerland) y WaveOne Gold, Dentsply Sirona Endodontics, Baillagues, Switzerland). La principal diferencia de los instrumentos endodónticos de NiTi térmicamente tratados con aleación Blue, respecto a los instrumentos endodónticos de NiTi con aleaciones CM-Wire o aleaciones Gold, es que los instrumentos endodónticos de NiTi térmicamente tratados con aleación Blue se mecanizan antes de recibir el tratamiento térmico (82).

La temperatura final de transformación a fase de alta temperatura de los instrumentos endodónticos de NiTi ProFile Vortex Blue se encuentra en 38.5°C (81), mientras que la temperatura inicial de transformación a fase de baja temperatura se encuentra en 31°C (20). Esta aleación presenta una mayor cantidad de martensita estable que las estructuras cristalinas de la aleación M-Wire, a pesar de presentar temperaturas de transformación más bajas, lo que le proporciona un efecto de control de memoria (60).

Por otra parte, los instrumentos endodónticos de NiTi con aleación Gold deben su color distintivo a una capa superficial. La temperatura final de transformación a fase de alta temperatura de los instrumentos endodónticos con aleación Gold se encuentra en 50.0°C (**¡Error! Marcador no definido.**), lo que induce a p ensar que estos instrumentos están constituidos por una microestructura cristalina en estado de alta temperatura o fase R.

Numerosos estudios han demostrado que los instrumentos endodónticos cuya microestructura cristalina está formulada en aleación Blue o Gold presentan mayor flexibilidad y resistencia a la fractura que los instrumentos endodónticos de NiTi convencional o formulados en M-Wire (73,60,83,84,85). Además, el sistema de instrumentación de NiTi Hyflex EDM presenta una resistencia significativamente mayor a la fatiga cíclica que los sistemas instrumentación de NiTi ProTaper Gold, WaveOne Gold y Reciproc Blue (78,86).

ALEACIÓN NiTi MAXWIRE

Actualmente, se han desarrollado dos sistemas de instrumentación endodóntica (XP-endo Shaper and XP-endo Finisher) a base de una nueva aleación de NiTi térmicamente tratada llamada MaxWire (Martensite-Austenite-electropolish-fileX) (FKG Dentaire), que combina el efecto de memoria de forma y superelasticidad.

En resumen, el tratamiento termomecánico de la aleación de NiTi permite un cambio en la composición de la microestructura cristalina que conduce a la aparición de martensita o fase R en condiciones clínicas, mientras que los instrumentos compuestos por aleaciones M-Wire y fase R mantienen un estado austenítico, las aleaciones CM-Wire, así como los instrumentos con tratamiento térmico Gold y Blue, están compuestos de cantidades sustanciales de martensita.

Los instrumentos compuestos por una microestructura cristalina en fase austenítica poseen propiedades superelásticas y proporcionan valores elevados de resistencia a la fractura, lo que recomienda su uso en conductos radiculares rectos o ligeramente curvos. Además, el uso de aleaciones de NiTi compuestas por una microestructura cristalina en fase austenítica puede compensar la menor resistencia a la torsión de limas de pequeño diámetro.

Los instrumentos compuestos por una microestructura cristalina en fase martensítica resultan más flexibles y presentan una mayor resistencia a la fatiga cíclica debido a una mayor cantidad de fase martensita. Se sabe que la

fatiga cíclica es más probable en curvaturas complejas y anatomías de conductos radiculares. Además, los instrumentos compuestos por una microestructura cristalina en fase martensítica se recomiendan en casos de sistemas de conductos radiculares con curvaturas severas o doble curvatura.

COMPLICACIONES ASOCIADAS AL INSTRUMENTAL ENDODÓNTICO DE NITI

El instrumental endodóntico de NiTi no está exento de experimentar complicaciones intraoperatorias durante su uso.

TRANSPORTE APICAL Y FALSA VÍA

La anatomía del sistema de conductos radiculares puede contribuir a la aparición de complicaciones intraoperatorias. La presencia de angulaciones y/o radios de curvatura radicular acentuados pueden influir sobre la aparición de transportes ectópicos del ápice, que puede dificultar al sellado de la constricción apical durante la obturación del sistema de conductos radiculares. La aparición de transportes apicales puede dificultar la desinfección y obturación del sistema de conductos radiculares, conduciendo a la aparición o persistencia de lesiones periapicales (87,88).

Por lo tanto, la microestructura de la aleación de NiTi y el diseño geométrico del instrumental endodóntico de NiTi puede influir sobre la aparición del transporte apical.

Actualmente, el desarrollo de nuevos sistemas de instrumentación de NiTi sometidos a tratamientos metalúrgicos y termomecánicos han incrementado la flexibilidad y la resistencia a la fatiga cíclica y torsional del instrumental endodóntico (89,90,91). Estas aleaciones proporcionan a los sistemas de instrumentación la capacidad de mantenerse centrados en el sistema de conductos radiculares, respetando la anatomía original del conducto radicular y

evitando la aparición de transportes apicales. Además, la sección transversal y conicidad de los instrumentos endodónticos de NiTi puede reducir la masa, dando como resultado instrumentos más flexibles con mejor adaptación al sistema de conductos radiculares (92).

Algunos autores han evidenciado que los sistemas de instrumentación rotatoria de NiTi de sección transversal trapezoidal descentrada, con una conicidad decreciente en dirección coronal, proporcionan una mayor flexibilidad y una instrumentación más centrada y por ende más adaptada a la anatomía original del sistema de conductos radiculares que otros sistemas de instrumentación rotatoria (93,94,95,96) y sistemas reciprocantes (97); sin embargo, la revisión sistemática realizada por Ahn et al concluyó que los sistemas de instrumentación reciprocante se mantenían más centrados en el conducto radicular además de proporcionar una mayor resistencia a la fatiga cíclica (98). Sin embargo, todos los sistemas de instrumentación analizados en los artículos seleccionados reflejaron transportes apicales inferiores a 300 µm, considerado un valor a partir del cual la capacidad de sellado del material de obturación puede verse afectado negativamente (99), por lo que ambos sistemas de instrumentación se consideran seguros en relación al transporte apical.

FRACTURA DEL INSTRUMENTAL ENDODÓNTICO

Diferentes autores han informado que la fractura de las limas manuales de acero inoxidable se encuentra entre el 2-6%, mientras que la incidencia del instrumental endodóntico rotatorio de NiTi varía entre el 1.67 y el 5% (100,101,102).

La fractura súbita e inesperada del instrumental endodóntico de NiTi puede ocasionarse por dos fenómenos físicos acontecidos durante la instrumentación del sistema de conductos radiculares.

FRACTURA POR TORSIÓN

La fractura por torsión se produce cuando el extremo del instrumental endodóntico sufre un bloqueo en el interior del sistema de conductos radiculares y el resto del instrumento se mantiene en rotación hasta que se deviene su fractura (100). Este tipo de fractura está asociada a sistemas de conductos radiculares obliterados (metamorfosis cálcica) en los que el instrumental endodóntico de NiTi experimenta un elevado grado de fricción contra las paredes de dentina radicular (103). En el momento en que la resistencia el corte es superior a la capacidad de corte el instrumento endodóntico de NiTi se detiene generalmente en su parte más apical, mientras el resto del instrumento endodóntico de NiTi continúa girando. La fractura del instrumento acontece tras producirse una deformación elástica inicial, seguida por una deformación plástica al superarse el límite elástico de la aleación de NiTi (66,104).

FRACTURA POR FLEXIÓN O FATIGA CÍCLICA

A diferencia de la anterior, la fractura por flexión no está relacionada con sistemas de conductos radiculares obliterados, sino con sistemas de conductos radiculares con una angulación y/o radio de curvatura radicular acentuados. En el punto de máxima curvatura se alternan ciclos de tensión-compresión a la velocidad de rotación angular programada en el motor de endodoncia (105). La fractura del instrumento se produce cuando se supera el límite elástico en el ángulo de máxima curvatura del sistema de conductos radiculares, que se refleja en la región del instrumento endodóntico de NiTi en el que se alternan los ciclos de tensión-compresión (106). La superficie externa del instrumento endodóntico de NiTi experimenta un fenómeno de tensión, mientras que la superficie interna del instrumento endodóntico de NiTi está sometido a compresión (73).

Los instrumentos endodónticos de NiTi experimentan tres etapas durante la fatiga por flexión que se suceden secuencialmente por acúmulo de fatiga o stress: Inicialmente, se generan microcracks en la superficie del instrumento

que pueden progresar en profundidad. A continuación, las fisuras se extienden a lo largo de la microestructura cristalográfica. En las microestructuras cristalinas formuladas en fase de baja temperatura, la adaptación cristalográfica de la martensita inducida por la tensión adoptando una geometría monoclinica, reduce su propagación. Finalmente se produce la deformación plástica y la fractura (107,108).

A pesar de que la fractura del instrumental endodóntico de NiTi es difícilmente atribuible a uno solo de estos conceptos y que ambos suelen contribuir a la fractura del instrumental, Parashos et al relaciona el 30% de las fracturas del instrumental endodóntico rotatorio de NiTi con la fractura torsional y el 70% a la fractura por torsión (100). Así mismo, resulta difícil aislar estas variables científicamente, tanto los estudios clínicos como los experimentales en condiciones controladas someten a los instrumentos endodónticos de NiTi a fatiga torsional y cíclica.

FACTORES QUE INFLUYEN SOBRE LA RESISTENCIA A LA FATIGA CÍCLICA DEL INSTRUMENTAL ENDODÓNTICO DE NiTi

Numerosos factores han demostrado su influencia sobre la resistencia a la fatiga cíclica del instrumental endodóntico de Ni-Ti. Principalmente, la etiología de la fractura del instrumental endodóntico se debe a factores relacionados con el diseño geométrico y composición metalúrgica del instrumental endodóntico de NiTi, así como a factores relacionados con el radio y ángulo de curvatura del sistema de conductos radiculares.

DIÁMETRO APICAL DEL INSTRUMENTAL ENDODÓNTICO DE NiTi (“*TIP*”)

La conicidad y el diámetro apical del instrumental endodóntico de NiTi condicionan el diámetro del instrumento en el punto de máxima curvatura del conducto, uno de los factores más destacados en la resistencia a la fatiga cíclica (109,110,111,112,113). Así mismo, el diámetro apical también influye sobre la capacidad de penetración del instrumental endodóntico en el sistema

de conductos radiculares y por tanto sobre el torque y tiempo de instrumentación (114).

Pruett et al destacó la menor resistencia a la fatiga cíclica los de instrumentos endodoónticos rotatorios de NiTi de mayor diámetro apical, respecto a instrumentos de menor diámetro y por tanto más flexibles (115).

Ehrhardt et al determinó que las limas 10.04 y 15.05 del sistema de instrumentación endodóntica Mtwo presentaban menor resistencia a la fatiga cíclica debido a su baja resistencia al torque y a la fatiga mecánica experimentada en conductos estrechos sin instrumentación previa (116). Sin embargo, Inan et Gonulol evidenciaron una resistencia significativamente mayor ($p > 0.05$) a la fractura cíclica debido a la flexibilidad proporcionada por su menor diámetro y conicidad (117).

CONICIDAD DEL INSTRUMENTAL ENDODÓNTICO DE NiTi (“*TAPER*”)

Otros autores han destacado el efecto de la conicidad del instrumental endodóntico rotatorio de NiTi sobre la resistencia a la fatiga cíclica. Gambarini et al observó que la resistencia a la fatiga cíclica del instrumental endodóntico de NiTi se reducía a medida que aumentaba la conicidad (118). Esto puede deberse a que la conicidad aumenta la superficie de contacto con el sistema de conductos radiculares, así como la masa del instrumento y por ende su rigidez, lo que resulta determinante en el comportamiento del instrumental endodóntico rotatorio de NiTi en conductos curvos. Además, los instrumentos de mayor conicidad acumulan más tensión durante los ciclos de tensión-compresión en el punto de máxima curvatura del sistema de conductos radiculares (119); los cuales también son dependientes de la velocidad angular (revoluciones por minuto) del micromotor de endodoncia. Así mismo, el aumento del diámetro también puede influir en un aumento de los valores de fatiga torsional (100).

Además, los instrumentos de conicidad constante han resultado ser poco conservadores con la dentina pericervical de los conductos radiculares; donde

el instrumento alcanza su máximo diámetro, fragilizando el diente y volviéndolo más susceptible a la fractura. Por este motivo, los fabricantes han introducido sistemas de instrumentación rotatoria de NiTi de conicidad variable que resultan más respetuosos con la dentina pericervical.

Actualmente, la tendencia se dirige a utilizar instrumentos endodónticos rotatorios de NiTi de menor conicidad o de conicidad variable con un comportamiento más conservador con la dentina radicular; especialmente a nivel vervical.

SECCIÓN TRANSVERSAL DEL INSTRUMENTAL ENDODÓNTICO DE NiTi

El diseño geométrico de la sección transversal del instrumental endodóntico de NiTi desempeña un papel esencial en la resistencia a la fatiga cíclica del instrumental endodóntico. El diseño de la sección transversal determina la masa del instrumento y por ende su elasticidad, su capacidad de corte y evacuación de residuos (120).

Así mismo, se ha demostrado que instrumentos con mismo tip, taper y microestructura cristalina de la aleación de NiTi, pero diferente diseño geométrico en la sección transversal, presentaban un comportamiento diferente frente a la fatiga cíclica (121).

Del mismo modo, otros autores encontraron una relación inversamente proporcional entre el área de la sección transversal del instrumento endodóntico rotatorio de NiTi y la resistencia a la fatiga cíclica del mismo, ya que una mayor superficie de la sección transversal proporciona mayor masa al instrumento haciéndolo más rígido y por ende menos flexible y resistente a la fatiga cíclica. Así mismo, los diseños de sección transversal con mayor área presentarán mayor superficie de contacto con el sistema de conductos radiculares, aumentando las tensiones y la fatiga en el interior del instrumento. Berutti et al compararon la resistencia a la fatiga cíclica de una lima con un diseño de sección transversal triangular convexo (ProTaper Universal) con otra

lima con un diseño de sección transversal triangular cóncava (ProFile), concluyendo que la menor masa del instrumento con sección transversal en "S" itálica presentaba un mejor comportamiento frente a la fatiga cíclica (27).

Así mismo, se ha analizado el comportamiento mecánico y la distribución del stress de diferentes diseños de sección transversal en condiciones de flexión y torsión. Berutti et al observaron que los instrumentos con un diseño de sección transversal en triple-U resultaban más flexibles que el diseño de sección transversal triangular; sin embargo, resultaban más resistentes en condiciones de torsión. Por otra parte, la distribución de las tensiones de los instrumentos de sección transversal triangular fue más baja y uniforme que en los instrumentos con diseño en triple-U (27). Además, Schäfer et al demostraron la relación entre el área de la sección transversal y la flexibilidad de los instrumentos (120).

SURCO DE EVACUACIÓN DE RESIDUOS (FLUTE)

La eficacia del surco de evacuación ("f*lute*") para remover los restos de tejido orgánico e inorgánico del interior del sistema de conductos radiculares está determinada por su profundidad, diseño, extensión ("*pitch*") y ángulo de corte.

La profundidad y la extensión del *flute* condiciona también la masa del material influyendo en su flexibilidad. Así mismo, su extensión condiciona el paso de roscar (*pitch*), lo que aumenta o reduce la superficie de contacto con el sistema de conductos radiculares y aumenta o reduce el fenómeno de atornillamiento del instrumento endodóntico rotatorio de NiTi en el interior del sistema de conductos radiculares. Además, un déficit en el espacio diseñado para evacuar los restos de tejido orgánico e inorgánico del interior del sistema de conductos radiculares puede influir en el aumento de las tensiones por torsión del instrumento durante su uso, ya que un excesivo acúmulo de los restos de tejido en el interior del sistema de conductos radiculares aumentará la fricción del instrumento y dificultará su avance.

Este parámetro (*flute*) no ha sido objeto de investigaciones ya que guarda estrecha relación con el *pitch* y el diseño de la sección transversal, que han sido ampliamente estudiados.

Así mismo, Parashos et Messer destacaron que longitud del *flute* también puede afectar a la resistencia a la fractura del instrumental endodóntico de NiTi (100).

ÁNGULO HELICOIDAL DEL INSTRUMENTAL ENDODÓNTICO DE NiTi

El ángulo formado por la arista de corte y el eje longitudinal del instrumento endodóntico de NiTi recibe el nombre de "ángulo helicoidal". Este rasgo geométrico del instrumental endodóntico influye sobre la capacidad de corte del instrumental endodóntico, y por ende sobre su capacidad de avance.

DISTANCIA ENTRE LAS ARISTAS DE CORTE DEL INSTRUMENTAL ENDODÓNTICO DE NiTi ("*PITCH*")

La distancia entre las aristas de corte (paso de rosca o "*pitch*") determina la capacidad de penetración y el fenómeno de atornillamiento del instrumental endodóntico de NiTi.

PROCESO TERMO-MECÁNICO DE FABRICACIÓN DEL INSTRUMENTAL ENDODÓNTICO

Inicialmente, el instrumental endodóntico manual se fabricó en acero inoxidable y posteriormente en NiTi. La mecanización de los procesos endodónticos ha motivado la aparición de nuevas aleaciones con el propósito de inducir cambios en su estructura cristalina para inferir mejoraras en las propiedades físico-mecánicas del instrumental endodóntico rotatorio de NiTi.

Inicialmente, se realizaba una fundición al vacío de los elementos aleantes de la aleación de NiTi, seguida de un proceso de forjado a alta temperatura y un proceso de enfriamiento para permitir laminar y estirar el material. Finalmente,

el material se sometía a una serie de tratamientos térmicos y un proceso de fresado a fin de obtener la morfología del instrumento (19). Sin embargo, estos procesos resultaban imprecisos y generaban tensiones internas en el material que ocasionaban defectos estructurales en el instrumento (18,30,104). Esto propició el desarrollo de las técnicas de implantación iónica y electropulido para eliminar los defectos estructurales y aumentar la resistencia de los instrumentos endodónticos rotatorios de NiTi (57).

A continuación, se desarrollaron le implementaron tratamientos termo-mecánicos en el proceso de fabricación de los instrumentos endodónticos rotatorios de NiTi, para controlar las características físico-mecánicas a través de las temperaturas de transformación de sus fases cristalográficas y por ende el comportamiento clínico del instrumental (20,21,122).

Se han descrito tres procedimientos de fabricación termo-mecánica de los instrumentos endodónticos de NiTi: M-Wire, fase R y CM-Wire. La aleación M-Wire se desarrolló a partir de NiTiNOL SE508 (NiTiNOL Devices & Components, Inc, Fremont, CA) sometido a un tratamiento termo-mecánico y se caracteriza por presentar tres fases cristalinas en su composición; incluyendo la martensita, la fase R y la austenita. Shen et al y Alapati et al, evidenciaron que los instrumentos endodónticos Protaper Next (Dentsply Maillefer, Baillagues, Switzerland), fabricados a base de una aleación M-Wire han demostrado una resistencia a la fatiga cíclica estadísticamente significativa respecto a los instrumentos endodónticos de NiTi convencional (57). Arias et al observaron que los instrumentos endodónticos rotatorios de NiTi GTX fabricados a base de una aleación M-Wire son más resistentes a la fatiga cíclica que los instrumentos endodónticos rotatorios de NiTi GT fabricados a base de una aleación de NiTi convencional (123). Así mismo, Pérez-Higueras et al demostraron que los instrumentos ProTaper Next fabricados en aleación M-Wire presentaban una mayor resistencia a la fatiga cíclica que los instrumentos ProTaper Universal fabricados en aleación SE-Wire (124); sin embargo, estos instrumentos difieren en su diseño geométrico, de forma que las diferencias entre ambos no pueden atribuirse únicamente a la aleación. Johnson et al demostraron que los instrumentos endodónticos rotatorios de

NiTi ProFile 25-04 fabricados en base a una aleación M-Wire presentaban un 390% más resistencia a la fatiga cíclica que los instrumentos endodónticos rotatorios de NiTi ProFile 25-04 fabricados en base a una aleación NiTiNOL SE508 (NiTiNOL Devices & Components, Inc, Fremont, CA) (125). Por otra parte, Gambarini et al, no observaron diferencias estadísticamente significativas en la resistencia a la fatiga cíclica de los instrumentos fabricados a base de una aleación M-Wire con aquellos fabricados en una aleación de NiTi convencional (56).

Más tarde, se desarrolló la aleación en fase R, la cual transformaba la aleación de NiTi previamente fresada en estado austenítico en una fase premartensítica al someterla a un proceso térmico en el que se alternan ciclos térmicos de calentamiento y enfriamiento para dotar a la aleación de un fenómeno de superelasticidad y resistencia a la fatiga cíclica. A continuación, se realiza el fenómeno de atornillamiento de las limas Twisted File (SybronEndo, Orange, CA, EEUU) (20). Tras completar la torsión, los instrumentos endodónticos rotatorios de NiTi con aleación en fase R se someten a un proceso térmico para conservar su forma, a la vez que su estructura cristalina torna en austenita (127).

Posteriormente, se desarrolló la aleación CM-Wire (DS Dental, Johnson City, TN, EEUU), caracterizada por un complejo tratamiento térmico y una reducción del porcentaje en peso atómico del níquel (52%) respecto a la aleación de NiTi convencional (54,5-57%) (24), lo cual aumenta la temperatura final de transformación de la fase austenítica hasta los 45°C, permitiendo que la microestructura cristalina de la aleación de NiTi presente un estado martensítico estable a temperatura corporal (38). Este proceso térmico se realiza posterior al fresado del instrumento endodóntico rotatorio de NiTi, incrementando su resistencia a la fatiga por flexión (300%); sin embargo, impide que el instrumento recupere su forma original durante la conformación del sistema de conductos radiculares, lo cual se asocia con un menor riesgo de transporte apical y perforaciones radiculares (126).

Actualmente, se han desarrollado dos nuevas aleaciones con el objeto de mejorar el comportamiento mecánico y aumentar la vida útil de los instrumentos endodónticos rotatorios de NiTi, especialmente en condiciones de torsión y/o flexión desfavorables. Estas aleaciones se someten a un tratamiento térmico que infiere en su microestructura cristalina aumentando el porcentaje de fase martensítica. La temperatura final de transformación a fase de alta temperatura de los instrumentos endodónticos con aleación Gold se encuentra en 50.0°C (60), lo que induce a pensar que estos instrumentos están constituidos por una microestructura cristalina en estado de alta temperatura o fase R. Sin embargo, La temperatura final de transformación a fase de alta temperatura de los instrumentos endodónticos con aleación Blue se encuentra en 38.5°C (81), mientras que la temperatura inicial de transformación a fase de baja temperatura se encuentra en 31°C (20).

Por último, los instrumentos endodónticos rotatorios de NiTi fabricados mediante electroerosión por hilo ("*Wirecut Electrical Discharge Machining"* WEDM)) permiten una precisión cercana al micrón y el estrés generado durante el proceso de mecanizado se limita a la superficie metálica de los instrumentos endodónticos de NiTi (127). Además, genera una superficie rugosa que proporciona propiedades abrasivas que mejoran la capacidad de corte de los instrumentos endodónticos rotatorios de NiTi. El sistema de instrumentación Neoniti (Neolix, Châtres-la-Forêt, France) está fabricado mediante este proceso de fabricación WEDM.

VELOCIDAD DEL INSTRUMENTAL ENDODÓNTICO DE NiTi

Una de las variables más influyentes en la resistencia a la fatiga cíclica es la velocidad angular del instrumental endodóntico de NiTi. Cabe destacar la importancia de seguir las recomendaciones del fabricante y programar las revoluciones por minuto recomendadas por este. Numerosos autores han destacado la relevancia del número de ciclos que realiza el instrumento endodóntico rotatorio de NiTi hasta la fractura. La exposición del instrumental a velocidades elevadas reduce el tiempo para alcanzar el número máximo de

ciclos hasta la fractura y aumenta la velocidad a la que se alternan los ciclos de tensión-compresión del instrumental endodóntico de NiTi, aumentando la acumulación de tensiones en la matriz de la aleación (128,129). Algunos autores han observado que la velocidad de rotación de los instrumentos no afecta a la resistencia a la fractura del instrumental endodóntico rotatorio de NITi (130); sin embargo, la mayoría de los autores ha evidenciado que la velocidad constituye un factor a considerar para prevenir la fatiga cíclica y torsional del instrumental endodóntico rotatorio de NiTi (131,132).

TIPO DE MOVIMIENTO (RECIPROCANTE/ROTACIONAL CONTINUO) DEL INSTRUMENTAL ENDODÓNTICO DE NiTi

La reducción progresiva del número de instrumentos endodónticos de NiTi, hasta la aparición de los sistemas de lima única, ha supuesto un cambio de paradigma en Endodoncia. Estos sistemas han motivado la aparición de nuevos movimientos de rotación del instrumental endodóntico de NiTi a fin de reducir la fatiga de instrumentos de elevada conicidad ("*taper*") y diámetro apical ("*tip*").

NÚMERO DE USOS DEL INSTRUMENTAL ENDODÓNTICO DE NiTi

Los fabricantes de instrumental endodóntico rotatorio de NiTi especifican en los blíster que estos instrumentos no son reutilizables ni esterilizables. Sin embargo, numerosos autores han demostrado que el instrumental fatigado muestra defectos e irregularidades estructurales microscópicas que reducen la capacidad de corte del instrumento y lo predisponen a la fractura por fatiga cíclica (109,112,133,134), incluso después del primer uso (135). Sin embargo, otros autores han indicado que el instrumental endodóntico rotatorio de NiTi puede reutilizarse hasta en 10 ocasiones sin que aumente el riesgo de fractura (136). Por lo que la decisión depende de un cúmulo de variables, incluyendo las propiedades metalúrgicas del instrumento, el ángulo y el radio de curvatura del sistema de conductos radiculares y la habilidad del operador.

NÚMERO DE CICLOS DE ESTERILIZACIÓN DEL INSTRUMENTAL ENDODÓNTICO DE NiTi

La reutilización de los instrumentos endodónticos rotatorios de NiTi constituye una práctica extendida entre los clínicos, a pesar de estar desaconsejada por los fabricantes y la comunidad científica. Esto requiere la esterilización de los instrumentos en el autoclave a elevadas temperaturas, lo que puede afectar a la microestructura cristalina de la aleación de NiTi (137,138). Hayashi et al demostraron que los ciclos térmicos aplicados durante el proceso de esterilización del instrumental influyen sobre la capacidad de flexión y la resistencia a la fatiga cíclica (139).

Sin embargo, la influencia de este tratamiento térmico no controlado por el fabricante debe analizarse junto al uso clínico del instrumental y no de forma aislada. Por lo que el resultado de los usos y los ciclos térmicos tiene un efecto acumulativo e irreversible sobre la microestructura cristalográfica de la aleación de NiTi, alterando la composición de las fases cristalinas, aumentando las irregularidades superficiales de los instrumentos endodónticos rotatorios de NiTi y, por ende, reduciendo las propiedades físico-mecánicas de los instrumentos y su resistencia a la fatiga cíclica (140).

RADIO Y ÁNGULO DE CURVATURA DEL SISTEMA DE CONDUCTOS RADICULARES

Existen dos parámetros que influyen sobre la resistencia a la fatiga cíclica del instrumental endodóntico rotatorio de NiTi que escapan al control del clínico: el ángulo y el radio de curvatura del sistema de conductos radiculares.

Numerosos autores han mostrado la relevancia de estas variables sobre la resistencia a la fractura del instrumental endodóntico de NiTi. Todos ellos coinciden en señalar que un aumento en el ángulo de curvatura y/o una reducción del radio de curvatura del sistema de conductos radiculares reduce la resistencia a la fatiga cíclica del instrumental endodóntico de NiTi (114,121,141). Concretamente, la reducción del radio de curvatura del sistema de conductos radiculares se asocia con una reducción de la capacidad para resistir fuerzas de torsión (142,143). Así mismo, el comportamiento mecánico

de los instrumentos endodónticos rotatorios de NiTi en el interior de sistemas de conductos radiculares con dos o más ángulos de curvatura es similar al modelo generado en sistemas de conductos simples, pero con la aparición de más localizaciones de concentración de stress que coinciden con los puntos de máximo ángulo de curvatura.

EXPOSICIÓN A SOLUCIONES IRRIGANTES: HIPOCLORITO SÓDICO

El hipoclorito sódico constituye el agente irrigador más empleado en endodoncia para la desinfección del sistema de conductos radiculares dada su alta capacidad bactericida y su alta capacidad para disolver material orgánico y tejido necrótico (144). Además, el hipoclorito sódico al 5.25% es capaz de eliminar el 90% del biofilm dentinario de *Enterococcus faecalis*, siempre que exista un contacto de unos 40-60 minutos entre el irrigante y la dentina infectada (145).

La exposición continuada de los instrumentos endodónticos rotatorios de NiTi al hipoclorito sódico ha demostrado inducir un fenómeno de corrosión sobre la aleación, lo que a su vez podría causar irregularidades superficiales que influyeran significativamente sobre la resistencia a la fractura del instrumental endodóntico rotatorio de NiTi. Concretamente, Stokes et al observó que el hipoclorito sódico formulado a concentraciones entre el 5-5.25% generaba un fenómeno de corrosión identificable (146). Por otra parte, otros autores han demostrado que la exposición del hipoclorito sódico sobre el instrumental endodóntico rotatorio de NiTi no influye sobre las propiedades mecánicas ni la capacidad de corte del instrumental (147).

VELOCIDAD DEL MOVIMIENTO DE PICOTEO DEL INSTRUMENTAL ENDODÓNTICO DE NiTi

El diseño geométrico del instrumental endodóntico rotatorio de NiTi favorece su penetración en el interior del sistema de conductos radiculares; sin embargo, se recomienda realizar movimientos de picoteo o de tracción-pulsión con el propósito de reducir su fatiga cíclica y torsional e el interior del sistema de

conductos radiculares. Yared et al recomendó realizar movimientos de picoteo con una presión apical ligera y breve para reducir la fatiga y por ende aumentar la resistencia a la fractura de instrumentos rotatorios de NiTi, así como un movimiento de picoteo constante e ininterrumpido para evitar el bloqueo del instrumento endodóntico rotatorio de NiTi en el interior del sistema de conductos radiculares (136). Sin embargo, este factor que influye directamente en el tiempo que permanece el instrumental endodóntico rotatorio de NiTi conformando el sistema de conductos radiculares requiere más estudios que analicen su influencia.

TEMPERATURA DEL INSTRUMENTAL ENDODÓNTICO DE NiTi

Estudios previos han destacado la importancia de la temperatura del instrumental endodóntico rotatorio o reciprocante durante los ensayos experimentales o durante su uso clínico. La Rosa et al demostraron que los estudios realizados a temperatura corporal perjudicaron la resistencia a la fatiga cíclica de la mayoría de los instrumentos endodónticos de NiTi (148). Además, Plotino et al informaron que la temperatura puede afectar a la transformación de la microestructura cristalina de NiTi, disminuyendo significativamente la resistencia a la fatiga cíclica a temperatura corporal (149).

PRONÓSTICO DE LA FRACTURA DEL INSTRUMENTAL ENDODÓNTICO DE NITI

La fractura del instrumental endodóntico de NiTi tiene una incidencia entre el 0.09 y el 5% (102). La fractura inesperada del instrumental endodóntico rotatorio o reciprocante de NiTi provoca un bloqueo del sistema de conductos radiculares, impidiendo la desinfección de las soluciones irrigantes más allá del instrumento fracturado (100,115, 150), conduciendo a una posible necrosis pulpar y la formación de lesiones periapicales (151). Así mismo, se ha demostrado que la presencia de un instrumento fracturado en el interior del sistema de conductos radiculares junto a la presencia de lesiones periapicales previas reduce la tasa de éxito del tratamiento de conductos (152).

Stridberg evidenció que la fractura del instrumental endodóntico rotatorio de NiTi en el interior del sistema de conductos radiculares mostró una reducción significativa en la tasa de éxito del tratamiento de conductos radiculares con presencia de patología periapical (153). Por otra parte, Sjögren et al destacaron la importancia de la reducción bacteriana durante los procedimientos de limpieza y desinfección del tratamiento de conductos radiculares en el pronóstico de la terapia endodóntica, e informó que la obtención de cultivos microbiológicos negativos obtenidos del sistema de conducto radicular condujeron a una tasa de éxito endodóntico cercana al 94%, mientras que los cultivos positivos redujeron la tasa de éxito al 68% (154). Además, Siqueira señaló que la carga bacteriana persistente constituye un factor etiológico relevante en el fracaso de la terapia endodóntica, así como en la instauración y desarrollo de infecciones endodónticas secundarias (155). Esta es la razón por la cual la resistencia a la fatiga cíclica de las limas endodónticas rotatorias de NiTi ha sido ampliamente analizada.

ACTITUD CLÍNICA FRENTE A LA FRACTURA DEL INSTRUMENTAL ENDODÓNTICO DE NITI

La extracción del instrumento endodóntico rotatoria de NiTi fracturado en el interior del sistema de conductos radiculares constituye la primera elección terapéutica; sin embargo, no siempre es posible ya que la requiere la remoción de dentina radicular (156), que puede afectar negativamente la integridad estructural del diente (157), incluso conducir a la perforación radicular y/o aumentar el riesgo de fractura vertical radicular, especialmente en el tercio apical.

Por lo tanto, un conocimiento más profundo de las variables que influyen en la fractura del instrumental endodóntico rotatorio de NiTi, ayudará a reducir el riesgo de fractura del instrumental.

Numerosos sistemas y técnicas de remoción del instrumental endodóntico rotatorio de NiTi han sido propuestas en la literatura para remover los fragmentos fracturados del interior del sistema de conductos (158) radiculares, incluyendo el kit Masseran (159), Endo Safety System (160), y Endo Extractor (161). Además, se han propuesto otras técnicas para la eliminación de instrumentos endodónticas rotatorias de NiTi fracturados, incluida la "*loop technique*" (162), "*spinal tap needle technique*" y la técnica Hedstrom (163), canceladores (164), lima de tubo y Hedstrom técnica (165), aguja hipodérmica (166), "*blunt needle and core paste technique*" (167) y el "*Instrument Removal System*" (IRS) (168). Sin embargo, todos estos procedimientos requieren que la una ampliación del coronal tercio del sistema de conductos radiculares para proporcionar acceso a la plataforma del instrumento fracturado, lo que implica una pérdida de tejido dentinario que puede afectar negativamente la integridad estructural del diente. El estudio "**Comparative Analysis of Ease of Removal of Fractured NiTi Endodontic Rotary Files from the Root Canal System—An In Vitro Study"** analizó y comparó la capacidad de extracción de instrumentos fracturados y el volumen de dentina removido por la técnica de remoción ultrasónica en comparación con el dispositivo "Endo Rescue" en conductos rectos y curvos. Los resultados La técnica de remoción basada en ultrasónidos permitió la extracción de ocho instrumentos fracturados (uno procedente del conducto radicular mesiovestibular y siete procedentes del conducto radicular distal), mientras que el dispositivo "Endo Rescue" permitió la extracción de tres instrumentos fracturados (procedentes del conducto radicular distal). Sin embargo, no se observaron diferencias estadísticamente significativas respecto al volumen de dentina removida por ambas técnicas de extracción en el conducto mesiovestibular (p = 0.9109) y distal (p = 0.8669). (169).

JUSTIFICACIÓN

La prognosis del tratamiento de conductos, y por ende la supervivencia del diente tratado, dependen de la asepsia alcanzada en el interior del sistema de conductos radiculares previa a la obturación del conducto radicular. La separación del instrumental rotatorio en el interior del sistema de conductos radiculares impide la desinfección de los mismos; predisponiendo la persistencia de las infecciones endodónticas primarias.

Un mayor conocimiento acerca del comportamiento del instrumental endodóntico de NiTi, aportará información sobre su resistencia a la fractura frente a diferentes variables relacionadas con la fatiga cíclica y contribuirá a evitar complicaciones intraoperatorias.

HIPÓTESIS

NULA (H_0)

No existen diferencias estadísticamente significativas en relación a las variables que influyen sobre la resistencia a la fatiga cíclica del instrumental endodóntico rotatorio de NiTi.

ALTERNATIVA (H_1)

Existen diferencias estadísticamente significativas en relación a las variables que influyen sobre la resistencia a la fatiga cíclica del instrumental endodóntico rotatorio de NiTi.

OBJETIVOS

PRINCIPAL

1. Analizar la influencia de las variables relacionadas con la fatiga cíclica en la resistencia a la fractura del instrumental endodóntico de NiTi.

SECUNDARIOS

2. Analizar la influencia del diámetro apical y la conicidad del instrumental endodóntico rotatorio de NiTi su resistencia a la fractura por fatiga cíclica.

3. Analizar la influencia del diseño de la sección transversal y el *pitch* en el comportamiento mecánico del instrumental endodóntico de NiTi bajo condiciones de flexión y torsión.

4. Analizar la influencia del diseño de la sección transversal del instrumental endodóntico rotatorio de NiTi en la resistencia a la fractura por fatiga cíclica.

5. Analizar la influencia de la aleación del instrumental endodóntico rotatorio de NiTi en la resistencia a la fractura por fatiga cíclica.

6. Analizar la influencia de la frecuencia del movimiento de picoteo del instrumental endodóntico rotatorio de NiTi sobre su resistencia a la fractura por fatiga cíclica.

7. Analizar la influencia del movimiento del instrumental endodóntico rotatorio y reciprocante de NiTi sobre su resistencia a la fractura por fatiga cíclica.

8. Analizar la influencia de los movimientos reciprocantes del instrumental endodóntico reciprocante de NiTi sobre su resistencia a la fractura por fatiga cíclica.

9. Analizar la influencia del número de usos y ciclos de esterilizaciones del instrumental endodóntico reciprocante de NiTi sobre su resistencia a la fractura por fatiga cíclica.

10. Analizar la resistencia a la fractura por fatiga cíclica de los nuevos sistemas endodónticos de NiTi.

11. Analizar la influencia del radio y ángulo de curvatura del sistema de conductos radiculares en el comportamiento mecánico del instrumental endodóntico de NiTi.

12. Analizar el desgaste volumétrico del instrumental endodóntico reciprocante de NiTi sometido a fatiga cíclica.

13. Analizar la capacidad de remoción del instrumental endodóntico rotatorio de NiTi separado en el interior del sistema de conductos radiculares y el desgaste de dentina radicular.

MATERIAL, MÉTODOS Y RESULTADOS

applied sciences

MDPI

Article

The Effect of Taper and Apical Diameter on the Cyclic Fatigue Resistance of Rotary Endodontic Files Using an Experimental Electronic Device

Vicente Faus-Llácer [1], Nirmine Hamoud Kharrat [1], Celia Ruiz-Sánchez [1], Ignacio Faus-Matoses [1], Álvaro Zubizarreta-Macho [2,*] and Vicente Faus-Matoses [1]

[1] Department of Stomatology, Faculty of Medicine and Dentistry, University of Valencia, 46010 Valencia, Spain; fausvj@uv.es (V.F.-L.); nirhak@alumni.uv.es (N.H.K.); celia.ruiz@uv.es (C.R.-S.); ignacio.faus@uv.es (I.F.-M.); vicente.faus@uv.es (V.F.-M.)

[2] Department of Endodontics, Faculty of Health Sciences, Alfonso X El Sabio University, 28691 Madrid, Spain

* Correspondence: amacho@uax.es

Abstract: The aim of this study was to analyze the effect of the taper and apical diameter of nickel–titanium (NiTi) endodontic rotary files on the dynamic cyclic fatigue resistance. A total of 50 unused conventional NiTi wire alloy endodontic rotary instruments were used in this study. All NiTi endodontic rotary files were submitted to a custom-made dynamic cyclic fatigue device until fracture occurred. The time to failure, the number of cycles to failure, the number of pecking movements, and the length of the fractured file tip were analyzed using the analysis of variance (ANOVA) test. In addition, the Weibull characteristic strength and Weibull modulus were also calculated. The paired *t*-test revealed statistically significant differences between the time to failure, number of cycles to failure, and number of cycles of in-and-out movement of both the apical diameter ($p < 0.001$) and the taper ($p < 0.001$) of NiTi endodontic rotary files; however, the results did not show statistically significant differences between the mean length of the fractured files regarding the apical diameter ($p = 0.344$) and taper study groups ($p = 0.344$). Increased apical diameter and taper of NiTi endodontic rotary files decreased their dynamic resistance to cyclic fatigue.

Keywords: Endodontics; cyclic fatigue; taper; apical diameter; rotary movement; endodontic rotary files

Citation: Faus-Llácer, V.; Kharrat, N.H.; Ruiz-Sánchez, C.; Faus-Matoses, I.; Zubizarreta-Macho, Á.; Faus-Matoses, V. The Effect of Taper and Apical Diameter on the Cyclic Fatigue Resistance of Rotary Endodontic Files Using an Experimental Electronic Device. *Appl. Sci.* **2021**, *11*, 863. https://doi.org/10.3390/app11020863

Received: 30 November 2020
Accepted: 14 January 2021
Published: 18 January 2021

1. Introduction

The introduction of nickel–titanium (NiTi) alloy in endodontic rotary instruments had a great impact on endodontics due to their combination of speed, quality, accuracy, and risk reduction [1]. However, the main drawback of the NiTi endodontic rotary instruments is the fracture of the endodontic files inside the root canal system during the shaping procedures, which prevents root canal system disinfection beyond the fractured instrument and can influence the prognosis of the root canal treatment [2,3].

The fracture of NiTi endodontic rotary files can occur as a consequence of excessive torsion or flexural fatigue [4,5]; the latter being the most frequent cause [6]. Flexural fatigue or cyclic fatigue is caused by the alternating compression and traction cycles that NiTi endodontic rotary files experience at the point of maximum curvature of the root canal system [7]. There are factors related to the cyclic fatigue resistance of NiTi endodontic rotary files: cross-section design [8], the diameter of the inner and outer core [2], the operating speed and torque [9,10], radius and angle of curvature [11], operator capability [12,13], anatomical configuration of the root canal system [14], irrigation solutions [15], sterilization cycles [16,17], and NiTi alloy [3,18].

However, the influence of the taper and apical diameter of NiTi endodontic rotary files on the cyclic fatigue resistance has never been reported, although research has highlighted that the fracture incidence of NiTi endodontic rotary files increased in curved root canal systems, possibly related to the apical diameter [19] and taper of the NiTi endodontic rotary files [20], mainly at the point of the maximum curvature. This is because large file tapers accumulate a greater amount of internal stress during stress-compression cycles when flexed to accommodate the curvature of the root canal system [21]. However, an increase in the diameter of the NiTi endodontic rotary files can contribute to increasing the resistance to torsional fracture [5].

In addition, many cyclic fatigue testing devices have been proposed in the literature; however, they differ mainly in the ability to reproduce the pecking movements of the operator statically or dynamically during the root canal shaping. Dynamic cyclic fatigue testing devices are recommended because they faithfully reproduce the operator pecking movements; moreover, Loios et al. reported that the pecking movements performed by dynamic cyclic fatigue testing devices extended the fatigue lifetime of the NiTi endodontic rotary files, compared to static cyclic fatigue testing devices [22]. Therefore, a dynamic cyclic fatigue testing device was used in this study.

The aim of this study was to analyze and compare the effect of the taper and apical diameter on the dynamic cyclic fatigue resistance of NiTi endodontic rotary files, with a null hypothesis (H0) stating that the taper and apical diameter would not affect the resistance of NiTi endodontic rotary files in dynamic cyclic fatigue.

2. Materials and Methods

2.1. Study Design

In this in vitro study, we utilized 50 unused conventional NiTi wire alloy endodontic rotary instruments (RaCe®, La Chaux-De-Fonds, Switzerland), 25 mm in length with a triangular cross-section. All NiTi endodontic rotary files were analyzed using scanning electron microscopy (SEM) (HITACHI S-4800, Fukuoka, Japan) in the Department of Mechanical, Energetic, and Materials Engineering of the School of Industrial Engineering of the University of Extremadura (Badajoz, Spain) under the following exposure parameters: acceleration voltage: 20 kV, magnification from 100× to 6500×, and a resolution between −1.0 nm at 15 kV and 2.0 nm at 1 kV, to confirm the taper (Figure 1) and apical diameter (Figure 2) values of the previously selected NiTi endodontic rotary files (RaCe®, La Chaux-De-Fonds, Switzerland).

None of the NiTi endodontic rotary files (RaCe®, La Chaux-De-Fonds, Switzerland) were discarded after analyzing for possible manufacture defects which could influence the cyclic fatigue resistance of the NiTi endodontic rotary files (RaCe®, La Chaux-De-Fonds, Switzerland). A controlled experimental trial was performed at the Dental Centre of Innovation and Advanced Specialties at Alfonso X El Sabio University (Madrid, Spain), between November and December 2020. The NiTi endodontic rotary files were selected and categorized into the following study groups: A: 250 μm apical diameter and 2% taper (n = 10) (25.02); B: 250 μm apical diameter and 4% taper (n = 10) (25.04); C: 250 μm apical diameter and 6% taper (n = 10) (25.06); D: 200 μm apical diameter and 6% taper (n = 10) (20.06); E: 300 μm apical diameter and 6% taper (n = 10) (30.06).

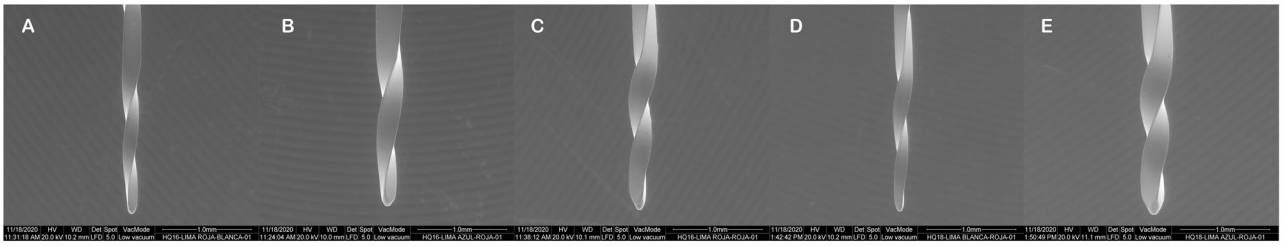

Figure 1. Scanning electron microscopy (SEM) analysis of the taper of (**A**) 25.02, (**B**) 25.04, (**C**) 25.06, (**D**) 20.06, and (**E**) 30.06 NiTi endodontic rotary files.

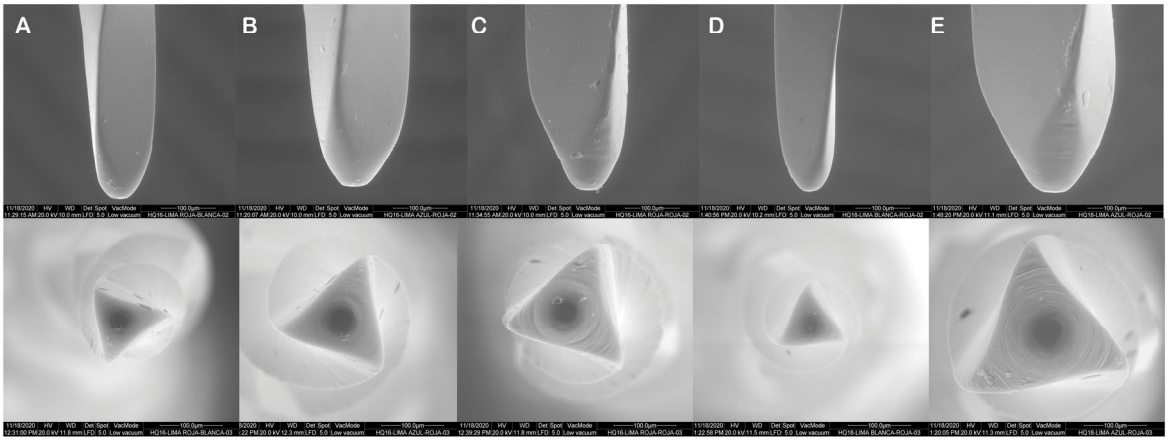

Figure 2. SEM analysis of the apical diameter of (**A**) 25.02, (**B**) 25.04, (**C**) 25.06, (**D**) 20.06, and (**E**) 30.06 NiTi endodontic rotary files.

2.2. Experimental Cyclic Fatigue Model

The selected NiTi endodontic rotary files (RaCe®, La Chaux-De-Fonds, Switzerland) were used in a custom-made device (utility model patent number ES1219520), designed by computer-aided design/computer-aided engineering (CAD/CAE) 2D/3D software (Midas FX+®, Brunleys, Milton Keynes, UK) and created using 3D printing (ProJet® 6000 3D Systems©, Rock Hill, SC, USA) (Figure 3A–D).

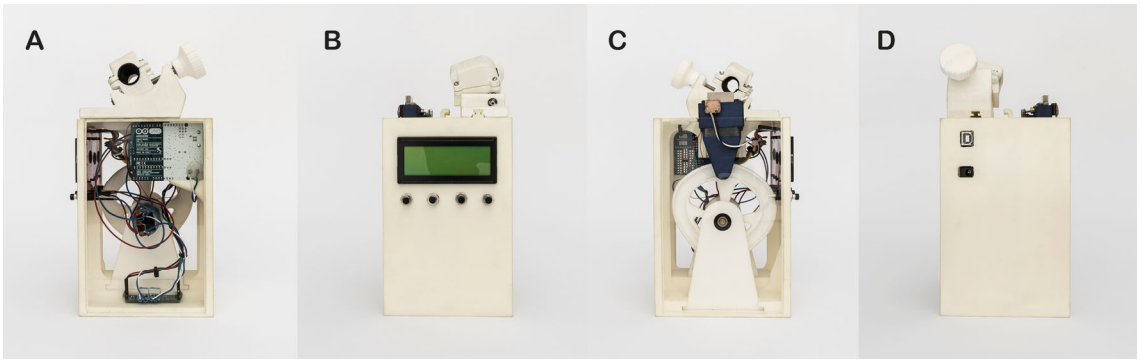

Figure 3. (**A**) Front, (**B**) back, and (**C**,**D**) lateral surfaces of the dynamic cyclic fatigue hardware device.

The endodontic rotary file (RaCe, La Chaux-De-Fonds, Switzerland) was submitted to micro computed tomography (Skyscan 1176, Bruker-MicroCT, Kontich, Belgium) with the following exposure parameters: 160.0 kilovolt peak, 56.0–58.0 microamperes, 500.0 ms, 720 projections, four frames, a tungsten target between 0.25 and 0.375 mm, a 3 μm

resolution, and a pixel size of 0.127 μm, to obtain a standard tessellation language digital file that allowed the design of an accurate artificial root canal regarding the outer measurements of the selected endodontic rotary file (RaCe, La Chaux-De-Fonds, Switzerland), which ensured intimate contact.

Each one of the previously selected NiTi endodontic rotary files (RaCe, La Chaux-De-Fonds, Switzerland) were introduced in a custom-made artificial root canal designed with a 60° curvature according to Schneider's measuring technique [23] and 3 mm radius of curvature, based on the outer geometry (taper and cross-sections diameters) of each NiTi endodontic rotary file (RaCe, La Chaux-De-Fonds, Switzerland). The artificial root canals were designed using computer aided design/computer aided engineering (CAD/CAE) 2D/3D software (Midas FX+®, Brunleys, Milton Keynes, UK) and manufactured by electrical discharge machining (EDM) molybdenum wire-cut technology (Cocchiola S.A., Buenos Aires, Argentina) from a stainless steel piece 2 mm in width.

The speed of the up-and-down movement of the artificial root canal were generated by the brushed DC gearmotor (Ref.: 1589, Pololu® Corporation, Las Vegas, NV, USA) regarding the signals emitted by the driver (Ref.: DRV8835, Pololu® Corporation, Las Vegas, NV, USA), which performed an H-bridge function that managed the speed of the up-and-down movement through Pulse Width Modulation (PWM) signals emitted by four switches modulated by transistors. The movement generated by the brushed DC gearmotor (Ref.: 1589, Pololu® Corporation, Las Vegas, NV, USA) was transferred to the artificial root canal support through a roller bearing system (Ref.: MR104ZZ, FAG, Schaeffler Herzogenaurach, Germany). The artificial root canal support moved in a pure axial motion through a lineal guide (Ref.: HGH35C 10249-1 001 MA, HIWIN Technologies Corp. Taichung, Taiwan).

The time to failure of the NiTi endodontic rotary files was detected by a light-dependent resistor (LDR) sensor (Ref.: C000025, Arduino LLC®, Ivrea, Italy) located at the apex of the artificial root canal, which received the continuous light source emitted by a high-brightness white light-emitting diode (LED) (20,000 mcd) (Ref.: 12.675/5/b/c/20k, Batuled, Coslada, Spain), which was located opposite to the artificial root canal. The light signals emitted by the LED sensor were detected by the LDR (Ref.: C000025, Arduino LLC®) sensor with a frequency of 50 ms to accurately identify the time of failure. The NiTi endodontic rotary files (RaCe®, La Chaux-De-Fonds, Switzerland) were used with a 6:1 reduction handpiece (X-Smart Plus, Dentsply Maillefer) and torque-controlled motor with continuous rotation at 1000 rpm and 1.5 N/cm torque, according to the manufacturer's instructions [24].

The reduction handpiece (X-Smart Plus, Dentsply Maillefer, Ballaigues, Switzerland) was submitted to an industrial scan (3D Geomagic Capture Wrap, 3D Systems©, Rock Hill, SC, USA) to obtain an STL digital file, which allowed the design (Midas FX+®, Brunleys) and manufacture (ProJet® 6000. 3D Systems©, Rock Hill, SC, USA) of a custom-made support piece placed on the top of the cyclic fatigue testing device to prevent undesirable movements of the reduction handpiece (X-Smart Plus, Dentsply Maillefer) and, hence, the NiTi endodontic rotary files (RaCe®, La Chaux-De-Fonds, Switzerland) inside the artificial root canal. (Figure 4).

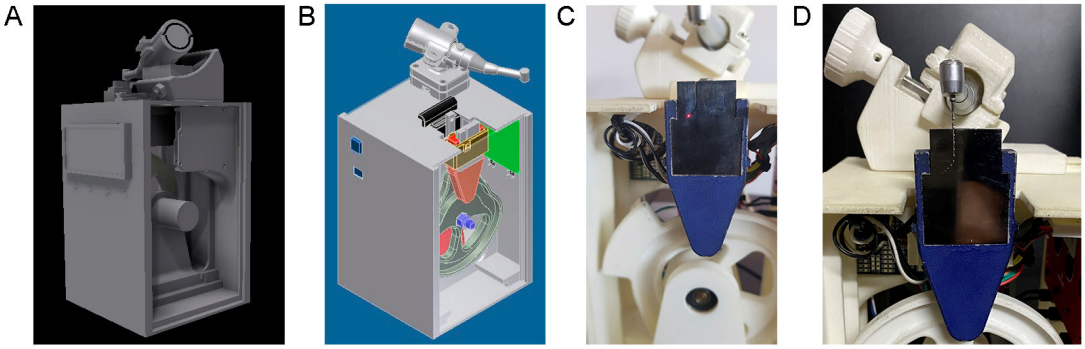

Figure 4. (**A**) Back and (**B**) front surfaces of the 3D design of the dynamic cyclic fatigue hardware device, with the reduction handpiece (**C**) located on the top of the dynamic cyclic fatigue hardware device and the NiTi endodontic rotary file (**D**) inside the artificial root canal.

The NiTi endodontic rotary files (RaCe®, La Chaux-De-Fonds, Switzerland) were used until fracture occurred to analyze the effect of the taper and apical diameter on the resistance of NiTi endodontic rotary files (RaCe®, La Chaux-De-Fonds, Switzerland) to cyclic fatigue. All NiTi endodontic rotary files (RaCe®, La Chaux-De-Fonds, Switzerland) were used in the dynamic cyclic fatigue device at a frequency of 60 pecking movements/min, according to a previous study [25]. To reduce the friction between the reciprocating files and the artificial canal walls, special high-flow synthetic oil designed for the lubrication of mechanical parts (Singer All-Purpose Oil; Singer Corp., Barcelona, Spain) was applied. All NiTi endodontic rotary files (RaCe®, La Chaux-De-Fonds, Switzerland) were used until fracture occurred. The time to failure, the number of cycles to failure, the number of cycles of in-and-out movements, and the length of the fractured file tip were measured and recorded.

2.3. Statistical Tests

Statistical analysis of all variables was carried out using SAS 9.4 (SAS Institute Inc., Cary, NC, USA). The descriptive statistics are expressed as the mean and standard deviation (SD) for quantitative variables. Comparative analysis was performed by comparing the time to failure (in seconds), the number of cycles to failure, the number of pecking movements (cycles of in-and-out movements) and the length of the fractured file tip (mm) using the ANOVA test. In addition, the Weibull characteristic strength and Weibull modulus were calculated. The statistical significance was set at $p < 0.05$.

3. Results

The mean and standard deviation (SD) values for time to failure (in seconds) regarding the apical diameter and taper are displayed in Table 1 and Figure 5A,B.

Table 1. Descriptive statistics of the time to failure in relation to the apical diameter and taper study groups.

Study Group	*n*	Mean	SD	Minimum	Maximum
20.06	10	361.91	18.07	328.18	382.91
25.02	10	410.39	13.11	387.28	428.19
25.04	10	294.27	10.50	279.87	310.33
25.06	10	225.77	11.73	210.79	241.83
30.06	10	102.91	15.41	81.29	127.91

The ANOVA test showed statistically significant differences between the time to failure of the apical diameter ($p < 0.001$) (Figure 5A) and taper ($p < 0.001$) (Figure 5B) of the NiTi endodontic rotary files.

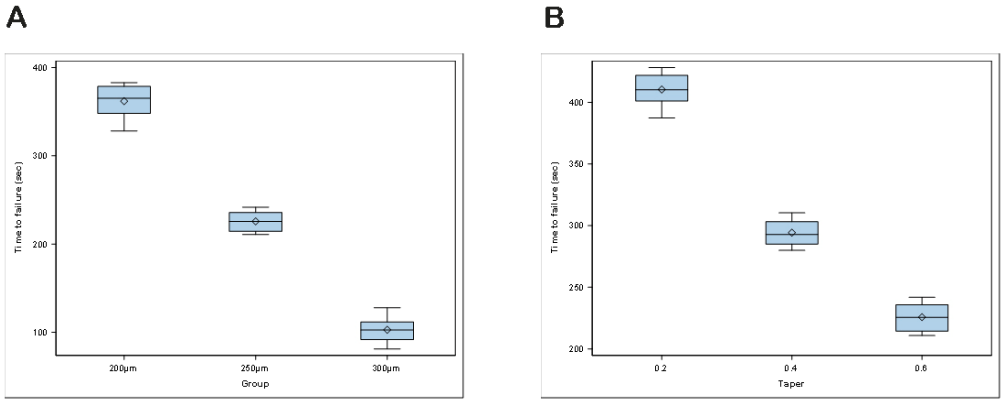

Figure 5. Box plots of the time to failure for the (**A**) apical diameter and (**B**) taper study groups. The horizontal line in each box represents the respective median value.

The scale distribution parameter (η) of the Weibull statistics showed statistically significant differences between the time to failure of the 20.06 and 25.06 apical diameter study groups ($p < 0.001$), 20.06 and 30.06 apical diameter study groups ($p < 0.001$) and 25.06 and 30.06 apical diameter study groups ($p < 0.001$). In addition, the shape distribution parameter (β) of the Weibull statistics showed statistically significant differences between the time to failure of the 20.06 and 25.06 apical diameter study groups ($p < 0.001$) and 20.06 and 30.06 apical diameter study groups ($p = 0.002$); however, it did not show statistically significant differences between the time to failure of the 25.06 and 30.06 apical diameter study groups ($p = 0.656$) (Table 2, Figure 6A).

The scale distribution parameter (η) of the Weibull statistics showed statistically significant differences between the time to failure of the 25.02 and 25.04 taper study groups ($p < 0.001$), 25.02 and 25.06 taper study groups ($p < 0.001$), and 25.04 and 25.06 taper study groups ($p < 0.001$). However, the shape distribution parameter (β) of the Weibull statistics did not show statistically significant differences between the time to failure of the 25.02 and 25.04 taper study groups ($p = 0.148$), 25.02 and 25.06 taper study groups ($p = 0.287$), and 25.04 and 25.06 taper study groups ($p = 0.702$) (Table 2, Figure 6B).

Table 2. The Weibull statistics of the time to failure for the apical diameter and taper study groups.

	Weibull Shape (β)				Weibull Scale (η)			
	Estimate	**St Error**	**Lower**	**Upper**	**Estimate**	**St Error**	**Lower**	**Upper**
20.06	26.22	6.75	15.83	43.43	369.77	4.70	360.67	379.09
25.02	37.02	9.08	22.89	59.86	416.37	3.76	409.05	423.81
25.04	32.42	7.98	20.01	52.52	299.13	3.09	293.14	305.25
25.06	22.37	5.53	13.78	36.31	231.14	3.46	224.45	238.02
30.06	7.62	1.84	4.74	12.23	109.38	4.81	100.34	119.24

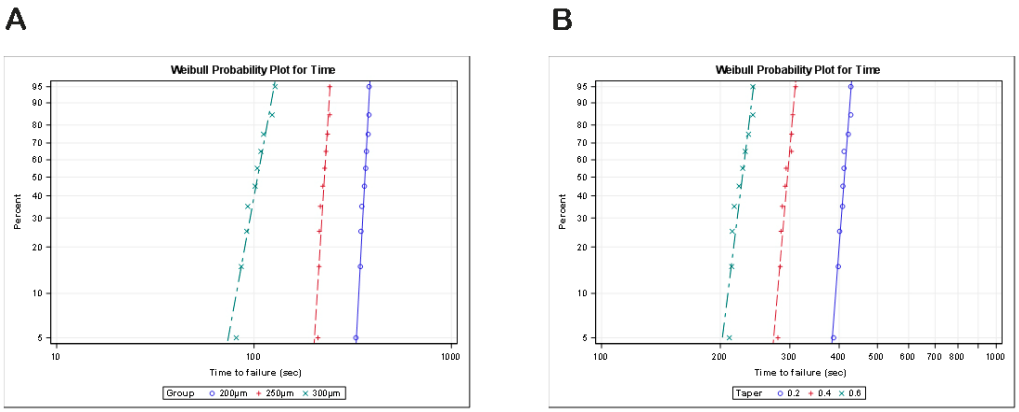

Figure 6. Weibull probability plots of the time to failure for the (**A**) apical diameter and (**B**) taper study groups.

The mean and SD values for number of cycles to failure regarding the apical diameter and taper are displayed in Table 3 and Figure 7A,B.

Table 3. Descriptive statistics of the number of cycles to failure in relation to the apical diameter and taper study groups.

Study Group	*n*	Mean	SD	Minimum	Maximum
20.06	10	3015.87	150.54	2734.90	3190.80
25.02	10	3419.80	109.28	3227.50	3568.30
25.04	10	2452.13	87.42	2332.50	2585.80
25.06	10	1880.60	98.59	1749.90	2014.90
30.06	10	857.57	128.32	677.40	1065.80

The ANOVA test showed statistically significant differences between the number of cycles to failure of the apical diameter ($p < 0.001$) (Figure 7A) and taper ($p < 0.001$) (Figure 7B) of NiTi endodontic rotary files.

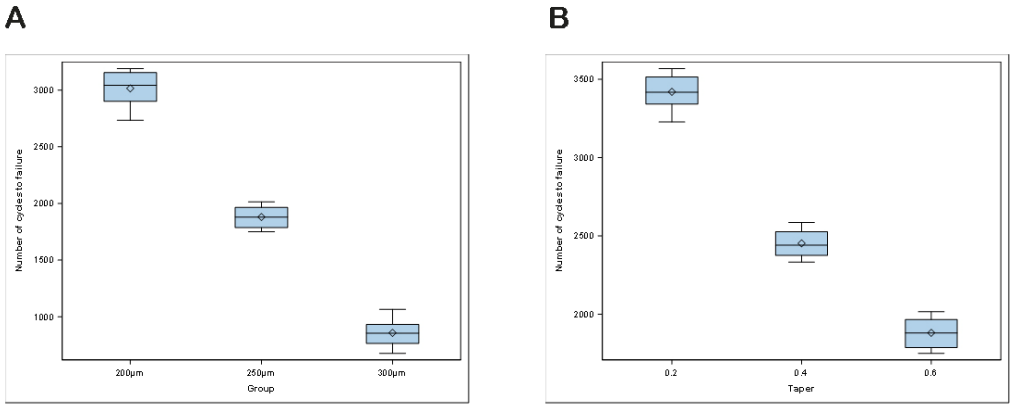

Figure 7. Box plots of the number of cycles to failure for the (**A**) apical diameter and (**B**) taper study groups. The horizontal line in each box represents the median value.

The scale distribution parameter (η) of the Weibull statistics showed statistically significant differences between the number of cycles to failure of the 20.06 and 25.06 apical diameter study groups ($p < 0.001$), 20.06 and 30.06 apical diameter study groups ($p < 0.001$), and 25.06 and 30.06 apical diameter study groups ($p < 0.001$). In addition, the shape distribution parameter (β) of the Weibull statistics showed statistically significant differences between the time to failure of the 20.06 and 25.06 apical diameter study groups ($p < 0.001$) and 20.06 and 30.06 apical diameter study groups ($p = 0.002$); however,

it did not show statistically significant differences between the time to failure of the 25.06 and 30.06 apical diameter study groups ($p = 0.644$) (Table 4, Figure 8A).

The scale distribution parameter (η) of the Weibull statistics showed statistically significant differences between the number of cycles to failure of 25.02 and 25.04 taper study groups ($p < 0.001$), 25.02 and 25.06 taper study groups ($p < 0.001$), and 25.04 and 25.06 taper study groups ($p < 0.001$). However, the shape distribution parameter (β) of the Weibull statistics did not show statistically significant differences between the number of cycles to failure of the 25.02 and 25.04 taper study groups ($p = 0.144$), 25.02 and 25.06 taper study groups ($p = 0.279$), and 25.04 and 25.06 taper study groups ($p = 0.705$) (Table 4, Figure 8B).

Table 4. The Weibull statistics of the number of cycles to failure for the apical diameter and taper study groups.

	Weibull Shape (β)				Weibull Scale (η)			
	Estimate	**St Error**	**Lower**	**Upper**	**Estimate**	**St Error**	**Lower**	**Upper**
20.06	26.24	6.76	15.84	43.47	3081.29	39.11	3005.58	3158.91
25.02	37.01	9.07	22.89	59.85	3469.64	31.38	3408.68	3531.68
25.04	32.46	7.99	20.03	52.58	2492.67	25.73	2442.74	2543.61
25.06	22.25	5.51	13.07	36.14	1925.63	28.99	1869.64	1983.29
30.06	7.62	1.84	4.74	12.24	911.45	40.08	836.17	993.49

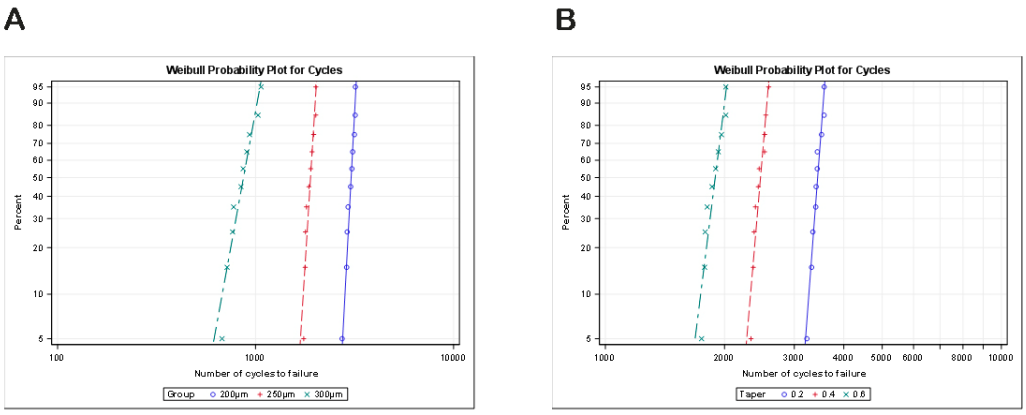

Figure 8. The Weibull probability plots of the number of cycles to failure for the (**A**) apical diameter and (**B**) taper study groups.

The mean and SD values for the number of cycles of in-and-out movements regarding the apical diameter and taper are displayed in Table 5 and Figure 9A,B.

Table 5. Descriptive statistics of the number of cycles of in-and-out movements in relation to the apical diameter and taper study groups.

Study Group	n	Mean	SD	Minimum	Maximum
20.06	10	361.91	18.07	328.18	382.91
25.02	10	410.39	13.11	387.28	428.19
25.04	10	294.27	10.50	279.87	310.33
25.06	10	225.77	11.73	210.79	241.83
30.06	10	102.91	15.41	81.29	127.91

The ANOVA test showed statistically significant differences between the number of cycles of in-and-out movements of the apical diameter ($p < 0.001$) (Figure 9A) and taper ($p < 0.001$) (Figure 9B) of the NiTi endodontic rotary files.

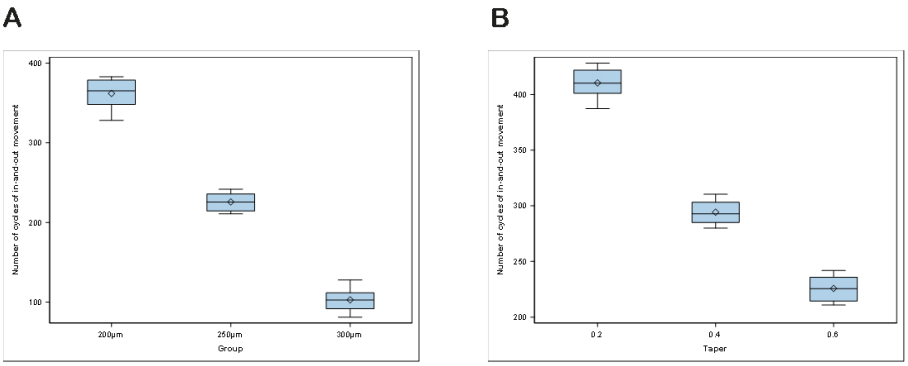

Figure 9. Box plots of the number of cycles of in-and-out movements for the (**A**) apical diameter and (**B**) taper study groups. The horizontal line in each box represents the respective median value.

The scale distribution parameter (η) of the Weibull statistics showed statistically significant differences between the number of cycles of in-and-out movements of the 20.06 and 25.06 apical diameter study groups ($p < 0.001$), 20.06 and 30.06 apical diameter study groups ($p < 0.001$), and 25.06 and 30.06 apical diameter study groups ($p < 0.001$). In addition, the shape distribution parameter (β) of the Weibull statistics showed statistically significant differences between the number of cycles of in-and-out movements of the 20.06 and 25.06 apical diameter study groups ($p < 0.001$) and 20.06 and 30.06 apical diameter study groups ($p = 0.002$); however, it did not show statistically significant differences between the number of cycles of in-and-out movements of the 25.06 and 30.06 apical diameter study groups ($p = 0.656$) (Table 6, Figure 10A).

The scale distribution parameter (η) and the shape distribution parameter (β) of the Weibull statistics showed statistically significant differences between the number of cycles of in-and-out movements of the 25.02 and 25.04 taper study groups ($p < 0.001$), 25.02 and 25.06 taper study groups ($p < 0.001$), and 25.04 and 25.06 taper study groups ($p < 0.001$) (Table 6, Figure 10B).

Table 6. The Weibull statistics of the number of cycles of in-and-out movements for the apical diameter and taper study groups.

	Weibull Shape (β)				Weibull Scale (η)			
	Estimate	**St Error**	**Lower**	**Upper**	**Estimate**	**St Error**	**Lower**	**Upper**
20.06	26.22	6.75	15.83	43.43	369.77	4.70	360.67	379.09
25.02	37.02	9.08	22.89	59.86	416.37	3.76	409.05	423.81
25.04	32.42	7.98	20.01	52.52	299.13	3.09	293.14	305.25
25.06	22.37	5.53	13.78	36.31	231.14	3.46	224.45	238.02
30.06	7.62	1.84	4.74	12.23	109.38	4.81	100.34	119.24

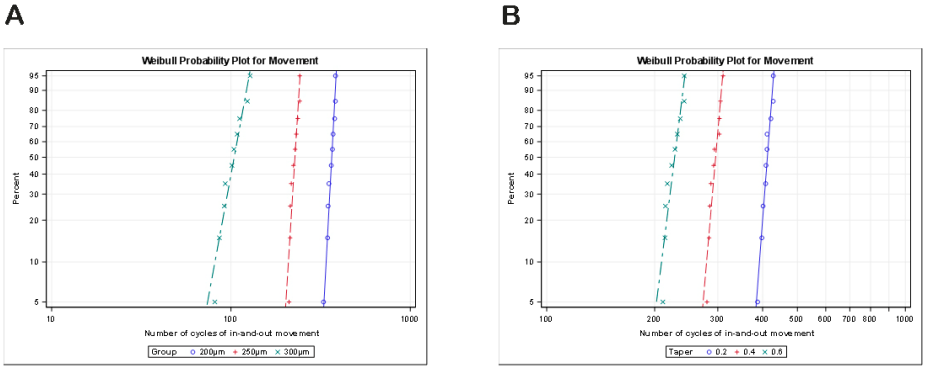

Figure 10. Weibull probability plots of the number of cycles of in-and-out movements for the (**A**) apical diameter and (**B**) taper study groups.

The ANOVA test did not show statistically significant differences between the mean length of the fractured files regarding the apical diameter study groups ($p = 0.344$) (Figure 11A) and taper study groups ($p = 0.344$) (Figure 11B).

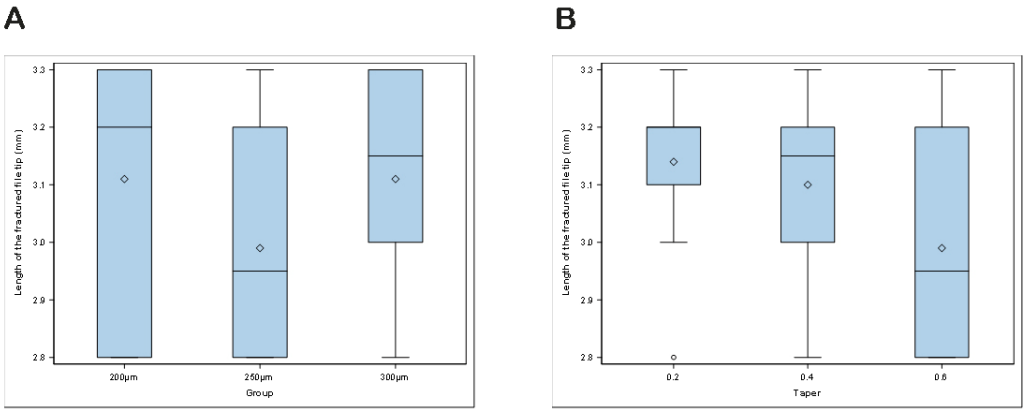

Figure 11. Box plots of the length of fractured files regarding the (**A**) apical diameter and (**B**) taper study groups. The horizontal line in each box represents the respective median value.

The scale distribution parameter (η) and the shape distribution parameter (β) of the Weibull statistics did not show statistically significant differences for either the apical diameter ($p > 0.05$) (Figure 12A) or taper ($p > 0.05$) (Figure 12B) study groups.

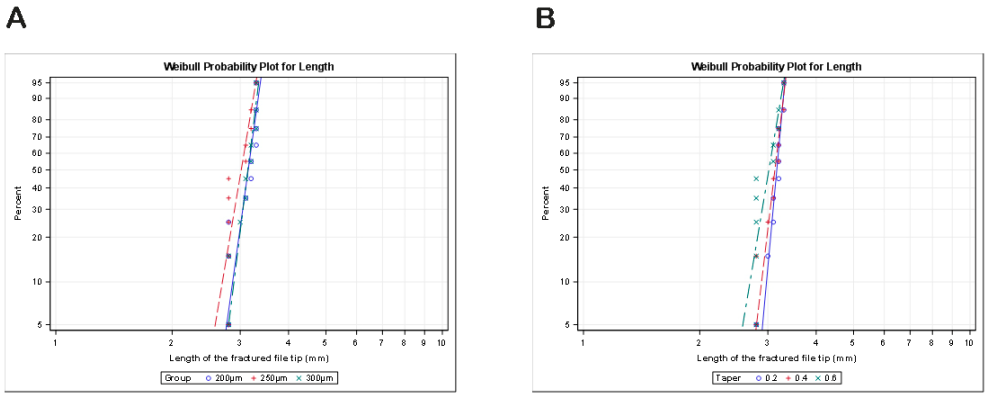

Figure 12. The Weibull probability plots of the length of fractured files regarding the (**A**) apical diameter and (**B**) taper study groups.

4. Discussion

The results obtained in the present study reject the null hypothesis (H_0) which stated that the apical diameter and taper would not affect the resistance of NiTi endodontic rotary files to dynamic cyclic fatigue.

Research reported a prevalence of fractures of NiTi endodontic rotary files between 0.9% [26] and 5% [27], and also highlighted the influence of this intraoperative complication on the outcome of root canal treatment. In addition, Stridberg stated that the fracture of an endodontic instrument inside a root canal system demonstrated a further significant periapical pathology decrease in the success rate of the root canal treatment [28]. Sjögren highlighted the importance of bacterial reduction during the cleaning and shaping procedures of a root canal treatment on the prognosis of the endodontic therapy, and reported that negative microbiological cultures obtained from the root canal system led to an endodontic success rate close to 94%, whereas positive cultures reduced the success rate to 68% [29].

Siqueira pointed out that the persistent bacterial load is the main aetiology factor of endodontic failure and secondary endodontic infections [30]. This is the reason why the cyclic fatigue resistance of NiTi endodontic rotary files has been widely analyzed. Previous studies were conducted to analyze the resistance of both NiTi endodontic rotary and reciprocating instruments to different conditions related to cyclic fatigue [31]. However, the absence of a normative which regulates the cyclic fatigue tests of the NiTi endodontic rotary and reciprocating files led to the appearance of a heterogeneous multitude of cyclic fatigue test devices, which makes comparison of the results difficult [32]. In the present study, a dynamic cyclic fatigue device was used because it reproduces the operator's movements more accurately, and the results can be extrapolated to the clinical situation [33].

Alcalde et al., showed that the 25.06 NiTi endodontic reciprocating files (ProDesigner R, Easy, Belo Horizonte, Brazil) presented higher ($p > 0.05$) cyclic fatigue resistance and angular rotation before fracture compared to 25.08 Ni Ti endodontic reciprocating files (Reciproc, VDW, Munich, Germany) and 25.07 (WaveOne Gold, Dentsply Sirona, Ballaigues, Switzerland) [34]. However, the different cross-section design, crystalline structure of the NiTi alloy and counterclockwise direction could influence the results obtained in this study.

The NiTi endodontic rotary system used in this study was selected because it provided NiTi endodontic rotary files with different apical diameters while maintaining the cross-sectional design, NiTi alloy crystal structure, and taper, as well as providing NiTi endodontic rotary files with different tapers while maintaining the same apical diameter, cross-sectional design, and crystal structure of the NiTi alloy. In addition, the selection of an NiTi endodontic rotary system instead of a reciprocating system was because the reciprocating movement associated with single-file systems has been shown to extend the lifetime of NiTi endodontic rotary files compared with continuous rotation, thus increasing the cyclic fatigue resistance of the reciprocating files [35].

Even the metallurgical characteristics and thermal treatments of the NiTi alloy influenced the flexibility and cyclic fatigue resistance of NiTi endodontic files [36,37]. For this reason, a conventional NiTi wire alloy endodontic rotary system was also selected. In addition, Gambarini reported the significantly higher cyclic fatigue resistance ($p < 0.01$) of 25.04 NiTi endodontic rotary files (ProFile, Maillefer, Baillagues, Switzerland) compared with 20.06 NiTi endodontic rotary files (ProFile, Maillefer, Baillagues, Switzerland) and 25.06 NiTi endodontic rotary files (ProFile, Maillefer, Baillagues, Switzerland). These results are in line with those of the present study and highlight the influence of the taper above the apical diameter.

Capar et al. also analyzed the cyclic fatigue resistance of rotary pathfinding instruments and reported that the 15.02 NiTi endodontic pathfinding rotary files (HyFlex GPF, Coltene-Whaledent, Allstetten, Switzerland) showed statistically higher cyclic fatigue resistance ($p < 0.05$) compared with the 12.03 NiTi endodontic pathfinding rotary files (G files, Micro-Mega, Besançon Cedex, France), 16.04 NiTi endodontic pathfinding rotary files (ProGlider, Dentsply Maillefer, Ballaigues, Switzerland), 16.02 NiTi endodontic pathfinding rotary files (Pathfile, Dentsply Maillefer, Ballaigues, Switzerland), and 15.02 NiTi endodontic pathfinding rotary files (Scout Race, FKG Dentaire, La Chaux-de-Fonds, Switzerland) [38].

These results agreed with those of the present study, and Camargo et al. reported that the 25.06 NiTi endodontic reciprocating files (ProDesigner R, Easy, Belo Horizonte, Brazil) showed similar canal transportation and centering abilities after preparation of the second mesiobuccal canals compared with the 25.08 NiTi endodontic reciprocating files (Reciproc, VDW, Munich, Germany); however, the 25.06 NiTi endodontic rotary files (ProDesigner R, Easy, Belo Horizonte, Brazil) removed less volume of the root canal dentine and presented an absence of root canal perforation [39].

Duque et al. also reported that the 35.06 NiTi endodontic reciprocating files (WaveOne Gold, Dentsply Sirona, Ballaigues, Switzerland) significantly increased ($p <$

0.05) the percentage of root canal dentine removal compared to the 35.05 NiTi endodontic reciprocating files (ProDesigner R, Easy, Belo Horizonte, Brazil); however, no statistically significant differences ($p > 0.05$) were observed between the apical transportation and percentage of untouched areas of the root canal systems using different apical diameters in curved canals [40].

These results can be summarized in that increasing the mass of the instrument based on an increase in the taper and/or the apical diameter negatively affected the resistance to cyclical fatigue of the instrument; influencing their flexibility and leading the instruments to cause excessive root canal dentine removal, apical transport, root perforations, and fractures [27,41,42]. The lengths of the fractured files were also measured to determine whether the fracture point would depend on the apical diameter or the taper of the NiTi endodontic rotary instruments, or if it were instead conditioned by the radius of the artificial root canal.

No statistically significant differences were observed between the mean length of the fractured files regarding the apical diameter study groups ($p = 0.344$) and taper study groups ($p = 0.344$); therefore, the length of the fractured files may be associated with the radius of the artificial root canals rather than the apical diameter and taper of the NiTi endodontic rotary instruments. Unfortunately, the limitations of the study prevented the analysis of more tapers and apical diameters and, even with different NiTi alloys, the reciprocating movement and cross-section designs. The study was not developed in a clinical environment due to the difficulty in standardizing the sample.

5. Conclusions

The conclusion derived from the present study is that the increase in the apical diameter and taper decreased the cyclic fatigue resistance of NiTi endodontic rotary files; therefore, we recommend enlarging the apical constriction by increasing the apical diameter with low taper instruments.

Author Contributions: Conceptualization, V.F.-L.; methodology, N.H.K.; validation, C.R.-S.; formal analysis, I.F.-M.; investigation, V.F.-M. and Á.Z.-M. All authors have read and agreed to the published version of the manuscript.

Funding: This research received no external funding.

Institutional Review Board Statement: Not applicable.

Informed Consent Statement: Not applicable.

Data Availability Statement: Data available on request due to restrictions eg privacy or ethical.

Acknowledgments: The authors would like to thank Roberto Gutiérrez González and Daniel Ortega Ufano their invaluable assistance in this study.

Conflicts of Interest: The authors declare no conflicts of interest.

References

1. Bhagabati, N.; Yadav, S.; Talwar, S. An in vitro cyclic fatigue analysis of different endodontic nickel-titanium rotary instruments. *J. Endod*. **2012**, *38*, 515–518.
2. McGuigan, M.B.; Louca, C.; Duncan, H.F. Clinical decision-making after endodontic instrument fracture. *Br. Dent. J*. **2013**, *214*, 395–400.
3. McGuigan, M.B.; Louca, C.; Duncan, H.F. The impact of fractured endodontic instruments on treatment outcome. *Br. Dent. J*. **2013**, *214*, 285–289.
4. Topçuoğlu, H.S.; Topçuoğlu, G. Cyclic Fatigue Resistance of Reciproc Blue and Reciproc Files in an S-shaped Canal. *J. Endod*. **2017**, *43*, 1679–1682.
5. Parashos, P.; Messer, H.H. Rotary NiTi instrument fracture and its consequences. *J. Endod*. **2006**, *32*, 1031–1043.
6. Shen, Y.; Zhou, H.; Campbell, L.; Wang, Z.; Wang, R.; Du, T.; Haapasalo, M. Fatigue and nanomechanical properties of K3XF nickel-titanium instruments. *Int. Endod. J*. **2014**, *47*, 1160–1167.
7. Kuhn, G.; Tavernier, B.; Jordan, L. Influence of structure on nickel-titanium endodontic instruments failure. *J. Endod*. **2001**, *27*, 516–520.

8. Xu, X.; Eng, M.; Zheng, Y.; Eng, D. Comparative study of torsional and bending properties for six models of nickel-titanium root canal instruments with different cross-sections. *J. Endod*. **2006**, *32*, 372–375.
9. Daugherty, D.W.; Gound, T.G.; Comer, T.L. Comparison of fracture rate, deformation rate, and efficiency between rotary endodontic instruments driven at 150 rpm and 350 rpm. *J. Endod*. **2001**, *27*, 93–95.
10. Martín, B.; Zelada, G.; Varela, P.; Bahillo, J.G.; Magán, F.; Ahn, S.; Rodríguez, C. Factors influencing the fracture of nickel-titanium rotary instruments. *Int. Endod. J*. **2003**, *36*, 262–266.
11. Topçuoğlu, H.S.; Demirbuga, S.; Düzgün, S.; Topçuoğlu, G. Cyclic fatigue resistance of new reciprocating files (Reciproc Blue, WaveOne Gold, and SmartTrack) in two different curved canals. *J. Investig. Clin. Dent*. **2018**, *9*, e12344.
12. Yared, G.M.; Kulkarni, G.K. Failure of ProFile Ni-Ti instruments used by an inexperienced operator under access limitations. *Int. Endod. J*. **2002**, *35*, 536–541.
13. Sonntag, D.; Delschen, S.; Stachniss, V. Root-canal shaping with manual and rotary Ni-Ti files performed by students. *Int. Endod. J*. **2003**, *36*, 715–723.
14. Peters, O.A.; Peters, C.I.; Schönenberger, K.; Barbakow, F. ProTaper rotary root canal preparation: Assessment of torque and force in relation to canal anatomy. *Int. Endod. J*. **2003**, *36*, 93–99.
15. Keles, A.; Uzunoglu Ozyurek, E.; Uyanik, M.O.; Nagas, E. Effect of Temperature of Sodium Hypochlorite on Cyclic Fatigue Resistance of Heat-treated Reciprocating Files. *J. Endod*. **2019**, *45*, 205–208.
16. Mize, S.B.; Clement, D.J.; Pruett, J.P.; Carnes, D.L., Jr. Effect of sterilization on cyclic fatigue of rotary nickel-titanium endodontic instruments. *J. Endod*. **1998**, *24*, 843–847.
17. Zubizarreta-Macho, A.; Alonso-Ezpeleta, O.; Albaladejo Martínez, A.; Faus Matoses, V.; Caviedes Brucheli, J.; Agustín-Panadero, R.; Mena Álvarez, J.; Vizmanos Martínez-Verganza, F. Novel Electronic Device to Quantify the Cyclic Fatigue Resistance of Endodontic Reciprocating Files after Using and Sterilization. *App. Sci*. **2020**, *10*, 4962.
18. Ruiz-Sánchez, C.; Faus-Llácer, V.; Faus-Matoses, I.; Zubizarreta-Macho, Á.; Sauro, S.; Faus-Matoses, V. The Influence of NiTi Alloy on the Cyclic Fatigue Resistance of Endodontic Files. *J. Clin. Med*. **2020**, 9, 3755.
19. Pruett, J.P.; Clement, D.J.; Carnes, D.L., Jr. Cyclic fatigue testing of nickel-titanium endodontic instruments. *J. Endod*. **1997**, *23*, 77–85.
20. Gambarini, G.; Gerosa, R.; De Luca, M.; Garala, M.; Testarelli, L. Mechanical properties of a new and improved nickel-titanium alloy for endodontic use: An evaluation of file flexibility. *Oral Surg. Oral Med. Oral Pathol. Oral Radiol. Endod*. **2008**, *105*, 798–800.
21. Al-Hadlaq, S.M. Evaluation of cyclic flexural fatigue resistance of 25/0.04 and 25/0.06 twisted file rotary nickel-titanium endodontic instruments. *Aust. Endod. J*. **2013**, *39*, 62–65.
22. Loios, G.; Martins, R.F.; Ginjeira, A.; Dragoi, M.V.; Buican, G. Fatigue Resistance of Rotary Endodontic Files Submitted to Axial Motion in Multiplanar Canals Manufactured by 3D Printing. *Procedia Eng.* **2016**, *160*, 117–122,.
23. Schneider, S.W. A comparison of canal preparations in straight and curved root canals. *Oral Surg. Oral Med. Oral Pathol*. **1971**, *32*, 271–275.
24. El Feky, H.M.; Ezzat, K.M.; Bedier, M.M.A. Cyclic fatigue resistance of M-Pro and RaCe Ni-Ti rotary endodontic instruments in artificial curved canals: A comparative in vitro study. *Restor. Dent. Endod*. **2019**, *44*, e44.
25. Zubizarreta-Macho, A.; Mena Álvarez, J.; Albadalejo Martínez, A.; Segura-Egea, J.J.; Caviedes Brucheli, J.; Agustín-Panadero, R.; López Píriz, R.; Alonso-Ezpeleta, O. Influence of the pecking motion on the cyclic fatigue resistance of endodontic rotary files. *J. Clin. Med*. **2020**, *9*, 45.
26. Arens, F.C.; Hoen, M.M.; Steiman, H.R.; Dietz, G.C., Jr. Evaluation of single-use rotary nickel-titanium instruments. *J. Endod*. **2003**, *29*, 664–666.
27. Parashos, P.; Gordon, I.; Messer, H.H. Factors influencing defects of rotary nickel-titanium endodontic instruments after clinical use. *J. Endod*. **2004**, *30*, 722—725.
28. Strindberg, L. The dependence of the results of pulp therapy on certain factors. *Acta Odontol. Scand*. **1956**, *14*, 1–175.
29. Sjögren, T.; Figdor, D.; Persson, S.; Sundqvist, G. Influence of infection at the time of root filling on the outcome of endodontic treatment of teeth with apical periodontitis. *Int. Endod. J*. **1997**, *30*, 297–306.
30. Siqueira, J.F., Jr. Aetiology of root canal treatment failure: Why well-treated teeth can fail. *Int. Endod. J*. **2001**, *34*, 1–10.
31. Yared, G.M.; Bou Dagher, F.E.; Machtou, P. Cyclic fatigue of ProFile rotary instruments after clinical use. *Int. Endod. J*. **2000,** *33*, 204–207.
32. Plotino, G.; Grande, N.M.; Cordaro, M.; Testarelli, L.; Gambarini, G. A review of cyclic fatigue testing of nickel-titanium rotary instruments. *J. Endod*. **2009**, *35*, 1469–1476.
33. Haikel, Y.; Serfaty, R.; Bateman, G.; Senger, B.; Allemann, C. Dynamic and cyclic fatigue of engine-driven rotary nickel-titanium endodontic instruments. *J. Endod*. **1999**, *25*, 434–440.
34. Alcalde, M.P.; Duarte MAH, Bramante, C.M.; de Vasconselos, B.C.; Tanomaru-Filho, M.; Guerreiro-Tanomaru, J.M.; Pinto, J.C.; Só, M.V.R.; Vivan, R.R. Cyclic fatigue and torsional strength of three different thermally treated reciprocating nickel-titanium instruments. *Clin. Oral Investig*. **2018**, *22*, 1865–1871.
35. Siddique, R.; Nivedhitha, M.S. Effectiveness of rotary and reciprocating systems on microbial reduction: A systematic review. *J. Conserv. Dent*. **2019**, *22*, 114–122.
36. Klymus, M.E.; Alcalde, M.P.; Vivan, R.R.; Só, M.V.R.; de Vasconselos, B.C.; Duarte, M.A.H. Effect of temperature on the cyclic fatigue resistance of thermally treated reciprocating instruments. *Clin. Oral Investig*. **2019**, *23*, 3047–3052.

37. Silva, E.J.N.L.; Vieira, V.T.L.; Hecksher, F.; Dos Santos Oliveira, M.R.S.; Dos Santos Antunes, H.; Moreira, E.J.L. Cyclic fatigue using severely curved canals and torsional resistance of thermally treated reciprocating instruments. *Clin. Oral Investig*. **2018**, *22*, 2633–2638.
38. Capar, I.D.; Kaval, M.E.; Ertas, H.; Sen, B.H. Comparison of the cyclic fatigue resistance of 5 different rotary pathfinding instruments made of conventional nickel-titanium wire, M-wire, and controlled memory wire. *J. Endod*. **2015**, *41*, 535–538.
39. Camargo, E.J.; Duarte, M.A.H.; Marques, V.A.S.; Só, M.V.R.; Duque, J.A.; Alcalde, M.P.; Vivan, R.R. The ability of three nickel-titanium mechanized systems to negotiate and shape MB2 canals in extracted maxillary first molars: A micro-computed tomographic study. *Int. Endod. J*. **2019**, *52*, 847–856.
40. Duque, J.A.; Vivan, R.R.; Duarte, M.A.H.; Alcalde, M.P.; Cruz, V.M.; Borges, M.M.B.; Bramante, C.M. Effect of larger apical size on the quality of preparation in curved canals using reciprocating instruments with different heat thermal treatments. *Int. Endod. J*. **2019**, *52*, 1652–1659.
41. Ounsi, H.F.; Salameh, Z.; Al-Shalan, T.; Ferrari, M.; Grandini, S.; Pashley, D.H.; Tay, F.R. Effect of clinical use on the cyclic fatigue resistance of ProTaper nickel-titanium rotary instruments. *J. Endod*. **2007**, *33*, 737–741.
42. Grande, N.M.; Plotino, G.; Pecci, R.; Bedini, R.; Malagnino, V.A.; Somma, F. Cyclic fatigue resistance and three-dimensional analysis of instruments from two nickel-titanium rotary systems. *Int. Endod. J*. **2006**, *39*, 755–763.

Journal of
Clinical Medicine

MDPI

Article

Influence of Cross-Section and Pitch on the Mechanical Response of NiTi Endodontic Files under Bending and Torsional Conditions—A Finite Element Analysis

Victor Roda-Casanova [1], Antonio Pérez-González [1], Alvaro Zubizarreta-Macho [2,3,*] and Vicente Faus-Matoses [4]

[1] Department of Mechanical Engineering and Construction, Universitat Jaume I, 12071 Castelló de la Plana, Spain; vroda@uji.es (V.R.-C.); aperez@uji.es (A.P.-G.)
[2] Department of Dentistry, Alfonso X el Sabio University, 28691 Madrid, Spain
[3] Department of Orthodontics, University of Salamanca, 37008 Salamanca, Spain
[4] Department of Stomatology, Faculty of Medicine and Dentistry, University of Valencia, 46010 Valencia, Spain; vfaus@clinicafaus.com
* Correspondence: amacho@uax.es

Abstract: In this article, the effects of cross-section and pitch on the mechanical response of NiTi endodontic files is studied by means of finite element analyses. The study was conducted over a set of eight endodontic rotary files, whose geometry was obtained from combinations of two cross-sections (square and triangular) and four pitches. Each file was subjected to bending and torsional analyses, simulating the testing conditions indicated in the ISO 3630 Standard, in order to assess their stiffness and mechanical strength. The results indicate that endodontic files with a square cross-section have double the stiffness of those with triangular cross-sections, both in terms of bending and torsion. For both loading modes, endodontic files with a triangular cross-section can undergo larger deformations before overload failure than those with a square cross-section: up to 20% more in bending and 40% in torsion. Moreover, under equivalent boundary conditions, endodontic files with triangular cross-sections present a higher fatigue life than those with square cross-sections: up to more than 300% higher for small pitches. The effect of pitch on the stiffness and strength of the file is smaller than that of the cross-section shape, but smaller pitches could be beneficial when using a triangular cross-section, as they increase the bending flexibility, fatigue life, and torsion stiffness. These results suggest a clinical recommendation for the use of files with a triangular-shaped cross-section and a small pitch in order to minimize ledging and maximize fatigue life. Finally, in this study, we reveal the sensitivity of the orientation of files with respect to the bending direction, which must be taken into account when designing, reporting, and interpreting test results under such loading conditions.

Keywords: endodontic file; cross-section; pitch; flexural bending; torsion; stress distribution; finite element analysis

Citation: Roda-Casanova, V.; Pérez-González, A.; Zubizarreta-Macho, A.; Faus-Matoses, V. Influence of Cross-Section and Pitch on the Mechanical Response of NiTi Endodontic Files under Bending and Torsional Conditions—A Finite Element Analysis. *J. Clin. Med.* **2022**, *11*, 2642. https://doi.org/10.3390/jcm11092642

Academic Editors: Massimo Amato, Giuseppe Pantaleo and Alfredo Iandolo

Received: 18 April 2022
Accepted: 5 May 2022
Published: 8 May 2022

1. Introduction

The introduction of nickel–titanium alloy (NiTi) for the manufacturing of root canal instruments entailed a great revolution in the field of endodontics, as the consequent endodontic files decreased the incidence of iatrogenic complications [1,2]. However, despite the continuous mechanical and chemical improvements made by manufacturers, the failure of endodontic files during root canal treatments remains a concern for clinicians [3], as the incidence of their fracture still ranges from 0.09% to 5% [4,5].

The fracture of rotary instruments occurs mainly due to two different mechanisms, usually referred to as torsion overload and flexural fatigue [6,7]. On one hand, the torsion overload failure mechanism corresponds to a static failure that typically occurs when the tip of the endodontic file becomes blocked in the root canal whilst the instrument continues

rotating [8]. In static failure, the file fails because the stress value reaches the elastic limit of the material, such that the file undergoes permanent deformation and finally fractures. On the other hand, flexural fatigue is a failure mechanism produced mainly by the alternating compressive and tensile stresses and strains that appear in any point of a file rotating inside a curved root canal [8,9]. This type of fatigue failure results in a sudden fracture of the file after a certain number of rotations, even if the stress levels are far below the elastic limit of the material, due to the nucleation and progression of small cracks in some stressed sections of the file. Thus, bending and torsion are essential conditions to evaluate the mechanical behavior of endodontic instruments [10]. The unexpected failure of NiTi endodontic files may condition the outcome of the root canal treatment by blocking the advancement of disinfecting agents beyond the fractured instrument [11–13], which may lead to subsequent pulp necrosis and the formation of periapical lesions [14], or decrease the success rate of root canal treatment of teeth with periapical pathology [15]. In addition, extraction of the fractured NiTi endodontic rotary file from the root canal system requires root dentin removal to provide access to the fractured instruments [16]. This causes a loss of dentin tissue, which can negatively affect the structural integrity of the tooth [17]. Furthermore, it can lead to root perforation and increase the risk of vertical root fracture, especially in the apical third [16]. For these reasons, a better understanding of the independent and combined effects of the different parameters that affect these failure mechanisms is desirable, and additional research must be addressed to this end.

Several works have been conducted to analyze the influence of both the NiTi alloy [18] and the geometrical parameters on the torsional and bending resistance of endodontic instruments. Both the chemical composition and crystalline structure of the NiTi alloy have been studied, and it has been shown that they highly influence the strength of the endodontic file [19]. In particular, endodontic rotary systems with a higher concentration of the martensitic phase and manufactured using electropolishing, ion implantation, cryogenic treatment, and heat treatments improve the mechanical behavior of NiTi endodontic rotary files, increasing their cyclic fatigue resistance. The geometric parameters of the endodontic files have also been reported to influence the instrument's performance, including the taper and apical diameter [20], cross-section design [21,22], flute length, helix angle, and pitch [23]. The influence of these variables has been analyzed using static and dynamic custom-made cyclic fatigue testing devices, which have not been submitted to a standardization normative, and do not allow for independently assessing the influence of each geometric parameter associated with flexural fatigue or torsional overload. There are other standardized testing devices, such as those described in ISO 3630-1:2008 [24], which allow for the independent assessment of both torsional and bending phenomena, although their capability to reproduce the actual operating conditions of endodontic files has not yet been verified.

Computer simulation has proven to be an interesting tool for studying the failure of endodontic rotary files. In the simplest cases, analytical methods can be used for such a purpose, which are usually based on the small strain theory of elasticity. In this line, Zhang et al. [25] have analyzed the mechanical behavior of NiTi endodontic files under torsional and bending loads. Tsao et al. [26] have developed analytical models to study the flexibility of NiTi instruments subjected to bending loads. These analytical models have the advantage of being fast and easy to implement, but their capabilities to consider non-linear behaviors (i.e., material non-linearity) or complex loading scenarios are limited. These limitations can be overcome by using numerical methods such as the finite element method.

The ability of the finite element method to reproduce the results obtained from experimental tests using endodontic rotary files has been proven in several works [7,10,27–29], whose main conclusions have been summarized in a recent bibliographical review [30]. This review concluded that the finite element method is a reliable tool for evaluating the behavior of NiTi rotary instruments, and has the advantage of reducing instrument development time and costs. Another important advantage of the finite element method is that it also allows us to assess aspects of the mechanical behavior of the instruments, such as the

stress distribution, which are difficult to obtain in laboratory tests [10]. The finite element method has been previously used to analyze the influence of cross-section design and pitch on the stiffness and stress distribution under bending and torsional conditions [10,31–37]. Appendix B collects detailed information about these previous studies, including their main conclusions and limitations. Some of these studies have used proprietary file models, such as ProTaper, ProFile, Mtwo, and others, which hampers the independent evaluation of parameters such as cross-section geometry, cross-section area, or pitch [10,32–35]. Other studies have used theoretical file models to avoid this problem, but with some limitations; for example, in [36], the authors analyzed four different cross-sections and three pitch values under torsion, but did not provide detailed information about the material model for the shape memory alloy (SMA) of the files or about the quality of the finite element mesh. In another study, Versluis et al. [33] analyzed the effects of pitch and cross-section geometry on flexural stiffness and stresses using a representative SMA material model. However, the boundary conditions were specified differently to those in ISO 3630-1:2008 [24] and the bending applied was low, leading to maximum von Mises stresses below the initial stress for transformation from austenite to martensite, and, thus, the effect of the super-elasticity of the files was not analyzed; furthermore, torsion behavior was not included in the study. In [37], the effect of cross-section geometry and pitch on the 'screw-in' tendency of the files was analyzed, but a linear material model was used for the file. A more recent study investigated different geometric options for the sides of a triangle-shaped cross-section (straight, convex, and concave), as well as the use of files with combinations of these geometries along the file [31], but the pitch effect was not analyzed.

Some of these finite element models are limited in their accuracy, in terms of representing the correct geometry and boundary conditions of the endodontic files, or use simplified material models that are incapable of representing their actual mechanical response under load. In this study, we address all of these partial limitations of previous studies by undertaking a comprehensive analysis of the effects of pitch and cross-section using an accurate finite element model that allows us to simulate the testing conditions of the ISO3630 Standard to the best extent possible. The method used to obtain the parametric geometrical representation of the endodontic instrument and the corresponding finite element mesh has been proposed in our previous work [38]. The use of an accurate numerical model in these tests can foster improvements in new generations of more resistant and flexible endodontic files, reducing the need for expensive and time-consuming experiments in the early design stages. From a clinical perspective, these improvements are expected to reduce the risk of failure of endodontic instruments, thus preventing clinical complications.

The aim of this study was to analyze and compare the effects of the cross-section and the pitch on the mechanical response (in terms of strength and stiffness) of NiTi endodontic files under bending and torsional conditions, similar to those indicated in the ISO 3630 Standard [24], using the finite element method. The study was conducted using a set of eight different endodontic rotary files whose geometries were obtained from combinations of two cross-sections (triangular and square) and four pitches (1 mm, 2 mm, 4 mm, and 8 mm). Under these conditions, the following individual objectives were pursued: (i) to develop a finite element model which reproduces the experimental tests conducted in the ISO 3630 Standard; (ii) to conduct a bending analysis of the selected endodontic rotary files, in order to predict the stiffness and strength of the files under static and cyclic loading conditions; and (iii) to conduct a torsional analysis of the selected endodontic rotary files, in order to predict the stiffness and the strength of the files under static loading conditions.

2. Materials and Methods

For this study, different endodontic instruments were analyzed using numerical simulation with finite elements. Figure 1 shows the geometries of the eight endodontic files considered. The different geometries were obtained by varying the cross-section (square and triangular) and the pitch ($p_z = \{1\text{ mm}, 2\text{ mm}, 4\text{ mm}, 8\text{ mm}\}$) of the files. All of them had a total length of $L_{total} = 25$ mm, the length of their active part was $L_a = 16$ mm, and

their tip and shaft diameters were $d_a = 0.25$ mm and $d_{sh} = 1.20$ mm, respectively. The taper of the endodontic files was 6%.

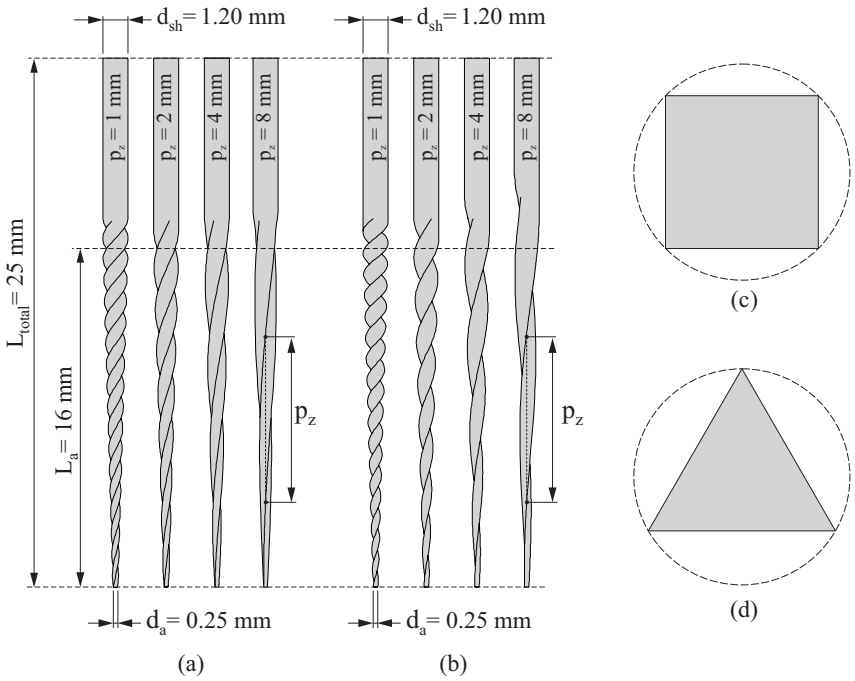

Figure 1. Geometries of the analyzed endodontic files: endodontic files with square cross-section (**a**); endodontic files with triangular cross-section (**b**); normalized square cross-section (**c**); and normalized triangular cross-section (**d**).

The material for all the files was considered to be NiTi, which exhibits a super-elastic stress–strain curve, as shown in Figure 2. Here, E_A and E_M represent the Young's moduli of austenite and martensite, respectively. The beginning and end of the loading phase transformation are denoted by σ_L^S and σ_L^E, respectively, whereas the beginning and the end of the unloading transformation phase are denoted by σ_U^S and σ_U^E. Finally, ε_L represents the uni-axial transformation strain, and σ_{ME}^E indicates the end of the martensitic elastic regime.

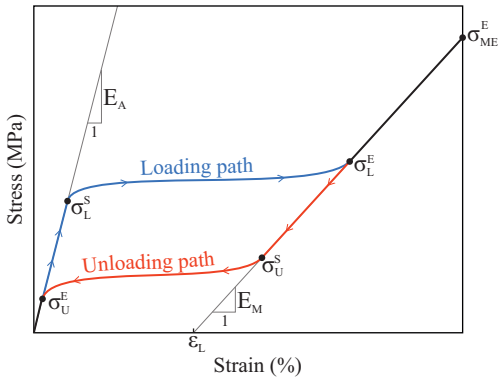

Figure 2. Sample stress–strain curve for NiTi material.

2.1. Devices for Experimental Bending and Torsion Analysis

Endodontic files are usually tested in terms of bending and torsional loads, and the typical standardized procedure for these tests has been described in the ISO 3630 Standard [24], as summarized in Figure 3. For the torsion analysis (Figure 3a), the last 3 mm at the tip of the endodontic file are inserted inside a clamping jaw. After checking that the endodontic file is properly fixed and aligned with the axis of rotation, the top of the file is rigidly connected to the torsion device. This torsion device is increasingly rotated

at angle θ_z, and the torsional moment M_z is measured using a torquemeter attached to the clamping jaw. The test ends with the failure of the endodontic file. At this point, the maximum rotated angle $\theta_{z,max}$ and maximum torsional moment $M_{z,max}$ are registered.

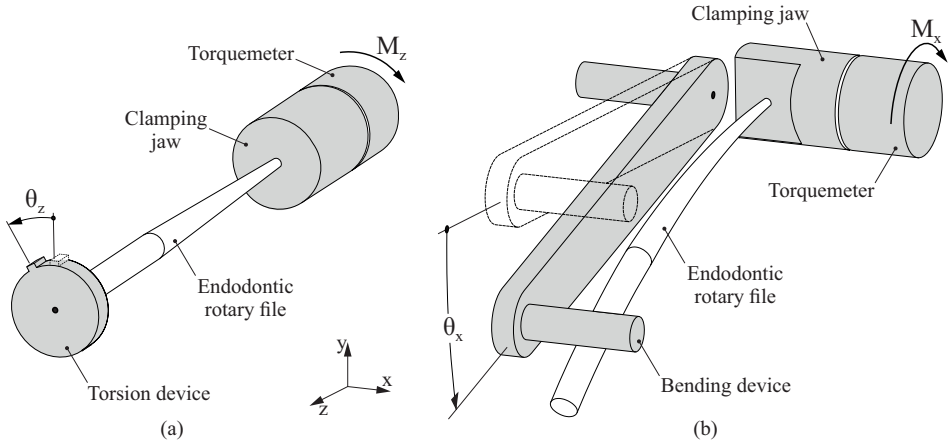

Figure 3. Devices used for torsion (**a**) and bending (**b**) analyses.

In a similar way, in the bending analysis (Figure 3b), the last 3 mm at the tip of the endodontic file are inserted inside a clamping jaw. After checking that the endodontic file is properly fixed and aligned with the axis of rotation, the bending device is positioned until it contacts the endodontic file. Then, the bending device is increasingly rotated at angle θ_x, and the bending moment M_x is measured using a torquemeter attached to the clamping jaw. The test ends with the failure of the endodontic file. At this point, the maximum rotated angle $\theta_{x,max}$ and maximum bending moment $M_{x,max}$ are registered.

2.2. Definition of the Finite Element Model for the NiTi Endodontic File

Figure 4 shows an example of the finite element model created for the endodontic file simulation experiments, as described in Section 2.1. Here, only the portion of the endodontic file subjected to stresses and strains was considered in the analysis (i.e., the part of the endodontic file inserted into the clamping jaw was not included in the finite element model). The geometry of the endodontic file was generated and then discretized into quadratic finite element tetrahedrons following the meshing procedure developed in our previous work [38]. Using this procedure, the finite element mesh of a endodontic file was automatically built from its geometrical parameters (d_{sh}, d_a, L_a, L_{total}, and p_z, as shown in Figure 1) and the average element size.

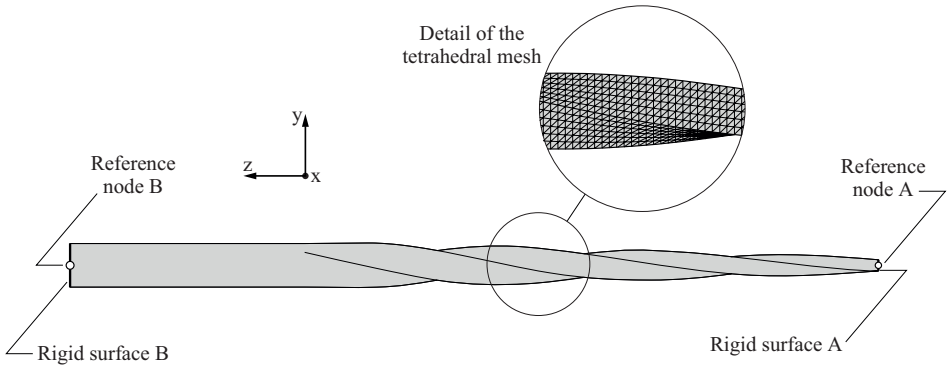

Figure 4. Definition of the finite element model.

To select the average element size, a mesh sensitivity study was conducted in our previous work [38] for a finite element model of an endodontic file with similar geometry, element type, boundary, and loading conditions, as described in Figure 4. In this study, the variations in the maximum element energy error and energy norm error with respect to the

average element size were observed, and it was concluded that an average element size equal to 0.1 mm provided a good compromise between accuracy and computational cost. For these reasons, this average element size was used to perform this study, resulting in a finite element model with 89,295 nodes and 58,749 elements.

The super-elastic behavior of the NiTi alloy used to manufacture the endodontic files was modeled using the material model developed by Auricchio [39]. The material properties that characterize this material model were extracted from [10], and are shown in Table 1.

Table 1. Material properties to characterize the super-elastic behavior of NiTi alloy. Reprinted/adapted with permission from Ref. [10]. 2014, Elsevier.

Parameter	Variable	Magnitude
Young's modulus of austenite	E_A	42,530 MPa
Austenite Poisson's ratio	ν_A	0.33
Young's modulus of martensite	E_M	12,828 MPa
Martensite Poisson's ratio	ν_M	0.33
Uni-axial transformation strain	ε_L	6%
Slope of the stress–temperature curve for loading	$(\delta\sigma/\delta T)_L$	6.7
Start of transformation loading	σ_L^S	492 MPa
End of transformation loading	σ_L^E	630 MPa
Reference temperature	T_0	22 °C
Slope of the stress–temperature curve for unloading	$(\delta\sigma/\delta T)_U$	6.7
Start of transformation unloading	σ_U^S	192 MPa
End of transformation unloading	σ_U^E	97 MPa
End of martensitic elastic regime	σ_{ME}^E	1200 MPa

The surface at the fixed end of the endodontic file was defined as a rigid surface (denoted as rigid surface A in Figure 4). This rigid surface was rigidly connected to reference node A, which was used to introduce the boundary conditions for the finite element model. To simulate the effect of the clamping jaw over the endodontic file, all of the degrees of freedom of reference node A were restricted. At the other side of the file, the top surface was also defined as a rigid surface (denoted as rigid surface B in Figure 4). This rigid surface was rigidly connected to reference node B, which was used to define the loading conditions of the model. Two different loading conditions were considered in the analyses, one for the bending analysis and the other for the torsional analysis:

- In the bending analysis, an increasing displacement was imposed at reference node B in the negative direction of the y-axis, until the maximum von Mises stress along the endodontic file σ_{max} reached the end of the martensitic elastic regime. As the results of the bending analyses are sensitive to the orientation of the endodontic file with respect to the bending direction, the analysis was conducted in 24 different angular positions, given by a rotation $\varphi_z = \{0°, 15°, 30°, \ldots, 360°\}$ of the endodontic file with respect to the z-axis.
- In the torsional analysis, an increasing rotation was imposed at reference node B along the positive direction of z-axis, until the maximum von Mises stress along the endodontic file σ_{max} reached the end of the martensitic elastic regime. Here, the results of the analysis do not depend on the orientation of the file.

The finite element model was solved through transient analysis using the large displacements formulation, which was conducted using the ABAQUS software. Hence, material and geometric non-linearities were considered in the study. In each one of these analyses, the rotation at reference node B (θ_x for bending analysis and θ_z for torsional analysis) and the reaction moment at reference node A (M_x for bending analysis and M_z for torsional analysis) were registered for each analysis frame. The maximum von Mises stress and the maximum principal strain were also retrieved for each analysis frame, using the

method indicated in Appendix A.1, in order to minimize possible numerical singularities in the model. Finally, the bending fatigue life was estimated following the method described in Appendix A.2, based on the Coffin–Manson relation, considering the material properties indicated in Table 2.

Table 2. Material properties used to characterize the fatigue behavior of NiTi alloy [28,40].

Parameter	Variable	Magnitude
Fatigue ductility coefficient	ε_F'	0.68
Fatigue strength coefficient	σ_F'	705 MPa
Fatigue ductility exponent	c	−0.6
Fatigue strength exponent	b	−0.06
Modulus of elasticity	E	42.5 GPa

3. Results

3.1. Bending Analysis

Figure 5 shows the von Mises stress plot for the bending analysis of two representative endodontic files with pitch $p_z = 4$ mm and analysis angular position given by $\varphi_z = 0°$, for the analysis frame in which the maximum von Mises stress in the model reaches the end of the loading transformation phase ($\sigma_{max} = \sigma_L^E$). Figure 5a shows the von Misses stress plot over an endodontic file with square cross-section and Figure 5b shows the von Misses stress plot over an endodontic file with triangular cross-section. The figure shows that, under these boundary conditions, the highest stresses were located in the apical third of the file.

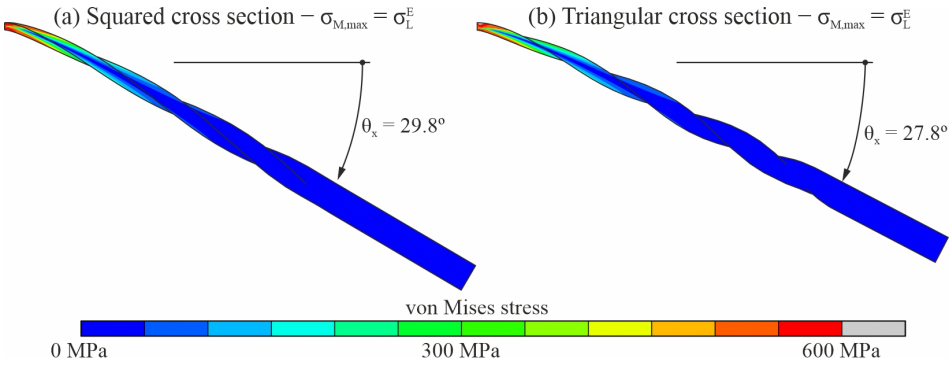

Figure 5. The von Mises stress plots for the bending analysis of endodontic files with $p_z = 4$ mm and $\varphi = 0°$.

Figure 6 shows the relationship between the rotation θ_x and the reaction bending moment M_x obtained from the bending analysis of the endodontic files with square (Figure 6a) and triangular (Figure 6b) cross-sections and pitch $p_z = 4$ mm. Here, the abscissa axis shows the rotation of the reference node B along the x-axis, while the ordinate axis shows the reaction bending moment at reference node A. The figure also shows the points where the maximum von Mises stress in the finite element model reaches the start of the phase transformation, the end of the phase transformation, and the end of the martensitic elastic regime. The curves in the figure exhibit a significant decrease in the slope for a rotation close to 20°, corresponding to a change in the stiffness of the file, as the transformation from austenite to martensite progresses in part of the file. As the bending response of an endodontic file is dependent on its orientation (given by the angle φ_z), different curves were obtained for each cross-section. For clarity, only the lower and upper curves are shown for each case, along with another intermediate representative curve. The figures also show the cross-section orientation at the encastré for each case.

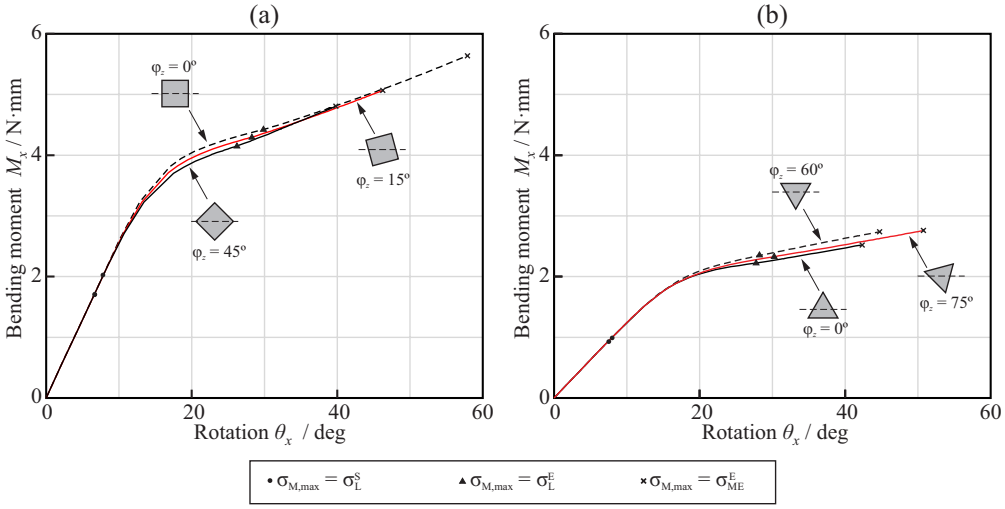

Figure 6. Bending moment–rotation relationships for the bending analysis of endodontic files with $p_z = 4$ mm: squared cross-section (**a**) and triangular cross-section (**b**).

Figure 7 shows the bending overload failure mechanism evaluation, which occurs when the maximum von Mises stress in the endodontic file reaches the end of the martensitic elastic regime ($\sigma_{max} = \sigma^E_{ME}$). On one hand, Figure 7a shows, for each considered pitch and cross-section, the rotation that needs to be applied at the free end of the endodontic files to reach the end of the martensitic elastic regime in the bending analysis. On the other hand, Figure 7b shows, for each considered pitch and cross-section, the maximum bending moment that can be applied at the free end of the endodontic files before they reach the end of the martensitic elastic regime in the bending analysis. As different angular positions were evaluated for each cross-section and pitch, the results shown are the range between the minimum and maximum obtained values. The bold lines represent the mean value within this range.

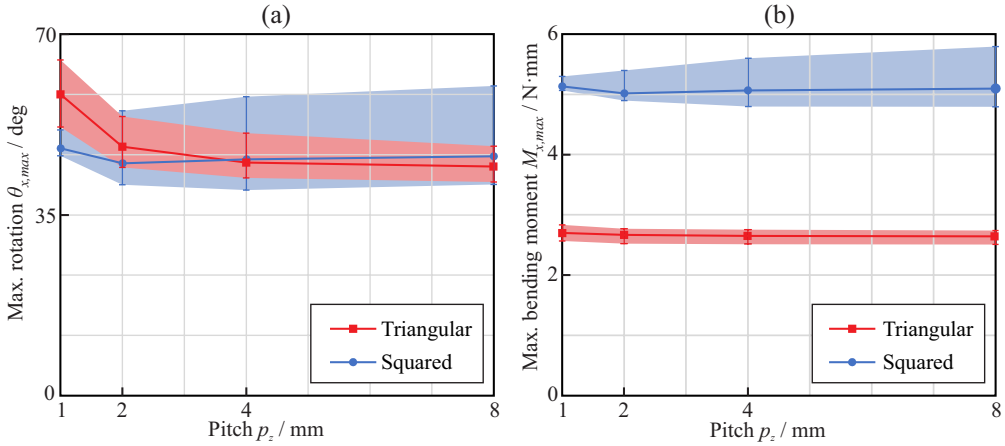

Figure 7. Bending analysis: effect of the pitch on the maximum rotation (**a**) and maximum applied torque (**b**) when the end of the martensitic elastic regime is reached.

Figure 7a shows that the maximum rotation was, on average, quite similar for triangular and square cross-sections when the pitch value was larger than 3 mm. For these pitch values, it was nearly independent of the pitch, but with a slight tendency to increase with the pitch when using a square cross-section and to decrease when using a triangular cross-section. For pitches below 3 mm, files with triangular cross-sections exhibited larger rotations than files with square cross-sections. From Figure 7b, it can be observed that the moment required to bend the square cross-section to failure was almost twice that for the triangular cross-section. The results shown in Figure 7a,b indicate that square cross-sections

are more sensitive to the orientation of the file (φ_z) than triangular cross-sections, as the results exhibited larger variability.

Figure 8 shows the bending stiffness of the endodontic rotary files for the austenite and transformation phases. The stiffness in the austenite phase was calculated as the slope of the bending moment–rotation curve before σ_L^S, while that in the transformation phase was calculated as the slope of the bending moment–rotation curve between σ_L^E and σ_{ME}^E. In general, it was observed that the stiffness of the endodontic files with square cross-sections was larger than that of the files with triangular cross-sections, both in the austenite and transformation phases. Moreover, the sensitivity to the orientation of the files with square cross-sections was larger than that of those with triangular cross-sections, especially in the austenite phase. The effect of the pitch on the stiffness was negligible for pitches larger than 3 mm. With smaller pitches, a reduction in the stiffness was observed, except for the austenite phase with the square cross-section.

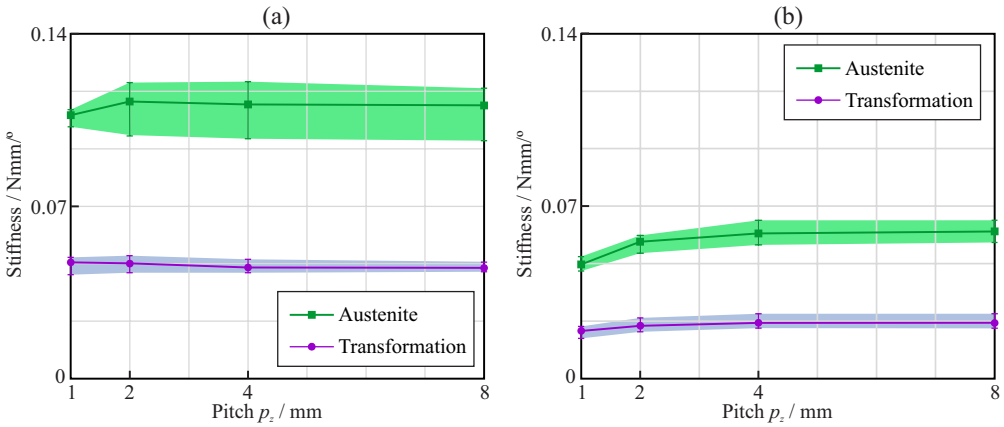

Figure 8. Bending analysis: bending stiffness of the endodontic rotary files with (**a**) square and (**b**) triangular cross-section.

Finally, Figure 9 shows the evaluation of the expected fatigue life of the endodontic files when cyclically subjected to a purely reversed bending, which produced a rotation of $\theta_x = 20°$ at the free end of the file. As explained in Appendix A.2, the bending fatigue life depends on the maximum principal strain in the file. Figure 9a shows the maximum principal strain predicted by the finite element model as a function of the pitch, for both square and triangular cross-sections. In both cases, the effect of file orientation with respect to the bending moment was significant, and the effect of the pitch was noted especially for pitches smaller than near 3 mm, for which a decrease in the strain was observed. For the square cross-section, the increase was almost linear; meanwhile, for the triangular cross-section, this increase approximated a logarithmic function. Figure 9b shows the number of cycles that the endodontic files could bear before bending fatigue failure, calculated from the maximum principal strains using the Coffin–Manson relation. It was observed that endodontic files with triangular cross-sections can withstand a larger number of cycles than those with square cross-sections, especially for small pitches.

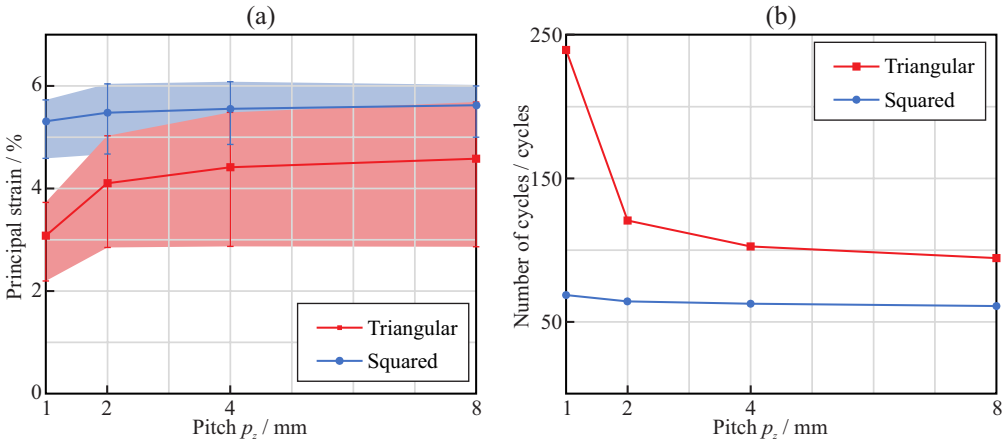

Figure 9. Bending analysis: effect of the pitch on the maximum principal strain (**a**) and the expected number of cycles (**b**) when the rotated angle is $\theta_x = 20°$.

3.2. Torsional Analysis

Figure 10 shows the von Mises stress plot for the torsional analysis of the endodontic files with square (Figure 10a) and triangular (Figure 10b) cross-sections and pitch $p_z = 4$ mm, for the analysis frames in which the maximum von Mises stress in the model reached the end of the loading transformation phase ($\sigma_{max} = \sigma_L^E$). As in the case of the bending analysis, the highest stresses were located near the apical part of the file.

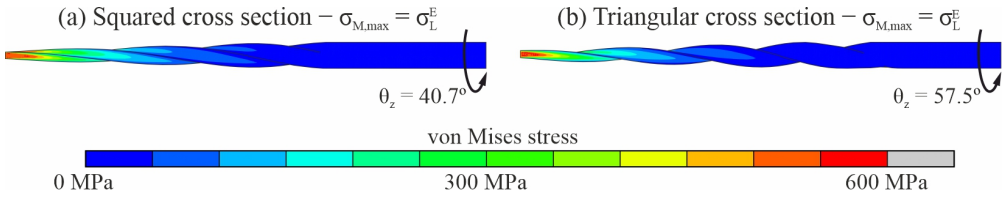

Figure 10. The von Mises stress plots for the torsional analysis of endodontic files with $p_z = 4$ mm.

Figure 11 shows the relationship between the rotation θ_z and the reaction torque M_z, obtained from the torsional analysis of the endodontic files with square (Figure 11a) and triangular (Figure 11b) cross-sections. Here, the abscissa axis shows the rotation of reference node B along the z-axis, while the ordinate axis shows the reaction torsional moment measured at reference node A. The figure also shows the points where the maximum von Mises stress in the finite element model reaches the start of the phase transformation, the end of the phase transformation, and the end of the martensitic elastic regime.

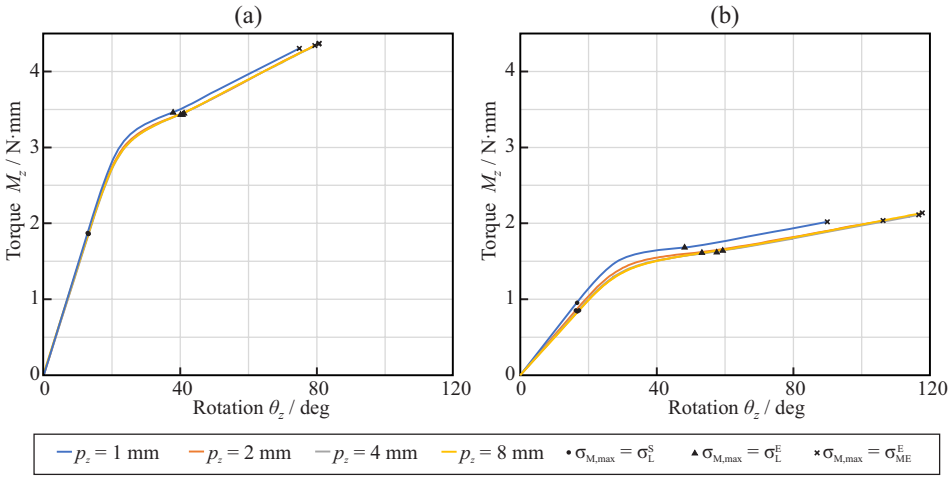

Figure 11. Torque–rotation relationships for the torsional analysis of endodontic files with different axial pitch: squared cross-section (**a**) and triangular cross-section (**b**).

Figure 12a shows, for each considered pitch and cross-section, the maximum rotation that needed to be applied at the free end of the endodontic files so that they reached the end of the martensitic elastic regime in the torsional analysis. The results show that the triangular cross-section was able to bear larger rotations before plastic deformation than the square cross-section. The rotation before failure was nearly independent of the pitch with the square cross-section, whereas it increased with the pitch for the triangular cross-section and pitch values between 1 mm and 4 mm. Figure 12b shows, for each considered pitch and cross-section, the maximum torque that could be applied at the free end of endodontic files before they reached the end of the martensitic elastic regime in the torsional analysis. It was observed that a square cross-section was able to bear almost double the torsional moment of the triangular cross-section. The strength of the files was independent of the pitch for these loading conditions.

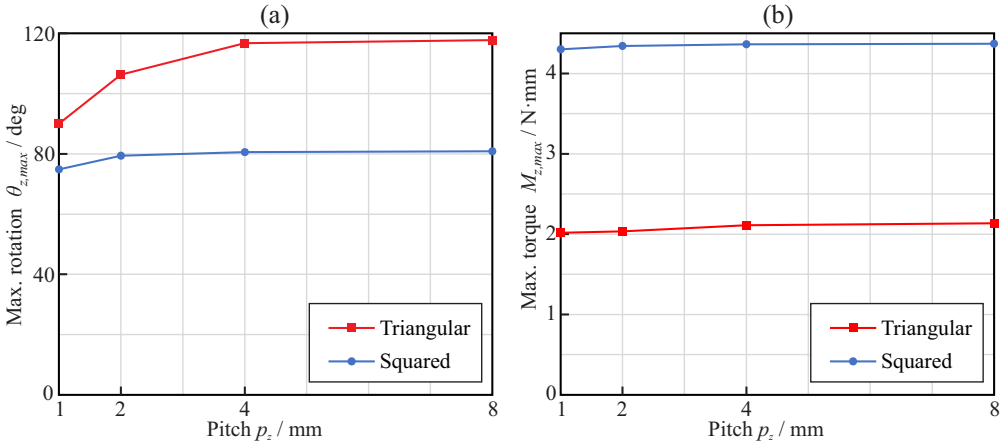

Figure 12. Torsional analysis: effect of the pitch on the applied torque (**a**) and rotation (**b**) when the end of the martensitic elastic regime is reached.

Finally, Figure 13 shows the torsional stiffness of the endodontic rotary files for the austenite and transformation phases. The stiffness in the austenite phase was calculated as the slope of the torque–rotation curve before σ_L^S, while the stiffness in the transformation phase was calculated as the slope of the torque–rotation curve between σ_L^E and σ_{ME}^E. In general, it was observed that the stiffness of the endodontic files with a square cross-section was larger than that of those with a triangular cross-section, both in the austenite and transformation phases.

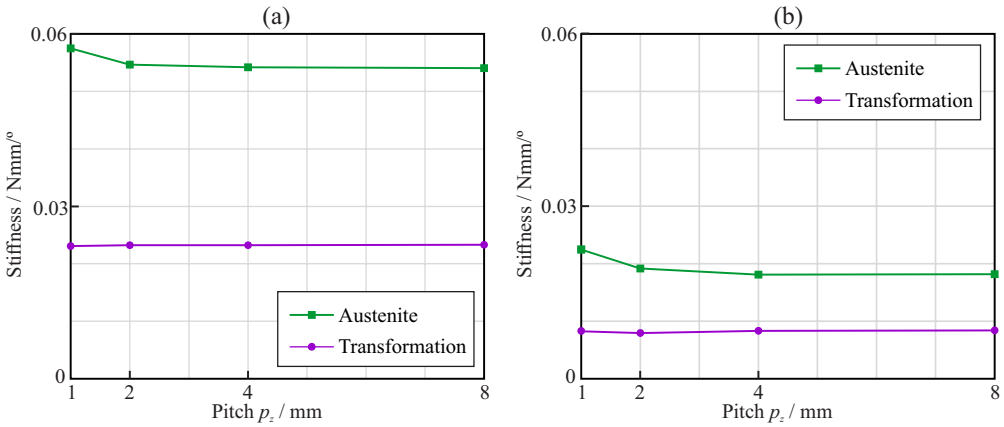

Figure 13. Torsional analysis: torsion stiffness of the endodontic rotary files with (**a**) square and (**b**) triangular cross-section.

4. Discussion

In this study, we applied an accurate non-linear finite element model to better understand the effects of the cross-section and pitch of NiTi endodontic files on their mechanical response under bending and torsion loads, according to the ISO 3630 Standard. Finite element analysis has been shown to be a good tool for this type of analysis, providing information about the stress distribution and circumventing experimental variability limitations [24]. Previous research using simulation with the same or similar objectives was first thoroughly analyzed, and the main conclusions and limitations of these studies are summarized in Appendix B, as a reference for further research. The importance of this research is supported by fact that the failure of endodontic files during root canal treatments remains a serious concern for clinicians.

The results of this study demonstrated that, for equal file diameter and taper, the cross-section shape, either triangular or square, has a greater effect than the pitch on the flexural and torsional stiffness of the file. The use of a square cross-section more than doubled the stiffness, compared to that of the triangular cross-section, as explained by the greater second moment of the area of the cross-section. The effect of pitch on stiffness was only appreciable for pitches lower than 3 mm, and was more important for triangular than for square cross-sections. When a NiTi file is bent or twisted, according to the conditions of ISO 3630, the super-elastic behavior of the material appears—which is evident from a significant decrease in the stiffness of the file—as a result of the progression of the transformation from the austenite to martensite phase in the most stressed areas of the file (see Figures 6 and 11). Our results indicate that, for a file with a shaft diameter of 1.2 mm and 6% taper, this change in stiffness appears when the rotation of the shank end section, with respect to the tip end section, is approximately 20° in bending or 30° in torsion. The stiffness of the file decreases by a factor greater than 2 after this transformation point (Figures 8 and 13). The file pitch has the opposite effect on the stiffness for torsion and bending: decreasing the pitch reduces the flexural stiffness, but increases the torsional stiffness. This effect is common for triangular and square cross-sections in the austenite phase, but it is less clear in the transformation phase, where the stiffness is less affected by pitch. This result is in agreement with those obtained in [33,36] for bending and torsion, respectively. As indicated in [33], pitch reduction could benefit both cutting efficiency, due to the higher torsional stiffness, and better adaptation to the canal shape, due to lower bending stiffness.

The obtained stress distributions (Figures 5 and 10) indicate that, for the boundary conditions imposed by the ISO 3630 Standard, the highest stresses were located near the tip of the file (where it is clamped), both in terms of bending and torsion and for both cross-section shapes. The stresses in the proximal part of the file were negligible when the stress corresponding to the end of the loading transformation phase ($\sigma_{max} = \sigma_L^E$) was reached in the tip of the file. This can be explained by the smaller section at the tip and, in the case of bending, by the higher bending moment in this area.

Static failure under bending was obtained for comparable rotations—close to 40° for pitch greater than 3 mm and ranging between 40° and 60°, depending on the pitch—for both triangular and square cross-sections (see Figure 7a). However, the bending moment necessary to reach this bending (and, thus, the reaction in the clamp) was quite different, given the difference in stiffness between the cross-section shapes (Figure 7b). This implies greater reaction forces (close to double) in the root canal with the square cross-section than with the triangular cross-section, for comparable bending deformations. The effect of the pitch on bending strength was only significant for pitches below 3 mm, where a progressive reduction in strain was observed when the pitch decreased (Figure 9a). This allows for bending of the file to a greater deformation before failure for small pitches, with a corresponding higher expected fatigue life for the same bending deformation (Figure 9b). This effect was especially observed for the triangular cross-section and, to a lesser extent, for the square cross-section. The analysis carried out to estimate the fatigue life also showed that, for the same pitch, the triangular cross-section had a higher expected life than the square cross-section, in agreement with [36], the difference being remarkable for

the smallest pitch analyzed (1 mm), for which the expected life may be more than three times longer.

Our results showed that the orientation of the bending moment, with respect to the cross-section, had a significant effect on the results, changing the results by up to 19.1° and 0.97 N · mm for the square cross-section and up to 13.0° and 0.27 N · mm for the triangular cross-section. This should be taken into account when designing, reporting, and interpreting experimental bending tests according to ISO 3630.

On the other hand, for torsion, the triangular cross-section files could be rotated to a higher angle before failure than those with a square cross-section, as can be observed from Figure 12. However, due to the difference in stiffness, this failure was reached for a torque less than half that for the square cross-section. The effect of the pitch was opposite to that observed in bending, with a reduction in the pitch leading to a lower strength, as shown by the lower possible rotation before failure, which was also in agreement with the results in [36].

From a clinical perspective, the results obtained in this study suggest that the use of a triangular-shaped cross-section with small pitch for endodontic files could be better for the safe shaping of curved root canals, as its lower stiffness would produce less reaction forces in the channel, thus reducing the possibility of ledging and canal transportation. At the same time, files with a triangular cross-section and 1 mm pitch could exhibit a fatigue life more than double that of files with higher pitches or with a square cross-section. This is accompanied by a lower rotational stiffness, which could be beneficial for improving cutting efficiency [36]. The use of a smaller pitch can only partially compensate for this lower torsional stiffness of the triangular cross-section.

The results obtained in this simulation study refer to the boundary conditions established for the tests described in ISO 3630; however, it should be noted that the stress distribution within the file in these tests is not always comparable to the clinical situation, as the bending of the file is also constrained by contact with the canal walls, resulting in a different deformation, depending on the root curvature. As shown in [38], in a curved canal, the maximum strain is usually located near the highest curvature of the curved root canal axis and the fatigue life is clearly dependent on the radius of curvature. Under the conditions of ISO 3630, the highest curvature of the deformed file is close to the tip, so the conclusions in this study are especially valid for root canals with the highest curvature located near the apical end.

Finally, this work has certain limitations that deserve to be mentioned. This investigation was conducted through theoretical studies, by means of finite element analyses of endodontic rotary files; as such, no experimental tests were conducted. Regarding the investigated endodontic file geometries, all of them had uniform parameters (pitch and cross-section) throughout their entire length, even though there exist endodontic instruments in which these parameters vary through their active length. Finally, the bending fatigue life of the endodontic instruments was assessed considering a fully reversed fatigue phenomenon corresponding to a continuous rotation motion of the file within the root canal. The study of the bending fatigue under other types of motion (e.g., reciprocating and adaptive motions) is left for future research.

5. Conclusions

In this study, we simulated the mechanical response of NiTi rotary endodontic files with different cross-sections and pitches using an accurate finite element model under bending and torsion according to the conditions of the ISO 3630 Standard.

From the results obtained, we can conclude that, with equivalent shaft diameter and taper, endodontic files with a square-shaped cross-section have more than double the stiffness of those with a triangular-shaped cross-section under both bending and torsion. The effect of the pitch on stiffness was less significant, but the use of a pitch lower than 3 mm made the files more flexible for bending and stiffer for torsion when using a triangular cross-section, with beneficial effects seen in clinical use. The phase transformation from

austenite to martensite led to a significant decrease in file stiffness both in bending and torsion, which was noticeable in the moment versus deformation curve. When the files were deformed under bending or torsion up to failure, a higher angle of rotation was possible before failure for the triangular section, especially in torsion and, for small pitches, in bending. A higher fatigue life can be expected in clinical use with the triangular-shaped cross-section than for the square cross-section under equivalent file deformations, especially with small pitch values. These results suggest a clinical recommendation for the use of files with triangular-shaped cross-sections and small pitch, in order to minimize ledging and maximize fatigue life.

Under the conditions of the ISO 3630 standard, the orientation of the bending plane with respect to the cross-section of the file had a significant effect on the stiffness and the strength of the file. This effect should be taken into account when designing, reporting, and interpreting similar test results.

Further works on this topic could be focused on studying the mechanical response of endodontic instruments with variable parameters (e.g., in terms of pitch and cross-section) throughout their active length. The bending fatigue life of the endodontic files in cases where the loading conditions do not represent a fully reversed fatigue phenomenon (e.g., adaptive or reciprocating motions) also deserves attention in future investigations.

Author Contributions: Conceptualization, A.P.-G. and V.R.-C.; methodology, A.P.-G. and V.R.-C.; software, V.R.-C.; investigation, A.P.-G. and V.R.-C.; resources, A.Z.-M. and V.F.-M.; writing—original draft preparation, A.P.-G.; writing—review and editing, V.R.-C.; supervision, A.Z.-M. and V.F.-M.; project administration, A.Z.-M. and V.F.-M. All authors have read and agreed to the published version of the manuscript.

Funding: This research received no external funding.

Institutional Review Board Statement: Not applicable.

Informed Consent Statement: Not applicable.

Data Availability Statement: Not applicable.

Conflicts of Interest: The authors declare no conflicts of interest.

Appendix A. Post-Processing of the Finite Element Analysis Results

Appendix A.1. Assessment of the Maximum von Mises Stress and Maximum Principal Strain Values in the Endodontic File

Due to the nature of the finite element method, stress and strain singularities may appear in the vicinity of those regions of the model where boundary conditions are applied or in those areas nearby geometric stress increases. These singularities imply that unrealistically large values of stress–strain are obtained as a consequence of the numerical treatment used to derive these magnitudes from the nodal displacement results. There are many researchers who have claimed that the stress–strain results at singularity points cannot be considered when evaluating the strength of endodontic files [41,42].

Several strategies can be found in the literature to address this issue. Żmudzki [43] proposed to exclude the stress results at these points, instead extrapolating the extreme value from the stress values in the surrounding nodes. A different approach has been used by Baek [36], who determined the maximum stress level as the mean value of the top 1% von Mises equivalent stress values in the finite element model. In this work, the maximum von Mises stress σ_{max} at a given analysis frame is defined as the maximum stress level that is reached by a certain amount λ of the total volume of the file (V_{tot}). To determine this magnitude, the steps below were followed:

- Let $i \in [1, n_e]$ refer to each of the n_e tetrahedral finite elements in the model, and $j \in [1, 4]$ refer to the integration points in each tetrahedral element. The von Mises stress at a given element and integration point is denoted as σ_{ij}, and the volume

associated with each integration point is denoted as $V_{ij} = V_i/4$ (where V_i is the volume of element i).

- The von Mises stress σ_{ij} and the volume V_{ij} at each integration point of the model are retrieved and stored in an array Σ with $n_i = 4 \cdot n_e$ rows. Each row m in Σ contains the von Mises stress and the volume associated with a given integration point, with the shape

$$\Sigma[m] = [\sigma_{ij}, V_{ij}]. \quad \text{(A1)}$$

- The rows in Σ are rearranged in such a way that the von Mises stresses are sorted in descending order. Then, the algorithm shown in Figure A1 is applied to determine the maximum von Mises stress in the analysis frame.

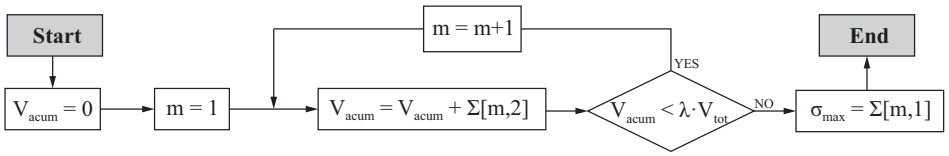

Figure A1. Algorithm to search for the maximum von Mises σ_{ij} stress in the analysis frame after the array Σ is created.

In this work, the magnitude of λ is set arbitrarily to 0.1‰, which has been shown to be a good value to avoid stress singularities while maintaining the actual stress level of the file. The same strategy was applied to determine the maximum principal strain in each analysis frame.

Appendix A.2. Determination of Bending Fatigue Life of the NiTi Endodontic Files

When the endodontic files are continuously rotated inside the root canal, they are typically subjected to a purely reversed fatigue phenomenon in which, for each rotation of the file, the bending strain alternates between nearly equal positive and negative peak values following a sinusoidal function [44]. The difference between these peak values is called the bending strain range, which is denoted by $\Delta\varepsilon$. Several studies [45–47] have demonstrated that the bending strain range and the number of cycles to failure (NCF) are correlated, and this correlation can be adequately represented by the Coffin–Manson relation:

$$\frac{\Delta\varepsilon}{2} = \varepsilon'_F \cdot N_f^c + \frac{\sigma'_F}{E} \cdot N_f^b, \quad \text{(A2)}$$

where N_f is equivalent to the NCF, ε'_F is the fatigue ductility coefficient, σ'_F is the fatigue strength coefficient, c is the fatigue ductility exponent, and b is the fatigue strength exponent.

Two issues arise when applying the Coffin–Manson relation to predict the NCF of the endodontic files from the strain results obtained from the proposed finite element model:

- On one hand, the Coffin–Manson relation is based on a uni-axial strain, but the strain results obtained from the finite element model correspond to a multi-axial strain state. Thus, a criterion to reduce the obtained multi-axial strain state to an equivalent uni-axial strain condition is required.
- On the other hand, the bending analysis conducted using the proposed finite element model does not represent the actual strain history of the endodontic file when it is rotating inside the root canal, as bending is applied in just one direction (uni-directional fatigue). Thus, a conversion method must be proposed to convert the obtained strains into a purely reversed fatigue phenomenon.

According to Roda-Casanova et al. [44], and in order to convert the multi-axial strain state into uni-axial strain, the bending strain range $\Delta\varepsilon_i$ at node i of the finite element model can be successfully approximated by:

$$\Delta\varepsilon_i = \max_{j=1\ldots n_f}(\varepsilon_{ij}^{max}) - \min_{j=1\ldots n_f}(\varepsilon_{ij}^{min}), \tag{A3}$$

where ε_{ij}^{max} and ε_{ij}^{min} are the maximum and the minimum principal strains that take place at node i at time frame j of the transient analysis, respectively. Considering that the endodontic file is continuously rotating inside the root canal, it is fair to assume that the maximum and minimum principal strains that take place at node i have the same modulus and different sign. Under this assumption, Equation (A3) can be simplified to:

$$\Delta\varepsilon_i = 2 \cdot \max_{j=1\ldots n_f}(\varepsilon_{ij}^{max}). \tag{A4}$$

Thus, by determining the maximum magnitude of the maximum principal strain in the finite element model and calculating the strain range $\Delta\varepsilon_i$ at such a node using Equation (A4), the NCF for a given specimen can be predicted through Equation (A2). The material parameters considered for the application of the Coffin–Manson relation are reflected in Table 2.

Appendix B. Literature Review

Table A1. Previous FE studies considering the effects of cross-section and pitch on rotary endodontic files.

Source	Section Type	Tip Diameter; Taper	Pitch (mm)	Material Model and Parameters	FE Code; Model Type	Boundary Conditions; Number of Nodes/Elements	Conclusions	Limitations
Xu et al., 2006 [32]	6 shapes (ProTaper, Hero642, Mtwo, ProFile, Quantec, NiTiflex)	0.4 mm, 4%	3.6	Multi-linear kinematic hardening plastic model E_A = 34.3 GPa, ν_A = 0.33, σ_L^S = 480 MPa, σ_L^E = 755 MPa	N/A, Static	Loads: progressive 0–2.5 Nmm torsion in shank, Constraints: fixed at tip, # nodes: Not available. # elements: Not available.	(1) Sections with higher core area show lower stresses for the same torque	(1) Sections analyzed have different total areas
Kim et al., 2009 [34]	4 shapes (ProFile, HeroShaper, Mtwo, NRT)	0.3 mm; 6%	Several, N/A	E_A = 36 GPa, ν_A = 0.3, σ_L^E = 504 MPa, σ_L^S = 755 MPa	ABAQUS; Static (cases I to IV) Dynamic (case V): Simulated shaping	Case I (or II), Load: 1 N (or 2 mm) bending in tip Constraint: shank fixed Case II (or III), Load: 2.5 Nmm (or 10°) torsion in shank Constraint: fixed at 4 mm from tip Case V, Constraint: shank rotation 240 rpm, file introduction in simulated root canal; # nodes: 7018–18,214 # elements: 5300–9440	(1) Rectangle-based sections have lower expected fatigue life than triangle-based sections	(1) Material model not clearly defined
Baek et al., 2011 [36]	4 theoretical shapes (triangle, slender rectangle, rectangle, square)	0.3 mm; 4.4%	3.2, 1.6, 1.1	E_A = 36 GPa, ν_A = 0.3	ABAQUS; Static	Load: 20° torsion in shank Constraint: fixed at 4 mm from tip; # nodes: Not available. # elements: Not available.	(1) Rectangle-based sections, even with smaller areas, have higher torsional stiffness than triangular section; (2) Reduction in pitch increases torsional stiffness	(1) Linear material model; (2) Mesh quality not provided
Arbab-Chirani et al., 2011 [35]	5 shapes (Hero, Hero Shaper, Mtwo, ProFile, ProTaper F1)	0.2mm; 6%	Several, N/A	SMA material model, E_A = 47 GPa, ν_A = 0.3 σ_L^S = 505 MPa	Cast3M; Static	Case 1: Load: bending at tip 3.8 mm, Constraint: shank fixed Case 2: Load: torsion at tip 22°, Constraint: shank fixed; # nodes: 66,023–73,561 # elements: 14,100–16,200	(1) ProTaper F1, Hero Shaper, and Hero are stiffer than Mtwo and ProFile; (2) Maximum stresses near the tip for both cases and similar for all the files	(1) Different pitch among files; (2) Deformations applied are low to extend martensitic transformation to a significant part of the file

Table A1. *Cont.*

Source	Section Type	Tip Diameter; Taper	Pitch (mm)	Material Model and Parameters	FE Code; Model Type	Boundary Conditions; Number of Nodes/Elements	Conclusions	Limitations
Versluis et al., 2012 [33]	4 theoretical shapes (triangle, slender rectangle, rectangle, square)	0.3 mm; 4%	3.2, 1.6, 1.1	SMA material model, E_A = 36 GPa, ν_A = 0.3 σ_L^S = 504 MPa, σ_L^E = 600 MPa	MSC.Marc; Static	Load: bending at tip 5 mm (all possible orientations with respect to the cross-section), Constraint: shank axis orientation and shank end location fixed; # nodes: Not available. # elements: Not available.	(1) Flexural stiffness and stress decreases with decreasing pitch; (2) Decreasing the pitch reduces the oscillation of stress when the file rotates; (3) Flexural stiffness and stress correlates with center-core area; (4) Effect of section greater than that of pitch; (5) Maximum stress is affected by bending orientation for rectangular section	(1) Deformations applied are low to extend martensitic transformation to a significant part of the file (max. stresses below 504 MPa)
De Arruda et al., 2014 [10]	3 shapes (Mtwo, RaCe, PTU F1)	0.25 mm; 6%	Several (Not available)	Shape-memory alloy material model implemented as ABAQUS sub-routine, E_A = 42.53 GPa, ν_A = 0.33 σ_L^S = 492 MPa, σ_L^E = 630 MPa	ABAQUS; Static	Case 1: Load: bending in shank from 0º to 45º (two perpendicular orientations), Constraint: fixed at 3 mm from tip Case 2: Load: 3 Nmm torsion in shank, Constraint: fixed at 3 mm from tip; # nodes: 84,126–91,372 # elements: 48,460–55,009	(1) Finite element analysis results agree with experimental results; (2) RaCe and Mtwo are more flexible than PTU F1 in bending and torsion; (3) Shape of the section affects the maximum stress and the variation in stress with bending orientation	(1) Only three section geometries and two orientations for bending considered; (2) Different pitch among files
Ha et al., 2015 [37]	4 theoretical shapes (triangle, slender rectangle, rectangle, square)	0.3 mm; 4.4%	3.2, 1.6, 1.1	E_A = 26 GPa, ν_A = 0.3	ABAQUS; Not available.	Load: Prescribed rotation inside the root canal, Constraint: Contact with friction in 3 simulated root canal (15º, 30º, 45º curvature), shank axis orientation & shank end location fixed; # nodes: 10,230–18,042 # elements: 8325–15,540	(1) The square cross-section shows the highest 'screw-in' force and reaction torque; (2) 'Screw-in' force and reaction torque are higher for greater pitch and higher root canal curvature	(1) Linear material model; (2) Very low friction coefficient (0.1) considered between file and root canal; (3) Solid surface used as root canal model; (4) Only 3 root canal geometries considered
Basser-Ahamed et al., 2018 [31]	5 theoretical shapes (triangle T, convex triangle C, concave triangle U, combined CTU, combinedUTC)	0.25 mm; 6%	1.6	File: E_A = 36 GPa, ν_A = 0.3 Root canal: E = 18.6 GPa, ν_A = 0.3	ANSYS; Not available.	Load: Torque 2 Nm, Constraint: Contact with simulated root canal (45º curvature), shank axis orientation and shank end location fixed, rotation of 180º at 240 rpm; File: # nodes: 16,750–42,785 # elements: 75,430–152,432 Root canal: # nodes: 3000 # elements: 3500	(1) A combined section CTU (C coronal third, T middle third, U apical third) presents lower stresses than constant section	(1) Geometry of the root canal not clearly defined defined; (2) Contact and friction conditions undefined; (3) Does not consider changes in dentin properties within the root canal; (4) Effect of pitch not analyzed

References

1. Walia, H.; Brantley, W.; Gerstein, H. An initial investigation of the bending and torsional properties of nitinol root canal files. *J. Endod.* **1988**, *14*, 346–351. https://doi.org/10.1016/S0099-2399(88)80196-1.
2. Esposito, P.; Cunningham, C. A comparison of canal preparation with nickel-titanium and stainless steel instruments. *J. Endod.* **1995**, *21*, 173–176. https://doi.org/10.1016/S0099-2399(06)80560-1.
3. Bergmans, L.; Van Cleynenbreugel, J.; Wevers, M.; Lambrechts, P. Mechanical root canal preparation with NiTi rotary instruments: Rationale, performance and safety. Status Report for the American Journal of Dentistry. *Am. J. Dent.* **2001**, *14*, 324–333.
4. Parashos, P.; Gordon, I.; Messer, H. Factors influencing defects of rotary nickel-titanium endodontic instruments after clinical use. *J. Endod.* **2004**, *30*, 722–725. https://doi.org/10.1097/01.DON.0000129963.42882.C9.
5. Spili, P.; Parashos, P.; Messer, H. The impact of instrument fracture on outcome of endodontic treatment. *J. Endod.* **2005**, *31*, 845–850. https://doi.org/10.1097/01.don.0000164127.62864.7c.
6. Plotino, G.; Grande, N.M.; Cordaro, M.; Testarelli, L.; Gambarini, G. A Review of Cyclic Fatigue Testing of Nickel-Titanium Rotary Instruments. *J. Endod.* **2009**, *35*, 1469–1476. https://doi.org/10.1016/j.joen.2009.06.015.
7. Scattina, A.; Alovisi, M.; Paolino, D.S.; Pasqualini, D.; Scotti, N.; Chiandussi, G.; Berutti, E. Prediction of cyclic fatigue life of nickel-titanium rotary files by virtual modeling and finite elements analysis. *J. Endod.* **2015**, *41*, 1867–1870. https://doi.org/10.1016/j.joen.2015.07.010.
8. Peters, O.; Barbakow, F. Dynamic torque and apical forces of ProFile .04 rotary instruments during preparation of curved canals. *Int. Endod. J.* **2002**, *35*, 379–389. https://doi.org/10.1046/j.0143-2885.2001.00494.x.
9. Kuhn, G.; Tavernier, B.; Jordan, L. Influence of structure on nickel-titanium endodontic instruments failure. *J. Endod.* **2001**, *27*, 516–520. https://doi.org/10.1097/00004770-200108000-00005.
10. De Arruda Santos, L.; López, J.; De Las Casas, E.; De Azevedo Bahia, M.; Buono, V. Mechanical behavior of three nickel-titanium rotary files: A comparison of numerical simulation with bending and torsion tests. *Mater. Sci. Eng. C* **2014**, *37*, 258–263. https://doi.org/10.1016/j.msec.2014.01.025.
11. Pruett, J.; Clement, D.; Carnes, D., Jr. Cyclic fatigue testing of nickel-titanium endodontic instruments. *J. Endod.* **1997**, *23*, 77–85. https://doi.org/10.1016/S0099-2399(97)80250-6.
12. Parashos, P.; Messer, H. Rotary NiTi Instrument Fracture and its Consequences. *J. Endod.* **2006**, *32*, 1031–1043. https://doi.org/10.1016/j.joen.2006.06.008.
13. Topçuoğlu, H.; Topçuoğlu, G. Cyclic Fatigue Resistance of Reciproc Blue and Reciproc Files in an S-shaped Canal. *J. Endod.* **2017**, *43*, 1679–1682. https://doi.org/10.1016/j.joen.2017.04.009.
14. Siqueira, J., Jr.; Rôças, I. Polymerase chain reaction-based analysis of microorganisms associated with failed endodontic treatment. *Oral Surgery Oral Med. Oral Pathol. Oral Radiol. Endod.* **2004**, *97*, 85–94. https://doi.org/10.1016/S1079-2104(03)00353-6.
15. Strindberg, L. The Dependence of the Results of Pulp Therapy on Certain Factors: An Analytic Study Based on Radiographic and Clinical Follow-Up Examinations. *Acta Odontol Scand* **1956**, *14*, 1–175.
16. Yang, Q.; Shen, Y.; Huang, D.; Zhou, X.; Gao, Y.; Haapasalo, M. Evaluation of Two Trephine Techniques for Removal of Fractured Rotary Nickel-titanium Instruments from Root Canals. *J. Endod.* **2017**, *43*, 116–120. https://doi.org/10.1016/j.joen.2016.09.001.
17. Fu, M.; Zhang, Z.; Hou, B. Removal of broken files from root canals by using ultrasonic techniques combined with dental microscope: A retrospective analysis of treatment outcome. *J. Endod.* **2011**, *37*, 619–622. https://doi.org/10.1016/j.joen.2011.02.016.
18. Ruiz-Sánchez, C.; Faus-Llacer, V.; Faus-Matoses, I.; Zubizarreta-Macho, A.; Sauro, S.; Faus-Matoses, V. The influence of niti alloy on the cyclic fatigue resistance of endodontic files. *J. Clin. Med.* **2020**, *9*, 3755. https://doi.org/10.3390/jcm9113755.
19. Zupanc, J.; Vahdat-Pajouh, N.; Schäfer, E. New thermomechanically treated NiTi alloys—A review. *Int. Endod. J.* **2018**, *51*, 1088–1103. https://doi.org/10.1111/iej.12924.
20. Faus-Llacer, V.; Kharrat, N.; Ruiz-Sanchez, C.; Faus-Matoses, I.; Zubizarreta-Macho, A.; Faus-Matoses, V. The effect of taper and apical diameter on the cyclic fatigue resistance of rotary endodontic files using an experimental electronic device. *Appl. Sci.* **2021**, *11*, 863. https://doi.org/10.3390/app11020863.
21. Turpin, Y.; Chagneau, F.; Vulcain, J. Impact of two theoretical cross-sections on torsional and bending stresses of nickel-titanium root canal instrument models. *J. Endod.* **2000**, *26*, 414–417. https://doi.org/10.1097/00004770-200007000-00009.
22. Sekar, V.; Kumar, R.; Nandini, S.; Ballal, S.; Velmurugan, N. Assessment of the role of cross section on fatigue resistance of rotary files when used in reciprocation. *Eur. J. Dent.* **2016**, *10*, 541–545. https://doi.org/10.4103/1305-7456.195171.
23. Kwak, S.; Ha, J.H.; Lee, C.J.; El Abed, R.; Abu-Tahun, I.; Kim, H.C. Effects of Pitch Length and Heat Treatment on the Mechanical Properties of the Glide Path Preparation Instruments. *J. Endod.* **2016**, *42*, 788–792. https://doi.org/10.1016/j.joen.2016.02.002.
24. *ISO 3630-1:2008*; Dentistry—Root-Canal Instruments—Part 1: General Requirements and Test Methods. International Organization for Standardization: Geneva, Switzerland, 2008.
25. Zhang, E.; Cheung, G.; Zheng, Y. A mathematical model for describing the mechanical behaviour of root canal instruments. *Int. Endod. J.* **2011**, *44*, 72–76. https://doi.org/10.1111/j.1365-2591.2010.01801.x.
26. Tsao, C.; Liou, J.; Wen, P.; Peng, C.; Liu, T. Study on bending behaviour of nickel-titanium rotary endodontic instruments by analytical and numerical analyses. *Int. Endod. J.* **2013**, *46*, 379–388. https://doi.org/10.1111/iej.12025.
27. Lee, M.H.; Versluis, A.; Kim, B.M.; Lee, C.J.; Hur, B.; Kim, H.C. Correlation between experimental cyclic fatigue resistance and numerical stress analysis for nickel-titanium rotary files. *J. Endod.* **2011**, *37*, 1152–1157. https://doi.org/10.1016/j.joen.2011.03.025.

28. Montalvão, D.; Shengwen, Q.; Freitas, M. A study on the influence of Ni-Ti M-Wire in the flexural fatigue life of endodontic rotary files by using Finite Element Analysis. *Mater. Sci. Eng. C* **2014**, *40*, 172–179. https://doi.org/10.1016/j.msec.2014.03.061.
29. Bonessio, N.; Pereira, E.; Lomiento, G.; Arias, A.; Bahia, M.; Buono, V.; Peters, O. Validated finite element analyses of WaveOne Endodontic Instruments: A comparison between M-Wire and NiTi alloys. *Int. Endod. J.* **2015**, *48*, 441–450. https://doi.org/10.1111/iej.12333.
30. Chien, P.Y.; Walsh, L.J.; Peters, O.A. Finite element analysis of rotary nickel-titanium endodontic instruments: A critical review of the methodology. *Eur. J. Oral Sci.* **2021**, *129*, e12802. https://doi.org/10.1111/eos.12802.
31. Basheer Ahamed, S.; Vanajassun, P.; Rajkumar, K.; Mahalaxmi, S. Comparative Evaluation of Stress Distribution in Experimentally Designed Nickel-titanium Rotary Files with Varying Cross Sections: A Finite Element Analysis. *J. Endod.* **2018**, *44*, 654–658. https://doi.org/10.1016/j.joen.2017.12.013.
32. Xu, X.; Eng, M.; Zheng, Y.; Eng, D. Comparative study of torsional and bending properties for six models of nickel-titanium root canal instruments with different cross-sections. *J. Endod.* **2006**, *32*, 372–375. https://doi.org/10.1016/j.joen.2005.08.012.
33. Versluis, A.; Kim, H.C.; Lee, W.; Kim, B.M.; Lee, C.J. Flexural stiffness and stresses in nickel-titanium rotary files for various pitch and cross-sectional geometries. *J. Endod.* **2012**, *38*, 1399–1403. https://doi.org/10.1016/j.joen.2012.06.008.
34. Kim, H.; Kim, H.; Lee, C.; Kim, B.; Park, J.; Versluis, A. Mechanical response of nickel-titanium instruments with different cross-sectional designs during shaping of simulated curved canals. *Int. Endod. J.* **2009**, *42*, 593–602. https://doi.org/10.1111/j.1365-2591.2009.01553.x.
35. Arbab-Chirani, R.; Chevalier, V.; Arbab-Chirani, S.; Calloch, S. Comparative analysis of torsional and bending behavior through finite-element models of 5 Ni-Ti endodontic instruments. *Oral Surgery Oral Med. Oral Pathol. Oral Radiol. Endodontology* **2011**, *111*, 115–121. https://doi.org/10.1016/j.tripleo.2010.07.017.
36. Baek, S.H.; Lee, C.J.; Versluis, A.; Kim, B.M.; Lee, W.; Kim, H.C. Comparison of torsional stiffness of nickel-titanium rotary files with different geometric characteristics. *J. Endod.* **2011**, *37*, 1283–1286. https://doi.org/10.1016/j.joen.2011.05.032.
37. Ha, J.H.; Cheung, G.S.; Versluis, A.; Lee, C.J.; Kwak, S.W.; Kim, H.C. 'Screw-in' tendency of rotary nickel-titanium files due to design geometry. *Int. Endod. J.* **2015**, *48*, 666–672. https://doi.org/10.1111/iej.12363.
38. Roda-Casanova, V.; Zubizarreta-Macho, A.; Sanchez-Marin, F.; Ezpeleta, O.; Martínez, A.; Catalán, A. Computerized generation and finite element stress analysis of endodontic rotary files. *Appl. Sci.* **2021**, *11*, 4329. https://doi.org/10.3390/app11104329.
39. Auricchio, F.; Petrini, L. A three-dimensional model describing stress-temperature induced solid phase transformations: Solution algorithm and boundary value problems. *Int. J. Numer. Methods Eng.* **2004**, *61*, 807–836. https://doi.org/10.1002/nme.1086.
40. El-Anwar, M.I.; Mandorah, A.O.; Yousief, S.A.; Soliman, T.A.; Abd El-Wahab, T.M. A finite element study on the mechanical behavior of reciprocating endodontic files. *Braz. J. Oral Sci.* **2015**, *14*, 52–59. https://doi.org/10.1590/1677-3225v14n1a11.
41. Stolk, J.; Verdonschot, N.; Huiskes, R. Management of stress fields around singular points in a finite element analysis. *Comput. Methods Biomech. Biomed. Eng.* **2001**, *3*, 57–62.
42. Chen, G.; Pettet, G.; Pearcy, M.; McElwain, D. Comparison of two numerical approaches for bone remodelling. *Med. Eng. Phys.* **2007**, *29*, 134–139. https://doi.org/https://doi.org/10.1016/j.medengphy.2005.12.008.
43. Żmudzki, J.; Chladek, W. Stress present in bone surrounding dental implants in FEM model experiments. *J. Achiev. Mater. Manuf. Eng.* **2008**, *27*, 71–74.
44. Roda-Casanova, V.; Pérez-González, A.; Zubizarreta-Macho, Á.; Faus-Matoses, V. Fatigue Analysis of NiTi Rotary Endodontic Files through Finite Element Simulation: Effect of Root Canal Geometry on Fatigue Life. *J. Clin. Med.* **2021**, *10*, 5692. https://doi.org/10.3390/jcm10235692.
45. Cheung, G.S.; Darvell, B.W. Fatigue testing of a NiTi rotary instrument. Part 1: Strain-life relationship. *Int. Endod. J.* **2007**, *40*, 612–618. https://doi.org/10.1111/j.1365-2591.2007.01262.x.
46. Figueiredo, A.M.; Modenesi, P.; Buono, V. Low-cycle fatigue life of superelastic NiTi wires. *Int. J. Fatigue* **2009**, *31*, 751–758. https://doi.org/10.1016/j.ijfatigue.2008.03.014.
47. Maletta, C.; Sgambitterra, E.; Furgiuele, F.; Casati, R.; Tuissi, A. Fatigue properties of a pseudoelastic NiTi alloy: Strain ratcheting and hysteresis under cyclic tensile loading. *Int. J. Fatigue* **2014**, *66*, 78–85. https://doi.org/10.1016/j.ijfatigue.2014.03.011.

Journal of
Clinical Medicine

MDPI

Article

Influence of the Geometrical Cross-Section Design on the Dynamic Cyclic Fatigue Resistance of NiTi Endodontic Rotary Files—An In Vitro Study

Vicente Faus-Llácer [1], Nirmine Hamoud-Kharrat [1], María Teresa Marhuenda Ramos [1], Ignacio Faus-Matoses [1], Álvaro Zubizarreta-Macho [2,3,*], Celia Ruiz Sánchez [1] and Vicente Faus-Matoses [1]

[1] Department of Stomatology, Faculty of Medicine and Dentistry, University of Valencia, 46010 Valencia, Spain; fausvj@uv.es (V.F.-L.); nirhak@alumni.uv.es (N.H.-K.); marhuen3@uv.es (M.T.M.R.); ignacio.faus@uv.es (I.F.-M.); celia.ruiz@uv.es (C.R.S.); vicente.faus@uv.es (V.F.-M.)
[2] Department of Endodontics, Faculty of Health Sciences, Alfonso X el Sabio University, 28691 Madrid, Spain
[3] Department of Surgery, Faculty of Medicine and Dentistry, University of Salamanca, 37008 Salamanca, Spain
* Correspondence: amacho@uax.es or alvaro.zubizarreta@usal.es

Abstract: The aim of this study was to analyze and compare the influence of the geometrical cross-section design on the dynamic cyclic fatigue resistance of NiTi endodontic rotary files. Materials and Methods: Forty sterile endodontic rotary files were selected and distributed into the following study groups: A: 25.06 double S-shaped cross-section NiTi alloy endodontic rotary files (Mtwo) (n = 10); B: 20.04 rectangular cross-section NiTi alloy endodontic rotary files (T Pro E1) (n = 10); C: 25.04 convex triangular cross-section NiTi alloy endodontic rotary files (T Pro E2) (n = 10); and D: 25.06 triangular cross-section NiTi alloy endodontic rotary files (T Pro E4) (n = 10). A cyclic fatigue device was used to conduct the static cyclic fatigue tests with stainless steel artificial root canal systems with 200 µm and 250 µm apical diameter, 60° curvature angle, 3 mm radius of curvature, 20 mm length, and 4% and 8% taper. The results were analyzed using the ANOVA test and Weibull statistical analysis. Results: All the pairwise comparisons presented statistically significant differences between the time to failure and number of cycles to failure for the cross-section design study groups ($p < 0.001$). Conclusions: the double S-shaped cross-section of Mtwo NiTi endodontic files shows higher cyclic fatigue resistance than the rectangular cross-section of T Pro E1 NiTi endodontic files, the convex triangular cross-section of T Pro E2 NiTi endodontic files, and the triangular cross-section of T Pro E4 NiTi endodontic files.

Keywords: endodontics; cyclic fatigue; cross-section design; NiTi; continuous rotation; energy-dispersive X-ray

Citation: Faus-Llácer, V.; Hamoud-Kharrat, N.; Marhuenda Ramos, M.T.; Faus-Matoses, I.; Zubizarreta-Macho, Á.; Ruiz Sánchez, C.; Faus-Matoses, V. Influence of the Geometrical Cross-Section Design on the Dynamic Cyclic Fatigue Resistance of NiTi Endodontic Rotary Files—An In Vitro Study. *J. Clin. Med.* **2021**, *10*, 4713. https://doi.org/10.3390/jcm10204713

Academic Editors: Massimo Amato, Giuseppe Pantaleo and Alfredo Iandolo

Received: 6 September 2021
Accepted: 11 October 2021
Published: 14 October 2021

1. Introduction

The introduction of nickel–titanium alloy (NiTi) in the manufacturing of root canal instruments entailed a great revolution in the field of endodontics, as these endodontic files decreased the iatrogenic complications [1,2]. However, the failure of endodontic rotary files is still a concern, despite the continuous mechanical and chemical improvements in the NiTi alloy endodontic rotary instruments made by manufacturers to reduce the incidence of complications during root canal treatment [3]. Nevertheless, the incidence of fracture of NiTi endodontic rotary files ranges from 0.09% to 5% [4,5]. The failure of NiTi endodontic rotary files occurs when fatigue resistance is overcome by torsional stress, flexural bending (cyclic) stress, or a combination of the two [6]. Specifically, torsional fatigue occurs when the tip of the endodontic file becomes blocked in the root canal while the instrument continues rotating [7], and flexural bending fatigue occurs by the alternating application of compressive and tensile stress cycles on a curved root canal, leading to overcoming plastic deformation and the subsequent failure of the endodontic rotary instrument [6,8].

In addition, the unexpected failure of the NiTi alloy endodontic rotary instruments might condition the outcome of the root canal treatment by blocking the advancement of disinfecting agents beyond the fractured instrument [9–11], which may lead to subsequent pulp necrosis and the formation of periapical lesions [12] or decrease the success rate of root canal treatment of teeth with periapical pathology [13]. Therefore, several reports have been conducted to analyze the influence of both the NiTi alloy and the geometrical parameters on the torsional and flexural bending resistance of endodontic rotary instruments to prevent the incidence of failure of endodontic rotary instruments. Both the chemical composition and crystalline structure of the NiTi alloy have been widely found to highly influence the fatigue resistance of endodontic rotary files, in particular, the endodontic rotary systems, composed of a higher concentration of the martensitic phase and manufactured by electropolishing, ion implantation, cryogenic treatment, and heat treatments, improve the mechanical behavior of NiTi endodontic rotary files, increasing their cyclic fatigue resistance [14]. However, some geometrical factors have also been reported to influence the instrument's performance, including the taper and apical diameter [15], cross-section design [16,17], flute length, helix angle, and pitch [18]. Unfortunately, the independent assessment of each factor associated with flexural bending fatigue may be difficult in a clinical setting due to the heterogeneous anatomy of the root canal system; thus, controlled experimental studies have been conducted to independently analyze each variable using custom-made cyclic fatigue devices [15].

The aim of this study was to analyze and compare the influence of the geometrical cross-section design on the dynamic cyclic fatigue resistance of NiTi endodontic rotary files, with a null hypothesis (H_0) stating that the geometry of the cross-section design would not affect the resistance of NiTi endodontic rotary files to dynamic cyclic fatigue.

2. Materials and Methods

2.1. Study Design

Forty (40) sterile and non-used NiTi alloy endodontic rotary instruments were used in this in vitro study. A controlled experimental trial was performed at the Department of Stomatology of the Faculty of Medicine and Dentistry at the University of Valencia (Valencia, Spain), between March and July 2021. The NiTi endodontic rotary files were selected and categorized into the following study groups: A: double S-shaped cross-section with 250 µm apical diameter and 6% taper conventional NiTi alloy endodontic rotary files mainly consisting of austenite phase at body temperature [19] (Ref.: 0236 025 025, Mtwo, VDW, Munich, Germany) (n = 10) (Mtwo); B: rectangular cross-section with 200 µm apical diameter and 4% taper austenite phase NiTi alloy endodontic rotary files (Ref.: 20010103, T Pro E1, Perfect Endo, Shenzhen Perfect Medical Instruments, Shanwei City, China) (n = 10) (T Pro E1); C: convex triangular cross-section with 250 µm apical diameter and 4% taper austenite phase NiTi alloy endodontic rotary file (Ref.: 20010103, T Pro E2, Perfect Endo, Shenzhen Perfect Medical Instruments, Shanwei City, China) (n = 10) (T Pro E2); and D: triangular cross-section with 250 µm apical diameter and 6% taper austenite phase NiTi alloy endodontic rotary file (Ref.: 20010103, T Pro E4, Perfect Endo, Shenzhen Perfect Medical Instruments, Shanwei City, China) (n = 10) (T Pro E4). All endodontic rotary files were manufactured in austenitic phase with an austenite finish (A_f), and the temperatures of the Mtwo, T Pro E1, T Pro E2, and T Pro E4 were approximately 15 °C [19], 15 °C, 20 °C, and 20 °C, respectively. The A_f temperatures of T Pro E1, T Pro E2, and T Pro E4 were provided by the manufacturer.

2.2. Scanning Electron Microscopy Analysis

All NiTi endodontic rotary files were initially analyzed under scanning electron microscopy (SEM) (HITACHI S-4800, Fukuoka, Japan) at ×30 and ×600 in the Central Support Service for Experimental Research of the University of Valencia (Burjassot, Spain) under the following exposure parameters: acceleration voltage: 20 kV, magnification from 100× to 6500×, and a resolution between −1.0 nm at 15 kV and 2.0 nm at 1 kV, to perform

a surface characterization to discard further surface defects in its manufacture and analyze and compare the geometrical design of the NiTi endodontic rotary files (Figure 1).

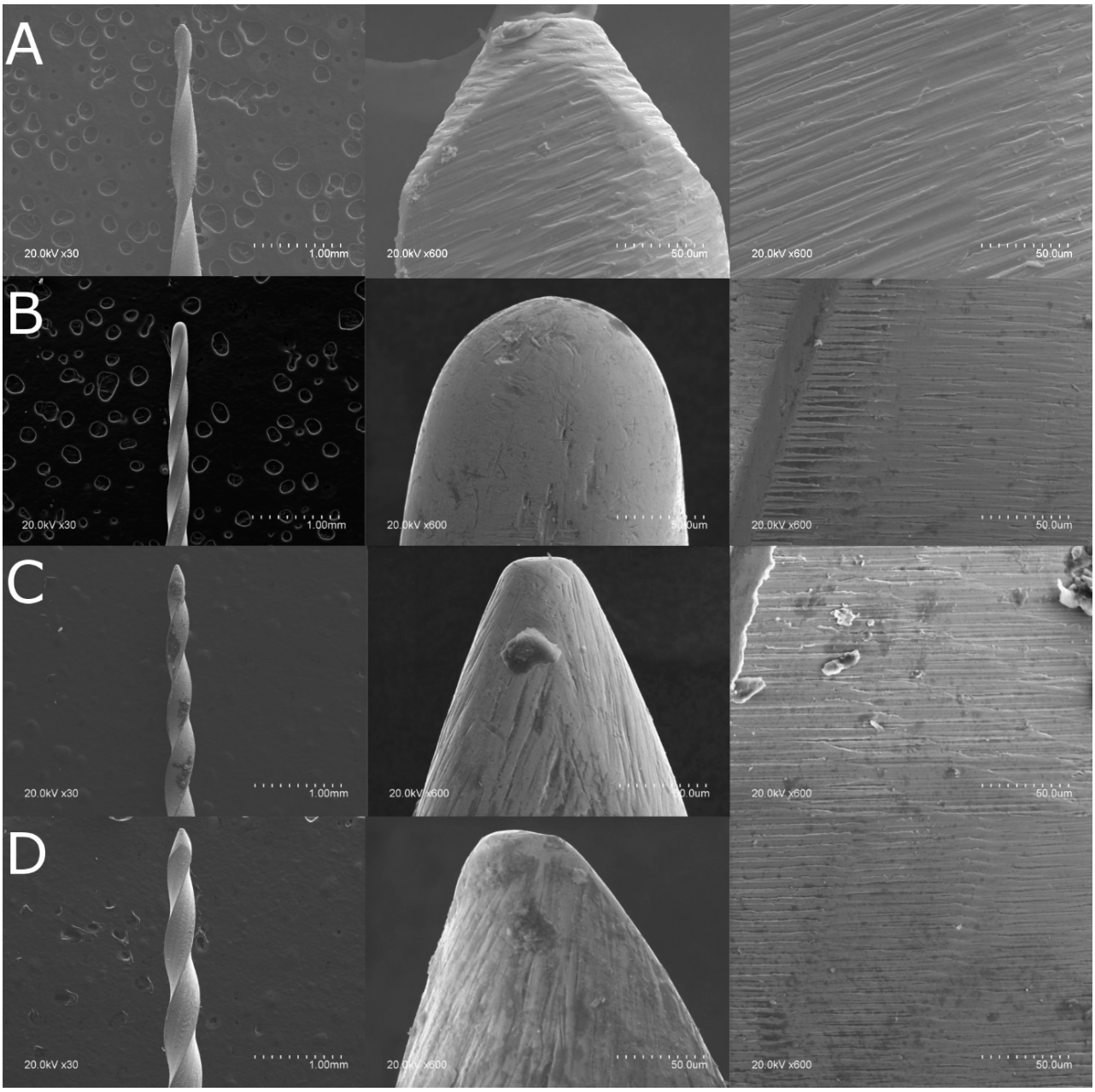

Figure 1. (**A**) SEM analysis of the Mtwo NiTi alloy endodontic rotary file, (**B**) T Pro E1 Gold-Wire NiTi alloy endodontic rotary file, (**C**) T Pro E2 Gold-Wire NiTi alloy endodontic rotary file, and (**D**) T Pro E4 Gold-Wire NiTi alloy endodontic rotary file.

2.3. Energy-Dispersive X-ray Spectroscopy Analysis

Additionally, an energy-dispersive X-ray spectroscopy (EDX) analysis was performed on all NiTi endodontic rotary files in the Central Support Service for Experimental Research of the University of Valencia (Burjassot, Spain) under the following exposure parameters: acceleration voltage: 20 kV; magnification: from 100× to 6500×; and a resolution between −1.0 nm at 15 kV and 2.0 nm at 1 kV, in order to analyze the elemental composition of the chemical elements of the NiTi endodontic rotary files used in the static fatigue tests, by means of the atomic weight percent measurement, at three randomized locations (Figure 2).

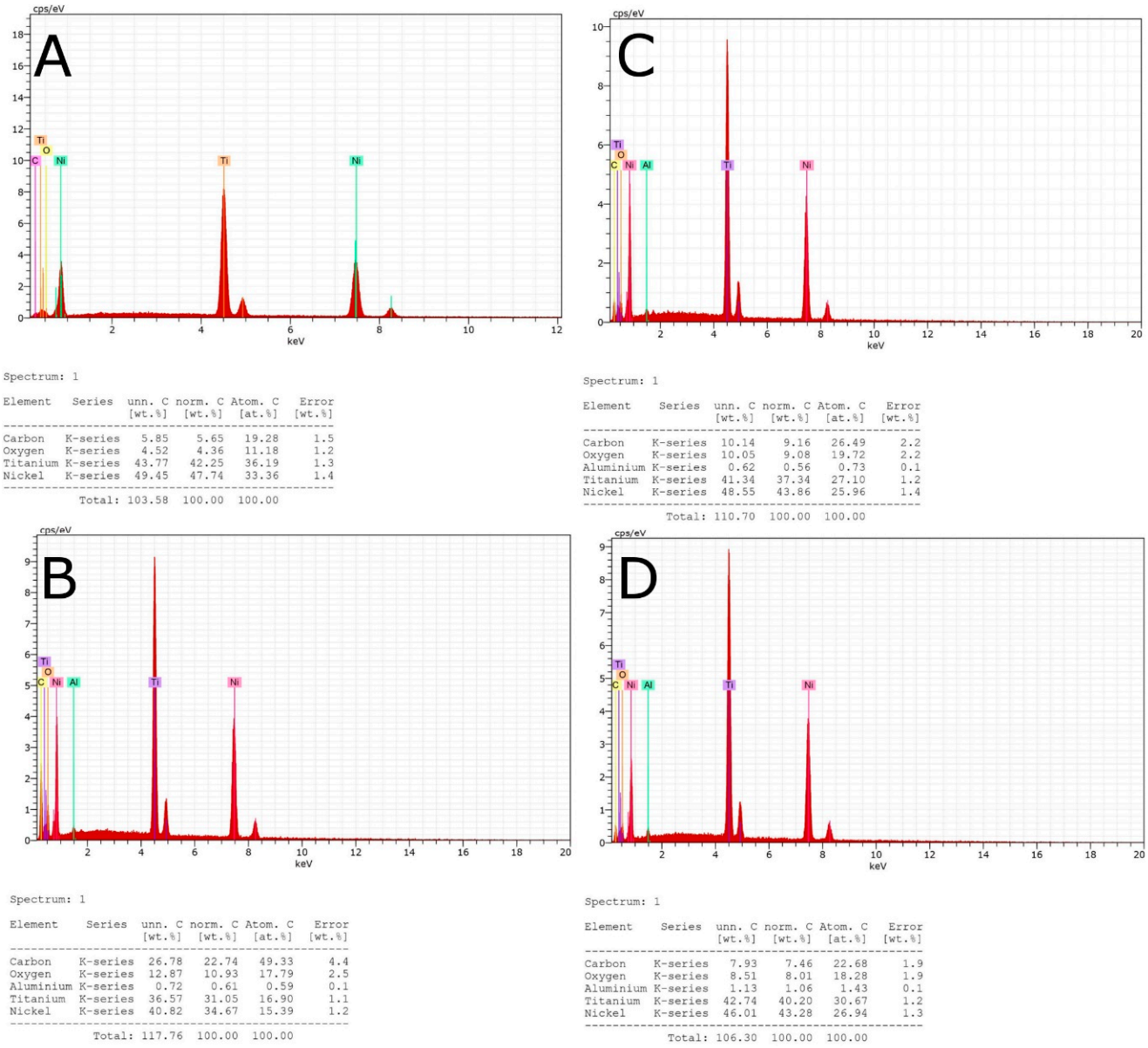

Figure 2. (**A**) EDX micro-analysis of the Mtwo NiTi alloy endodontic rotary file, (**B**) T Pro E1 austenite phase NiTi alloy endodontic rotary file, (**C**) T Pro E2 austenite phase NiTi alloy endodontic rotary file, and (**D**) T Pro E4 austenite phase NiTi alloy endodontic rotary file.

2.4. Experimental Cyclic Fatigue Model

Dynamic cyclic fatigue tests were performed using the previously described custom-made device (utility model patent number ES1219520) [20]. The structure of the dynamic cyclic fatigue test device was designed by computer aided design/computer aided engineering (CAD/CAE) 2D/3D software (Midas FX+®, Brunleys, Milton Keynes, UK) and created using 3D printing (ProJet® 6000 3D Systems©, Rock Hill, SC, USA) (Figure 3).

The custom-made artificial root canals were performed with a 60° curvature according to Schneider's measuring technique [21] and 3 mm radius of curvature using CAD/CAE 2D/3D software for inverse engineering technology. The artificial root canal was created from stainless steel using electrical discharge machining (EDM) molybdenum wire-cut technology (Cocchiola S.A., Buenos Aires, Argentina). This process ensured intimate contact between the NiTi endodontic reciprocating files and the artificial root canal walls. The artificial root canal was positioned on its support, and failure of the endodontic rotary

instrument was detected using a Light-Dependent Resistor (LDR) sensor (Ref.: C000025, Arduino LLC®, Ivrea, Italy) located at the apex of the artificial root canal. The LDR sensor quantifies the continuous light source emitted by a high-brightness white Light-Emitting Diode (LED) (20000 mcd) (Ref.: 12.675/5/b/c/20k, Batuled, Coslada, Spain), which is located opposite the artificial root canal. The light signals emitted by the LED sensor were detected by the LDR (Ref.: C000025, Arduino LLC®) sensor with a frequency of 50 ms to accurately identify the precise time of failure.

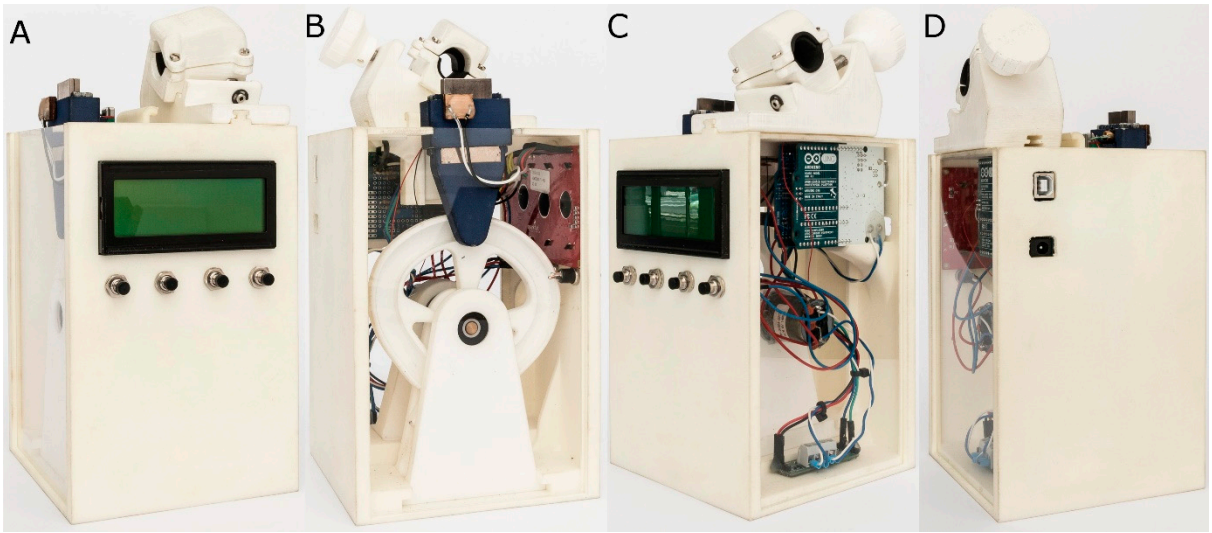

Figure 3. (**A**) Front, (**B**) back, (**C**) right, and (**D**) left surfaces of the dynamic cyclic fatigue device.

The direction and speed of the movement generated by the brushed DC gear motor (Ref.: 1589, Pololu® Corporation, Las Vegas, NV, USA) and controlled by the driver (Ref.: DRV8835, Pololu® Corporation, Las Vegas, NV, USA) were transferred to the artificial root canal support through a roller bearing system (Ref.: MR104ZZ, FAG, Schaeffler Herzogenaurach, Germany). The artificial root canal support moved in a pure axial motion using a lineal guide (Ref.: HGH35C 10249-1 001 MA, HIWIN Technologies Corp. Taichung, Taiwan). All the NiTi endodontic rotary files were used with a 6:1 reduction handpiece (X-Smart plus, Dentsply Maillefer, Baillagues, Switzerland) and torque-controlled motor. Mtwo NiTi alloy endodontic rotary files (Ref.: 0236 025 025, Mtwo, VDW, Munich, Germany) were used at 250 rpm and 2.3 N/cm torque, T Pro E1 austenite phase NiTi alloy endodontic rotary files (Ref.: 20010103, T Pro E1, Perfect Endo, Shenzhen Perfect Medical Instruments, Shanwei City, China) were used at 250 rpm and 2 N/cm torque, T Pro E2 austenite phase NiTi alloy endodontic rotary files (Ref.: 20010103, T Pro E1, Perfect Endo, Shenzhen Perfect Medical Instruments, Shanwei City, China) were used at 250 rpm and 2 N/cm torque, and T Pro E4 austenite phase NiTi alloy endodontic rotary files (Ref.: 20010103, T Pro E1, Perfect Endo, Shenzhen Perfect Medical Instruments, Shanwei City, China) were used at 250 rpm and 2 N/cm torque, according to the manufacturer's instructions.

All NiTi endodontic files were used in the dynamic cyclic fatigue device at a frequency of 60 pecking movements/min according to a previous study [20]. To reduce the friction between the rotating files and the artificial canal walls, special high-flow synthetic oil designed for the lubrication of mechanical parts (Singer All-Purpose Oil; Singer Corp., Barcelona, Spain) was applied.

All NiTi endodontic rotary files were used until fracture occurred. The time to failure and the number of cycles to failure were measured and recorded.

2.5. Statistical Tests

Statistical analysis of all the variables was carried out using SAS 9.4 (SAS Institute Inc., Cary, NC, USA). Descriptive statistics are expressed as the mean and standard deviation

(SD) for quantitative variables. Comparative analysis was performed by comparing the time to failure (in seconds) and the number of cycles to failure using the ANOVA test. For the comparisons, the p-values were adjusted using the Tukey method to correct the type I error. In addition, Weibull characteristic strength and Weibull modulus were calculated. The statistical significance was set at $p < 0.05$.

3. Results

SEM analysis of the T Pro E2 NiTi endodontic rotary files (Ref.: 20010103, T Pro E1, Perfect Endo, Shenzhen Perfect Medical Instruments, Shanwei City, China) showed accumulation of organic matter, but none of the NiTi endodontic rotary files showed relevant structural alterations. Moreover, manufacturing lines were distributed perpendicularly to the longitudinal axis in all of the endodontic rotary files and also parallel to each other due to the manufacturing process by laser machining. The width and spacing of the manufacturing lines and tubular porosity correspond to the precision and intensity of the laser machining process. In addition, the macroscopically geometrical design of the double S-shaped cross-section of Mtwo NiTi alloy endodontic rotary files (Ref.: 0236025025, Mtwo, VDW, Munich, Germany) showed a higher pitch than the rectangular cross-section of T Pro E1 NiTi endodontic files (Ref.: 20010103, T Pro E1, Perfect Endo, Shenzhen Perfect Medical Instruments, Shanwei City, China), the convex triangular cross-section of T Pro E2 NiTi endodontic files (Ref.: 20010103, T Pro E1, Perfect Endo, Shenzhen Perfect Medical Instruments, Shanwei City, China), and the triangular cross-section of T Pro E4 NiTi endodontic files (Ref.: 20010103, T Pro E1, Perfect Endo, Shenzhen Perfect Medical Instruments, Shanwei City, China).

EDX micro-analysis of the double S-shaped cross-section of Mtwo NiTi alloy endodontic rotary files (Ref.: 0236025025, Mtwo, VDW, Munich, Germany), the rectangular cross-section of T Pro E1 NiTi endodontic files (Ref.: 20010103, T Pro E1, Perfect Endo, Shenzhen Perfect Medical Instruments, Shanwei City, China), the convex triangular cross-section of T Pro E2 NiTi endodontic files (Ref.: 20010103, T Pro E1, Perfect Endo, Shenzhen Perfect Medical Instruments, Shanwei City, China), and the triangular cross-section of T Pro E4 NiTi endodontic files (Ref.: 20010103, T Pro E1, Perfect Endo, Shenzhen Perfect Medical Instruments, Shanwei City, China) was performed at 20 kV as this allowed a deeper analysis of the NiTi endodontic rotary files surface. In summary, the double S-shaped cross-section of Mtwo NiTi alloy endodontic rotary files (Ref.: 0236025025, Mtwo, VDW, Munich, Germany) differs in the chemical elements present in the metal alloy, in accordance with the rectangular cross-section of T Pro E1 NiTi endodontic files (Ref.: 20010103, T Pro E1, Perfect Endo, Shenzhen Perfect Medical Instruments, Shanwei City, China), the convex triangular cross-section of T Pro E2 NiTi endodontic files (Ref.: 20010103, T Pro E1, Perfect Endo, Shenzhen Perfect Medical Instruments, Shanwei City, China), and the triangular cross-section of T Pro E4 NiTi endodontic files (Ref.: 20010103, T Pro E1, Perfect Endo, Shenzhen Perfect Medical Instruments, Shanwei City, China), which include aluminum in the chemical composition of the metal alloy (Table 1).

Table 1. Mean atomic weight percent (%) of Mtwo NiTi alloy endodontic rotary files, T Pro E1 austenite phase NiTi alloy endodontic rotary files, T Pro E2 austenite phase NiTi alloy endodontic rotary files, and T Pro E4 austenite phase NiTi alloy endodontic rotary files.

Spectrum	C	O	Al	Ti	Ni
Mtwo 20 kV (1–3)	20.92	10.89	-	37.60	30.58
T Pro E1 20 kV (1–3)	42.51	21.15	0.52	19.48	16.34
T Pro E2 20 kV (1–3)	26.49	19.72	0.73	27.10	25.96
T Pro E4 20 kV (1–3)	39.52	19.25	2.43	20.58	18.23

The mean and SD values for the time to failure (in seconds) for each of the study groups are displayed in Table 2 and Figure 4.

Table 2. Descriptive statistics of the time to failure of Mtwo NiTi alloy endodontic rotary files, T Pro E1 austenite phase NiTi alloy endodontic rotary files, T Pro E2 austenite phase NiTi alloy endodontic rotary files, and T Pro E4 austenite phase NiTi alloy endodontic rotary files.

Study Group	*n*	Mean	SD	Minimum	Maximum
Mtwo	10	500.06 [a]	9.22	484.90	512.90
T Pro E1	10	256.05 [b]	7.96	242.90	269.20
T Pro E2	10	349.29 [c]	7.02	339.00	358.20
T Pro E14	10	400.64 [d]	8.72	387.10	411.60

[a,b,c,d] Statistically significant differences between groups ($p < 0.05$).

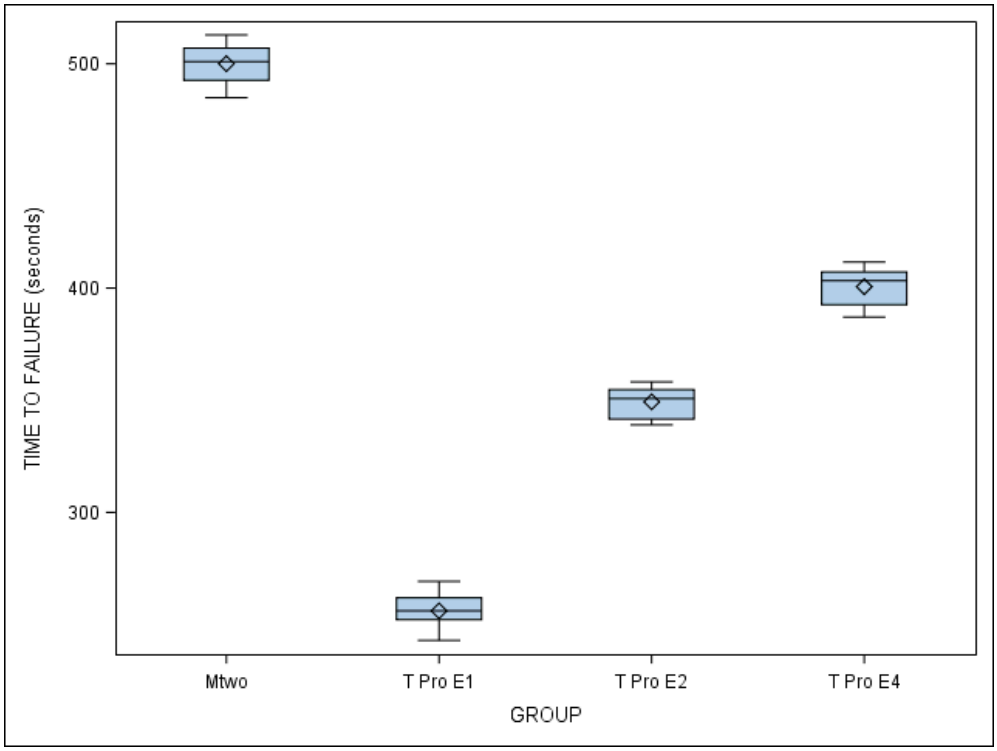

Figure 4. Box plot of the time to failure of Mtwo NiTi alloy endodontic rotary files, T Pro E1 austenite phase NiTi alloy endodontic rotary files, T Pro E2 austenite phase NiTi alloy endodontic rotary files, and T Pro E4 austenite phase NiTi alloy endodontic rotary files.

The ANOVA test showed statistically significant differences between the time to failure of all NiTi endodontic rotary files ($p < 0.001$) (Figure 4). The results related to the number of cycles to failure are similar as the dynamic cyclic fatigue device had a frequency of 60 pecking movements/min.

The scale distribution parameter (η) of the Weibull statistical analysis found statistically significant differences between the time to failure of all NiTi endodontic rotary files ($p < 0.001$) (Table 3, Figure 5). However, the shape distribution parameter (β) of the Weibull analysis found no statistically significant differences between the time to failure of any of the NiTi endodontic rotary files ($p > 0.05$). The results related to the number of cycles to failure are similar as the dynamic cyclic fatigue device had a frequency of 60 pecking movements/min (Table 3, Figure 5).

Table 3. Weibull statistics of time to failure of replica-like and original brand NiTi endodontic rotary files study groups.

	Weibull Shape (β)				Weibull Scale (η)			
Study Group	**Estimate**	**St Error**	**Lower**	**Upper**	**Estimate**	**St Error**	**Lower**	**Upper**
Mtwo	67.0256	16.7296	41.0943	109.3202	504.2430	2.5132	499.3413	509.1928
T Pro E1	37.0114	8.8527	23.1599	59.1472	259.6936	2.3498	255.1287	264.3402
T Pro E2	64.0224	16.4767	38.6606	106.0220	352.4523	1.8358	348.8725	356.0689
T Pro E14	59.2617	15.1900	35.8586	97.9388	404.5474	2.2760	400.1110	409.0329

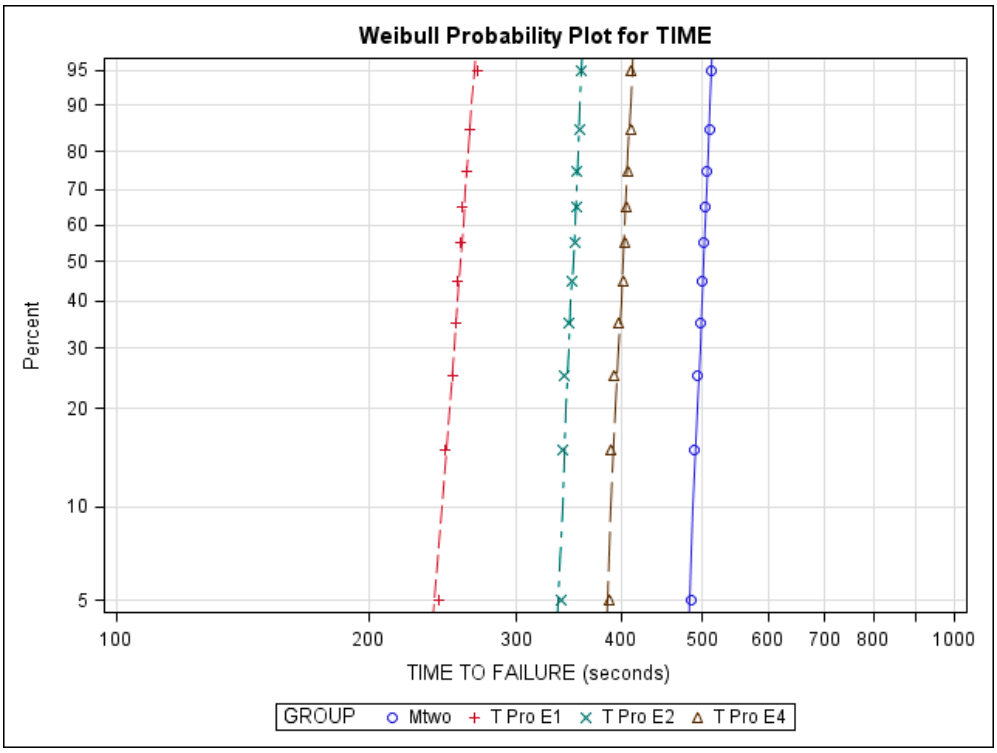

Figure 5. Weibull probability plot of time to failure of Mtwo NiTi alloy endodontic rotary files, T Pro E1 austenite phase NiTi alloy endodontic rotary files, T Pro E2 austenite phase NiTi alloy endodontic rotary files, and T Pro E4 austenite phase NiTi alloy endodontic rotary files.

4. Discussion

The results obtained in the present study reject the null hypothesis (H_0) that stated that the geometry of the cross-section design would not affect the resistance of NiTi endodontic rotary files to dynamic cyclic fatigue.

The results derived in the present study reported that Mtwo NiTi alloy endodontic rotary files with double S-shaped cross-section showed higher resistance to dynamic cyclic fatigue than T Pro E1 austenite phase NiTi alloy endodontic rotary files with rectangular cross-sections, T Pro E2 austenite phase NiTi alloy endodontic rotary files with convex triangular cross-sections, and T Pro E4 austenite phase NiTi alloy endodontic rotary files with triangular cross-sections. The results can be summarized in that with the increase in the mass and the contact points between the instrument surface and the dentin walls of the root canal, the cyclic fatigue resistance of the NiTi endodontic rotary files decreases. This can also influence the flexibility of the NiTi endodontic rotary files and lead the instrument to cause excessive root canal dentine removal, apical transportation [22], root perforations, and fractures [4,23,24].

The persistent bacterial load present in the root canal system after endodontic therapy has been highlighted as a relevant etiologic factor in the endodontic failure and secondary endodontic infections [25]; moreover, Sjögren established a relationship between the bacte-

rial load reduction during the root canal treatment and the prognosis of the endodontic therapy, and reported that negative microbiological cultures obtained from the root canal system led to an endodontic success rate close to 94%, whereas positive cultures reduced the success rate to 68% [26]. This is the reason that the cyclic fatigue resistance of NiTi endodontic rotary files has been widely analyzed.

The design of the anatomical-based artificial root canal used in the present study was based on the method described by Schneider [21], selecting a 5 mm radius and 60° curvature angle and adapting the geometry to the NiTi endodontic rotary files included in this study. Previous studies have shown that the fatigue resistance of endodontic rotary files decreases as the angle of curvature increases and the radius of curvature decreases [10,27,28], since the stress accumulation on the endodontic rotary file is inversely proportional to the radius of curvature of the canal. As a result, in more abrupt root canals, there is an augmentation of the torsion and flexural bending fatigue that ultimately results in instrument fracture [10,21]. Moreover, clinical or even ex vivo experimental studies would be desirable to reproduce clinical conditions and extrapolate the cyclic fatigue results to the clinical setting; however, the difficulty to homogenize the radius, curvature angle, apical diameter, hardness, and cross-section of the root canals can bias the study by introducing more variables [28]. Therefore, custom-made static and dynamic cyclic fatigue devices have been developed to independently analyze the influence of the variable under study; unfortunately, there is neither a norm that regulates the characteristics of the custom-made cyclic fatigue devices nor an international standard for testing the cyclic fatigue behavior of NiTi endodontic rotary instruments with taper higher than 2% [29].

Static and dynamic testing devices have been used to analyze the cyclic fatigue. In the static cyclic fatigue testing models, the NiTi endodontic files are rotated until fracture occurs and the tension–compression cycles are concentrated in the maximum curvature angle of the root canal, resulting in microstructural alterations in the file and subsequent failure. Therefore, dynamic cyclic fatigue testing devices are preferable to better reproduce the clinical conditions, especially the pecking motion of the NiTi endodontic rotary files. Thus, this study used a dynamic cyclic fatigue testing model, an anatomical-based artificial root canal and an automatic detection system to objectively and accurately identify failures of endodontic rotary files [28,30,31].

Previous studies have analyzed the influence of cross-section design on the mechanical behavior of the NiTi endodontic rotary files. Sekar et al. analyzed the role of the cross-section on the cyclic fatigue resistance of NiTi endodontic rotary files under continuous and reciprocation motion and reported that the 25.06 Mtwo rotary files were significantly more resistant to failure than Revo-S SU and One Shape files in both continuous ($p < 0.001$) and reciprocating motion ($p < 0.001$) [17]. These findings are consistent with the results of our study, which concluded that the double S-shaped cross-section of Mtwo NiTi endodontic files showed higher cyclic fatigue resistance than the rectangular cross-section of T Pro E1 NiTi endodontic files, the convex triangular cross-section of T Pro E2 NiTi endodontic files, and the triangular cross-section of T Pro E4 NiTi endodontic files. In addition, de Menezes et al. reported that ProDesign endodontic rotary files with a modified double S-shaped cross-section design presented a significantly higher ($p < 0.05$) number of cycles to failure (910.37 $\pm$ 472.10) than Wave One Gold endodontic reciprocating files with a parallelogram cross-section design (264.76 $\pm$ 305.42) in artificial root canals with a 60° curvature and 5 mm radius of curvature [32]. Moreover, Adiguzel et al. showed that XP-endo Shaper endodontic rotary files with triangular cross-sections design presented a significantly higher ($p < 0.05$) number of cycles to failure (3064.0 $\pm$ 248.1) than HyFlex CM endodontic rotary files with a variable cross-section design (from triangular to trapezoidal and quadratic) (1120.5 $\pm$ 106.1) in artificial root canals with a 60° curvature and 3 mm radius of curvature [33]; however, Uygun et al. showed that HyFlex EDM endodontic rotary files with a variable cross-section design (from triangular to trapezoidal and quadratic) presented a significantly higher ($p < 0.05$) number of cycles to failure (1710.42 $\pm$ 114.89) than Vortex Blue endodontic rotary files with a convex triangular cross-section design

(548.39 ± 77.64), ProTaper Gold endodontic rotary files with a convex triangular cross-section design (600.83 ± 66.49), and One Curve endodontic rotary files with a variable cross-section design (from double S-shaped to triangular) (959.58 ± 61.18) in artificial root canals with a 60° curvature and 3 mm radius of curvature [34].

Unfortunately, the limitations of the present study prevented the analysis of more cross-section designs to standardize the NiTi alloy, apical diameter, pitch, helix angle, manufacturing process, speed, and taper. In addition, the study was not developed in a clinical environment due to the difficulty in standardizing the sample.

5. Conclusions

The conclusion derived from the present study is that the double S-shaped cross-section of Mtwo NiTi endodontic files shows higher cyclic fatigue resistance than the rectangular cross-section of T Pro E1 NiTi endodontic files, the convex triangular cross-section of T Pro E2 NiTi endodontic files, and the triangular cross-section of T Pro E4 NiTi endodontic files.

Author Contributions: Conceptualization, V.F.-L., N.H.-K. and Á.Z.-M.; design, I.F.-M.; data acquisition, C.R.S.; formal analysis, V.F.-M.; statistical analyses, Á.Z.-M. and V.F.-L.; review and editing, N.H.-K. and M.T.M.R. All authors have read and agreed to the published version of the manuscript.

Funding: This research received no external funding.

Institutional Review Board Statement: Not applicable.

Informed Consent Statement: Not applicable.

Data Availability Statement: Data are available on request due to restrictions, e.g., privacy or ethical.

Conflicts of Interest: The authors declare no conflict of interest.

References

1. Walia, H.; Brantley, W.A.; Gerstein, H. An initial investigation of the bending and torsional properties of nitinol root canal files. *J. Endod.* **1988**, *14*, 346–351. [CrossRef]
2. Esposito, P.T.; Cunningham, C.J. A comparison of canal preparation with nickel-titanium and stainless steel instruments. *J. Endod.* **1995**, *21*, 173–176. [CrossRef]
3. Bergmans, L.; Van Cleynenbreugel, J.; Wevers, M.; Lambrechts, P. Mechanical root canal preparation with NiTi rotary instruments: Rationale, performance and safety. Status report for the American Journal of Dentistry. *Am. J. Dent.* **2001**, *14*, 324–333. [PubMed]
4. Parashos, P.; Gordon, I.; Messer, H.H. Factors Influencing Defects of Rotary Nickel-Titanium Endodontic Instruments After Clinical Use. *J. Endod.* **2004**, *30*, 722–725. [CrossRef] [PubMed]
5. Spili, P.; Parashos, P.; Messer, H.H. The Impact of Instrument Fracture on Outcome of Endodontic Treatment. *J. Endod.* **2005**, *31*, 845–850. [CrossRef] [PubMed]
6. Sattapan, B.; Nervo, G.J.; Palamara, J.E.; Messer, H.H. Defects in Rotary Nickel-Titanium Files After Clinical Use. *J. Endod.* **2000**, *26*, 161–165. [CrossRef] [PubMed]
7. Peters, O.; Barbakow, F. Dynamic torque and apical forces of ProFile .04 rotary instruments during preparation of curved canals. *Int. Endod. J.* **2002**, *35*, 379–389. [CrossRef]
8. Kuhn, G.; Tavernier, B.; Jordan, L. Influence of Structure on Nickel-Titanium Endodontic Instruments Failure. *J. Endod.* **2001**, *27*, 516–520. [CrossRef] [PubMed]
9. Pruett, J.P.; Clement, D.J.; Carnes, D.L., Jr. Cyclic fatigue testing of nickel-titanium endodontic instruments. *J. Endod.* **1997**, *23*, 77–85. [CrossRef]
10. Parashos, P.; Messer, H.H. Rotary NiTi Instrument Fracture and its Consequences. *J. Endod.* **2006**, *32*, 1031–1043. [CrossRef]
11. Topçuoğlu, H.S.; Topçuoğlu, G. Cyclic Fatigue Resistance of Reciproc Blue and Reciproc Files in an S-shaped Canal. *J. Endod.* **2017**, *43*, 1679–1682. [CrossRef]
12. Siqueira, J.F., Jr.; Rôças, I.N. Polymerase chain reaction–based analysis of microorganisms associated with failed endodontic treatment. *Oral. Surg. Oral. Med. Oral. Pathol. Oral. Radiol. Endod.* **2014**, *97*, 85–94. [CrossRef]
13. Strindberg, L. The Dependence of the Results of Pulp Therapy on Certain Factors: An Analytic Study Based on Radiographic and Clinical Follow-up Examinations. *Acta Odontol. Scand.* **1956**, *14*, 1–175.
14. Zupanc, J.; Vahdat-Pajouh, N.; Schäfer, E. New thermomechanically treated NiTi alloys—A review. *Int. Endod. J.* **2018**, *51*, 1088–1103. [CrossRef] [PubMed]

15. Faus-Llácer, V.; Kharrat, N.H.; Ruiz-Sánchez, C.; Faus-Matoses, I.; Zubizarreta-Macho, Á.; Faus-Matoses, V. The Effect of Taper and Apical Diameter on the Cyclic Fatigue Resistance of Rotary Endodontic Files Using an Experimental Electronic Device. *Appl. Sci.* **2021**, *11*, 863. [CrossRef]
16. Turpin, Y.L.; Chagneau, F.; Vulcain, J.M. Impact of Two Theoretical Cross-Sections on Torsional and Bending Stresses of Nickel-Titanium Root Canal Instrument Models. *J. Endod.* **2000**, *26*, 414–417. [CrossRef] [PubMed]
17. Sekar, V.; Kumar, R.; Nandini, S.; Ballal, S.; Velmurugan, N. Assessment of the role of cross section on fatigue resistance of rotary files when used in reciprocation. *Eur. J. Dent.* **2016**, *10*, 541–545. [CrossRef] [PubMed]
18. Kwak, S.W.; Ha, J.-H.; Lee, C.-J.; El Abed, R.; Abu-Tahun, I.H.; Kim, H.-C. Effects of Pitch Length and Heat Treatment on the Mechanical Properties of the Glide Path Preparation Instruments. *J. Endod.* **2016**, *42*, 788–792. [CrossRef] [PubMed]
19. Keskin, C.; Yilmaz, Ö.S.; Keleş, A.; Inan, U. Comparison of cyclic fatigue resistance of Rotate instrument with reciprocating and continuous rotary nickel–titanium instruments at body temperature in relation to their transformation temperatures. *Clin. Oral Investig.* **2021**, *25*, 151–157. [CrossRef] [PubMed]
20. Zubizarreta-Macho, Á.; Álvarez, J.M.; Martínez, A.A.; Segura-Egea, J.J.; Brucheli, J.C.; Agustín-Panadero, R.; Píriz, R.L.; Alonso-Ezpeleta, Ó. Influence of the Pecking Motion Frequency on the Cyclic Fatigue Resistance of Endodontic Rotary Files. *J. Clin. Med.* **2019**, *9*, 45. [CrossRef] [PubMed]
21. Schneider, S.W. A comparison of canal preparations in straight and curved root canals. *Oral Surg. Oral Med. Oral Pathol.* **1971**, *32*, 271–275. [CrossRef]
22. Freire, L.G.; Gavini, G.; Cunha, R.S.; Dos Santos, M. Assessing apical transportation in curved canals: Comparison between cross-sections and micro-computed tomography. *Braz. Oral Res.* **2012**, *26*, 222–227. [CrossRef] [PubMed]
23. Ounsi, H.F.; Salameh, Z.; Al-Shalan, T.; Ferrari, M.; Grandini, S.; Pashley, D.H.; Tay, F.R. Effect of Clinical Use on the Cyclic Fatigue Resistance of ProTaper Nickel-Titanium Rotary Instruments. *J. Endod.* **2007**, *33*, 737–741. [CrossRef] [PubMed]
24. Grande, N.M.; Plotino, G.; Pecci, R.; Bedini, R.; Malagnino, V.A.; Somma, F. Cyclic fatigue resistance and three-dimensional analysis of instruments from two nickel–titanium rotary systems. *Int. Endod. J.* **2006**, *39*, 755–763. [CrossRef] [PubMed]
25. Siqueira, J.F., Jr. Aetiology of root canal treatment failure: Why well-treated teeth can fail. *Int. Endod. J.* **2001**, *34*, 1–10. [CrossRef]
26. Sjögren, T.; Figdor, D.; Persson, S.; Sundqvist, G. Influence of infection at the time of root filling on the outcome of endodontic treatment of teeth with apical periodontitis. *Int. Endod. J.* **1997**, *30*, 297–306. [CrossRef]
27. Azimi, S.; Delvari, P.; Hajarian, H.C.; Saghiri, M.A.; Karamifar, K.; Lotfi, M. Cyclic Fatigue Resistance and Fractographic Analysis of Race and Protaper Rotary NiTi Instruments. *Iran. Endod. J.* **2011**, *6*, 80–86.
28. Haïkel, Y.; Serfaty, R.; Bateman, G.; Senger, B.; Allemann, C. Dynamic and cyclic fatigue of engine-driven rotary nickel-titanium endodontic instruments. *J. Endod.* **1999**, *25*, 434–440. [CrossRef]
29. ISO. *Dentistry—Root Canal Instruments—Part 1: General Requirements and Test Methods; ISO 3630–3631; ISO; Geneva, Switzerland, 2008.*
30. Whipple, S.J.; Kirkpatrick, T.C.; Rutledge, R.E. Cyclic Fatigue Resistance of Two Variable-taper Rotary File Systems: ProTaper Universal and V-Taper. *J. Endod.* **2009**, *35*, 555–558. [CrossRef]
31. Gambarini, G. Cyclic Fatigue of Nickel-Titanium Rotary Instruments after Clinical Use with Low-and High-Torque Endodontic Motors. *J. Endod.* **2001**, *27*, 772–774. [CrossRef]
32. De Menezes, S.E.A.C.; Batista, S.M.; Lira, J.O.P.; de Melo Monteiro, G.Q. Cyclic Fatigue Resistance of WaveOne Gold, ProDesign R and ProDesign Logic Files in Curved Canals In Vitro. *Iran Endod. J.* **2017**, *12*, 468–473. [PubMed]
33. Adiguzel, M.; Isken, I.; Pamukcu, I.I. Comparison of cyclic fatigue resistance of XP-endo Shaper, HyFlex CM, FlexMaster and Race instruments. *J. Dent. Res. Dent. Clin. Dent. Prospect.* **2018**, *12*, 208–212. [CrossRef] [PubMed]
34. Uygun, A.D.; Unal, M.; Falakaloglu, S.; Guven, Y. Comparison of the cyclic fatigue resistance of hyflex EDM, vortex blue, protaper gold, and onecurve nickel-Titanium instruments. *Niger J. Clin. Pract.* **2020**, *23*, 41–45. [PubMed]

Journal of
Clinical Medicine

MDPI

Article

The Influence of NiTi Alloy on the Cyclic Fatigue Resistance of Endodontic Files

Celia Ruiz-Sánchez [1], Vicente Faus-Llácer [1], Ignacio Faus-Matoses [1], Álvaro Zubizarreta-Macho [2,*], Salvatore Sauro [3,4] and Vicente Faus-Matoses [1]

[1] Department of Stomatology, Faculty of Medicine and Dentistry, University of Valencia, 46010 Valencia, Spain; celia.ruiz@uv.es (C.R.-S.); fausvj@uv.es (V.F.-L.); ignacio.faus@uv.es (I.F.-M.); vicente.faus@uv.es (V.F.-M.)

[2] Department of Endodontics, Faculty of Health Sciences, Alfonso X El Sabio University, 28691 Madrid, Spain

[3] Department of Dentistry, Faculty of Health Sciences, CEU Cardenal Herrera University, 46115 Valencia, Spain; salvatore.sauro@uchceu.es

[4] Department of Therapeutic Dentistry, I.M. Sechenov First Moscow State Medical University, 119146 Moscow, Russia

* Correspondence: azubimac@hotmail.com

Received: 30 October 2020; Accepted: 20 November 2020; Published: 21 November 2020

Abstract: Background: The aim of this study was to analyze the influence of NiTi alloy in endodontic rotary instruments on cyclic fatigue resistance. Methods: One hundred and sixty-four (164) sterile endodontic rotary files were selected and distributed into the following study groups: A: 25.08 F2 ProTaper Universal (PTU) (n = 41); B: 25.06 X2 ProTaper Next (PTN) (n = 41); C: 25.08 F2 ProTaper Gold (PTG) (n = 41), and D: 25.06 ProFile Vortex Blue (PVB) (n = 41). A cyclic fatigue device was designed to conduct the static cyclic fatigue tests with stainless steel artificial root canals systems with 250 µm apical diameter, 60° curvature angle, 5 mm radius of curvature, 20 mm length, and 6% (25.06) and 8% taper (25.08). Failure of the endodontic rotary instrument was detected by a single operator through direct observation and was also filmed to allow measurement of the exact time to failure. Results were analyzed using the ANOVA test and Weibull statistical analysis. Results: All pairwise comparisons presented statistically significant differences between the time to failure for the NiTi alloy study groups ($p < 0.001$), except between the PTN and PVB study groups ($p = 0.379$). In addition, statistically significant differences between the number of cycles to failure for the NiTi alloy study groups ($p < 0.001$) were also observed. Conclusions: The NiTi CM-Gold wire alloy of the ProTaper Gold endodontic rotary files resulted in greater resistance to cyclic fatigue than ProFile Vortex Blue, ProTaper Next, and ProTaper Universal endodontic rotary files.

Keywords: endodontics; cyclic fatigue; NiTi alloy; M-Wire; CM-Gold Wire; CM-Blue Wire

1. Introduction

Endodontic rotary files have experienced continuous development since nickel–titanium (NiTi) files were introduced in the 1980s [1]. This alloy improved the flexibility and strength properties of endodontic rotary files compared with conventional stainless-steel endodontic instruments [2], and it simplified the treatment of root canals by improving the speed, accuracy, and safety of root canal shaping [3]. Despite continuous enhancements in the design and manufacture of NiTi endodontic rotary files to reduce the occurrence of complications during root canal treatment [4], failures remain a concern. Machado et al. retrospectively reported a fracture incidence of ProTaper Universal endodontic rotary files of 4.4% in 1031 teeth, mainly in mandibular first (8.8%) and second (9.6%)

molars [5]; however, Bueno et al. reported no fractures in any of the 1104 Wave One Gold endodontic reciprocating files [6]. The more martensitic crystalline structure of the NiTi alloy of Wave One Gold endodontic reciprocating files allows higher flexibility and resistance than conventional austenitic endodontic rotary files. In addition, the removal of fractured fragments from NiTi endodontic rotary files within the root canal system is a challenge for the clinician because it prevents the disinfection of the entire root canal system [7].

Many variables can contribute to NiTi endodontic rotary file separation, such as root canal shape, instrument geometry, rotational speed, torque, sterilization cycles, the number of clinical uses, and the angle and radius of the curvature of the root canal system; however, researchers have focused their attention on the NiTi alloys, new surface treatments, and design improvements as prominent factors in the fracture resistance of NiTi endodontic rotary files [8–11]. Therefore, the surface treatments such as electropolishing, ion implantation, cryogenic treatment, and heat treatments improve the physical properties of NiTi endodontic rotary files, increasing their cyclic fatigue resistance [12]. Currently, the most widely used surface treatment is heat treatment, which consists of heat treating the NiTi alloy in a temperature range of around 450–550 °C and is carried out during or after the NiTi endodontic rotary file manufacturing process [12].

NiTi endodontic rotary systems are classified according to the crystal structure of the NiTi alloy: conventional NiTi, NiTi M-Wire, and R-Phase alloy endodontic rotary systems composed of an austenitic crystal structure, NiTi CM-Wire alloy endodontic rotary instruments composed of a martensitic crystal structure, and finally NiTi endodontic rotary systems that contain both austenitic and martensitic crystal structures [12]. Currently, novel endodontic rotary systems are developed with a higher concentration of the martensitic phase to improve the physical properties of hyperelasticity, shape memory, and fracture resistance compared to conventional NiTi alloys [12,13]. Conventional NiTi alloy of ProTaper Universal endodontic rotary files have lower cyclic fatigue resistance of endodontic rotary files compared to NiTi M-Wire of ProTaper Next endodontic rotary files [14–18]. Furthermore, NiTi CM-Wire alloy of Profile Vortex Blue and ProTaper Gold endodontic rotary files have shown a significantly ($p < 0.05$) higher cyclic fatigue resistance compared to the NiTi M-Wire alloy of endodontic rotary files [17,19–23].

The purpose of the present study was to analyze and compare the effect of the NiTi alloy on the static cyclic fatigue resistance of NiTi endodontic rotary files, with a null hypothesis (H_0) stating that NiTi alloy of the endodontic rotary files would have no effect on the static cyclic fatigue resistance of NiTi endodontic rotary files.

2. Materials and Methods

2.1. Study Design

One hundred and sixty-four (164) sterile unused endodontic rotary files with a 250 μm apical diameter were used in this in vitro study. All NiTi endodontic rotary files were first inspected under magnification (OPMI pico, Zeiss, Oberkochen, Germany), and none were discarded. A controlled experimental trial was performed at the Department of Stomatology of the Faculty of Medicine and Dentistry at the University of Valencia (Valencia, Spain), between September 2019 and July 2020. The NiTi endodontic rotary files were categorized into the following study groups: A: 25.08 F2 conventional NiTi alloy ProTaper Universal (Dentsply Maillefer, Baillagues, Switzerland) (PTU) (n = 41); B: 25.06 X2 NiTi M-Wire alloy ProTaper Next (Dentsply Maillefer, Baillagues, Switzerland) (PTN) (n = 41); C: 25.08 F2 NiTi CM-Gold Wire alloy ProTaper Gold (Dentsply Maillefer, Baillagues, Switzerland) (PTG) (n = 41); and D: 25.06 NiTi CM-Blue Wire alloy ProFile Vortex Blue (Dentsply Tulsa Dental, Tulsa, OK, USA) (PVB) (n = 41).

2.2. Experimental Cycling Fatigue Procedure

Static fatigue procedures were performed through the cyclic fatigue device previously described [24–26] and based on the cyclic fatigue device developed by Plotino et al. [27]. The 16:1 reduction handpiece (X-Smart Plus, Dentsply Maillefer, Baillagues, Switzerland) was placed and

fixed on a square polymethyl methacrylate structure using four fixations and the artificial root canals systems were placed in a square polymethyl methacrylate structure fixed by two fixations to the previous polymethyl methacrylate structure (Figure 1).

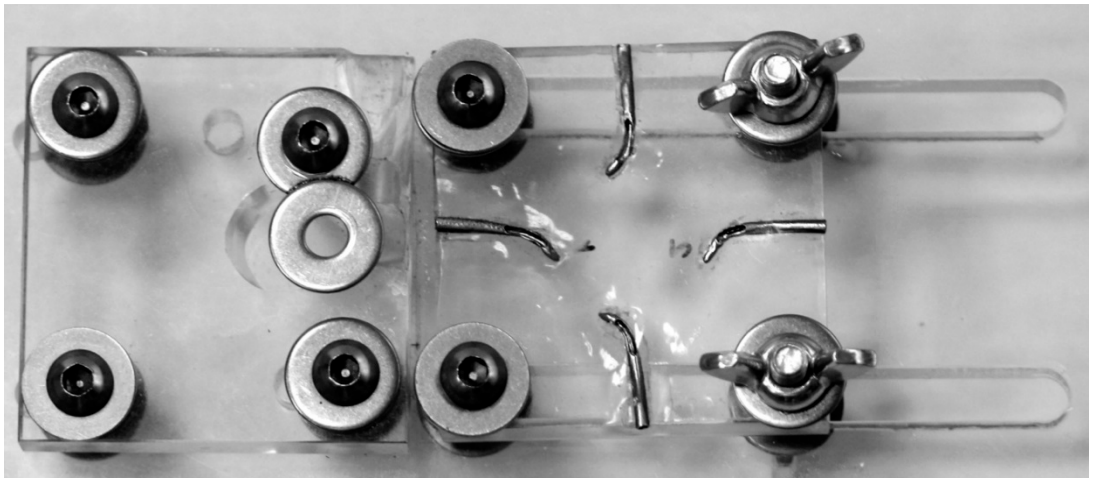

Figure 1. Static cyclic fatigue device with embedded stainless steel artificial root canal systems.

Two artificial root canal systems were constructed with 250 μm apical diameter, 60° curvature angle, 5 mm radius of curvature, 20 mm length, and 8% (25.08) (Figure 2A) and 6% taper (25.06) (Figure 2B). The artificial root canal systems were formed from a stainless-steel cylinder (Cocchiola S.A., Buenos Aires, Argentina) based on the anatomy of each NiTi endodontic rotary file to ensure an intimate contact between the artificial root canal system walls and the NiTi endodontic rotary files. The stainless-steel artificial root canal systems were partially removed to allow the identification of the exact time to failure of the tested endodontic rotary instruments (Figure 2A,B). Furthermore, all the static fatigue procedures were filmed to allow the measurement of the exact time to failure. The NiTi endodontic rotary files were placed inside the artificial root canal systems at their full working length before the static fatigue test started (Figure 2A,B).

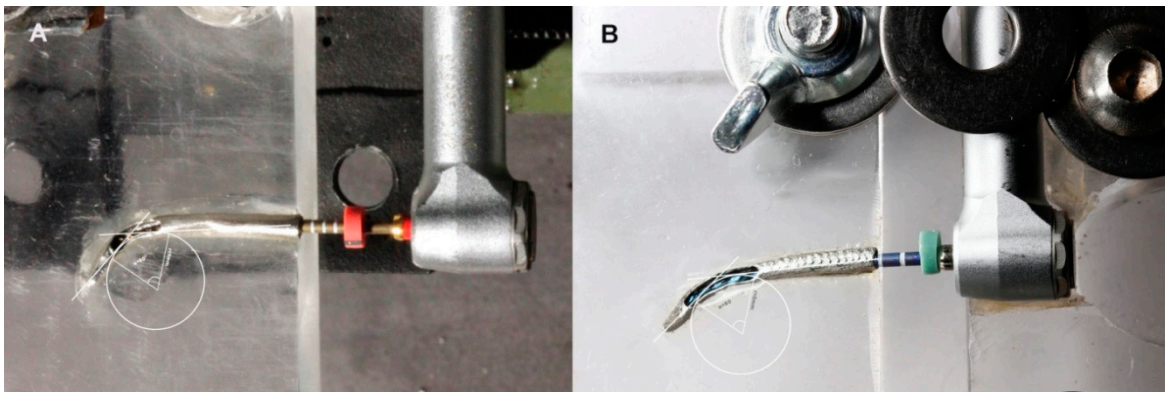

Figure 2. (**A**) ProTaper Gold (PTG) endodontic rotary file inside the 8% taper artificial root canal system and (**B**) ProFile Vortex Blue (PVB) endodontic rotary file inside the 6% taper artificial root canal system.

The NiTi endodontic rotary files were used with a 16:1 reduction handpiece (X-Smart Plus, Dentsply Maillefer, Baillagues, Switzerland) according to the manufacturer's instructions. The PTU, PTN and PTG endodontic rotary files were used at 300 revolutions per minute (rpm) and 5.2 N/cm torque; however, PVB endodontic rotary files were used at 500 rpm and 2.8 N/cm torque. The NiTi endodontic rotary files were used until fracture occurred in order to analyze the time to failure and the number of cycles to failure were measured and recorded with a digital chronometer (Timex, Middlebury, CT, USA).

To reduce the friction between the reciprocating files and the artificial canal walls, high-flow synthetic oil designed for the lubrication of the artificial root canal systems (Singer All-Purpose Oil; Singer Corp., Barcelona, Spain) was applied [28,29].

2.3. Scanning Electron Microscopy and Energy Dispersive X-ray Spectroscopy Analysis

A Scanning Electron Microscopy (SEM) and an Energy Dispersive X-Ray Spectroscopy (EDX) analysis were performed in the Department of Mechanical, Energetic, and Materials Engineering of the School of Industrial Engineering of the University of Extremadura (Badajoz, Spain) to perform a surface characterization and analyze the elemental composition of the chemical elements of the NiTi endodontic rotary files used in the static fatigue tests by means of the atomic weight percent measurement at three different locations (1, 2 and 3). SEM analysis (HITACHI S-4800, Fukuoka, Japan) of the NiTi endodontic rotary files was performed with the following exposure parameters: acceleration voltage: 20 kV, magnification from 100× to 6500× and a resolution between −1.0 nm at 15 kV and 2.0 nm at 1 kV.

2.4. Statistical Tests

Statistical analysis was performed by means of SAS 9.4 (SAS Institute Inc., Cary, NC, USA). Descriptive analysis included the mean and standard deviation (SD) for quantitative data. Comparative statistics was carried out by comparing the time to failure (minutes) and the number of cycles to failure using the ANOVA test. Weibull statistical analysis was also conducted. Descriptive analysis of the SEM and EDX analysis of the endodontic rotary files was also described. Statistical significance level was established at $p < 0.05$.

3. Results

The mean and SD values for time to failure (minutes) for each of the study groups are displayed in Table 1 and Figure 3.

Table 1. Descriptive analysis of the time to failure (minutes).

Study Group	*n*	Mean	SD	Minimum	Maximum
PTU	41	1.24 [a]	0.21	0.33	1.58
PTN	41	2.63 [b]	0.58	1.83	4.20
PTG	41	3.42 [c]	0.85	1.68	5.89
PVB	41	2.86 [b]	0.82	1.41	4.89

[a,b,c,d] Statistically significant differences between groups ($p < 0.05$). PTU: ProTaper Universal; PTN: ProTaper Next; PTG: ProTaper Gold; PVB: ProFile Vortex Blue.

The ANOVA analysis showed statistically significant differences between time to failure of PTG and PTN ($p < 0.001$), PTG and PTU ($p < 0.001$), PTG and PVB ($p = 0.001$), PTN and PTU ($p < 0.001$), and PTU and PVB ($p < 0.001$) NiTi endodontic rotary file study groups (Figure 3). However, no statistically significant differences were observed between time to failure of PTN and PVB ($p = 0.379$) (Figure 3).

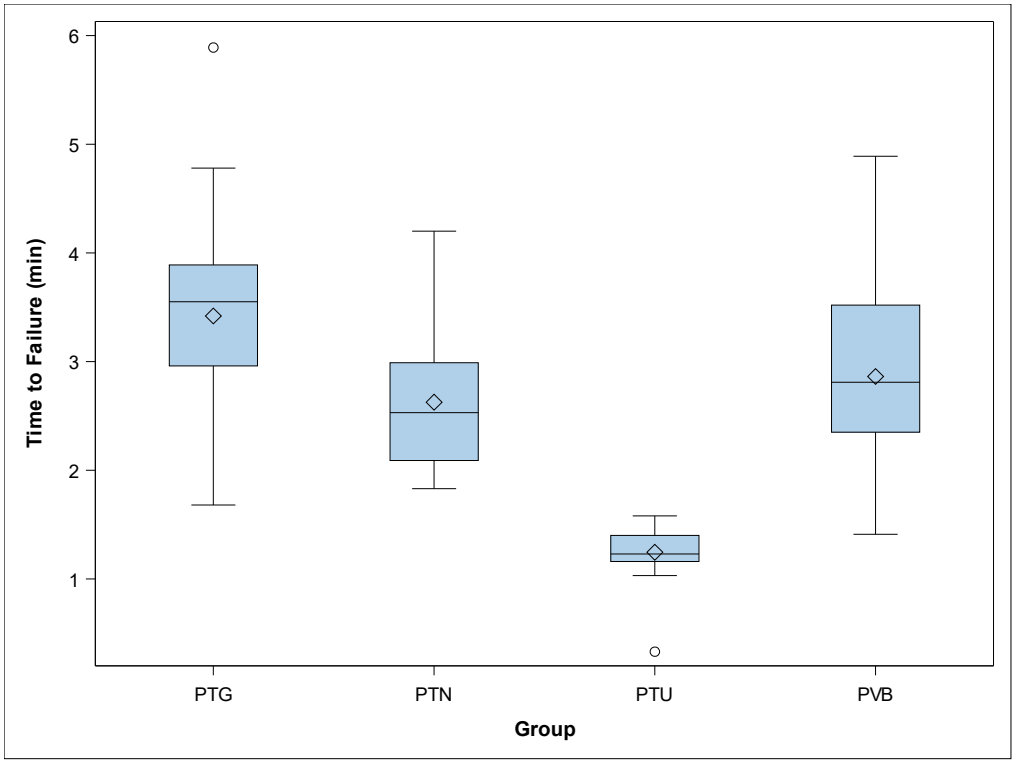

Figure 3. Box plot of the time to failure. The horizontal line in each box represents the respective median value of the study groups.◊; Mean value of the box plots. PTU: ProTaper Universal; PTN: ProTaper Next; PTG: ProTaper Gold; PVB: ProFile Vortex Blue.

The scale distribution parameter (η) of Weibull statistics found statistically significant differences between the time to failure of PTG and PVB ($p = 0.003$), PTU and PVB ($p < 0.001$), PTG and PTU ($p < 0.001$), PTN and PTU ($p < 0.001$), and PTG and PVB ($p < 0.001$) NiTi endodontic rotary files (Table 2, Figure 4); however, there were no statistically significant differences between the time to failure of PTN and PVB ($p = 0.067$) NiTi endodontic rotary file study groups (Table 2, Figure 4). The shape distribution parameter (β) of Weibull statistics found statistically significant differences between the time to failure of PTU and PVB ($p < 0.001$), PTG and PTU ($p = 0.001$), and PTN and PTU ($p = 0.003$) NiTi endodontic rotary files (Table 2, Figure 4). However, no statistically significant differences were observed between the time to failure of PTG and PVB ($p = 0.467$), PTN and PVB ($p = 0.228$), and PTG and PVB ($p = 0.628$) (Table 2, Figure 4) study groups. Briefly, the behavior of the endodontic rotary systems was very predictable, because most endodontic rotary files of each endodontic rotary system fractured at almost the same time. The less-steep slope generated by PTU NiTi endodontic rotary files indicates that the behavior is more predictable than in the other endodontic rotary systems, but they fracture earlier. The PTG NiTi endodontic rotary files showed a higher cyclic fatigue resistance than the PTU, PTN, and PVB NiTi endodontic rotary files.

Table 2. Weibull statistics of time to failure of the study groups.

Study Group	Weibull Shape (β)				Weibull Scale (η)			
	Estimate	St Error	Lower	Upper	Estimate	St Error	Lower	Upper
PTU	7.7054	0.9453	6.0585	9.8000	1.3203	0.0279	1.2666	1.3762
PTN	4.7196	0.5369	3.7764	5.8983	2.8604	0.1005	2.6701	3.0643
PTG	4.3641	0.5001	3.4862	5.4632	3.7429	0.1414	3.4758	4.0307
PVB	3.8689	0.4629	3.0601	4.8914	3.1652	0.1350	2.9114	3.4410

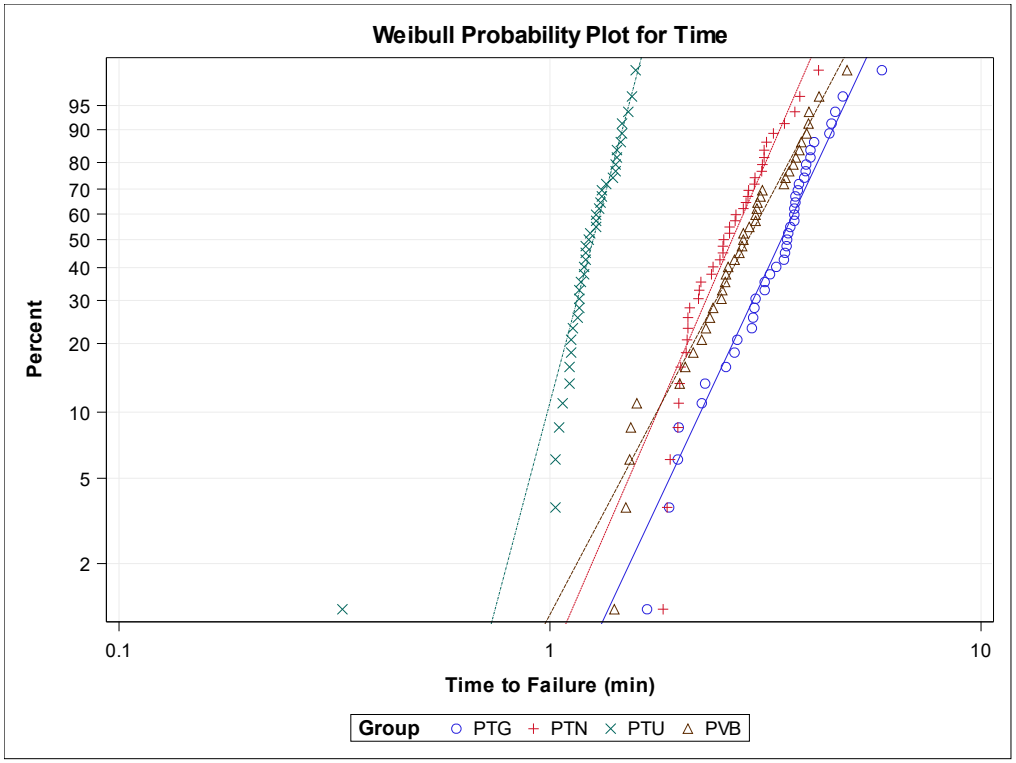

Figure 4. Weibull probability plot of time to failure for the study groups.

The mean and SD values for number of cycles to failure for each of the study groups are displayed in Table 3 and Figure 5.

Table 3. Descriptive statistics of the number of cycles to failure of the study groups.

Study Group	*n*	Mean	SD	Minimum	Maximum
PTU	41	373.46 [a]	62.40	99.00	474.00
PTN	41	787.90 [b]	173.91	549.00	1260.00
PTG	41	1021.49 [c]	264.81	415.00	1767.00
PVB	41	1431.46 [d]	411.60	705.00	2445.00

[a,b,c,d] Statistically significant differences between groups ($p < 0.05$).

The ANOVA analysis showed statistically significant differences between the number of cycles to failure of PTG and PTN ($p = 0.001$), PTG and PTU ($p < 0.001$), PTG and PVB ($p < 0.001$), PTN and PTU ($p < 0.001$), PTN and PVB ($p < 0.001$), and PTU and PVB ($p < 0.001$) NiTi endodontic rotary file study groups (Figure 5).

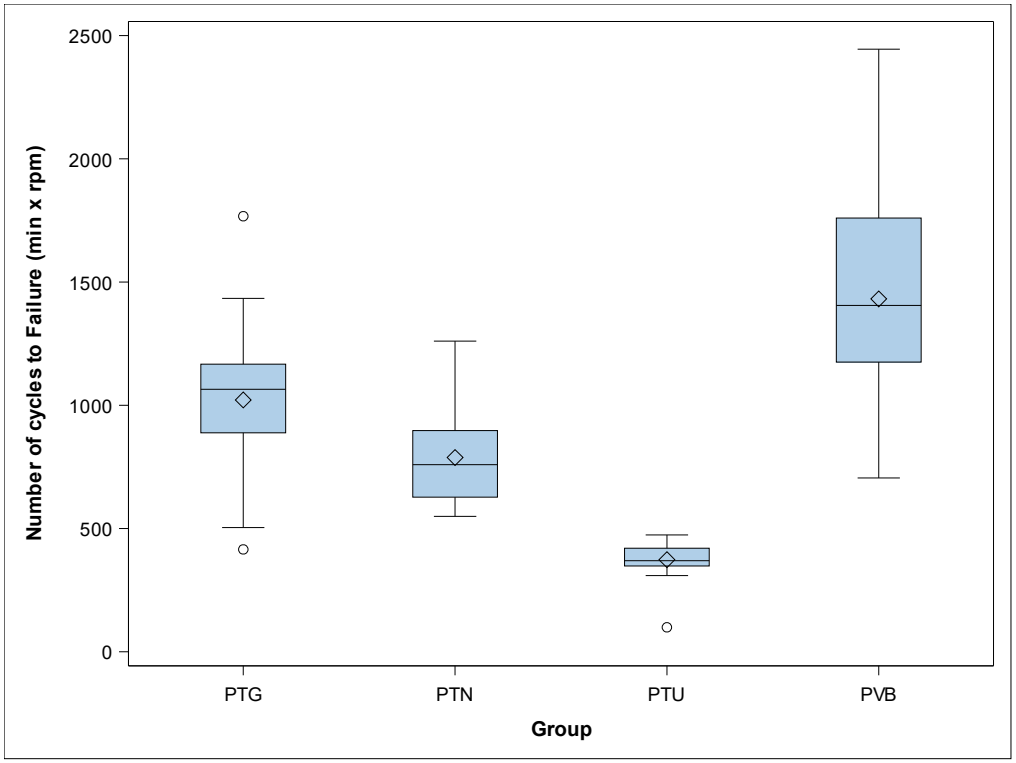

Figure 5. Box plot of the number of cycles to failure. The horizontal line in each box represents the respective median value of the study groups.○: Mean value of the box plots.

The scale distribution parameter (η) of Weibull statistics found statistically significant differences between the number of cycles to failure of PTG and PVB ($p < 0.001$), PTN and PVB ($p < 0.001$), PTU and PVB ($p < 0.001$), PTG and PTU ($p < 0.001$), PTN and PTU ($p < 0.001$), and PTG and PVB ($p < 0.001$) NiTi endodontic rotary files (Table 4, Figure 6). The shape distribution parameter (β) of the Weibull statistics found statistically significant differences between the number of cycles to failure of PTU and PVB ($p < 0.001$), PTG and PTU ($p < 0.001$), and PTN and PTU ($p = 0.003$) NiTi endodontic rotary files (Table 4, Figure 6). However, no statistically significant differences were observed between the number of cycles to failure of PTG and PVB ($p = 0.557$), PTN and PVB ($p = 0.228$), and PTG and PVB ($p = 0.535$) (Table 4, Figure 6). Briefly, the behavior of the endodontic rotary systems is very predictable, because most endodontic rotary files of each endodontic rotary system break almost at the same time. The less steep slope generated by PTU NiTi endodontic rotary files indicates that the behavior is more predictable than in the other endodontic rotary systems, but they fracture earlier. The PVB NiTi endodontic rotary files showed a higher cyclic fatigue resistance than did the PTU, PTN, and PTG NiTi endodontic rotary files.

Table 4. Weibull statistics of the number of cycles to failure for the study groups.

Study Group	Weibull Shape (β)				Weibull Scale (η)			
	Estimate	St Error	Lower	Upper	Estimate	St Error	Lower	Upper
PTU	7.7054	0.9453	6.0585	9.8000	396.0883	8.3847	379.9908	412.8678
PTN	4.7196	0.5369	3.7764	5.8983	858.1237	30.1478	801.0235	919.2942
PTG	4.2673	0.4950	3.3995	5.3566	1119.912	43.1923	1038.377	1207.8487
PVB	3.8689	0.4629	3.0601	4.8914	1582.588	67.4766	1455.711	1720.5229

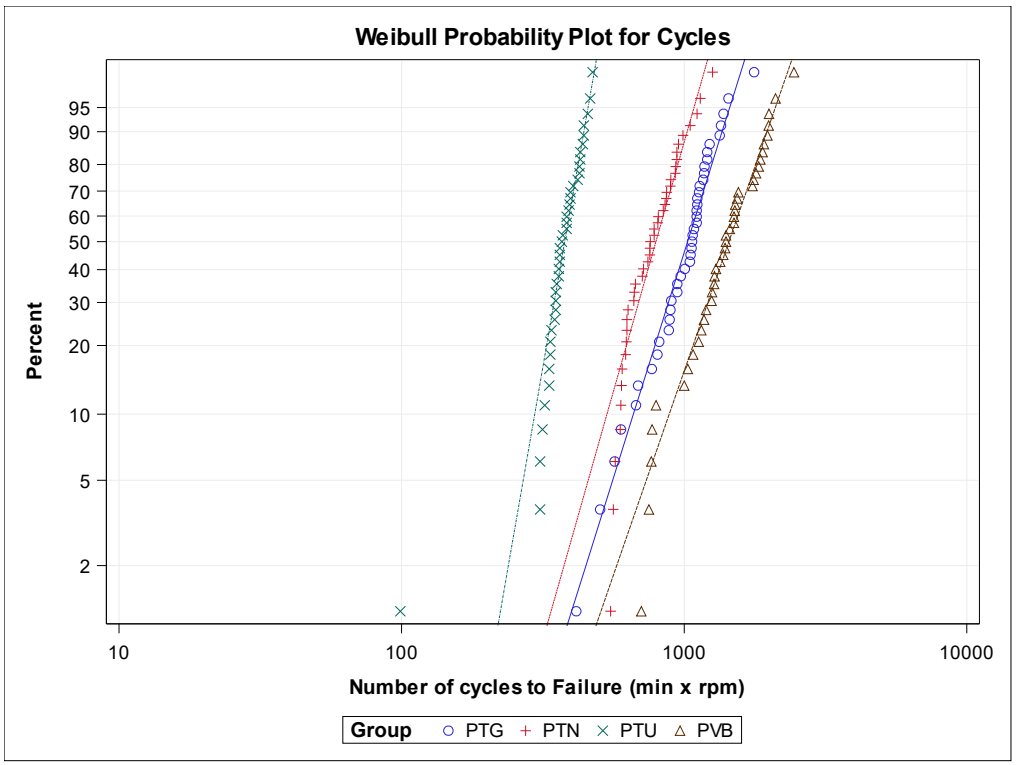

Figure 6. Weibull probability plot of the number of cycles to failure for the study groups.

SEM analysis of the NiTi alloy PTU endodontic rotary files did not show accumulation of organic matter or structural alterations. Furthermore, manufacturing lines were distributed perpendicularly to the longitudinal axis of the endodontic rotary files and also parallel to each other due to the laser machining manufacturing process. The width and distance between the manufacturing lines corresponded to the precision and intensity of the laser machining process. Tubular porosity due to the laser machining process was also observed. Furthermore, all NiTi alloy PTU endodontic rotary files exhibited tubular porosity resulting from the combination of Ti alloys with other chemicals elements (Figure 7A–C).

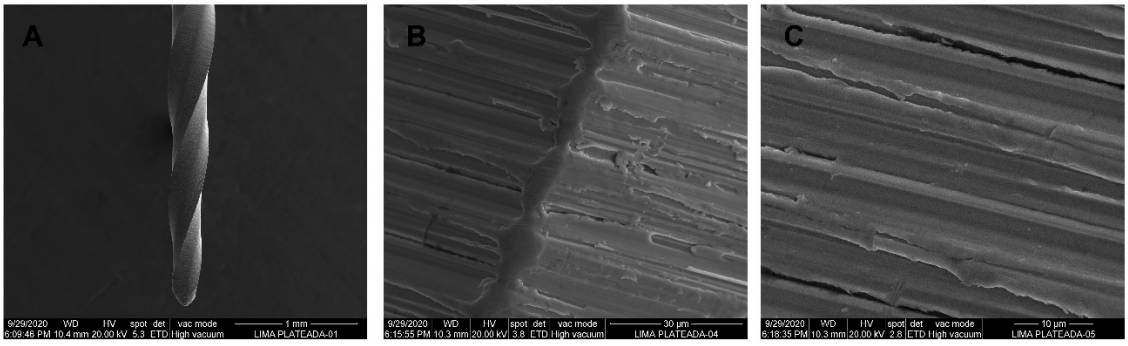

Figure 7. SEM images of NiTi alloy ProTaper Universal (PTU) endodontic rotary files at (**A**) 100×, (**B**) 3600×, and (**C**) 6500×.

EDX micro-analysis of PTU, PTN, PTG, and PVB NiTi endodontic rotary files was performed at 20 kV at three different locations, which allowed for a deep and accurate analysis of the NiTi endodontic rotary files composition. EDX micro-analysis at 20 kV showed that PTU NiTi endodontic rotary files were composed of C (2.17–3.18 wt.%), O (1.48–1.61 wt.%), Ti (42.72–43.25 wt.%), and Ni (52.56–52.97 wt.%) (Table 5 and Figure 8A–C).

Table 5. Mean atomic weight percent (%) of NiTi alloy PTU endodontic rotary files at 15 kV and 20 kV and three different locations (1, 2 and 3).

Spectrum	C	O	Ti	Ni
PTU 20 kV (1)	2.17	1.61	43.25	52.97
PTU 20 kV (2)	3.18	1.54	42.72	52.56
PTU 20 kV (3)	2.65	1.48	42.99	52.87
Sigma	0.55	0.65	0.46	0.53

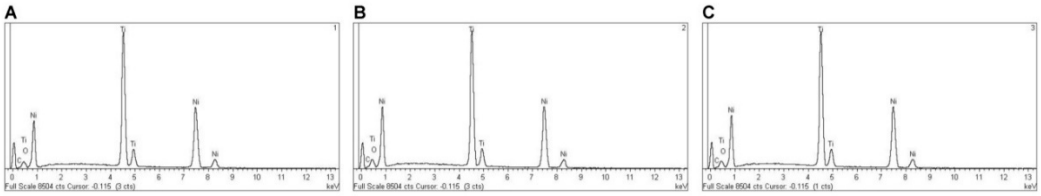

Figure 8. EDX micro-analysis of NiTi alloy PTU endodontic rotary files in location (**A**) 1, (**B**) 2, and (**C**) 3.

SEM analysis of the NiTi M-Wire alloy PTN endodontic rotary files did not show accumulation of organic matter or structural alterations. Furthermore, manufacturing lines were distributed perpendicularly to the longitudinal axis of the endodontic rotary files and also parallel to each other due to the laser machining manufacturing process. Lower width and distance between the manufacturing lines was observed compared to the NiTi alloy PTU endodontic rotary files. Tubular porosity due to the laser machining process was also observed (Figure 9A–C).

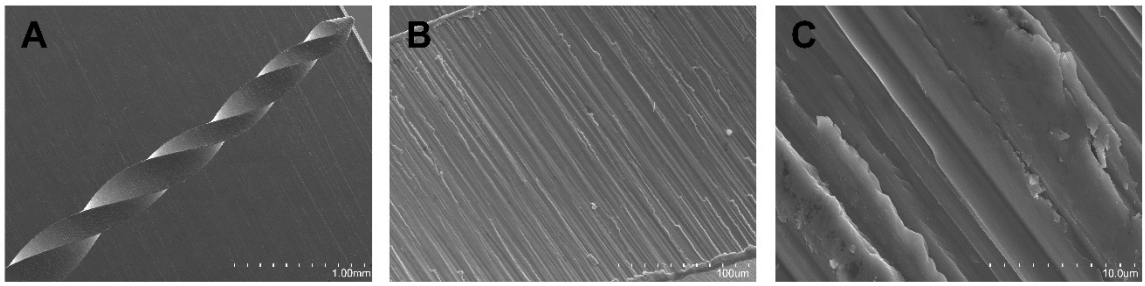

Figure 9. SEM images of M-Wire alloy ProTaper Next (PTN) endodontic rotary files at (**A**) 100×, (**B**) 3600×, and (**C**) 6500×.

EDX micro-analysis at 20 kV in three different locations showed that M-Wire alloy PTN endodontic rotary files were composed of C (3.31–4.43 wt.%), Al (0.56–1.39 wt.%), Ti (50.39–51.03 wt.%), and Ni (43.31–45.10 wt.%) (Table 6 and Figure 10A–C).

Table 6. Mean atomic weight percent (%) of M-Wire alloy PTN endodontic rotary files at 15 kV and 20 kV and three different locations (1, 2, and 3).

Spectrum	C	Al	Ti	Ni
PTN 20 kV (1)	4.43	1.24	51.03	43.31
PTN 20 kV (2)	3.31	1.39	50.39	44.90
PTN 20 kV (3)	3.43	0.56	50.91	45.10
Sigma	0.61	0.44	0.34	0.98

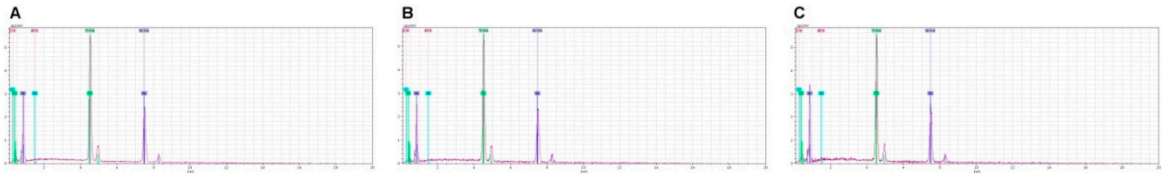

Figure 10. EDX micro-analysis of M-Wire alloy PTN endodontic rotary files at locations (**A**) 1, (**B**) 2, and (**C**) 3.

SEM analysis of the NiTi CM-Gold Wire alloy PTG endodontic rotary files did not show accumulation of organic matter or structural alterations. Furthermore, manufacturing lines were distributed perpendicularly to the longitudinal axis of the endodontic rotary files and also parallel to each other due to the laser machining manufacturing process (Figure 11A–C).

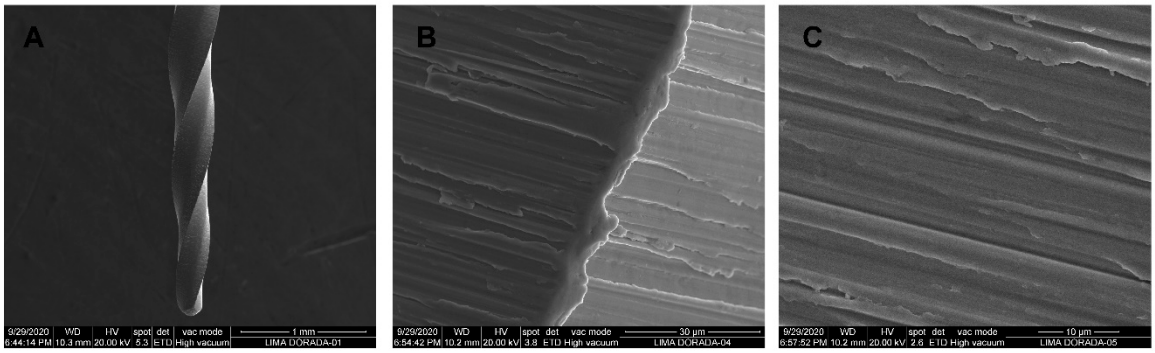

Figure 11. SEM images of CM-Gold Wire alloy PTG endodontic rotary files at (**A**) 100×, (**B**) 3600×, and (**C**) 6500×.

EDX micro-analysis at 20 kV in three different locations showed that CM-Gold Wire PTG endodontic rotary files were composed of C (2.11–2.20 wt.%), O (6.87–7.54 wt.%), Ti (40.49–40.82 wt.%), and Ni (49.59–50.20 wt.%) (Table 7 and Figure 12A–C).

Table 7. Mean atomic weight percent (%) of CM-Gold Wire alloy PTG endodontic rotary files at 15 kV and 20 kV at three different locations (1, 2 and 3).

Spectrum	C	O	Ti	Ni
PTG 20 kV (1)	2.11	6.87	40.82	50.20
PTG 20 kV (2)	2.12	7.35	40.49	50.04
PTG 20 kV (3)	2.20	7.54	40.67	49.59
Sigma	0.54	0.67	0.44	0.53

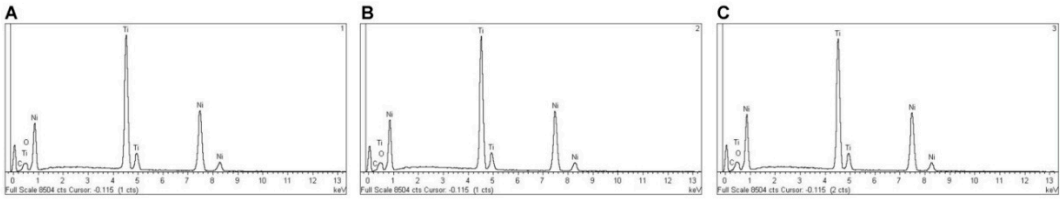

Figure 12. EDX micro-analysis of CM-Gold Wire PTG endodontic rotary files in location (**A**) 1, (**B**) 2, and (**C**) 3.

SEM analysis of the CM-Blue Wire alloy PVB endodontic rotary files did not show accumulation of organic matter or structural alterations. Furthermore, manufacturing lines were distributed perpendicularly to the longitudinal axis of the endodontic rotary files and also parallel to each other due to the laser machining manufacturing process (Figure 13A–C).

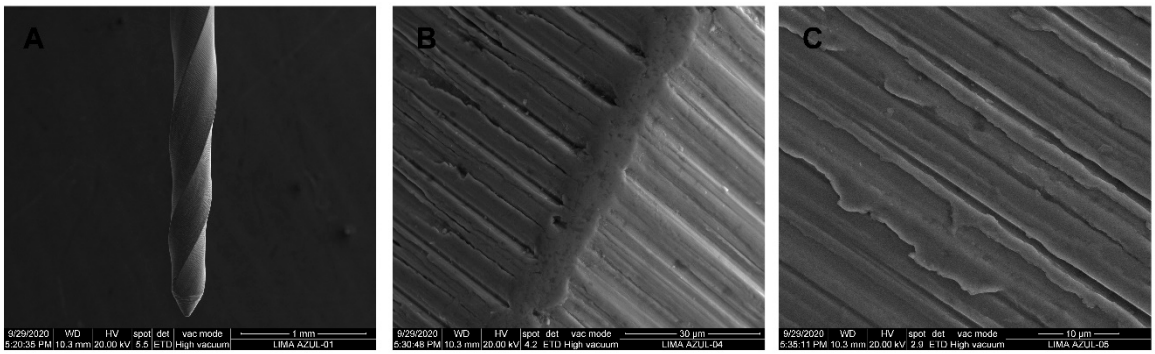

Figure 13. SEM images of CM-Blue Wire PVB endodontic rotary files at (**A**) 100×, (**B**) 3600×, and (**C**) 6500×.

EDX micro-analysis at 20 kV at three different locations showed that CM-Blue Wire PVB NiTi endodontic rotary files were composed of C (2.26–2.71 wt.%), O (11.37–13.30 wt.%), Ti (37.87–38.98 wt.%), and Ni (46.17–47.56 wt.%) (Table 8, Figure 14A–C).

Table 8. Mean atomic weight percent (%) of CM-Blue Wire PVB endodontic rotary files at 15 kV and 20 kV at three different locations (1, 2 and 3).

Spectrum	C	O	Ti	Ni
PVB 20 kV (1)	2.66	13.30	37.87	46.17
PVB 20 kV (2)	2.26	11.80	38.38	47.56
PVB 20 kV (3)	2.71	11.37	38.98	46.94
Sigma	0.58	0.69	0.44	0.53

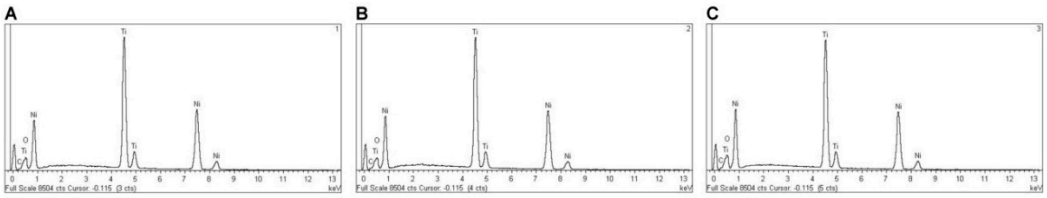

Figure 14. EDX micro-analysis of CM-Blue Wire PVB endodontic rotary files at locations (**A**) 1, (**B**) 2, and (**C**) 3.

4. Discussion

The results obtained in the present study reject the null hypothesis (H_0) that states that the NiTi alloy of the endodontic rotary files has no effect on the static cyclic fatigue resistance of NiTi endodontic rotary files.

NiTi endodontic rotary files suffer unexpected fractures inside the root canal system despite their greater flexibility [4,30], which are produced by the stress caused by cyclic fatigue, torsional fatigue, or a combination of both [31,32]. The incidence of fracture of NiTi endodontic rotary files ranges from 0.09% to 5% [33,34] and influences the prognosis of the root canal system as the fractured fragment blocks the access to the apex, preventing disinfection of the root canal system. Furthermore, it has been reported that the presence of a previous periapical pathology combined with the fracture of an endodontic instrument represents a significant decrease in the success of the root canal treatment [35]. This is the reason why the cyclic fatigue resistance of NiTi endodontic rotary files has been widely analyzed.

In 2002, the American National Standard Institute and the American Dental Association established a standardization procedure to assess the cyclic and torsional fatigue resistance of stainless steel endodontic hand files [36]. The fatigue resistance was also described by the

International Standards Organization (ISO) (ISO 3630/1) for 2% taper stainless steel endodontic hand files [37]; however, no specifications for the cyclic fatigue resistance of NiTi endodontic rotary systems above 2% taper exist, so many different static and dynamic cyclic fatigue devices have been developed to analyze the cyclic fatigue resistance of NiTi endodontic rotary files. A static cyclic fatigue device was used for this study because it allowed the analysis of an accumulative stress concentration located in the curvature area of the artificial root canal system that caused microstructural changes in the NiTi alloy responsible for the cyclic fatigue resistance of NiTi endodontic rotary files [38]. However, the static cyclic fatigue resistance comparison of different NiTi endodontic rotary systems is highly complicated due to difficulty in isolating its differences while respecting transversal designs, tapers, angular speeds, and NiTi alloy. For this reason, the most similar files for each endodontic rotary system were selected based on their length, apical diameter, cross section, angular movement, and speed and taper, although this represents a limitation within the study. In addition, the different speed values at which the NiTi endodontic rotary systems were used could influence the study results, but the NiTi endodontic rotary systems were used at the speed values recommended by the manufacturers. PTU, PTN, and PTG NiTi endodontic rotary systems were used at 300 rpm, while the PVB NiTi endodontic rotary system was used at 500 rpm; however, most authors agree that rotation speed appears to have no effect on the resistance of NiTi endodontic rotary systems [32,39,40].Gao et al. showed no statistical significant differences ($p > 0.05$) between the NiTi endodontic rotary files made of the same NiTi alloy and the same apical diameter but operated at different rotation speeds to cyclic fatigue resistance [41].

Previous studies have also analyzed the influence of the NiTi alloy on the cyclic fatigue resistance of endodontic rotary files, and most agree that the martensitic phase of NiTi alloy is the crystalline structure most resistant to cyclic fatigue [42]. In this study, the comparison of the static cyclic fatigue resistance of conventional NiTi alloy of PTU endodontic rotary files (1.24 ± 0.21 min) and NiTi M-Wire alloy of PTN endodontic rotary files (2.63 ± 0.58 min) showed a significantly ($p < 0.001$) higher static cyclic fatigue resistance of PTN NiTi endodontic rotary files compared to PTU endodontic rotary files. In addition, the comparison between conventional NiTi alloy of PTU endodontic rotary files (1.24 ± 0.21 min) and NiTi CM-Gold Wire alloy of PTG endodontic rotary files (3.42 ± 0.85 min) was influenced by fewer variables compared to the rest of the NiTi endodontic rotary systems because they presented similar cross-sections and designs. These NiTi endodontic rotary systems showed a significantly ($p < 0.001$) higher static cyclic fatigue resistance for PTG NiTi endodontic rotary files than PTU endodontic rotary files, which highlights the influence of the NiTi alloy on the cyclic fatigue resistance of NiTi endodontic rotary files, as was already shown in previous studies [16,19]. Furthermore, the comparison between the NiTi CM-Gold Wire alloy of PTG endodontic rotary files (3.42 ± 0.85 min) and the NiTi CM-Blue Wire alloy of PVB endodontic rotary files (2.86 ± 0.82 min) also showed significantly ($p < 0.001$) higher static cyclic fatigue resistance of PTG NiTi endodontic rotary files than PVB endodontic rotary files; however, it is difficult to isolate the most relevant variable or the most determinant variable combination in cyclic fatigue resistance of NiTi endodontic rotary files. These results differ when comparing the cyclic fatigue resistance of the NiTi CM-Blue Wire alloy of Reciproc Blue endodontic reciprocating system with the NiTi CM-Gold Wire alloy from the Wave One Gold endodontic reciprocating system. The cyclic fatigue resistance of the Reciproc Blue endodontic reciprocating system showed a higher resistance to cyclic fatigue than the Wave One Gold endodontic reciprocating system, probably due to the cross-sectional design [43,44]. The influence of the cross-sectional design on the cyclic fatigue resistance was also analyzed by comparing the NiTi M-Wire alloy of the Reciproc endodontic reciprocating system with the NiTi M-Wire alloy of the Wave One endodontic reciprocating system and showed that the Reciproc endodontic reciprocating system had significantly ($p < 0.001$) higher static cyclic fatigue resistance than the Wave One endodontic reciprocating system [45].

The novel heat treatments of NiTi alloys show more resistance to cyclic fatigue than conventional NiTi alloys. Elanghy et al. reported a statistically significant ($p < 0.001$) higher cyclic fatigue resistance of ProTaper Next and ProTaper Gold compared to conventional NiTi alloys of TRUShape and ProTaper Universal NiTi endodontic rotary systems [46], and Uygun et al. reported

similar results when comparing ProFile Vortex Blue and ProTaper Next with the conventional NiTi alloy of ProTaper Universal [47]. These results agreed with those obtained in the present study and highlight the relevance of the alloying elements in the allotropic transformation of the crystalline structure of the NiTi alloy, which in turn influences the physical and mechanical properties of the endodontic rotary files [47]. Titanium is an allotropic metal which can present two crystalline structures: compact hexagonal (α or austenite) and body-centered cubic (β or martensite). Depending on the stabilizing effect of the α and β phases, the alloying elements of titanium are classified as neutral elements, betagenic elements, or stabilizers of the α phase and alphagenic elements or stabilizers of the β phase. The stabilization of the phases implies the increase or decrease of the transition temperature β [48]; specifically, alphagenic elements increase the transition temperature β. Among the alphagenic elements, Al is the most important alloying element, although O, C, and N can also be used. The results obtained from the EDX micro-analysis showed the presence of the above mentioned alloying elements. The atomic weight of the alloying elements showed an upward trend from the conventional NiTi alloy of PTU endodontic rotary files (C (2.17–3.18 wt.%) and O (1.48–1.61 wt.%)), to the NiTi M-Wire alloy of PTN endodontic rotary files (C (3.31–4.43 wt.%) and Al (0.56–1.39 wt.%)), to the NiTi CM-Blue Wire alloy of PVB endodontic rotary files (C (2.26–2.71 wt.%) and O (11.37–13.30 wt.%)), and finally to the NiTi CM-Gold Wire alloy of PTG endodontic rotary files (C (2.11–2.20 wt.%) and O (6.87–7.54 wt.%)); this leads to more crystalline structures that are more martensitic and therefore more flexible and resistant to fracture, which is consistent with the time to failure observed in the study of resistance to static cyclic fatigue.

5. Conclusions

NiTi CM-Gold wire alloy of the ProTaper Gold endodontic rotary files is more resistance to cyclic fatigue than ProFile Vortex Blue, ProTaper Next, and ProTaper Universal endodontic rotary files, due to the elements of the alloy present in the crystalline structure that give the ProTaper Gold endodontic rotary files greater flexibility and resistance.

Author Contributions: All of the authors contributed to the investigation, supervision, writing, review, and editing of the study. Conceptualization, C.R.-S. and V.F.-L.; data curation, I.F.-M. and V.F.-M.; formal analysis, S.S.; visualization, Á.Z.-M. All authors have read and agreed to the published version of the manuscript.

Funding: This research received no external funding.

Conflicts of Interest: The authors declare no conflict of interest.

References

1. Gavini, G.; Santos, M.D.; Caldeira, C.L.; Machado, M.E.L.; Freire, L.G.; Iglecias, E.F.; Peters, O.A.; Candeiro, G.T.M. Nickel-titanium instruments in endodontics: A concise review of the state of the art. *Braz. Oral Res*. **2018,** *32* (Suppl. 1), e67.
2. Peralta-Mamani, M.; Rios, D.; Duarte, M.A.H.; Santiago Junior, J.F.; Honório, H.M. Manual vs. rotary instrumentation in endodontic treatment of permanent teeth: A systematic review and meta-analysis. *Am. J. Dent*. **2019**, *32*, 311–324.
3. Uslu, G.; Gundogar, M.; Özyurek, T.; Plotino, G. Cyclic fatigue resistance of reduced-taper nickel-titanium (NiTi) instruments in doubled-curved (S-shaped) canals at body temperature. *J. Dent. Res. Dent. Clin. Dent. Prospects*. **2020**, *14*, 111–115.
4. Bergmans, L.; van Cleynenbreugel, J.; Wevers, M.; Lambrechts, P. Mechanical root canal preparation with NiTi rotary instruments: Rationale, performance and safety. Status report for the American Journal of Dentistry. *Am. J. Dent*. **2001**, *14*, 324–333.
5. Machado, R.; Júnior, C.S.; Colombelli, M.F.; Picolli, A.P.; Junior, J.S.; Cosme-Silva, L.; Garcia, L.D.F.R.; Alberton, L.R. Incidence of ProTaper Universal System Instrument Fractures—A Retrospective Clinical Study. *Eur. Endod. J*. **2018**, *3*, 77–81.
6. Bueno, C.S.P.; Oliveira, D.P.; Pelegrine, R.A.; Fontana, C.E.; Rocha, D.G.P.; Gutmann, J.L.; Bueno, C.E.S. Fracture incidence of WaveOne Gold files: A prospective clinical study. *Int. Endod. J*. **2020,** *53*, 1192–1198.

7. Cheung, G.S.P. Instrument fracture: Mechanisms, removal of fragments, and clinical outcomes. *Endod. Top.* **2009**, *16*, 1–26.
8. McGuigan, M.B.; Louca, C.; Duncan, H.F. The impact of fractured endodontic instruments on treatment outcome. *Br. Dent. J.* **2013**, *214*, 285–289.
9. Zhou, H.; Peng, B.; Zheng, Y.-F. An overview of the mechanical properties of nickeltitanium endodontic instruments. *Endod. Top.* **2013**, *29*, 42–54.
10. Shen, Y.; Zhou, H.; Zheng, Y.; Peng, B.; Haapasalo, M. Current challenges and concepts of the thermomechanical treatment of nickel-titanium instruments. *J. Endod*. **2013**, *39*, 163–172.
11. Testarelli, L.; Plotino, G.; Al-Sudani, D.; Vincenzi, V.; Giansiracusa, A.; Grande, N.M.; Gambarini, G. Bending properties of a new nickel-titanium alloy with a lower percent by weight of nickel. *J. Endod*. **2011**, *37*, 1293–1295.
12. Zupanc, J.; Vahdat-Pajouh, N.; Schäfer, E. New thermomechanically treated NiTi alloys—A review. *Int. Endod. J.* **2018**, *51*, 1088–1103.
13. Zhou, H.; Shen, Y.; Zheng, W.; Li, L.; Zheng, Y.; Haapasalo, M. Mechanical properties of controlled memory and superelastic nickel-titanium wires used in the manufacture of rotary endodontic instruments. *J. Endod*. **2012**, *38*, 1535–1540.
14. Gutmann, J.L.; Gao, Y. Alteration in the inherent metallic and surface properties of nickel-titanium root canal instruments to enhance performance, durability and safety: A focused review. *Int. Endod. J.* **2012**, *45*, 113–128.
15. Pérez-Higueras, J.J.; Arias, A.; de la Macorra, J.C.; Peters, O.A. Differences in cyclic fatigue resistance between ProTaper Next and ProTaper Universal instruments at different levels. *J. Endod*. **2014**, *40*, 1477–1481.
16. Uygun, A.D.; Kol, E.; Topcu, M.K.C.; Seckin, F.; Ersoy, I.; Tanriver, M. Variations in cyclic fatigue resistance among ProTaper Gold, ProTaper Next and ProTaper Universal instruments at different levels. *Int. Endod. J.* **2016**, *49*, 494–499.
17. González-Chapela, J.; Castelo-Baz, P.; Varela-Patiño, P.; Martín-Biedma, B.; Ruíz-Piñón, M. Alternating versus continuous rotation: Root canal transportation and centering ratio with the ProTaper Next. *J. Conserv. Dent*. **2017**, *20*, 255–259.
18. Elnaghy, A.M. Cyclic fatigue resistance of ProTaper Next nickel-titanium rotary files. *Int. Endod. J.* **2014**, *47*, 1034–1039.
19. Hieawy, A.; Haapasalo, M.; Zhou, H.; Wang, Z.; Shen, Y. Phase transformation behavior and resistance to bending and cyclic fatigue of ProTaper Gold and ProTaper Universal instruments. *J. Endod*. **2015**, *41*, 1134–1138.
20. Elnaghy, A.M.; Elsaka, S.E. Mechanical properties of ProTaper Gold nickel-titanium rotary instruments. *Int. Endod. J.* **2016**, *49*, 1073–1078.
21. Algahtani, F.; Huang, X.; Haapasalo, M.; Wang, Z.; Hieawy, A.; Zhang, D.; Aleksejuniene, J.; Shen, Y. Fatigue resistance of ProTaper gold exposed to high-concentration sodium hypochlorite in double curvature artificial canal. *Bioact. Mater*. **2019**, *4*, 245–248.
22. Keskin, C.; Inan, U.; Guler, D.H.; Kalyoncuoğlu, E. Cyclic fatigue resistance of XP-Endo Shaper, K3XF, and ProTaper Gold nickel-titanium instruments. *J. Endod*. **2018**, *44*, 1164–1167.
23. Özyürek, T.; Yılmaz, K.; Uslu, G. The effects of autoclave sterilization on the cyclic fatigue resistance of ProTaper Universal, ProTaper Next, and ProTaper Gold nickeltitanium instruments. *Restor. Dent. Endod*. **2017**, *42*, 301–308.
24. Ruiz-Sánchez, C.; Faus-Matoses, V.; Alegre-Domingo, T.; Faus-Matoses, I.; Faus-Llácer, V.-J. An in vitro cyclic fatigue resistance comparison of conventional and new generation nickel-titanium rotary files. *J. Clin. Exp. Dent*. **2018**, *10*, e805–e809.
25. Castelló-Escrivá, R.; Alegre-Domingo, T.; Faus-Matoses, V.; Román-Richon, S.; FausLlácer, V.J. In vitro comparison of cyclic fatigue resistance of ProTaper, WaveOne, and Twisted Files. *J. Endod*. **2012**, *38*, 1521–1524.
26. Montenegro-Santillan, R.; Alegre-Domingo, T.; Faus-Matoses, V.; Faus-Llacer, V. An in vitro comparison of cyclic fatigue resistance of ProTaper Universal and GT series X files. *Med. Oral Patol. Oral Cir. Bucal* **2013**, *18*, e533–e536.
27. Plotino, G.; Grande, N.M.; Cordaro, M.; Testarelli, L.; Gambarini, G. A review of cyclic fatigue testing of nickel-titanium rotary instruments. *J. Endod*. **2009**, *35*, 1469–1476.

28. Zubizarreta-Macho, Á.; Mena Álvarez, J.; Albaladejo Martínez, A.; Segura-Egea, J.J.; Caviedes Brucheli, J.; Agustín-Panadero, R.; López Píriz, R.; Alonso-Ezpeleta, Ó. Influence of the Pecking Motion Frequency on the Cyclic Fatigue Resistance of Endodontic Rotary Files. *J. Clin. Med*. **2019**, *9*, 45.
29. Zubizarreta-Macho, A.; Alonso-Ezpeleta, O.; Albaladejo Martínez, A.; Faus Matoses, V.; Caviedes Brucheli, A.; Agustín-Panadero, R.; Mena Álvarez, J.; Vizmanos Martínez-Berganza, F. Novel Electronic Device to Quantify the Cyclic Fatigue Resistance of Endodontic Reciprocating Files after Using and Sterilization. *Appl. Sci*. **2020**, *10*, 4962.
30. Pruett, J.P.; Clement, D.J.; Carnes, D.L., Jr. Cyclic fatigue testing of nickel-titanium endodontic instruments. *J. Endod*. **1997**, *23*, 77–85.
31. Wei, X.; Ling, J.; Jiang, J.; Huang, X.; Liu, L. Modes of failure of ProTaper nickel-titanium rotary instruments after clinical use. *J. Endod*. **2007**, *33*, 276–279.
32. Gambarini, G. Cyclic fatigue of nickel-titanium rotary instruments after clinical use with low-and high-torque endodontic motors. *J. Endod*. **2001**, *27*, 772–774.
33. Parashos, P.; Gordon, I.; Messer, H.H. Factors influencing defects of rotary nickel-titanium endodontic instruments after clinical use. *J. Endod*. **2004**, *30*, 722–725.
34. Spili, P.; Parashos, P.; Messer, H.H. The impact of instrument fracture on outcome of endodontic treatment. *J. Endod*. **2005**, *31*, 845–850.
35. Strindberg, L. The dependence of the results of pulp therapy on certain factors. *Acta Odontol. Scand*. **1956**, *14*, 1–175.
36. ANSI/ADA Specification Nº 28-2002. *Root Canal Files and Reamers, Type K for Hand Use*; American Dental Association: Chicago, IL, USA, 2002.
37. ISO 3630-3631:2008. *Dentistry—Root Canal Instruments—Part 1: General Requirements and Test Methods*; ISO: Geneva, Switzerland, 2008.
38. Lopes, H.P.; Britto, I.M.; Elias, C.N.; de Machado Oliveira, J.C.; Neves, M.A.; Moreira, E.J.; Siqueira, J., Jr. Cyclic fatigue resistance of ProTaper Universal instruments when subjected to static and dynamic tests. *Oral Surg. Oral Med. Oral Pathol. Oral Radiol. Endod*. **2010**, *110*, 401–404.
39. Zelada, G.; Varela, P.; Martin, B.; Bahillo, J.; Magan, F.; Ahn, S. The Effect of rotational speed and the curvature of root canals on the breakage of rotary endodontic instruments. *J. Endod*. **2002**, *28*, 540–542.
40. Kitchens, G.G.; Liewehr, F.R.; Moon, P.C. The effect of operational speed on the fracture of nickel-titanium rotary instruments. *J. Endod*. **2007**, *33*, 52–54.
41. Gao, Y.; Shotton, V.; Wilkinson, K.; Phillips, G.; ben Johnson, W. Effects of raw material and rotational speed on the cyclic fatigue of ProFile Vortex rotary instruments. *J. Endod*. **2010**, *36*, 1205–1209.
42. Santoro, M.; Nicolay, O.F.; Cangialosi, T.J. Pseudoelasticity and thermoelasticity of nickel-titanium alloys: A clinically oriented review. Part I: Temperature transitional ranges. *Am. J. Orthod. Dentofac. Orthop*. **2001**, *119*, 587–593.
43. Gundogar, M.; Ozyurek, T. Cyclic fatigue resistance of OneShape, HyFlex EDM, WaveOne Gold, and Reciproc Blue nickel-titanium instruments. *J. Endod*. **2017**, *43*, 1192–1196.
44. Keskin, C.; Inan, U.; Demiral, M.; Keles, A. Cyclic fatigue resistance of Reciproc Blue, Reciproc, and WaveOne Gold reciprocating instruments. *J. Endod*. **2017**, doi:10.1016/j.joen.2017.03.036.
45. Arias, A.; Perez-Higueras, J.J.; de la Macorra, J.C. Differences in cyclic fatigue resistance at apical and coronal levels of Reciproc and WaveOne new files. *J. Endod*. **2012**, *38*, 1244–1248.
46. Elnaghy, A.M.; Elsaka, S.E. Laboratory comparison of the mechanical properties of TRUShape with several nickel-titanium rotary instruments. *Int. Endod. J*. **2017**, *50*, 805–812.
47. Zafar, M.S. Impact of Endodontic Instrumentation on Surface Roughness of Various Nickel-Titanium Rotary Files. *Eur. J. Dent*. **2020**, doi:10.1055/s-0040-1718469.
48. Seracchiani, M.; Miccoli, G.; Di Nardo, D.; Zanza, A.; Cantore, M.; Gambarini, G.; Testarelli, L. Effect of flexural stress on torsional resistance of NiTi instruments. *J. Endod*. **2020**, doi:10.1016/j.joen.2020.10.011.

Journal of
Clinical Medicine

MDPI

Article

Influence of the Pecking Motion Frequency on the Cyclic Fatigue Resistance of Endodontic Rotary Files

Álvaro Zubizarreta-Macho [1,*], Jesús Mena Álvarez [1], Alberto Albaladejo Martínez [2], Juan José Segura-Egea [3], Javier Caviedes Brucheli [4], Rubén Agustín-Panadero [5], Roberto López Píriz [6] and Óscar Alonso-Ezpeleta [7]

1 Department of Endodontics, Faculty of Health Sciences, Alfonso X el Sabio University, 28691 Madrid, Spain; jmenaalvarez@gmail.com
2 Department of Dentistry, School of Medicine, University of Salamanca, 37008 Salamanca, Spain; albertoalbaladejo@hotmail.com
3 Faculty of Dentistry, University of Sevilla, C/Avicena s/n, 41009 Sevilla, Spain; segurajj@us.es
4 Centro de Investigaciones Odontológicas (CIO) Pontificia, Universidad Javeriana, Bogotá 1101, Colombia; javiercaviedes@gmail.com
5 Department of Stomatology, Faculty of Medicine and Dentistry, University of Valencia, 46010 Valencia, Spain; rubenagustinpanadero@gmail.com
6 Institute of Materials Science of Madrid, Superior Council of Scientific Investigations, 28222 Madrid, Spain; lopezpiriz@gmail.com
7 Department of Endodontics, School of Health Sciences, University of Zaragoza, 22006 Aragorn, Spain; lalonezp@unizar.es
* Correspondence: amacho@uax.es

Received: 2 November 2019; Accepted: 20 December 2019; Published: 24 December 2019

Abstract: Purpose: To analyze the influence of the pecking motion frequency on the cyclic fatigue resistance of endodontic rotary files. Material and Methods: Sixty PlexV 25.06 endodontic rotary files were selected and distributed into three groups: 30 movements/min (n = 20), 60 movements/min (n = 20), and 120 movements/min (n = 20). A dynamic cyclic fatigue device was designed using Computer Aided Design/ Computer Aided Engineering (CAD/CAE) technology and manufactured by 3D impressions to simulate the pecking motion performed by an operator. Failures of the endodontic rotary files were detected by a Light-Emitting Diode (LED)/Light-Dependent Resistor (LDR) system controlled by an Arduino-Driver complex and management software. Endodontic rotary files were tested on an artificial root canal manufactured by wire electrical discharge machining (EDM), with similar dimensions to those of the instrument under examination. Endodontic rotary files were used following the manufacturer's recommendations. The results were analyzed by ANOVA and Weibull statistics. Results: All pairwise comparisons revealed statistically significant differences in all three variables, except for the difference in the number of cycles between the groups with 60 and 120 movements/min (p = 0.298). The scale distribution parameter of Weibull statistics showed statistically significant differences in all three variables, except for the differences in the number of cycles between groups with 30 and 60 movements/min (p = 0.0722). No statistically significant differences in the three variables were observed for the shape distribution parameter. Conclusion: A low frequency of pecking motion is recommended to reduce the risk of failure of endodontic rotary files associated with cyclic fatigue.

Keywords: endodontics; cyclic fatigue; pecking motion; endodontic rotary files; NiTi rotary files

1. Introduction

Endodontic rotary files have experienced continuous development since nickel–titanium (NiTi) files were introduced in the 1980s [1]. This alloy increases the flexibility and strength of rotary files compared with stainless-steel instruments [2], and it simplifies the endodontic procedure by improving the speed, accuracy, and safety of root canal shaping [3]. Despite continuous enhancements in the design and manufacture of NiTi rotary files to reduce the occurrence of failure during root canal shaping [4], failures can still occur. Many variables can contribute to file separation, but the main causes are cyclic bending fatigue and torsional overload [5–8]. Torsional overload is caused by the blockage of the endodontic files during rotational movement [9]. However, NiTi instrument failures are primarily caused by cyclic fatigue, which occurs when a NiTi endodontic instrument rotates in a curved root canal [10]. During rotation, the structure of the endodontic instrument is alternately subjected to compressive and tensile stress cycles, which produce microstructural changes that lead to the failure of the endodontic rotary file [11]. Root canal shape, instrument geometry, rotational speed, torque, instrument surface treatments, sterilization cycles, the number of clinical uses, and the chemical composition of NiTi alloys are the main factors that affect the number of cycles to failure (NCF) of NiTi rotary instruments [12,13]. However, the influence of the pecking motion (frequency of in-and-out movement) on the cyclic fatigue resistance of endodontic rotary instruments has never been tested. In 2002, the American National Standard Institute and the American Dental Association standardized a protocol for testing the torsional and flexibility resistance of stainless-steel manual files [14], which was also addressed in the 3630-1 norm by the International Organization for Standardization (ISO) [15] for endodontic instruments with a taper of 2%. However, there is no international standard for testing the cyclic fatigue behavior of NiTi endodontic rotary instruments [11], and several self-designed devices and methods have been used [11]. However, none of these custom-made devices have been capable of dynamically testing the cyclic fatigue of NiTi endodontic rotary instruments in vitro with an automatic detection system and an anatomically based artificial root canal.

The aim of this work was to analyze the influence of the pecking motion on the cyclic fatigue resistance of endodontic rotary instruments; the null hypothesis (H0) asserts that the frequency of the pecking motion does not significantly affect the time to failure, the NCF, or the cyclic fatigue resistance of endodontic rotary instruments.

2. Materials and Methods

2.1. Study Design

Sixty sterile NiTi CM Wire endodontic rotary instruments 25.06 (Plex V2®, Orodeka, Italia) were involved in this study. Before the experiment, every endodontic rotary instrument was inspected for defects or deformities under a stereomicroscope (SZR-10, Optika, Bergamo, Italy), and none were discarded. A randomized controlled experimental trial was performed at the Dental Centre of Innovation and Advanced Specialties at the Alfonso X el Sabio University (Madrid, Spain) between February and July 2019. The endodontic rotary instruments were randomized (Epidat 4.1, Galicia, Spain) and distributed into the three groups: (A) 30 pecking movements/min (n = 20), (B) 60 pecking movements/min (n = 20), and (C) 120 pecking movements/min (n = 20).

2.2. The Experimental Cyclic Fatigue Model

The cyclic fatigue tests were performed using a custom-made device (Utility Model Patent number ES1219520) that provides information about the behavior of an endodontic rotary file during a root canal treatment. The endodontic rotary instruments were neither used nor submitted to sterilization cycles before the tests. The structure was designed by 2D/3D Computer-Aided Design/Computer-Aided Engineering (CAD/CAE) (Midas FX+®, Brunleys, MK, UK) and manufactured by 3D impression (ProJet® 6000. 3D Systems©, Rock Hill, SC, USA) (Figure 1).

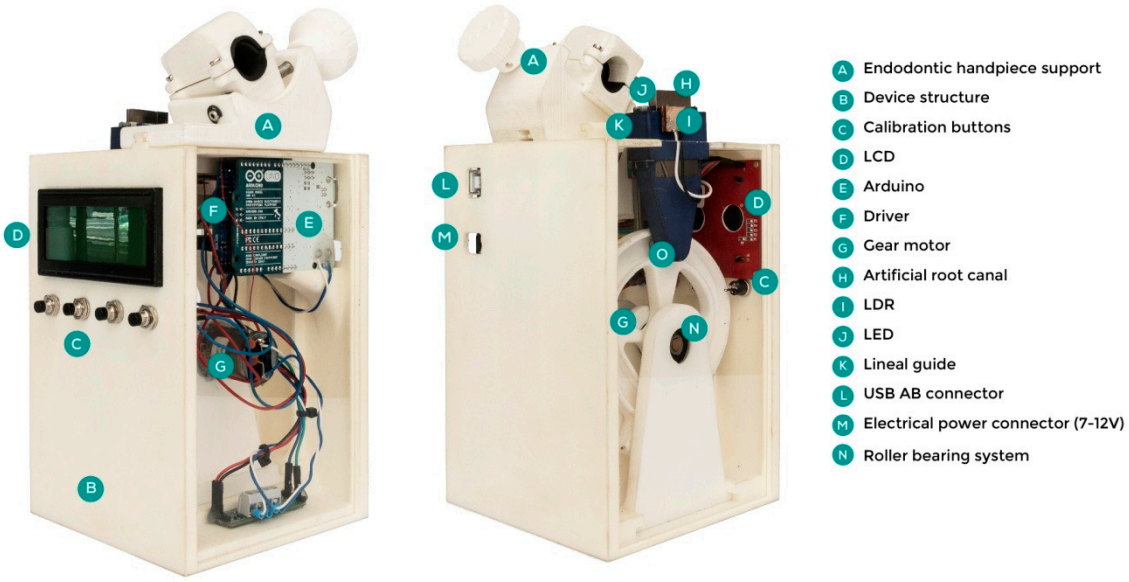

Figure 1. Parts of the hardware of the cyclic fatigue test device.

The endodontic handpiece (X-Smart Plus, Dentsply Maillefer, Baillagues, Switzerland) was scanned (3D Geomagic Capture Wrap, 3D Systems©, Rock Hill, SC, USA) to create an accurate design for its support piece by means of inverse engineering technology (Midas FX+®, Brunleys) and 3D impression manufacture (ProJet® 6000. 3D Systems©, Rock Hill, SC, USA). This support was firmly attached to the main structure and enabled the angular displacement of the endodontic handpiece by means of a spindle to test different file lengths. The support also allowed the files to be removed during the cyclic fatigue tests.

The direction and speed of the movement were produced by the brushed DC gearmotor (Ref.: 1589, Pololu® Corporation, Las Vegas, NV, USA) controlled by the driver (Ref.: DRV8835, Pololu® Corporation, Las Vegas, NV, USA), which performed an H-bridge function that controlled the speed movement through Pulse Width Modulation (PWM) signals emitted by four switches modulated by transistors. The movement was transferred to the artificial root canal support through a roller bearing system (Ref.: MR104ZZ, FAG, Schaeffler Herzogenaurach, Germany). The artificial root canal support moved in a pure axial motion through a lineal guide (Ref.: HGH35C 10249-1 001 MA, HIWIN Technologies Corp., Taichung, Taiwan). The endodontic rotary file selected (Plex V2®, Orodeka) was digitized using a micro Computer Tomography (Skyscan 1176, Bruker-MicroCT, Kontich, Belgium) to obtain a stereolithography (STL) file (Figure 2A) that was needed to design an accurate artificial root canal regarding the measurements of the endodontic rotary file tested (Figure 2B). The artificial root canal piece was manufactured with stainless steel with a 1 mm width. The artificial root canal form was anatomically based and designed using 2D/3D CAD/CAE software (Midas FX+®, Brunleys), and it was manufactured by electrical discharge machining (EDM) molybdenum wire-cut technology (Cocchiola S.A., Buenos Aires, Argentina) (Figure 2C) to simulate the tested endodontic rotary instrument's apical size, taper, and length and enable intimate contact between the endodontic rotary file and the artificial root canal, with a 60° curvature according to Schneider's measure technique [16] and a 3 mm radius of curvature (Figure 2D).

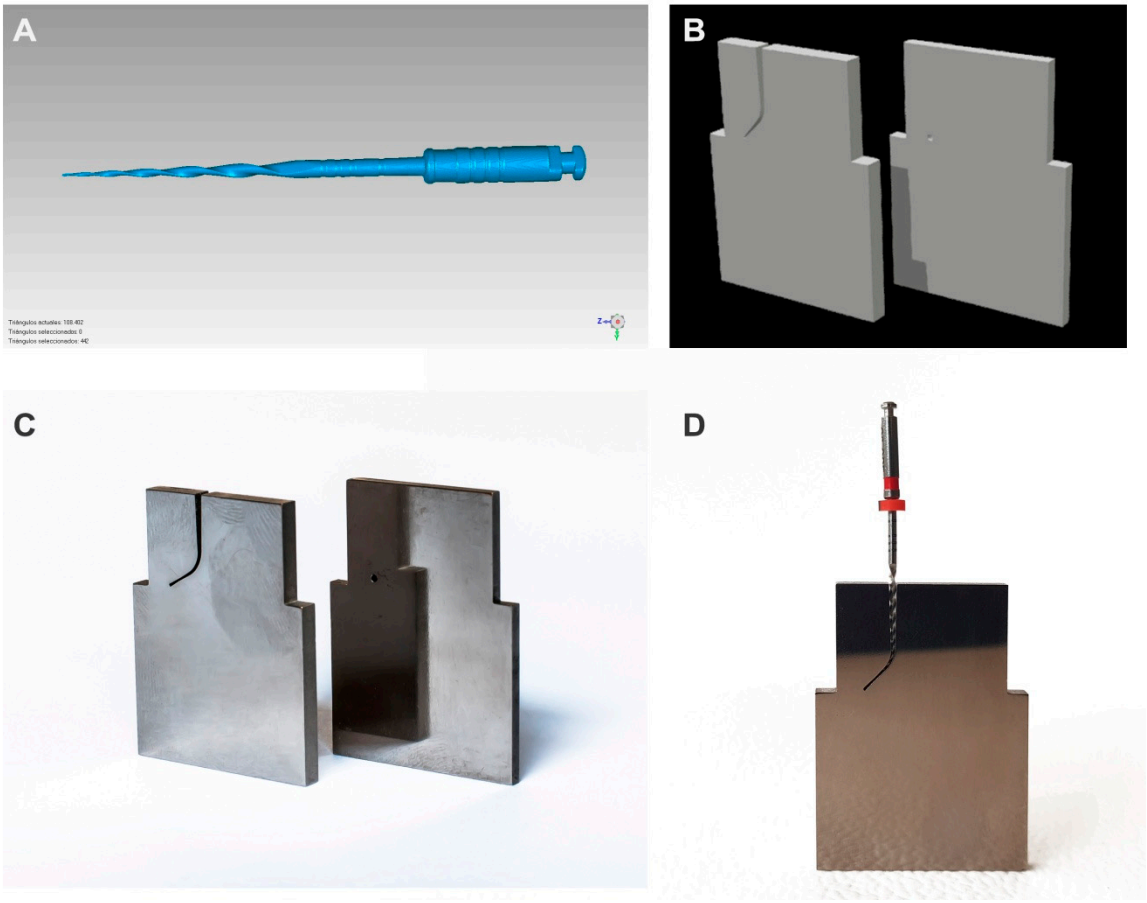

Figure 2. (**A**) Stereolithography (STL) file of the endodontic rotary file; (**B**) STL file of the artificial root canal; (**C**) artificial root canal manufactured by electrical discharge machining (EDM) and (**D**) endodontic rotary file in intimate contact with the artificial root canal (**D**).

The failure of the endodontic rotary instrument (Figure 2B) was detected through a Light-Dependent Resistor (LDR) sensor (Ref.: C000025, Arduino LLC®, Ivrea, Italy) located at the apex of the artificial root canal. The LDR sensor quantifies the continuous light source emitted by a high-brightness white Light-Emitting Diode (LED) (20000 mcd) (Ref.: 12.675/5/b/c/20k, Batuled, Coslada, Spain), which is opposite to the artificial root canal (Figure 1). The LDR (Ref.: C000025, Arduino LLC®) sensor data were conditioned by a processor (Arduino UNO Rev. 3, Arduino LLC®, Ivrea, Italy) (Figure 1) to detect values from 0 (endodontic rotary instrument inside the artificial root canal) to 1024 (endodontic rotary instrument outside the artificial root canal). The time to failure was determined when the LDR (Ref.: C000025, Arduino LLC®) sensor detected no variations in light values for 50 ms. The hardware was managed by software that receives input signals from the Arduino board (Figure 3A–C). The signals were detected by the LDR (Ref.: C000025, Arduino LLC®) sensor with a frequency of 50 ms to accurately detect the time of failure.

Once the LDR (Ref.: C000025, Arduino LLC®) sensor detects the failure of the endodontic rotary instrument, the brushed DC gearmotor stops immediately, and the time to failure and the test parameters are saved by the management software. In addition, the manager application sends output data that start each cyclic fatigue test and control the speed of the pecking motion of the artificial root canal. The speed of the movement and the LDR (Ref.: C000025, Arduino LLC®) sensor values were also shown in real time on a Liquid Crystal Display (LCD) (Ref.: LCD-09568, Spark Fun Electronics, Niwot, CO, USA) placed on the structure of the device (Figure 1).

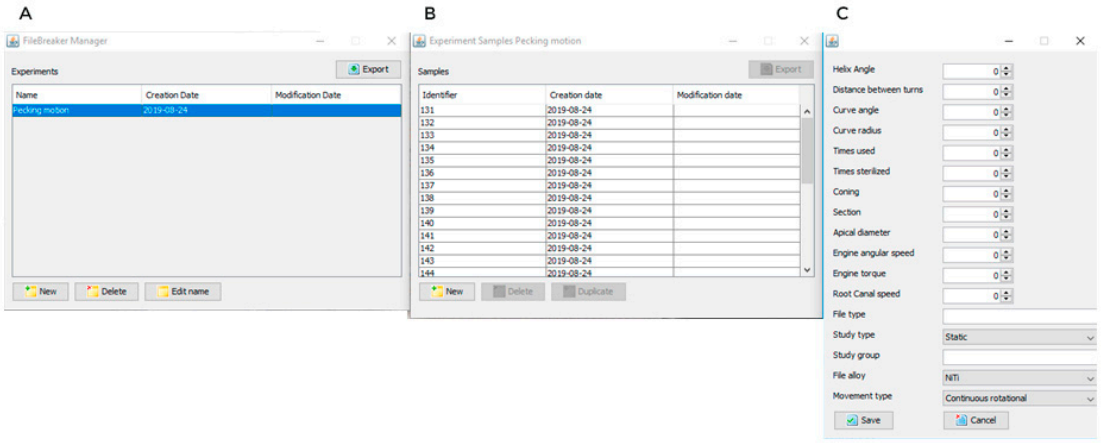

Figure 3. The management software (**A**,**B**) that managed the cyclic fatigue device with configurable parameters (**C**).

The endodontic rotary instruments were operated by a 6:1 reduction handpiece (X-Smart Plus, Dentsply Maillefer) and a torque-controlled motor with continuous rotation at 400 rpm and 3.5 N/cm torque according to the manufacturer's instructions. The friction between the file and the artificial canal walls was reduced by applying special high-flow synthetic oil designed for the lubrication of mechanical parts (Singer All-Purpose Oil; Singer Sewing Company, Barcelona, Spain).

All endodontic rotary instruments were rotated until fracture occurred. The number of cycles to fracture (NCF) for each instrument was calculated by using the following formula: NCF = time (seconds) to failure × rotational speed (rpm)/60 seconds [17]. The time to failure, the NCF, the number of in-and-out movements, and the length of the fracture file tip were also measured and recorded. Fractographic analysis of the failure was performed under a scanning electron microscope (ZEISS Supra 35VP; Oberkochen, GmBH, Germany) to examine topographic features of the fractured endodontic rotary files.

2.3. Statistical Tests

Statistical analysis of all variables was carried out using SAS 9.4 (SAS Institute Inc., Cary, NC, USA). Descriptive statistics are expressed as means and standard deviations (SD) for quantitative variables and as absolute numbers and percentages for qualitative variables. Comparative analysis was performed by comparing the time to failure, the NCF, and the number of pecking movements (cycles of in-and-out movements) using ANOVA. In addition, Weibull characteristic strength (σ0) and Weibull modulus (m) were calculated. The statistical significance was set at $p < 0.05$.

3. Results

The means and SD values for the time to failure (seconds), the NCF, and the number of cycles of in-and-out movement in the study groups are displayed in Tables 1–3, respectively.

Table 1. Descriptive statistics of the time to failure.

	n	Mean	SD	Minimum	Maximum	Fracture Length (mm)
30 MOV/MIN	20	423.66 [a]	84.61	216.23	544.40	3.23
60 MOV/MIN	20	234.23 [b]	60.56	127.00	378.21	3.04
120 MOV/MIN	20	163.06 [c]	45.95	81.80	241.16	3.81

SD, standard deviations; [a], [b], [c], different superscript means statistically significant differences between groups ($p < 0.05$).

Table 2. Descriptive statistics of the NCF.

	n	Mean	SD	Minimum	Maximum	Fracture Length (mm)
30 MOV/MIN	20	2824.37 [a]	564.05	1441.55	3629.35	3.23
60 MOV/MIN	20	1560.55 [b]	401.23	846.69	2501.41	3.04
120 MOV/MIN	20	1087.06 [c]	306.34	545.33	1607.73	3.81

NCF, the number of cycles to failure; [a], [b], [c], different superscript means statistically significant differences between groups ($p < 0.05$).

Table 3. Descriptive statistics of the number of cycles of in-and-out movement.

	n	Mean	SD	Minimum	Maximum	Fracture Length (mm)
30 MOV/MIN	20	211.60 [a]	42.66	108.12	272.20	3.23
60 MOV/MIN	20	234.23 [b]	60.56	127.00	378.21	3.04
120 MOV/MIN	20	326.12 [b]	91.90	163.59	482.32	3.81

[a], [b], different superscript means statistically significant differences between groups ($p < 0.05$).

The ANOVA revealed statistically significant differences in all three variables. The differences revealed by pairwise comparisons were all statistically significant, except for the difference in the number of cycles between the groups with 60 and 120 movements/min ($p = 0.298$). The scale distribution parameter (η) of Weibull statistics showed statistically significant differences in all three variables, except for the difference in the number of cycles between the groups with 30 and 60 movements/min ($p = 0.0722$) (Tables 4–6).

Table 4. Weibull statistics of the time to failure.

	m = Weibull Shape (β)				σ_0 = Weibull Scale (η)			
	Estimate	St Error	Lower	Upper	Estimate	St Error	Lower	Upper
30 MOV/MIN	6.3802	1.1533	4.4768	9.0927	455.9851	16.7468	424.3155	490.0185
60 MOV/MIN	4.2152	0.6990	3.0456	5.8341	257.1689	14.4489	230.3531	287.1065
120 MOV/MIN	4.4090	0.8177	3.0653	6.3417	179.5190	9.5319	161.7759	199.2080

Table 5. Weibull statistics of the NCF.

	m = Weibull Shape (β)				σ_0 = Weibull Scale (η)			
	Estimate	St Error	Lower	Upper	Estimate	St Error	Lower	Upper
30 MOV/MIN	6.3802	1.1533	4.4768	9.0927	3039.9005	111.6454	2828.7697	3266.7895
60 MOV/MIN	4.2540	0.7079	3.0702	5.8944	1712.7561	95.3373	1535.7306	1910.1877
120MOV/MIN	4.4090	0.8177	3.0653	6.3417	1196.7927	63.5463	1078.5059	1328.0528

Table 6. Weibull statistics of the number of cycles of in-and-out movement.

	m = Weibull Shape (β)				σ_0 = Weibull Scale (η)			
	Estimate	St Error	Lower	Upper	Estimate	St Error	Lower	Upper
30 MOV/MIN	6.3342	1.1474	4.4412	9.0341	227.8707	8.4275	211.9375	245.0018
60 MOV/MIN	4.2152	0.6990	3.0456	5.8341	257.1689	14.4489	230.3531	287.1065
120 MOV/MIN	4.4090	0.8177	3.0653	6.3416	359.0376	19.0640	323.5513	398.4160

However, the shape distribution parameter (β) showed no statistically significant differences in the time to failure between the groups with 30 and 60 movements/min ($p = 0.0911$), 30 and 120 movements/min ($p = 0.1537$), and 60 and 120 movements/min ($p = 0.8568$) (Figures 4 and 5).

There were no statistically significant differences in the β value of the NCF between the groups with 30 and 60 movements/min ($p = 0.0990$), 30 and 120 movements/min ($p = 0.1537$), and 60 and 120 movements/min ($p = 0.8858$) (Figures 6 and 7).

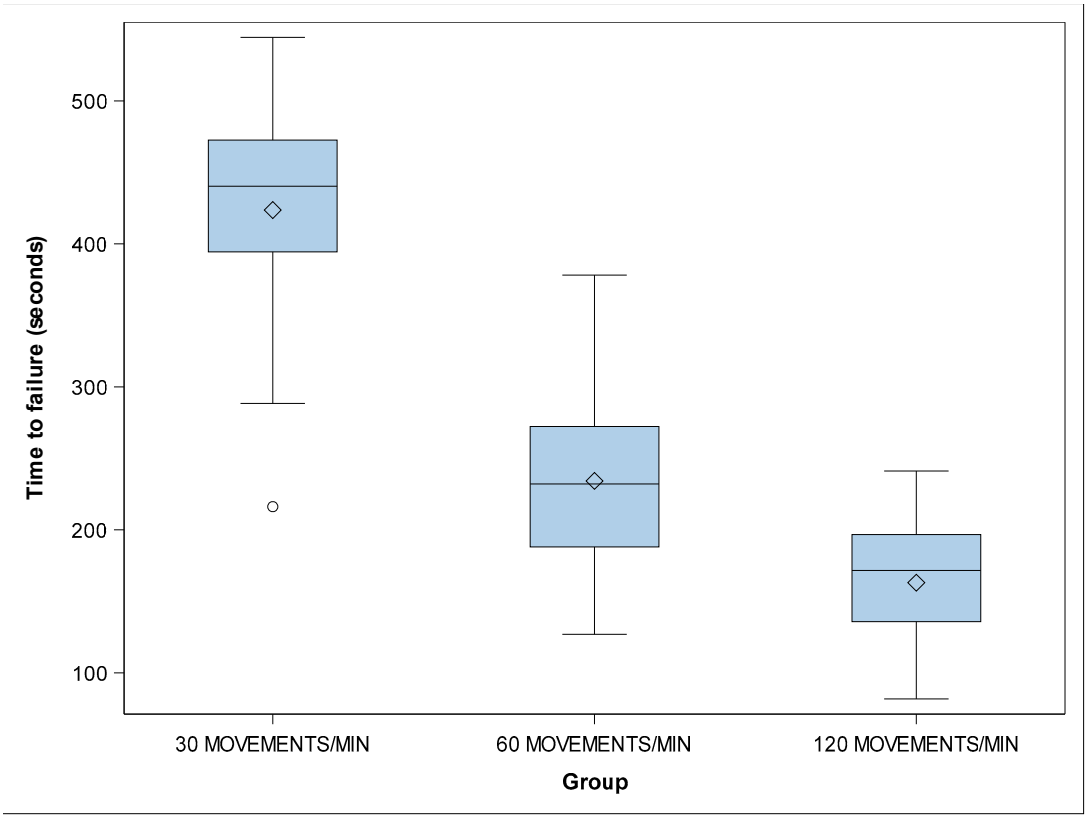

Figure 4. Boxplots of the time to failure of the experimental groups. The horizontal line in each box represents the median value.

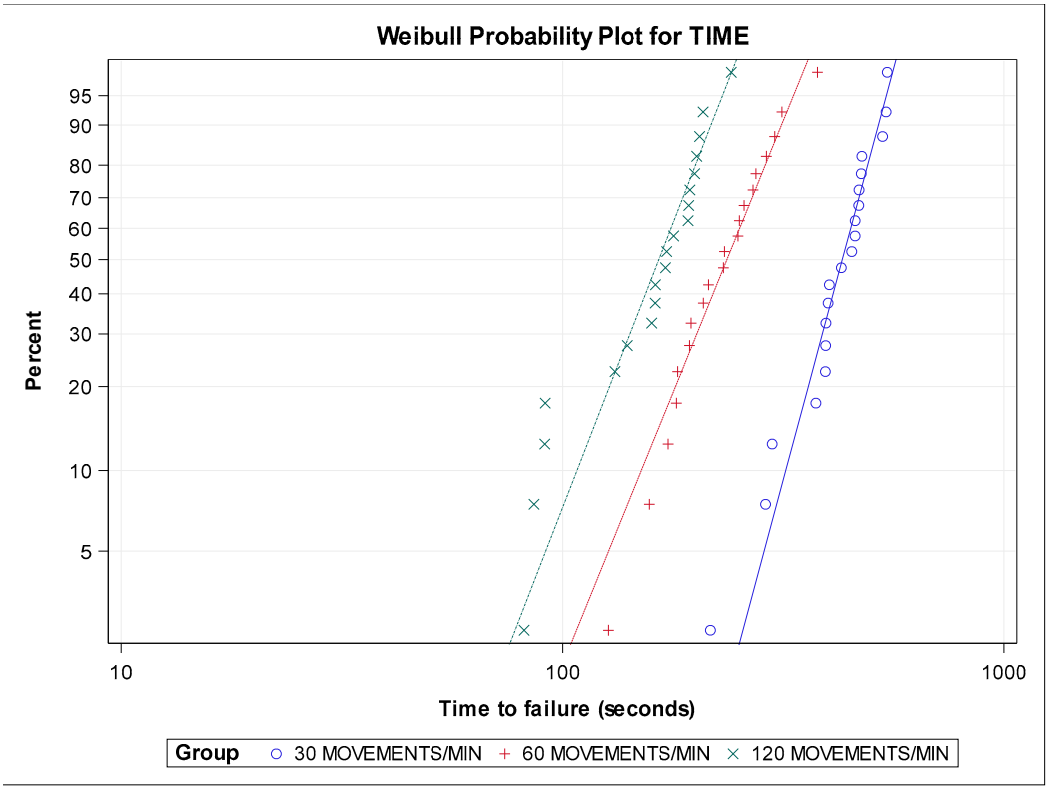

Figure 5. Weibull probability plot of the time to failure.

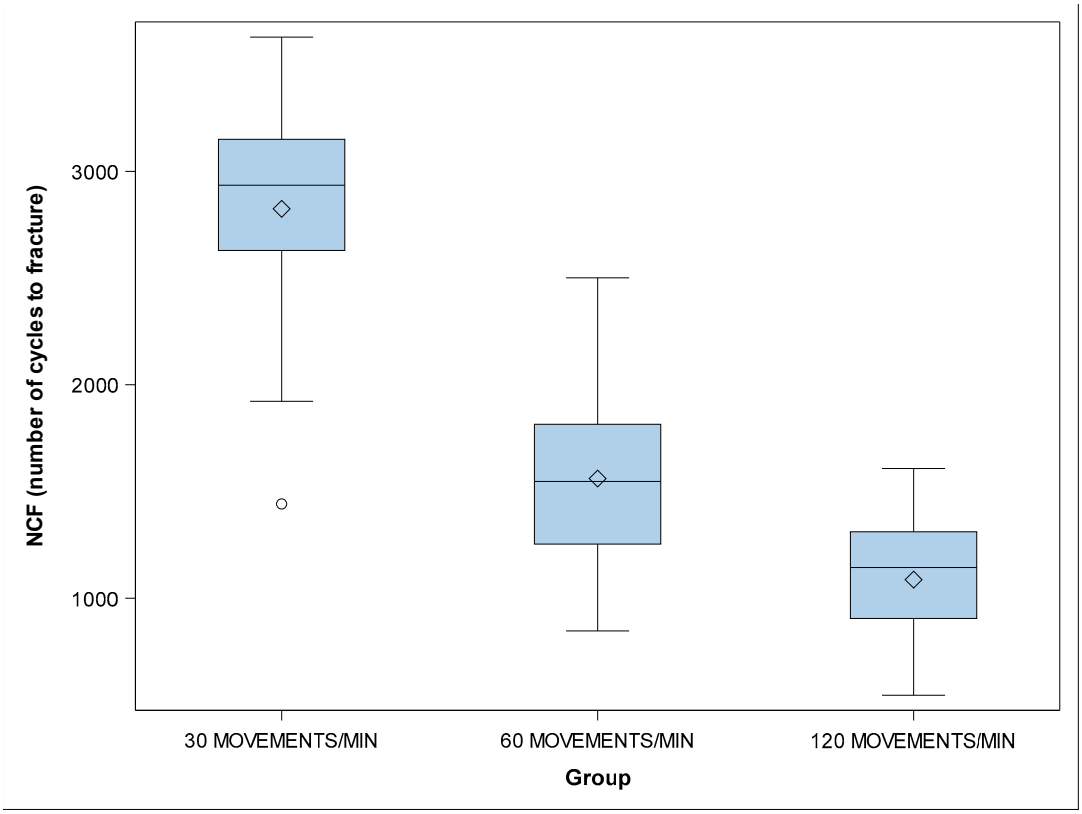

Figure 6. Boxplots of the NCF of the experimental groups. The horizontal line in each box represents the median value.

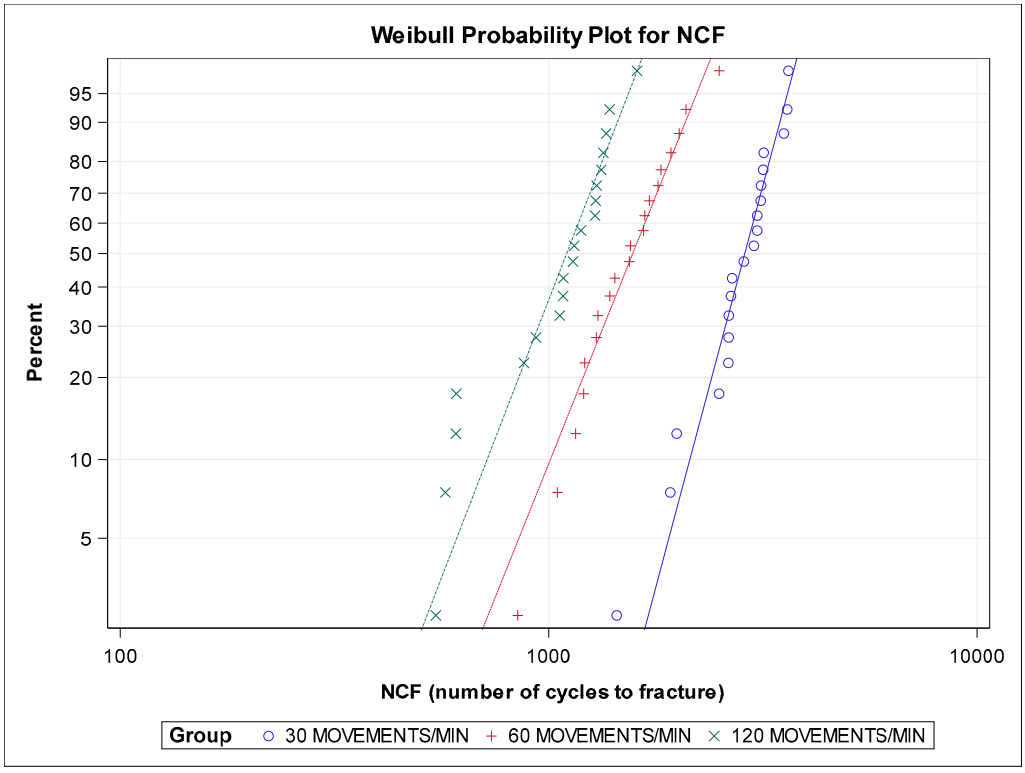

Figure 7. Weibull probability plot of the NCF.

There were no statistically significant differences in the β value of the number of cycles of in-and-out movement between the groups with 30 and 60 movements/min (p = 0.0990), 30 and 120 movements/min (p = 0.1537), and 60 and 120 movements/min (p = 0.8858) (Figures 8 and 9).

The lifespan of the endodontic rotary files submitted to 30 movements/min was higher (430.53 ± 77.71 s than that of instruments submitted to 60 movements/min (235.75 ± 62.55 s) and 120 movements/min (165.20 ± 42.03 s). The mean lengths of the fractured fragments were not statistically significantly different for any of the instruments tested ($p > 0.05$).

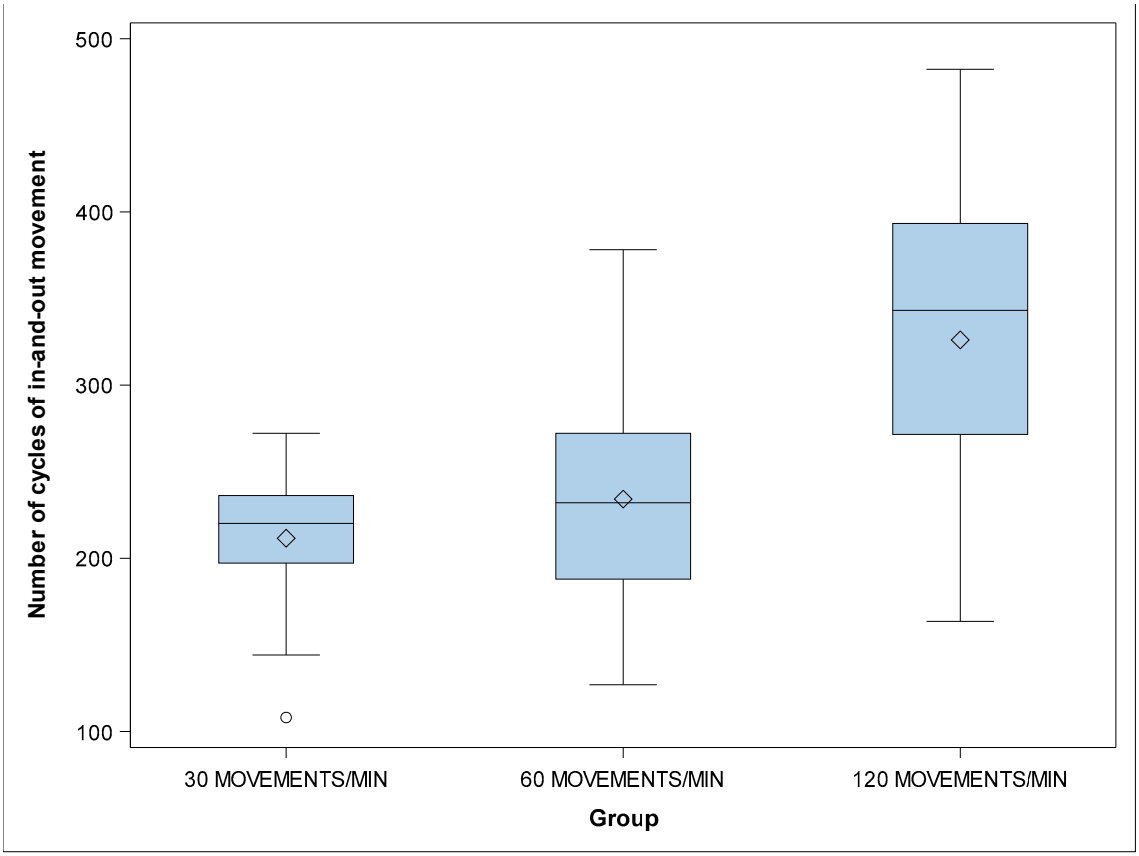

Figure 8. Boxplots of the number of cycles of in-and-out movement of the experimental groups. The horizontal line in each box represents the median value.

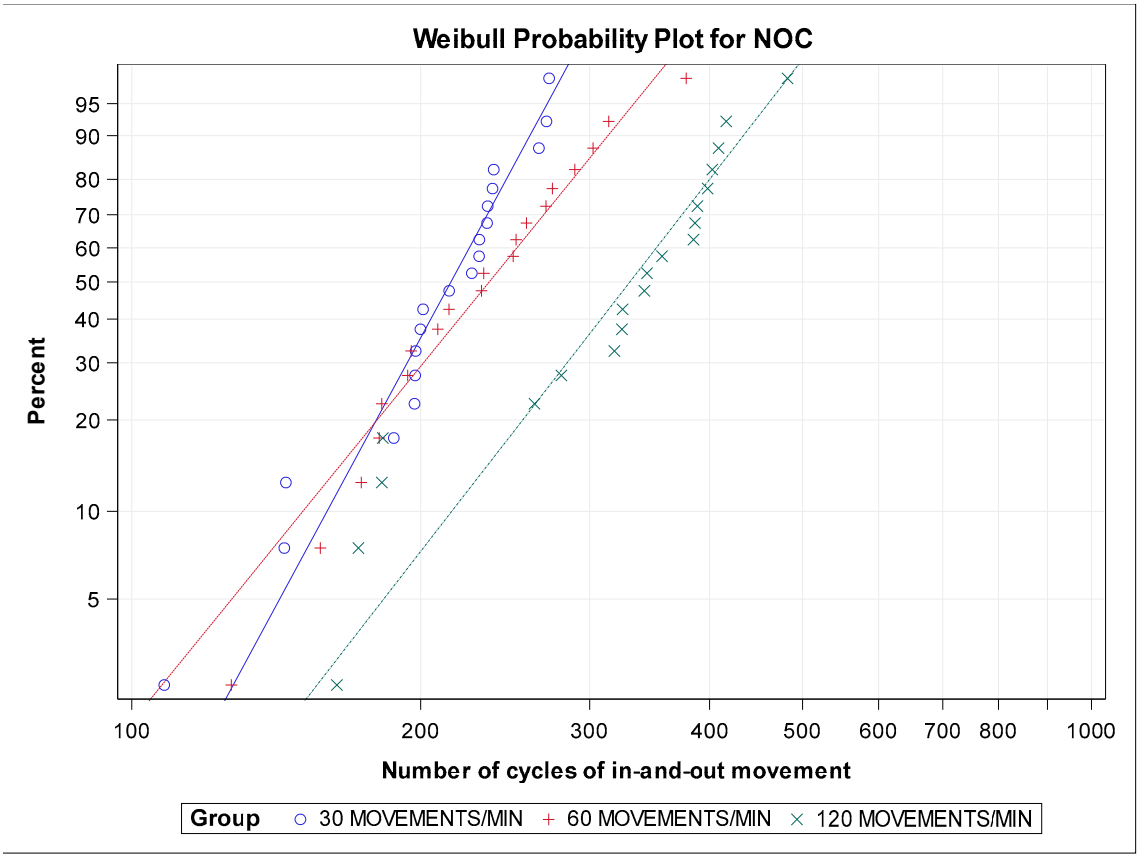

Figure 9. Weibull probability plot of the number of cycles of in-and-out movement.

4. Discussion

The results obtained in the present study lead to the rejection of the null hypothesis (H0), which states that the frequency of pecking motion has no statistically significant effect on the cyclic fatigue resistance of endodontic rotary instruments.

Different causes of fractures of endodontic instruments have been proposed by many authors and include operator experience [18,19], rotational speed [20,21], the number of uses [22], the number of rotations [23], pre-flaring [24], glide path [25], the angle and radius of the curvature [20,26], and the sterilization of instruments [27]. However, the influence of the frequency of pecking motion performed by the operator on the cyclic fatigue resistance of endodontic rotary instruments has not yet been analyzed.

Cyclic fatigue resistance has been experimentally analyzed by using several custom-made devices; however none of them have been capable of testing the cyclic fatigue resistance of NiTi endodontic rotary instruments using an anatomically based artificial root canal that allows intimate contact between the artificial root canal and the endodontic rotary instrument along the file, which might alter the cyclic fatigue resistance of the endodontic rotary instruments and hence the results of the experiment [11]. The dynamic motion produced by a cyclic fatigue test device can be made comparable to the pecking motion performed by the operator during a root canal treatment. The automatic detection system is able to objectively and accurately identify failures of endodontic rotary files.

Dederich and Zakariasen (1986) were first to develop a dynamic testing device, which allowed the endodontic rotary instruments to realize displacement in a pure axial movement [28]. Ray et al. (2007) also performed dynamic cyclic fatigue studies with standardized axial movement, and they concluded that the pecking motion increased the lifespan of the endodontic rotary instruments submitted to cyclic fatigue compared with the results obtained from static cyclic fatigue studies [29]. Hülsmann

et al. (2019) reported similar findings to ours and highlighted the differences between static and dynamic cyclic fatigue tests [30]. Nevertheless, only 12% of published cyclic fatigue studies have used a dynamic fatigue device [30]. Most studies that have compared static and dynamic cyclic fatigue studies have concluded that the time to fracture of endodontic rotary instruments submitted to dynamic cyclic fatigue studies was approximately 20–40% higher than that found in static cyclic fatigue studies [26,31–35]. Previous dynamic cyclic fatigue devices have been unable to accurately identify the causes of endodontic rotary instrument failures because of the absence of standardization of the axial direction of the pecking motion. Lateral movements during the pecking motion of an endodontic rotary instrument can lead to a second bending point at the beginning of the artificial root canal, thus distorting the outcome of cyclic fatigue tests. In addition, Plotino et al. (2010) reported the influence of the shape of the artificial root canal on the contact between the endodontic rotary instrument and the artificial root canal. They concluded that artificial root canals must be designed with a focus on the shape of the endodontic rotary file being studied [36]. However, the above-described artificial root canals had a cylindrically shaped circular section that did not allow intimate contact with the endodontic rotary instrument. In an attempt to simulate real clinical conditions, the present study involved an artificial root canal that was designed by using the measurements of the endodontic rotary instrument being studied.

The higher β values observed for the group with 30 movements/min for all three variables reveal more predictable behavior of the failure of the endodontic rotary instruments in this study group, and the lower η values found in the groups with 60 and 120 movements/min for all three variables indicate a lower cyclic fatigue resistance of the endodontic rotary instruments in these study groups. The location of the crystal structure transformation is changed in the endodontic rotary instrument during the pecking motion, which increases the cyclic fatigue resistance [30].

The conclusion derived from this study is that a high frequency of pecking motion decreases the cyclic fatigue resistance of endodontic rotary files.

Nevertheless, further research is needed to determine the influence of the frequency of pecking motion and working time on the cyclic fatigue resistance of endodontic rotary files.

5. Conclusions

In conclusion, within the limitations of this study, our results show that a high frequency of pecking motion decreases the cyclic fatigue resistance of endodontic rotary instruments. A low frequency of pecking motion is recommended to reduce the risk of fractures of endodontic rotary instruments associated with cyclic fatigue.

Author Contributions: All of the authors contributed to the investigation, supervision, writing, review, and editing of the study. The study was conceptualized by R.A.-P., J.M.Á., A.A.M., Á.Z.-M., and J.J.S.-E. Data curation, data visualization, and analysis were carried out by J.C.B., R.L.P., and Ó.A.-E. All authors have read and agreed to the published version of the manuscript.

Acknowledgments: The authors would like to thank Santiago López Martínez for his invaluable assistance in this study.

Conflicts of Interest: The authors declare no conflict of interest.

References

1. Peters, O.A. Current challenges and concepts in the preparation of root canal systems: A review. *J. Endod.* **2004**, *30*, 559–567. [CrossRef] [PubMed]
2. Pedullà, E.; Lo Savio, F.; Boninelli, S.; Plotino, G.; Grande, N.M.; La Rosa, G.; Rapisarda, E. Torsional and Cyclic Fatigue Resistance of a New Nickel-Titanium Instrument Manufactured by Electrical Discharge Machining. *J. Endod.* **2016**, *42*, 156–159. [CrossRef] [PubMed]
3. Walia, H.; Brantley, W.A.; Gerstein, H. An initial investigation of the bending and torsional properties of Nitinol root canal files. *J. Endod.* **1988**, *14*, 346–351. [CrossRef]

4. Li, U.M.; Lee, B.S.; Shih, C.T.; Lan, W.H.; Lin, C.P. Cyclic fatigue of endodontic nickel titanium rotary instruments: Static and dynamic tests. *J. Endod.* **2002**, *28*, 448–451. [CrossRef] [PubMed]
5. Gutmann, J.L.; Gao, Y. Alteration in the inherent metallic and surface properties of nickel-titanium root canal instruments to enhance performance, durability and safety: A focused review. *Int. Endod. J.* **2012**, *45*, 113–128. [CrossRef]
6. Pirani, C.; Cirulli, P.P.; Chersoni, S.; Micele, L.; Ruggeri, O.; Prati, C. Cyclic fatigue testing and metallographic analysis of nickel-titanium rotary instruments. *J. Endod.* **2011**, *37*, 1013–1016. [CrossRef]
7. De Arruda Santos, L.; Bahia, M.G.; de Las Casas, E.B.; Buono, V.T. Comparison of the mechanical behaviour between controlled memory and superelastic nickel-titanium files via Finite Element Analysis. *J. Endod.* **2013**, *39*, 1444–1447. [CrossRef]
8. Plotino, G.; Testarelli, L.; Al-Sudani, D.; Pongione, G.; Grande, N.M.; Gambarini, G. Fatigue resistance of rotary instruments manufactured using different nickel-titanium alloys: A comparative study. *Odontology* **2014**, *102*, 31–35. [CrossRef]
9. Sattapan, B.; Nervo, G.J.; Palamara, J.E.; Messer, H.H. Defects in rotary nickel titanium files after clinical use. *J. Endod.* **2000**, *26*, 161–165. [CrossRef]
10. Inan, U.; Gonulol, N. Deformation and fracture of Mtwo rotary nickel-titanium instruments after clinical use. *J. Endod.* **2009**, *35*, 1396–1399. [CrossRef]
11. Plotino, G.; Grande, N.M.; Cordaro, M.; Testarelli, L.; Gambarini, G. A review of cyclic fatigue testing of nickel-titanium rotary instruments. *J. Endod.* **2009**, *35*, 1469–1476. [CrossRef] [PubMed]
12. Bhagabati, N.; Yadav, S.; Talwar, S. An in vitro cyclic fatigue analysis of different endodontic nickel-titanium rotary instruments. *J. Endod.* **2012**, *38*, 515–518. [CrossRef] [PubMed]
13. Lopes, H.P.; Gambarra-Soares, T.; Elias, C.N.; Siqueira, J.F.; Inojosa, I.F.; Lopes, W.S.; Vieira, V.T. Comparison of the mechanical properties of rotary instruments made of conventional nickel-titanium wire, M-wire, or nickel-titanium alloy in R-phase. *J. Endod.* **2013**, *39*, 516–520. [CrossRef] [PubMed]
14. ANSI/ADA. *Root Canal Files and Reamers, Type K for Hand Use*; Specification N° 28–2002; American Dental Association: Chicago, IL, USA, 2002.
15. ISO. *ISO 3630–3631: Dentistry—Root Canal Instruments—Part 1: General Requirements and Test Methods*; ISO: Geneva, Switzerland, 2008.
16. Schneider, S.W. A comparison of canal preparations in straight and curved root canals. *Oral Surg. Oral Med. Oral Pathol.* **1971**, *32*, 271–275. [CrossRef]
17. Topçuoğlu, H.S.; Topçuoğlu, G.; Akti, A.; Düzgün, S. In vitro comparison of cyclic fatigue resistance of ProTaper Next, HyFlex CM, OneShape, and ProTaper Universal instruments in a canal with a double curvature. *J. Endod.* **2016**, *42*, 969–971. [CrossRef]
18. Mandel, E.; Adib-Yazdi, M.; Benhamou, L.M.; Lachkar, T.; Mesgouez, C.; Sobel, M. Rotary Ni-Ti profile systems for preparing curved canals in resin blocks: Influence of operator on instrument breakage. *Int. Endod. J.* **1999**, *32*, 436–443. [CrossRef]
19. Yared, G.M.; Dagher, F.E.; Machtou, P.; Kulkarni, G.K. Influence of rotational speed, torque and operator proficiency on failure of Greater Taper files. *Int. Endod. J.* **2002**, *35*, 7–12. [CrossRef]
20. Zelada, G.; Varela, P.; Martín, B.; Bahillo, J.G.; Magán, F.; Ahn, S. The effect of rotational speed and the curvature of root canals on the breakage of rotary endodontic instruments. *J. Endod.* **2002**, *28*, 540–542. [CrossRef]
21. Martín, B.; Zelada, G.; Varela, P.; Bahillo, J.G.; Magán, F.; Ahn, S.; Rodríguez, C. Factors influencing the fracture of nickel-titanium rotary instruments. *Int. Endod. J.* **2003**, *36*, 262–266. [CrossRef]
22. Parashos, P.; Gordon, I.; Messer, H.H. Factors influencing defects of rotary nickel-titanium instruments after clinical use. *J. Endod.* **2004**, *30*, 722–725. [CrossRef]
23. Ferreira, F.; Adeodato, C.; Barbosa, I.; Aboud, L.; Scelza, P.; Zaccaro Scelza, M. Movement kinematics and cyclic fatigue of NiTi rotary instruments: A systematic review. *Int. Endod. J.* **2017**, *50*, 143–152. [CrossRef] [PubMed]
24. Roland, D.D.; Andelin, W.E.; Browning, D.F.; Hsu, G.-H.R.; Torabinejad, M. The effect of preflaring on the rates of separation for 0.04 taper nickel titanium rotary instruments. *J. Endod.* **2002**, *28*, 543–545. [CrossRef] [PubMed]
25. Patiño, P.V.; Biedma, B.M.; Liébana, C.R.; Cantatore, G.; Bahillo, J.G. The influence of manual glide path on the separation rate of NiTi rotary instruments. *J. Endod.* **2005**, *31*, 114–116. [CrossRef] [PubMed]

26. Gambarini, G.; Galli, M.; Di Nardo, D.; Seracchiani, M.; Donfrancesco, O.; Testarelli, L. Differences in cyclic fatigue lifespan between two different heat treated NiTi endodontic rotary instruments: WaveOne Gold vs EdgeOne Fire. *J. Clin. Exp. Dent.* **2019**, *11*, 609–613. [CrossRef] [PubMed]
27. Hilfer, P.B.; Bergeron, B.E.; Mayerchak, M.J.; Roberts, H.W.; Jeansonne, B.G. Multiple autoclave cycle effects on cyclic fatigue of nickel-titanium rotary files produced by new manufacturing methods. *J. Endod.* **2011**, *37*, 72–74. [CrossRef] [PubMed]
28. Dederich, D.N.; Zakariasen, K.L. The effects of cyclical axial motion on rotary endodontic instrument fatigue. *Oral Surg. Oral Med. Oral Pathol.* **1986**, *61*, 192–196. [CrossRef]
29. Ray, J.J.; Kirkpatrick, T.C.; Rutledge, R.E. Cyclic fatigue of EndoSequence and K3 rotary files in a dynamic model. *J. Endod.* **2007**, *33*, 1469–1472. [CrossRef]
30. Hülsmann, M.; Donnermeyer, D.; Schäfer, E. A critical appraisal of studies on cyclic fatigue resistance of enginedriven endodontic instruments. *Int. Endod. J.* **2019**, *52*, 1427–1445. [CrossRef]
31. Lopes, H.P.; Britto, I.M.; Elias, C.N.; Machado de Oliveira, J.C.; Neves, M.A.; Moreira, E.J.; Siqueira, J.F. Cyclic fatigue resistance of ProTaper Universal instruments when subjected to static and dynamic tests. *Oral Surg. Oral Med. Oral Pathol. Oral Radiol. Endod.* **2010**, *110*, 401–404. [CrossRef]
32. Lopes, H.P.; Elias, C.N.; Vieira, M.V.; Siqueira, J.F.; Mangelli, M.; Lopes, W.S.; Vieira, V.T.; Alves, F.R.; Oliveira, J.C.; Soares, T.G. Fatigue life of Reciproc and Mtwo instruments subjected to static and dynamic tests. *J. Endod.* **2013**, *39*, 693–696. [CrossRef]
33. Rodrigues, R.C.; Lopes, H.P.; Elias, C.N.; Amaral, G.; Vieira, V.T.; De Martin, A.S. Influence of different manufacturing methods on the cyclic fatigue of rotary nickel-titanium endodontic instruments. *J. Endod.* **2011**, *37*, 1553–1557. [CrossRef] [PubMed]
34. Gambarra-Soares, T.; Lopes, H.P.; Olivieira, J.C.M.; Chaves Souza, L.; Vieira, V.T.L.; Elias, C.N. Dynamic or static cyclic fatigue tests: Which best determines the lifespan of endodontic files? *ENDO Endod. Pract. Today* **2013**, *7*, 101–104.
35. De-Deus, G.; Vieira, V.T.; da Silva, E.J.; Lopes, H.; Elias, C.N.; Moreira, E.J. Bending resistance and dynamic and static cyclic fatigue life of Reciproc and WaveOne large instruments. *J. Endod.* **2014**, *40*, 575–579. [CrossRef] [PubMed]
36. Plotino, G.; Grande, N.; Mazza, C.; Petrovic, R.; Testarelli, L.; Gambarini, G. Influence of size and taper of artificial canals on the trajectory of NiTi instruments in cyclic fatigue studies. *Oral Surg. Oral Med. Oral Pathol. Oral Radiol. Endod.* **2010**, *109*, 60–66. [CrossRef]

Journal of
Clinical Medicine

MDPI

Article

Effect of Rotational Speed on the Resistance of NiTi Alloy Endodontic Rotary Files to Cyclic Fatigue—An In Vitro Study

Vicente Faus-Matoses [1], Vicente Faus-Llácer [1], Celia Ruiz-Sánchez [1], Sharon Jaramillo-Vásconez [1], Ignacio Faus-Matoses [1,*], Benjamín Martín-Biedma [2] and Álvaro Zubizarreta-Macho [3,4]

[1] Department of Stomatology, Faculty of Medicine and Dentistry, University of Valencia, 46010 Valencia, Spain; vicente.faus@uv.es (V.F.-M.); fausvj@uv.es (V.F.-L.); ceruizsan@gmail.com (C.R.-S.); sjavas@alumni.uv.es (S.J.-V.)
[2] Department of Surgery and Medical-Surgical Specialties, School of Medicine and Dentistry, Universidad de Santiago de Compostela, 15705 Santiago de Compostela, Spain; benjamin.martin@usc.es
[3] Department of Implant Surgery, Faculty of Health Sciences, Alfonso X El Sabio University, 28691 Madrid, Spain; amacho@uax.es.
[4] Department of Surgery, Faculty of Medicine and Dentistry, University of Salamanca, 37008 Salamanca, Spain
* Correspondence: ignacio.faus@uv.es

Abstract: The present study aims to evaluate and contrast the function of the rotational speed of NiTi alloy endodontic rotary files on how resistant they are to dynamic cyclic fatigue. Methods: A total of 150 NiTi alloy endodontic rotary files with similar geometrical design and metallurgical properties were randomly divided into study groups: Group A: 200 rpm (n = 30); Group B: 350 rpm (n = 30); Group C: 500 rpm (n = 30); Group D: reciprocating movement at 350 rpm with 120° counterclockwise and 30° clockwise motion (350 rpm+) (n = 30); and Group E: reciprocating movement at 400 rpm with 120° counterclockwise and 30° clockwise motion (400 rpm+) (n = 30). A dynamic device was designed to carry out dynamic cyclic fatigue tests using artificial root canal systems made from stainless steel with an apical diameter of 250 μm, 5 mm radius of curvature, 60° curvature angle, and 6% taper, and 20 mm in length. A Weibull statistical analysis and ANOVA test were used to analyze the results. Results: The ANOVA analysis showed differences in time to failure among all the study groups that were of statistical significance ($p < 0.001$). Conclusions: NiTi alloy endodontic rotary files using reciprocating movement at 350 rpm with 120° counterclockwise and 30° clockwise motion exhibit greater resistance to dynamic cyclic fatigue than files used with a reciprocating movement at 400 rpm with 120° counterclockwise and 30° clockwise motion, continuous rotational speed at 200 rpm, continuous rotational speed at 350 rpm, or continuous rotational speed at 500 rpm; it is therefore advisable to use reciprocating movements at a low speed.

Keywords: continuous rotation; cyclic fatigue; endodontics; endodontic rotary file; reciprocating; speed; resistance

Citation: Faus-Matoses, V.; Faus-Llácer, V.; Ruiz-Sánchez, C.; Jaramillo-Vásconez, S.; Faus-Matoses, I.; Martín-Biedma, B.; Zubizarreta-Macho, Á. Effect of Rotational Speed on the Resistance of NiTi Alloy Endodontic Rotary Files to Cyclic Fatigue—An In Vitro Study. *J. Clin. Med.* **2022**, *11*, 3143. https://doi.org/10.3390/jcm11113143

Academic Editors: Massimo Amato, Giuseppe Pantaleo, Alfredo Iandolo and Gianrico Spagnuolo

Received: 2 May 2022
Accepted: 30 May 2022
Published: 31 May 2022

1. Introduction

Chemical disinfection and mechanical instrumentation of the root canal system are crucial in the prevention of apical periodontitis that arises due to treatment, or to cure it if already established [1]. However, the failure of nickel–titanium (NiTi) alloy endodontic rotatory files remains a major dilemma for endodontists during root canal treatment, despite the NiTi alloy undergoing continuous chemical and mechanical enhancements by manufacturers so as to help prevent complications during endodontic therapy [2]. The fracture of NiTi alloy endodontic rotary files can be caused by torsional fatigue, cyclic fatigue, or some combination thereof [3]. Torsional failure happens when the end of a NiTi alloy endodontic rotary file has become trapped on one of the root canal walls while the

instrument is still rotating, causing the file to fracture once the elasticity of the material has been exceeded [4,5]. Flexural bending fatigue is caused by the repeated application of compression and traction cycles that the NiTi alloy endodontic rotary file experiences at the site of maximum curvature of the root canal; these stresses subsequently lead to plastic deformation, which can result in unexpected file fracture [3,6].

Several studies have reported that a fractured fragment of the NiTi alloy endodontic rotary file may block the curved canal, negatively affecting the treatment outcome, as disinfecting agents can no longer reach the infected root canal areas [1,7,8]. Additionally, root canal systems that have not been properly disinfected may have a lower likelihood of healing in teeth with periapical lesions [9].

Several additional factors have been linked to the fracture of NiTi alloy endodontic rotary files, including instruments with a cross-section design [10], taper and apical diameter [11], flute length, pitch, and helix angle [12]. In addition, the dynamics of the instrument, such as torque [13] and canal geometry [8], as well as the manufacturing process, whether electropolishing, heat treatment, or ion implantation [14], can influence the risk of fracture.

It remains unclear whether or not rotational speed affects the resistance to cyclic fatigue of NiTi alloy endodontic rotary files. Yared et al. and Martín et al. have found that rotational speed does indeed influence the prevalence of fracture in NiTi alloy endodontic rotary files [15,16]. However, Pruett et al. showed that rotational speed had no significant impact on the risk of fracture of NiTi alloy endodontic rotary files [8]. Additionally, some studies have reported that reciprocating motion may overextend the cyclic fatigue life of NiTi alloy endodontic files in comparison to continuous motion [17,18].

The present study aims to evaluate and assess the effect of the rotational speed of NiTi alloy endodontic rotary files on their resistance to dynamic cyclic fatigue, with a null hypothesis (H_0) postulating that rotational speed has no effect on how resistant NiTi alloy endodontic rotary files are to dynamic cyclic fatigue.

2. Materials and Methods

2.1. Study Design

One hundred and fifty (150) sterile, brand new endodontic rotary files with a parallelogram cross-section design, 6% taper, and 250 μm apical diameter (Ref.: IRE 02506, D, Endogal, Galician Endodontics Company, Lugo, Spain) were randomly distributed among different study groups: Group A: continuous rotational speed at 200 rpm (200 rpm) (n = 30); Group B: continuous rotational speed at 350 rpm (350 rpm) (n = 30); Group C: continuous rotational speed at 500 rpm (500 rpm) (n = 30); Group D: reciprocating movement at 350 rpm with 120° counterclockwise and 30° clockwise motion (350 rpm+) (n = 30); and Group E: reciprocating movement at 400 rpm with 120° counterclockwise and 30° clockwise motion (400 rpm+) (n = 30). The final total of experimental units included was 150, with these being assigned to one of the five study groups in keeping with the proportions determined by the researchers. The power was set at 80% and testing the null hypothesis H_0 resulted in an effect size of 0.606. A single-factor ANOVA test for independent samples was used to make equal the mean values of the five groups, and the significance level was set at 5%. A microscope (OPMI pico, Zeiss, Oberkochen, Germany) was used to examine all NiTi alloy endodontic rotary files (Ref.: IRE 02506, D, Endogal, Galician Endodontics Company, Lugo, Spain) prior to use, with no files discarded. Between January and July 2022, this controlled experiment was conducted at the Department of Stomatology of the Faculty of Medicine and Dentistry at the University of Valencia (Valencia, Spain).

2.2. Analysis with Scanning Electron Microscopy

A scanning electron microscope (SEM) (HITACHI S-4800, Fukuoka, Japan) was used at ×30 and ×600 for the initial inspection of the NiTi alloy endodontic rotary files (Ref.: IRE

02506, D, Endogal, Galician Endodontics Company, Lugo, Spain). This analysis was conducted at the Central Support Service for Experimental Research of the University of Valencia in Burjassot, Spain. The analysis was carried out with the following exposure parameters: 20 kV acceleration voltage; magnification from 100× to 6500×; and resolution ranging from −1.0 nm at 15 kV to 2.0 nm at 1 kV. Researchers did this to evaluate the surface characteristics and ensure there were no manufacturing surface defects.

2.3. Analysis with Energy-Dispersive X-ray Spectroscopy

In addition, energy-dispersive X-ray spectroscopy (EDX) was also used to analyze all the NiTi alloy endodontic rotary files (Ref.: IRE 02506, D, Endogal, Galician Endodontics Company, Lugo, Spain). This was conducted at the Central Support Service for Experimental Research at the University of Valencia in Burjassot, Spain. This inspection used these exposure parameters: 20 kV acceleration voltage; magnification from 100× to 6500×; and resolution ranging from −1.0 nm at 15 kV to 2.0 nm at 1 kV. These parameters were used to assess the elemental makeup of the chemicals in the files used to test their resistance to static fatigue. The researchers also evaluated the atomic weight percent, taking measurements from three different sections (apical third, medium third, and coronal third of the NiTi alloy endodontic files).

2.4. Experimental Model Simulating Dynamic Cyclic Fatigue

The researchers conducted tests of resistance to dynamic cyclic fatigue at room temperature (20 °C) to evaluate the mechanical behavior of the instruments, according to Martins et al. [19], using the aforementioned customized device (Utility Model Patent No. ES1219520) [20]. CAD/CAE 2D/3D software (Midas FX+®, Brunleys, Milton Keynes, UK) was used to design the structure of the device, which was subsequently created with 3D-printing software (ProJet® 6000 3D Systems©, Rock Hill, SC, USA) (Figure 1).

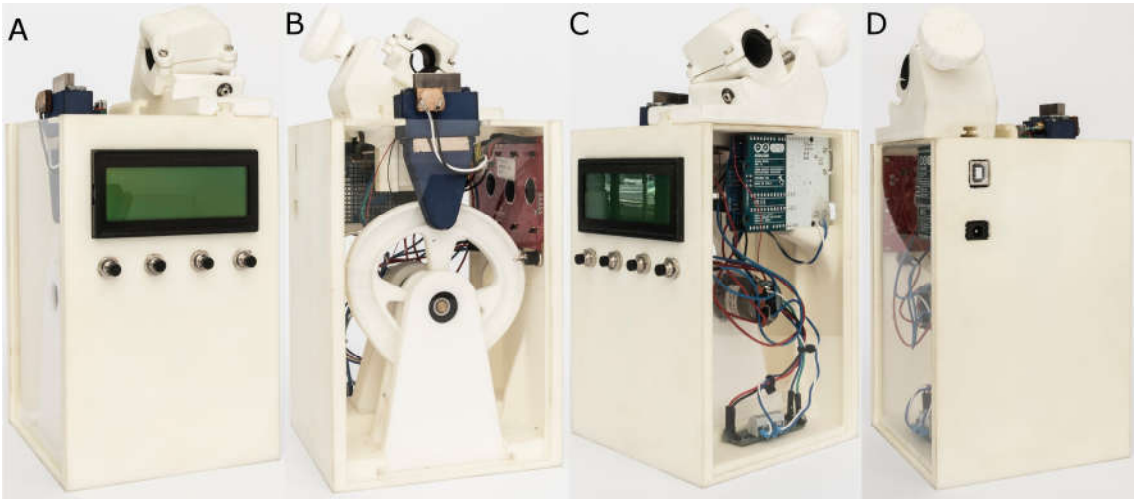

Figure 1. (**A**) Front, (**B**) back, (**C**) right, and (**D**) left sides of the dynamic cyclic fatigue device.

The customized artificial root canals were performed using Schneider's measuring technique, with a curvature of 60° [21] and a 5 mm curvature radius. The inverse engineering software used for this purpose was CAD/CAE 2D/3D. Molybdenum wire-cut technology (Cocchiola S.A., Buenos Aires, Argentina) was used with electrical discharge machining (EDM) to create the artificial root canal from stainless steel. Researchers also ensured that the NiTi files were flush with the walls of the artificial root canal. This newly created artificial canal was then positioned on its support, and a light-dependent resistor (LDR) sensor (Ref.: C000025, Arduino LLC®, Ivrea, Italy) placed at the apex of the canal was used to identify any failures in the endodontic rotary instruments (Ref.: IRE 02506, D,

Endogal, Galician Endodontics Company, Lugo, Spain). This device works by measuring the light source continuously generated by a very strong white LED (20,000 mcd) (Ref.: 12.675/5/b/c/20k, Batuled, Coslada, Spain). The LED was positioned opposite the artificial root canal. An LED LDR sensor (Ref.: C000025, Arduino LLC®) at 50 ms was used to interpret the LED signals so as to identify the precise time of failure.

A roller bearing system (Ref.: MR104ZZ, FAG, Schaeffler Herzogenaurach, Herzogenaurach, Germany) was used to apply the movement direction and speed indicated by the operator (Ref.: DRV8835, Pololu® Corporation, Las Vegas, NV, USA) and created by the brushed DC gear motor (Ref.: 1589, Pololu® Corporation, Las Vegas, NV, USA) to the artificial support. The support was maneuvered in an exclusively axial motion with the help of a linear guide (Ref.: HGH35C 10249-1 001 MA, HIWIN Technologies Corp. Taichung, Taiwan). A torque-controlled motor and 6:1 reduction handpiece (X-Smart plus, Dentsply Maillefer, Baillagues, Switzerland) were used in conjunction with the NiTi endodontic rotary files.

A frequency of 60 pecks per minute was used for the NiTi endodontic files within the dynamic cyclic fatigue device, following the parameters of a prior study [19]. Researchers also applied a high-flow synthetic oil (Singer All-Purpose Oil; Singer Corp., Barcelona, Spain) to help prevent friction between the NiTi endodontic files and the walls of the artificial root canal; this oil is specifically formulated for the lubrication of mechanical parts.

The files were all used until failure. The researchers recorded and evaluated both the length of time and the number of cycles the files took to fracture.

2.5. Statistical Tests

Statistical analysis of all variables was performed using SAS 9.4 (SAS Institute Inc., Cary, NC, USA). The mean value and SD were used to express the descriptive statistics of the quantitative variables. The researchers then used an ANOVA test to perform a comparative analysis of the number of cycles to failure and the time to failure (in seconds). In 2-to-2 comparisons, the Tukey method was used to determine the p-values and correct any Type I errors. The researchers also calculated the Weibull modulus and Weibull characteristic strength. Statistical significance was defined as $p < 0.05$.

3. Results

Scanning electron microscopy (SEM) analysis of the NiTi alloy endodontic rotary files did not detect any structural alterations or accumulated organic matter. Additionally, due to the laser machining process used to make them, the manufacturing lines were parallel to each other and perpendicular to the longitudinal axis of the files. The distance and width between these manufacturing lines were indicators of the precision and intensity of the laser machining manufacturing process. The laser machining process also resulted in tubular porosity that was observed in the files. Additionally, tubular porosity was visible in all of the NiTi alloy endodontic rotary files as a result of the combination of other chemical elements with the Ti alloys (Figure 2).

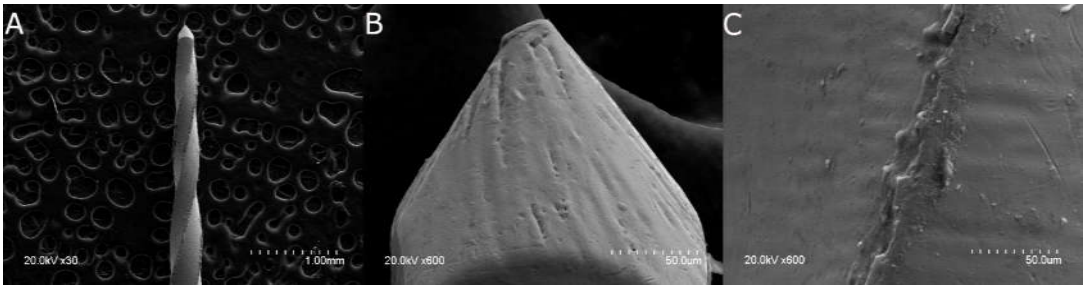

Figure 2. (**A**) SEM images of the full-length NiTi alloy endodontic rotary files (Ref.: IRE 02506, D, Endogal, Galician Endodontics Company, Lugo, Spain) at × 30, (**B**) and specifically of the end of the file at × 600 and (**C**) the surface of the file at × 600.

EDX micro-analysis of the NiTi alloy endodontic rotary files was performed at three different locations at 20 kV, enabling a thorough and precise analysis of the composition of the NiTi alloy endodontic rotary files. Through EDX micro-analysis at 20 kV, the NiTi alloy endodontic rotary files were found to comprise Ti (37.59–34.52 wt.%) and Ni (34.19–38.81 wt.%), although O and C were also observed (Figure 3).

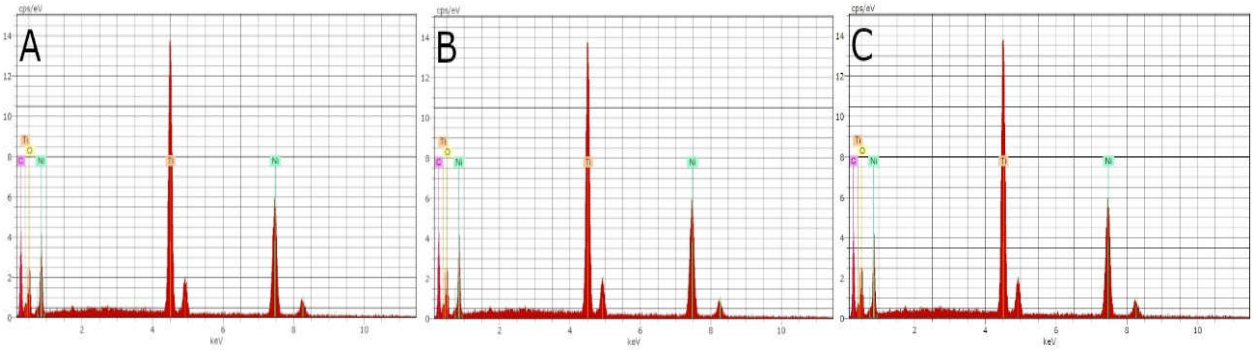

Figure 3. EDX micro-analysis of the NiTi alloy endodontic rotary files at locations (**A**) 1, (**B**) 2, and (**C**) 3.

Table 1 and Figure 4 show the mean and SD values of the time to failure (in seconds) across all study groups.

Table 1. Descriptive analysis of time to failure (seconds).

Study Group	*n*	Mean	SD	Minimum	Maximum
200 rpm	30	364.30 [a]	6.71	352.38	375.49
350 rpm	30	282.42 [b]	7.19	261.90	293.71
500 rpm	30	143.84 [c]	5.70	132.08	152.39
350 rpm +	30	590.38 [d]	11.19	561.37	608.08
400 rpm +	30	488.44 [e]	12.93	462.19	512.33

[a, b, c, d, e] Statistically significant differences among groups ($p < 0.05$).

The ANOVA analysis found there were differences of statistical significance among all of the study groups with regard to the time to failure ($p < 0.001$) (Figure 5). The results of the time to failure could be applied to the "number of cycles to failure" since all of the NiTi endodontic files were used at a frequency of 60 pecks per minute within the dynamic cyclic fatigue device.

The Weibull statistics scale distribution parameter (η) identified differences of statistical significance among all of the study groups with regard to the time to failure ($p < 0.001$) (Table 2, Figure 5). The Weibull statistics shape distribution parameter (β) revealed differences great enough to be statistically significant with regard to time to failure between the 200 rpm and 400 rpm+ groups ($p = 0.0236$), the 500 rpm and 350 rpm+ groups ($p = 0.0003$), the 350 rpm+ and 400 rpm+ groups ($p = 0.0154$), the 350 rpm and 500 rpm groups ($p = 0.0152$), and the 200 rpm and 500 rpm groups ($p = 0.0005$). However, there were not enough differences observed in the time to failure between the 350 rpm and 400 rpm+ groups ($p = 0.2283$), the 500 rpm and 400 rpm groups ($p = 0.1908$), the 200 rpm and 350 rpm+ groups ($p = 0.08925$), the 350 rpm and 350 rpm+ groups ($p = 0.2492$), and the 200 rpm and 350 rpm groups ($p = 0.3123$) to be statistically significant (Table 2, Figure 5). In short, the NiTi alloy endodontic rotary systems exhibited very predictable behavior, as it took about the same amount of time for the majority of the endodontic rotary files within each study group to reach the point of failure. The more gradual slope seen when using the NiTi endodontic rotary files at 350 rpm+ would indicate that this behavior is easier to predict than other kinematics. The NiTi alloy endodontic rotary files at 350 rpm+ were shown to be the most

resistant to cyclic fatigue, followed by the NiTi alloy endodontic rotary files at 400 rpm+, 200 rpm, 350 rpm, and 500 rpm.

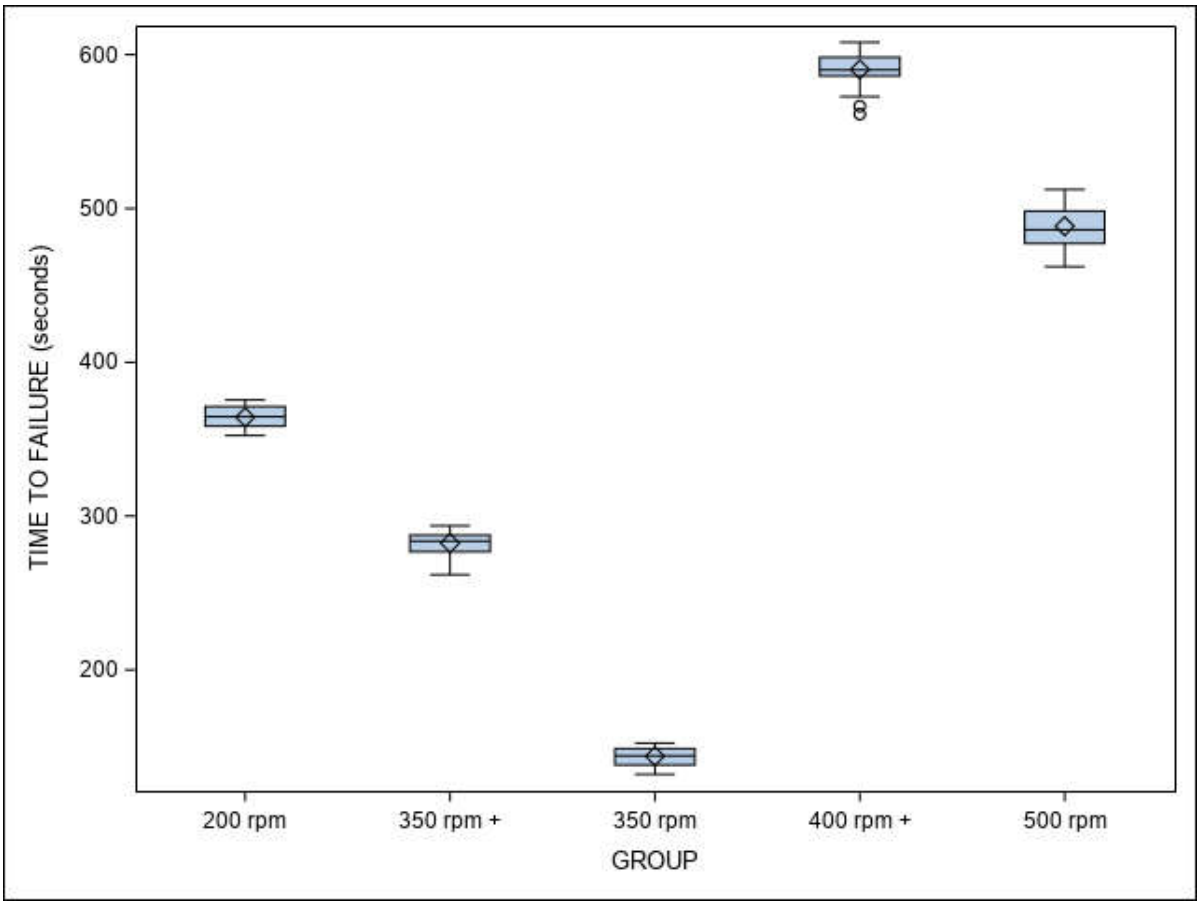

Figure 4. Box plot of time to failure. The median value of the respective study groups is represented by the horizontal line in each box. ◊—Box plot mean value. O—Extrema value.

Table 2. Weibull statistics for the time to failure across the study groups.

Study Group	Weibull Shape (β)				Weibull Scale (η)			
	Estimate	St Error	Lower	Upper	Estimate	St Error	Lower	Upper
200 rpm	61.9124	8.8223	46.8258	81.8598	367.5283	1.1471	365.2868	369.7836
350 rpm	50.3905	7.3394	37.8766	67.0388	285.6319	1.0898	283.5039	287.7759
500 rpm	30.5162	4.4688	22.9024	40.6611	146.4785	0.9251	144.6765	40.6611
350 rpm+	63.6086	8.9083	48.3399	83.7000	595.4815	1.8047	591.9549	599.0291
400 rpm+	39.6357	5.3913	30.3603	51.7449	494.7559	2.4189	490.0376	499.5197

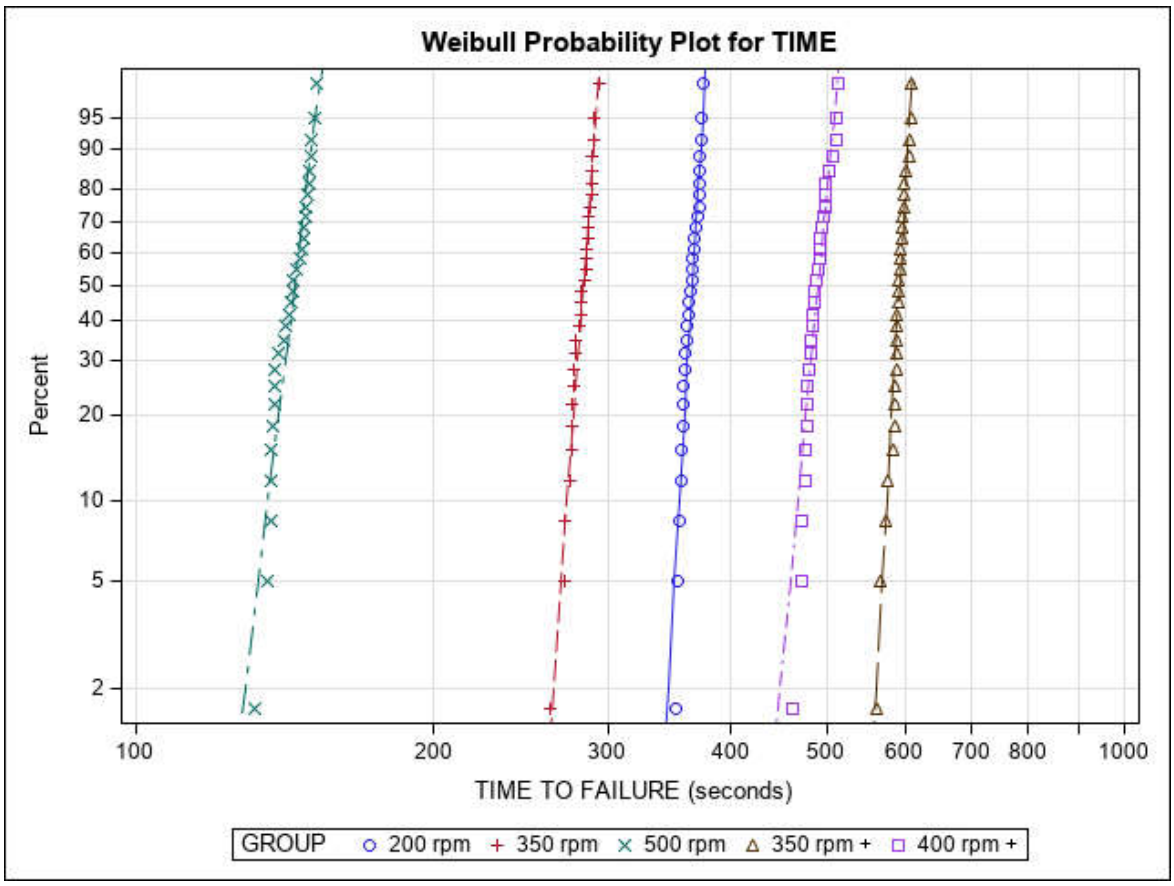

Figure 5. Weibull probability plot displaying time to failure across study groups.

4. Discussion

The findings of the present study do not accept the null hypothesis (H_0), which postulates that rotational speed does not affect the dynamic fatigue resistance of NiTi alloy endodontic rotary files.

The present study used the same NiTi alloy endodontic instruments in rotary and reciprocating kinematic motion since the manufacturer reported that the geometrical design of the NiTi alloy endodontic files allows for its use in both kinematic movements; therefore, manufacturers recommend its use with both continuous and reciprocating rotations. Furthermore, other instrumentation systems can be used with continuous or reciprocating rotation, and it is necessary to have a motor in which the angles can be adjusted. Clear examples can be found in the studies of Yared 2008 [22] and De Deus 2010 [17], where they used instruments that cut clockwise in a reciprocating mode.

Previous studies have analyzed the effects of rotational speed on the number of cycles to fracture of rotary NiTi instruments. Lopes et al. subjected ProTaper Universal instruments F3 and F4 to 300 and 600 rpm; however, the speed values selected were too distant, a cylindrical tube was used as the artificial root canal, and the fracture detection of the NiTi alloy endodontic rotary files was subjective and therefore imprecise. Furthermore, they did not carry out any additional measurement methods [23]. Additionally, some reviews have been conducted with the aim of analyzing the mechanical and metallurgical behavior of endodontic instruments under different testing conditions and methodologies [24–26].

The results derived from the present study indicate that the resistance of NiTi alloy endodontic rotary files to cyclic fatigue is inversely proportional to the rotational speed. In addition, reciprocating movements were shown to be more resistant to cyclic fatigue

when compared with continuous rotational movements. Moreover, the results derived from the present study present a direct application to the clinical setting, since the reciprocating systems provided higher resistance to cyclic fatigue, followed by the lower values of rotational speed. Therefore, clinicians should choose reciprocating motion systems or reduce the rotational speed of the endodontic torque-controlled motor if the NiTi endodontic rotary or reciprocating file is expected to experience high cyclic fatigue, particularly in root canal systems with a pronounced angle and/or curvature radius.

Specification #28 of the American Dental Association/American National Standards Institute (ADA/ANSI) outlines tests used to measure how flexible stainless steel hand files are, as well as their strength under torsion. These same tests were also adopted under ISO 3630/1, which is meant for instruments with a 0.02 ISO taper. Currently, there are still no specifications or international standards with regard to testing the resistance of endodontic rotary instruments to cyclic fatigue [27]. The ideal model would entail curved canals being instrumented in natural teeth. That being said, each tooth can only be used once with these tests, and instrumentation causes changes to the shape of the root canal, rendering it impossible to establish standardized experimental conditions. Therefore, various methods and devices have been used to analyze the in vitro resistance of NiTi rotary endodontic instruments to cyclic fatigue fractures [28]. Cyclic fatigue is considered a dynamic event itself since the movement of the NiTi alloy endodontic rotary or reciprocating instruments inside the root canal system gives it dynamism. Cyclic fatigue tests have been carried out in a static model under well-controlled experimental conditions; however, the novel pecking movement of the endodontic handpiece of the present cyclic fatigue device provides an additional dynamic movement more representative of the in-and-out motion made by the operator. That being said, studies have shown that the number of cycles to failure is significantly higher in the dynamic model, regardless of the brand or manufacturing processes [29–31]. In the static testing model, there is no up-and-down movement applied to the instrument, causing stresses to accumulate at a fixed point. With the dynamic model, however, these stresses are spread out along the full length of the instrument, thereby increasing its cyclic fatigue resistance [23]. Furthermore, researchers have found that the up-and-down motion should not exceed 1, 2, or 3 mm/s in the dynamic testing model so as to simulate clinical conditions [24]. An automatic detection system can be used to identify the precise point of failure of endodontic rotary files [19]. Given this, the present study used an anatomically based artificial root canal design in accordance with Schneider's method [20], using a 60° curvature angle and radius of 5 mm, and modifying the geometry to adapt to the NiTi endodontic rotary files used in this study [11].

The findings of this study corroborate the findings of Kim et al., who found that the Reciproc R25 and WaveOne Primary heat-treated NiTi alloy endodontic reciprocating files were more resistant to torsion and cyclic fatigue when compared with ProTaper F2 NiTi alloy endodontic rotary files used under continuous rotation [32]. Similarly, De Deus et al. found that the ProTaper F2 NiTi alloy endodontic rotary file also exhibited significantly greater resistance to cyclic fatigue when employed using reciprocating movement rather than continuous rotational motion [17]. Furthermore, several other studies have emphasized the increase in the lifespan of NiTi alloy endodontic rotary files when using reciprocating movement as opposed to continuous rotational motion [33,34]. That being said, there are several studies that have analyzed the impact of rotational speed on how resistant NiTi alloy endodontic rotary files are to cyclic fatigue, although the findings remain controversial. Lopes et al. found that the ProFile NiTi alloy endodontic rotary instrument exhibited greater susceptibility to accidental fracture at higher rotational speeds, and they found that the total number of cycles to failure was about 30% lower in ProTaper instruments when the rotational speed was increased from 300 to 600 rpm [23]. On the other hand, Martin et al. reported that unexpected fracture of NiTi alloy endodontic rotary instruments was correlated with the rotational speed, as the ProTaper NiTi alloy endodontic rotary instrument was more susceptible to fracture at 350 rpm than at 250 or 150 rpm [16]. However, Gao et al. reported no statistically significant differences ($p > 0.05$)

between files that had similar NiTi alloys and apical diameters when used at different rotational speeds [35]. The discrepancies in these findings may be due to differing study designs, NiTi alloys, or geometrical designs of the instruments under study. Additionally, not only the asymmetric oscillatory counterclockwise motion (reciprocation motion) but also the asymmetric oscillatory clockwise motion can be used with any rotary instrument. Martins et al. evaluated the cyclic fatigue resistance of three replicate rotary instruments compared with their original brand systems using continuous rotation and optimum torque reverse kinematics. They reported that reciprocating files showed greater resistance to cyclic fatigue than continuous rotation files, and the replicas showed higher cyclic fatigue resistance than the original brand instruments and higher transition temperatures to the austenitic phase [36].

The results found by Ray et al. were corroborated by those obtained in the present study using an analysis of dynamic cyclic fatigue when employing a standardized axial movement, increasing the durability of NiTi alloy endodontic rotary instruments subjected to cyclic fatigue in comparison with the results observed in static cyclic fatigue devices [37]. Most studies comparing dynamic and static cyclic fatigue appliances have concluded endodontic rotary instruments exhibited a time to fracture roughly 20–40% longer when undergoing dynamic cyclic fatigue than the time to fracture found in studies of static cyclic fatigue, with this also being more similar to the clinical setting [38–40].

The cyclic fatigue testing was performed in a room temperature setting, according to the results by La Rosa et al., who showed that studies at body temperature impaired the cyclic fatigue resistance of most files [41]. In addition, Plotino et al. reported that the surrounding temperature affected the NiTi crystalline phase transformation, significantly decreasing the cyclic fatigue resistance at body temperature [42].

Regrettably, the limitations of this study precluded analyzing any additional kinematic movements, under both reciprocating and continuous rotation movements. Future studies ought to include more NiTi alloys, apical diameters, pitch, helix angles, manufacturing processes, and tapers. Furthermore, due to difficulties with the standardization of samples, the present study was not conducted in a clinical setting. However, the present study provided multimethod research, including SEM, EDX, and an accurate dynamic cyclic fatigue device, increasing the knowledge of the mechanical behavior of NiTi endodontic rotary files under different kinematic conditions.

5. Conclusions

NiTi alloy endodontic rotary files used with a reciprocating movement at 350 rpm with 120° counterclockwise and 30° clockwise motion were more resistant to dynamic cyclic fatigue than those used with a reciprocating movement at 400 rpm with 120° counterclockwise and 30° clockwise motion, continuous rotational speed at 200 rpm, continuous rotational speed at 350 rpm, and continuous rotational speed at 500 rpm. It is therefore advisable to use reciprocating movements at a low speed.

Author Contributions: Conceptualization, V.F.-M., S.J.-V.; data acquisition, V.F.-L.; design, I.F.-M.; review and editing, B.M.-B.; Formal analysis, C.R.-S.; all statistical analyses, Á.Z.-M. All authors have read and agreed to the published version of the manuscript.

Funding: This research did not receive any external funding.

Institutional Review Board Statement: Not applicable.

Informed Consent Statement: Not applicable.

Data Availability Statement: Information available upon request, subject to relevant restrictions (such as privacy or ethical).

Conflicts of Interest: The authors declare no conflict of interest.

References

1. Siqueira, J.F., Jr.; Rôças, I.N.; Ricucci, D.; Hülsmann, M. Causes and management of post-treatment apical periodontitis. *Br. Dent. J.* **2014**, *216*, 305–312. https://doi.org/10.1038/sj.bdj.2014.200.
2. Bergmans, L.; Van Cleynenbreugel, J.; Wevers, M.; Lambrechts, P. Mechanical root canal preparation with NiTi rotary instruments: Rationale, performance and safety. Status report for the American Journal of Dentistry. *Am. J. Dent.* **2001**, *14*, 324–333.
3. Sattapan, B.; Nervo, G.J.; Palamara, J.E.; Messer, H.H. Defects in rotary nickel-titanium files after clinical use. *J. Endod.* **2000**, *26*, 161–165. https://doi.org/10.1097/00004770-200003000-00008.
4. Peters, O.A.; Barbakow, F. Dynamic torque and apical forces of ProFile.04 rotary instruments during preparation of curved canals. *Int. Endod. J.* **2002**, *35*, 379–389. https://doi.org/10.1046/j.0143-2885.2001.00494.x.
5. Varghese, N.O.; Pillai, R.; Sujathen, U.N.; Sainudeen, S.; Antony, A.; Paul, S. Resistance to torsional failure and cyclic fatigue resistance of ProTaper Next, WaveOne, and Mtwo files in continuous and reciprocating motion: An in vitro study. *J. Conserv. Dent.* **2016**, *19*, 225–230. https://doi.org/10.4103/0972-0707.181937.
6. Kuhn, G.; Tavernier, B.; Jordan, L. Influence of structure on nickel-titanium endodontic instruments failure. *J. Endod.* **2001**, *27*, 516–520. https://doi.org/10.1097/00004770-200108000-00005.
7. Cheung, G.S. Instrument fracture: Mechanisms, removal of fragments, and clinical outcomes. *Endod. Top.* **2007**, *16*, 1–26.
8. Pruett, J.P.; Clement, D.J.; Carnes, D.L., Jr. Cyclic fatigue testing of nickel-titanium endodontic instruments. *J. Endod.* **1997**, *23*, 77–85. https://doi.org/10.1016/S0099-2399(97)80250-6.
9. Sjogren, U.; Hagglund, B.; Sundqvist, G.; Wing, K. Factors affecting the long-term results of endodontic treatment. *J. Endod.* **1990**, *16*, 498–504. https://doi.org/10.1016/S0099-2399(07)80180-4.
10. Faus-Llácer, V.; Hamoud-Kharrat, N.; Marhuenda Ramos, M.T.; Faus-Matoses, I.; Zubizarreta-Macho, Á.; Ruiz Sánchez, C.; Faus-Matoses, V. Influence of the Geometrical Cross-Section Design on the Dynamic Cyclic Fatigue Resistance of NiTi Endodontic Rotary Files-An In Vitro Study. *J. Clin. Med.* **2021**, *10*, 4713. https://doi.org/10.3390/jcm10204713.
11. Faus-Llácer, V.; Kharrat, N.H.; Ruiz-Sánchez, C.; Faus-Matoses, I.; Zubizarreta-Macho, Á.; Faus-Matoses, V. The Effect of Taper and Apical Diameter on the Cyclic Fatigue Resistance of Rotary Endodontic Files Using an Experimental Electronic Device. *Appl. Sci.* **2021**, *11*, 863. https://doi.org/10.3390/app11020863.
12. Kwak, S.W.; Ha, J.H.; Lee, C.J.; El Abed, R.; Abu-Tahun, I.H.; Kim, H.C. Effects of Pitch Length and Heat Treatment on the Mechanical Properties of the Glide Path Preparation Instruments. *J. Endod.* **2016**, *42*, 788–792. https://doi.org/10.1016/j.joen.2016.02.002.
13. Gambarini, G. Cyclic fatigue of nickel-titanium rotary instruments after clinical use with low- and high-torque endodontic motors. *J. Endod.* **2001**, *27*, 772–774. https://doi.org/10.1097/00004770-200112000-00015.
14. Gutmann, J.L.; Gao, Y. Alteration in the inherent metallic and surface properties of nickel-titanium root canal instruments to enhance performance, durability and safety: A focused review. *Int. Endod. J.* **2012**, *45*, 113–128. https://doi.org/10.1111/j.1365-2591.2011.01957.x.
15. Yared, G.M.; Bou Dagher, F.E.; Machtou, P. Cyclic fatigue of Profile rotary instruments after simulated clinical use. *Int. Endod. J.* **1999**, *32*, 115–119. https://doi.org/10.1046/j.1365-2591.1999.00201.x.
16. Martín, B.; Zelada, G.; Varela, P.; Bahillo, J.G.; Magán, F.; Ahn, S.; Rodríguez, C. Factors influencing the fracture of nickel-titanium rotary instruments. *Int. Endod. J.* **2003**, *36*, 262–266. https://doi.org/10.1046/j.1365-2591.2003.00630.x.
17. De-Deus, G.; Moreira, E.J.; Lopes, H.P.; Elias, C.N. Extended cyclic fatigue life of F2 ProTaper instruments used in reciprocating movement. *Int. Endod. J.* **2010**, *43*, 1063–1068. https://doi.org/10.1111/j.1365-2591.2010.01756.x.
18. Pedullà, E.; Grande, N.M.; Plotino, G.; Gambarini, G.; Rapisarda, E. Influence of continuous or reciprocating motion on cyclic fatigue resistance of 4 different nickel-titanium rotary instruments. *J. Endod.* **2013**, *39*, 258–261. https://doi.org/10.1016/j.joen.2012.10.025.
19. Martins, J.N.R.; Silva, E.J.N.L.; Marques, D.; Belladonna, F.; Simões-Carvalho, M.; Vieira, V.T.L.; Antunes, H.S.; Braz Fernandes, F.M.B.; Versiani, M.A. Design, metallurgical features, mechanical performance and canal preparation of six reciprocating instruments. *Int. Endod. J.* **2021**, *54*, 1623–1637. https://doi.org/10.1111/iej.13529.
20. Zubizarreta-Macho, A.; Mena Álvarez, J.; Albadalejo Martínez, A.; Segura-Egea, J.J.; Caviedes Brucheli, J.; Agustín-Panadero, R.; López Píriz, R.; Alonso-Ezpeleta, O. Influence of the pecking motion on the cyclic fatigue resistance of endodontic rotary files. *J. Clin. Med.* **2020**, *9*, e45.
21. Schneider, S.W. A comparison of canal preparations in straight and curved root canals. *Oral Surg. Oral Med. Oral Pathol.* **1971**, *32*, 271–275.
22. Yared, G. Canal preparation using only one Ni-Ti rotary instrument: Preliminary observations. *Int. Endod. J.* **2008**, *41*, 339–344. https://doi.org/10.1111/j.1365-2591.2007.01351.x.
23. Lopes, H.P.; Ferreira, A.A.; Elias, C.N.; Moreira, E.J.; de Oliveira, J.C.; Siqueira, J.F., Jr. Influence of rotational speed on the cyclic fatigue of rotary nickel-titanium endodontic instruments. *J. Endod.* **2009**, *35*, 1013–1016. https://doi.org/10.1016/j.joen.2009.04.003.

24. Zanza, A.; D'Angelo, M.; Reda, R.; Gambarini, G.; Testarelli, L.; Di Nardo, D. An Update on Nickel-Titanium Rotary Instruments in Endodontics: Mechanical Characteristics, Testing and Future Perspective-An Overview. *Bioengineering* **2021**, *16*, 218. https://doi.org/10.3390/bioengineering8120218.
25. Schäfer, E.; Bürklein, S.; Donnermeyer, D. A critical analysis of research methods and experimental models to study the physical properties of NiTi instruments and their fracture characteristics. *Int. Endod. J.* **2022**, *55*, 72–94. https://doi.org/10.1111/iej.13673.
26. Ferreira, F.; Adeodato, C.; Barbosa, I.; Aboud, L.; Scelza, P.; Zaccaro Scelza, M. Movement kinematics and cyclic fatigue of NiTi rotary instruments: A systematic review. *Int. Endod. J.* **2017**, *50*, 143–152. https://doi.org/10.1111/iej.12613.
27. ANSI/ADA Specification Nº 28-2002. *Root Canal Files and Reamers, Type K for Hand Use*; American Dental Association: Chicago, IL, USA, 2002.
28. Plotino, G.; Grande, N.M.; Cordaro, M.; Testarelli, L.; Gambarini, G. A review of cyclic fatigue testing of nickel-titanium rotary instruments. *J. Endod*. **2009**, *35*, 1469–1476. https://doi.org/10.1016/j.joen.2009.06.015.
29. Rodrigues, R.C.; Lopes, H.P.; Elias, C.N.; Amaral, G.; Vieira, V.T.; De Martin, A.S. Influence of different manufacturing methods on the cyclic fatigue of rotary nickel-titanium endodontic instruments. *J. Endod*. **2011**, *37*, 1553–1537. https://doi.org/10.1016/j.joen.2011.08.011.
30. Li, U.M.; Lee, B.S.; Shih, C.T.; Lan, W.H.; Lin, C.P. Cyclic fatigue of endodontic nickel titanium rotary instruments: Static and dynamic tests. *J. Endod*. **2002**, *28*, 448–451. https://doi.org/10.1097/00004770-200206000-00007.
31. Lopes, H.P.; Elias, C.N.; Vieira, M.V.; Siqueira, J.F., Jr.; Mangelli, M.; Lopes, W.S.; Vieira, V.T.; Alves, F.R.; Oliveira, J.C.; Soares, T.G. Fatigue Life of Reciproc and Mtwo instruments subjected to static and dynamic tests. *J. Endod*. **2013**, *39*, 693–696. https://doi.org/10.1016/j.joen.2012.11.048.
32. Kim, H.C.; Kwak, S.W.; Cheung, G.S.; Ko, D.H.; Chung, S.M.; Lee, W. Cyclic fatigue and torsional resistance of two new nickel-titanium instruments used in reciprocation motion: Reciproc versus WaveOne. *J. Endod*. **2012**, *38*, 541–544. https://doi.org/10.1016/j.joen.2011.11.014.
33. Varela-Patiño, P.; Ibañez-Párraga, A.; Rivas-Mundiña, B.; Cantatore, G.; Otero, X.L.; Martin-Biedma, B. Alternating versus continuous rotation: A comparative study of the effect on instrument life. *J. Endod*. **2010**, *36*, 157–159. https://doi.org/10.1016/j.joen.2009.09.023.
34. You, S.Y.; Bae, K.S.; Baek, S.H.; Kum, K.Y.; Shon, W.J.; Lee, W. Lifespan of one nickel-titanium rotary file with reciprocating motion in curved root canals. *J. Endod*. **2010**, *36*, 1991–1994. https://doi.org/10.1016/j.joen.2010.08.040.
35. Gao, Y.; Shotton, V.; Wilkinson, K.; Phillips, G.; Johnson, W.B. Effects of raw material and rotational speed on the cyclic fatigue of ProFile Vortex rotary instruments. *J. Endod*. **2010**, *36*, 1205–1209. https://doi.org/10.1016/j.joen.2010.02.015.
36. Martins, J.N.R.; Nogueira Leal Silva, E.J.; Marques, D.; Ginjeira, A.; Braz Fernandes, F.M.; De Deus, G.; Versiani, M.A. Influence of Kinematics on the Cyclic Fatigue Resistance of Replicalike and Original Brand Rotary Instruments. *J. Endod*. **2020**, *46*, 1136–1143. https://doi.org/10.1016/j.joen.2020.05.001.
37. Ray, J.J.; Kirkpatrick, T.C.; Rutledge, R.E. Cyclic fatigue of EndoSequence and K3 rotary files in a dynamic model. *J. Endod*. **2007**, *33*, 1469–1472. https://doi.org/10.1016/j.joen.2007.07.041.
38. Gambarini, G.; Galli, M.; Di Nardo, D.; Seracchiani, M.; Donfrancesco, O.; Testarelli, L. Differences in cyclic fatigue lifespan between two different heat treated NiTi endodontic rotary instruments: WaveOne Gold vs EdgeOne Fire. *J. Clin. Exp. Dent*. **2019**, *11*, e609–e613. https://doi.org/10.4317/jced.55839.
39. Lopes, H.P.; Britto, I.M.; Elias, C.N.; Machado de Oliveira, J.C.; Neves, M.A.; Moreira, E.J.; Siqueira, J.F., Jr. Cyclic fatigue resistance of ProTaper Universal instruments when subjected to static and dynamic tests. *Oral Surg. Oral Med. Oral Pathol. Oral Radiol. Endod*. **2010**, *110*, 401–404. https://doi.org/10.1016/j.tripleo.2010.05.013.
40. De-Deus, G.; Leal Vieira, V.T.; Nogueira da Silva, E.J.; Lopes, H.; Elias, C.N.; Moreira, E.J. Bending resistance and dynamic and static cyclic fatigue life of Reciproc and WaveOne large instruments. *J. Endod*. **2014**, *40*, 575–579. https://doi.org/10.1016/j.joen.2013.10.013.
41. La Rosa, G.R.M.; Shumakova, V.; Isola, G.; Indelicato, F.; Bugea, C.; Pedullà, E. Evaluation of the Cyclic Fatigue of Two Single Files at Body and Room Temperature with Different Radii of Curvature. *Materials* **2021**, *14*, 2256. https://doi.org/10.3390/ma14092256.
42. Plotino, G.; Grande, N.M.; Mercadé Bellido, M.; Testarelli, L.; Gambarini, G. Influence of Temperature on Cyclic Fatigue Resistance of ProTaper Gold and ProTaper Universal Rotary Files. *J. Endod*. **2017**, *43*, 200–202. https://doi.org/10.1016/j.joen.2016.10.014.

BMC Oral Health

RESEARCH ARTICLE

Open Access

Influence of the type of reciprocating motion on the cyclic fatigue resistance of reciprocating files in a dynamic model

Álvaro Zubizarreta-Macho[1], Alberto Albaladejo Martínez[2], Carlos Falcão Costa[3], Norberto Quispe-López[1], Ruben Agustín-Panadero[4] and Jesús Mena-Álvarez[1,5*]

Abstract

Background: The aim of this study was to compare the influence of two novel reciprocating movements on the cyclic fatigue resistance of endodontic reciprocating files.

Methods: 30 Procodile® (Komet Medical, Lemgo, Germany) files were selected in this study and distributed according to the following study groups depending on the movements to be performed: ReFlex Dynamic ($n = 10$), ReFlex Smart ($n = 10$) and Reciproc ($n = 10$) reciprocating movement. These files were fixed to a specific dynamic cyclic fatigue device designed and manufactured by 3D impression to simulate the pecking motion performed by the operator. The time to failure and the number of cycles of in-and-out of the endodontic files was registered. The results were analyzed by ANOVA and Weibull statistics.

Results: Statistically significant differences were found when the number of cycles of in-and-out movement and the time to failure of ReFlex Dynamic and Reciproc reciprocating movement ($p < 0.001$) and between ReFlex Smart and Reciproc reciprocating movement ($p < 0.001$) were compared in pairs. However, no statistically significant differences were observed between time to failure and number of cycles of in-and-out movement of ReFlex Dynamic and ReFlex Smart reciprocating movement ($p = 0.253$).

Conclusions: The ReFlex Smart reciprocating movement increased the cyclic fatigue resistance of endodontic reciprocating files compared with traditional reciprocating movement.

Keywords: Endodontics, Cyclic fatigue, Nitinol, Reciprocating movement

Background

Nickel–titanium (NiTi) rotary files have improved accuracy, reduced apical foramen transportation and reduced working time, with respect to traditional stainless steel endodontic files [1]. However, the failure of NiTi rotary files is still a complication related to endodontic rotary instruments difficult to solve [2]. Failure of NiTi rotary files can occur by cyclic bending fatigue or torsional overload [3]. Torsional overload occurs when the tip of the file is locked inside the root canal system. Cyclic bending fatigue is caused when the file is submitted to alternating compressive and tensile stress cycles at the maximum curvature of the curved root canal [4]. The arrival of reciprocating single-file systems with speed- and torque-controlled motor systems has had a great impact on the field of endodontics. Single-file systems have demonstrated the ability to clean and shape the root canal system with fewer instruments, which implies a reduced working time. In addition, they have

*Correspondence: jmenaalvarez@gmail.com
[1] Department of Endodontics, Faculty of Dentistry, Alfonso X el Sabio University, 28691 Madrid, Spain
Full list of author information is available at the end of the article

shown a negative effect on postoperative pain after root canal treatment [5], a high capability to maintain the original canal anatomy without removing excess dentin and enhancing a more centered preparation compared with rotary multiple-file systems [6]; these files have a short learning curve [7] although they do not show statistically significant differences regarding their antibacterial efficacy compared to rotary multiple-file systems [8]. However, single-file systems are submitted to high levels of cyclic and torsional fatigue, which might lead to fracturing of reciprocating files [9]. The reciprocating movement associated with single-file systems has been shown to extend the lifetime of NiTi rotary files compared with continuous rotation, thus increasing the cyclic fatigue resistance of reciprocating files [8]. The previously described Wave One and Reciproc reciprocating movement instruments perform wide and continuously counter clockwise (CCW) (170° and 150°, respectively) movement and reduce the fatigue of the reciprocating files by moving in a smaller angle in the clockwise (CW) direction (50° and 30°, respectively) [10, 11,]. The large CCW reciprocating angle allows the reciprocating file to cut the root canal dentine and advance in the root canal system, whereas the smaller CW reciprocating angle allows the reciprocating file to disengage from the dentine to reduce the screwing effect and file breakage. However, the ReFlex Dynamic reciprocating movement performed by EndoPilot® endodontic handpiece (Komet Medical, Lemgo, Germany) starts moving the reciprocating files (Procodile®, Komet Medical, Lemgo, Germany) with a widely CCW movement, but stops and continues moving CCW without turning in reverse if no resistance of the files is detected by the handpiece management software. However, if the handpiece management software detects resistance of the reciprocating files, EndoPilot® is able to change the movement of the fatigued files in the reverse direction (CW). The ReFlex Smart reciprocating movement performed by EndoPilot® handpiece starts making the same movement as the ReFlex Dynamic reciprocating movement, but it is also able to turn twice in the reverse direction (CW) if the handpiece management software detects resistance on the fatigued files.

Taking those facts into account, the aim of this work was to analyze and compare the influence of two novel reciprocating movements on the cyclic fatigue resistance of endodontic reciprocating files, with a null hypothesis (H0) stating that there would be no difference between the reciprocating movements with regard to the cyclic fatigue resistance. The incorporation of a new movement and a new design in the endodontic file justifies this study. It should be noted that Procodile file is made of a conventional NiTi alloy.

Methods

Study design

Procodile® (Komet Medical, Lemgo, Germany) is a NiTi endodontic reciprocating file with one-file system. Procodile has a double-S cross-section, variable tapered core, 0.25 mm tip diameter, 6% continous taper, 25 mm in length and CCW reciprocating motion. A sample of 30 new files were utilized in this in vitro study. Previously to use, all endodontic files were inspected under a stereomicroscope (SZR-10, Optika, Bergamo, Italy) to observe possible defects and none were discarded. The endodontic files were randomized (Epidat 4.1, Galicia, Spain) and distributed into the following study groups: A: ReFlex Dynamic reciprocating movement (n = 10); B: ReFlex Smart reciprocating movement (n = 10); and C: Reciproc reciprocating movement (n = 10).

Dynamic cyclic fatigue test device

To perform the dynamic cyclic fatigue tests was used a custom-made device (utility model patent number ES1219520) previously described [12]. The structure of experimental cyclic fatigue model was designed by computer aided design/computer aided engineering (CAD/CAE) 2D/3D software (Midas FX+®, Brunleys, Milton Keynes, UK) and manufactured by 3D impression (ProJet® 6000 3D Systems©, Rock Hill, SC, USA).

To obtain an accurate stereolithography (STL) file, endodontic reciprocating file (Procodile 25.06) underwent microcomputerized tomography scan (Skyscan 1176, Bruker-MicroCT, Kontich, Belgium) (Fig. 1a). STL file was used to design an anatomically based artificial root canal with a 60° curvature according to Schneider's measuring technique [13] and 3 mm radius of curvature by inverse engineering technology using the CAD/CAE 2D/3D software (Fig. 1b). The artificial root canal was manufactured by electrical discharge machining (EDM) molybdenum wire-cut technology (Cocchiola S.A., Buenos Aires, Argentina). This process allowed intimate contact between endodontic reciprocating files and artificial root canal walls (Fig. 1c, d).

The endodontic reciprocating files randomly assigned to groups A and B were used with the ReFlex Dynamic and ReFlex Smart reciprocating movements respectively, and both were performed with a 6:1 reduction handpiece (EndoPilot® endodontic handpiece) and torque-controled motor (EndoPilot®, Schlumbohm, Brokstedt, Germany). It is not possible to provide torque and revolutions per minute (rpm), because handpiece management software adapts the reciprocating movement of files with regard to their resistance inside the artificial root canal, to reduce cyclic and torsional fatigue and, hence, to increase the fracture resistance. The handpiece management software continuously analyzes the resistance

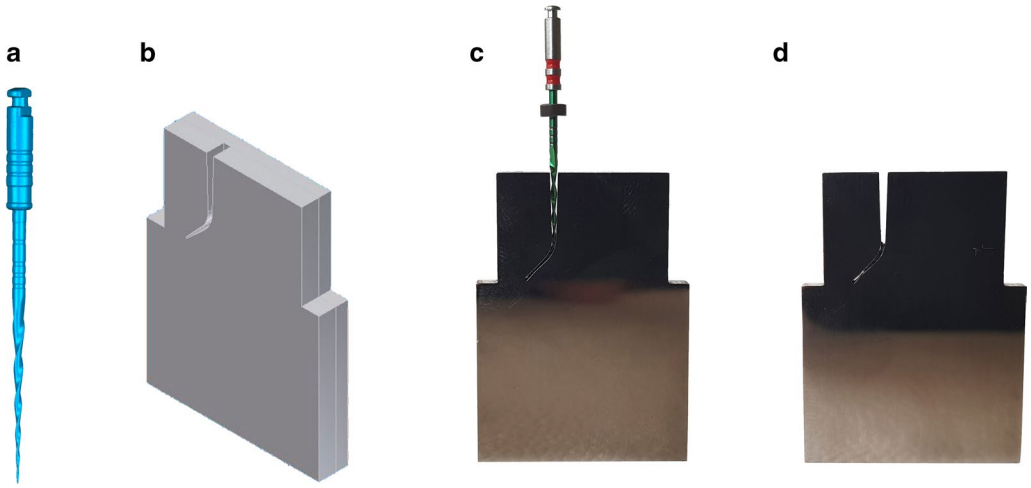

Fig. 1 **a** STL file of the endodontic reciprocating file, **b** STL file of the artificial root canal, **c** adjustment of the endodontic reciprocating file with the artificial root canal walls and **d** fracture of the endodontic reciprocating file inside the artificial root canal

experienced by the reciprocating files inside the artificial root canal through an accurate mathematical algorithm. The Procodile files randomly assigned to group C were used by a 6:1 reduction handpiece, a torque-controlled motor (Silver Reciproc®; VDW, Munich, Germany) and Reciproc® reciprocating movement was performed by the Silver Reciproc endodontic handpiece according to the manufacturer's instructions [14].

To allow accurate adjustment with their respective endodontic handpiece supports during the dynamic cyclic fatigue tests, both endodontic handpieces were scanned (3D Geomagic Capture Wrap, 3D Systems©, Rock Hill, SC, USA).

All endodontic reciprocating files were used in the dynamic cyclic fatigue device to a frequency of 60 pecking movements/min according to a previous study [12]. To reduce the friction between the reciprocating files and the artificial canal walls, special high-flow synthetic oil (Singer All-Purpose Oil; Singer Corp., Barcelona, Spain) designed for lubrication of mechanical parts was applied.

All files were used until fracture occurred and the time to failure, the number of cycles of in-and-out movements and the length of fractured files tip were measured and recorded.

Statistical tests

SAS 9.4 (SAS Institute Inc., Cary, NC, USA) was used to statistical analysis of all variables. Descriptive statistics are expressed as mean and standard deviation (SD) for quantitative variables. By comparing the time to failure (seconds) and the number of pecking movements (cycles of in-and-out movements), comparative analysis was performed using ANOVA. In addition, Weibull characteristic strength and Weibull modulus were calculated and their 95% confidence interval for each group. The statistical significance was set at $p < 0.05$.

Results

The means and SD values for time to failure (seconds) of the study groups are displayed in Table 1 and Fig. 2. The mean time to fracture of Procodile Reflex Dynamic was 261.95 s and SD 83.32, while that of Procodile Reflex Smart was 527.43 s and SD 89.31; the mean time to fracture for Procodile with the Reciproc movement was 308.07 s and SD 92.04.

ANOVA revealed statistically significant differences between the time to failure of ReFlex Dynamic and Reciproc reciprocating movement ($p < 0.001$), and between ReFlex Smart and Reciproc reciprocating

Table 1 Descriptive statistics of time to failure

	n	Mean	SD	Minimum	Maximum	Fracture length
Procodile ReFlex Dynamic	10	261.95[a]	83.32	128.28	401.69	3.18
Procodile ReFlex Smart	10	527.43[b]	89.31	403.35	691.90	3.15
Procodile Reciproc	10	308.07[c]	92.04	208.82	512.92	3.18

[a,b,c] Statistically significant differences between groups ($p < 0.05$)

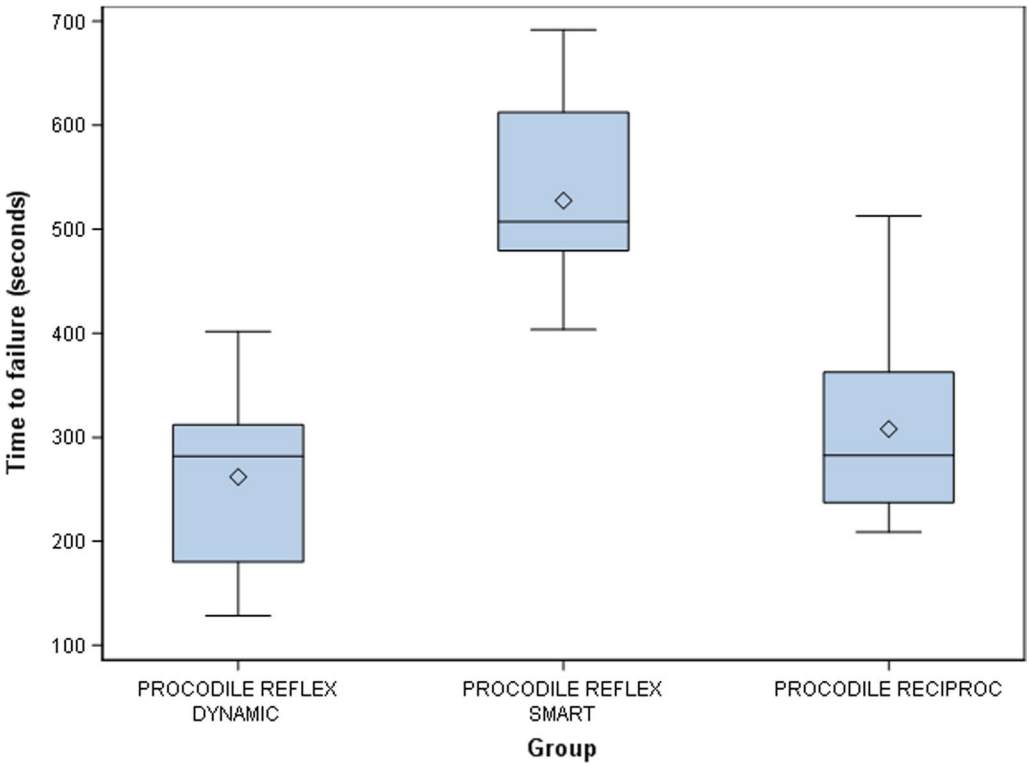

Fig. 2 Box plots of time to failure of experimental groups. Horizontal line in each box represents median value

movement ($p < 0.001$). However, no statistically significant differences were observed between the time to failure of ReFlex Dynamic and ReFlex Smart reciprocating movement ($p = 0.253$).

The scale distribution parameter (η) of Weibull statistics showed statistically significant differences between the time to failure of ReFlex Dynamic and Reciproc reciprocating movement ($p < 0.001$), and between ReFlex Smart and Reciproc reciprocating movement ($p < 0.001$). However, no statistically significant differences were observed between the time to failure of ReFlex Dynamic and ReFlex Smart reciprocating movement ($p = 0.215$) (Table 2 and Fig. 3). The shape distribution parameter (β) of Weibull statistics did not show statistically significant differences between the time to failure of ReFlex Dynamic and Reciproc reciprocating movement ($p = 0.069$), between ReFlex Smart and Reciproc reciprocating movement ($p = 0.112$), and between ReFlex Dynamic and ReFlex Smart reciprocating movement ($p = 0.889$). ReFlex Smart reciprocating movement presented the highest shape distribution parameter of Weibull statistics (6.4889), therefore the highest predictability compared to ReFlex Dynamic and Reciproc, which showed the lowest shape distribution parameter of Weibull statistics (3.5825) and the largest scatter of fracture point, hence the least predictable cyclic fatigue resistance behaviour (Table 2 and Fig. 3).

The means and SD values for the number of cycles of in-and-out movement of the study groups are displayed in Table 3 and Fig. 4. The results for the number

Table 2 Weibull statistics of time to failure

	Weibull shape (β)				Weibull scale (η)			
	Estimate	SE	Lower	Upper	Estimate	SE	Lower	Upper
Procodile ReFlex Dynamic	37.555	0.9442	2.944	61.472	290.668	277.881	2.442.749	3.458.726
Procodile ReFlex Smart	64.889	15.332	40.837	103.108	5.645.218	292.099	5.100.788	6.247.758
Procodile Reciproc	35.825	0.8125	22.969	55.876	3.411.025	320.377	2.837.505	4.100.466

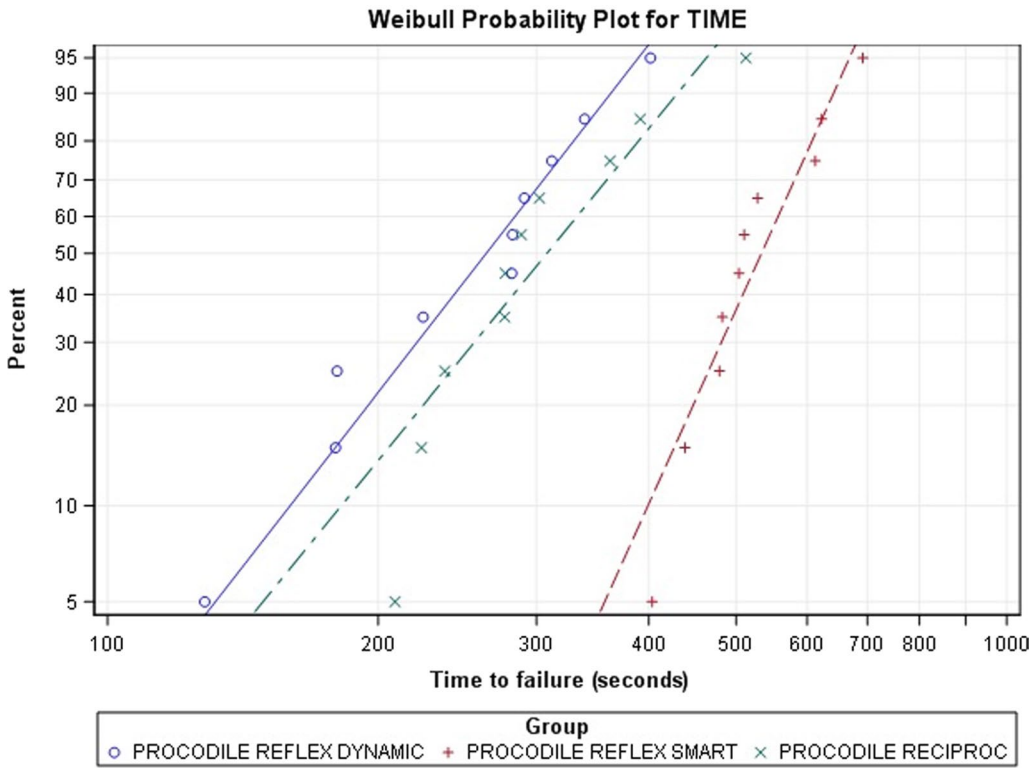

Fig. 3 Weibull probability plot of time to failure

Table 3 Descriptive statistics of the number of cycles of in-and-out movement

	n	Mean	SD	Minimum	Maximum	Fracture length
Procodile ReFlex Dynamic	10	261.95[a]	83.32	128.28	401.69	3.18
Procodile ReFlex Smart	10	527.43[b]	89.31	403.35	691.90	3.15
Procodile Reciproc	10	308.07[c]	92.04	208.82	512.92	3.18

[a,b,c] Statistically significant differences between groups ($p < 0.05$)

of cycles of in-and-out movement were the same as for the time to failure since a frequency of 60 pecking movements/min was used during for the process.

ANOVA, in relation to the number of cycles of in-and-out movement, showed the same results as the time to failure, due to a frequency of 60 pecking movements/min was used during the dynamic cyclic fatigue tests.

The scale (η) and shape (β) distribution parameters of Weibull statistics related to the number of cycles of in-and-out movement also showed the same results as the time to failure because a frequency of 60 pecking movements/min was used during the dynamic cyclic fatigue tests (Table 4 and Fig. 5).

The mean length of the fractured fragments was 3.18 mm in Procodile Reflex Dynamic and Procodile Reciproc, and 3.15 mm in Procodile Reflex Smart. These results were not statistically significantly different among all instruments tested ($p > 0.05$) (Tables 1, 3).

Discussion

The results obtained in the present study reject the null hypothesis (H0), which states that there would be no difference between the effects of reciprocating movements on the cyclic fatigue resistance of endodontic rotary instruments.

When comparing cyclic fatigue resistance of reciprocating systems and conventional rotary systems, most studies have reported that reciprocating motion improves the cyclic fatigue resistance of endodontic

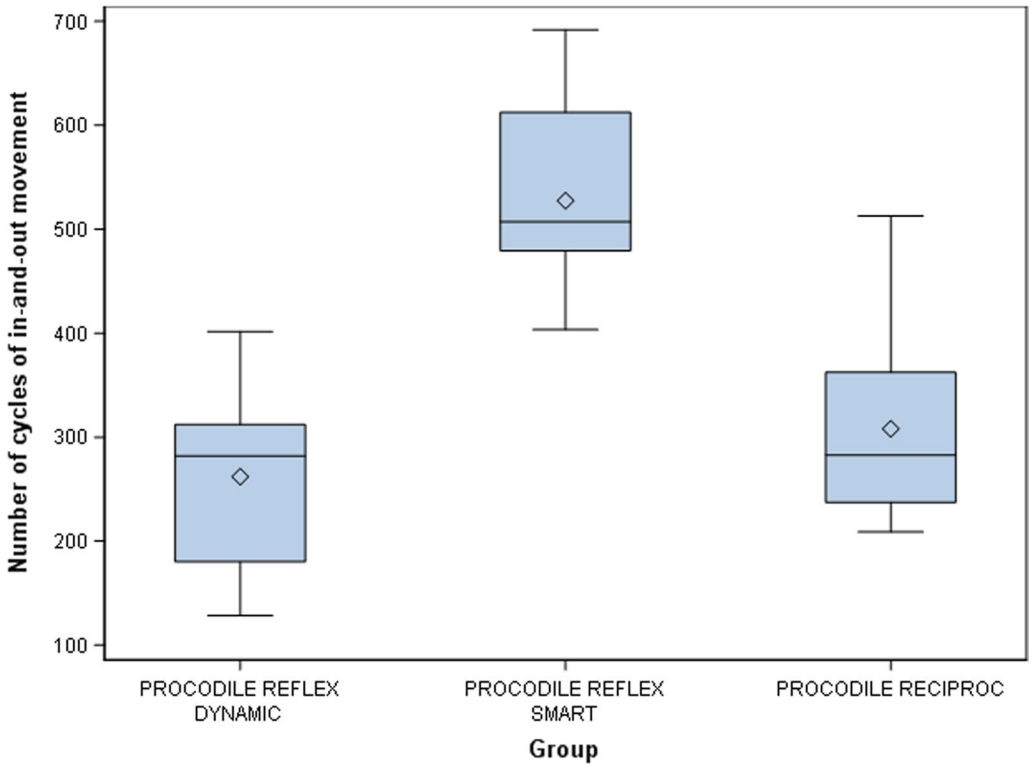

Fig. 4 Box plots of number of cycles of in-and-out movement of experimental groups. Horizontal line in each box represents median value

Table 4 Weibull statistics of number of cycles of in-and-out movement

	Weibull shape (β)				Weibull scale (η)			
	Estimate	SE	Lower	Upper	Estimate	SE	Lower	Upper
Procodile ReFlex Dynamic	37.555	0.9442	2.944	61.472	290.668	277.881	2.442.749	3.458.726
Procodile ReFlex Smart	64.889	15.332	40.837	103.108	5.645.218	292.099	5.100.788	6.247.758
Procodile Reciproc	35.825	0.8125	22.969	55.876	3.411.025	320.377	2.837.505	4.100.466

instruments versus continuous rotation [15]. Cyclic fatigue has been tested in artificial canals using tubes, curved metal guiding slopes, plastic blocks and needles with curvatures; however, the artificial root canal should be custom-designed to ensure immediate contact with the endodontic file. In addition, only dynamic devices simulate the pecking movement performed by the operator, which represents the time during which the file remains in the canal. Olcay et al. [16] demonstrated that Wave One Gold endodontic reciprocating files showed a significant difference ($p=0.00$) in time to failure (239.60 ± 12.84 s) compared to Protaper Next (161.40 ± 6.68 s) and 2Shape (77.73 ± 2.61 s) conventional rotary files; however, this was a static cyclic fatigue test with an artificial root canal with 1.5 mm wide parallel walls and 5 mm radius of curvature and different cross-sections and alloys. Scott et al. [17] analyzed the alloy influence on the cyclic fatigue resistance of reciprocating systems by comparing Wave One Primary, Wave One Gold Primary and EdgeFile X1, and concluded that endodontic reciprocating files manufactured with novel heat-treated alloys showed better cyclic fatigue resistance than those made with traditional M-Wire alloys; however, this was also a static cyclic fatigue test with an artificial root canal of parallel walls and 5 mm radius of curvature and different apical diameters. Al-Obaida et al. [18] also compared the cyclic fatigue resistance of five novel heat-treated manufactured NiTi reciprocating systems in canals with single and double curvature and demonstrated that Reciproc Blue (421.92 ± 155.09/251

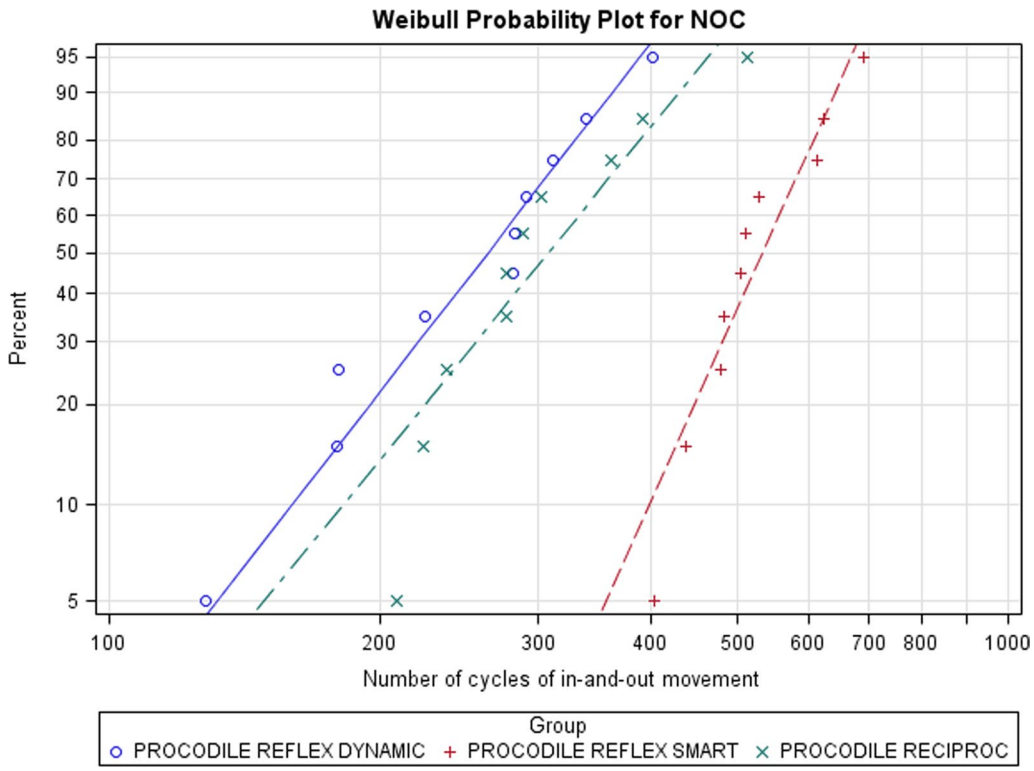

Fig. 5 Weibull probability plot of number of cycles to failure (NOC)

.25 ± 47.05 s) endodontic reciprocating files exhibited significantly ($p < 0.05$) higher cyclic fatigue resistance, followed by Reciproc (180.42 ± 35.43/160.58 ± 29.98 s) and Wave One Gold (167.67 ± 26.73/122.92 ± 26.54 s) for both types of artificial root canals. Regardless of the alloy of the reciprocating system, the cross-section that showed the best response to cyclic fatigue was the double-S cross-section of Reciproc and Reciproc Blue, which was the same as Procodile. Similarly, Sekar et al. [19] reported in their study that the cross-section that had the most influence on cyclic fatigue resistance was the double-S cross-section of Mtwo endodontic rotary files. Alsilani et al. [20] stated that the double-S cross-section of the Reciproc system presented a statistically significantly ($p < 0.001$) mean time to failure (301.13 ± 54.463/836.53 ± 67.960 s) compared to One Shape (187.73 ± 33.457/275 .27 ± 58.410 s) and Revo-S SU (116.67 ± 37.663/197.60 ± 41.092 s) in both continuous rotation and reciprocating movement. Furthermore, Di Nardo et al. [21] compared the cyclic fatigue resistance of an NiTi and a novel heat-treated manufactured NiTi reciprocating system (Reziflow and Wave One Gold, respectively) and showed that the NiTi system presented significantly ($p < 0.05$) higher cyclic fatigue resistance (50.75 ± 20.06 s) than the heat-treated system (30.13 ± 9.40 s). Although this was also a static cyclic fatigue test with an artificial root canal of parallel walls and 90° and 5 mm radius of curvature, Reziflow has a similar design and manufacturing process as Procodile. These findings might suggest that the cross-section design of the endodontic files might also be a factor to consider in the results of cyclic fatigue tests above the manufacturing process. The longer time to failure results associated with the ReFlex Smart reciprocating movement (527.43 ± 89.31 s) can be attributed to the double reverse direction performed by EndoPilot endodontic handpiece, which allows reduced cyclic fatigue of the files. The dynamic cyclic fatigue test could also have an influence on the high results obtained compared to studies of static cyclic fatigue tests. Keleş et al. [22] reported that cyclic fatigue resistance was significantly ($p < 0.05$) greater in dynamic than static cyclic fatigue tests at room temperature for four endodontic reciprocating files—Wave One (177.9 ± 46.9/106.2 ± 36.6 s), Wave One Gold (258.9 ± 47.9/175.3 ± 60.3 s), Reciproc (292.4 ± 81.3/196.7 ± 55.6 s), and Reciproc Blue (275.9 ± 86.4/214.4 ± 108.4 s)—and provided a better simulation of the clinical environment, because compression and tensile stresses are distributed over a wider area along the file surface [23].

In this study, the time to failure and the number of cycles of in-and-out movement were analyzed to determine the influence of novel reciprocating movement on the cyclic fatigue resistance of NiTi endodontic reciprocating files; however, it was not possible to calculate the number of cycles to fracture in groups A and B because the rpm could vary during the tests by EndoPilot handpiece management software. This has been considered a limitation of the present study and highlights the need for an international standard for testing the cyclic fatigue resistance of NiTi endodontic reciprocating files, because several self-designed devices and methods have been used with different results [24]. However, none of these custom-made devices have been capable of dynamically testing the cyclic fatigue of NiTi endodontic reciprocating files in vitro with an automatic detection system and an anatomically based artificial root canal. We have not found comparative studies on the resistance to fracture of the Procodile files and the Smart and Reflex movements to be able to discuss our results.

An angle of curvature of 60° was selected to design the artificial root canal, because Topçuoğlu et al. [25] reported that artificial root canals with a 45° angle of curvature did not exhibit significant ($p > 0.05$) differences between the cyclic fatigue resistance of R-Pilot (394.5 ± 45.3 s) and WaveOne Gold (412.4 ± 55.2 s) glider files; however, artificial root canals with 60° angle of curvature showed that WaveOne Gold (368.3 ± 44.1 s) had significantly ($p < 0.05$) greater cyclic fatigue resistance than R-Pilot (247.2 ± 36.2 s).

Although there are differences between reciprocating motions (speed and angle), further studies are needed to determine the most favorable motions for root canal treatment. Iacono et al. [26] analyzed the influence of reciprocating motion and reciprocating system alloys on cyclic fatigue resistance and stated that the experimental movement with different rotation angles, based on sinusoidal acceleration, showed a positive impact on the cyclic fatigue resistance of reciprocating instruments. The different values of CW and CCW reciprocating angles between ReFlex and the number of cycles of reciprocation per second could explain the statistical differences between the cyclic fatigue resistance of reciprocating movements. The CW and CCW reciprocating angles are specific for the endodontic reciprocating systems, and the CCW reciprocating angle should be smaller than the elastic limit of each system material. Ha et al. [27] reported a distortion angle and torsional load at the pseudo-elastic limit for the Reciproc system of 214 ± 25° and 1.78 ± 0.18 Ncm, respectively. However, the Reciproc Blue system showed a distortion angle and torsional load at the pseudo-elastic limit of 253 ± 19° and 1.57 ± 0.21 Ncm, respectively. The distortion angle of both systems is greater than the CCW reciprocating angle (150°), keeping the instrument below its pseudo-elastic limit [28] while extending its lifespan and clinical efficiency. In addition, it is probable that the angular speed (ω) of the angular displacement (θ) (mainly at the CCW angle) could increase the metal fatigue of the files, although it remains a concern [29]. It is known that the Reciproc reciprocating movements perform a θ of 2617 rad (150°) and a ω of 31.415 rad/s (300 rpm) at the CCW angle [11]; however, Wave One performs a θ of 2967 rad (170°) and a ω of 36.651 rad/s (350 rpm) [10, 11]. It is probable that the higher θ and ω values of Wave One compared to Reciproc and the higher cutting surface contact of Wave One (convex triangular cross-section) compared to Reciproc and Procodile (double-S cross-section) could also affect the cyclic fatigue resistance of these reciprocating instruments. Procodile also presents a double-S cross-section, but unlike the others, it is made of conventional NiTi alloy; however, its variable internal taper offers greater flexibility.

The conclusion derived from this study is that novel reciprocating movements increase the cyclic fatigue resistance of endodontic reciprocating files compared with traditional reciprocating movements. Nevertheless, further research are needed to determine the influence of these novel reciprocating movements on the cyclic fatigue resistance of heat-treated manufactured NiTi reciprocating systems.

Conclusions

In conclusion, within the limitations of this study, our results showed that ReFlex Smart reciprocating movement increased the cyclic fatigue resistance of endodontic reciprocating files compared with ReFlex Dynamic and Reciproc reciprocating movements.

Abbreviations

CAD/CAE: Computer-aided design/computer-aided engineering.; CCW: Counterclockwise; CW: Clockwise; EDM: Electrical discharge machining; LED/LDR: Light-emitting diode/light-dependent resistor; NOC: Cycles to failure; NiTi: Nickel–titanium; RPM: Revolutions per minute; SD: Standard deviation; STL: Standard Triangle Language.

Acknowledgements

Not applicable.

Authors' contributions

All of the authors contributed to the investigation, supervision, writing, review, and editing of the study. The study was conceptualized by JMÁ, AZM and RA-P. Data curation, data visualization, and formal analysis were carried out by AAM, NQL and CFC. All authors have read and agreed to the published version of the manuscript.

Funding

There was no financial support for this study.

Availability of data and materials
The datasets used and/or analysed during the current study are available from the corresponding author on reasonable request.

Declarations

Ethics approval and consent to participate
A randomized controlled experimental trial was performed at the Dental Centre of Innovation and Advanced Specialties at Alfonso X El Sabio University (Madrid, Spain), between September and November 2019. Not applicable.

Consent to publish
Not applicable.

Competing interests
None of the authors has declared any conflict of interest or financial disclosures.

Author details
[1] Department of Endodontics, Faculty of Dentistry, Alfonso X el Sabio University, 28691 Madrid, Spain. [2] Department of Dentistry, School of Medicine, University of Salamanca, 37008 Salamanca, Spain. [3] Faculty of Health Sciences, Fernando Pessoa University, 4150-518 Porto, Portugal. [4] Department of Stomatology, Faculty of Medicine and Dentistry, University of Valencia, 46010 Valencia, Spain. [5] Department of Endodontics, Faculty of Dentistry, Alfonso X El Sabio University, Albarracin 35, 28037 Madrid, Spain.

Received: 31 July 2020 Accepted: 25 March 2021
Published online: 07 April 2021

References

1. Parashos P, Messer HH. Rotary NiTi instrument fracture and its consequences. J Endod. 2006;32(11):1031–43. https://doi.org/10.1016/j.joen.2006.06.008.
2. Gambarini G, Gergi R, Naaman A, Osta N, Al SD. Cyclic fatigue analysis of twisted file rotary NiTi instruments used in reciprocating motion. Int Endod. 2012;45(9):802–6. https://doi.org/10.1111/j.1365-2591.2012.02036.x.
3. Pedullà E, Lo Savio F, Boninelli S, Plotino G, Grande NM, La Rosa G, Rapisarda E. Torsional and cyclic fatigue resistance of a new nickel-titanium instrument manufactured by electrical discharge machining. J Endod. 2016;42(1):156–9. https://doi.org/10.1016/j.joen.2015.10.004.
4. Pirani C, Cirulli PP, Chersoni S, Micele L, Ruggeri O, Prati C. Cyclic fatigue testing and metallographic analysis of nickel-titanium rotary instruments. J Endod. 2011;37(7):1013–6. https://doi.org/10.1016/j.joen.2011.04.009.
5. Martins CM, De Souza Batista VE, Andolfatto Souza AC, Andrada AC, Mori GG, Gomes Filho JE. Reciprocating kinematics leads to lower incidences of postoperative pain than rotary kinematics after endodontic treatment: a systematic review and meta-analysis of randomized controlled trial. J Conserv Dent. 2019;22(4):320–31. https://doi.org/10.4103/JCD.JCD_439_18.
6. Singh S, Abdul MSM, Sharma U, Sainudeen S, Jain C, Kalliath JT. An in vitro comparative evaluation of volume of removed dentin, canal transportation, and centering ratio of 2shape, WaveOne Gold, and ProTaper gold files using cone-beam computed tomography. J Int Soc Prev Community Dent. 2019;9(5):481–5. https://doi.org/10.4103/jispcd.JISPCD_444_18.
7. Muñoz E, Forner L, Garcet S, Rodríguez-Lozano FJ, Llena C. Canal shaping with a reciprocating system is easy to learn. Int Endod J. 2019;52(8):1244–9. https://doi.org/10.1111/iej.13111.
8. Siddique R, Nivedhitha MS. Effectiveness of rotary and reciprocating systems on microbial reduction: a systematic review. J Conserv Dent. 2019;22(2):114–22. https://doi.org/10.4103/JCD.JCD_523_18.
9. Plotino G, Testarelli L, Al-Sudani D, Pongione G, Grande NM, Gambarini G. Fatigue resistance of rotary instruments manufactured using different nickel-titanium alloys: a comparative study. Odontology. 2014;102(1):31–5. https://doi.org/10.1007/s10266-012-0088-8.
10. Varghese NO, Pillai R, Sujathen UN, Sainudeen S, Antony A, Paul S. Resistance to torsional failure and cyclic fatigue resistance of ProTaper Next, WaveOne, and Mtwo files in continuous and reciprocating motion: an in vitro study. J Conserv Dent. 2016;19(3):225–30. https://doi.org/10.4103/0972-0707.181937.
11. Yılmaz K, Özyürek T. Cyclic fatigue life of Tango-Endo, WaveOne GOLD, and Reciproc NiTi instruments. Restor Dent Endod. 2017;42(2):134–9. https://doi.org/10.5395/rde.2017.42.2.134.
12. Zubizarreta-Macho A, Mena Álvarez J, Albadalejo Martínez A, Segura-Egea JJ, Caviedes Brucheli J, Agustín-Panadero R, López Píriz R, Alonso-Ezpeleta O. Influence of the pecking motion on the cyclic fatigue resistance of endodontic rotary files. J Clin Med. 2019;9(1):45. https://doi.org/10.3390/jcm9010045.
13. Schneider SW. A comparison of canal preparations in straight and curved root canals. Oral Surg Oral Med Oral Pathol. 1971;32(2):271–5. https://doi.org/10.1016/0030-4220(71)90230-1.
14. Rubio J, Zarzosa JI, Pallarés A. A comparative study of cyclic fatigue of 10 different types of endodontic instruments: an in vitro study. Acta Stomatol Croat. 2019;53(1):28–36. https://doi.org/10.15644/asc53/1/3.
15. Ferreira F, Adeodato C, Barbosa I, Aboud L, Scelza P, Zaccaro SM. Movement kinematics and cyclic fatigue of NiTi rotary instruments: a systematic review. Int Endod. 2017;50(2):143–52. https://doi.org/10.1111/iej.12613.
16. Olcay K, Eyuboglu TF, Erkan E. Cyclic fatigue resistance of wave one gold, protaper next and 2shape nickel titanium rotary instruments using a reliable method for measuring temperature. Niger J Clin Pract. 2019;22(10):1335–40. https://doi.org/10.4103/njcp.njcp_655_18.
17. Scott R, Arias A, Macorra JC, Govindjee S, Peters OA. Resistance to cyclic fatigue of reciprocating instruments determined at body temperature and phase transformation analysis. Aust Endod J. 2019;45(3):400–6. https://doi.org/10.1111/aej.12374.
18. Al-Obaida MI, Merdad K, Alanazi MS, Altwaijry H, AlFaraj M, Alkhamis AA, Al-Madi EM. Comparison of cyclic fatigue resistance of 5 heat-treated nickel-titanium reciprocating systems in canals with single and double curvatures. J Endod. 2019;45(10):1237–41. https://doi.org/10.1016/j.joen.2019.06.011.
19. Sekar V, Kumar R, Nandini S, Ballal S, Velmurugan N. Assessment of the role of cross section on fatigue resistance of rotary files when used in reciprocation. Eur J Dent. 2016;10(4):541–5. https://doi.org/10.4103/1305-7456.195171.
20. Alsilani R, Jadu F, Bogari DF, Jan AM, Alhazzazi TY. Single file reciprocating systems: a systematic review and meta-analysis of the literature: comparison of reciproc and WaveOne. J Int Soc Prev Community Dent. 2016;6(5):402–9. https://doi.org/10.4103/2231-0762.192945.
21. Di Nardo D, Galli M, Morese A, Seracchiani M, Ferri V, Miccoli G, Gambarini G, Testarelli L. A comparative study of mechanical resistance of two reciprocating files. J Clin Exp Dent. 2019;11(3):e231–5. https://doi.org/10.4317/jced.55487.
22. Keleş A, Eymirli A, Uyanık O, Nagas E. Influence of static and dynamic cyclic fatigue tests on the lifespan of four reciprocating systems at different temperatures. Int Endod J. 2019;52(6):880–6. https://doi.org/10.1111/iej.13073.
23. Hülsmann M. Research that matters: studies on fatigue of rotary and reciprocating NiTi root canal instruments. Int Endod J. 2019;52(10):1401–2. https://doi.org/10.1111/iej.13194.
24. Plotino G, Grande NM, Cordaro M, Testarelli L, Gambarini G. A review of cyclic fatigue testing of nickel-titanium rotary instruments. J Endod. 2009;35(11):1469–76. https://doi.org/10.1016/j.joen.2009.06.015.
25. Topçuoğlu HS, Topçuoğlu G, Kafdağ Ö, Arslan H. Cyclic fatigue resistance of new reciprocating glide path files in 45- and 60-degree curved canals. Int Endod J. 2018;51(9):1053–8. https://doi.org/10.1111/iej.12915.

26. Iacono F, Pirani C, Arias A, de la Macorra JC, Generali L, Gandolfi MG, Prati C. Impact of a modified motion on the fatigue life of NiTi reciprocating instruments: a Weibull analysis. Clin Oral Investig. 2019;23(7):3095–102. https://doi.org/10.1007/s00784-018-2730-5.
27. Ha JH, De-Deus G, Versluis A, Kwak SW, Kim HC. Safe pseudoelastic limit range under torsional loading with Reciproc Blue. Int Endod J. 2019;52(2):244–9. https://doi.org/10.1111/iej.12988.52,244-249.
28. Kim JW, Ha JH, Cheung GSP, Versluis A, Kwak SW, Kim HC. Safety of the factory preset rotation angle of reciprocating instruments. J Endod. 2014;40(10):1671–5. https://doi.org/10.1016/j.joen.2014.06.002.
29. Plotino G, Grande NM, Testarelli L, Gambarini G. Cyclic fatigue of Reciproc and WaveOne reciprocating instruments. Int Endod J. 2012;45(7):614–8. https://doi.org/10.1111/j.1365-2591.2012.02015.x.

Publisher's Note

applied sciences

MDPI

Article

Novel Electronic Device to Quantify the Cyclic Fatigue Resistance of Endodontic Reciprocating Files after Using and Sterilization

Álvaro Zubizarreta-Macho [1], Óscar Alonso-Ezpeleta [2], Alberto Albaladejo Martínez [3], Vicente Faus Matoses [4], Javier Caviedes Brucheli [5], Rubén Agustín-Panadero [4,*], Jesús Mena Álvarez [1] and Fernando Vizmanos Martínez-Berganza [1]

1 Department of Endodontics, Faculty of Health Sciences, Alfonso X El Sabio University, 28691 Madrid, Spain; amacho@uax.es (Á.Z.-M.); jmenaalvarez@gmail.com (J.M.Á.); fvizmmar@myuax.com (F.V.M.-B.)
2 Department of Endodontics, School of Health Sciences, University of Zaragoza, 22006 Zaragosa, Spain; lalonezp@unizar.es
3 Department of Dentistry, School of Medicine, University of Salamanca, 37008 Salamanca, Spain; albertoalbaladejo@hotmail.com
4 Department of Stomatology, Faculty of Medicine and Dentistry, University of Valencia, 46010 Valencia, Spain; vfaus@clinicafaus.com
5 Centro de Investigaciones Odontológicas (C.I.O.) Pontificia, Universidad Javeriana, Bogotá 1101, Colombia; javiercaviedes@gmail.com
* Correspondence: ruben.agustin@uv.es; Tel.: +34-963-864-034

Received: 26 June 2020; Accepted: 16 July 2020; Published: 19 July 2020

Abstract: Background: The aim of this study was to analyze the effects of the time of use (TU) and sterilization cycles (SC) of endodontic reciprocating files on cyclic fatigue resistance. Methods: One-hundred-and-twenty (120) Procodile NiTi endodontic reciprocating instruments were selected at random and distributed into the following study groups: A: 0 sterilization cycles/0s time of use ($n = 10$); B: 0/60 ($n = 10$); C: 0/120 ($n = 10$); D: 1/0 ($n = 10$); E: 1/60 ($n = 10$); F: 1/120 ($n = 10$); G: 5/0 ($n = 10$); H: 5/60 ($n = 10$); I: 5/120 ($n = 10$); J: 10/0 ($n = 10$); K: 10/60 ($n = 10$); and L: 10/120 ($n = 10$). A dynamic cyclic fatigue device was designed using computer-aided design/computer-aided engineering (CAD/CAE) technology and created with a 3D printer to simulate the pecking motion performed by the clinician. Failure of the endodontic rotary instrument was detected by a light-emitting diode-light-dependent resistor (LED-LDR) system controlled by an Arduino driver complex and management software. The results were analyzed using the ANOVA test. Results: All pairwise comparisons presented statistically significant differences between the time to failure, number of cycles to failure and number of cycles of in-and-out movement for the time of use study groups ($p < 0.001$), but not in the number of sterilization cycles ($p > 0.05$). Conclusions: The time of use of NiTi endodontic reciprocating files negatively affects dynamic cyclic fatigue resistance. Dynamic cyclic resistance is not affected by the number of sterilization cycles.

Keywords: endodontics; cyclic fatigue; time of use; sterilization cycles; reciprocating movement

1. Introduction

Nickel–titanium (NiTi) endodontic rotary instruments and the subsequent development of mechanical preparation has improved the prognosis of root canal treatment, as their increased taper and automated motion enable more effective cleaning and shaping of the root canal system [1]. Many advances have been made in the last few years, including innovations in instrument design, new NiTi alloys, thermal treating of NiTi alloys, and the addition of new movements to instrumentation

systems. The changes produced in the martensitic phase of the NiTi alloy, led with little or no memory, and the decrease in the tendency of the file to straighten during use, results in a more flexible file [2] with greater resistance to both cyclic fatigue as a torsional fracture [3].

However, the possible separation of instruments remains a major concern during clinical use of NiTi files. Failure due to cyclic fatigue or torsional fracture occurs unexpectedly, without any sign of previous permanent plastic deformation. It is caused by alternating tension-compression cycles, which are generated in the instrument when it is turned in a curved channel. Many variables that can influence resistance to fracture due to cyclic fatigue and torsional stress of NiTi rotary files have been investigated, including operating speed, instrument design, metal surface treatments, effect of irrigation solutions, and the sterilization cycles to which rotary files are subjected [4].

NiTi rotary files are often reused in clinical practice for cost-saving reasons. The sterilization procedure follows the steps of disinfection, cleaning, washing, drying, packaging, and heat sterilization [5]. The disinfection and cleaning steps reduce the bacterial load and remove debris from the blades of the instrument, and the sterilization step kills any form of microorganism, including spores [6]. The most widely used method for sterilization in the dental field described in the scientific literature is heat sterilization [7].

Repeated autoclave sterilization is necessary to prevent cross-contamination between patients [8]. The heat used during sterilization procedures may affect the mechanical and physical properties of these files [9]. Previous research has found that autoclave sterilization resulted in an increase in the surface roughness of NiTi rotary files, which affects the mechanical properties [10,11]. These changes can affect the external surfaces in the form of micropitting and/or corrosion [12], reduction in cutting capacity, and/or by impairing resistance to cyclic fatigue or torsional fatigue [4]. Other studies hypothesize that after repeated clinical uses and sterilizations, there is a change in the austenite finishing temperature closest to the clinical operating temperatures. This would alter the proportions of austenite and microstructural phases of NiTi of martensite, ultimately affecting the mechanical properties of the files [2,3,13].

On the other hand, other studies suggest that autoclaving could improve the mechanical properties of instruments manufactured using a type of heat treatment, although this does not necessarily apply to other heat treatment methods. NiTi as an alloy is very "sensitive" to both thermal and mechanical (machining) tension that may occur during the raw material manufacturing processes and subsequent use of endodontic instruments. Adequate control of transition temperatures is essential to ensure optimum super-elastic properties. In addition, any other machining process will affect transition temperatures. This may explain why the performance of NiTi rotary instruments is affected by manufacturing quality processes and different thermal treatments [4,14].

Therefore, the most recent scientific literature does not always agree on the effects of sterilization. These differences may be due to the heterogeneity of the instruments researched. The endodontic instruments manufactured by various brands differ not only in diameter and the cone at the tip, but also in shape of the sections and the characteristics of alloys [15,16]. The scientific literature provides conflicting findings regarding the effects of heat sterilization on the properties of NiTi and steel instruments used in endodontics.

However, there have been no published studies analyzing the influence of clinical use and autoclaving cycles on the cyclic fatigue resistance of NiTi reciprocating files.

The aim of this study was to analyze and compare the effect of time of use and number of sterilization cycles on the dynamic cyclic fatigue resistance of NiTi endodontic reciprocating files, with a null hypothesis (H0) stating that the time of use and number of sterilization cycles would not affect the resistance of NiTi endodontic reciprocating files to dynamic cyclic fatigue.

2. Materials and Methods

2.1. Study Design

One-hundred-and-twenty (120) sterile 250 µm apical diameter and 6% taper (25.06) austenite NiTi endodontic reciprocating files (Procodile®, Komet Medical, Lemgo, Germany) with a variable tapered core, one-file system, 25 mm in length, counter-clockwise (CCW) reciprocating motion, and double-S cross-section were utilized in this in vitro study. All NiTi endodontic reciprocating files were first inspected under magnification (SZR-10, Optika, Bergamo, Italy), and all samples were included. A randomized controlled experimental trial was performed at the Department of Endodontics of the Faculty of Health Sciences at Alfonso X El Sabio University (Madrid, Spain), between September and November 2019. The NiTi endodontic reciprocating files were randomized (Epidat 4.1, Galicia, Spain) and categorized into the following study groups: A: 0 sterilization cycles and 0 seconds of dynamic cyclic fatigue (n = 10); B: 0 sterilization cycles and 60 s of dynamic cyclic fatigue (n = 10); C: 0 sterilization cycles and 120 s of dynamic cyclic fatigue (n = 10); D: 1 sterilization cycles and 0 s of dynamic cyclic fatigue (n = 10); E: 1 sterilization cycles and 60 s of dynamic cyclic fatigue (n = 10); F: 1 sterilization cycles and 120 s of dynamic cyclic fatigue (n = 10); G: 5 sterilization cycles and 0 s of dynamic cyclic fatigue (n = 10); H: 5 sterilization cycles and 60 s of dynamic cyclic fatigue (n = 10); I: 5 sterilization cycles and 120 s of dynamic cyclic fatigue (n = 10); J: 10 sterilization cycles and 0 s of dynamic cyclic fatigue (n = 10); K: 10 sterilization cycles and 60 s of dynamic cyclic fatigue (n = 10); and L: 10 sterilization cycles and 120 s of dynamic cyclic fatigue (n = 10).

2.2. Experimental Cycling Fatigue Procedure

Dynamic fatigue procedures were performed regarding the previously described cyclic fatigue device (utility model patent number ES1219520) [17]. The structure of the dynamic cyclic fatigue test device was planned by computer aided design/computer aided engineering (CAD/CAE) 2D/3D software (Midas FX+®, Brunleys, Milton Keynes, UK) and created using 3D printing (ProJet® 6000 3D Systems©, Rock Hill, SC, USA) (Figure 1A–F).

The Procodile 25.06 NiTi endodontic reciprocating file (Komet Medical, Lemgo) was assessed using a microcomputed tomography scan (Skyscan 1176, Bruker-MicroCT, Kontich, Belgium) to design an accurate standard tessellation language (STL) digital file. The STL file was used to generate a replica of an artificial root canal of 60° angle and 3 mm radius of curvature using the CAD/CAE 2D/3D software for inverse engineering technology (Figure 2A) [18]. The artificial root canal was created by means of a highly accurate subtractive technique from a stainless steel piece (Cocchiola S.A., Buenos Aires, Argentina). This process ensured intimate contact between the NiTi endodontic reciprocating files (Procodile®, Komet Medical, Lemgo) and the artificial root canal walls (Figure 1H). The artificial root canal was positioned on its own support (Figure 2B) and failure of the endodontic reciprocating files was detected by analyzing the amount of light using emitted from a Light-Emitting Diode (LED) (20000 mcd) (Ref.: 12.675/5/b/c/20k, Batuled, Coslada, Spain) (Figure 1G) by a Light-Dependent Resistor (LDR) sensor (Ref.: C000025, Arduino LLC®, Ivrea, Italy) located opposite at 3 mm of the working length, with a frequency of 50 ms to accurately detect the time of failure. The axial pecking movement of the NiTi endodontic reciprocating files affects the measurement of the light signal received by the LDR sensor, which were shown in real time on a Liquid Crystal Display (LCD) (Ref.: LCD-09568, Spark Fun Electronics, Niwot, CO, USA). Therefore, the absence of variation in light values during three cycles of light analysis was interpreted as the NiTi endodontic reciprocating file's failure. The sensor data was conditioned by a processor (Arduino UNO Rev. 3, Arduino LLC®, Ivrea, Italy), and the hardware was managed by software that receives input signals from the Arduino board.

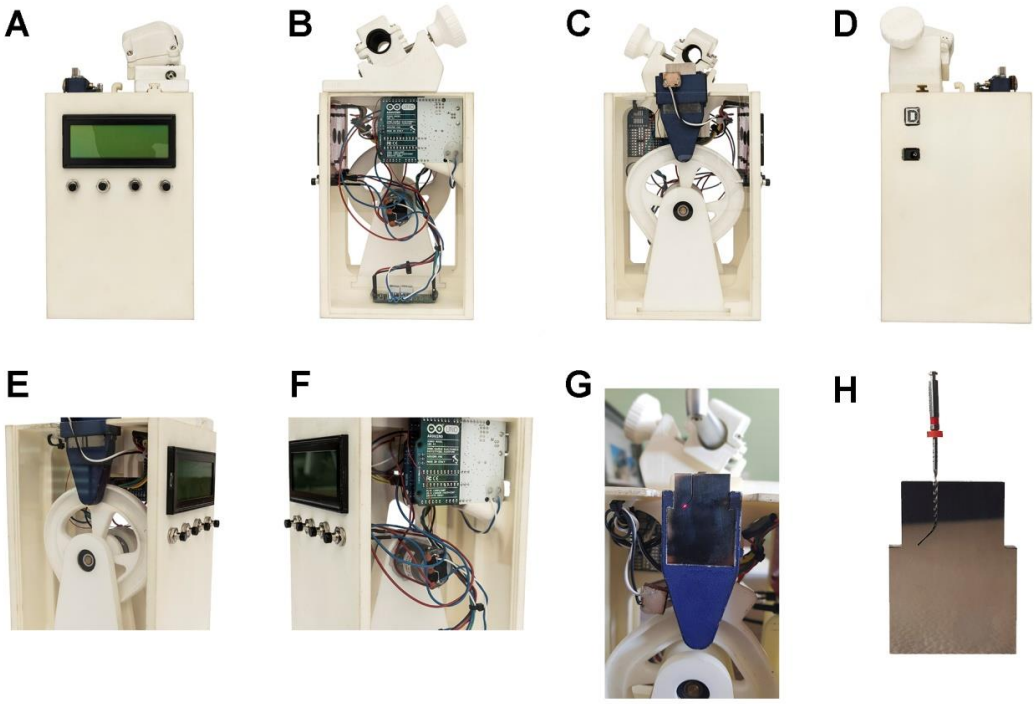

Figure 1. (**A**–**D**) Different views of the dynamic cyclic fatigue hardware device, (**E**) detail of the artificial root canal inside the artificial root canal support with the LDR sensor placed at working lenght, (**F**) detail of the Arduino board, gear motor, (**G**) detail of the artificial root canal and LED at 3 mm from working length, and (**H**) detail of the intimate contact between the artificial root canal and the NiTi endodontic reciprocating file.

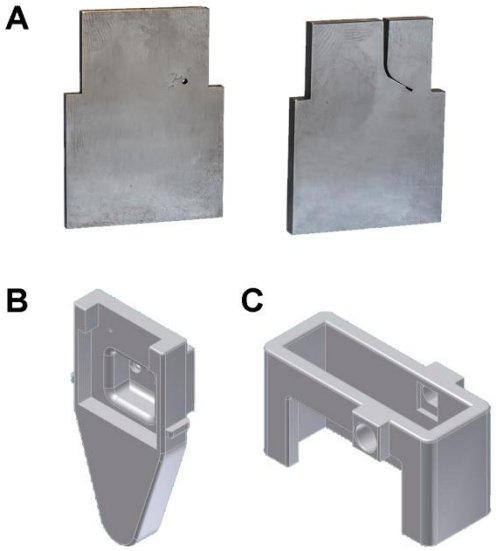

Figure 2. (**A**) Stainless steel artificial root canal plates, (**B**) CAD/CAE 2D/3D design of the artificial root canal support, and (**C**) CAD/CAE 2D/3D design of the LED-LDR detection complex.

The lineal displacement of the artificial root canal support on the lineal guide (Ref.: HGH35C 10249-1 001 MA, HIWIN Technologies Corp. Taichung, Taiwan) was generated by the gear motor (Ref.: 1589, Pololu® Corporation, Las Vegas, NV, USA) and controlled by the driver (Ref.: DRV8835, Pololu® Corporation, Las Vegas, NV, USA) through a roller bearing system (Ref.: MR104ZZ, FAG, Schaeffler Herzogenaurach, Germany). The NiTi endodontic reciprocating files (Procodile®, Komet Medical, Lemgo) were used with a 6:1 reduction handpiece (EndoPilot, Komet Medical, Lemgo) and

reciprocating motion, according to the manufacturer's instructions [19]. The endodontic handpiece (EndoPilot, Komet Medical, Lemgo) was digitalized (3D Geomagic Capture Wrap, 3D Systems©, Rock Hill, SC, USA) to enable accurate adjustment to the endodontic handpiece supports during the dynamic cyclic fatigue tests. Initially, the NiTi endodontic reciprocating files (Procodile®, Komet Medical, Lemgo) were randomly (Epidat 4.1, Galicia, Spain) unsterilized or pre-sterilized 1, 5 or 10 times using the following parameters: 3 bar, 134 °C and 45 min. Next, the NiTi endodontic reciprocating files (Procodile®, Komet Medical, Lemgo) were randomly (Epidat 4.1, Galicia, Spain) subjected to no fatigue, fatigued for 60 s or fatigued for 120 s in the dynamic cycle fatigue device. The NiTi endodontic reciprocating files (Procodile®, Komet Medical, Lemgo) were used until fracture occurred in order to analyze the effect of sterilization cycles and the time of use on the resistance of NiTi endodontic reciprocating files to cyclic fatigue.

All NiTi endodontic reciprocating files (Procodile®, Komet Medical, Lemgo) were used in the dynamic cyclic fatigue device at a frequency of 60 pecking movements/min according to a previous study [17]. To reduce the friction between the reciprocating files and the artificial canal walls, a special high-flow synthetic oil designed for the lubrication of mechanical parts (Singer All-Purpose Oil; Singer Corp., Barcelona, Spain) was applied.

All NiTi endodontic reciprocating files (Procodile®, Komet Medical, Lemgo) were used until fracture occurred. The time to failure, the number of cycles to failure, the number of cycles of in and out movements, and the length of the fractured file tip were measured and recorded.

2.3. Statistical Tests

Statistical analysis was performed by means of SAS 9.4 (SAS Institute Inc., Cary, NC, USA). Descriptive analysis is described as mean and standard deviation (SD) for quantitative data. Comparative statistics was carried out by comparing the time to failure (in seconds), the number of cycles to failure, the number of pecking movements (cycles of in-and-out movements), and the length of the fractured file tip (mm) using the ANOVA test. Furthermore, Weibull statistical analysis was also calculated. Statistical significance level was established at $p < 0.05$.

3. Results

The mean and SD values for time to failure (in seconds) and the mean length of the fractured file tip (mm) for each of the study groups are displayed in Table 1 and Figure 3.

Table 1. Descriptive analysis of the time to failure in relation to time of use and number of sterilization cycles.

Time of Use	Sterilization Cycles	*n*	Mean	SD	Minimum	Maximum	Fracture Length
0 s	0 [a]	10	235.29	45.07	153.20	282.83	3.06
	1 [a]	10	239.55	35.54	176.75	276.66	3.10
	5 [a]	10	225.26	32.04	164.10	265.31	3.17
	10 [a]	10	235.30	32.83	182.28	276.91	3.04
60 s	0 [b]	10	195.59	45.56	112.84	242.92	3.13
	1 [b]	10	191.45	31.82	136.77	234.89	3.06
	5 [b]	10	182.64	28.97	132.47	216.00	3.01
	10 [b]	10	191.18	29.71	145.94	234.33	3.04
120	0 [c]	10	88.58	12.39	61.82	102.35	3.11
	1 [c]	10	80.85	9.70	61.91	92.87	3.08
	5 [c]	10	86.90	9.56	72.16	102.01	2.99
	10 [c]	10	97.62	10.40	82.09	121.11	3.02

[a,b,c] Statistically significant differences between groups ($p < 0.05$).

The ANOVA analysis showed statistically significant differences between time to failure and the time of use of NiTi endodontic reciprocating files ($p < 0.001$) (Figure 3). However, no statistically significant differences were observed between time to failure and the number of sterilization cycles

applied to NiTi endodontic reciprocating files ($p = 0.848$) (Figure 3). The mean length of the fractured file tip did not show statistically significant differences between time to failure of the time of use ($p > 0.05$) and the sterilization cycles ($p > 0.05$) of the NiTi endodontic reciprocating files (Figure 3).

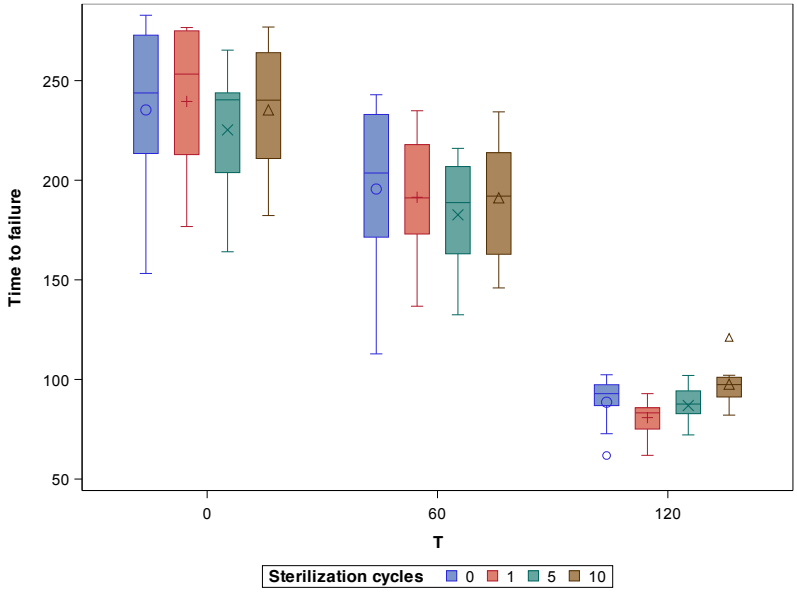

Figure 3. Box plot of the time to failure for the time of use and the sterilization cycles study groups. The horizontal line in each box represents the respective median value.

The scale distribution parameter (η) of Weibull statistics found statistically significant differences between time to failure and the time of use of NiTi endodontic reciprocating files ($p > 0.001$) (Table 2, Figure 4A); however, there were no statistically significant differences in time to failure between the number of sterilization cycles applied to NiTi endodontic reciprocating files ($p > 0.05$) (Table 2, Figure 4B). The shape distribution parameter (β) of Weibull statistics found no statistically significant differences between time to failure in relation to time of use ($p > 0.05$) (Table 2, Figure 4A), and the sterilization cycles applied to NiTi endodontic reciprocating files ($p > 0.05$) (Table 2, Figure 4B).

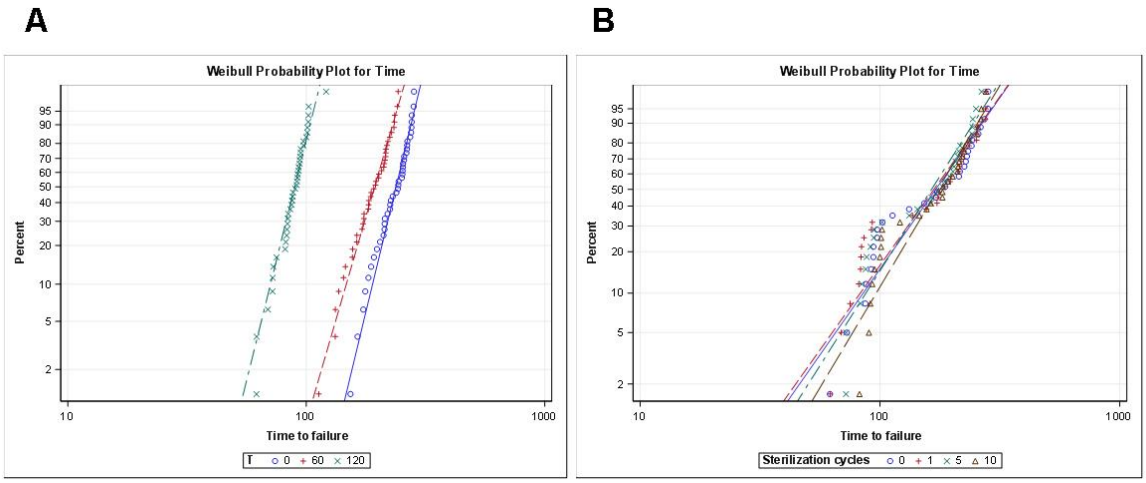

Figure 4. (**A**) Weibull probability plot of time to failure for the time of use and (**B**) sterilization cycles study groups.

Table 2. Weibull statistics of time to failure for the time of use and the sterilization cycles study groups.

Study Group	Weibull Shape (β)				Weibull Scale (η)			
	Estimate	St Error	Lower	Upper	Estimate	St Error	Lower	Upper
0 s	8.3142	1.0833	6.4404	10.7332	248.5615	4.9655	239.0173	258.4868
60 s	6.8989	0.8808	5.3716	8.8603	203.9091	4.9179	194.4944	213.7794
120 s	8.0777	0.9119	6.4743	10.0782	93.5190	1.9349	89.8025	97.3892
0 cycles	2.7040	0.4074	2.0127	3.6328	195.6014	13.9108	170.1516	224.8576
1cycle	2.6640	0.4060	1.9761	3.5913	192.7207	13.8859	167.3392	221.9521
5 cycles	2.9873	0.4529	2.2195	4.0208	185.5872	11.9333	163.6121	210.5138
10 cycles	3.1770	0.4761	2.3685	4.2617	195.9868	11.8612	174.0652	220.6693

The mean and SD values for number of cycles to failure and the length of the fractured file tip (mm) of the study groups are displayed in Table 3 and Figure 5.

Table 3. Descriptive statistics of the number of cycles to failure of the time of use and the sterilization cycles study groups.

Time of Use	Sterilization Cycles	*n*	Mean	SD	Minimum	Maximum	Fracture Length
0 s	0 [a]	10	1176.35	225.32	766.00	1414.00	3.06
	1 [a]	10	1259.40	162.90	989.50	1500.00	3.10
	5 [a]	10	1120.85	156.52	820.50	1316.50	3.17
	10 [a]	10	1176.44	164.09	911.35	1384.50	3.04
60 s	0 [b]	10	977.90	227.76	564.00	1214.50	3.13
	1 [b]	10	954.80	157.00	684.00	1174.50	3.06
	5 [b]	10	913.30	144.78	662.50	1080.00	3.01
	10 [b]	10	955.80	148.54	729.50	1171.50	3.04
120	0 [c]	10	442.96	61.98	309.10	512.00	3.11
	1 [c]	10	404.26	48.51	309.55	464.35	3.08
	5 [c]	10	431.98	48.33	360.80	510.00	2.99
	10 [c]	10	488.12	51.96	410.45	605.50	3.02

[a,b,c] Statistically significant differences between groups ($p < 0.05$).

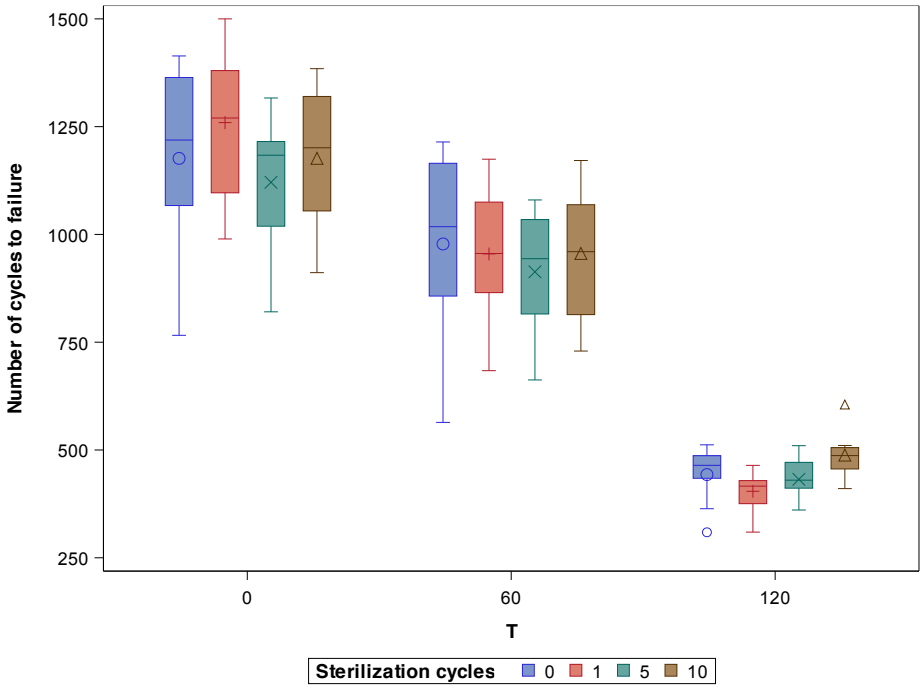

Figure 5. Box plot of the number of cycles to failure for the time of use and the sterilization cycles study groups. The horizontal line in each box represents the median value.

The ANOVA test revealed statistically significant differences between the number of cycles to failure and the time of use of NiTi endodontic reciprocating files ($p < 0.001$) (Figure 5). However, no statistically significant differences were observed between the number of cycles to failure and the number of sterilization cycles applied to NiTi endodontic reciprocating files ($p = 0.848$) (Figure 5). The mean length of the fractured file tip did not show statistically significant differences between the number of cycles to failure and the time of use ($p > 0.05$) and number of sterilization cycles ($p > 0.05$) applied to the NiTi endodontic reciprocating files (Figure 5).

The scale distribution parameter (η) of Weibull statistics showed statistically significant differences between the number of cycles to failure and the time of use of NiTi endodontic reciprocating files ($p < 0.001$) (Table 4, Figure 6A); however, there were no statistically significant differences between the number of cycles to failure and the number of sterilization cycles applied to NiTi endodontic reciprocating files ($p > 0.05$) (Table 4, Figure 6B). The shape distribution parameter (β) of Weibull statistics did not show statistically significant differences between the number of cycles to failure and the time of use ($p > 0.05$) (Table 4, Figure 6A), nor the number of sterilization cycles applied to NiTi endodontic reciprocating files ($p > 0.05$) (Table 4, Figure 6B).

Table 4. Weibull statistics of the number of cycles to failure for the time of use and sterilization cycles study groups.

Study Group	Weibull Shape (β)				Weibull Scale (η)			
	Estimate	St Error	Lower	Upper	Estimate	St Error	Lower	Upper
0 s	8.1790	1.0424	6.3712	10.4999	1257.379	25.5617	1208.264	1308.4906
60 s	6.9078	0.8808	5.3803	8.8690	1018.7335	24.5392	971.7553	1067.9829
120 s	8.0244	0.9069	6.4301	10.0141	467.0982	9.7300	448.4118	486.5633
0 cycles	2.7040	0.4074	2.0127	3.6328	195.6014	13.9108	170.1516	224.8576
1cycle	2.6640	0.4060	1.9761	3.5913	192.7207	13.8859	167.3392	221.9521
5 cycles	2.9873	0.4529	2.2195	4.0208	185.5872	11.9333	163.6121	210.5138
10 cycles	3.1770	0.4761	2.3685	4.2617	195.9868	11.8612	174.0652	220.6693

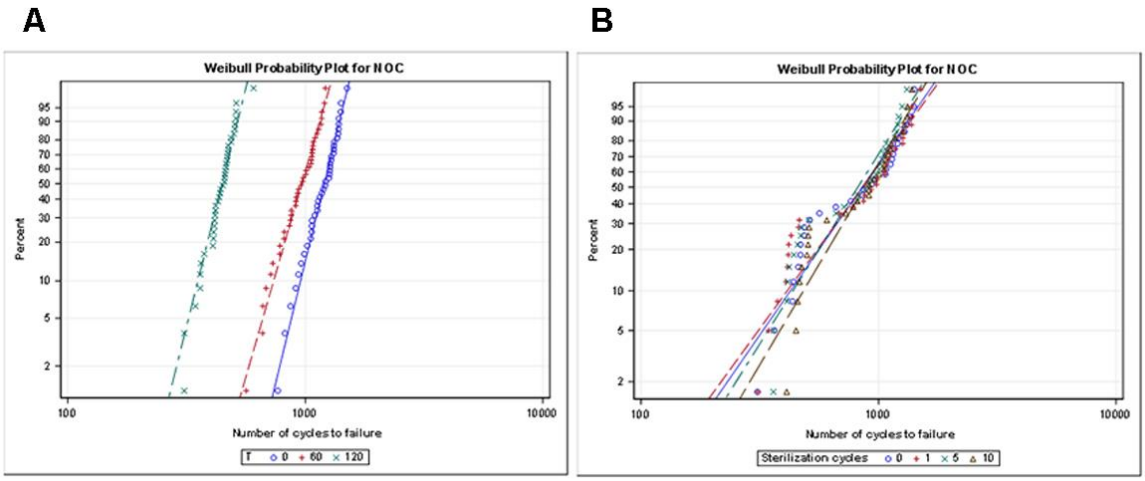

Figure 6. (**A**) Weibull probability plot of the number of cycles to failure for the time of use and (**B**) sterilization cycles study groups.

The mean and SD values for the number of cycles of in-and-out movement and the length of the fractured file tip (mm) of the study groups are displayed in Table 5 and Figure 7.

Table 5. Descriptive statistics of the number of cycles of in-and-out movement for the time of use and sterilization cycles study groups.

Time of Use	Sterilization Cycles	*n*	Mean	SD	Minimum	Maximum	Fracture Length
0s	0 [a]	10	235.29	45.07	153.20	282.83	3.06
	1 [a]	10	239.55	35.54	176.75	276.66	3.10
	5 [a]	10	225.26	32.04	164.10	265.31	3.17
	10 [a]	10	229.30	46.31	122.28	276.91	3.04
60s	0 [b]	10	214.69	30.30	162.27	251.10	3.13
	1 [b]	10	205.45	38.46	136.77	265.01	3.06
	5 [b]	10	186.64	38.88	132.47	246.87	3.01
	10 [b]	10	183.18	48.23	113.82	264.33	3.04
120	0 [c]	10	88.58	12.39	61.82	102.35	3.11
	1 [c]	10	80.85	9.70	61.91	92.87	3.08
	5 [c]	10	86.90	9.56	72.16	102.01	2.99
	10 [c]	10	97.62	10.40	82.09	121.11	3.02

[a,b,c] Statistically significant differences between groups ($p < 0.05$).

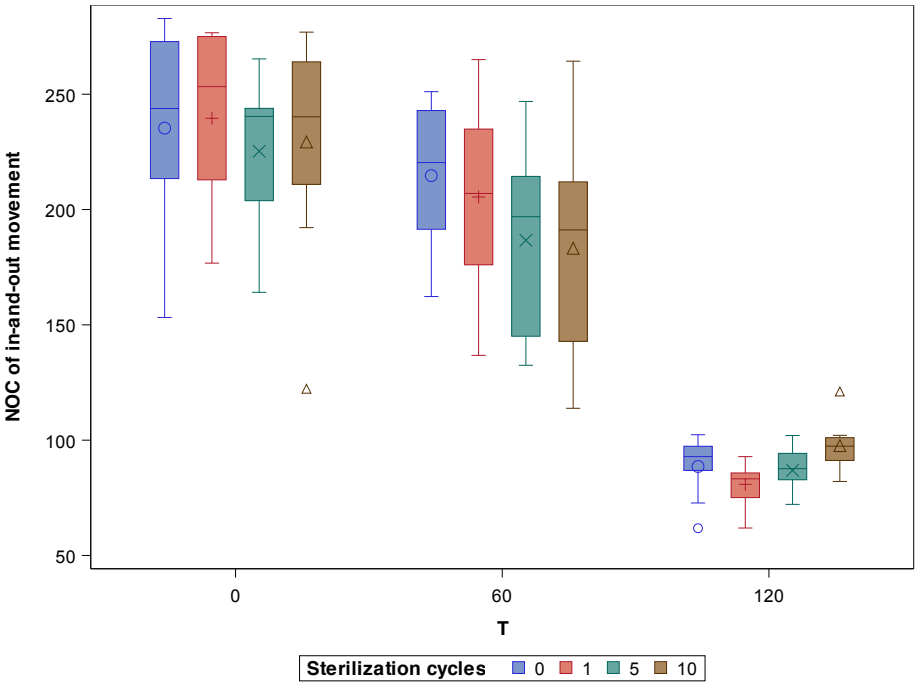

Figure 7. Box plot of the number of cycles of in-and-out movement for the time of use and sterilization cycles study groups. The horizontal line in each box represents the median value.

The ANOVA test revealed statistically significant differences between the number of cycles of in and out movement and the time of use of NiTi endodontic reciprocating files ($p < 0.001$) (Figure 7). However, no statistically significant differences were observed between the number of cycles of in and out movement and the number of sterilization cycles applied to NiTi endodontic reciprocating files ($p = 0.848$) (Figure 7). The mean length of the fractured file tip did not show statistically significant differences between the number of cycles of in-and-out movement and the time of use ($p > 0.05$) or the number of sterilization cycles ($p > 0.05$) applied to the NiTi endodontic reciprocating files (Figure 7).

The scale distribution parameter (η) of Weibull statistics showed statistically significant differences between the number of cycles of in-and-out movement and the time of use of NiTi endodontic reciprocating files ($p < 0.001$) (Table 6, Figure 8A); however, no statistically significant differences were found between the number of cycles of in-and-out movement and the number of sterilization cycles applied to the NiTi endodontic reciprocating files ($p > 0.05$) (Table 6, Figure 8B). The shape distribution parameter (β) of Weibull statistics did not show statistically significant differences between the number

of cycles of in-and-out movement and the time of use ($p > 0.05$) (Table 6, Figure 8A) or the number of sterilization cycles applied to the NiTi endodontic reciprocating files ($p > 0.05$) (Table 6, Figure 8B).

Table 6. Weibull statistics of the number of cycles of in-and-out movements for the time of use and sterilization cycles study groups.

Study Group	Weibull Shape (β)				Weibull Scale (η)			
	Estimate	St Error	Lower	Upper	Estimate	St Error	Lower	Upper
0 s	7.8371	1.0332	6.0526	10.1478	247.8093	5.2331	237.7620	258.2813
60 s	5.9056	0.7502	4.6039	7.5752	213.5034	6.0177	202.0287	225.6298
120 s	8.0777	0.9119	6.4743	10.0782	93.5190	1.9349	89.8025	97.3892
0 cycles	2.8397	0.4369	2.1004	3.8391	202.3470	13.6633	177.2639	230.9795
1cycle	2.6486	0.4087	1.9573	3.5841	198.0170	14.3348	171.8235	228.2036
5 cycles	2.9091	0.4413	2.1610	3.9163	187.3384	12.3756	164.5872	213.2345
10 cycles	2.8747	0.4233	2.1540	3.8366	191.7153	12.8646	168.0889	218.6626

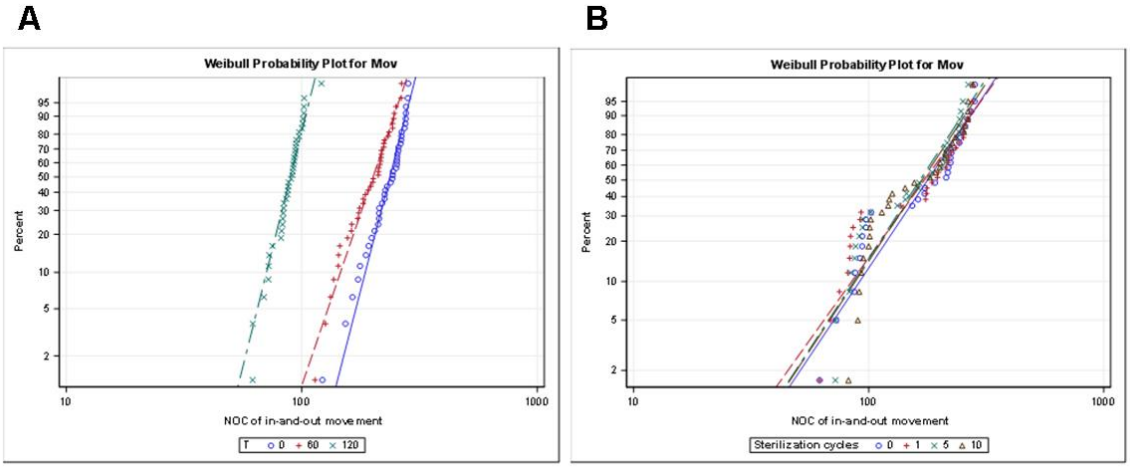

Figure 8. (**A**) Weibull probability plot of the number of cycles of in-and-out movements for the time of use and (**B**) sterilization cycles study groups.

4. Discussion

The results obtained in the present study reject the null hypothesis (H0) that states that time of use would have no effect on the dynamic cyclic fatigue resistance of NiTi endodontic reciprocating files. However, it also accepts the null hypothesis (H0) that states that the number of sterilization cycles applied to NiTi endodontic reciprocating files would have no effect on their resistance to dynamic cyclic fatigue.

The cyclic fatigue resistance of NiTi endodontic rotary and reciprocating instruments has been widely compared with regard to the NiTi alloy used, cross-section design, curvature angle, radius, pecking motion frequency, etc., with both static and dynamic custom-made cyclic fatigue devices having been used [20,21]. However, dynamic custom-made cyclic fatigue devices are the only ones that faithfully simulate the pecking movement performed by the clinician, more accurately representing the amount of time during which the NiTi endodontic rotary instrument remains in the artificial root canal. In addition, the artificial root canal should be custom-designed for the specific NiTi endodontic rotary instrument being tested in order to ensure immediate contact with the artificial root canal (as happens in a clinical setting). This also ensures that compression and tensile stress cycles are localized at the maximum flexure point [22], distributes the shear resistance homogeneously along the NiTi endodontic rotary instrument surface, and leads to the formation of microcracks on the instruments' microstructure [23] without any signs of plastic deformation in the static model; the area of these stresses spreads through the instrument shaft in the dynamic model [21]. Most of the static and dynamic custom-made cyclic fatigue devices provided a non-instrument-based artificial root

canal [24,25], so the results extracted from these studies should be carefully considered and not applied to clinical practice. Di Nardo et al. reported statistically significant differences ($p < 0.05$) between the time to failure of Wave One Gold NiTi endodontic reciprocating files (50.75 ± 20.06 s) and Reziflow (30.13 ± 9.40) conventional NiTi endodontic rotary instruments [26]. Although this was a static cyclic fatigue test with an artificial root canal of parallel walls and 90° and 5 mm curvature radius, Reziflow has a similar design and manufacturing process as Procodile. In this study, a curvature angle of 60° was designed, because Topçuoğlu et al. reported that artificial root canals with a 45° angle of curvature did not show statistically significant differences ($p > 0.05$) between the time to failure of WaveOne Gold (412.4 ± 55.2 s) and R-Pilot (394.5 ± 45.3 s) glider files; however, artificial root canals with a curvature angle of 60° showed statistically significant differences ($p < 0.05$) between the time to failure of WaveOne Gold (368.3 ± 44.1 s) and R-Pilot (247.2 ± 36.2 s) endodontic instruments [27].

Kim et al. state that the endodontic reciprocating instruments must be disposed of after the first use because the mechanical properties, metallurgical features and risk of failure of the endodontic reciprocating instruments result from repeated usage [28]. Furthermore, Generali et al. reported that the continued usage of Reciproc and Reciproc Blue endodontic reciprocating instruments reduced resistance to cyclic fatigue, also reducing the martensite and R-phase in Reciproc Blue endodontic reciprocating instruments and causing microcracks near the tip of both endodontic reciprocating instruments after usage. In addition, there were statistically significant differences ($p < 0.05$) between the cyclic fatigue resistance of new and used Reciproc Blue endodontic reciprocating instruments, in keeping with the findings of the present study. However, no statistically significant differences ($p > 0.05$) were observed between the cyclic fatigue resistance of new and used Reciproc endodontic reciprocating instruments. Regardless of the NiTi alloy of the endodontic reciprocating system, the double-S cross-section design of Reciproc and Reciproc Blue endodontic reciprocating instruments and the reciprocating movement are similar to the Procodile NiTi endodontic reciprocating instruments; even the DSC curves confirm that the Reciproc Blue endodontic reciprocating instruments are made up of a mix of austenite and R-phase, as observed in XRD patterns [29]. However, this was a static cyclic fatigue test with an artificial root canal machined on a quenched martensitic carbon steel plate. The endodontic instruments are designed to cut dentin, but not materials with different cutting resistance values, so the results of the present study can hardly be accurately extrapolated to a clinical setting. However, in the present study, the NiTi endodontic reciprocating instruments were selected in the austenite phase due to their physical and metallurgical properties in terms of hardness and cutting capability in order to ensure the advance of the NiTi endodontic reciprocating instrument inside the stainless steel artificial root canal. In addition, the automatic, objective detection of the NiTi endodontic reciprocating instruments failure process using a LED-LDR system provided an accurate and standardizable measurement procedure, regardless of the subjective measurement protocol used in most studies to detect the precise moment of failure of the endodontic instrument tip. No statistically significant difference was found between the mean lengths of fractured file tips, whose maximum area of stress corresponded to the mid-point arc of the apical curvature, in keeping with the findings of Pruett et al. [22]. This result confirms the correct and repeated positioning of the tested NiTi endodontic reciprocating instruments within the artificial root canal.

Some researchers have postulated that the gamma-ray and autoclave sterilization processes used for fully sterile packaged Hyflex EDM and TRUShape endodontic rotary instruments might impact on the life span of NiTi martensitic endodontic rotary instruments in terms of their resistance to fatigue [30]. Furthermore, the heat sterilization method can also cause changes in the physical and mechanical properties of NiTi endodontic rotary instruments and even impact the torsional properties of NiTi endodontic rotary instruments [31]. Yang et al. reported that the surface roughness of K3XF R-phase NiTi endodontic rotary instruments increased after autoclaving, but this did not affect the cyclic fatigue resistance after 30 sterilization cycles [32]. Pedullà et al. found that repeated sterilization cycles did not impact resistance of NiTi endodontic rotary instruments to fatigue except for Twisted Files R-phase NiTi endodontic rotary instruments, which showed a significant decrease

in flexural resistance after three sterilization cycles ($p < 0.05$) [33]. Champa et al. showed that multiple sterilization cycles significantly increased the cyclic fatigue resistance of Reciproc M-Wire NiTi endodontic reciprocating instruments, but decreased the cyclic fatigue resistance of Wave One M Wire NiTi endodontic reciprocating instruments in an artificial root canal (not anatomically modeled) with 60° of curvature in a static cyclic fatigue device [34]. Özyürek et al. also reported that the sterilization cycles significantly increased the cyclic fatigue resistance of Protaper Next M-Wire NiTi endodontic rotary instruments ($p < 0.05$) and Protaper Gold alloy NiTi endodontic rotary instruments ($p < 0.05$) [35]. Zhao et al. showed that the cyclic fatigue resistance of pre-sterilized HyFlex CM CM Wire NiTi endodontic rotary instruments and K3XF R-phase NiTi endodontic rotary instruments increased significantly ($p < 0.05$) after 10 sterilization cycles in an artificial root canal (not anatomically modeled) with a curvature of 60° and a radius of 3 mm in a static cyclic fatigue device [36]. Most of the martensitic endodontic rotary instruments (M-Wire alloys) have demonstrated an increase in cyclic fatigue resistance after heat sterilization procedures. However, in the present study, the cyclic fatigue resistance of austenite NiTi endodontic reciprocating files was not affected after 10 autoclave sterilization cycles ($p > 0.05$). The thermal treating of M-Wire endodontic rotary instruments makes the martensitic phase of NiTi alloy less subject to breakage during clinical use and stabilizes the NiTi alloy. The thermal heating induced by heat sterilization procedures make it even more stable, increasing cyclic fatigue resistance [31].

5. Conclusions

The conclusion derived from the present study is that the time of use of austenite NiTi endodontic reciprocating files negatively affects their dynamic cyclic fatigue resistance; however, resistance to dynamic cyclic fatigue is not affected by the number of sterilization cycles.

Author Contributions: All of the authors contributed to the investigation, supervision, writing, review, and editing of the study. The study was conceptualized by J.M.Á., A.A.M., Á.Z.-M., and R.A.-P. Data curation, data visualization, and analysis were carried out by V.F.M., J.C.B., F.V.M.-B. and Ó.A.-E. All authors have read and agreed to the published version of the manuscript.

Funding: This research received no external funding.

Conflicts of Interest: The authors declare no conflicts of interest.

References

1. Gavini, G.; Santos, M.D.; Caldeira, C.L.; Machado, M.; Freire, L.G.; Iglecias, E.F.; Peters, O.A.; Candeiro, G. Nickel-titanium instruments in endodontics: A concise review of the state of the art. *Braz. Oral. Res.* **2018**, *32*, 67. [CrossRef] [PubMed]
2. Shen, Y.; Zhou, H.M.; Zheng, Y.F.; Campbell, L.; Peng, B.; Haapasalo, M. Metallurgical characterization of controlled memory wire nickel-titanium rotary instruments. *J. Endod.* **2011**, *37*, 1566–1571. [CrossRef]
3. Testarelli, L.; Plotino, G.; Al-Sudani, D.; Vincenzi, V.; Giansiracusa, A.; Grande, N.M.; Gambarini, G. Bending properties of a new nickel-titanium alloy with a lower percent by weight of nickel. *J. Endod.* **2011**, *37*, 1293–1295. [CrossRef] [PubMed]
4. Plotino, G.; Costanzo, A.; Grande, N.M.; Petrovic, R.; Testarelli, L.; Gambarini, G. Experimental evaluation on the influence of autoclave sterilization on the cyclic fatigue of new nickel-titanium rotary instruments. *J. Endod.* **2012**, *38*, 222–225. [CrossRef] [PubMed]
5. Laneve, E.; Raddato, B.; Dioguardi, M.; Di Gioia, G.; Troiano, G.; Lo Muzio, L. Sterilisation in Dentistry: A Review of the Literature. *Int. J. Dent.* **2019**, *2019*, 650728. [CrossRef] [PubMed]
6. Sheth, N.C.; Rathod, Y.V.; Shenoi, P.R.; Shori, D.D.; Khode, R.T.; Khadse, A.P. Evaluation of new technique of sterilization using biological indicator. *J. Conserv. Dent.* **2017**, *20*, 346–350. [CrossRef]
7. Raju, T.B.V.G.; Garapati, S.; Agrawal, R.; Reddy, S.; Razdan, A.; Kumar, S.K. Sterilizing Endodontic Files by four different sterilization methods to prevent cross-infection. An In-vitro Study. *J. Int. Oral. Health* **2013**, *5*, 108–112.

8. Spagnuolo, G.; Ametrano, G.; D'antò, V.; Rengo, C.; Simeone, M.; Riccitiello, F.; Amato, M. Effect of autoclaving on the surfaces of TiN-coated and conventional nickel–titanium rotary instruments. *Int. Endod. J.* **2012**, *45*, 1148–1155. [CrossRef]
9. Casper, R.B.; Roberts, H.W.; Roberts, M.D.; Himel, V.T.; Bergeron, B.E. Comparison of autoclaving effects on torsional deformation and fracture resistance of three innovative endodontic file systems. *J. Endod.* **2011**, *37*, 1572–1575. [CrossRef]
10. Valois, C.R.; Silva, L.P.; Azevedo, R.B. Multiple autoclave cycles affect the surface of rotary nickel-titanium files: An atomic force microscopy study. *J. Endod.* **2008**, *34*, 859–862. [CrossRef]
11. Alapati, S.B.; Brantley, W.A.; Svec, T.A.; Powers, J.M.; Nusstein, J.M.; Daehn, G.S. SEM observations of nickel-titanium rotary endodontic instruments that fractured during clinical use. *J. Endod.* **2005**, *31*, 40–43. [CrossRef]
12. Grassi, F.R.; Pappalettere, C.; Di Comite, M.; Corsalini, M.; Mori, G.; Ballini, A.; Crincoli, V.; Pettini, F.; Rapone, B.; Boccaccio, A. Effect of different irrigating solutions and endodontic sealers on bond strength of the dentin-post interface with and without defects. *Int. J. Med. Sci.* **2012**, *9*, 642–654. [CrossRef] [PubMed]
13. Seago, S.T.; Bergeron, B.E.; Kirkpatrick, T.C.; Roberts, M.D.; Roberts, H.W.; Himel, V.T.; Sabey, K.A. Effect of Repeated Simulated Clinical Use and Sterilization on the Cutting Efficiency and Flexibility of Hyflex CM Nickel-Titanium Rotary Files. *J. Endod.* **2015**, *41*, 725–728. [CrossRef] [PubMed]
14. Hilfer, P.B.; Bergeron, B.E.; Mayerchak, M.J.; Roberts, H.W.; Jeansonne, B.G. Multiple autoclave cycle effects on cyclic fatigue of nickel-titanium rotary files produced by new manufacturing methods. *J. Endod.* **2011**, *37*, 72–74. [CrossRef] [PubMed]
15. Alfoqom Alazemi, M.; Bryant, S.T.; Dummer, P.M. Deformation of HyFlex CM instruments and their shape recovery following heat sterilization. *Int. Endod. J.* **2015**, *48*, 593–601. [CrossRef] [PubMed]
16. Ferreira, F.; Adeodato, C.; Barbosa, I.; Aboud, L.; Scelza, P.; Zaccaro Scelza, M. Movement kinematics and cyclic fatigue of NiTi rotary instruments: A systematic review. *Int. Endod. J.* **2017**, *50*, 143–152. [CrossRef] [PubMed]
17. Zubizarreta-Macho, A.; Mena Álvarez, J.; Albadalejo Martínez, A.; Segura-Egea, J.J.; Caviedes Brucheli, J.; Agustín-Panadero, R.; López Píriz, R.; Alonso-Ezpeleta, O. Influence of the pecking motion on the cyclic fatigue resistance of endodontic rotary files. *J. Clin. Med.* **2020**, *9*, 45. [CrossRef] [PubMed]
18. Schneider, S.W. A comparison of canal preparations in straight and curved root canals. *Oral. Surg. Oral. Med. Oral. Pathol.* **1971**, *32*, 271–275. [CrossRef]
19. Rubio, J.; Zarzosa, J.I.; Pallarés, A. A Comparative Study of Cyclic Fatigue of 10 Different Types of Endodontic Instruments: An in Vitro Study. *Acta Stomatol. Croat.* **2019**, *53*, 28–36. [CrossRef]
20. De-Deus, G.; Vieira VT, L.; da Silva EJ, N.; Lopes, H.; Elias, C.N.; Moreira, E.J. Bending resistance and dynamic and static cyclic fatigue life of Reciproc and WaveOne large instruments. *J. Endod.* **2014**, *40*, 575–579. [CrossRef]
21. Keleş, A.; Eymirli, A.; Uyanık, O.; Nagas, E. Influence of static and dynamic cyclic fatigue tests on the lifespan of four reciprocating systems at different temperatures. *Int. Endod. J.* **2019**, *52*, 880–886. [CrossRef] [PubMed]
22. Pruett, J.P.; Clement, D.J.; Carnes, D.L., Jr. Cyclic fatigue testing of nickel-titanium endodontic instruments. *J. Endod.* **1997**, *23*, 77–85. [CrossRef]
23. Hulsmann, M.; Donnermeyer, D.; Schäfer, E. A critical appraisal of studies on cyclic fatigue resistance of engine-driven endodontic instruments. *Int. Endod. J.* **2019**, *52*, 1427–1445. [CrossRef] [PubMed]
24. Olcay, K.; Eyuboglu, T.F.; Erkan, E. Cyclic fatigue resistance of wave one gold, protaper next and 2shape nickel titanium rotary instruments using a reliable method for measuring temperature. *Niger. J. Clin. Pract.* **2019**, *22*, 1335–1340. [CrossRef]
25. Scott, R.; Arias, A.; Macorra, J.C.; Govindjee, S.; Peters, O.A. Resistance to cyclic fatigue of reciprocating instruments determined at body temperature and phase transformation analysis. *Aust. Endod. J.* **2019**, *45*, 400–406. [CrossRef]
26. Di Nardo, D.; Galli, M.; Morese, A.; Seracchiani, M.; Ferri, V.; Miccoli, G.; Gambarini, G.; Testarelli, L. A comparative study of mechanical resistance of two reciprocating files. *J. Clin. Exp. Dent.* **2019**, *11*, 231–235. [CrossRef]
27. Topçuoğlu, H.S.; Topçuoğlu, G.; Kafdağ, Ö.; Arslan, H. Cyclic fatigue resistance of new reciprocating glide path files in 45- and 60-degree curved canals. *Int. Endod. J.* **2018**, *51*, 1053–1058. [CrossRef]

28. Kim, J.W.; Ha, J.H.; Cheung, G.S.P.; Versluis, A.; Kwak, S.W.; Kim, H.C. Safety of the factory preset rotation angle of reciprocating instruments. *J. Endod.* **2014**, *40*, 1671–1675. [CrossRef]
29. Generali, L.; Puddu, P.; Borghi, A.; Brancolini, S.; Lusvarghi, L.; Bolelli, G.; Consolo, U.; Pedullà, E. Mechanical properties and metallurgical features of new and ex vivo used Reciproc Blue and Reciproc. *Int. Endod. J.* **2020**, *53*, 250–264. [CrossRef]
30. Arias, A.; Macorra, J.C.; Govindjee, S.; Peters, O.A. Effect of gamma-ray sterilization on phase transformation behavior and fatigue resistance of contemporary nickel-titanium instruments. *Clin. Oral. Investig.* **2020**, *20*. [CrossRef]
31. Dioguardi, M.; Sovereto, D.; Aiuto, R.; Laino, L.; Illuzzi, G.; Laneve, E.; Raddato, B.; Caponio, V.C.A.; Dioguardi, A.; Zhurakivska, K.; et al. Effects of Hot Sterilization on Torsional Properties of Endodontic Instruments: Systematic Review with Meta-Analysis. *Materials (Basel)* **2019**, *12*, 2190. [CrossRef] [PubMed]
32. Yang, Y.J.; Hou, B.X.; Hou, X.M. Effect of autoclave on surface microstructure and cyclic fatigue resistance of R-phase rotary instruments. *Beijing Da Xue Xue Bao Yi Xue Ban* **2018**, *50*, 882–886. [PubMed]
33. Pedullà, E.; Benites, A.; La Rosa, G.M.; Plotino, G.; Grande, N.M.; Rapisarda, E.; Generali, L. Cyclic Fatigue Resistance of Heat-treated Nickel-titanium Instruments after Immersion in Sodium Hypochlorite and/or Sterilization. *J. Endod.* **2018**, *44*, 648–653. [CrossRef]
34. Champa, C.; Divya, V.; Srirekha, A.; Karale, R.; Shetty, A.; Sadashiva, P. An analysis of cyclic fatigue resistance of reciprocating instruments in different canal curvatures after immersion in sodium hypochlorite and autoclaving: An in vitro study. *J. Conserv. Dent.* **2017**, *20*, 194–198. [PubMed]
35. Özyürek, T.; Yılmaz, K.; Uslu, G. The effects of autoclave sterilization on the cyclic fatigue resistance of ProTaper Universal, ProTaper Next, and ProTaper Gold nickel-titanium instruments. *Restor. Dent. Endod.* **2017**, *42*, 301–308. [CrossRef] [PubMed]
36. Zhao, D.; Shen, Y.; Peng, B.; Haapasalo, M. Effect of autoclave sterilization on the cyclic fatigue resistance of thermally treated Nickel-Titanium instruments. *Int. Endod. J.* **2016**, *49*, 990–995. [CrossRef]

International Journal of
Environmental Research and Public Health

MDPI

Article

Comparative Study of the SEM Evaluation, EDX Assessment, Morphometric Analysis, and Cyclic Fatigue Resistance of Three Novel Brands of NiTi Alloy Endodontic Files

Vicente Faus-Matoses [1], Raúl Pérez García [1], Vicente Faus-Llácer [1], Ignacio Faus-Matoses [1,*], Óscar Alonso Ezpeleta [2], Alberto Albaladejo Martínez [3] and Álvaro Zubizarreta-Macho [3,4,†]

[1] Department of Stomatology, Faculty of Medicine and Dentistry, University of Valencia, 46010 Valencia, Spain; vicente.faus@uv.es (V.F.-M.); raulpe8@alumni.uv.es (R.P.G.); fausvj@uv.es (V.F.-L.)
[2] Department of Endodontics, School of Health Sciences, University of Zaragoza, 22006 Zaragoza, Spain; lalonezp@unizar.es
[3] Department of Surgery, Faculty of Medicine and Dentistry, University of Salamanca, 37008 Salamanca, Spain; albertoalbaladejo@hotmail.com (A.A.M.); alvaro.zubizarreta@usal.es or amacho@uax.es (Á.Z.-M.)
[4] Department of Endodontics, Faculty of Health Sciences, Alfonso X El Sabio University, 28691 Madrid, Spain
* Correspondence: ignacio.faus@uv.es
† Current address: Department of Implant Surgery, Faculty of Health Sciences, Alfonso X El Sabio University, Avda., Universidad, 1, 28691 Villanueva de la Cañada, Spain.

Abstract: In this study, we compare and analyze the scanning electron microscopy (SEM), energy-dispersive X-ray spectroscopy (EDX), morphometry and cyclic fatigue resistance of Endogal, Path-Max, and Smarttrack novel brands of nickel–titanium (NiTi) alloy endodontic files. Material and Methods: Thirty sterile NiTi endodontic rotary files were randomly selected and assigned to one of the following study groups: A: 25.08 F2 Endogal (EDG) (n = 10); B: 25.08 F2 Path Max Pro (PMP) (n = 10); and C: 25.06 Smarttrack (ST) (n = 10). Dynamic cyclic fatigue tests were conducted using a cyclic fatigue device in stainless steel artificial root canal systems with an apical diameter of 250 µm, curvature angle of 60°, radius of curvature of 3 mm, and taper of 6%. Additionally, we analyzed the NiTi endodontic rotary files using EDX, SEM, and morphometry after micro-CT scanning. The results were analyzed using Weibull statistical analysis and ANOVA testing. Results: SEM, EDX, and morphometric analyses showed differences between the three novel brands of NiTi endodontic rotary files. Moreover, statistically significant differences were observed between the number of cycles to failure and time to failure of the three novel brands of NiTi endodontic rotary files ($p < 0.001$). Conclusions: Smarttrack NiTi alloy endodontic reciprocating files display greater resistance to cyclic fatigue than Endogal and Path Max Pro NiTi alloy endodontic rotary files, due to the reciprocating movement and metallurgical composition.

Keywords: cyclic fatigue; endodontics; energy-dispersive X-ray; scanning electron microscopy; morphometry; reciprocating; continuous rotation; NiTi

Citation: Faus-Matoses, V.; Pérez García, R.; Faus-Llácer, V.; Faus-Matoses, I.; Alonso Ezpeleta, Ó.; Albaladejo Martínez, A.; Zubizarreta-Macho, Á. Comparative Study of the SEM Evaluation, EDX Assessment, Morphometric Analysis, and Cyclic Fatigue Resistance of Three Novel Brands of NiTi Alloy Endodontic Files. *Int. J. Environ. Res. Public Health* **2022**, *19*, 4414. https://doi.org/10.3390/ijerph19074414

Received: 8 March 2022
Accepted: 4 April 2022
Published: 6 April 2022

1. Introduction

The use of nickel–titanium (NiTi) alloy for the manufacturing of instruments used in root canals has revolutionized the field of endodontics, with these new endodontic instruments reducing iatrogenic complications [1,2]. Nevertheless, failure of these instruments is still a concern for clinicians. Despite the continued chemical and mechanical improvements to the NiTi alloy endodontic rotary instruments by their manufacturers in an effort to prevent potential root canal treatment complications [3], fractures of NiTi endodontic rotary files still occur, with an incidence rate between 0.09% and 5% [4,5]. These nickel–titanium alloy endodontic rotary files fail when their resistance to fatigue is surpassed by flexural bending (cyclic) stress, torsional stress or a combination thereof [6]. More

precisely, torsional fatigue is seen when the tip of the endodontic file becomes blocked within the root canal as the instrument still rotates [7]. Flexural bending fatigue occurs when alternating tensile and compressive stress cycles applied on a curved root canal result in plastic deformities and the endodontic rotary instrument subsequently fails [7,8], despite the centering ability and contact pressure distribution of the NiTi endodontic rotary file against the root canal walls during shaping of the root canal system [9,10].

Furthermore, unexpected failures of NiTi alloy endodontic rotary instruments can inhibit good clinical outcomes by blocking disinfecting agents from penetrating past the fractured instrument [11–13], potentially leading to pulp necrosis and causing periapical lesions to form [14]. This can also affect the success rates of root canal treatments in teeth with periapical pathologies [15]. In an effort to address these issues, several studies have assessed the effect of both nickel–titanium alloys and geometric parameters on the resistance to flexural bending and torsional fatigue of endodontic rotary instruments, with the aim of lowering the incidence of failure in these instruments. The crystalline structure and chemical make-up of the nickel–titanium alloy have both been extensively analyzed as factors affecting the fatigue resistance of endodontic rotary files, especially in endodontic rotary systems with a more highly concentrated martensitic phase or those manufactured by electro-polishing, ion implantation, cryogenic treatment, and heat treatment to improve the mechanical behaviors of NiTi endodontic rotary files; particularly, increasing their resistance to cyclic fatigue [16]. Nevertheless, researchers have reported that certain geometric factors also influence instrument performance, including the apical diameter and taper [17], flute length, cross-section design [18,19], pitch [18], brushing movement [20], and helix angle. In addition, Nóvoa et al. evidenced the corrosive effect of a sodium hypochlorite irrigating solution on NiTi alloy endodontic rotary files [21]. However, Cavalleri et al. reported that this corrosive effect does not increase the risk of fracture of the NiTi alloy endodontic rotary instrument [22]. Unfortunately, it is difficult to independently assess each factor that is linked to flexural bending fatigue within a clinical setting, due to the heterogeneous anatomical make-up of root canal systems. As a result, controlled experimental studies have enabled the independent analysis of each variable using custom-made cyclic fatigue devices.

More recently, novel brands of NiTi alloy endodontic instruments, such as Endogal, PathMax, and Smarttrack, have emerged to enhance the mechanical properties and reduce the rates of failure of current instrumentation systems [23]. However, the absence of literature related to the geometrical design, metallurgical composition, and mechanical properties require a study to analyze the metallurgical composition and compare the cyclic fatigue resistance of these instruments.

In the present study, we aim to analyze and compare the scanning electron microscopy, energy-dispersive X-ray spectroscopy, morphometry and cyclic fatigue resistance of Endogal, PathMax, and Smarttrack novel brands of NiTi alloy endodontic files, with a null hypothesis (H_0) stating that Endogal, PathMax, and Smarttrack novel brands of NiTi alloy endodontic files do not show differences in the scanning electron microscopy, energy-dispersive X-ray spectroscopy, morphometry and cyclic fatigue resistance.

2. Materials and Methods

2.1. Study Design

Thirty unused NiTi alloy endodontic instruments were utilized for this in vitro study. The endodontic rotary files were supplied as sterile by the manufacturer. A total of 30 experimental units were included, distributed among the 3 groups, in accordance with the proportions set by the researcher, and a power of 80% was set. In addition, an effect size of 0.606 can be detected when testing the null hypothesis H_0: The means of the 3 groups were equal by the means of a 1-factor ANOVA test for independent samples, taking into account that the level of significance is 5%. Between March and July 2021, a controlled experimental study was carried out at the Department of Stomatology of the

Faculty of Medicine and Dentistry at the University of Valencia (Valencia, Spain). NiTi alloy endodontic rotary files were randomly selected and distributed among the following study groups: A: 250 μm apical diameter and 6% taper gold-wire NiTi alloy endodontic rotary file (Ref.: IRE 02506, D, Endogal, Galician Endodontics Company, Lugo, Spain) (n = 10) (EDG); B: 250 μm apical diameter and 6% taper heat-treated NiTi alloy endodontic rotary file (Ref.: 121 812, PathMax Pro, Nikinc Dental B.V., Eindhoven, The Netherlands) (n = 10) (PMP), and C: 250 μm apical diameter and 6% taper heat-treated NiTi alloy endodontic reciprocating file (Ref.: 121 104, 25, Smarttrack, Nikinc Dental B.V., Eindhoven, The Netherlands) (n = 10) (ST).

2.2. Scanning Electron Microscopy Analysis

All of the NiTi alloy endodontic files were initially analyzed using a scanning electron microscope (SEM) (HITACHI S-4800, Fukuoka, Japan) at 30× and 600× magnification. This analysis was carried out at the Central Support Service for Experimental Research of the University of Valencia in Burjassot, Spain, and was conducted using the following exposure parameters: 20 kV acceleration voltage, resolution ranging from − 1.0 nm at 15 kV to 2.0 nm at 1 kV, and magnification from 100× to 6500×. This was carried out for surface characterization and to rule out further surface defects due to manufacturing, as well as to compare and contrast the geometric designs of the Endogal, PathMax, and Smarttrack novel brands of NiTi alloy endodontic files.

2.3. Energy-Dispersive X-ray Spectroscopy Analysis

In addition, an energy-dispersive X-ray spectroscopy (EDX) analysis was carried out on all of the NiTi files. This was conducted at the Central Support Service for Experimental Research of the University of Valencia in Burjassot, Spain, and the following exposure parameters were used: Acceleration voltage of 20 kV, resolution ranging from −1.0 nm at 15 kV to 2.0 nm at 1 kV, and magnification from 100× to 6500×. This analysis was carried out to assess the elemental make-up of the chemical elements of the files. Moreover, we assessed atomic weight percentages, with measurements taken at three different locations.

2.4. Micro-Computed Tomography Scan and Morphometric Analyses

Finally, a micro-CT scan (Skyscan 1176, Bruker-MicroCT, Kontich) was performed to obtain accurate Digital Imaging and Communications in Medicine (DICOM) digital files of the NiTi alloy endodontic files, at the Department of Mechanical, Energetic, and Materials Engineering of the School of Industrial Engineering at the University of Valencia (Valencia, Spain), under the following exposure parameters: 56.0–58.0 microamperes, 160.0 kilovolt peak, 500.0 ms, 4 frames, 720 projections, 3 μm resolution, a tungsten target from 0.25–0.375 mm, and pixel size of 0.127 μm. Thereafter, morphometric analysis of the pitch and helix angle of the NiTi endodontic rotary files was carried out using Fiji/ImageJ (Oviedo, Spain), an open-source Java-based image processing software [24]. Subsequently, each DICOM digital file was segmented from the micro-CT volume to quantify its pitch and helix angle, by thresholding the original volume to obtain a 3D binary mask. Then, the longitudinal axis of the NiTi alloy endodontic files was established by interpolating the center of each Z-slice (file section). Thereafter, the maximum (peak) and minimum (valley) distances were defined in a longitudinal view between the file edge and the longitudinal axis to define the different pitches. Finally, the direction of the cutting edge over the longitudinal axis was overlapped to determine the helix angle. The pitch and helix angle measurement was recorded at all of the pitches from the file tip.

In addition, the DICOM digital files were transferred to Standard Tessellation Language (STL) digital files for the Endogal, PathMax, and Smarttrack novel brands of NiTi alloy endodontic files to illustrate the values of the pitch and helix angle, as well as to contrast the geometric designs of the files.

Furthermore, the cross-section geometry of Endogal, PathMax, and Smarttrack novel brands of NiTi alloy endodontic files was analyzed.

2.5. Experimental Cyclic Fatigue Model

We conducted dynamic cyclic fatigue resistance tests using a custom-made device (Utility Model Patent No. ES1219520) [25]. The structure of the device was designed using CAD/CAE 2D/3D software (Midas FX+®, Brunleys, Milton Keynes, UK), and printed using the 3D printing software (ProJet® 6000 3D Systems©, Rock Hill, SC, USA); see Figure 1.

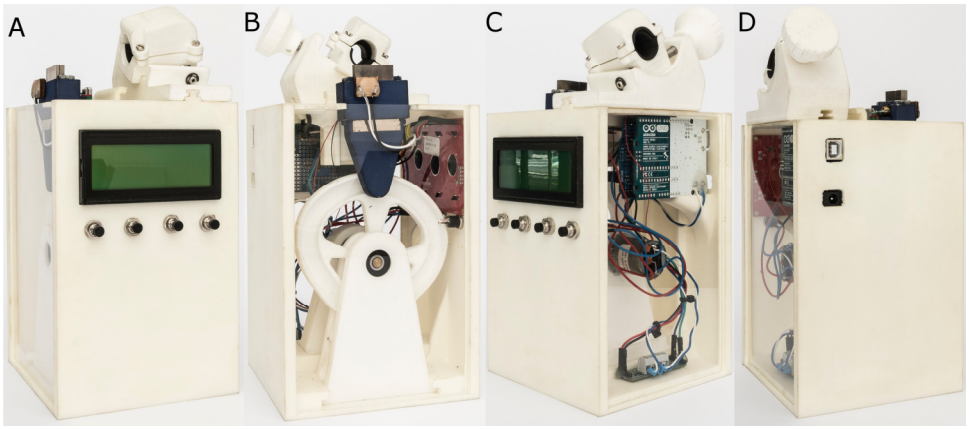

Figure 1. (**A**) Front, (**B**) back, (**C**) right side, and (**D**) left side of the dynamic cyclic fatigue device.

The custom-made artificial root canals were designed with a 60° curvature, as per Schneider's measuring technique [26], with a radius of curvature of 3 mm. For this, the CAD/CAE 2D/3D inverse engineering software was used. The artificial root canal was manufactured from stainless steel with electrical discharge machining (EDM) molybdenum wire-cut technology (Cocchiola S.A., Buenos Aires, Argentina), thereby ensuring close contact between the NiTi files and the walls of the artificial root canal (Figure 2).

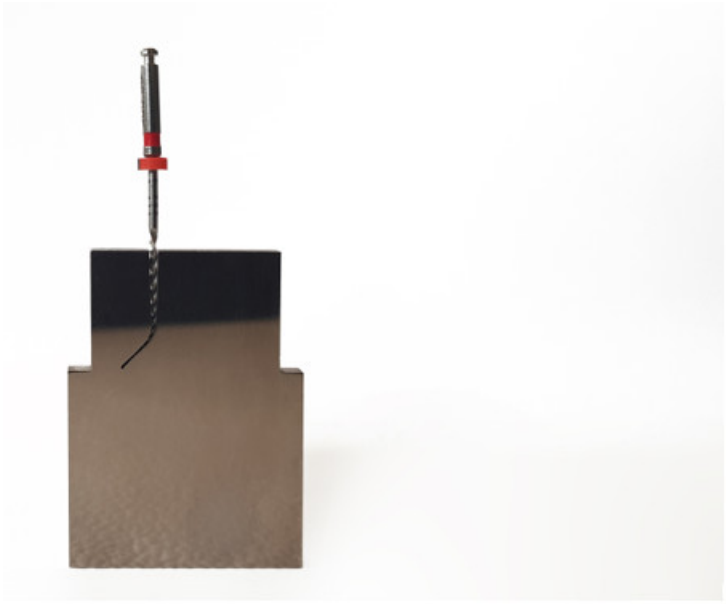

Figure 2. Artificial root canal manufactured from stainless steel with EDM molybdenum wire-cut technology in close contact with a NiTi alloy endodontic rotary file.

Then, the manufactured canal was positioned on its support, and any failures in the endodontic rotary instruments were detected using a light-dependent resistor (LDR)

sensor (Ref.: C000025, Arduino LLC®, Ivrea, Italy) positioned at the apex of the canal. The LDR sensor measures the continuous light source of a very bright white LED (20000 mcd) (Ref.: 12.675/5/b/c/20 k, Batuled, Coslada, Spain). This LED was placed opposite to the artificial root canal (Figure 1). The LED signals were picked up by the LDR sensor (Ref.: C000025, Arduino LLC®) every 50 ms to pinpoint the exact time of failure.

The speed and movement direction were controlled by a driver (Ref.: DRV8835, Pololu® Corporation, Las Vegas, NV, USA), generated by a brushed DC gear motor (Ref.: 1589, Pololu® Corporation, Las Vegas, NV, USA), and applied to the artificial support using a roller bearing system (Ref.: MR104ZZ, FAG, Schaeffler Herzogenaurach, Germany). The support moved in a solely axial motion using a lineal guide (Ref.: HGH35C 10249-1 001 MA, HIWIN Technologies Corp. Taichung, Taiwan). A 6:1 reduction handpiece (X-Smart plus, Dentsply Maillefer, Baillagues, Switzerland) and torque-controlled motor were used, in accordance with the manufacturer's instructions (Table 1).

Table 1. Characteristics of the movement performed by each study group, in terms of speed, torque/direction of movement, and type of movement.

Study Group	Speed	Torque/Direction	Movement
EDG	250 rpm	4 N/cm	Continuous rotational
PMP	250 rpm	4 N/cm	Continuous rotational
ST	350 rpm	170° CCW/50° CW	Reciprocant

CCW: Counterclockwise; CW: Clockwise.

All of the NiTi alloy endodontic files were used at a frequency of 60 pecks per minute within the dynamic cyclic fatigue device, as per a prior study. To prevent friction between the reciprocating files and the artificial root canal walls, we applied a specialized high-flow synthetic oil (Singer All-Purpose Oil; Singer Corp., Barcelona, Spain) formulated for use in lubricating mechanical parts.

All of the files were used until they fractured. We measured and recorded the time to failure and the number of cycles to failure.

2.6. Statistical Tests

All of the variables were statistically analyzed using the SAS 9.4 software (SAS Institute Inc., Cary, NC, USA). The descriptive statistics of quantitative variables were expressed as mean and SD. Then, we performed a comparative analysis, using the ANOVA test to compare the time to failure (in seconds) and number of cycles to failure. In 2-to-2 comparisons, Tukey's test was used to adjust the *p*-values to correct for Type I error. Furthermore, the Weibull modulus and characteristic strength were calculated. The statistical significance was defined as $p < 0.05$.

3. Results

SEM analysis of the Endogal, PathMax, and Smarttrack novel brands of NiTi alloy endodontic files showed accumulated organic matter, but no structural alterations were observed in any of the files. Manufacturing lines were perpendicularly distributed, in relation to the longitudinal axis, in all of the files. They were also parallel, as a result of manufacturing with laser machining. The tubular porosity as well as the width and spacing of the manufacturing lines both correspond to the intensity and precision of the laser machining process. Furthermore, the microscopic geometric design of EDG NiTi alloy endodontic rotary files, PMP NiTi alloy endodontic rotary files, and ST NiTi alloy endodontic reciprocating files clearly differed in the tip design; particularly, in the direction of the helix angle of ST NiTi alloy endodontic reciprocating files (Figure 3).

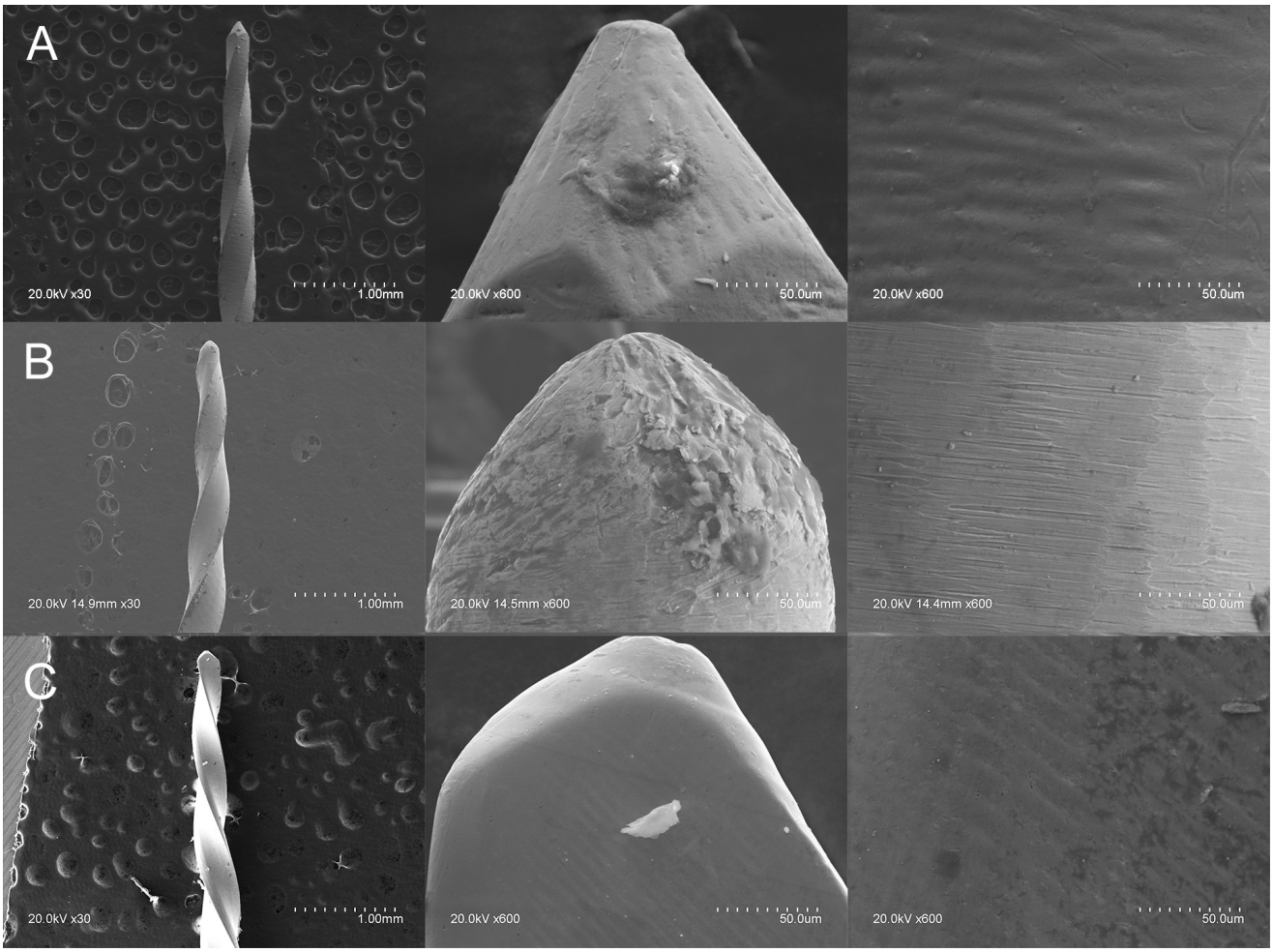

Figure 3. SEM analysis (at 30× and 600×) of: (**A**) EDG NiTi alloy endodontic rotary file, (**B**) PMP heat-treated NiTi alloy endodontic rotary file, and (**C**) ST heat-treated NiTi alloy endodontic reciprocating file.

EDX micro-analysis of EDG, PMP, and ST NiTi alloy endodontic files was carried out at 15 and 20 kV. However, the 20 kV acceleration voltage results were more determinant than those at 15 kV. In summary, the EDG, PMP, and ST NiTi alloy endodontic files differed in atomic weight percentages, although the elements present in the chemical composition were similar (Figure 4 and Table 2).

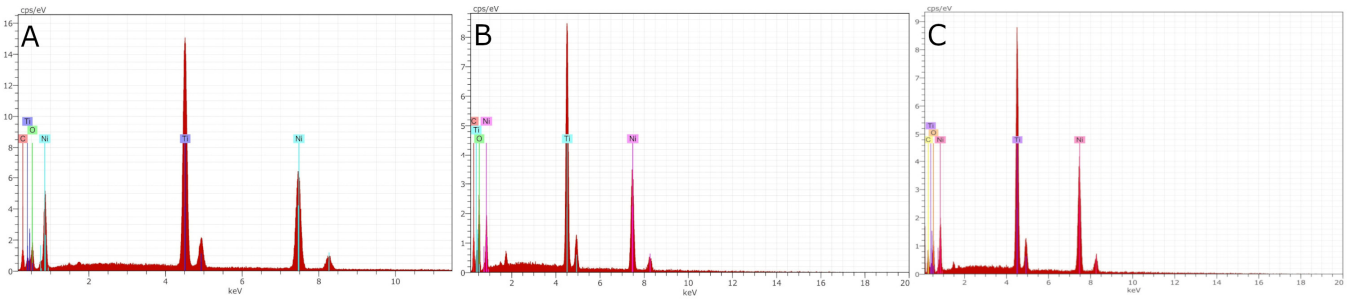

Figure 4. EDX micro-analysis of: (**A**) EDG NiTi alloy endodontic rotary file, (**B**) PMP heat-treated NiTi alloy endodontic rotary file, and (**C**) ST heat-treated NiTi alloy endodontic reciprocating file.

Table 2. Mean atomic weight percentages (%) of EDG NiTi alloy endodontic rotary file, PMP heat-treated NiTi alloy endodontic rotary file, and ST heat-treated NiTi alloy endodontic reciprocating file at 15 and 20 kV in three different locations (1–3).

Spectrum	C	O	Ti	Ni
EDG 15 kV (1–3)	27.66	24.05	25.98	22.31
PMP 15 kV (1–3)	28.79	39.78	17.32	14.10
ST 15 kV (1–3)	29.57	27.57	22.69	20.18
EDG 20 kV (1–3)	45.60	25.41	16.13	12.86
PMP 20 kV (1–3)	30.74	38.79	16.44	14.03
ST 20 kV (1–3)	30.64	24.79	22.45	22.11

The morphometric analysis showed a lower pitch of the EDG NiTi alloy endodontic rotary file (6 pitches), compared with the PMP heat-treated NiTi alloy endodontic rotary file (10 pitches) and ST heat-treated NiTi alloy endodontic reciprocating file (10 pitches) (Figure 5). In addition, the EDG NiTi alloy endodontic rotary file showed a more pronounced gradual reduction of pitch to the tip, followed by the PMP heat-treated NiTi alloy endodontic rotary file and ST heat-treated NiTi alloy endodontic reciprocating file (Figure 5). Moreover, the replica-like EDG NiTi endodontic rotary files did not show measuring lines in the non-cutting part (Figure 5). Furthermore, the morphometric analysis showed different cross-sectional geometries between the novel brands of NiTi alloy endodontic files; particularly, between the EDG NiTi alloy endodontic rotary files and PMP heat-treated NiTi alloy endodontic rotary file and ST heat-treated NiTi alloy endodontic reciprocating file (Figure 6).

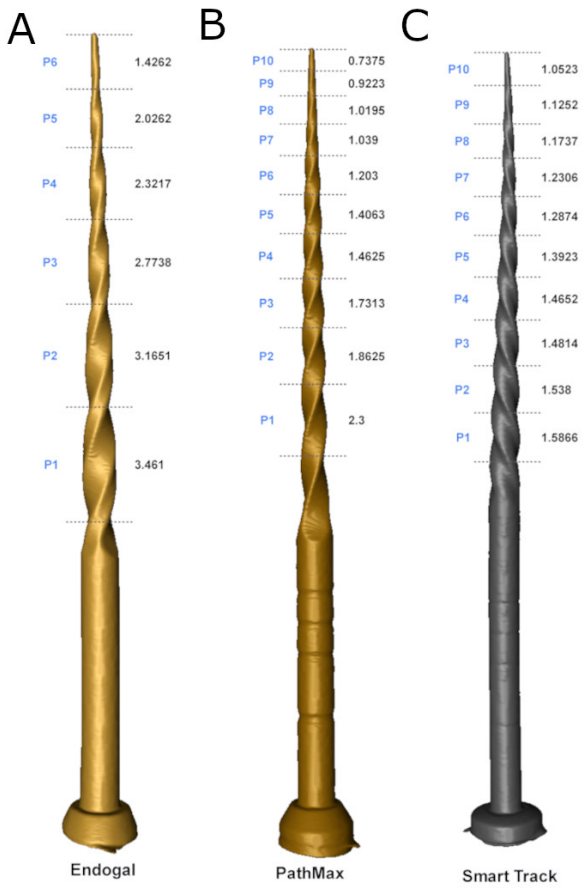

Figure 5. (**A**) STL digital files of EDG NiTi alloy endodontic rotary file, (**B**) PMP heat-treated NiTi alloy endodontic rotary file, and (**C**) ST heat-treated NiTi alloy endodontic reciprocating file.

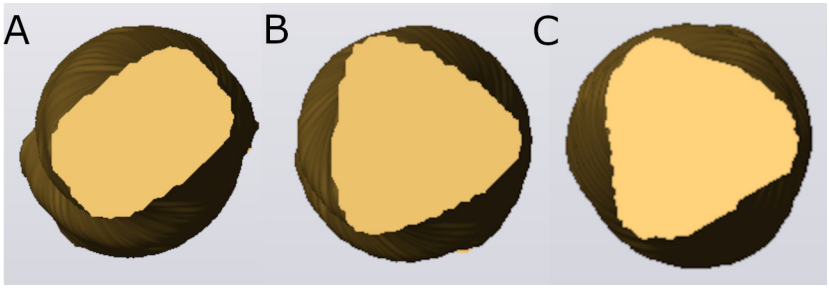

Figure 6. STL digital files of the cross-section geometries of: (**A**) EDG NiTi alloy endodontic rotary file, (**B**) PMP heat-treated NiTi alloy endodontic rotary file, and (**C**) ST heat-treated NiTi alloy endodontic reciprocating file.

In addition, EDG NiTi endodontic rotary files showed a gradual reduction of the helix angle from the tip. However, ST heat-treated NiTi alloy endodontic reciprocating files showed a slight gradual reduction of the helix angle and PMP heat-treated NiTi alloy endodontic rotary files did not show variations of the helix angle along the cutting surface, which is a similar helix angle along the cutting part of the files (Table 3). Furthermore, ST heat-treated NiTi alloy endodontic reciprocating files showed a different direction of the helix angle, compared with EDG NiTi endodontic rotary files and PMP heat-treated NiTi alloy endodontic rotary files (Figure 5).

Table 3. Mean helix angle measurements (°) at all of the pitches to the tip of novel brands of NiTi alloy endodontic files.

Study Group	P1	P2	P3	P4	P5	P6	P7	P8	P9
EDG	26.7	23.3	21.9	18.3	15.1	13.6			
PMP	25.5	25.4	26	24.9	25.7	26.3	26	26.6	25.2
ST	35.8	33.7	32.7	31.2	28	25.5	22.3	20.2	17.1

The mean and SD values of time to failure (in seconds) for each of the study groups can be seen in Table 4.

Table 4. Descriptive statistics regarding time to failure of the novel brands of NiTi alloy endodontic files.

	n	Mean	SD	Minimum	Maximum
EDG	10	420.78 [a]	5.83	413.00	431.10
PMP	10	463.97 [b]	7.55	455.90	477.50
ST	10	675.95 [c]	8.07	664.70	689.60

[a,b,c] Statistically significant differences between groups ($p < 0.05$).

The ANOVA test revealed statistically significant differences between the mean time to failure for all novel brands of NiTi alloy endodontic files ($p < 0.001$). In addition, Tukey's test indicated statistically significant differences between NiTi endodontic rotary files and NiTi endodontic reciprocating files ($p < 0.001$). The results for number of cycles to failure were similar, as the dynamic cyclic fatigue device was set at a frequency of 60 pecks per minute.

The Weibull statistic scale distribution parameter (η) indicated statistically significant differences in time to failure across all of the novel brands of NiTi alloy endodontic files ($p < 0.001$; Table 5, Figure 7). On the other hand, the shape distribution parameter (β) revealed no statistically significant differences in time to failure for any of the novel brands of NiTi alloy endodontic files ($p > 0.05$). The results for number of cycles to failure were similar, as the dynamic cyclic fatigue device was set at a frequency of 60 pecks per minute (Table 5, Figure 7).

Table 5. Weibull statistics of time to failure for the EDG, PMP, and ST novel brands of NiTi alloy endodontic files.

	Weibull Shape (β)				Weibull Scale (η)			
Study Group	Estimate	Std. error	Lower	Upper	Estimate	Std. Error	Lower	Upper
EDG	76.9	18.0	48.5	121.9	423.5	1.8	419.9	427.2
PMP	65.6	15.4	41.4	104.1	467.6	2.3	462.9	472.3
ST	91.1	21.6	57.2	145.2	679.8	2.5	674.9	684.7

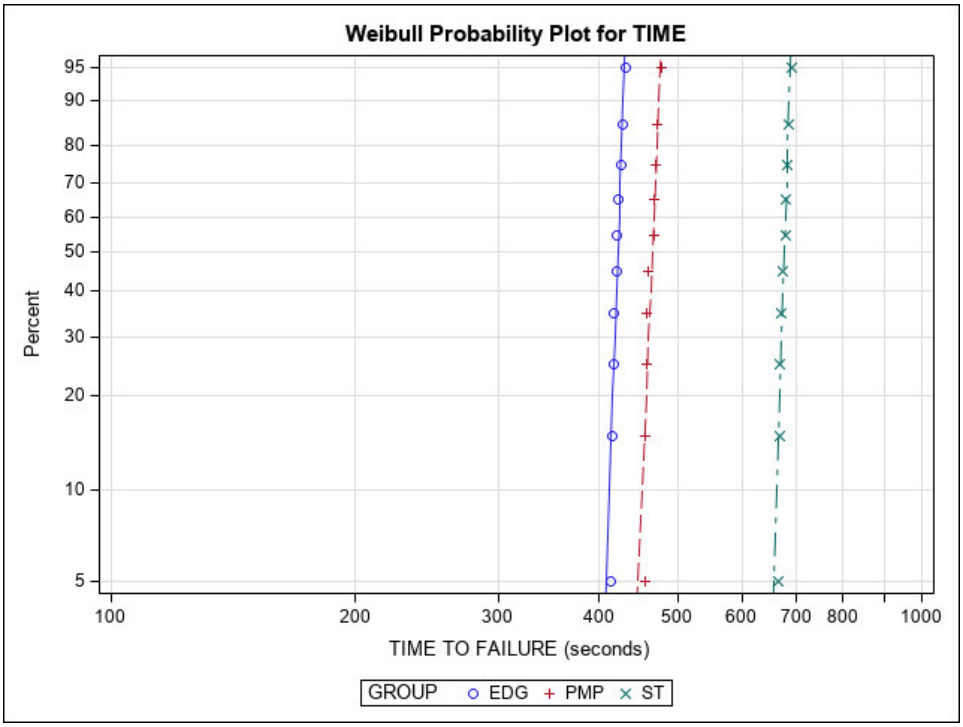

Figure 7. Weibull probability plot of time to failure for the EDG, PMP, and ST novel brands of NiTi alloy endodontic files.

4. Discussion

Our results reject the null hypothesis (H_0) and Tukey's test also found that Endogal, PathMax, and Smarttrack novel brands of NiTi alloy endodontic files do not show differences in the scanning electron microscopy, energy-dispersive X-ray spectroscopy, morphometry and cyclic fatigue resistance.

The results of the SEM analysis indicated that the microscopic geometric design of the EDG NiTi alloy endodontic rotary files, PMP heat-treated NiTi alloy endodontic rotary files, and ST heat-treated NiTi alloy endodontic reciprocating files were clearly different. Furthermore, EDX micro-analysis showed that the atomic weight percentages were different in the atomic weight percentage, although the elements present in the chemical composition were similar. The largest difference in chemical composition was shown in the EDG NiTi alloy endodontic rotary file, since it incorporated a high concentration of C in the chemical make-up of the NiTi alloy (27.66–45.60 wt%). Titanium is an allotropic metal with compact hexagonal (α or austenite) or body-centered cubic (β or martensite) structures. Depending on the stabilizing effects of the α and β phases, titanium's alloying elements are defined as neutral elements (i.e., stabilizers of the α phase or betagenic elements) or as alphagenic elements (i.e., stabilizers of the β phase). Phase stabilization signifies a higher or lower transition temperature β [27]. More specifically, alphagenic elements increase the transition temperature β. Of the alphagenic elements, Al is the most significant alloying element, although C, O, and N can also be used. The results of the

EDX micro-analysis revealed the presence of C and O alloying elements, leading to a more martensitic crystalline structure. Therefore, this makes them more flexible and fracture-resistant. A higher atomic weight percentage of oxygen was shown after the EDX micro-analysis of PMP heat-treated NiTi alloy endodontic rotary files (38.79–39.78 wt%), compared with EDG NiTi alloy endodontic rotary files (24.05–25.41 wt%) and ST heat-treated NiTi alloy endodontic reciprocating files (24.79–27.57 wt%), which would lead to the higher resistance to cyclic fatigue of the PMP heat-treated NiTi alloy endodontic rotary files.

Furthermore, morphometric analysis of the novel brands of NiTi alloy endodontic files showed differences at the pitch and helix angle and the cross-section geometric design; particularly between the EDG NiTi alloy endodontic rotary file (trapezoidal) and the PMP heat-treated NiTi alloy endodontic rotary file (convex triangular) and ST heat-treated NiTi alloy endodontic rotary file (convex triangular). PMP heat-treated NiTi alloy endodontic rotary file and ST heat-treated NiTi alloy endodontic rotary file showed a higher number of threads than the EDG NiTi alloy endodontic rotary file. Moreover, Versluis et al. experimentally reported that the number of threads directly increases the flexural stiffness [28]. However, Al Raeesi et al. found that a shorter pitch design increased the resistance to cyclic fatigue of glide path instruments [29]. The EDG NiTi alloy endodontic rotary file and ST heat-treated NiTi alloy endodontic rotary file showed a gradual trend of reducing the helix angle to the tip. However, the PMP heat-treated NiTi alloy endodontic rotary file maintained a continuous helix angle along the cutting part of the endodontic rotary file. In addition, Rui et al. experimentally demonstrated that an increase in the helix angle value improves the mechanical behavior of the instrument under torsional and bending conditions [30].

Furthermore, Faus-Llacer et al., found that two NiTi-alloy endodontic rotary files with a double S-shaped cross-section were more resistant to dynamic cyclic fatigue than T Pro E1 austenite phase nickel–titanium alloy endodontic rotary files with a rectangular cross-section, T Pro E2 austenite phase NiTi alloy endodontic rotary files with a convex triangular cross-section, and T Pro E4 austenite phase NiTi alloy endodontic rotary files with a triangular cross-section [31]. These results indicate that, by increasing the mass and contact points between the instrument surface and dentin walls of the root canal, the resistance to cyclic fatigue of the NiTi alloy endodontic rotary files decrease. The flexibility of NiTi alloy endodontic rotary file may also be affected, resulting in excessive root canal dentine removal, root perforations, apical transport [32], and fractures [4,33,34]. Briefly, the results derived from the cyclic fatigue analysis demonstrated that the ST novel brand NiTi alloy endodontic reciprocating files had greater resistance to cyclic fatigue than the EDG and PMP novel brands of NiTi alloy endodontic rotary files.

The anatomical-based root canal design used in this study was based on Schneider's method [19], using a radius of 3 mm and curvature angle of 60°. Herein, the geometry was adapted to the aforementioned NiTi endodontic rotary files. Prior studies have shown that the resistance to fatigue of files becomes lower as the radius of curvature decreases and the angle of curvature increases [12,35,36], as the stress accumulating on the file is inversely proportional to the radius of the canal's curvature. Consequently, more abrupt root canals have greater torsion and flexural bending fatigue, which may ultimately lead to instrument fracture [17]. Furthermore, clinical or even ex vivo experimental studies are recommended, to better replicate clinical conditions and to make it possible to apply these cyclic fatigue results to a clinical setting. However, difficulties in homogenizing the curvature angle, radius, apical diameter, cross-section, and hardness of the root canals may bias the study results by adding more variables. Therefore, custom-made dynamic and static cyclic fatigue devices have been developed to independently analyze the effects of the variables under study. Unfortunately, at present, there are no norms regulating the characteristics of these custom-built devices, nor are there any international standards for testing the cyclic fatigue behaviors of NiTi alloy endodontic rotary instruments with a taper larger than 2% [37]. The development of additive manufacturing processes based on

three-dimensional printing has allowed for the acquisition of anatomical-based dental replicas, which can be used for the analysis of the cyclic fatigue resistance of NiTi alloy endodontic rotary files [38]. However, the physical properties of the printed plastic material used in three-dimensional printing highly differ from those of the root dentin. Therefore, translation of the obtained results to clinical settings is difficult.

Cyclic fatigue has been studied using both static and dynamic testing. In static cyclic fatigue testing models, NiTi alloy endodontic files are rotated until they fracture, with tension–compression cycles concentrated in the maximum curvature angle of the root canal, causing microstructural changes to the file, and triggering its subsequent failure. Therefore, dynamic cyclic fatigue testing devices are preferred, as they can better simulate clinical conditions; particularly, the pecking motion of nickel–titanium endodontic rotary files. As a result, in this study, we employed an anatomically accurate artificial root canal, dynamic cyclic fatigue testing, and an automatic detection system to accurately and objectively identify failure of the endodontic rotary files [39,40].

Unfortunately, limitations to the present study prevented the NiTi alloy, pitch, helix angle, speed or manufacturing process from standardization. Furthermore, this study was not carried out in a clinical setting, as the associated samples are difficult to standardize.

5. Conclusions

The results obtained in the present study led us to conclude that: Smarttrack novel brand of NiTi alloy endodontic reciprocating files display greater resistance to cyclic fatigue than Endogal and Path Max Pro novel brands of NiTi alloy endodontic rotary files, due to the reciprocating movement and metallurgical composition.

Author Contributions: Conceptualization, V.F.-L., R.P.G. and Á.Z.-M.; data acquisition, I.F.-M.; design, V.F.-M.; formal analysis, Ó.A.E.; writing—review and editing, A.A.M.; statistical analyses, Á.Z.-M. and V.F.-M. All authors reviewed and approved the published version of the manuscript. All authors have read and agreed to the published version of the manuscript.

Funding: No external funding was granted for this study.

Institutional Review Board Statement: Not applicable.

Informed Consent Statement: Not applicable.

Data Availability Statement: Data available upon request, in accordance with relevant considerations (e.g., ethical privacy restrictions).

Conflicts of Interest: The authors declare no conflict of interest.

References

1. Walia, H.M.; Brantley, W.A.; Gerstein, H. An initial investigation of the bending and torsional properties of Nitinol root canal files. *J. Endod*. **1988**, *14*, 346–351.
2. Esposito, P.T.; Cunningham, C.J. A comparison of canal preparation with nickel-titanium and stainless steel instruments. *J. Endod.* **1995**, *21*, 173–176.
3. Bergmans, L.; van Cleynenbreugel, J.; Wevers, M.; Lambrechts, P. Mechanical root canal preparation with NiTi rotary instruments: Rationale, performance and safety. Status report for the American Journal of Dentistry. *Am. J. Dent*. **2001**, *14*, 324–333.
4. Parashos, P.; Gordon, I.; Messer, H.H. Factors influencing defects of rotary nickel-titanium endodontic instruments after clinical use. *J. Endod*. **2004**, *30*, 722–725.
5. Spili, P.; Parashos, P.; Messer, H.H. The impact of instrument fracture on outcome of endodontic treatment. *J. Endod*. **2005**, *31*, 845–850.
6. Sattapan, B.; Nervo, G.J.; Palamara, J.E.; Messer, H.H. Defects in rotary nickel-titanium files after clinical use. *J. Endod*. **2000**, *26*, 161–165.
7. Peters, O.A.; Barbakow, F. Dynamic torque and apical forces of ProFile.04 rotary instruments during preparation of curved canals. *Int. Endod. J.* **2002**, *35*, 379–389.
8. Kuhn, G.; Tavernier, B.; Jordan, L. Influence of structure on nickel-titanium endodontic instruments failure. *J. Endod*. **2001**, *27*, 516–520.

9. Carpegna, G.; Alovisi, M.; Salvatore Paolino, D.; Marchetti, A.; Gibello, U.; Scotti, N.; Pasqualini, D.; Scattina, A.; Chiandussi, G.; Berutti, E. Evaluation of Pressure Distribution against Root Canal Walls of NiTi Rotary Instruments by Finite Element Analysis. *Appl. Sci*. **2020**, *10*, 2981. https://doi.org/10.3390/app10082981.
10. Alovisi, M.; Pasqualini, D.; Scotti, N.;·Carpegna, G.; Comba, A.; Bernardi, M.; Tutino, F.; Dioguardi, M.; Berutti, E. Micro-CT evaluation of rotary and reciprocating glide path and shaping systems outcomes in maxillary molar curved canals. *Odontology* **2022**, *110*, 54–61.
11. Pruett, J.P.; Clement, D.J.; Carnes, D.L., Jr. Cyclic fatigue testing of nickel-titanium endodontic instruments. *J. Endod*. **1997**, *23*, 77–85.
12. Parashos, P.; Messer, H.H. Rotary NiTi instrument fracture and its consequences. *J. Endod*. **2006**, *32*, 1031–1043.
13. Topçuoğlu, H.S.; Topçuoğlu, G. Cyclic fatigue resistance of reciproc blue and reciproc files in an s-shaped canal. *J. Endod*. **2017**, *43*, 1679–1682.
14. Siqueira, J.F., Jr.; Rôças, I.N. Polymerase chain reaction–based analysis of microorganisms associated with failed endodontic treatment. *Oral Surg. Oral Med. Oral Pathol. Oral Radiol. Endod.* **2014**, *97*, 85–94.
15. Heydari, A.; Rahmani, M.; Heydari, M. Removal of a Broken Instrument from a Tooth with Apical Periodontitis Using a Novel Approach. *Iran. Endod. J*. **2016**, *11*, 237–240. https://doi.org/10.7508/iej.2016.03.018.
16. Zupanc, J.; Vahdat-Pajouh, N.; Schäfer, E. New thermomechanically treated NiTi alloys—A review. *Int. Endod. J*. **2018**, *51*, 1088–1103.
17. Faus-Llácer, V.; Kharrat, N.H.; Ruiz-Sánchez, C.; Faus-Matoses, I.; Zubizarreta-Macho, Á.; Faus-Matoses, V. The effect of taper and apical diameter on the cyclic fatigue resistance of rotary endodontic files using an experimental electronic device. *Appl. Sci*. **2021**, *11*, 863.
18. Turpin, Y.L.; Chagneau, F.; Vulcain, J.M. Impact of two theoretical cross-sections on torsional and bending stresses of nickel-titanium root canal instrument models. *J. Endod*. **2000**, *26*, 414–417.
19. Sekar, V.; Kumar, R.; Nandini, S.; Ballal, S.; Velmurugan, N. Assessment of the role of cross section on fatigue resistance of rotary files when used in reciprocation. *Eur. J. Dent*. **2016**, *10*, 541–545.
20. Alovisi, M.; Pasqualini, D.; Carpegna, G.; Comba, A.; Moccia, E.; Multari, S.; Dioguardi, M.; Scotti, N.; Berutti, E. The influence of brushing movement on geometrical shaping outcomes: A micro-ct study. *Appl. Sci*. **2020**, *10*, 4805. https://doi.org/10.3390/app10144805.
21. Nóvoa, X.R.; Martin-Biedma, B.; Varela-Patiño, P.; Collazo, A.; Macías-Luaces, A.; Cantatore, G.; Pérez, M.C.; Magán-Muñoz, F. The corrosion of nickel-titanium rotary endodontic instruments in sodium hypochlorite. *Int. Endod. J*. **2007**, *40*, 36–44. https://doi.org/10.1111/j.1365-2591.2006.01178.x.
22. Cavalleri, G.; Cantatore, G.; Costa, A.; Grillenzoni, M.; Comin Chiaramonti, L.; Gerosa, R. The corrosive effects of sodium hypochlorite on nickel-titanium endodontic instruments: Assessment by digital scanning microscope. *Minerva Stomatol*. **2009**, *58*, 225–231.
23. Martins, J.N.R.; Nogueira Leal Silva, E.J.; Marques, D.; Ginjeira, A.; Braz Fernandes, F.M.; De Deus, G.; Versiani, M.A. Influence of kinematics on the cyclic fatigue resistance of replicalike and original brand rotary instruments. *J. Endod*. **2020**, *46*, 1136–1143.
24. Schneider, C.A.; Rasband, W.S.; Eliceiri, K.W. NIH Image to ImageJ: 25 years of image analysis. *Nat. Methods*. **2012**, *9*, 671–675.
25. Zubizarreta-Macho, A.; Mena Álvarez, J.; Albadalejo Martínez, A.; Segura-Egea, J.J.; Caviedes Brucheli, J.; Agustín-Panadero, R.; López Píriz, R.; Alonso-Ezpeleta, O. Influence of the pecking motion on the cyclic fatigue resistance of endodontic rotary files. *J. Clin. Med*. **2020**, *9*, 45.
26. Schneider, S.W. A comparison of canal preparations in straight and curved root canals. *Oral Surg. Oral Med. Oral Pathol*. **1971**, *32*, 271–275.
27. Seracchiani, M.; Miccoli, G.; Di Nardo, D.; Zanza, A.; Cantore, M.; Gambarini, G.; Testarelli, L. Effect of flexural stress on torsional resistance of NiTi instruments. *J. Endod*. **2020**, *47*, 472-476 https://doi.org/10.1016/j.joen.2020.10.011.
28. Versluis, A.; Kim, H.C.; Lee, W.; Kim, B.M.; Lee, C.J. Flexural stiffness and stresses in nickel-titanium rotary files for various pitch and cross-sectional geometries. *J. Endod*. **2012**, *38*, 1399–1403. https://doi.org/10.1016/j.joen.2012.06.008.
29. Al Raeesi, D.; Kwak, S.W.; Ha, J.H.; Sulaiman, S.; El Abed, R.; Kim, H.C. Mechanical properties of glide path preparation instruments with different pitch lengths. *J. Endod*. **2018**, *44*, 864–868. https://doi.org/10.1016/j.joen.2018.01.022.
30. He, R.; Ni, J. Design improvement and failure reduction of endodontic files through finite element analysis: Application to V-Taper file designs. *J Endod*. **2010**, *36*, 1552–1557. https://doi.org/10.1016/j.joen.2010.06.002.
31. Faus-Llacer, V.; Hamoud-Kharrat, N.; Marhuenda Ramos, M.T.; Faus-Matoses, I.; Zubizarreta-Macho, A.; Ruiz-Sánchez, C.; Faus-Matoses, V. Efficacy of a novel influence of the geometrical cross-section design on the dynamic cyclic fatigue resistance of niti endodontic rotary files. An In Vitro Study. *J. Clin. Med*. **2021**, *10*, 4713.
32. Freire, L.G.; Gavini, G.; Cunha, R.S.; Santos, M. Assessing apical transportation in curved canals: Comparison between cross-sections and micro-computed tomography. *Braz. Oral Res*. **2012**, *26*, 222–227.
33. Ounsi, H.F.; Salameh, Z.; Al-Shalan, T.; Ferrari, M.; Grandini, S.; Pashley, D.H.; Tay, F.R. Effect of clinical use on the cyclic fatigue resistance of ProTaper nickel-titanium rotary instruments. *J. Endod*. **2007**, *33*, 737–741.
34. Grande, N.M.; Plotino, G.; Pecci, R.; Bedini, R.; Malagnino, V.A.; Somma, F. Cyclic fatigue resistance and three-dimensional analysis of instruments from two nickel-titanium rotary systems. *Int. Endod. J*. **2006**, *39*, 755–763.
35. Azimi, S.; Delvari, P.; Hajarian, H.C.; Saghiri, M.A.; Karamifar, K.; Lotfi, M. Cyclic fatigue resistance and fractographic analysis of race and protaper rotary niti instruments. *Iran. Endod. J*. **2011**, *6*, 80–86.

36. Haikel, Y.; Serfaty, R.; Bateman, G.; Senger, B.; Allemann, C. Dynamic and cyclic fatigue of engine-driven rotary nickel-titanium endodontic instruments. *J. Endod*. **1999**, *25*, 434–440.
37. *ISO 3630–3631*; Dentistry—Root Canal Instruments—Part 1: General Requirements and Test Methods. ISO: Geneva, Switzerland, 2008.
38. Peters, O.; Scott, R.; Arias, A.; Lim, E.; Paque, F.; Almassi, S.; Hejlawy, S. Evaluation of dental students´skills acquisition in endodontics using a 3D printed tooth model. *Eur. Endod. J*. **2021**, *6*, 290–294.
39. Whipple, S.J.; Kirkpatrick, T.C.; Rutledge, R.E. Cyclic fatigue resistance of two variable-taper rotary file systems: ProTaper universal and V-Taper. *J. Endod*. **2009**, *35*, 555–558.
40. Gambarini, G. Cyclic fatigue of nickel-titanium rotary instruments after clinical use with low- and high-torque endodontic motors. *J. Endod*. **2001**, *27*, 772–774.

applied sciences

MDPI

Article

Computerized Generation and Finite Element Stress Analysis of Endodontic Rotary Files

Victor Roda-Casanova [1,*], Álvaro Zubizarreta-Macho [2,3], Francisco Sanchez-Marin [1], Óscar Alonso Ezpeleta [4], Alberto Albaladejo Martínez [3] and Agustín Galparsoro Catalán [2]

1 Mechanical Engineering and Construction Department, Universitat Jaume I, 12071 Valencia, Spain; ftsan@uji.es
2 Department of Dentistry, Alfonso X el Sabio University, 28691 Madrid, Spain; amacho@uax.es (Á.Z.-M.); agalpcat@uax.es (A.G.C.)
3 Department of Orthodontics, University of Salamanca, 37008 Salamanca, Spain; albertoalbaladejo@usal.es
4 Department of Endodontics, University of Zaragoza, 50009 Zaragoza, Spain; lalonezp@unizar.es
* Correspondence: vroda@uji.es

Abstract: Introduction: The finite element method has been extensively used to analyze the mechanical behavior of endodontic rotary files under bending and torsional conditions. This methodology requires elevated computer-aided design skills to reproduce the geometry of the endodontic file, and also mathematical knowledge to perform the finite element analysis. In this study, an automated procedure is proposed for the computerized generation and finite element analysis of endodontic rotary files under bending and torsional conditions. **Methods:** An endodontic rotary file with a 25 mm total length, 0.25 mm at the tip, 1.20 mm at 16 mm from the tip, 2 mm pitch and squared cross section was generated using the proposed procedure and submitted for analysis under bending and torsional conditions by clamping the last 3 mm of the endodontic rotary file and applying a transverse load of 0.1 N and a torsional moment of 0.3 N · cm. **Results:** The results of the finite element analyses showed a maximum von Mises stress of 398 MPa resulting from the bending analysis and a maximum von Mises stress of 843 MPa resulting from the torsional analysis, both of which are next to the encastre point. **Conclusions:** The automated procedure allows an accurate description of the geometry of the endodontic file to be obtained based on its design parameters as well as a finite element model of the endodontic file from the previously generated geometry.

Keywords: endodontic file; bending; torsion; stress distribution; finite element analysis

Citation: Roda-Casanova, V.; Zubizarreta-Macho, A.; Sanchez-Marin, F.; Alonso, O.; Albaladejo, A.; Galparsoro, A. Computerized Generation and Finite Element Stress Analysis of Endodontic Rotary Files. *Appl. Sci.* **2021**, *11*, 4329. https://doi.org/10.3390/app11104329

Academic Editor: Jaroslaw Zmudzki

Received: 20 April 2021
Accepted: 8 May 2021
Published: 11 May 2021

1. Introduction

Endodontic rotary files have experienced continuous development, both in the chemical composition of alloys and geometrical design, which has improved their mechanical behavior during operation [1]. However, unexpected fractures of endodontic rotary files within the root canal system are still a concern and remain a challenge for clinicians despite continuous enhancements in their geometrical design and manufacture processes to reduce the incidence of fractures [2], which ranges from 0.09% to 5% [3,4].

Previous studies have suggested that flexural failure (bending) and torsional failure are the main causes for endodontic rotary file fractures [5–7]. Torsional failure is caused by the blockage of the endodontic files during rotational movement [5]; however, endodontic rotary instrument failures are mainly caused by cyclic bending fatigue, which occurs when a endodontic rotary instrument rotates in a curved root canal [8]. In addition, endodontic rotary files can be simultaneously subjected to cumulative torsional and bending stress during root canal shaping, which can lead to the fracture of endodontic rotary files and therefore affect the prognosis of root canal treatment as the fractured fragment blocks the access to the apex, preventing root canal system disinfection [9,10].

In addition, root canal dentine removal during the retrieval procedures of separated files can weaken the tooth structure up to 4.25 ± 0.68 mm^3 [11]. Moreover, fractures of endodontic instruments on teeth with periapical pathology significantly decrease the success rate of root canal treatment [12]. Therefore, improvements of the chemical composition of the alloy and geometrical design may increase torsional and bending resistance, preventing the fracture of the endodontic rotary instruments [13]. Furthermore, some geometrical factors have been highlighted as influencing the instrument's performance, such as taper [14], apical diameter [7,14], cross section [15], flute length, helix angle and pitch [16]; however, most studies were conducted experimentally using custom-made cyclic fatigue devices, hardly reproducing the clinical setting and the absence of regulation prevents data comparison [17].

However, finite element (FE) analysis is an alternative that allows the mechanical behavior and stress distribution of endodontic rotary instruments subjected to different conditions to be simulated through mathematical analysis [18]. Moreover, FE analyses have been previously used in endodontics to assess both the mechanical behavior of endodontic instruments [19] and stress distribution during root canal treatments [16].

Two different approaches can be found in recent works when developing FE models for the stress analysis of endodontic files, which differ in the way in which the endodontic file geometry is obtained. In both cases, the obtained geometry must be converted to a finite element model by means of a FE analysis pre-processor, in order to proceed to its analysis. In addition, elevated solid mechanics knowledge is required in both cases, in order to define a finite element model that can accurately reproduce the physics of the problem.

In the most conventional approach [1,20,21], the generation of the geometry of the file is conducted through computer-aided design (CAD) software. This approach requires elevated CAD knowledge to accurately reproduce the geometric characterization of the endodontic rotary file parameters. In fact, there are several cases in which the generated geometries cannot accurately reproduce the geometry of the actual endodontic file, especially at the transition between the active part and the shaft.

In another approach [22], the geometry of the endodontic file is obtained from a tomography scanner. This approach requires expensive equipment in order to obtain the computer representation from the tomography scanner and elevated knowledge to manipulate the obtained geometry files.

Both processes are costly in terms of time and have to be accomplished for each assigned case of design of various geometries and cases of investigation. Therefore, generating an automated procedure that simplifies the procedures described above and enables the performance of FE analyses without the need for this knowledge will help us to better understand the mechanical behavior of endodontic rotary files under various conditions. Thus, the aims of this work are as follows:

- To develop an automated procedure to obtain an accurate description of the geometry of the endodontic file from its design parameters;
- To develop an automated procedure to obtain an FE model of the endodontic file from the generated geometry;
- To demonstrate the capabilities of the proposed procedures.

2. Materials and Methods

This section describes a new method developed for the computerized generation of endodontic files and the obtention of FE models for their stress analysis. The geometry considered for the endodontic file is shown in Figure 1a. It is defined with respect to a coordinate system S_f, whose z_f axis is alined with the theoretical axis of rotation of the endodontic file and its origin O_f is at the tip of the endodontic file. The geometry of the endodontic file is fully parametrized by the following set of parameters:

- The diameter of the shaft, d_{sh};
- The diameter of the tip of the active part, d_{ap};
- The length of the active part, L_{ap};

- The total length of the file, L_{total};
- The pitch of the active part, p_z, which represents the distance between adjacent points in the cutting edge.

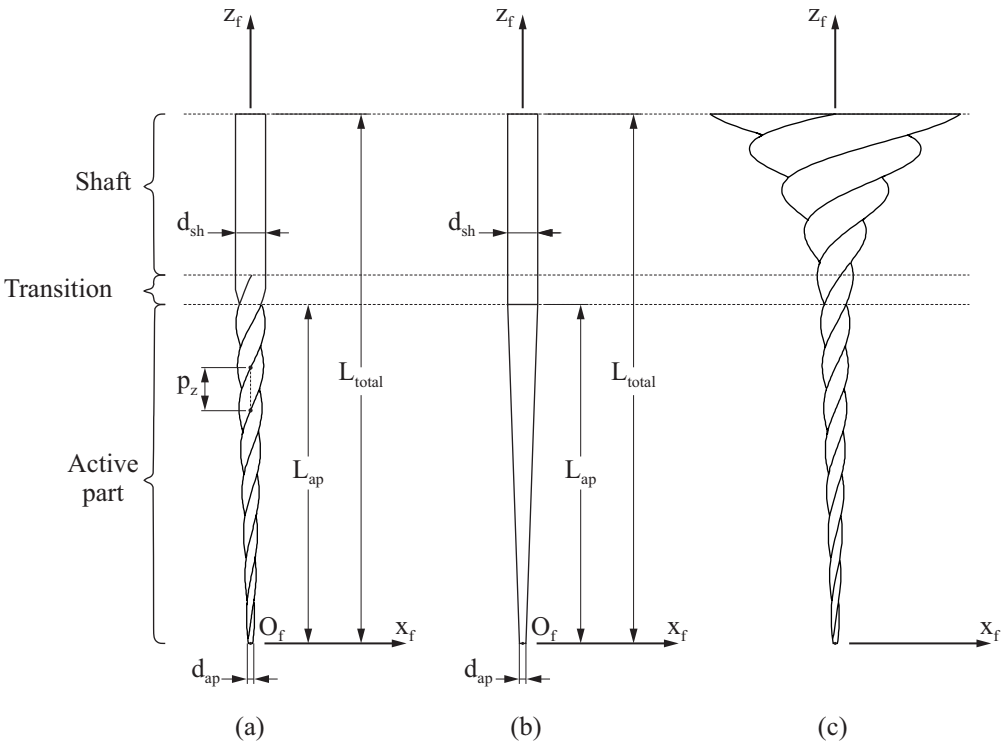

Figure 1. Definition of the geometry of the endodontic file (**a**), the raw material (**b**) and the machined material (**c**).

Three different parts can be identified for this endodontic file: the active part, the shaft and the transition part. The active part contains the cutting edges and has an arbitrary cross section (squared, triangular, etc.). The shaft has a circular cross section and connects the active part with the support of the endodontic file (which is not included in this model). Finally, the transition part allows for a smooth transition from the cross section of the active part to the cross section of the shaft. Figure 2 shows an example of the cross section of the endodontic file at each one of these parts.

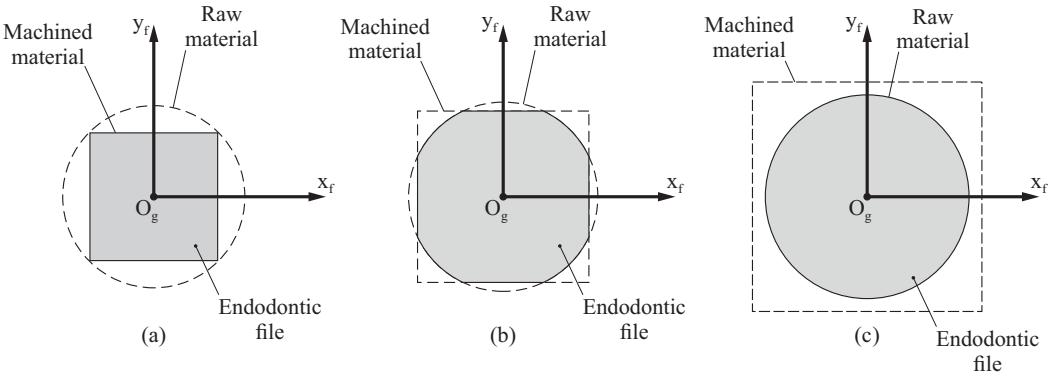

Figure 2. Cross-sections of the endodontic file at different positions along the z_g axis: active part (**a**), transition area (**b**) and shaft (**c**).

The computerized generation of this endodontic file is achieved as the intersection of two different geometries: the raw material (Figure 1b) and the machined material (Figure 1c). The raw material corresponds to a geometry of the endodontic file before the cutting edges are machined over it, and its generation is described in Section 2.1. The geometry of the machined material is an auxiliary geometry that is used to generate the cutting edges of the endodontic file, and its generation is described in Section 2.2. The intersection of both geometries and the obtention of the final geometry of the endodontic file is described in Section 2.3.

Having a computational description of the geometry of the endodontic file allows for an automated generation of FE models for its stress analysis. Section 2.4 provides further details on how to obtain these FE models.

2.1. Definition of the Geometry of the Raw Material for the Endodontic File

The raw material (Figure 1b) has an axisymmetric geometry that consists of two different parts:

- A cylindrical part, which corresponds to the shaft, characterized by its length ($L_{total} - L_{ap}$) and its diameter (d_{sh});
- A truncated cone, which corresponds to the active part. It is characterized by its length (L_a) and its diameters at the front (d_{ap}) and back ends (d_{sh}).

The position of a point P on the surface of the raw material is given by the parametric equation $\mathbf{r}_f^{'}(\theta, v)$, which provides the coordinates of point P in coordinate system S_f from its parametric coordinates $\theta \in [0°, 360°]$ and $v \in [0, L_{total}]$:

$$\mathbf{r}_f^{'}(\theta, v) = \left[\frac{\lambda^{'}(v)}{2} \cdot \cos\left(\theta + \varphi^{'}(v)\right) \qquad \frac{\lambda^{'}(v)}{2} \cdot \sin\left(\theta + \varphi^{'}(v)\right) \qquad v \right]^T \tag{1}$$

where angle $\varphi^{'}(v)$ is defined as a function of v; assuming a constant pitch p_z along the endondontic file, it can be defined as

$$\varphi^{'}(v) = \frac{v}{p_z} \cdot 2\pi \text{ rad} \tag{2}$$

On the other hand, $\lambda^{'}(v)$ represents the diameter of the raw material at coordinate v, and it is defined as

$$\lambda^{'}(v) = \begin{cases} d_{ap} + v \cdot \frac{d_{sh} - d_{ap}}{L_{ap}}, & \text{if } 0 \leq v < L_{ap} \\ d_{sh}, & \text{if } L_{ap} \leq v < L_{total} \end{cases} \tag{3}$$

2.2. Definition of the Geometry of the Machined Material for the Endodontic File

The machined material (Figure 1c) is an auxiliary geometry that is used for the generation of the geometry of the endodontic file, and it is obtained from the transformation (rotation, translation and scalation) of an arbitrary cross section.

For the definition of this geometry, let us consider an auxiliary coordinate system S_g, whose z_g axis is parallel to the z_f axis of coordinate system S_f, as indicated in Figure 3 left. The origin of coordinate system S_g is located on axis z_f at a distance v from O_f, and S_g is rotated with respect to S_f an angle $\varphi(v)$.

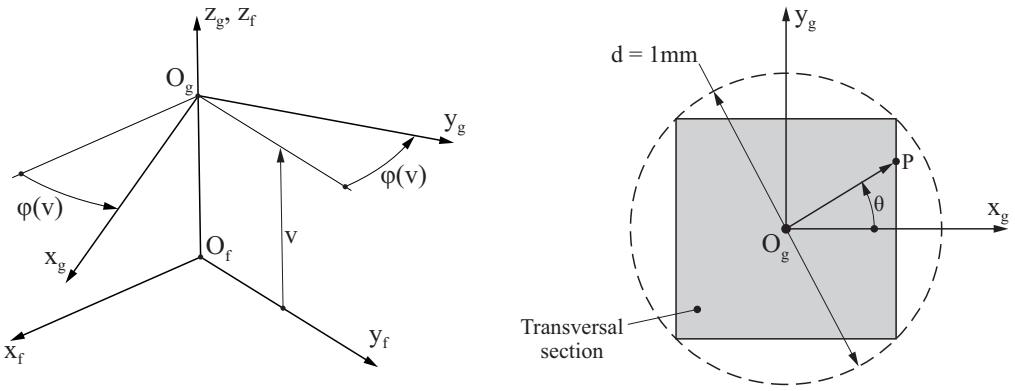

Figure 3. (**Left**) Definition of coordinate systems S_f and S_g and (**Right**) definition of a sample squared cross section for the endodontic file.

The cross section of the machined material is defined with respect to coordinate system S_g, and it is circumscribed into a normalized circumference (d = 1 mm), as illustrated in Figure 3 right for the particular case of a squared cross section. The position of any point P over the contour of the file section is defined by a parametric function $\mathbf{r}_g(\theta)$ that provides, for a given parametric coordinate $\theta \in [0°, 360°]$, the homogeneous coordinates [23] of point P in coordinate system S_g:

$$\mathbf{r}_g(\theta) = \begin{bmatrix} x_g(\theta) & y_g(\theta) & z_g(\theta) & 1 \end{bmatrix}^T \tag{4}$$

where $z_g(\theta) = 0$, since the cross section is contained in the $x_g y_g$ plane. In the particular case of squared transversal cross section, $x_g(\theta)$ and $y_g(\theta)$ can be defined as

$$x_g(\theta) = \frac{d \cdot \sqrt{2}}{4} \cdot \begin{cases} \tan(90° - \theta), & \text{if } 45° \leq \theta < 135° \\ -1, & \text{if } 135° \leq \theta < 225° \\ -\tan(270° - \theta), & \text{if } 225° \leq \theta < 315° \\ 1, & \text{otherwise} \end{cases} \tag{5a}$$

$$y_g(\theta) = \frac{d \cdot \sqrt{2}}{4} \cdot \begin{cases} 1, & \text{if } 45° \leq \theta < 135° \\ \tan(180° - \theta), & \text{if } 135° \leq \theta < 225° \\ -1, & \text{if } 225° \leq \theta < 315° \\ \tan\theta, & \text{otherwise} \end{cases} \tag{5b}$$

where d = 1 mm is the diameter of the normalized circumference. The definitions of $x_g(\theta)$ and $y_g(\theta)$ for other transversal cross sections can be trivially derived.

The position of a point P on the surface of the machined material is given by the parametric equation $\mathbf{r}_f(\theta, v)$, which provides the homogeneous coordinates of point P in coordinate system S_f from its parametric coordinates $\theta \in [0°, 360°]$ and $v \in [0, L_{total}]$:

$$\mathbf{r}_f(\theta, v) = \mathbf{M}_{fg}(v) \cdot \mathbf{r}_g(\theta) \tag{6}$$

where $\mathbf{r}_g(\theta)$ is given by Equation (4), v is a distance coordinate (see Figure 3) and $\mathbf{M}_{fg}(v)$ is a transformation matrix defined as

$$\mathbf{M}_{fg}(v) = \begin{bmatrix} \lambda(v) \cdot \cos\varphi(v) & -\lambda(v) \cdot \sin\varphi(v) & 0 & 0 \\ \lambda(v) \cdot \sin\varphi(v) & \lambda(v) \cdot \cos\varphi(v) & 0 & 0 \\ 0 & 0 & 1 & v \\ 0 & 0 & 0 & 1 \end{bmatrix} \tag{7}$$

The advantage of using homogeneous coordinates is that the transformation matrix $\mathbf{M}_{fg}(v)$ allows three simultaneous transformations of the transversal cross section of the machined material to be performed:

- The translation of the cross section a distance v along the z_f axis;
- The rotation of the cross section at an angle $\varphi(v)$ around the z_f axis;
- The scaling of the cross section in the $x_f y_f$ plane by a factor $\lambda(v)$.

The angle $\varphi(v)$ is defined as a function of v and, assuming a constant pitch p_z along the endondontic file, this angle can be defined as

$$\varphi(v) = \frac{v}{p_z} \cdot 2\pi \text{ rad} \tag{8}$$

Note that the equality $\varphi(v) = \varphi^{'}(v)$ must be satisfied to guarantee the robustness of the proposed formulation. On the other hand, the scale factor $\lambda(v)$ is defined as

$$\lambda(v) = \begin{cases} d_{ap} + v \cdot \frac{d_{sh} - d_{ap}}{L_{ap}}, & \text{if } 0 \leq v < L_{ap} \\ d_{ap} + v \cdot \frac{d_{sh} - d_{ap}}{L_{ap}} + a_{sh} \cdot \left(v - L_{ap}\right)^2, & \text{if } L_{ap} \leq v < L_{total} \end{cases} \tag{9}$$

In the interval corresponding to the active part, it is fulfilled that $\lambda(v) = \lambda^{'}(v)$. In the transition part and the shaft, $\lambda(v) > \lambda^{'}(v)$, because a quadratic term is included in the definition of $\lambda(v)$. This quadratic term allows for a smooth transition from the machined material to the raw material, and it is characterized by the parabola coefficient a_{sh}.

2.3. Definition of the Geometry of the Endodontic File

The final geometry of the endodontic file is obtained from the intersection of the geometries of the raw material and machined material, as described above. In order to compute this intersection, it is necessary to compute the inner point of these geometries for the same θ and v coordinates. For such a purpose, the distance from any point in the cross section to the z_f axis needs to be calculated. Distances $d'(v)$ and $d(\theta, v)$ are defined for the raw material and the machined material (respectively) as

$$d^{'}(v) = \frac{\lambda^{'}(v)}{2} \tag{10a}$$

$$d(\theta, v) = \left| \mathbf{r}_f(\theta, v) - \mathbf{r}_f(\theta, v) \cdot \mathbf{k}_f \right| \tag{10b}$$

where $\mathbf{k}_f$ is the unit vector in the direction given by the z_f axis of the coordinate system S_f.

Note that $d^{'}(v)$ does not depend on θ because the raw material has a circular cross section and, in consequence, all the points within the section are at the same distance of z_f. According to the definition of the scaling factors for the geometries of the raw material and the machine material, the following statements are fulfilled (see Figure 2):

- In the active part of the endodontic file, $d(\theta, v) \leq d^{'}(v)$;
- In the shaft of the endodontic file, $d(\theta, v) > d^{'}(v)$;
- In the transition part of the endodontic file, the relation between $d(\theta, v)$ and $d^{'}(v)$ cannot be known in advance.

Taking this into account, the geometry of the endodontic file is represented in coordinate system S_f by function $\mathbf{q}_f(\theta, v)$ as

$$\mathbf{q}_f(\theta, v) = \begin{cases} \mathbf{r}_f(\theta, v), & \text{if } d(\theta, v) < d^{'}(v) \\ \mathbf{r}_f^{'}(\theta, v), & \text{otherwise} \end{cases} \tag{11}$$

2.4. Development of an Fe Model for Stress Analysis of Endodontic Files

This section describes a new procedure for the automated development of FE models for the stress analysis of endodontic files. This procedure covers the typical steps in the generation of an FE model for stress analysis, which include the discretization of the volume of the endodontic file into finite elements, the definition of the material properties for the finite elements of the model and the definition of the loading and boundary conditions of the model.

In the first step, the volume of the endodontic file is discretized into tetrahedral elements by means of a constrained Delaunay tetrahedralization [24]. The constrained Delaunay tetrahedralization requires the boundary surfaces of the endodontic file to be represented by a set of triangles, which will constitute the external faces of the tetrahedrons once the mesh is generated. This boundary representation is achieved following these steps:

1. The external surfaces that define the volume of the endodontic file are represented analytically considering the parametric equation $\mathbf{q}_f(\theta, v)$ (Equation (11)), which provides the Cartesian coordinates of a point in the surface of the endodontic file from its parametric coordinates $\theta \in [0°, 360°]$ and $v \in [0, L_{total}]$;
2. The analytical determination of the position of the nodes in the surface of the endodontic file is performed, taking into account the number of desired elements in the longitudinal (n_v) and angular directions (n_θ). Let us reiterate that all nodes of the FE mesh are determined analytically using Equation (11);
3. Discretization of the surface of the endodontic file into triangular faces is accomplished using the nodes determined previously.

Using this boundary representation of the endodontic file, the tetrahedral mesh is constructed using the constrained Delaunay tetrahedralization implemented in the TetGen library [25]. This tetrahedralization does not change the position of the nodes defined for the endodontic file surface, and the resulting tetrahedrons keep the faces provided as input information.

When the FE mesh is generated, mechanical properties are assigned to its elements. The mechanical response of a material in its elastic range can be defined by the elastic modulus E and the Poisson's coefficient ν. Assuming the endondontic file is manufactured using a NiTi alloy, these material parameters are established as $E = 36$ GPa and $\nu = 0.3$ [1]. Of course, the user can specify other values.

In the last step, the loading and boundary conditions for the FE model are established. Endodontic files are usually tested for bending and torsional loads, and the typical procedure for these tests is described in [26] and summarized in Figure 4. In these analyses, the endodontic file is approached to a cantilever beam. A fixed support is defined at a distance d_{enc} from the tip of the endodontic file, in such a way that all the nodes below that dimension have all their degrees of freedom constrained. Typical magnitudes for d_{enc} are between 3 mm [2,20,22,27,28] and 4 mm [29], although other values could be considered [1,21].

Loads are specified at the other part of the endodontic file. For such a purpose, a rigid surface is defined comprising all the nodes within the end face. A reference node is defined at the center of this face, whose movements are coupled to the movements of the rigid surface by means of a multi-point constraint. Loads are applied directly over this reference node. Two different load cases are derived to study the bending (Figure 4a) and torsional (Figure 4b) response of the endodontic file. In the first of them (Figure 4a), a tangential load F_t is introduced over the reference node; in the second (Figure 4b), a torsional moment M_z is considered over this reference node.

This procedure provides an input file for the FE solver that contains the entire definition of the FE model. It must be emphasized that this implementation allows for the development of fully parametrized FE models, in which the geometry, the mesh density, the material parameters and the loading conditions can be specified by the user without using any other third-party software.

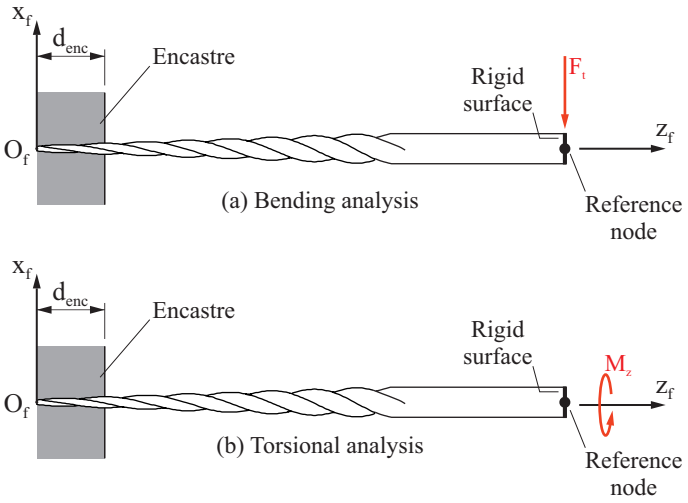

Figure 4. Definition of loading and boundary conditions.

3. Results

The developed procedure has been implemented in Matlab R2018 [30] (MathWorks Inc., Natick, MA, USA). A graphical interface, which is shown in Figure 5, has been programmed to ease the specification of the endodontic file geometry and the configuration of the FE model. After completing all the parameters that define the model, this software provides an input file for the FE solver, which contains the entire definition of the FE model.

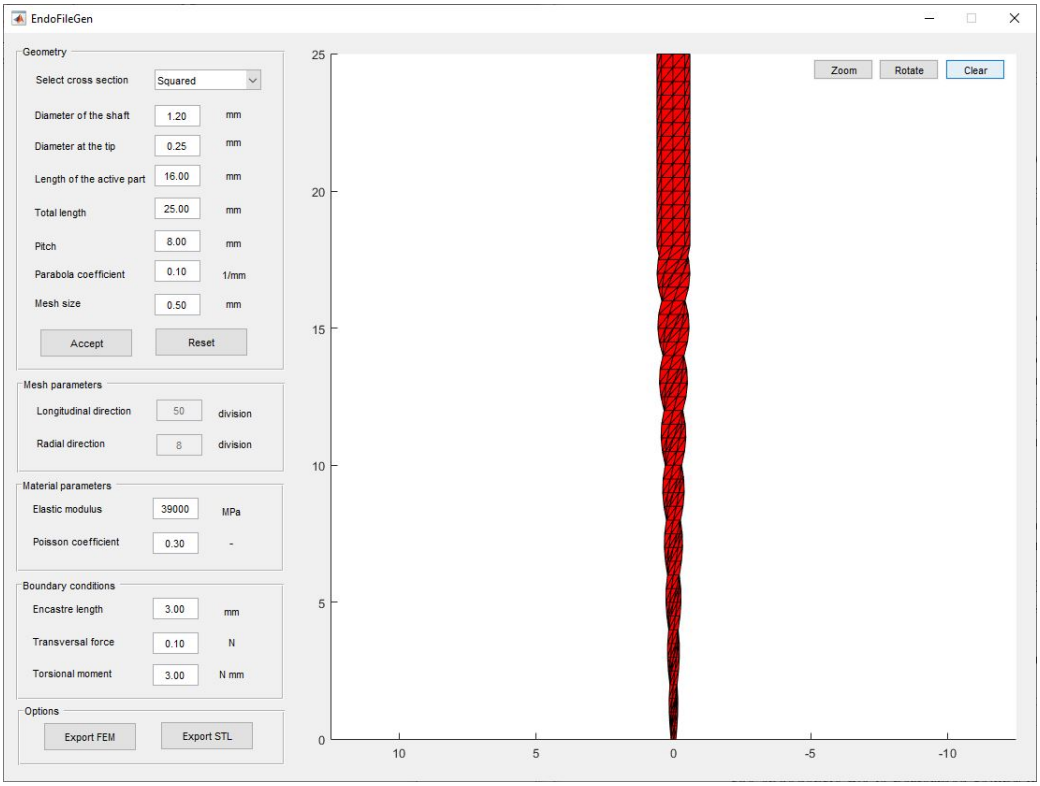

Figure 5. Graphical interface for the developed computer program.

The performance of the proposed procedure and its computational implementation is illustrated with the generation and stress analysis of an endodontic file, which is defined by the set of parameters shown in Table 1.

Table 1. Definition of cases of study.

Name	Magnitude
Cross section	Squared
Diameter of the shaft, d_{sh}	1.20 mm
Diameter of the tip, d_{ap}	0.25 mm
Length of the active part, L_{ap}	16.00 mm
Total length of the file, L_{total}	25.00 mm
Taper, c	6%
Pitch of the active part, p_z	2.00 mm
Parabola coefficient transition area, a_{sh}	0.10 mm^{-1}

Two different load cases are considered in this study, according to Bonessio et al. [27] and De Arruda Santos et al. [28]. In the first load case, the bending behavior of the endodontic file is studied by considering a transversal force $F_t = 0.1$ N. In the second load case, the torsional behavior of the endodontic file is studied by considering a torsional moment $M_z = 0.3\ \text{N} \cdot \text{cm}$. In both cases, the length of the encastre is $d_{enc} = 3$ mm.

3.1. Mesh Convergence Study

A mesh convergence study has been conducted to establish the optimum size and type for the elements of the mesh. In this study, several finite element models are obtained for the endodontic file, in which the density of the mesh is progressively increased by varying the magnitudes of n_v and n_θ. Four different average element sizes have been considered in the analysis, which vary from 0.05 mm to 0.20 mm, and both linear and quadratic tetrahedral elements have been taken into account. Figure 6 shows one of the meshes used in this study, in which the endodontic file is meshed using quadratic tetrahedrons with an average element size of 0.10 mm ($n_\theta = 24$ and $n_v = 250$). The resulting FE models were analyzed using ABAQUS [31] (Dassault Systèmes Simulia Corp, Providence, RI, USA).

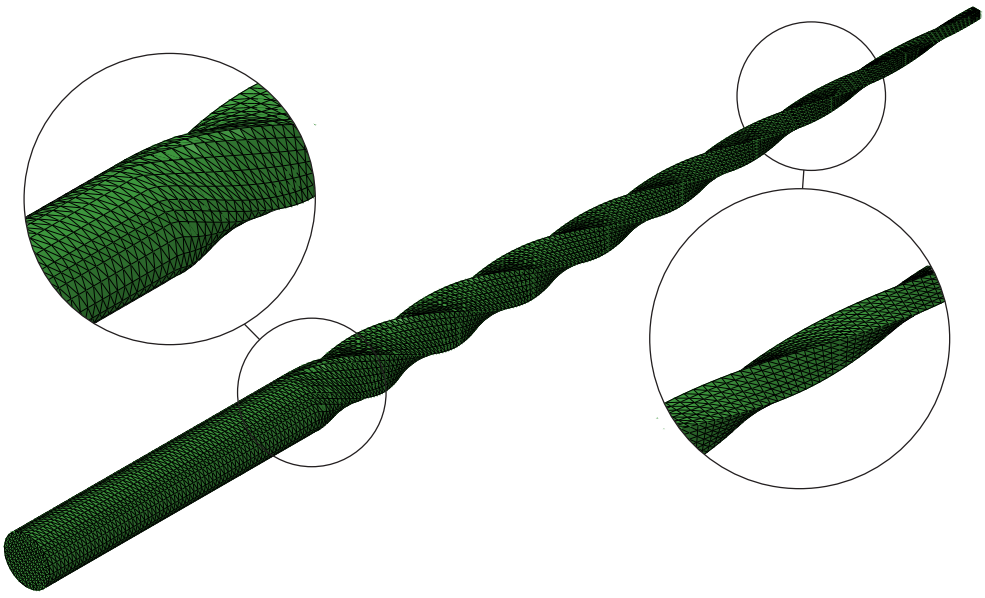

Figure 6. Finite element mesh for the endodontic file; the average element size is 0.10 mm ($n_\theta = 24$ and $n_v = 250$).

As suggested by Żmudzki [32,33], the convergence of the mesh can be assessed by means of an error energy norm E. In this error estimator, the stress vector $\hat{\boldsymbol{\sigma}}$ and the averaged stress vector $\boldsymbol{\sigma}^*$ are used to determine a stress error vector $\Delta\boldsymbol{\sigma}$:

$$\Delta\boldsymbol{\sigma} = \boldsymbol{\sigma}^* - \hat{\boldsymbol{\sigma}} \tag{12}$$

Then, for a given element i of the mesh and following the ideas presented by Zienkiewicz [34], an element energy error e_i is determined as:

$$e_i = \frac{1}{2} \cdot \int_{V_i} \Delta\boldsymbol{\sigma}^T \cdot \boldsymbol{D}^{-1} \cdot \Delta\boldsymbol{\sigma} \cdot dV_i \tag{13}$$

where $\boldsymbol{D}^{-1}$ is the material elasticity matrix and V_i denotes the volume of element i. The energy error e is estimated for the whole finite element model as the sum of the error contributions of all the elements in the mesh:

$$e = \sum_{i=1}^{N_e} e_i \tag{14}$$

where N_e denotes the number of elements in the mesh. Finally, and considering the total strain energy of the finite element model U, the error energy norm E is calculated as:

$$E = \sqrt{\frac{e}{U+e}} \tag{15}$$

Figure 7a shows the evolution of the error energy norm E as a function of the average element size, determined for each load case (torsion and bending) and element type (linear and quadratic). In all the cases, it can be observed that reducing the average element size also decreases the error in energy norm. For any load case and average element size, the error energy norm is significantly smaller when the problem is solved using quadratic elements than when it is solved using linear elements.

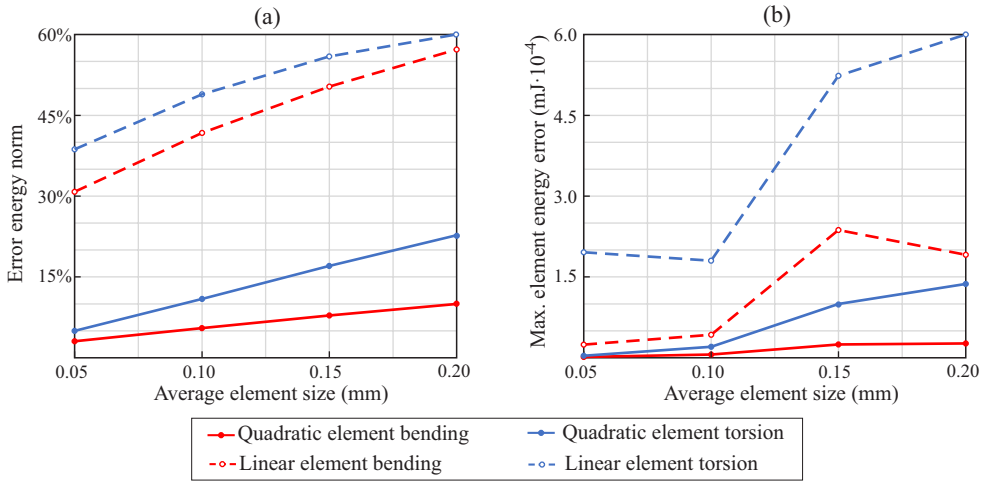

Figure 7. Results for the convergence study: (**a**) error energy norm of the whole model and (**b**) maximum element energy error.

Figure 7b shows the maximum element energy error $(\max(e_i))$ determined for each load case (torsion and bending) and element type (linear and quadratic), as a function of the average element size. The trends observed in this figure are similar to the ones observed in Figure 7a. In general, the maximum element energy error is reduced as the average element size is decreased, and quadratic elements demonstrate a better performance than linear elements. In all the cases the element with the maximum element energy error is found in the vicinity of the encastre, indicating that this is the region of the finite element model where mesh refinement is more needed.

Although there is no universal agreement over which is the error in energy norm that can be used as a threshold to validate the convergence of a given finite element mesh, an error in energy norm of 15% has been used in some works [35] for such a purpose. Taking this into consideration, and examining the results shown in Figure 7a, it could be said that

in this case the mesh convergence is achieved when the finite element model is built using quadratic elements and the average element size is equal or less than 0.10 mm.

3.2. Interpretation of the Results of the Stress Analysis

Figure 8 shows a von Mises stress plot along the endodontic file, which is obtained from a torsional analysis in which the finite element model is built with quadratic elements with an average element size of 0.05 mm. The maximum von Mises stress reached in this analysis is 843 MPa, and it is produced in the vicinity of the encastre (but not in the encastre itself, as it can be observed in the detail of Figure 8). The figure also shows the stress distribution along the cross section where maximum von Mises stress takes place. In both cases, the stress results follow the expected distribution for this type of analyses. The rotation at the free end of the file 0.39 rad.

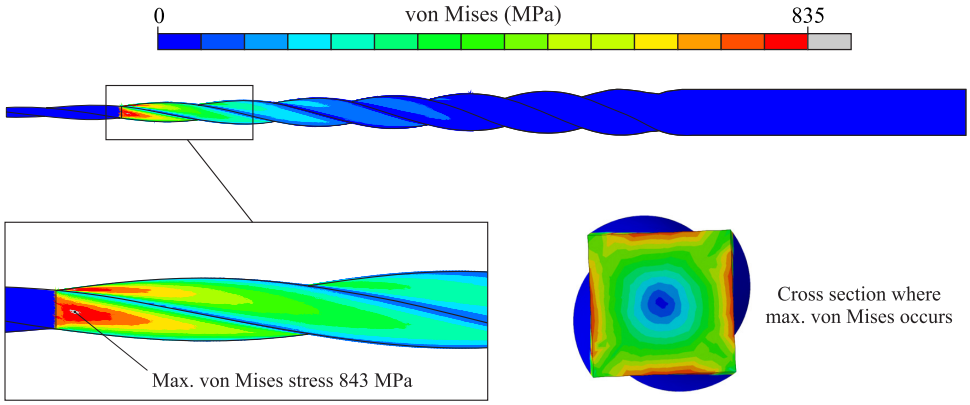

Figure 8. Stress results for torsional analysis (undeformed plot).

Figure 9 shows a von Mises stress plot along the endodontic file, which is obtained from a bending analysis in which the finite element model is built with quadratic elements with an average element size of 0.05 mm. The maximum von Mises stress reached in this analysis is 613 MPa, and it is produced in the vicinity of the encastre. The figure also shows the stress distribution along the cross section where the maximum stress is found. In both cases, the stress results follow the expected distribution for this type of analyses. The deflection at the free end of the file is 3.21 mm.

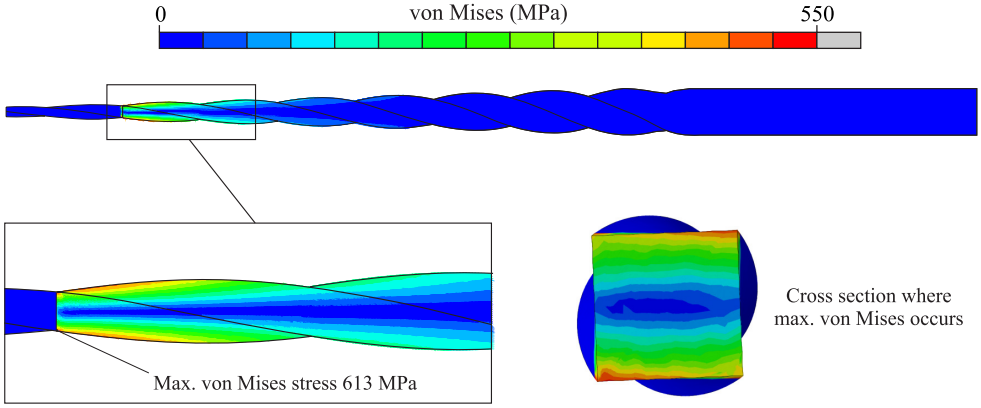

Figure 9. Stress results for bending analysis (undeformed plot).

Unlike in the torsional analysis, in the bending analysis the maximum von Mises stress occurs in a node where a boundary condition is applied and, as a consequence, a numerical singularity is produced that leads to unrealistic stress values. This issue is illustrated in Figure 10a, where a detail of the von Mises stress plot over the area where the bending stresses reach their maximum value is shown. This figure also displays the von Misses stress values at the nodes of the edge where the maximum stress takes place.

It can be observed that the maximum value of 613 MPa, produced at the node in the corner of the encastre section, is unreasonably high considering the stress magnitude at the surrounding nodes.

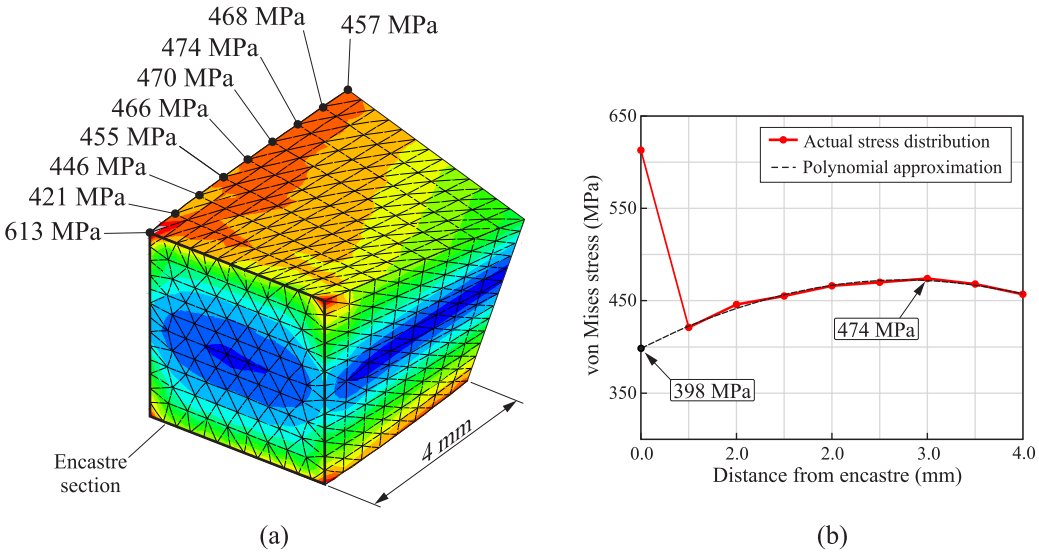

Figure 10. Stress results for bending analysis: (**a**) detail of the region where maximum von Mises stress takes place and (**b**) evolution of the von Mises stresses along the edge.

According to many researchers [36,37], these stress results at singularity points cannot be considered to evaluate the strength of the endodontic file. To get around this issue, Żmudzki [32] proposes to exclude the stress results at these points and then extrapolate the extreme value from the stress values in the remaining nodes. Following this idea, Figure 10b shows a plot of the evolution of the von Mises stress along the observed edge. A polynomial approximation to the stress values has been obtained, discarding the maximum value of 613 MPa. Following this approximation, the predicted von Misses stress value at the encastre is 398 MPa, leaving the maximum von Mises stress of the model at 474 MPa.

3.3. Parametric Study

The developed procedure allows for a simple and fast generation of finite element models of endodontic files, and, in consequence, it is especially suitable for performing parametric and optimization studies. In this section, the performance of the proposed procedure is illustrated with three parametric studies, in which the pitch of the active part, the length of the active part and the diameter of the tip were varied. In each parametric study, only one parameter was varied and the rest were kept constant and equal to those shown in Table 1.

Figure 11 shows the results obtained from the parametric study in which the pitch of the active part was varied. Four different magnitudes were considered for the pitch of the active part, which were between 1 mm and 4 mm. In each case, the endodontic file has been conveniently rotated so the orientation of the cross section at the encastre coincides with that shown in Figure 9. Figure 11a shows the results for the bending analysis. It can be observed that both the maximum von Mises stress and tip deflection reduced as the pitch of the active part increased. The maximum von Mises stress decreased from 517 MPa (when $p_z = 1$ mm) to 451 MPa (when $p_z = 4$ mm). The tip deflection decreased from 3.38 mm (when $p_z = 1$ mm) to 3.17 mm (when $p_z = 4$ mm).

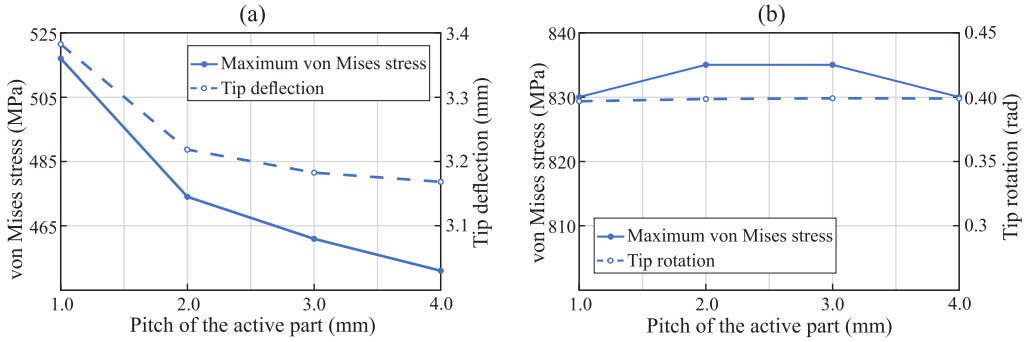

Figure 11. Results of the parametric study of the pitch of the active part: (**a**) bending analysis and (**b**) torsional analysis.

On the other hand, Figure 11b shows the results for the torsional analysis. In this case, minor variations are observed for the maximum von Mises stress and the tip rotation, indicating that these parameters may be independent of the pitch of the active part (at least in the observed range).

Figure 12 shows the results obtained from the parametric study in which the length of the active part was varied. Five different magnitudes were considered for the length of the active part, which were between 14 mm and 18 mm. Figure 12a shows the results for the bending analysis. It can be observed that both the maximum von Mises stress and tip deflection increased as the length of the active part increased. The maximum von Mises stress increased from 399 MPa (when $L_{ap} = 14$ mm) to 554 MPa (when $L_{ap} = 18$ mm). The tip deflection increased from 2.44 mm (when $L_{ap} = 14$ mm) to 4.05 mm (when $L_{ap} = 18$ mm).

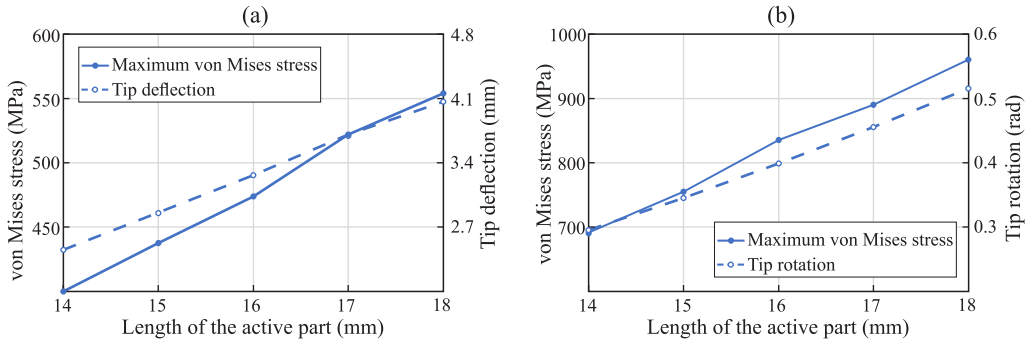

Figure 12. Results of the parametric study of the length of the active part: (**a**) bending analysis and (**b**) torsional analysis.

On the other hand, Figure 12b shows the results for the torsional analysis. As happened in the bending analysis, both the maximum von Mises stress and tip rotation increased as the length of the active part increased. The maximum von Mises stress increased from 690 MPa (when $L_{ap} = 14$ mm) to 960 MPa (when $L_{ap} = 18$ mm). The tip rotation increased from 0.30 rad (when $L_{ap} = 14$ mm) to 0.52 rad (when $L_{ap} = 18$ mm).

Finally, Figure 13 shows the results obtained from the parametric study in which the diameter of the tip of the active part was varied. Four different magnitudes were considered for the diameter of the tip of the active part, which were between 0.20 mm and 0.35 mm. Figure 13a shows the results for the bending analysis. It can be observed that both the maximum von Mises stress and tip deflection decreased as the diameter of the tip of the active part increased. The maximum von Mises stress decreased from 630 MPa (when $d_{ap} = 0.20$ mm) to 295 MPa (when $d_{ap} = 0.35$ mm). The tip deflection decreased from 4.20 mm (when $d_{ap} = 0.20$ mm) to 2.01 mm (when $d_{ap} = 0.35$ mm).

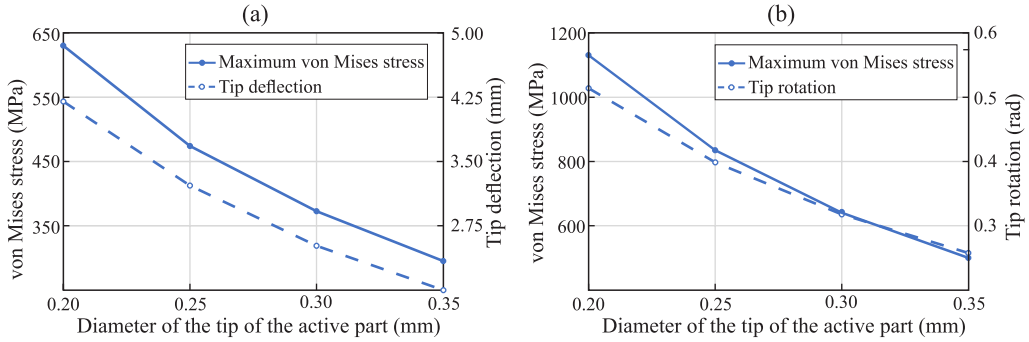

Figure 13. Results of the parametric study of the diameter of the tip of the active part: (**a**) bending analysis and (**b**) torsional analysis.

On the other hand, Figure 13b shows the results for the torsional analysis. As happened in the bending analysis, both the maximum von Mises stress and tip rotation decreased as the diameter of the tip of the active part increased. The maximum von Mises stress decreased from 1130 MPa (when $d_{ap} = 0.20$ mm) to 500 MPa (when $d_{ap} = 0.35$ mm). The tip rotation decreased from 0.51 mm (when $d_{ap} = 0.20$ mm) to 0.26 mm (when $d_{ap} = 0.35$ mm).

4. Discussion

FE models have been proposed to analyze the mechanical performance of endodontic rotary files, isolating the variables independently under controlled settings [38] to facilitate the comparison between the mechanical behavior and stress distribution of existing endodontic rotary files and even to allow the design of new endodontic rotary instruments by reducing time and costs [27]. In addition, He and Ni used FE methods to improve the geometrical design of existing endodontic rotary instruments and therefore the mechanical behavior under bending and torsional loads to reduce the prevalence of failure [2].

He and Ni also analyzed the influence of the helix angle, taper and flute length on the bending flexibility and torsional stiffness of endodontic files (V-Taper) through numerical simulations and concluded that the geometric features influence on the mechanical performance of endodontic files under bending and torsional conditions [2]. Arbab-Chirani et al. compared numerically the mechanical behavior of Hero, HeroShaper, ProFile, Wtwo and ProTaper F1 endodontic rotary NiTi instruments under bending and torsional conditions and showed that the different designs for tapers, pitch and cutting blades influence on the bending and torsional mechanical behavior [39]. Baek et al. evaluated the effect from pitch and cross-section design on torsional stiffness of NiTi endodontic rotary instruments and evidenced that torsional deformation and fracture of NiTi rotary files might be reduced by reducing the pitch and increasing the cross-sectional areas rather than the center core area [40].

Although metallurgical properties and metallurgical treatments have been shown to influence the properties of NiTi endodontic rotary instruments, geometrical design has been highlighted to be directly related to the stiffness [41], clinical efficiency and cutting performance of endodontic rotary files [29,42]. The cross-section design of endodontic rotary files has experienced a continuous development; Versluis et al. reported that increasing the cross-sectional surface area lead to a decrease in the flexibility of endodontic rotary files by a stress accumulation at the upper and lower edges of the cross section during bending tests, compared with smaller cross-sectional surface areas [17].

In addition, cross-sectional morphology has been also widely analyzed, and Galal and Hamdy reported that a convex triangular cross-section design showed maximum von Misses stresses upon bending tests (1962 MPa), followed by a triangular cross-section design (1535 MPa), parallelogram cross-section design (870 MPa) and rectangular cross-section design (814 MPa); however, a convex triangular cross-section design showed maximum von Misses stresses upon torsional tests (4321 MPa), followed by a triangular

cross-section design (4285 MPa), rectangular cross-section design (2659 MPa) and parallelogram cross-section design (2307 MPa).

Additionally, the stress distribution pattern was localized at the cutting edges under bending tests and more concentrated in the base of the flutes in the first 2 mm of the triangular cross-section design under torsional tests [43]. These results agree with the findings reported by Tsao et al., who showed a maximum von Misses stress of 1170 MPa at the cutting edges of a triangular cross-section design endodontic rotary file after applying a transverse load of 1 N at the tip of the endodontic rotary file during bending tests [44]; additionally, Prados-Privado et al. showed a maximum von Misses stress of 1146.6 MPa at the convex triangular cross-section design of a Wave One endodontic reciprocating file, followed by the S-shaped cross-section design of Reciproc (942.48 MPa), the parallelogram cross-section design of WaveOne Gold (847.35 MPa) and the S-shaped cross-section design of Reciproc Blue (614.21 MPa) under bending conditions.

However, torsional resistance tests showed a maximum von Misses stress of 990.14 MPa at the WaveOne endodontic reciprocating files, followed by Reciproc (678.69 MPa), Reciproc Blue (669.75 MPa) and WaveOneGold (481 MPa) [20]; however, these results are not aligned with those obtained in the present study, possibly because the authors used a different cross-section design (squared) and also a lower transverse load (0.1 N).

However, FE methods require elevated CAD knowledge to accurately reproduce the geometric characterization of the endodontic rotary file parameters as well as numerical analysis knowledge to simulate the mechanical behavior and stress distribution during bending and torsional resistance tests. In addition, some drawbacks related to FE models have been highlighted as they used to be difficult and expensive to build, complex and time-consuming; furthermore, the formulations can be complicated and they have difficulty in dealing with complex geometry problems [29]. Therefore, the analytical model proposed in this study represents a solution to generate FE models repeatably.

5. Conclusions

In this work, a new procedure for the computerized generation of the geometry of endodontic rotary files and the automated creation of finite element models for the stress analysis of endodontic files is proposed. This new procedure allows us to create fully parametrized finite element models of the endodontic files directly from their design and material parameters.

The proposed procedure has been used to implement computer software, and its performance has been demonstrated by means of numerical examples. In general, it can be said that the proposed procedure can help to increase the accuracy with which the geometry of the finite element models of the rotary files can be generated and, at the same time, simplifies the analysis process and reduces time consumption.

Author Contributions: Conceptualization, V.R.-C. and Á.Z.-M.; methodology, V.R.-C. and F.S.-M.; software, V.R.-C. and F.S.-M.; investigation, V.R.-C. and Á.Z.-M.; resources, Ó.A.E., A.A.M. and A.G.C.; writing—original draft preparation, V.R.-C. and Á.Z.-M.; writing—review and editing, V.R.-C. and Á.Z.-M.; visualization, V.R.-C.; project administration, Ó.A.E., A.A.M. and A.G.C. All authors have read and agreed to the published version of the manuscript.

Funding: This research received no external funding.

Institutional Review Board Statement: Not applicable.

Informed Consent Statement: Not applicable.

Data Availability Statement: Data available on request due to restrictions (privacy and ethical).

Conflicts of Interest: The authors declare no conflict of interest.

References

1. Basheer Ahamed, S.; Vanajassun, P.; Rajkumar, K.; Mahalaxmi, S. Comparative Evaluation of Stress Distribution in Experimentally Designed Nickel-titanium Rotary Files with Varying Cross Sections: A Finite Element Analysis. *J. Endod.* **2018**, *44*, 654–658. [CrossRef]
2. He, R.; Ni, J. Design improvement and failure reduction of endodontic files through finite element analysis: Application to V-Taper file designs. *J. Endod.* **2010**, *36*, 1552–1557. [CrossRef]
3. Parashos, P.; Gordon, I.; Messer, H. Factors influencing defects of rotary nickel-titanium endodontic instruments after clinical use. *J. Endod.* **2004**, *30*, 722–725. [CrossRef] [PubMed]
4. Spili, P.; Parashos, P.; Messer, H. The impact of instrument fracture on outcome of endodontic treatment. *J. Endod.* **2005**, *31*, 845–850. [CrossRef] [PubMed]
5. Sattapan, B.; Nervo, G.; Palamara, J.; Messer, H. Defects in rotary nickel-titanium files after clinical use. *J. Endod.* **2000**, *26*, 161–165. [CrossRef]
6. Barbosa, F.; Ponciano Gomes, J.; de Araújo, M. Fractographic Analysis of K3 Nickel-Titanium Rotary Instruments Submitted to Different Modes of Mechanical Loading. *J. Endod.* **2008**, *34*, 994–998. [CrossRef]
7. Plotino, G.; Grande, N.; Cordaro, M.; Testarelli, L.; Gambarini, G. A Review of Cyclic Fatigue Testing of Nickel-Titanium Rotary Instruments. *J. Endod.* **2009**, *35*, 1469–1476. [CrossRef]
8. Inan, U.; Gonulol, N. Deformation and Fracture of Mtwo Rotary Nickel-Titanium Instruments After Clinical Use. *J. Endod.* **2009**, *35*, 1396–1399. [CrossRef] [PubMed]
9. McGuigan, M.; Louca, C.; Duncan, H. Clinical decision-making after endodontic instrument fracture. *Br. Dent. J.* **2013**, *214*, 395–400. [CrossRef]
10. Mcguigan, M.; Louca, C.; Duncan, H. The impact of fractured endodontic instruments on treatment outcome. *Br. Dent. J.* **2013**, *214*, 285–289. [CrossRef]
11. Yang, Q.; Shen, Y.; Huang, D.; Zhou, X.; Gao, Y.; Haapasalo, M. Evaluation of Two Trephine Techniques for Removal of Fractured Rotary Nickel-titanium Instruments from Root Canals. *J. Endod.* **2017**, *43*, 116–120. [CrossRef]
12. Strindberg, L. The Dependence of the Results of Pulp Therapy on Certain Factors: An Analytic Study Based on Radiographic and Clinical Follow-up Examinations. *Acta Dontol. Scand.* **1956**, *14* (Suppl. 21), 1–175, N.G. Mauritzons Boktryckerl.
13. Kim, H.; Kim, H.; Lee, C.; Kim, B.; Park, J.; Versluis, A. Mechanical response of nickel-titanium instruments with different cross-sectional designs during shaping of simulated curved canals. *Int. Endod. J.* **2009**, *42*, 593–602. [CrossRef] [PubMed]
14. Faus-Llácer, V.; Kharrat, N.H.; Ruiz-Sánchez, C.; Faus-Matoses, I.; Zubizarreta-Macho, Á.; Faus-Matoses, V. The Effect of Taper and Apical Diameter on the Cyclic Fatigue Resistance of Rotary Endodontic Files Using an Experimental Electronic Device. *Appl. Sci.* **2021**, *11*, 863. [CrossRef]
15. Sekar, V.; Kumar, R.; Nandini, S.; Ballal, S.; Velmurugan, N. Assessment of the role of cross section on fatigue resistance of rotary files when used in reciprocation. *Eur. J. Dent.* **2016**, *10*, 541–545. [CrossRef]
16. Kwak, S.; Ha, J.H.; Lee, C.J.; El Abed, R.; Abu-Tahun, I.; Kim, H.C. Effects of Pitch Length and Heat Treatment on the Mechanical Properties of the Glide Path Preparation Instruments. *J. Endod.* **2016**, *42*, 788–792. [CrossRef] [PubMed]
17. Hülsmann, M. Research that matters: Studies on fatigue of rotary and reciprocating NiTi root canal instruments. *Int. Endod. J.* **2019**, *52*, 1401–1402. [CrossRef]
18. Zienkiewicz, O.; Taylor, R.; Zhu, J. *The Finite Element Method: Its Basis and Fundamentals*; Elsevier Science: Amsterdam, The Netherlands, 2005.
19. Berutti, E.; Chiandussi, G.; Gaviglio, I.; Ibba, A. Comparative analysis of torsional and bending stresses in two mathematical models of nickel-titanium rotary instruments: ProTaper versus ProFile. *J. Endod.* **2003**, *29*, 15–19. [CrossRef]
20. Prados-Privado, M.; Rojo, R.; Ivorra, C.; Prados-Frutos, J. Finite element analysis comparing WaveOne, WaveOne Gold, Reciproc and Reciproc Blue responses with bending and torsion tests. *J. Mech. Behav. Biomed. Mater.* **2019**, *90*, 165–172. [CrossRef]
21. Scattina, A.; Alovisi, M.; Paolino, D.; Pasqualini, D.; Scotti, N.; Chiandussi, G.; Berutti, E. Prediction of cyclic fatigue life of nickel-titanium rotary files by virtual modeling and finite elements analysis. *J. Endod.* **2015**, *41*, 1867–1870. [CrossRef]
22. De Arruda Santos, L.; De Azevedo Bahia, M.; De Las Casas, E.; Buono, V. Comparison of the mechanical behavior between controlled memory and superelastic nickel-titanium files via finite element analysis. *J. Endod.* **2013**, *39*, 1444–1447. [CrossRef] [PubMed]
23. Lou, Y.; Li, Z.; Hervé, J. *Projective, Affine and Euclidean Geometric Transformations and Mobility in Mechanisms*; LAP Lambert Academic Publishing: Chisinau, Moldova, 2011; pp. 1–18.
24. Shewchuk, J. General-dimensional constrained delaunay and constrained regular triangulations, I: Combinatorial properties. *Discret. Comput. Geom.* **2008**, *39*, 580–637. [CrossRef]
25. Si, H. TetGen, a Delaunay-Based Quality Tetrahedral Mesh Generator. *ACM Trans. Math. Softw.* **2015**, *41*, 1–36. [CrossRef]
26. *ISO 3630-1:2008-Dentistry-Root-Ccanal Instruments-Part 1: General Requirements and Test Methods*; Standard, International Organization for Standardization: Geneva, Switzerland, 2008.
27. Bonessio, N.; Pereira, E.; Lomiento, G.; Arias, A.; Bahia, M.; Buono, V.; Peters, O. Validated finite element analyses of WaveOne Endodontic Instruments: A comparison between M-Wire and NiTi alloys. *Int. Endod. J.* **2015**, *48*, 441–450. [CrossRef]
28. De Arruda Santos, L.; López, J.; De Las Casas, E.; De Azevedo Bahia, M.; Buono, V. Mechanical behavior of three nickel-titanium rotary files: A comparison of numerical simulation with bending and torsion tests. *Mater. Sci. Eng. C* **2014**, *37*, 258–263. [CrossRef]

29. Montalvão, D.; Alçada, F.; Braz Fernandes, F.; De Vilaverde-Correia, S. Structural characterisation and mechanical fe analysis of conventional and m-wire Ni-Ti alloys used in endodontic rotary instruments. *Sci. World J.* **2014**, *2014*. [CrossRef]
30. MATLAB. *9.4.0.813654 (R2018a)*; The MathWorks Inc.: Natick, MA, USA, 2018.
31. *Abaqus Theory Guide*; Dassault Systèmes Simulia Corp: Johnston, RI, USA, 2015.
32. Zmudzki, J.; Walke, W.; Chladek, W. Influence of model discretization density in FEM numerical analysis on the determined stress level in bone surrounding dental implants. *Adv. Soft Comput.* **2008**, *47*, 559–567. [CrossRef]
33. Zmudzki, J.; Walke, W.; Chladek, W. Stresses present in bone surrounding dental implants in FEM model experiments. *J. Achiev. Mater. Manuf. Eng.* **2008**, *27-1*, 71–74.
34. Zienkiewicz, O.C.; Zhu, J.Z. A simple error estimator and adaptive procedure for practical engineerng analysis. *J. Achiev. Mater. Manuf. Eng.* **1987**, *24*, 337–357. [CrossRef]
35. Patil, H.; Jeyakarthikeyan, P. Mesh convergence study and estimation of discretization error of hub in clutch disc with integration of ANSYS. *IOP Conf. Ser. Mater. Sci. Eng.* **2018**, *402*, 012065. [CrossRef]
36. Stolk, J.; Verdonschot, N.; Huiskes, R. Management of stress fields around singular points in a finite element analysis. *Comput. Methods Biomech. Biomed. Eng.* **2001**, *3*, 57–62.
37. Chen, G.; Pettet, G.; Pearcy, M.; McElwain, D. Comparison of two numerical approaches for bone remodelling. *Med. Eng. Phys.* **2007**, *29*, 134–139. [CrossRef] [PubMed]
38. Versluis, A.; Kim, H.C.; Lee, W.; Kim, B.M.; Lee, C.J. Flexural Stiffness and Stresses in Nickel-Titanium Rotary Files for Various Pitch and Cross-sectional Geometries. *J. Endod.* **2012**, *38*, 1399–1403. [CrossRef] [PubMed]
39. Arbab-Chirani, R.; Chevalier, V.; Arbab-Chirani, S.; Calloch, S. Comparative analysis of torsional and bending behavior through finite-element models of 5 Ni-Ti endodontic instruments. *Oral Surg. Oral Med. Oral Pathol. Oral Radiol. Endodontol.* **2011**, *111*, 115–121. [CrossRef] [PubMed]
40. Baek, S.H.; Lee, C.J.; Versluis, A.; Kim, B.M.; Lee, W.; Kim, H.C. Comparison of torsional stiffness of nickel-titanium rotary files with different geometric characteristics. *J. Endod.* **2011**, *37*, 1283–1286. [CrossRef] [PubMed]
41. Hamdy, T.M.; Galal, M.; Ismail, A.G.; Abdelraouf, R.M. Evaluation of Flexibility, Microstructure and Elemental Analysis of Some Contemporary Nickel-Titanium Rotary Instruments. *Open Access Maced. J. Med Sci.* **2019**, *7*, 3647–3654. [CrossRef]
42. Omar, N.; Ismail, A.; Galal, M.; Zaazou, M.H.; Mohamed, M.D.A. A comparative finite analysis of the mechanical behavior of ProTaper NEXT and WaveOne rotary files. *Bull. Natl. Res. Cent.* **2019**, *43*, 1–6. [CrossRef]
43. Galal, M.; Hamdy, T.M. Evaluation of stress distribution in nickel-titanium rotary instruments with different geometrical designs subjected to bending and torsional load: A finite element study. *Bull. Natl. Res. Cent.* **2020**, *44*, 1–11. [CrossRef]
44. Tsao, C.; Liou, J.; Wen, P.; Peng, C.; Liu, T. Study on bending behaviour of nickel-titanium rotary endodontic instruments by analytical and numerical analyses. *Int. Endod. J.* **2013**, *46*, 379–388. [CrossRef] [PubMed]

Journal of
Clinical Medicine

MDPI

Article

Fatigue Analysis of NiTi Rotary Endodontic Files through Finite Element Simulation: Effect of Root Canal Geometry on Fatigue Life

Victor Roda-Casanova [1], Antonio Pérez-González [1], Álvaro Zubizarreta-Macho [2,3,*] and Vicente Faus-Matoses [4]

1 Department of Mechanical Engineering and Construction, Universitat Jaume I, 12071 Castelló de la Plana, Spain; vroda@uji.es (V.R.-C.); aperez@uji.es (A.P.-G.)
2 Department of Dentistry, Alfonso X el Sabio University, 28691 Madrid, Spain
3 Department of Orthodontics, University of Salamanca, 37008 Salamanca, Spain
4 Department of Stomatology, Faculty of Medicine and Dentistry, University of Valencia, 46010 Valencia, Spain; vicente.faus@uv.es
* Correspondence: amacho@uax.es

Abstract: This article describes a numerical procedure for estimating the fatigue life of NiTi endodontic rotary files. An enhanced finite element model reproducing the interaction of the endodontic file rotating inside the root canal was developed, which includes important phenomena that allowed increasing the degree of realism of the simulation. A method based on the critical plane approach was proposed for extracting significant strain results from finite element analysis, which were used in combination with the Coffin–Manson relation to predict the fatigue life of the NiTi rotary files. The proposed procedure is illustrated with several numerical examples in which different combinations of endodontic rotary files and root canal geometries were investigated. By using these analyses, the effect of the radius of curvature and the angle of curvature of the root canal on the fatigue life of the rotary files was analysed. The results confirm the significant influence of the root canal geometry on the fatigue life of the NiTi rotary files and reveal the higher importance of the radius of curvature with respect to the angle of curvature of the root canal.

Keywords: endodontic rotary files; finite element analysis; fatigue analysis

Citation: Roda-Casanova, V.; Pérez-González, A.; Zubizarreta-Macho, A.; Faus-Matoses, V. Fatigue Analysis of NiTi Rotary Endodontic Files through Finite Element Simulation: Effect of Root Canal Geometry on Fatigue Life. *J. Clin. Med.* **2021**, *10*, 5692. https://doi.org/10.3390/jcm10235692

Academic Editors: Massimo Amato, Giuseppe Pantaleo and Alfredo Iandolo

Received: 5 November 2021
Accepted: 29 November 2021
Published: 3 December 2021

1. Introduction

The use of nickel-titanium (NiTi) rotary files for shaping root canals has spread in endodontics during the last decades, in detriment of manual preparation with traditional stainless-steel instruments. The superelasticity of NiTi and its lower Young's modulus reduce the risk of canal transportation and ledging in the treatment of curved root canals [1]. The superelasticity of the NiTi refers to the capacity of the material for undergoing large elastic deformations that can be restored after the forces producing the deformation are released. During these large deformations of the superelastic material, a phase transformation is induced within the material from austenite to martensite at a nearly constant stress. Due to this superelastic behaviour, files made of NiTi can adapt easily to strongly curved root canals. Successive modifications introduced during the last two decades in these instruments have allowed improving the quality of the cleaning and shaping, as well as saving time for both clinicians and patients [2–4]. However, the main problem that persists is the fracture of the files inside the root canal [5].

Fracture of rotary instruments occurs mainly by two different mechanisms, usually referred to as torsion overload and flexural fatigue [6,7]. A torsion overload mechanism corresponds to a static failure and occurs when a section of the file is locked within the canal, and the shank continues to rotate. In this static failure, the file fails because the stress value reaches the elastic limit of the material, and the file undergoes permanent

deformations and finally it fractures. Flexural fatigue is a failure mechanism produced mainly by the alternating compressive and tensile stresses and strains that appear in any point of a file rotating inside a curved root canal. This fatigue failure results in a sudden fracture of the file after a certain number of rotations, even if the stress levels are far below the elastic limit of the material due to the nucleation and progression of small cracks in some stressed sections of the file. The typical number of cycles to failure (NCF) is between some hundreds to several thousands [8]. This is equivalent to an expected life below some few minutes if a typical speed of rotation of 300 rpm is considered.

There is no definitive conclusion about which is the predominant mechanism of failure in the clinical practice [6]. Satappan et al. [9] indicated a higher prevalence of torsional fracture (55.7%) than flexural fatigue (44.3%). However, Peng et al. [10] and Wei et al. [11] observed the opposite, with a clear preponderance of flexural fatigue. Notwithstanding, flexural fatigue seems to be the main concern for clinicians, because there is no easy method to avoid or anticipate this failure [7], resulting in a common practice of discarding the files after a certain number of uses to prevent it. However, there is no clear rule about the recommended number of uses, mainly due to the variety of factors potentially affecting NCF, such as root canal anatomy, file geometry or the operator's experience, among others [12]. Therefore, a better understanding of the independent and combined effect of the different parameters on the flexural fatigue failure mechanism is desirable and additional research should be addressed to this end.

Experimental and simulated approaches have been used in the literature to analyse the effect of clinical and design parameters on the expected life of NiTi rotary files. Experimental approach has been mainly tackled by using in vitro studies in order to improve reproducibility. In general, those studies make the file rotate inside a curved path, reproducing the root canal geometry and registering NCF [6]. However, the differences among previous studies in the methodology and the setup used to bend the file hamper the comparability of results and limit their clinical relevance [6,12]. Due to this, a call for an international standard on the cyclic fatigue testing of rotary endodontic instruments is recurrent in the literature [6,13]. Despite these difficulties, the results from previous experimental studies on experimental fatigue tests on NiTi wires, or directly on endodontic files, have allowed drawing some conclusions about the fatigue behaviour of NiTi:

- The strain–life relationship is similar to that observed in low-cycle fatigue for metals, with a decrease in NCF for higher strain amplitudes, corresponding to highly curved canals [14].
- The fatigue life increases for files with a higher fraction of martensite, both by initial composition of the material or induced by phase transformation under deformation [15,16].
- The oral temperature and other parameters affecting the file temperature, such as rotational speed, can change the expected life, because they influence the phase fractions present in different points of the file in clinical use [17–19].
- Apart from the 'structural fatigue' resulting in the final fracture, NiTi exhibits 'functional fatigue', a significant and asymptotic change in the stress–strain curve and the phase transformation stresses during the first 100–140 cycles, resulting in a reduction in hysteresis cycle area and an increase in residual permanent strains after cycling [20].

These previous experimental studies have shown that, under constant value for other parameters, strain amplitude and NCF for NiTi wires are correlated, and this correlation can be adequately represented by the Coffin–Manson relation [14,16,20].

The simulated approach for analysing flexural fatigue has been mainly undertaken through the use of finite element (FE) models. FE analysis is a mathematical technique that can be used for predicting the state of stress and strain in a body or group of bodies under applied external loads and constraints. It is based on a fine discretisation of the geometry of bodies in a high number of small finite elements. This method allows gaining some insight into the stress and strain distributions inside the file, helping gain a better understanding of the failure mechanism. A recent study made a critical review of the use of this method applied to NiTi endodontic instruments [21] and highlighted some of the main limitations

of the analyses performed to date. According to this study, very few studies modelled cyclic fatigue using FE simulation. The authors cited those of Lee et al. [8], Scattina et al. [7] and Ha et al. [22].

In [8] the authors performed a simulation of four different file models on three root canal geometries with different curvature and compared the results with those obtained from in vitro tests on equivalent systems. In the FE model, the file was rotated inside the simulated FE model of the root canal, and the maximum von Mises stress on the file nodes was analysed. They found that the location of the maximum von Mises stress in the FE model is a good predictor of the fractured section observed experimentally. Additionally, they confirmed a negative correlation between the maximum von Mises stress in the file and the NCF. The authors cited computational problems that forced them to reduce the rotational speed to 240 rpm and to consider a friction coefficient of 0.01 in order to avoid nodal binding. The non-linear behaviour of the material was considered by using data from [23], which did not include the lower plateau in the stress–strain curve characteristic of the phase transformation for the unloading path, which corresponds to a lower stress level than that observed for the loading phase.

Scattina et al. [7] tried to predict NCF using FE simulations. They compared in vitro tests and FE simulations for three file models on a single root canal geometry. The model considered the contact between the file and the root canal, represented with rigid shell elements, and the simulation included the rotation of the file and the analysis of the stress state every 0.2 s during 2 s at a rotation speed of 300 rpm. The authors used a multiaxial random fatigue criterion [24] to predict the NCF based on the stress history. They tuned the material properties with an optimisation procedure to match NCF predictions with experimental results on two of the file models and used these properties to predict NCF for the third model, finding a good agreement with experiments in both NCF and fracture location. However, the paper neither cited the final material parameters obtained from this optimisation nor the specific parameters considered.

In [22], the authors used FE simulation to develop a new file model intermediate between G-1 and G-2 models (Dentsply Maillefer, Ballaigues, Switzerland), but in this case the FE model did not include a fatigue simulation.

Cheung et al. [25] also performed an FE based fatigue analysis for comparing two different cross section geometries for the file, NiTi and steel based on a fully reversed bending analysis without including the root canal in the model. They applied the Coffin–Manson equation for predicting NCF.

The objective of the present study is to contribute to a better understanding of the effect of root canal geometry on the expected life of NiTi rotary files using FE simulation. To our knowledge, only Lee et al. [8] attempted a similar study, but they only considered three canal geometries with a different curvature, without changing the length of the straight part at the entrance of the root canal. Moreover, they based their analysis on the von Mises stress instead of analysing strain, which is the relevant parameter for predicting the fatigue life for low-cycle fatigue, according to the Coffin–Manson relation [25]. They also used a constitutive material model that did not include the hysteresis cycle formed in the stress–strain cycle due to the different stress levels corresponding to the phase transformation during loading and unloading.

In the present study, we used transient FE simulation for analysing the fatigue behaviour of a NiTi endodontic file with two different pitch values on a greater variety of root canal geometries, with changes in both the angle between the initial part and the apical part of the root and the radius of curvature in the connection between both sections. The model also includes a more comprehensive constitutive model for NiTi material and a very detailed discretisation of the file into quadratic finite elements. It simulates the introduction of the file into the canal and its rotation, including contact and friction. With this model, we calculated the strain range during a cycle for each point of the file. We used the Coffin–Manson relation to predict the expected NCF of the file in each root canal geometry.

2. Materials and Methods

The present investigation was conducted by using finite element analysis of a set of cases of study in which several combinations of endodontic rotary files and root canal geometries were studied.

Two different geometries of endodontic rotary file were considered, which are denoted as P2 (Figure 1a) and P3 (Figure 1b). Both of them have a convex ProTaper cross section shown in Figure 1c, their total length being $L_{total} = 25$ mm, the length of their active part is $L_{ap} = 16$ mm and the diameter of their shaft and their tip is $d_{sh} = 1.20$ mm and $d_{ap} = 0.25$ mm, respectively. The only difference between P2 and P3 resides in their axial pitch: $p_z = 2$ mm for P2 and $p_z = 3$ mm for P3.

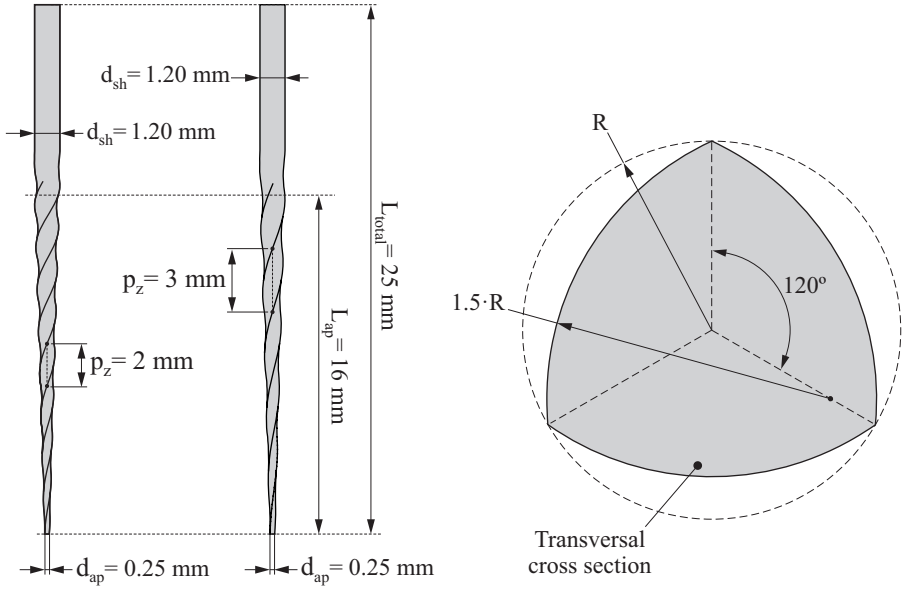

Figure 1. Geometry of the endodontic files P2 (**a**) and P3 (**b**) and normalised transversal cross section for both of them (**c**).

On the other hand, the geometry of the root canal was constructed as follows (Figure 2):

1. Segment AB has a length of $AB_{RC} = 10$ mm, and it is perpendicular to the external surface, as indicated in Figure 2a. Line L_1 passes through point B, and it is inclined at angle θ_{RC} with respect to segment AB.
2. A fillet, for which its radius is given by r_{RC}, is defined between segment AB and line L_1, as illustrated in Figure 2b. The tangency points of the fillet with the existing segments are denoted by D and E.
3. Point F is located over line L_1 in such a manner that the total length from point A to point F is $L_{RC} = 16$ mm. By performing this, the entire active part of the endodontic rotary files can be inserted within the canal. The resulting curve ADEF is the neutral axis of the root canal.
4. Finally, a conic surface is created by sweeping a circumference along the neutral axis of the root canal, as illustrated in Figure 2c. At the entrance of the canal, the diameter of this circumference is $D_{RC} = 1.26$ mm, and at the end of the canal it is $d_{RC} = 0.26$ mm.

The resulting geometry of the root canal depends on two parameters: the angle of curvature θ_{RC} and the radius of curvature r_{RC}, according to the method proposed by Pruett [26]. The variation of these parameters allows us to consider different geometries for the root canal. In this study, three different values for the angle of curvature $\theta_{RC} = [30^\circ, 45^\circ, 60^\circ]$ and three different radii of curvature $r_{RC} = [5\text{ mm}, 10\text{ mm}, 15\text{ mm}]$

were considered. Combining these variables, 9 different geometries of the root canal were obtained, which are shown in Figure 3 (denoted as RC1, RC2, ..., RC9).

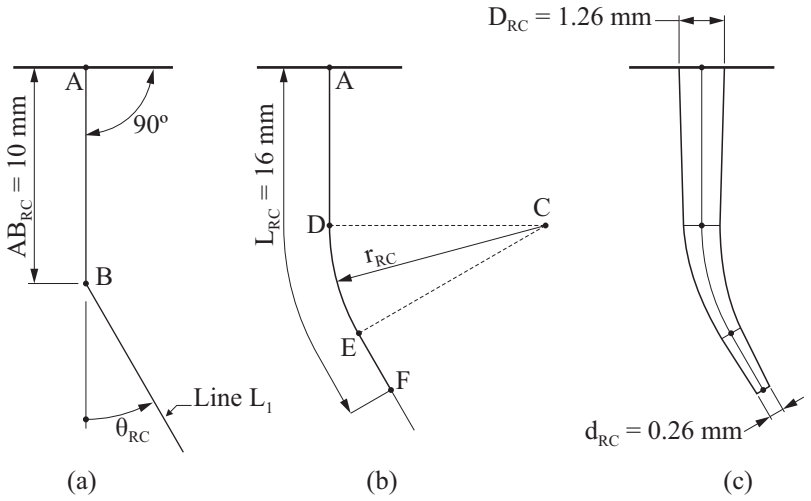

Figure 2. Parametrisation of the geometry of the root canal: (**a**) definition of the segment AB_{RC} and line L_1, (**b**) definition of the fillet and (**c**) definition of the root canal surface.

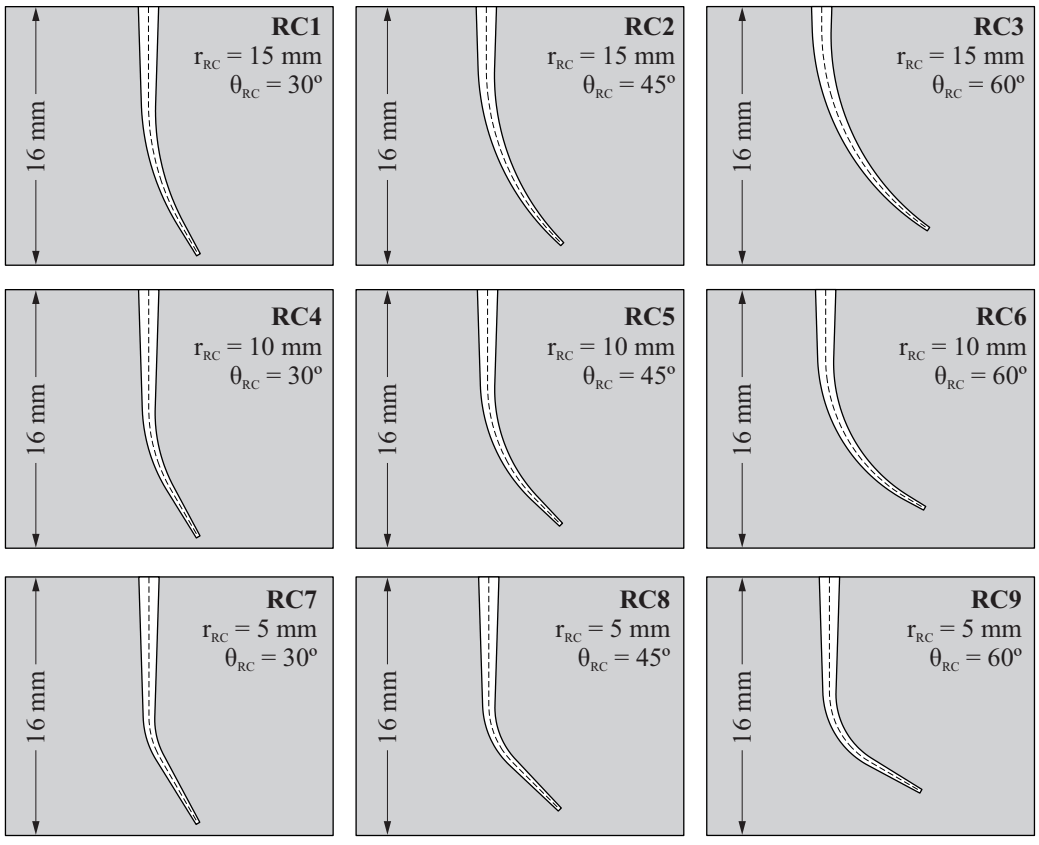

Figure 3. Geometries of root canal considered for the study.

2.1. Definition of the Finite Element Model

Figure 4 shows the finite element model used in this study, which consists of an endodontic rotary file and a root canal. The root canal is modelled as a rigid surface under the assumption that its deformations are so small compared to the deformations of the endodontic rotary file that they can be neglected. The root canal remains immovable during the analysis.

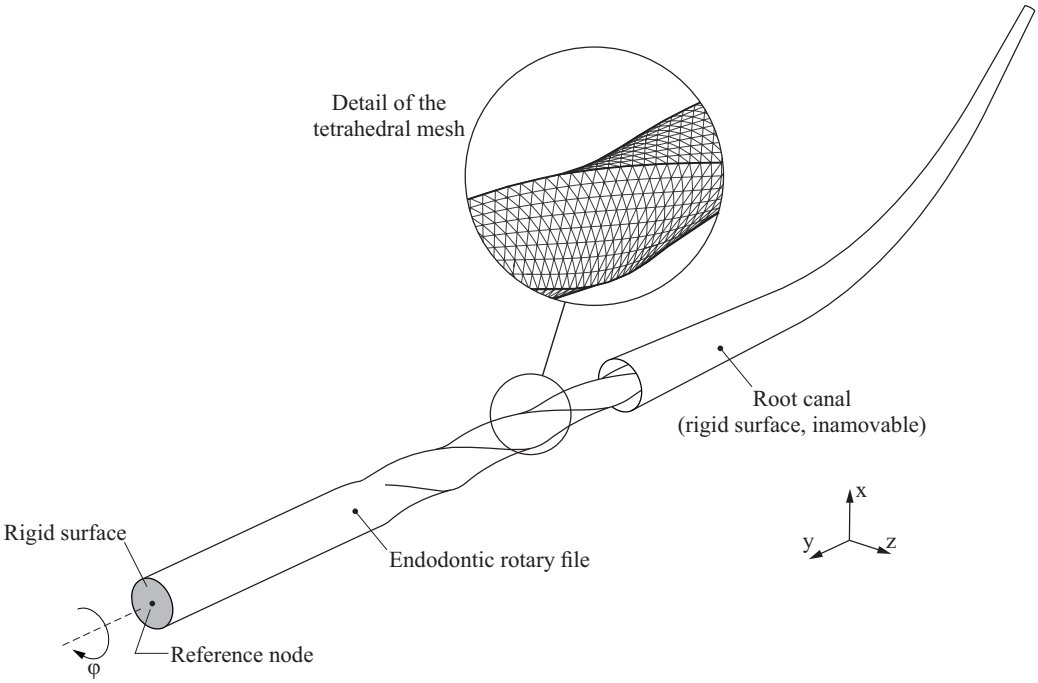

Figure 4. Definition of the finite element model.

The geometry of the endodontic file is generated and then discretised into quadratic finite element tetrahedrons following the ideas provided in [27]. The average element size has been set to 0.1 mm, which has proven to provide a good compromise between accuracy and computational cost. The resulting finite element model has 103,609 nodes and 68,367 elements.

The top surface of the endodontic rotary file is defined as a rigid surface (shaded in grey in Figure 4), and its movements are coupled to the movements of a reference node that is used to define the boundary conditions of the endodontic rotary file.

The superelastic behaviour of the NiTi alloy was modelled by using the material model developed by Auricchio [28], which is summarized in Figure 5. Here, E_A and E_M represent the Young's modulus of austenite and martensite, respectively. The beginning and the end of the loading transformation phase are given by σ_L^S and σ_L^E, respectively, whereas the beginning and the end of the unloading transformation phase are given by σ_U^S and σ_U^E. Finally, ε_L represents the uniaxial transformation strain, and σ_{ME}^E indicates the end of the martensitic elastic regime. In this work, the material properties that characterise this material model were extracted from [29].

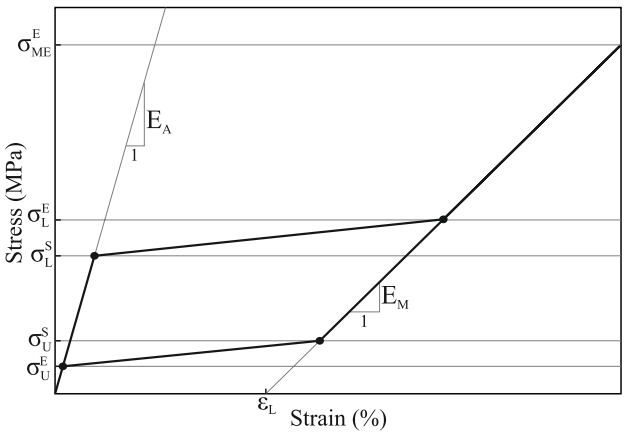

Figure 5. Definition of the stress–strain curve for the constitutive model of the superelastic NiTi alloy.

The mechanical interaction between the root canal and the endodontic rotary file was considered by using a node-to-surface contact. A penalty-based constraint enforcement method was selected in order to enhance the convergency of the numerical solution. The tangential behaviour of the contact was also taken into account in the finite element model, with a constant coefficient of friction $\mu = 0.1$ [30].

The finite element model was solved by using transient analysis, which was conducted by using a large displacement formulation, and performed in two sequential steps:

1. Insertion step: In the first step, the endodontic rotary file is inserted into the root canal. This is performed by prescribing a displacement at its reference node, which takes place along the y axis and has a magnitude equal to the length of the active part of the endodontic rotary file (L_{ap}). The rest of the movements of the reference node (displacements in x and y directions and all the rotations) are restricted in this step.
2. Rotation step: In the second step, after the active part of the endodontic rotary file is inserted in the root canal, the endodontic rotary file performs a complete revolution along its axis of rotation. This is performed by prescribing a 360° rotation along the y axis, while the rest of the movements of the reference node are restricted (rotations along x and z axes and all the displacements). The rotated angle is denoted by φ.

2.2. Fatigue Life Estimation from the Results of the Finite Element Analysis

The objective of this study was to predict the fatigue life of NiTi rotary files as they are rotating inside the root canal. For such a purpose, the strain results obtained from the rotation step of the finite element analysis were used in combination with the Coffin–Manson relation. This relation is conveniently expressed by the following equation:

$$\frac{\Delta\varepsilon}{2} = \varepsilon'_F \cdot N_f^c + \frac{\sigma'_F}{E} \cdot N_f^b \quad (1)$$

where N_f is equivalent to NCF, ε'_F is the fatigue ductility coefficient, σ'_F is the fatigue strength coefficient, c is the fatigue ductility exponent, b is the fatigue strength exponent, $\Delta\varepsilon$ is the total strain range and $\Delta\varepsilon/2$ is the strain amplitude. The prime in the equation indicates that the properties correspond to the cyclic properties, i.e., those after the initial 100–140 cycles.

In this equation, the first addend of the right side corresponds to the plastic strain amplitude $\Delta\varepsilon_p/2$ and the second one to the elastic strain amplitude $\Delta\varepsilon_e/2$. Figure 6 shows a logarithmic plot of the Equation (1), showing the contribution of these two terms, with the parameters for NiTi used in the present study, taken from [25]. The exponents b and c in the equation are negative, because the number of cycles correlates negatively with the strain amplitude. For high strain amplitudes, the plastic strain is much higher than the elastic strain, and the number of cycles to failure is low (low-cycle fatigue, LCF); for very low strain amplitudes, the second term of the equation is dominant because there is no significant plastic strain, and the number of cycles to failure is high (high-cycle fatigue, HCF). The transition between LCF and HCF can be observed as a change in the slope of the curve, which is typically located close to 10^3–10^4 cycles.

Since the Coffin–Manson relation is based on a uniaxial strain, a criterion to reduce the obtained multiaxial strain state to an equivalent uniaxial strain condition is required. The critical plane concept has been extensively used for such a purpose, with successful results both for high and low cycle fatigue [31]. In the critical plane approach, the assessment of the fatigue failure is carried out in the material plane where the amplitude of some stress/strain components (or a combination of them) exhibits a maximum [24]. In the discretised finite element model of the endodontic rotary file, each node i on the surface will have an associated critical plane Π_i characterised by its normal direction $\vec{n}_i$.

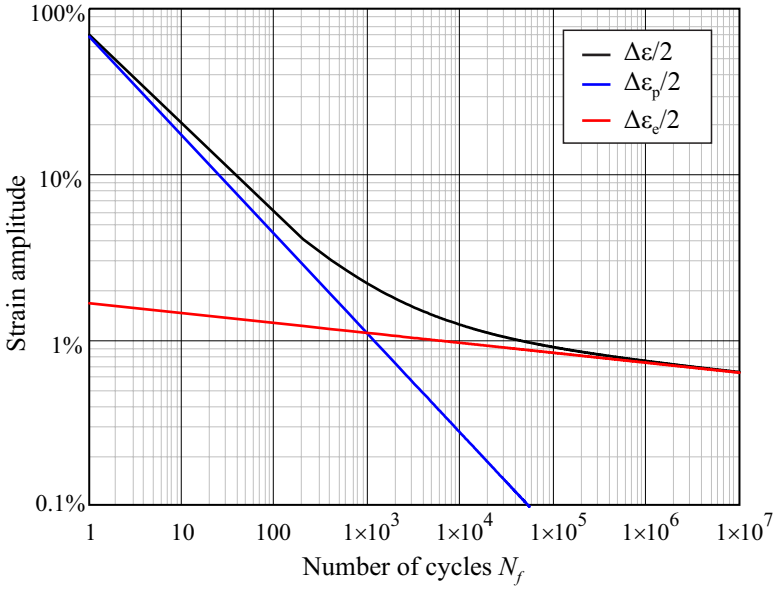

Figure 6. Coffin–Manson relation between strain amplitude and number of cycles to failure (NCF). Parameters for NiTi from [25]: $\varepsilon'_F = 0.68$, $\sigma'_F = 705$ MPa, $E = 42.5$ GPa, $c = -0.6$, $b = -0.06$.

In this study, the critical plane Π_i was defined in such a manner that its normal direction $\vec{n}_i$ is parallel to the direction of the maximum principal strain produced in node i, when the amplitude of this maximum principal strain reaches its maximum value. The direction $\vec{n}_i$ could be determined by observing the maximum principal strain at each frame of the analysis. However, in order to speed up the calculations, in this study it will be assumed that this maximum principal strain is normal to the plane that contains the trajectory of the observed node, as illustrated in Figure 7. Hence, $\vec{n}_i$ will be normal to the plane of rotation of node i.

After the critical plane Π_i is determined for node i, a bending strain value $\varepsilon_{i,j}$ can be then obtained for that node at each analysis frame j by transforming the strain tensor and selecting the strain component in the direction of $\vec{n}_i$. Finally, the total strain range $\Delta\varepsilon_i$ for node i is defined as follows.

$$\Delta\varepsilon_i = \max_{j=1\ldots n}(\varepsilon_{i,j}) - \min_{j=1\ldots n}(\varepsilon_{i,j}) \tag{2}$$

This total strain range $\Delta\varepsilon_i$ can be used in the Coffin–Manson relation to assess the fatigue life associated to node i. The material parameters considered for the application of the Coffin–Manson relation were extracted from [25].

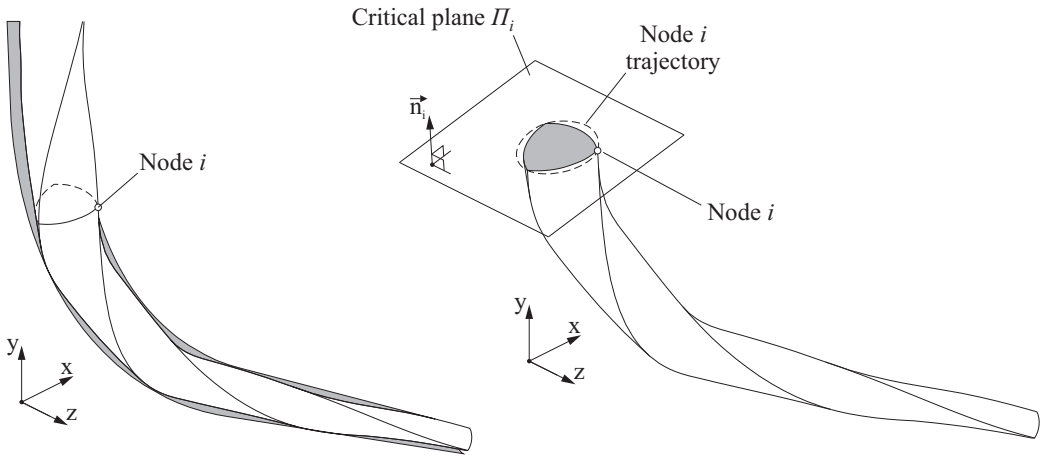

Figure 7. Determination of the critical plane and bending strain for node i.

The fatigue life of the endodontic rotary file was defined by the minimum value of fatigue life considering all the nodes in the surface of the endodontic rotary file. The node where $\Delta\varepsilon_i$ reaches a maximum value is the critical node, and it is denoted as $i = crit$.

3. Results

Figure 8 shows the strain results for endodontic rotary files P2 and P3 when they are rotating inside the most curved root canal RC9. Figure 8a shows the maximum principal strain plot for the case of study P2/RC9 in the instant of the rotation step of the analysis where the bending strain at the critical node reaches its maximum value. Figure 8b shows the minimum principal strain plot, for the same case of study, in the instant of the rotation step of the analysis where the bending strain at the critical node reaches its minimum value. The figure also shows the location of the critical node in both instants of time, as well as the critical plane for such a node. Figure 8c,d show the equivalent results for case P3/RC9 in which the file has a different pitch. The highest strains, both in tension and compression, are located at the edge in the surface of the file.

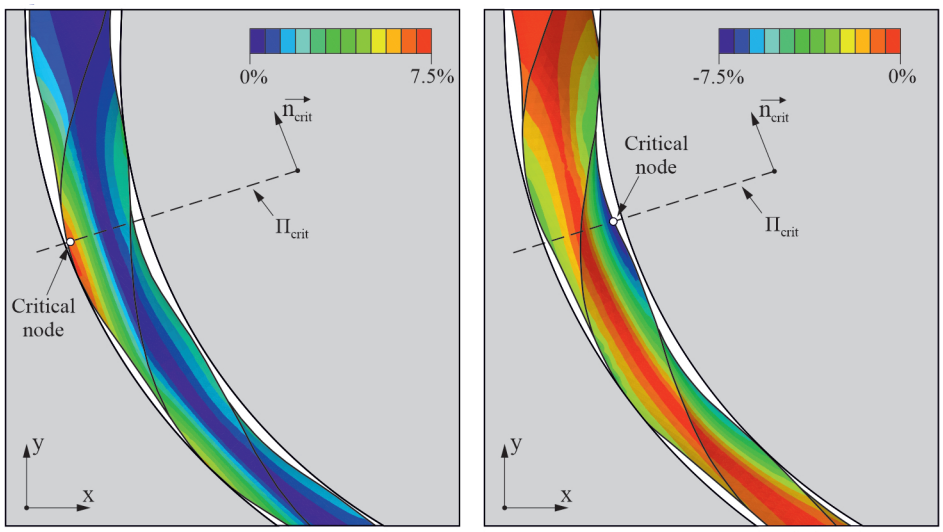

(a) P2/RC9 - Max. principal strain - φ=3.6º (b) P2/RC9 - Min. principal strain - φ=201.6º

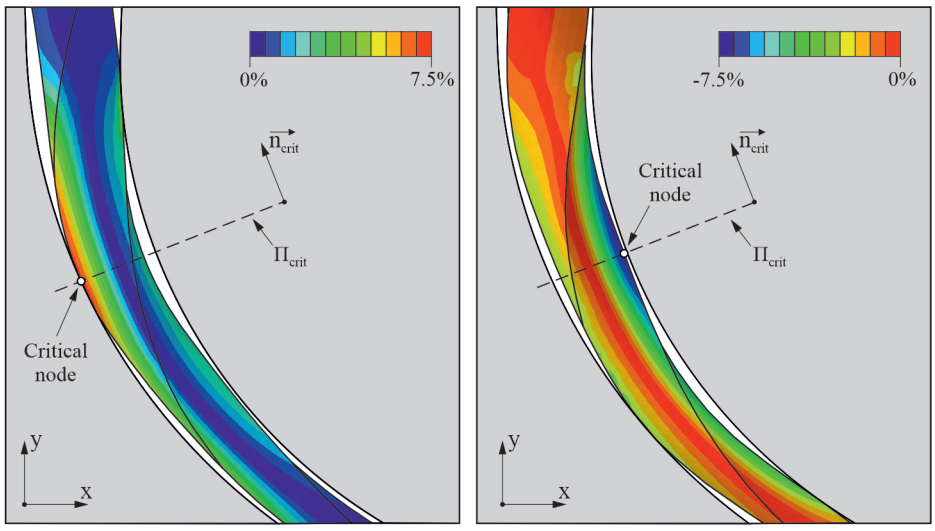

(c) P3/RC9 - Max. principal strain - φ=269.4º (d) P3/RC9 - Min. principal strain - φ=93.4º

Figure 8. Principal strains in two different analysis frames for cases of study P2/RC9 and P3/RC9.

The evolution of the bending strain and the maximum and minimum principal strains during an entire rotation of the file are shown in Figure 9 for P2/RC9 and P3/RC9, reflecting

a similar pattern for both files, but with a slightly higher strain range for the file with pitch 3 mm. The phase shift is due to a different orientation of the edges of the file in the critical plane. The points marked with a star correspond to the frames of maximum and minimum bending strain values, shown in Figure 8.

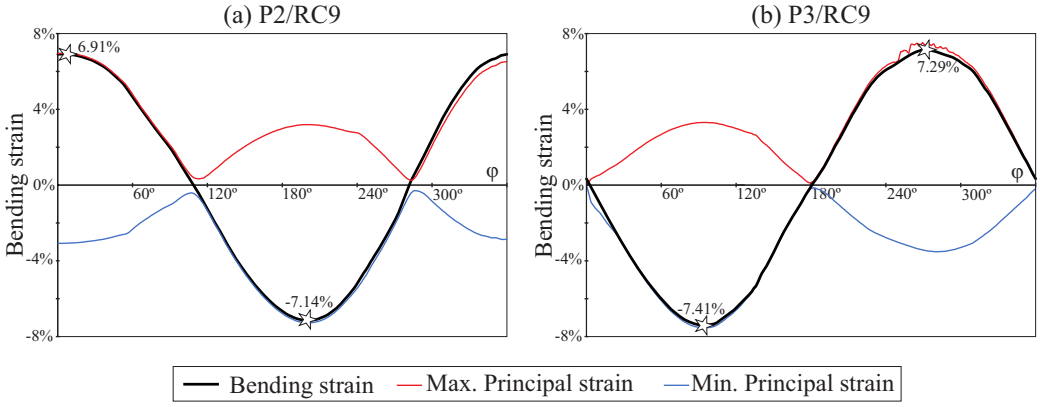

Figure 9. Strain history at critical nodes of cases of study P2/RC9 (**a**) and P3/RC9 (**b**).

The strain ranges obtained for all the studied cases are summarised in Figure 10. In these plots, the horizontal axis indicates the angle of curvature of the root canal and the vertical axis indicates the radius of curvature. The black dots indicate the combinations of radius and angle of curvature that have been studied, and the isolines are interpolated from these results.

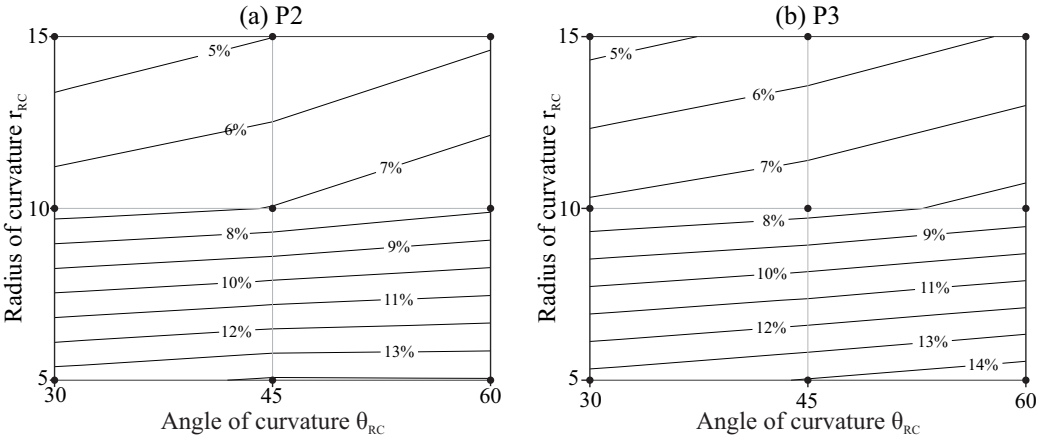

Figure 10. Maximum bending strain range as a function of the geometry of the root canal.

Figure 11 shows the expected life for each file as a function of the radius and the angle of curvature of the root canal, calculated as indicated in Section 2.2, also with interpolated isolines.

The results in Figures 10 and 11 indicate that root canals with higher curvatures (higher angles of curvature or/and smaller radii of curvature) force the files to a higher strain range and reduce their fatigue life. The effect of the angle of curvature is less significant for smaller radii of curvature, as indicated by the lower inclination of the isolines in the bottom of the figures. The file with pitch 3 mm (P3) showed higher strain and shorter fatigue life as compared with that of pitch 2 mm (P2), but this effect is slight, especially for less curved canals.

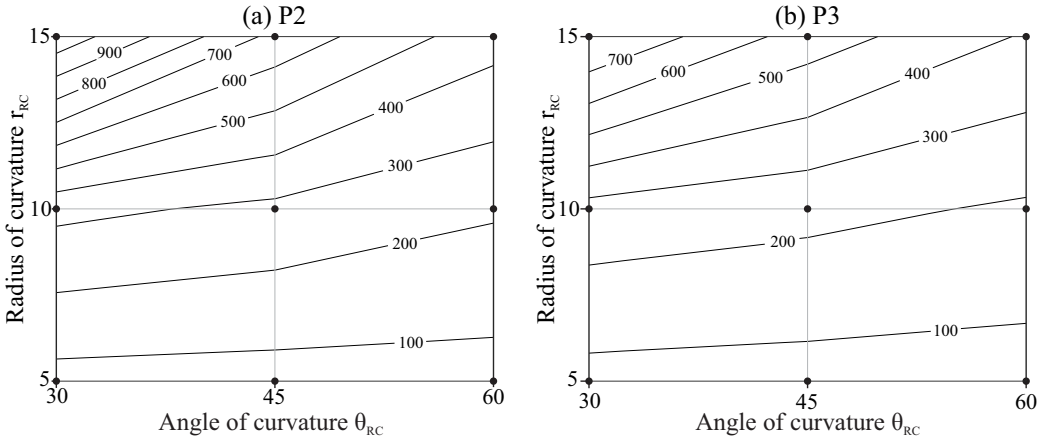

Figure 11. Expected life in number of fatigue cycles N_f as a function of the geometry of the root canal. (**a**) P2 and (**b**) P3.

Finally, Figure 12 summarizes the effect of the degree of insertion of the endodontic rotary file inside the root canal for the case of study P2/RC9. Here, the degree of insertion of the rotary file inside the root canal is expressed as the percentage of the active part that is inserted. Figure 12a shows the evolution of the bending strain at the critical node during a entire revolution of the file for different degrees of insertion of the file inside the root canal (70%, 85% and 100%).

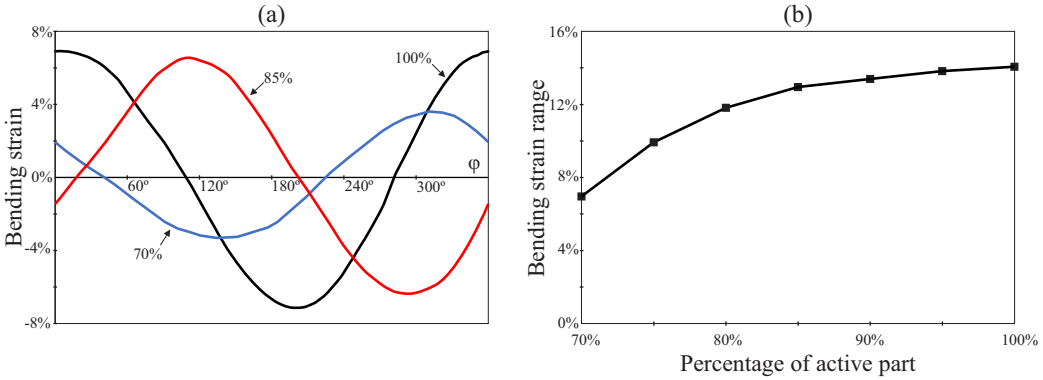

Figure 12. Effect of the degree of insertion of the endodontic file within the root canal. (**a**) Bending strain history at critical nodes and (**b**) bending strain range as a function of the degree of insertion.

Figure 12b shows the evolution of the bending strain range with the degree of insertion of the endodontic rotary file inside the root canal. Here, additional data points are considered for a better observation of the evolution of this magnitude. This figure shows that the bending strain range is reduced as the degree of insertion of the endodontic rotary file inside the root canal is decreased.

4. Discussion

This study analysed numerically the effect of the root canal geometry on the bending fatigue life of NiTi rotary instruments. Some previous studies have shown the predictive capacity of this simulated approach based on the use of FE models to predict the location of the file fracture [7,8]. However, a recent review highlighted some limitations introduced in previous FE studies in this field, especially in the representation of the boundary conditions, the accuracy of the mesh to represent the real file geometry or the lack of consideration of friction in the FE analysis [21]. Our investigation solved these main limitations, with a very accurate mesh of quadratic elements for the file, and undertook a transient non-linear simulation of the introduction of the file inside the root canal and its rotation inside the canal, including contact and friction simulation. We also used the Coffin–Manson relation

to estimate the expected life for the file working on a representative set of root canal geometries, proposing an adequate methodology for translating FE results to clinically relevant variables, which can be useful for manufacturers of NiTi rotary instruments.

Our results confirm that more curved canals are prone to reduce fatigue life, which was also previously observed in several in vitro studies [5,8,14]. We also found that the radius of curvature of the canal has a higher effect than the angle between the shaft and the apical portion of the file, especially for the lower radii of curvature. Changing the radius of curvature from 15 mm to 5 mm multiplies the strain amplitude by a factor of close to three for curvature angles of 30° and by a factor close to 2.5 for curvature angles of 60°. Due to the logarithmic relationship between strain and NCF, this effect is higher in the expected life, which is reduced by a factor close to ten for 30° of curvature angle and by a factor six for 60°. This result is in agreement with the experimental study by Chi et al. [5], although their setup was different because the curved part of the file reached the apical end for all conditions.

In most of the experimental studies, NCF is represented against a theoretical bending strain value obtained from geometrical approximations of the radius of curvature of the file and its diameter at the failure section using Equation (3) [14,16,17]:

$$\varepsilon_a = \frac{d}{2R} \tag{3}$$

where d is the file diameter, and R is the approximate radius of curvature of the file. Thus, the higher effect of the radius of curvature is expected from a theoretical point of view, because the ideal strain amplitude in bending is defined by Equation (3), depending only on the diameter of the file and the radius of curvature. However, the angle between the entrance and the apical portion of the root canal and also the clearance between the file and the canal walls affect the actual deformation of the file, which can be different to that defined by the geometrical approximation indicated by Equation (3), as observed in Figure 8. This would explain the effect observed for the angle of curvature.

The difference in strain amplitude and fatigue life for the files with pitch 2 mm and 3 mm is limited, with a slightly higher fatigue life for P2 and more pronounced for less curved root canals. Ha et al. [30] also observed lower stresses for closer pitch when analysing the screw-in tendency of NiTi rotary files with a transient FE model.

In Figure 12, we also studied the effect that the degree of insertion of the rotary file has on bending strain range. We observed that the bending strain range at the critical node decreases with a reduction in the degree of insertion. According to the Coffin–Manson relation, this increases the fatigue life of the rotary file. This reduction in the bending strain range could be explained because the diameter d of the rotary file at the curved part of the root canal is smaller with partial insertion and, according to Equation (3), this results in a reduction in the bending strain. Additionally, the greater clearance between the rotary file and root canal implies that the effective curvature radius of the file is higher than that of the root canal. Again, according to Equation (3), this implies an additional contribution to the reduction in bending strain range.

In this study, we based the analysis of file behaviour on the strain values observed, as recommended for LCF with significant strain values and fatigue life below some thousands of cycles [25]. We also proposed a method for calculating the strain amplitude during the cyclic rotation of the file, based on the use of a critical plane defining the direction of the maximum and minimum principal strains in the critical points. The results shown in Figure 9 reveal that the method proposed here for defining the critical plane is correct, because when the bending strain reaches its maximum and minimum points, its values coincide with the maximum and minimum principal strains, respectively.

This study has some limitations. We only considered a geometry of the file section, with a constant taper and pitch through its length. We also limited the analysis to root canals for which its geometrical axis can be represented by a planar curve. Moreover, despite our work trying to be as representative as possible of the clinical situation of the

file rotating inside the root canal, some possible improvements remain and are commented in the following paragraphs. They can be observed as challenges for future studies trying to improve the accuracy of the model.

The material model used in this study is non-linear and included the phase transformation plateaus in the stress–strain curve and the different Young's modulus of martensite and austenite. However, heat dissipated due to the hysteresis loop in the loading–unloading curve, and heat generated by sliding friction between the file and the canal can also induce phase transformations from martensite to austenite due to the shape memory effect of the material, adding a complex thermal–mechanical coupling that is not considered here. On the other hand, we have made estimations of the fatigue life based on the Coffin–Manson equation, but the fatigue ductility coefficient and fatigue ductility exponent were taken from the literature. We have not considered the effect of the phase transformations between austenite and martensite on fatigue response and, hence, on these parameters. Previous studies have shown that higher strains did not necessarily imply less cycles to failure, because a higher fraction of martensite results in a better response under cyclic loads [16]. To our knowledge, there is no clear approach for the moment to include this effect in the FE simulations.

In this study, we considered a transient simulation, but this simulation does not include the dynamical effects, which are dependent on the rotational speed of the file. Moreover, our model included normal and shear contact between the file and root canal walls, but these walls are simplified as rigid elements. Considering the dentine properties for the walls would be necessary for estimating the risk of canal transportation or ledging.

We have proposed a method for dealing with the multiaxial strain state in order to predict fatigue life, but the fatigue phenomenon in shape memory alloys is still under investigation [32], and there is no clearly established fatigue criterion for analysing multiaxial fatigue in those materials [7,32].

In addition, since the first introduction of NiTi rotary instruments in the last decade of the twentieth century, several changes have been introduced to new families of files in terms of composition, manufacturing methods and thermomechanical treatments, which is not always publicly known, affecting greatly the percentage of martensite or austenite present in the file in clinical use and also the fatigue life of instruments [15,33].

5. Conclusions

This numerical study confirms that the geometry of the root canal affects the fatigue life of rotary NiTi instruments. More curved root geometries, either by a higher inclination of the apical part of the canal with respect to the initial part at the entrance or by a lower radius of curvature, result in higher strain amplitudes in the file surface and to lower fatigue life. The radius of curvature in the curves of the root canal has a greater effect than the angle of curvature. Changes in the radius of curvature from 15 mm to 5 mm in the root canal can reduce fatigue life by factors close to ten. A change in the file pitch between 2 mm and 3 mm does not have an important effect on the fatigue life for the root canal geometries analysed, although the higher pitch exhibited a slightly lower life for root canals with low curvature. The degree of insertion of the file inside the root canal significantly affects the strain range obtained in the critical point of the file, and the strain range is reduced when the file is partially inserted within the file.

Author Contributions: Conceptualization, A.P.-G. and V.R.-C.; methodology, A.P.-G. and V.R.-C.; software, V.R.-C.; investigation, A.P.-G. and V.R.-C.; resources, Á.Z.-M. and V.F.-M.; writing—original draft preparation, A.P.-G.; writing—review and editing, V.R.-C.; supervision, Á.Z.-M. and V.F.-M.; project administration, Á.Z.-M. and V.F.-M. All authors have read and agreed to the published version of the manuscript.

Funding: This research received no external funding.

Institutional Review Board Statement: Not applicable.

Informed Consent Statement: Not applicable.

Conflicts of Interest: The authors declare no conflicts of interest.

References

1. Bürklein, S.; Schäfer, E. Critical evaluation of root canal transportation by instrumentation. *Endod. Top.* **2013**, *29*, 110–124. [CrossRef]
2. Iandolo, A.; Amato, A.; Martina, S.; Latif, D.A.; Pantaleo, G. Management of severe curvatures in root canal treatment with the new generation of rotating files using a safe and predictable protocol. *Open Dent. J.* **2020**, *14*, 421–425. [CrossRef]
3. Iandolo, A.; Abdellatif, D.; Pantaleo, G.; Sammartino, P.; Amato, A. Conservative shaping combined with three-dimensional cleaning can be a powerful tool: Case series. *J. Conserv. Dent.* **2020**, *23*, 648–652. [CrossRef]
4. Kuzekanani, M. Nickel-titanium rotary instruments: Development of the single-file systems. *J. Int. Soc. Prev. Community Dent.* **2018**, *8*, 386–390. [CrossRef]
5. Chi, C.W.; Li, C.C.; Lin, C.P.; Shin, C.S. Cyclic fatigue behavior of nickel–titanium dental rotary files in clinical simulated root canals. *J. Formos. Med. Assoc.* **2017**, *116*, 306–312. [CrossRef] [PubMed]
6. Plotino, G.; Grande, N.M.; Cordaro, M.; Testarelli, L.; Gambarini, G. A Review of Cyclic Fatigue Testing of Nickel-Titanium Rotary Instruments. *J. Endod.* **2009**, *35*, 1469–1476. [CrossRef]
7. Scattina, A.; Alovisi, M.; Paolino, D.S.; Pasqualini, D.; Scotti, N.; Chiandussi, G.; Berutti, E. Prediction of cyclic fatigue life of nickel-titanium rotary files by virtual modeling and finite elements analysis. *J. Endod.* **2015**, *41*, 1867–1870. [CrossRef]
8. Lee, M.H.; Versluis, A.; Kim, B.M.; Lee, C.J.; Hur, B.; Kim, H.C. Correlation between experimental cyclic fatigue resistance and numerical stress analysis for nickel-titanium rotary files. *J. Endod.* **2011**, *37*, 1152–1157. [CrossRef] [PubMed]
9. Sattapan, B.; Nervo, G.J.; Palamara, J.E.; Messer, H.H. Defects in rotary nickel-titanium files after clinical use. *J. Endod.* **2000**, *26*, 161–165. [CrossRef] [PubMed]
10. Peng, B.; Shen, Y.; Cheung, G.S.; Xia, T.J. Defects in ProTaper S1 instruments after clinical use: Longitudinal examination. *Int. Endod. J.* **2005**, *38*, 550–557. [CrossRef] [PubMed]
11. Wei, X.; Ling, J.; Jiang, J.; Huang, X.; Liu, L. Modes of Failure of ProTaper Nickel-Titanium Rotary Instruments after Clinical Use. *J. Endod.* **2007**, *33*, 276–279. [CrossRef]
12. McGuigan, M.B.; Louca, C.; Duncan, H.F. Endodontic instrument fracture: Causes and prevention. *Br. Dent. J.* **2013**, *214*, 341–348. [CrossRef] [PubMed]
13. Lo Savio, F.; Rosa, G.L.; Bonfanti, M.; Alizzio, D.; Rapisarda, E.; Pedullà, E. Novel Cyclic Fatigue Testing Machine for Endodontic Files. *Exp. Tech.* **2020**, *44*, 649–665. [CrossRef]
14. Cheung, G.S.; Darvell, B.W. Fatigue testing of a NiTi rotary instrument. Part 1: Strain-life relationship. *Int. Endod. J.* **2007**, *40*, 612–618. [CrossRef]
15. Tabassum, S.; Zafar, K.; Umer, F. Nickel-titanium rotary file systems: What's new? *Eur. Endod. J.* **2019**, *4*, 111–117. [CrossRef]
16. Figueiredo, A.M.; Modenesi, P.; Buono, V. Low-cycle fatigue life of superelastic NiTi wires. *Int. J. Fatigue* **2009**, *31*, 751–758. [CrossRef]
17. Eggeler, G.; Hornbogen, E.; Yawny, A.; Heckmann, A.; Wagner, M. Structural and functional fatigue of NiTi shape memory alloys. *Mater. Sci. Eng. A* **2004**, *378*, 24–33. [CrossRef]
18. Vilaverde Correia, S.; Nogueira, M.T.; Silva, R.J.C.; Pires Lopes, L.; Braz Fernandes, F.M. Phase Transformations in NiTi Endodontic Files and Fatigue Resistance. In *European Symposium on Martensitic Transformations*; EDP Sciences: Les Ulis, France, 2009; p. 07004. [CrossRef]
19. Dornelas Silva, J.; Lopes Buono, V.T. Effect of the initial phase constitution in the low-cycle fatigue of NiTi wires. *SN Appl. Sci.* **2019**, *1*, 1591. [CrossRef]
20. Maletta, C.; Sgambitterra, E.; Furgiuele, F.; Casati, R.; Tuissi, A. Fatigue properties of a pseudoelastic NiTi alloy: Strain ratcheting and hysteresis under cyclic tensile loading. *Int. J. Fatigue* **2014**, *66*, 78–85. [CrossRef]
21. Chien, P.Y.; Walsh, L.J.; Peters, O.A. Finite element analysis of rotary nickel-titanium endodontic instruments: A critical review of the methodology. *Eur. J. Oral Sci.* **2021**, *129*, e12802. [CrossRef]
22. Ha, J.H.; Lee, C.J.; Kwak, S.W.; El Abed, R.; Ha, D.; Kim, H.C. Geometric optimization for development of glide path preparation nickel-titanium rotary instrument. *J. Endod.* **2015**, *41*, 916–919. [CrossRef] [PubMed]
23. Xu, X.; Eng, M.; Zheng, Y.; Eng, D. Comparative study of torsional and bending properties for six models of nickel-titanium root canal instruments with different cross-sections. *J. Endod.* **2006**, *32*, 372–375. [CrossRef] [PubMed]
24. Carpinteri, A.; Spagnoli, A.; Vantadori, S.; Bagni, C. Structural integrity assessment of metallic components under multiaxial fatigue: The C-S criterion and its evolution. *Fatigue Fract. Eng. Mater. Struct.* **2013**, *36*, 870–883. [CrossRef]
25. Cheung, G.S.; Zhang, E.W.; Zheng, Y.F. A numerical method for predicting the bending fatigue life of NiTi and stainless steel root canal instruments. *Int. Endod. J.* **2011**, *44*, 357–361. [CrossRef] [PubMed]
26. Pruett, J.P.; Clement, D.J.; Carnes, D.L. Cyclic fatigue testing of nickel-titanium endodontic instruments. *J. Endod.* **1997**, *23*, 77–85. [CrossRef]
27. Roda-Casanova, V.; Zubizarreta-Macho, A.; Sanchez-Marin, F.; Alonso Ezpeleta, O.; Albaladejo Martinez, A.; Galparsoro Catalan, A. Computerized Generation and Finite Element Stress Analysis of Endodontic Rotary Files. *Appl. Sci.* **2021**, *11*, 4329. [CrossRef]
28. Auricchio, F.; Petrini, L. A three-dimensional model describing stress-temperature induced solid phase transformations: Solution algorithm and boundary value problems. *Int. J. Numer. Methods Eng.* **2004**, *61*, 807–836. [CrossRef]

29. de Arruda Santos, L.; López, J.B.; de Las Casas, E.B.; de Azevedo Bahia, M.G.; Buono, V.T.L. Mechanical behavior of three nickel-titanium rotary files: A comparison of numerical simulation with bending and torsion tests. *Mater. Sci. Eng. C* **2014**, *37*, 258–263. [CrossRef]
30. Ha, J.H.; Cheung, G.S.; Versluis, A.; Lee, C.J.; Kwak, S.W.; Kim, H.C. 'Screw-in' tendency of rotary nickel-titanium files due to design geometry. *Int. Endod. J.* **2015**, *48*, 666–672. [CrossRef]
31. Karolczuk, A.; Macha, E. Selection of the critical plane orientation in two-parameter multiaxial fatigue failure criterion under combined bending and torsion. *Eng. Fract. Mech.* **2008**, *75*, 389–403. [CrossRef]
32. Kang, G.; Song, D. Review on structural fatigue of NiTi shape memory alloys: Pure mechanical and thermo-mechanical ones. *Theor. Appl. Mech. Lett.* **2015**, *5*, 245–254. [CrossRef]
33. Gavini, G.; dos Santos, M.; Caldeira, C.L.; Machado, M.E.d.L.; Freire, L.G.; Iglecias, E.F.; Peters, O.A.; Candeiro, G.T.d.M. Nickel-titanium instruments in endodontics: A concise review of the state of the art. *Braz. Oral Res.* **2018**, *32*, e67. [CrossRef] [PubMed]

International Journal of
Environmental Research and Public Health

MDPI

Article

A Novel Digital Technique to Analyze the Wear of CM-Wire NiTi Alloy Endodontic Reciprocating Files: An In Vitro Study

Vicente Faus-Matoses [1], Vicente Faus-Llácer [1], Álvaro Aldeguer Muñoz [1], Jorge Alonso Pérez-Barquero [1], Ignacio Faus-Matoses [1,*], Celia Ruiz-Sánchez [1] and Álvaro Zubizarreta-Macho [2,3]

[1] Department of Stomatology, Faculty of Medicine and Dentistry, University of Valencia, 46010 Valencia, Spain; vicente.faus@uv.es (V.F.-M.); fausvj@uv.es (V.F.-L.); alalmu@alumni.uv.es (Á.A.M.); jorgealonso86@gmail.com (J.A.P.-B.); ceruizsan@gmail.com (C.R.-S.)
[2] Department of Endodontics, Faculty of Health Sciences, Alfonso X El Sabio University, 28691 Madrid, Spain; amacho@uax.es
[3] Department of Surgery, Faculty of Medicine and Dentistry, University of Salamanca, 37008 Salamanca, Spain
* Correspondence: ignacio.faus@uv.es

Abstract: The present study seeks to describe a novel digital measurement technique for analyzing the wear volume of controlled memory (CM)-wire NiTi alloy endodontic reciprocating files after clinical use. Material and Methods: Ten CM-wire NiTi endodontic reciprocating files were randomly used in ten first upper molar teeth within four root canals. The CM-wire NiTi alloy endodontic reciprocating files were subjected to preoperative and postoperative micro-computed tomography (micro-CT) scans to obtain accurate digital imaging and communication on medicine (DICOM) digital files, which were segmented using intensity-based thresholding and an exclusive OR (XOR) logical operation (Boolean algebra logical operator) to obtain a mask of the location to localize and quantify the wear volume of the CM-wire NiTi alloy endodontic reciprocating files. Gage repeatability and reproducibility statistical analysis was applied to assess the reproducibility and repeatability of this measurement technique. Results: The analysis showed a repeatability and reproducibility of 0.00% for the digital measurement technique used to analyze the wear volume of CM-wire NiTi alloy endodontic reciprocating files after clinical use. Wear was mostly identified at the tip and cutting edges of the CM-wire NiTi alloy endodontic reciprocating files. Conclusions: This novel digital measurement technique is a repeatable, reproducible, and accurate method of quantifying the wear volume of CM-wire NiTi alloy endodontic reciprocating files after clinical use.

Keywords: endodontics; cyclic fatigue; wear; NiTi; reciprocating movement; micro-computed tomography

Citation: Faus-Matoses, V.; Faus-Llácer, V.; Aldeguer Muñoz, Á.; Alonso Pérez-Barquero, J.; Faus-Matoses, I.; Ruiz-Sánchez, C.; Zubizarreta-Macho, Á. A Novel Digital Technique to Analyze the Wear of CM-Wire NiTi Alloy Endodontic Reciprocating Files: An In Vitro Study. *Int. J. Environ. Res. Public Health* **2022**, *19*, 3203. https://doi.org/10.3390/ijerph19063203

Academic Editors: Alberto De Biase, Marco Lollobrigida and Luca Lamazza

Received: 5 January 2022
Accepted: 1 March 2022
Published: 9 March 2022

1. Introduction

The removal of bacteria from the root canal system is one of the most significant factors influencing the prognosis of root canal treatment [1]; as a result, techniques for cleaning and shaping procedures are continuously being developed to help reduce bacterial loads within the root canal system with a view to preventing endodontic failure caused by persistent or secondary dental infections [2]. Additionally, novel trends are being developed to promote dentin–pulp formation using polymer-based instructive scaffolds [3,4].

There is also the ongoing development of endodontic rotary files, regarding both the chemical composition of metal alloys and their geometrical design, which improves the mechanical resistance of endodontic rotary files to bending and torsional stress [5]. Other characteristics of the geometrical design of endodontic rotary files that reportedly influence instrument performance include the cross section [6]; the helix angle, flute length, and pitch [7]; and the taper and apical diameter [4]. More specifically, a larger apical diameter and taper are correlated with lower cyclic fatigue resistance in nickel–titanium (NiTi) endodontic rotary files, with the files becoming more liable to fracture unexpectedly [3]. NiTi endodontic rotary files fracture at a rate of between 0.09% and 5% [8,9], with both

flexural (bending) and torsional failure having been identified as the primary factors leading to endodontic rotary file fractures [10,11]. When endodontic files become blocked during movement, this can result in torsional failure [8], and if they rotate within a curved root canal, this can lead to cyclic bending fatigue [12]. The root canal shaping process can potentially apply simultaneous cumulative torsional and bending stress, potentially leading to wear and tear, affecting the structure of NiTi endodontic rotary files and even leading to their fracture. This negatively affects the prognosis of root canal treatment because the fractured piece impedes access to the apex, making it difficult to disinfect the root canal system [13]. Shen et al. found that NiTi endodontic rotary instruments most often fracture in the apical 3–5 mm [14], which indicates that the last millimeters of the files are subjected to more flexural and torsional failure during shaping. Yared proposed a novel root canal preparation technique that employs a non-specific clockwise-cutting rotary file in a reciprocating movement [15] based on the balanced force technique [16]. NiTi endodontic reciprocating files have subsequently been developed with a view to improving and simplifying the shaping of the root canal system. Since these systems were first developed, these single-file NiTi endodontic reciprocating systems have gained popularity in the dental industry. In addition, manufacturers have also developed several thermally treated NiTi alloys with controlled memory wire that optimizes their microstructure and transformation behavior. This, in turn, has more of an impact on the mechanical behavior of NiTi endodontic reciprocating files [17]. However, torsional and bending stress can damage the structure of NiTi endodontic reciprocating files during the shaping process, leading to wear and deformation [18], negatively impacting cutting efficiency and increasing the risk of unexpected fracture [19,20]. Different measurement techniques have been used to assess the wear and deformation of NiTi endodontic files, including scanning electron microscopy (SEM) [13] and stereomicroscopy [18]. However, these measurement techniques cannot accurately analyze the volume of NiTi endodontic rotary files lost after clinical use.

The present study seeks to describe a novel digital measurement technique for analyzing the wear volume of controlled memory (CM)-wire NiTi alloy endodontic reciprocating files after clinical use, with a null hypothesis (H_0) that there is no difference between the morphometric measurement protocols used when it comes to accurately measuring the wear level of CM-wire NiTi alloy endodontic reciprocating files after use.

2. Materials and Methods

2.1. Study Design

Ten CM-wire NiTi alloy endodontic reciprocating files (R40, Reciproc; VDW, Munich, Germany) were randomly (Epidat 4.1, Galicia, Spain) used in ten first upper molar teeth in four root canals extracted for periodontal reasons using Schneider's method. All of the selected teeth had curvature angles of $\leq 20^{\circ}$, [21], a root length of greater than 16 mm, mature roots, and no prior incidence of root canal treatment, root resorption, or calcium metamorphosis. The study was carried out between July 2020 and October 2021 at the Department of Stomatology of the University of Valencia (Valencia, Spain). A randomized, controlled experimental trial was carried out in accordance with the statement of the German Ethics Committee on using organic tissues for medical research. The study was approved by the ethics committee of the University of Valencia (Process No. 12151). All patients provided their informed consented for their teeth to be transferred for use in the study.

2.2. Experimental Procedure

Tooth crowns were removed under the cement–enamel junction to achieve a standardized root length of 16 mm for all teeth. They were then scanned via digital radiography in both the buccolingual and mesiodistal directions to evaluate the root canal system anatomy. The root canal systems were performed using sterile 40.06 CM-wire NiTi alloy endodontic reciprocating files (Reciproc; VDW, Munich, Germany). The files had been analyzed under magnification (SZR-10, Optika, Bergamo, Italy) to rule out any surface defects from the

manufacturing process. Next, the working length was determined by inserting a size 8 K file (Dentsply Maillefer, Baillagues, Switzerland) into the root canal system until it became visible at the apical foramen under the operative microscope at a magnification of 10 × (Zeiss Dental Microscope, Oberkochen, Germany). The root canal systems were carried out with a 6:1 reduction handpiece (Reciproc; VDW, Munich, Germany) using the crown-down technique with a torque-controlled motor with reciprocant motion (Reciproc; VDW, Munich, Germany) for a duration of 73.1 s, according to the study performed by Bürklein et al. [22]. The same clinician performed all root canal treatments.

2.3. Micro-CT Scanning Procedures and Evaluation

The files were subjected to preoperative and postoperative micro-computed tomography (micro-CT) scans (Skyscan 1176, Bruker-MicroCT, Kontich) with the following exposure parameters: 56.0–58.0 microamperes, 160.0 kilovolt peak, 720 projections, 500.0 msec, 4 frames, a 3 µm resolution, a tungsten target between 0.25 and 0.375 mm, and a pixel size of 0.127 µm. These scans provided DICOM digital files of the endodontic files. The first micro-CT scan (Micro-CAT II, Siemens Preclinical Solutions, Knoxville, TN, USA) was taken prior to the root canal treatment (DICOM1) (Figure 1A), and the second micro-CT scan was taken after the root canal treatments had been completed (DICOM2) (Figure 1B).

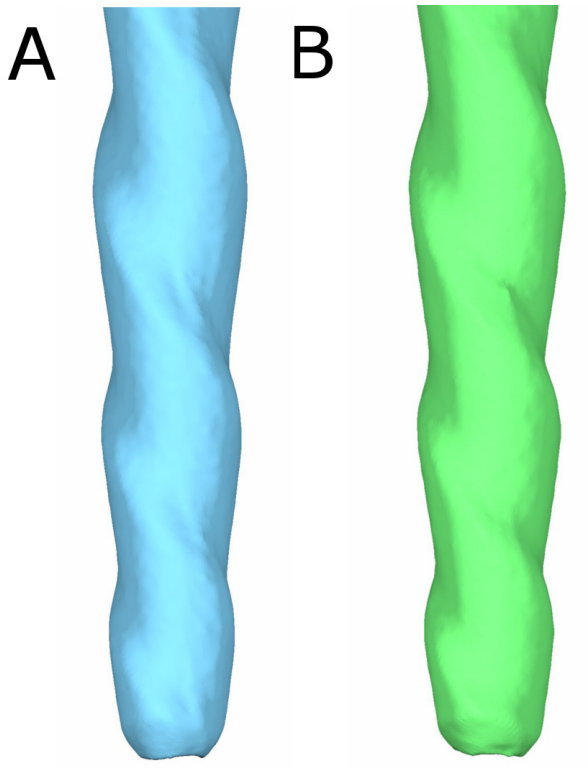

Figure 1. Three-dimensional reconstruction of the (**A**) preoperative and (**B**) postoperative micro-CT scans of a CM-wire NiTi alloy endodontic reciprocating file.

2.4. Alignment Procedure

Once the preoperative (DICOM1) and postoperative (DICOM2) digital files from the micro-CT scans of the endodontic files had been aligned into a common coordinate space by image registration using an in-house MeVisLab network (MeVis Medical Solutions AG), the digital files were further processed using Fiji/ImageJ, an open-source, Java-based image processing software product [23]. The preoperative (DICOM1) and postoperative (DICOM2) digital files were subsequently segmented via intensity-based thresholding. An exclusive OR (XOR) logical operation (Boolean algebra logical operator) was then applied to obtain a mask of the wear location of the endodontic files (Figure 2).

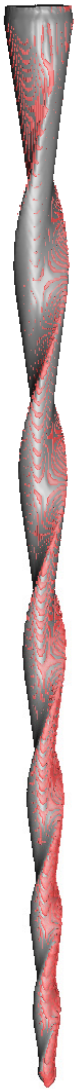

Figure 2. The procedure for alignment between the preoperative (red) and postoperative (grey) digital files and identification of the localization of the CM-wire NiTi alloy endodontic reciprocating files.

2.5. Measurement Procedure

After the alignment procedure, the volume of the resulting masks (mm^3) of the preoperative (DICOM1) and postoperative (DICOM2) digital files from the micro-CT scans of the CM-wire NiTi alloy endodontic reciprocating files was assessed, with the active part segmented to quantify the level of wear caused to the files. Finally, 3D images were rendered using Amira 3D software (Termo Scientific, Waltham, MA, USA) for preclinical analysis. The locations of wear were analyzed between the DICOM1 and DICOM2 digital files (Figure 3A) at 1 mm (Figure 3B), 2 mm (Figure 3C), 3 mm (Figure 3D), 4 mm (Figure 3E), 5 mm (Figure 3F), and 6 mm (Figure 3G) from the tip of the CM-wire NiTi alloy endodontic reciprocating files. All the plugins were developed by the imaging platform at the Center for Applied Medical Research (Navarra, Spain).

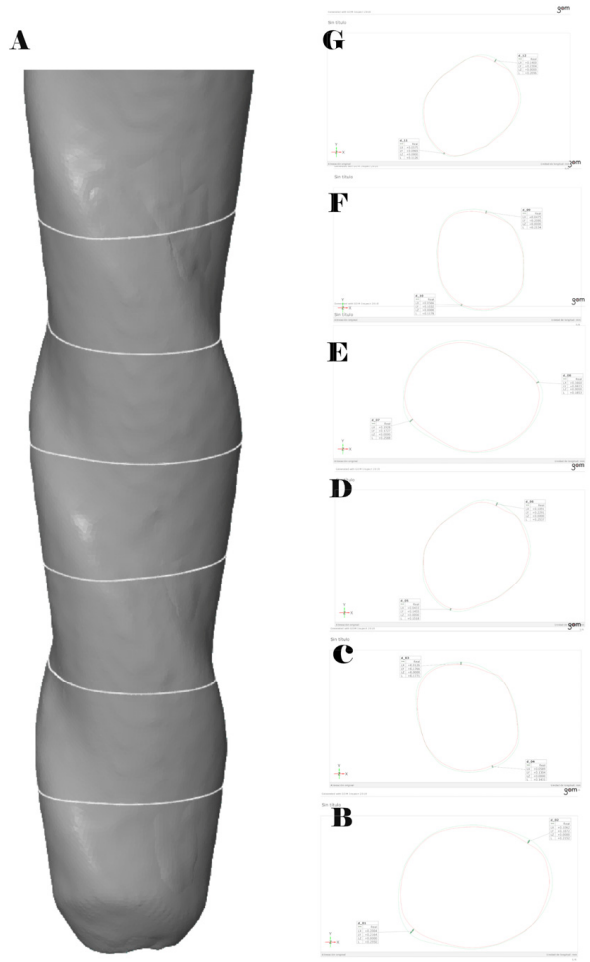

Figure 3. (**A**) Three-dimensional reconstruction of the aligned preoperative and postoperative digital files of the CM-wire NiTi alloy endodontic reciprocating files and cross sections at (**B**) 1 mm, (**C**) 2 mm, (**D**) 3 mm, (**E**) 4 mm, (**F**) 5 mm, and (**G**) 6 mm from the tip of the files.

In addition, the aligned preoperative (DICOM1) and postoperative (DICOM2) digital files from the micro-CT scans of the CM-wire NiTi alloy endodontic reciprocating files (Figure 4B) were isolated (Figure 4B) and measured in volume (Figure 4C) to analyze the wear of the CM-wire NiTi alloy endodontic reciprocating files after use.

2.6. Confirmation of Repeatability and Reproducibility

To confirm the repeatability of this novel digital measurement technique, a single operator (operator A) calculated the aforementioned measurements six times. A second operator (operator B) calculated the measurements six times to validate the reproducibility of this novel digital measurement technique.

2.7. Statistical Tests

Statistical analysis was conducted using SAS 9.4 (SAS Institute Inc., Cary, NC, USA) to evaluate the measured valuables. Descriptive statistics are expressed as the mean and standard deviation (SD) for quantitative variables. Gage repeatability and reproducibility statistical analysis was carried out to assess the reproducibility and repeatability of this measurement technique.

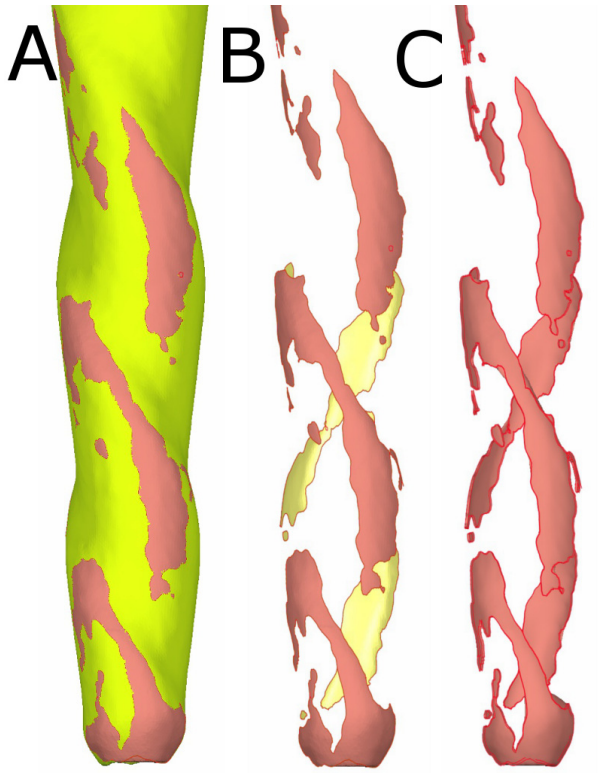

Figure 4. (**A**) Three-dimensional reconstruction of the aligned preoperative (yellow) and postoperative (red) digital files to isolate and measure the (**B**) wear area and (**C**) wear volume.

3. Results

Table 1 shows the mean and SD values for the wear volume (mm^3) of the CM-wire NiTi alloy endodontic reciprocating files between the operators.

Table 1. Quantitative statistics regarding the wear volume (mm^3) of the CM-wire NiTi alloy endodontic reciprocating files between the operators.

Operator		*n*	Mean	SD	Minimum	Maximum
A	1	6	0.070	0.000	0.070	0.070
	2	6	0.149	0.000	0.149	0.149
	3	6	0.161	0.000	0.161	0.161
	4	6	0.197	0.000	0.197	0.197
	5	6	0.036	0.000	0.036	0.036
	6	6	0.015	0.000	0.015	0.015
	7	6	0.028	0.000	0.028	0.028
	8	6	0.089	0.000	0.089	0.089
	9	6	0.104	0.000	0.104	0.104
	10	6	0.073	0.000	0.073	0.073
B	1	6	0.070	0.000	0.070	0.070
	2	6	0.149	0.000	0.149	0.149
	3	6	0.161	0.000	0.161	0.161
	4	6	0.197	0.000	0.197	0.197
	5	6	0.036	0.000	0.036	0.036
	6	6	0.028	0.000	0.028	0.028
	7	6	0.089	0.000	0.089	0.089
	8	6	0.104	0.000	0.104	0.104
	9	6	0.073	0.000	0.073	0.073
	10	6	0.028	0.000	0.028	0.028

SD: standard deviation.

Additionally, wear was mostly registered at the tip and cutting edges of the CM-wire NiTi alloy endodontic reciprocating files.

The Gage repeatability and reproducibility statistical analysis of the wear volume observed in the CM-wire NiTi alloy endodontic reciprocating files after use found that the variability attributable to the digital technique for measuring wear volume had a repeatability value of 0.00% of the total variability of the samples. As repeatability values must be below 1% in order to constitute high repeatability, the morphometric measurement technique demonstrates a high repeatability rate for volume measurement. Moreover, the correlation coefficient among operators was 1. In addition, the Gage repeatability and reproducibility statistical analysis of the wear volume of the files after use revealed that the variability attributable to the measurement technique performed by the two operators had a reproducibility value of 0.00% of the total variability of the samples. Reproducibility values must be below 1% to demonstrate high reproducibility; therefore, it can be concluded that this morphometric measurement technique has a high level of reproducibility when evaluating the wear volume in CM-wire NiTi alloy endodontic reciprocating files after use (see Figures 5 and 6).

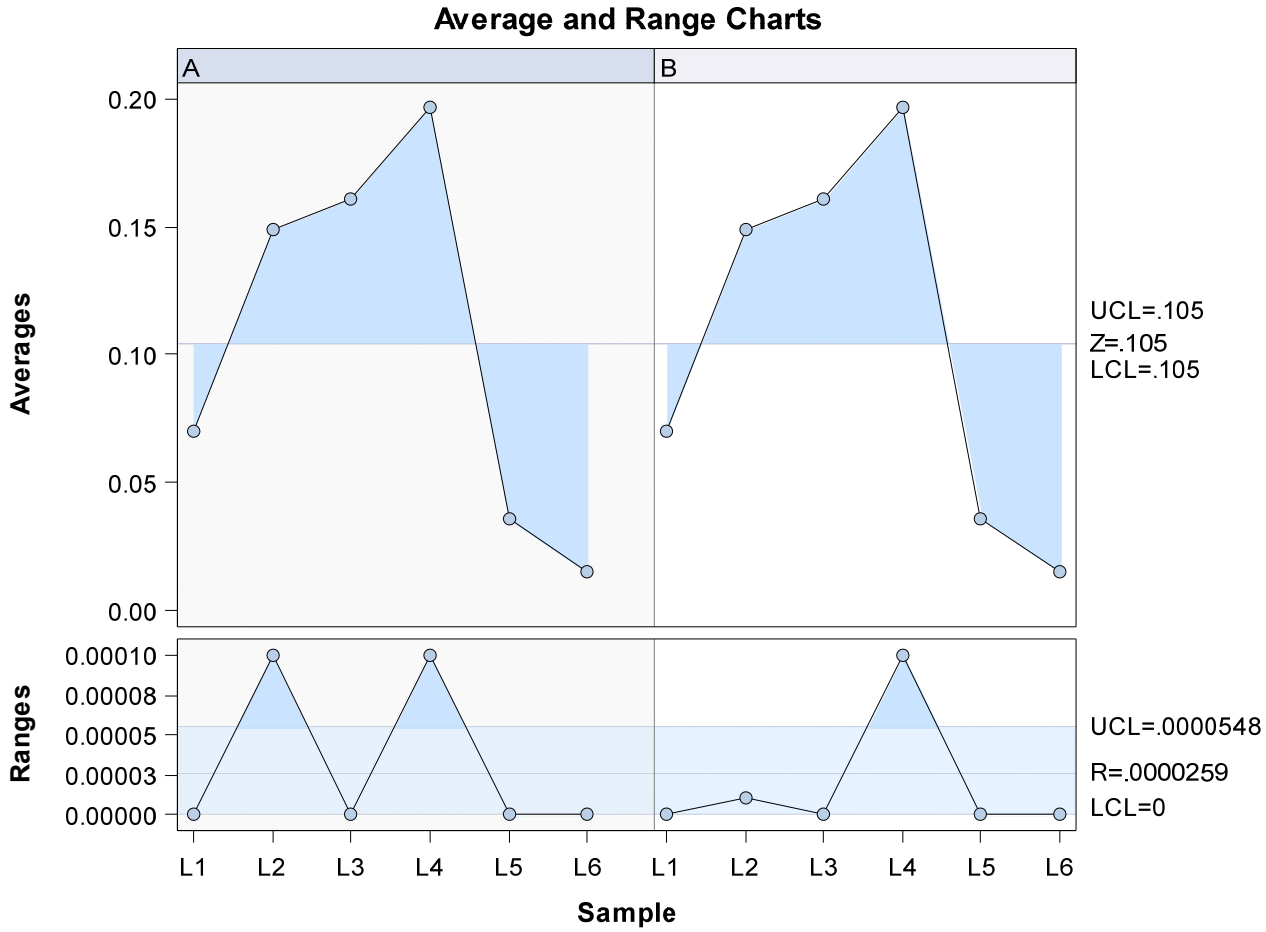

Figure 5. Mean values of the six measurements of the volume wear of CM-wire NiTi alloy endodontic reciprocating files after use, performed by operators A and B (average), and the differences between the six measurements of the volume wear of CM-wire NiTi alloy endodontic reciprocating files after use (range).

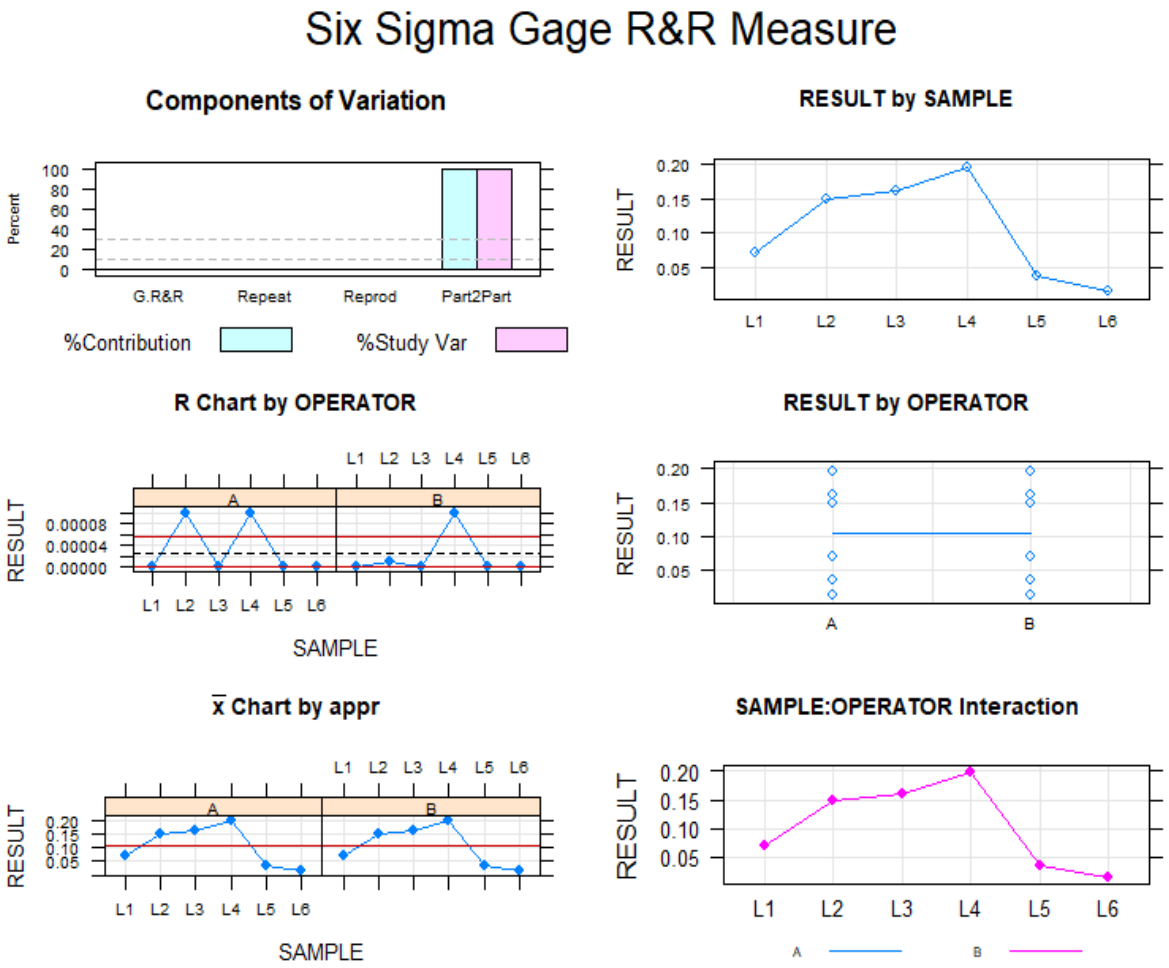

Figure 6. Measurement evaluation chart of the measurements of the volume wear of CM-wire NiTi alloy endodontic reciprocating files after use indicating the difference between the measurements of each observer to evaluate the impact of each variable on the total variation obtained (components of variation) with a mean control chart and a range control chart (R chart by operator and x chart by appr), graphed measurement points (result by sample and result by operator), and interactions (sample–operator interaction). The values are within the confidence limits.

4. Discussion

The results of the present study reject the null hypothesis (H_0) that there is no difference between morphometric measurement protocols in the accuracy of measuring the volume wear of CM-wire NiTi alloy endodontic reciprocating files after use.

The digital technique presented herein provides a repeatable, reproducible, and accurate method for quantifying the volume wear of endodontic reciprocating files after use in clinical settings.

The fatigue resistance of endodontic rotary or reciprocating files may be influenced by the metallurgical characteristics of the NiTi alloy, which affect the physical properties of the files [24,25]. Additionally, the kinematics of the NiTi alloy endodontic rotary files may also influence the cyclic fatigue resistance to rotary or reciprocating movement, increasing the resistance to cyclic fatigue of the endodontic files [26]. Furthermore, pecking motion frequency has been reported to affect the resistance to cyclic fatigue of NiTi alloy endodontic rotary files [27].

The geometrical parameters of the NiTi alloy endodontic files may also influence the level of resistance to cyclic fatigue of NiTi alloy endodontic rotary and reciprocating files. Sekar et al. [6] and Zhang et al. [28] analyzed the effect of cross-section design on

resistance to cyclic fatigue, finding that apical diameter and taper were linked to a higher risk of fracture.

However, speed does not affect the resistance to cyclic fatigue of NiTi alloy endodontic rotary files [29,30], unless the endodontic rotary file is already close to reaching the critical number of rotations [31].

Surface wear located at the cutting edge of NiTi alloy endodontic rotary files may also influence the effectiveness of endodontic instruments during use [14]. Spicciareli et al. reported morphological alterations and reduced cutting efficiency of CM-wire NiTi alloy endodontic reciprocating files after repeated use by analyzing seven deteriorating variables assessed using micrographs taken before and after use. Fatigue cracks and metal strips/metal flash were observed in the gradual wear of the cutting edge, which could negatively affect the cutting efficiency of the NiTi alloy endodontic reciprocating files [32]. In addition, Zubizarreta-Macho et al. pointed to the influence of the number of uses on resistance to cyclic fatigue of NiTi alloy endodontic rotary files [33], and Vieira et al. observed the appearance of transversal crack defects in the surface of NiTi alloy endodontic rotary files under flexural stress, as well as longitudinal crack defects in the surface of files after use. They reported that the cumulative effect of fatigue on NiTi alloy endodontic rotary files more significantly influences flexural fatigue conduct in comparison with torsional resistance [34].

Different protocols have been used to measure wear volume in NiTi alloy endodontic rotary files. Peters et al. used a high-resolution tomography scan to observe changes in extracted teeth before and after the use of NiTi K-Files, Lightspeed, ProFile.04 Instruments, and GT-Rotaries; however, the pre- and post-operative images were not aligned to evaluate the localization of wear [34]. Aracena et al. analyzed the deterioration of Wave One CM-wire NiTi alloy reciprocating files under a microscope after cutting them into three cross-sections, observing differences in irregularities and rake angles between the unused and used instruments [35]. In the present study, the NiTi alloy endodontic rotary files were virtually sectioned into six cross-sections. Inan et al. assessed the deformation and incidence of fracture in Mtwo NiTi alloy endodontic rotary files after clinical use by measuring the total length of the Mtwo NiTi alloy endodontic rotary files with a digital caliper; however, this provides a more subjective measurement procedure [18].

Tripi et al. assessed the effect of NiTi alloy endodontic rotary instruments using SEM analysis, identifying small holes, cracks, and detritus that may increase the potential risk of failure and reduce the cutting efficiency of NiTi alloy endodontic rotary instruments [3]. In addition, Inan et al. analyzed structural defects in NiTi alloy endodontic rotary instruments using stereomicroscopy and reported cracks, untwisting, loops, or deflections.

In the past, micro-CT analysis has been used to analyze the effects of root canal preparations on canal volume and tooth surface. Peters et al. studied the effects of four different shaping systems on the removal of dentine using 3D replicas of root canal systems of upper molar teeth [36]. Connert et al. used a micro-CT scan to assess the accuracy of electronic apex locators in determining the levels of apical constriction during root canal treatment [37]. Zuolo et al. also used a micro-CT scan to measure the frequency of microcracks caused by root canal preparation with TRUShape and Self-Adjusting Files [38]. In addition, the micro-CT measurement technique has been used to analyze the amount of root canal filling material remaining inside the root canal system after root canal retreatment [39], and Perez et al. evaluated the relationship between the depth of insertion of the irrigation needle and the removal of hard tissue detritus [39]. Micro-CT scans have also been used to assess anatomical changes in the root canal system after preparation, with findings indicating that NiTi alloy endodontic rotary instruments can cause morphological alterations in the root canal system anatomy directly linked to the geometrical design and metallurgical alloy of the file. Root canal anatomy also has a large impact on the way that an endodontic instrument works. However, micro-CT scans had not previously been used to analyze changes in the surface of NiTi alloy endodontic rotary files after use.

In the present study, we used CM-wire NiTi alloy endodontic reciprocating files to prevent flexion and torsion of the files during use, which prevents the alignment of DICOM files for the purpose of analyzing the wear location. One limitation observed in the present study is that NiTi alloy endodontic files with smaller diameters, as well as files with metallurgical composition or thermal treatments that allow more flexibility, may compromise the alignment procedure.

5. Conclusions

The results of the present study indicate that this novel digital measurement technique is a reproducible, repeatable, and accurate method for quantifying the volume wear of CM-wire NiTi alloy endodontic reciprocating files after clinical use.

Author Contributions: Conceptualization, V.F.-L., Á.A.M. and Á.Z.-M.; design, V.F.-M. and J.A.P.-B.; data acquisition, I.F.-M.; formal analysis, C.R.-S.; statistical analyses, Á.Z.-M. and V.F.-M.; review and editing, Á.Z.-M. All authors have read and agreed to the published version of the manuscript.

Funding: This research received no external funding.

Data Availability Statement: Data are available upon request in accordance with relevant restrictions (e.g., ethical or privacy concerns).

Conflicts of Interest: The authors state that they have no conflicts of interest.

References

1. Siqueira, J.F., Jr.; Rôças, I.N. Polymerase chain reaction–based analysis of microorganisms associated with failed endodontic treatment. *Oral Surg. Oral Med. Oral Pathol. Oral Radiol. Endod.* **2014**, *97*, 85–94. [CrossRef]
2. Sjögren, T.; Figdor, D.; Persson, S.; Sundqvist, G. Influence of infection at the time of root filling on the outcome of endodontic treatment of teeth with apical periodontitis. *Int. Endod. J.* **1997**, *30*, 297–306. [CrossRef] [PubMed]
3. Zein, N.; Harmouch, E.; Lutz, J.-C.; De Grado, G.F.; Kuchler-Bopp, S.; Clauss, F.; Offner, D.; Hua, G.; Benkirane-Jessel, N.; Fioretti, F. Polymer-Based Instructive Scaffolds for Endodontic Regeneration. *Materials* **2019**, *12*, 2347. [CrossRef]
4. Cao, Y.; Morrissey, T.G.; Acome, E.; Allec, S.I.; Wong, B.M.; Keplinger, C.; Wang, C. A transparent, self-healing, highly stretchable ionic conductor. *Adv. Mater.* **2017**, *29*, 1605099. [CrossRef]
5. Ahamed, S.B.B.; Vanajassun, P.P.; Rajkumar, K.; Mahalaxmi, S. Comparative Evaluation of Stress Distribution in Experimentally Designed Nickel-titanium Rotary Files with Varying Cross Sections: A Finite Element Analysis. *J. Endod.* **2018**, *44*, 654–658. [CrossRef]
6. Sekar, V.; Kumar, R.; Nandini, S.; Ballal, S.; Velmurugan, N. Assessment of the role of cross section on fatigue resistance of rotary files when used in reciprocation. *Eur. J. Dent.* **2016**, *10*, 541–545. [CrossRef] [PubMed]
7. Kwak, S.W.; Ha, J.-H.; Lee, C.-J.; El Abed, R.; Abu-Tahun, I.H.; Kim, H.-C. Effects of Pitch Length and Heat Treatment on the Mechanical Properties of the Glide Path Preparation Instruments. *J. Endod.* **2016**, *42*, 788–792. [CrossRef] [PubMed]
8. Parashos, P.; Gordon, I.; Messer, H.H. Factors Influencing Defects of Rotary Nickel-Titanium Endodontic Instruments After Clinical Use. *J. Endod.* **2004**, *30*, 722–725. [CrossRef]
9. Spili, P.; Parashos, P.; Messer, H.H. The Impact of Instrument Fracture on Outcome of Endodontic Treatment. *J. Endod.* **2005**, *31*, 845–850. [CrossRef]
10. Sattapan, B.; Nervo, G.J.; Palamara, J.E.; Messer, H.H. Defects in Rotary Nickel-Titanium Files After Clinical Use. *J. Endod.* **2000**, *26*, 161–165. [CrossRef]
11. Barbosa, F.O.G.; Gomes, J.A.D.C.P.; de Araújo, M.C.P. Fractographic Analysis of K3 Nickel-Titanium Rotary Instruments Submitted to Different Modes of Mechanical Loading. *J. Endod.* **2008**, *34*, 994–998. [CrossRef] [PubMed]
12. Plotino, G.; Grande, N.M.; Cordaro, M.; Testarelli, L.; Gambarini, G. A Review of Cyclic Fatigue Testing of Nickel-Titanium Rotary Instruments. *J. Endod.* **2009**, *35*, 1469–1476. [CrossRef] [PubMed]
13. Inan, U.; Gonulol, N. Deformation and Fracture of Mtwo Rotary Nickel-Titanium Instruments After Clinical Use. *J. Endod.* **2009**, *35*, 1396–1399. [CrossRef] [PubMed]
14. McGuigan, M.B.; Louca, C.; Duncan, H.F. Clinical decision-making after endodontic instrument fracture. *Br. Dent. J.* **2013**, *214*, 395–400. [CrossRef]
15. Shen, Y.; Zhou, H.-M.; Zheng, Y.; Peng, B.; Haapasalo, M. Current Challenges and Concepts of the Thermomechanical Treatment of Nickel-Titanium Instruments. *J. Endod.* **2013**, *39*, 163–172. [CrossRef]
16. Yared, G. Canal preparation using only one Ni-Ti rotary instrument: Preliminary observations. *Int. Endod. J.* **2007**, *41*, 339–344. [CrossRef]
17. Roane, J.B.; Sabala, C.L.; Duncanson, M.G., Jr. The "balanced force" concept for instrumentation of curved canals. *J. Endod.* **1985**, *11*, 203–211. [CrossRef]

18. De-Deus, G.; Silva, E.; Vieira, V.; Belladonna, F.; Elias, C.; Plotino, G.; Grande, N.M. Blue Thermomechanical Treatment Optimizes Fatigue Resistance and Flexibility of the Reciproc Files. *J. Endod.* **2017**, *43*, 462–466. [CrossRef]
19. Yamazaki-Arasaki, A.; Cabrales, R.; Dos Santos, M.; Kleine, B.M.; Prokopowitsch, I. Topography of four different endodontic rotary systems, before and after being used for the 12th time. *Microsc. Res. Tech.* **2012**, *75*, 97–102. [CrossRef]
20. Arantes, W.B.; da Silva, C.M.; Lage-Marques, J.L.; Habitante, S.; da Rosa, L.C.; de Medeiros, J.M. SEM analysis of defects and wear on Ni-Ti rotary instruments. *Scanning* **2014**, *36*, 411–418. [CrossRef]
21. Schneider, S.W. A comparison of canal preparations in straight and curved root canals. *Oral Surg. Oral Med. Oral Pathol. Oral Radiol. Endod.* **1971**, *32*, 271–275. [CrossRef]
22. Bürklein, S.; Hinschitza, K.; Dammaschke, T.; Schäfer, E. Shaping ability and cleaning effectiveness of two single-file systems in severely curved root canals of extracted teeth: Reciproc and WaveOne versus Mtwo and ProTaper. *Int. Endod. J.* **2011**, *45*, 449–461. [CrossRef] [PubMed]
23. Schneider, C.A.; Rasband, W.S.; Eliceiri, K.W. NIH Image to ImageJ: 25 Years of image analysis. *Nat. Methods* **2012**, *9*, 671–675. [CrossRef] [PubMed]
24. Ruiz-Sánchez, C.; Faus-Llácer, V.; Faus-Matoses, I.; Zubizarreta-Macho, Á.; Sauro, S.; Faus-Matoses, V. The Influence of NiTi Alloy on the Cyclic Fatigue Resistance of Endodontic Files. *J. Clin. Med.* **2020**, *9*, 3755. [CrossRef] [PubMed]
25. Zupanc, J.; Vahdat-Pajouh, N.; Schäfer, E. New thermomechanically treated NiTi alloys—A review. *Int. Endod. J.* **2018**, *51*, 1088–1103. [CrossRef] [PubMed]
26. Ferreira, F.; Adeodato, C.; Barbosa, I.; Aboud, L.; Scelza, P.; Scelza, M.Z. Movement kinematics and cyclic fatigue of NiTi rotary instruments: A systematic review. *Int. Endod. J.* **2016**, *50*, 143–152. [CrossRef]
27. Zubizarreta-Macho, Á.; Martínez, A.A.; Costa, C.F.; Quispe-López, N.; Agustín-Panadero, R.; Mena-Álvarez, J. Influence of the type of reciprocating motion on the cyclic fatigue resistance of reciprocating files in a dynamic model. *BMC Oral Health* **2021**, *21*, 179. [CrossRef]
28. Zhang, E.-W.; Cheung, G.S.; Zheng, Y.-F. Influence of Cross-sectional Design and Dimension on Mechanical Behavior of Nickel-Titanium Instruments under Torsion and Bending: A Numerical Analysis. *J. Endod.* **2010**, *36*, 1394–1398. [CrossRef]
29. Pedullà, E.; Plotino, G.; Grande, N.M.; Scibilia, M.; Pappalardo, A.; Malagnino, V.A.; Rapisarda, E.G. Influence of rotational speed on the cyclic fatigue of Mtwo instruments. *Int. Endod. J.* **2013**, *47*, 514–519. [CrossRef]
30. Kitchens, G.G., Jr.; Liewehr, F.R.; Moon, P.C. The effect of operational speed on the fracture of nickel-titanium rotary instruments. *J. Endod.* **2007**, *33*, 52–54. [CrossRef]
31. Spicciarelli, V.; Corsentino, G.; Ounsi, H.F.; Ferrari, M.; Grandini, S. Shaping effectiveness and surface topography of reciprocating files after multiple simulated uses. *J. Oral Sci.* **2019**, *61*, 45–52. [CrossRef] [PubMed]
32. Zubizarreta-Macho, A.; Alonso-Ezpeleta, O.; Albaladejo Martínez, A.; Faus Matoses, V.; Caviedes Brucheli, J.; Agustín-Panadero, R.; Mena Álvarez, J.; Vizmanos Martínez-Berganza, F. Novel Electronic Device to Quantify the Cyclic Fatigue Resistance of Endodontic Reciprocating Files after Using and Sterilization. *Appl. Sci.* **2020**, *10*, 4962. [CrossRef]
33. Vieira, E.P.; Nakagawa, R.K.L.; Buono, V.T.L.; Bahia, M.G.D.A. Torsional behaviour of rotary NiTi ProTaper Universal instruments after multiple clinical use. *Int. Endod. J.* **2009**, *42*, 947–953. [CrossRef]
34. Aracena, D.; Borie, E.; Betancourt, P.; Aracena, A.; Guzmán, M. Wear of the Primary WaveOne single file when shaping vestibular root canals of first maxillary molar. *J. Clin. Exp. Dent.* **2017**, *9*, e368–e371. [CrossRef] [PubMed]
35. Peters, O.A.; Schönenberger, K.; Laib, A. Effects of four Ni-Ti preparation techniques on root canal geometry assessed by micro computed tomography. *Int. Endod. J.* **2001**, *34*, 221–230. [CrossRef] [PubMed]
36. Connert, T.; Judenhofer, M.S.; Hülber-J, M.; Schell, S.; Mannheim, J.G.; Pichler, B.J.; Löst, C.; ElAyouti, A. Evaluation of the accuracy of nine electronic apex locators by using Micro-CT. *Int. Endod. J.* **2018**, *51*, 223–232. [CrossRef]
37. Zuolo, M.L.; De-Deus, G.; Belladonna, F.G.; Silva, E.J.; Lopes, R.T.; Souza, E.M.; Versiani, M.A.; Zaia, A.A. Micro-computed Tomography Assessment of Dentinal Micro-cracks after Root Canal Preparation with TRUShape and Self-adjusting File Systems. *J. Endod.* **2017**, *43*, 619–622. [CrossRef]
38. Faus-Matoses, V.; Pasarín-Linares, C.; Faus-Matoses, I.; Foschi, F.; Sauro, S.; Faus-Llácer, V.J. Comparison of Obturation Removal Efficiency from Straight Root Canals with ProTaper Gold or Reciproc Blue: A Micro-Computed Tomography Study. *J. Clin. Med.* **2020**, *9*, 1164. [CrossRef]
39. Perez, R.; Neves, A.A.; Belladonna, F.G.; Silva, E.J.N.L.; Souza, E.M.; Fidel, S.; Versiani, M.A.; Lima, I.; Carvalho, C.; De-Deus, G. Impact of needle insertion depth on the removal of hard-tissue debris. *Int. Endod. J.* **2017**, *50*, 560–568. [CrossRef]

International Journal of
Environmental Research and Public Health

MDPI

Article

Comparative Analysis of Ease of Removal of Fractured NiTi Endodontic Rotary Files from the Root Canal System—An In Vitro Study

Vicente Faus-Matoses [1], Eva Burgos Ibáñez [1], Vicente Faus-Llácer [1], Celia Ruiz-Sánchez [1], Álvaro Zubizarreta-Macho [2,3,*] and Ignacio Faus-Matoses [1]

[1] Department of Stomatology, Faculty of Medicine and Dentistry, University of Valencia, 46010 Valencia, Spain; vicente.faus@uv.es (V.F.-M.); eburi@alumni.uv.es (E.B.I.); fausvj@uv.es (V.F.-L.); ceruizsan@gmail.com (C.R.-S.); ignacio.faus@uv.es (I.F.-M.)
[2] Department of Endodontics, Faculty of Health Sciences, Alfonso X El Sabio University, 28691 Madrid, Spain
[3] Department of Surgery, Faculty of Medicine and Dentistry, University of Salamanca, 37008 Salamanca, Spain
* Correspondence: amacho@uax.es

Abstract: This study aimed at analyzing and comparing the ease of removal of fractured nickel–titanium (NiTi) endodontic rotary files from the root canal system between the ultrasonic tips and the Endo Rescue appliance removal systems, as well as comparing the volume of dentin removed between ultrasonic tips and the Endo Rescue appliance using a micro-computed tomography (micro-CT) scan. Material and Methods: Forty NiTi endodontic rotary files were intentionally fractured in 40 root canal systems of 20 lower first molar teeth and distributed into the following study groups: A: Ultrasonic tips (n = 20) (US) and B: Endo Rescue device (n = 20) (ER). Preoperative and postoperative micro-CT scans were uploaded into image processing software to analyze the volumetric variations of dentin using an algorithm that enables progressive differentiation between neighboring pixels after defining and segmenting the fractured NiTi endodontic rotary files and the root canal systems in both micro-CT scans. A non-parametric Mann–Whitney–Wilcoxon test or t-test for independent samples was used to analyze the results. Results: The US and ES study groups saw 8 (1 mesiobuccal and 7 distal root canal system) and 3 (distal root canal system) fractured NiTi endodontic rotary files removed, respectively. No statistically significant differences were found in the amount of dentin removed between the US and ER study groups at the mesiobuccal (p = 0.9109) and distal root canal system (p = 0.8669). Conclusions: Ultrasonic tips enable greater ease of removal of NiTi endodontic rotary files from the root canal system, with similar amounts of dentin removal between the two methods.

Keywords: endodontics; cyclic fatigue; endodontic rotary file removal; dentin removal; ultrasonics; Endo Rescue

Citation: Faus-Matoses, V.; Burgos Ibáñez, E.; Faus-Llácer, V.; Ruiz-Sánchez, C.; Zubizarreta-Macho, Á.; Faus-Matoses, I. Comparative Analysis of Ease of Removal of Fractured NiTi Endodontic Rotary Files from the Root Canal System—An In Vitro Study. *Int. J. Environ. Res. Public Health* **2022**, *19*, 718. https://doi.org/10.3390/ijerph19020718

Academic Editors: Alberto De Biase, Marco Lollobrigida and Luca Lamazza

Received: 13 December 2021
Accepted: 5 January 2022
Published: 10 January 2022

1. Introduction

Nickel–titanium (NiTi) alloy endodontic rotary files are widely used to clean and shape the root canal system because they have been shown to significantly increase the success rate of root canal treatments [1]. However, the unexpected fracture of NiTi alloy endodontic rotary files during the root canal treatment can sometimes influence outcomes [2], with the incidence of fracture of NiTi alloy endodontic rotary files estimated between 0.4% to 4.6% [3,4] by torsional fatigue or bending fatigue [5]. Several procedures can be used to remove fractured instruments [6], including the Masseran kit [6], Endo Safety System [7], and Endo Extractor [8]. Additionally, other techniques have been proposed for the removal of fractured NiTi alloy endodontic rotary files, including the wire loop technique [9], spinal tap needle-and-Hedstrom file technique [10], Cancelliers [11], Tube-and-Hedstrom file technique [12], hypodermic needle [13], blunt needle and core paste technique [14], and the

Instrument Removal System (IRS) [15]. However, all these procedures require that the coronal third of the root canal system be adequately enlarged to provide access to the fractured instruments [1]. This implies a loss of dentin tissue, which can negatively affect the structural integrity of the tooth [16]. Furthermore, it can result in perforated roots or potentially put teeth at risk of vertical root fracture, particularly in the apical third [1]. Additionally, the use of magnification in combination with ultrasonic has been widely recognized as the best technique for removing separated instruments, especially the technique proposed by Ruddle, who recommended preparing a platform in the pre-enlarged root canal system using ultrasonic tips. The removal of the fractured instruments can be performed using a range of techniques, many of them employing some type of microtube since the direct application of ultrasonic energy cannot remove fractured instruments [1]. As a result, there is no universal procedure for removing fractured instruments, and removals are often performed using an array of techniques and devices, with inherent risks and limitations.

Today, micro-computed tomography (micro-CT) scans are used to study root canal anatomy and assess changes in root canal morphology after root canal treatment [17–19]. Madarati et al. used a micro-CT scan to analyze changes in the root canal space after removal of fractured instruments in canine teeth using ultrasonics [20]. However, many studies have shown that the separation of fractured endodontic instruments occurs mostly in curved and narrow root canal systems, such as the mesiobuccal root canal of upper molars or the mesial root canal of lower molars, due to their complex anatomy and curved canal structure [10].

The objective of the present study was to assess and compare the ease of removal of fractured NiTi alloy endodontic rotary files from the root canal system between the ultrasonic tips and Endo Rescue appliance removal systems, as well as to compare the volume of dentin removed between ultrasonic tips and Endo Rescue appliance using a micro-CT scan. The null hypothesis is (H_0) that there is no difference in ease of removal of fractured NiTi endodontic rotary files between the ultrasonic tips and Endo Rescue appliance, and there is no difference in the dentin removal of fractured NiTi alloy endodontic rotary files between ultrasonic tips and Endo Rescue appliance.

2. Materials and Methods

2.1. Study Design

Forty root canal systems (20 mesial and 20 distal) extracted from twenty lower first molar teeth for periodontal reasons were selected for this study. The systems had mature roots and no incidence of previous root canal treatment, root resorption, or calcium metamorphosis. The study was carried out from February to October 2021 at the Department of Stomatology of the University of Valencia (Valencia, Spain). The study was a randomized controlled experimental trial in accordance with the statement by the German Ethics Committee (Zentrale Ethikkommission, 2003) on the use of organic tissues in medical research. The study design was approved by the Ethics Committee of Alfonso X El Sabio University (Process no. 24/2020). All patients provided their informed consent to transfer their teeth for the study.

2.2. Experimental Procedure

Digital preoperative radiographs were taken buccolingually and mesiodistally to analyze the root canal system anatomy of the teeth selected for the study. A single operator then performed the endodontic access cavities using the technique outlined by Rover et al. [21]. The working length of the root canal was established with a stainless steel #10 K-file (Dentsply Maillefer, Ballaigues, Switzerland) inserted until the tip became visible through the apical foramen. The canals were prepared using a Protaper Gold endodontic rotary system (Dentsply Maillefer, Ballaigues, Switzerland) and endodontic rotary file up to F1. They were irrigated with 5 mL of 5.25% NaOCl (Clorox; Oakland, CA, USA), 5 mL of sterile saline solution (Braun, Jaén, Spain), and 5 mL of 17% EDTA (SmearClear; SybronEndo, CA, USA) using an endodontic needle (Miraject Endo Luer; Hager & Werken,

Duisburg, Germany) with an apical diameter of 0.3 mm inserted up to 1 mm of the working length. The apical 4 mm of the F2 endodontic rotary files (Protaper Gold, Dentsply Maillefer, Ballaigues, Switzerland) was then partially cut with a low-speed 0.3 diamond disk (Brasseler, GA, USA, Savannah, GA, USA) and intentionally fractured in the mesiobuccal and distal root canals, 5 mm to the apical foramen coronally, as per Terauchi et al. [22]. The root canal systems were then randomly distributed (Epidat 4.1, Galicia, Spain) into one of two removal techniques: Group A: Ultrasonic tips (ET25; Satelec Corp, Merignac Cedex, France) (n = 20) (US) or Group B: Endo Rescue (Komet Medical, Lemgo, Germany) (n = 20) (ER). A bilateral Student's t-test was used with two independent samples to achieve a power of 80.00% for evaluating differences from the null hypothesis H_0: $\mu_1 = \mu_2$; factoring in the significance level of 5.00, 40 fractured NiTi endodontic rotary files were needed. The fractured NiTi alloy endodontic rotary files in the US study group were removed using the technique outlined by Ruddle et al., which uses fine ultrasonic tips (ET25; Satelec Corp, Merignac, France) in a counterclockwise motion to remove 1–1.5 mm of dentin around the coronal surface of the fractured file [15]. The obstruction begins to loosen and start spinning during this ultrasonic motion. The ultrasonic generator (Newtron P5, Satelec Corp) power was set to 6 (Figure 1A).

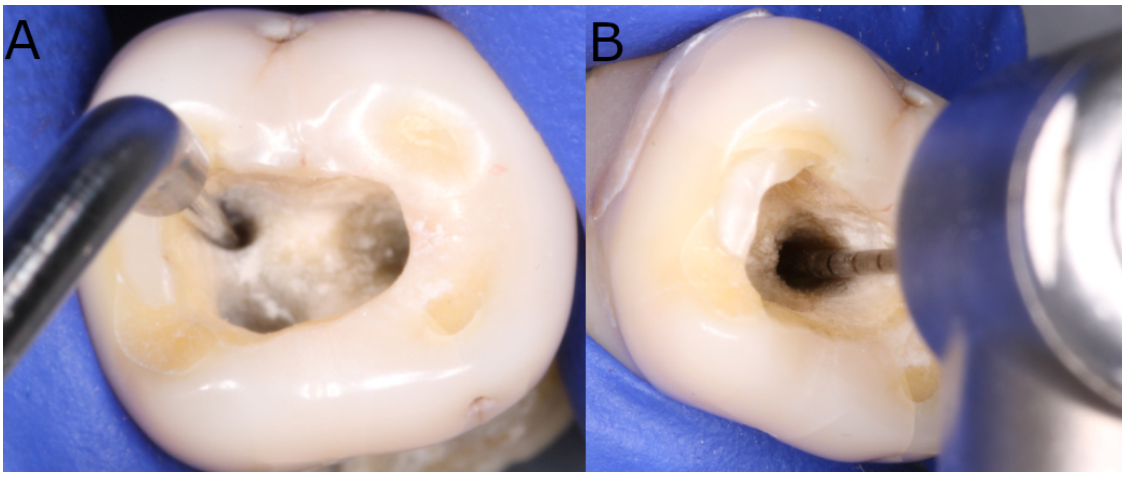

Figure 1. Removal of NiTi endodontic rotary files using (**A**) ultrasonic tip and (**B**) Endo Rescue appliance.

The fractured NiTi endodontic rotary files in the ER study group were removed using the Endo Rescue Kit (Komet Medical, Lemgo, Germany). First, dentin was removed in order to enlarge the root canal entrance using an endodontic bur (H269GK.315.016, Komet Medical, Lemgo, Germany) at a speed of 100,000 rpm. The canal curvature of the coronal root canal third was then straightened, using axial movements with a stainless-steel Gates-Glidden reamer (G180A.204.110, Komet Medical, Lemgo, Germany). Subsequently, a second stainless-steel Gates-Glidden reamer (G180A.204.090, Komet Medical, Lemgo, Germany) was used to create direct access to the fractured file (Protaper Gold, Dentsply Maillefer, Ballaigues, Switzerland). The coronal surface of the files was subsequently exposed by drilling around (RKP. 204.090, Komet Medical, Lemgo, Germany) them at 300 rpm. Finally, the file (Protaper Gold, Dentsply Maillefer, Ballaigues, Switzerland) was removed using the Endo Rescue trepan bur (RKT.204.090, Komet Medical, Lemgo, Germany) at 300 rpm in a counterclockwise movement (Figure 1B).

The NiTi alloy endodontic rotary files (Protaper Gold, Dentsply Maillefer, Ballaigues, Switzerland) in both the US and ER study groups were removed under magnification (OPMI Pico, Zeiss Dental Microscope, Oberkochen, Germany). The time it took to remove the files (Protaper Gold, Dentsply Maillefer, Ballaigues, Switzerland) was recorded in both the US and ER study groups in cases where the files were successfully removed from the root canal system. The working time for removal was established as 90 min for both groups [6].

The teeth were subsequently kept in an incubator (mco-18aic, Sanyo, Moriguchi, Osaka, Japan) (37 °C, 100% relative humidity). The same clinician, who has 10 year's experience in endodontics, performed all the root canal procedures.

2.3. Micro-CT Scanning

A micro-CT scan (Micro-CAT II, Siemens Preclinical Solutions, Knoxville, TN, USA) was performed pre- and postoperatively to analyze the volumetric variations in the amount of dentin removed after root canal procedures to extricate the fractured files (Protaper Gold, Dentsply Maillefer, Ballaigues, Switzerland). The scan was performed using the following exposure parameters: 88 µA, 360° rotation, 90 kV, and isotropic resolution of 50 µm. The 3D tomographic images of the entire tooth had a total of 512 slices, with isotropic 50-micron voxels and a 512 × 512 resolution, according to a previous study [23].

2.4. Measurement Procedure

Volumetric analysis of the dentin removed in the distal and mesiobuccal root canal systems subsequent to root canal procedures was performed using image processing software (ImageJ, National Institutes of Health, Bethesda, MD, USA) after identifying and segmenting the fractured NiTi endodontic rotary files (Protaper Gold, Dentsply Maillefer, Ballaigues, Switzerland), as well as the distal and mesiobuccal root canal systems (ROI: 10 × 10 × 10 mm) established using the preoperative and postoperative micro-CT scans (Micro-CAT II, Siemens Preclinical Solutions, Knoxville, TN, USA) (Figure 2).

Next, the teeth were reconstructed, with a 25-micron resolution per voxel (Quantum 3.0, San Jose, CA, USA). An advanced image segmentation technique based on partial differential equations (Level Sets, National Institutes of Health, Bethesda, MD, USA) was then used to divide mesiobuccal and distal root canal systems, enabling progressive differentiation between neighboring pixels and assessment of the anatomy of the root canal systems. The algorithm was initiated manually in the first slice of the volume's axial view, in which the user traces a contour closely around the channel. With the segmentation technique method, this contour is then deformed towards the inside until it converges, i.e., when the first slice of the root canal system is segmented. Next, the calculated contour was expanded by 6 pixels to initiate the next slice, to which the segmentation technique is once again applied. This process was then applied to each axial slice until the entire channel was 3D segmented. Finally, the difference in the volume of dentin subsequent to removal of the files was calculated in the coronal, medial, and apical third (Figure 3).

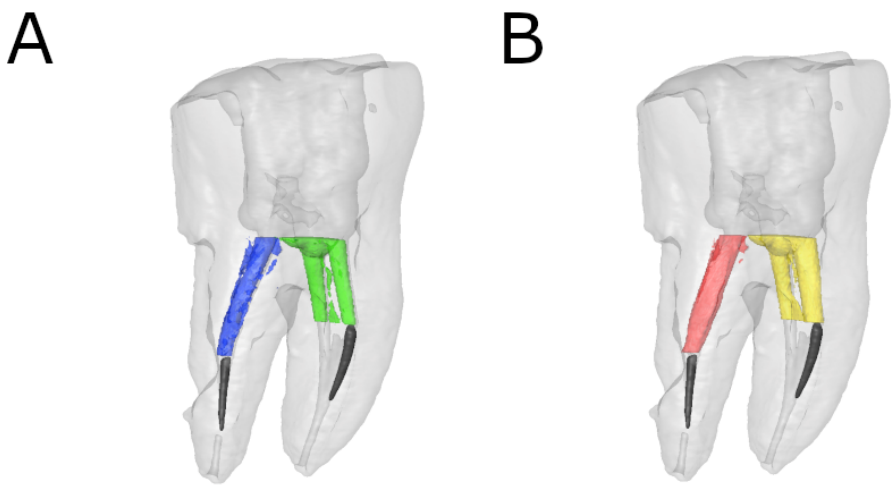

Figure 2. *Cont.*

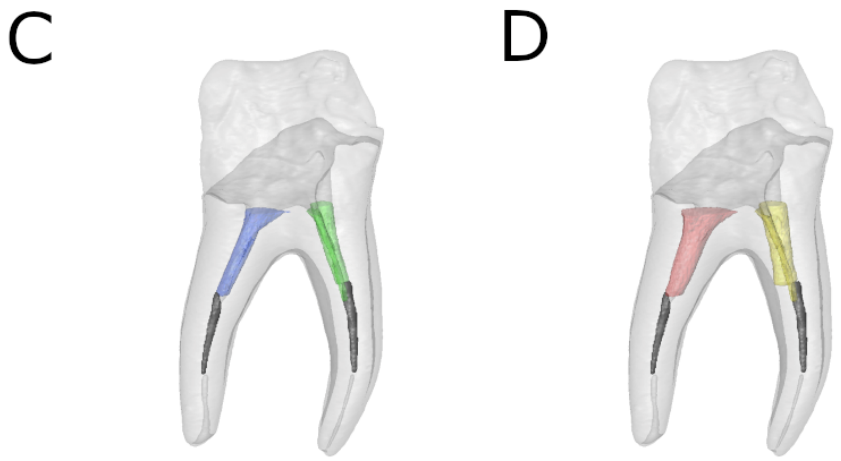

Figure 2. Reconstructed 3D micro-CT images of (**A**) preoperative and (**B**) postoperative ER study group and (**C**) preoperative and (**D**) postoperative US study group. Preoperative (blue) and postoperative (red) distal root canal and preoperative (green) and postoperative (yellow) mesial root canals were isolated. The fractured NiTi endodontic rotary files (black) were also isolated in both distal and mesiobuccal root canal systems.

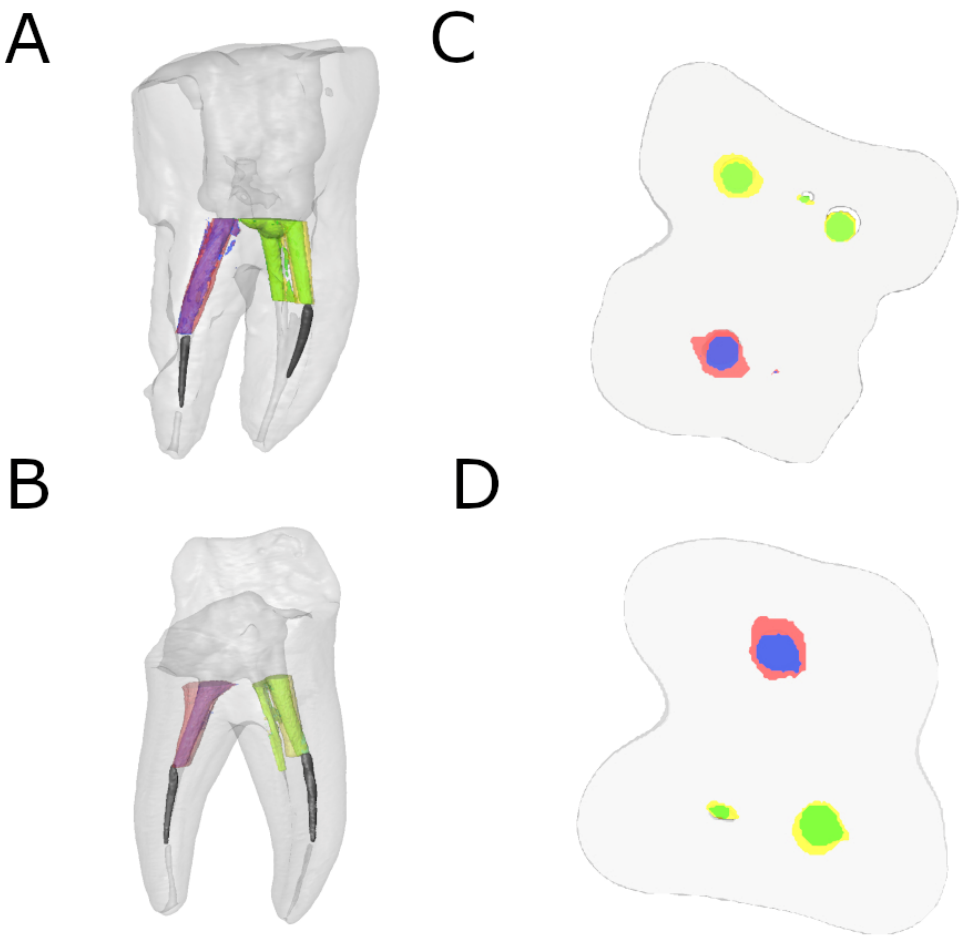

Figure 3. Reconstructed 3D micro-CT images of (**A**) preoperative and postoperative alignment and (**B**) cross-section of ER study group and reconstructed 3D micro-CT images of (**C**) preoperative and postoperative alignment and (**D**) cross-section of US study group. Preoperative (blue) and postoperative (red) distal root canal and preoperative (green) and postoperative (yellow) mesial root canals were aligned. The fractured NiTi endodontic rotary files (black) were also isolated in both distal and mesiobuccal root canal systems.

2.5. Statistical Tests

The studied variables were recorded for statistical analysis (SPSS 22.00, Microsoft Inc., Redmond, WA, USA). Statistical analysis of quantitative variables was performed out using the mean, median, and standard deviation (SD). A comparative analysis was carried out by evaluating the difference between preoperative and postoperative values using the Student's *t*-test for independent samples or the non-parametric Mann–Whitney–Wilcoxon test, depending on which test they best fit the criteria for. Statistical significance was set as $p < 0.05$.

3. Results

Table 1 shows the means and SD values of the preoperative and postoperative differences in dentin volume (mm^3) between the US and ER study groups at the coronal, medial, and apical level.

Table 1. Descriptive values of the preoperative and postoperative volumetric differences (mm^3) between the US and ER study groups at the coronal, medial, and apical level.

Study Group	Root	Root Third	Time	*n*	Mean	SD	Minimum	Maximum
US	Mesial	Coronal	Pre-op	10	1.62 [a]	1.48	0.44	5.08
			Post-op	10	2.38 [a]	1.94	0.58	6.85
		Medial	Pre-op	10	1.03 [a]	0.76	0.39	2.48
			Post-op	10	1.59 [a]	0.95	0.45	3.56
		Apical	Pre-op	10	0.78 [a]	0.59	0.29	2.13
			Post-op	10	1.21 [a]	0.62	0.37	2.37
	Distal	Coronal	Pre-op	10	2.71 [a]	3.42	0.56	11.94
			Post-op	10	3.64 [a]	4.39	0.69	15.64
		Medial	Pre-op	10	1.37 [a]	1.62	0.40	5.84
			Post-op	10	1.98 [a]	1.94	0.48	7.22
		Apical	Pre-op	10	0.83 [a]	0.42	0.33	1.45
			Post-op	10	1.35 [a]	0.66	0.43	2.79
ER	Mesial	Coronal	Pre-op	10	2.08 [a]	1.57	0.18	5.44
			Post-op	10	2.65 [a]	1.90	0.29	6.12
		Medial	Pre-op	10	1.36 [a]	0.97	0.16	3.67
			Post-op	10	1.75 [a]	1.03	0.28	4.16
		Apical	Pre-op	10	1.03 [a]	0.71	0.12	2.49
			Post-op	10	1.53 [a]	0.77	0.28	2.80
	Distal	Coronal	Pre-op	10	2.54 [a]	3.83	0.11	14.31
			Post-op	10	3.38 [a]	2.21	0.21	14.31
		Medial	Pre-op	10	1.31 [a]	1.69	0.11	5.79
			Post-op	10	1.96 [a]	2.04	0.21	7.24
		Apical	Pre-op	10	0.62 [a]	0.52	0.08	1.50
			Post-op	10	1.07 [a]	0.71	0.21	2.09

US: ultrasonic tips; ER: Endo Rescue [a]: statistical significance.

The paired *t*-test found no statistically significant differences ($p = 0.9109$) in changes in volume between the US (1.75 ± 1.70 mm^3) and ER (1.43 ± 0.89 mm^3) study groups in the mesiobuccal root canal system. In addition, there were no statistically significant differences ($p = 0.8669$) in changes in volume between the US (2.06 ± 1.68 mm^3) and ER (1.94 ± 1.50 mm^3) study groups in the distal root canal system (Table 1).

No statistically significant differences ($p = 0.9109$) were found in changes in volume in the coronal root third between the US (0.77 ± 0.96 mm^3) and ER (0.57 ± 0.58 mm^3) study groups in the mesiobuccal root canal system. In addition, there were no statistically significant differences ($p = 0.8814$) in changes in volume in the distal root canal system (Figure 4).

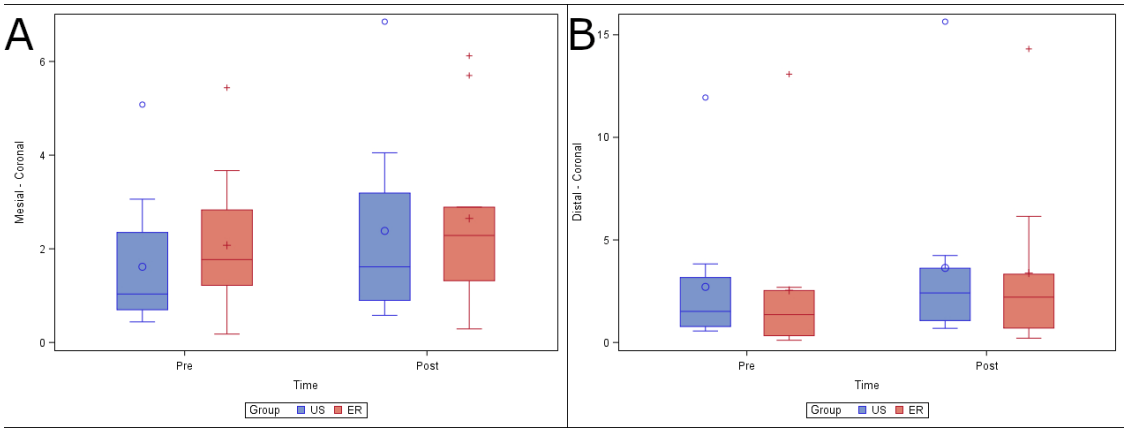

Figure 4. (**A**) Box plot of volume of dentin removed preoperatively and postoperatively, comparing the US and ER study groups at the coronal level in the mesiobuccal and (**B**) distal root canal systems.

No statistically significant differences ($p = 0.3232$) were found in the changes in volume at the medial root third between the US (0.56 ± 0.47 mm^3) and ER (0.39 ± 0.21 mm^3) study groups in the mesiobuccal root canal system. In addition, there were no statistically significant differences ($p = 0.8447$) in the change in volume between the US (0.61 ± 0.45 mm^3) and ER (0.65 ± 0.47 mm^3) study groups in the distal root canal system (Figure 5).

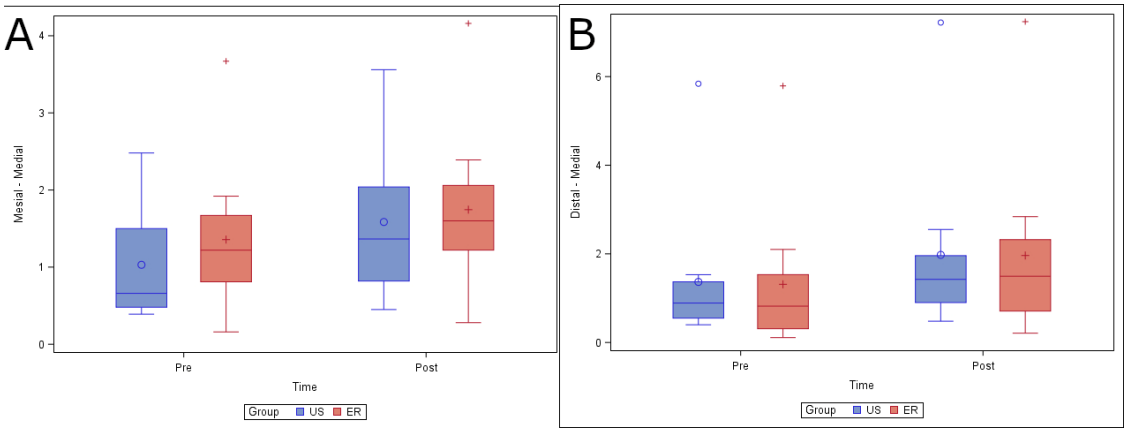

Figure 5. (**A**) Box plot of volume of dentin removed preoperatively and postoperatively, comparing the US and ER study groups at the medial level in the mesiobuccal and (**B**) distal root canal systems.

Finally, no statistically significant differences ($p = 0.5990$) were found in changes in volume at the apical root third between the US (0.43 ± 0.35 mm^3) and ER (0.50 ± 0.30 mm^3) study groups in the mesiobuccal root canal system. In addition, there were no statistically significant differences ($p = 0.6592$) in the change in volume between the US (0.53 ± 0.44 mm^3) and ER (0.45 ± 0.27 mm^3) study groups in the distal root canal system (Figure 6).

The time it took to remove the NiTi alloy endodontic rotary files randomly assigned to the ER study group ranged between 9–25 min, and 18–90 min for the files assigned to the US group.

Finally, the relationship between the dentin removal and the working time of the removal systems was also analyzed; however, no statistically significant differences were shown at the messiobuccal root canal system ($p = 0.0252$) (Figure 7A) neither the distal root canal system ($p = 0.0116$) (Figure 7B).

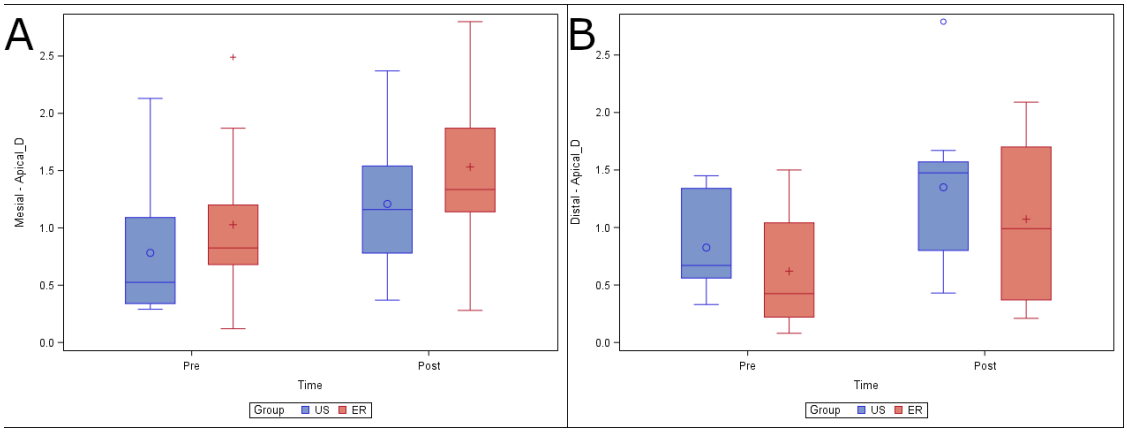

Figure 6. (**A**) Box plot of volume of dentin removed preoperatively and postoperatively, comparing the US and ER study groups at the apical level in the mesiobuccal and (**B**) distal root canal systems.

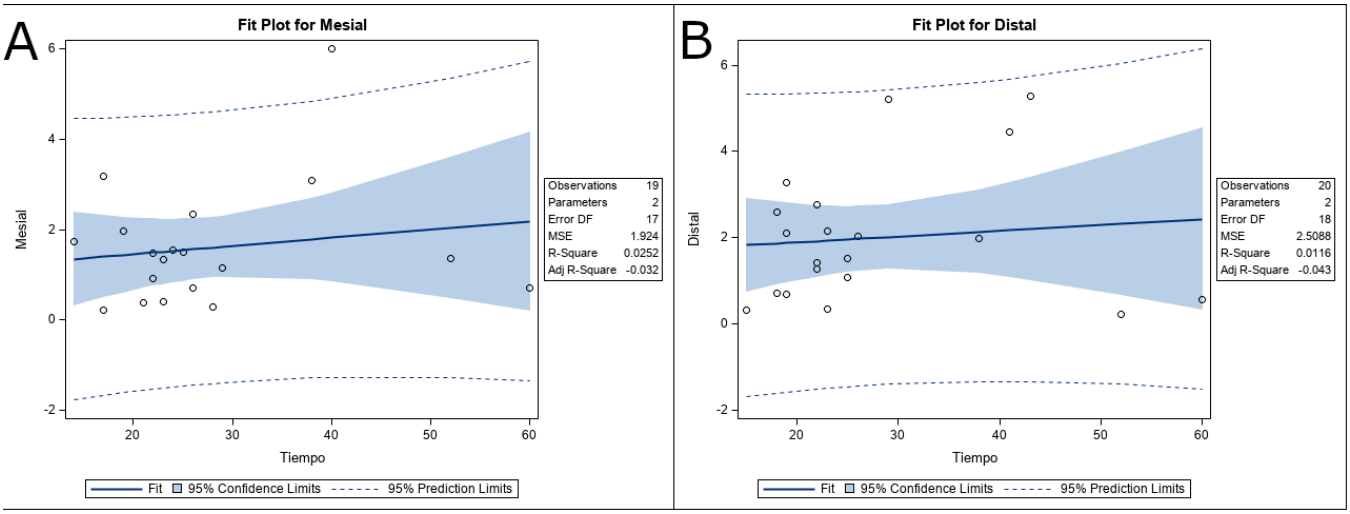

Figure 7. (**A**) Fit plot of the relationship between the dentin removal and the working time of the removal systems at the messiobuccal and (**B**) distal root canal systems. In summary, no differences in overall change in dentin volume were observed between the US and ER study groups after dentin removal. The most important result is that the US study group allowed the removal of 8 out of 20 fractured NiTi endodontic rotary files (1 in the mesiobuccal root canal system and 7 in the distal root canal system) from the root canal system; meanwhile, the ER study group allowed the removal of 3 out of 20 fractured NiTi endodontic rotary files (all in the distal root canal system) from the root canal system. Therefore, the US removal system is recommended for the removal of fractured files from the root canal system.

4. Discussion

The results of the present study rejected the null hypothesis (H_0) that there is no difference in ease of removal of fractured NiTi alloy endodontic rotary files between ultrasonic tips and the Endo Rescue appliance; however, the present study does accept the null hypothesis (H_0) that there is no difference in the volume of dentin removal between ultrasonic tips and the Endo Rescue appliance.

NiTi alloy endodontic rotary files removal systems whose removal techniques were different were selected, to analyze the removal capability and dentin removal of each removal system. This is the reason why the ultrasonic tips and the Endo Rescue appliance were used in this study. As these NiTi alloy endodontic rotary files removal systems and techniques have only been recently developed, this highlights that there is still no standardized procedure for safe removal of fractured instruments. A trephine removal

technique, using ultrasonics or trepan burs, in combination with a grabbing technique, such as the Masseran Extractor or the Instrument Removal System (Dentsply Tulsa Dental, Johnson City, TN, USA) has been widely used. However, these techniques have shown some limitations and may potentially lead to a weakening of the remaining root [16]. In addition, there are many variables correlated with the success rate of removal of fractured instruments, but these are mainly related to root canal system anatomy in terms of ratio and curvature angle [24,25]. Unexpected instrument fracture often occurs in narrow and curved canals, particularly in mesial root canal systems of lower molars and mesiobuccal root canal systems of upper molars [21]. Furthermore, in the present study, all files were fractured in the mesiobuccal root canal system, similar to a previous study [22], but distal root canal systems were also included in the study to assess the effect of root canal system anatomy on the ease of removal of fractured NiTi alloy endodontic rotary files, compared with the ease of removal of files fractured in the mesial root canal systems. It has also been reported in the literature that NiTi alloy endodontic rotary files tend to fracture more at the midpoint of root canal curvature [26]. However, even though the samples were matched between groups, there could still be some variations, for example, in isthmus size or other interconnections within the main root canal system [1]. The original canal shape should ideally be preserved as much as possible throughout the process of cleaning and shaping that are part of the root canal treatment, as root canal system enlargement of up to 40 to 50% of the root's width can increase susceptibility to vertical fracture [27,28]. Furthermore, Nevares et al. reported that a digital optical microscope (DOM) made it easier to visualize the fractured files [29]; therefore, an operating microscope was used to enable the visualization of all fragments throughout the removal procedures.

Root perforations were observed in three of the roots randomly assigned to the US group, while no root perforations were identified in the ER group. This could be due to the vibrating tip leading to excessive cutting of dentin tissue. The ultrasonic tip used for the present study was the ET 25, one of the most commonly used ultrasonic tips for removal of fractured NiTi alloy endodontic rotary files [30] due to its small diameter (0.3 mm) and low taper of 3%. The diameter of the root canal system after inserting the ultrasonic tip up to 1 mm was 1.16 mm; the diameter of the root canal system after trephining dentin with the Endo Rescue system was 0.7 mm. A previous study found that the minimal remaining thickness in mandibular molars was 0.60 mm in an ultrasonic study group and 0.66 mm in a trepan bur study group for the fragment located 5 mm below the root canal entrance [1]; however, the present study found no statistically significant differences in the remaining thickness of dentin between both study groups. The ER system was able to remove three fractured NiTi alloy endodontic rotary instruments, while the US technique removed eight fractured NiTi alloy endodontic rotary instruments. However, it is worth mentioning that operator skill and experience may also influence end results.

Suter et al. recommended not taking more than 45 to 60 min to remove fractured NiTi alloy endodontic rotary instruments, because success rates may drop as treatment time increases [12]. They attributed this lower success rate to operator fatigue or over-enlargement of the root canal system, which can compromise tooth integrity and increase the risk of root perforation. Time is generally recorded from the starting straight-line access preparation until the instrument has been successfully removed [1]. For the present study, treatment time was defined as being from beginning to trephine the dentin around the fragment until the instrument was successfully removed or the time limit exceeded. The time needed to remove files in the ER group ranged from 9 to 25 min, while the US group ranged from 18 min to over 1 h. Nagai et al. reported that the time required to remove fractured NiTi alloy endodontic rotary files using an ultrasonic technique ranged from 3 to 40 min, and the time needed to remove fractured NiTi alloy endodontic rotary files using the Masseran technique ranged from 20 min to several hours [31]. In the present study, treatment time was shorter in the trepan bur group than in the ultrasonic group. Therefore, the small-diameter trepan bur technique is recommended for removing instruments that have been fractured coronally or at the curvature of root canals.

Removing separated endodontic rotary files from curved canals poses a challenge for clinicians since these fragments tend to become blocked outside the wall of a curved canal, often causing the retrieval process to be unsuccessful. Therefore, the approach to removing the separated fragments should always include a combination of new techniques and devices that are most likely to be successful, while also minimizing the amount of dentin volume lost and length of treatment time [29]. Therefore, this type of study that assesses and compares the ease of removal of fractured NiTi alloy endodontic rotary files from the root canal system between two different removal systems in straight and curved root canal systems, as well as the volume of dentin removed, can help clinicians select a more effective extraction system for fractured NiTi alloy endodontic rotary files removal.

The standardization of the root canal system anatomy, in ex vivo studies, is a limitation. However, randomization of the sample was carried out. In addition, in future studies, the authors recommend clinical studies with more removal systems.

5. Conclusions

Within the limitations of this in vitro study, the results indicate that ultrasonic tips enable greater ease of removal of fractured NiTi endodontic rotary files from the root canal system, with little to no difference in the amount of dentin removed.

Author Contributions: Conceptualization, V.F.-M., E.B.I. and Á.Z.-M.; data acquisition, I.F.-M.; design, V.F.-L.; formal analysis, V.F.-M. and C.R.-S.; writing—review and editing, V.F.-L.; performed all statistical analyses, Á.Z.-M. and E.B.I. All authors have read and agreed to the published version of the manuscript.

Funding: No external funding was granted for this research.

Institutional Review Board Statement: The study was approved by the Ethics Committee of Alfonso X El Sabio University (Process no. 24/2020).

Informed Consent Statement: Informed consent was obtained from all subjects involved in the study.

Data Availability Statement: Data available on request due to restrictions eg privacy or ethical.

Conflicts of Interest: The authors have no conflict of interest.

References

1. Yang, Q.; Shen, Y.; Huang, D.; Zhou, X.; Gao, Y.; Haapasalo, M. Evaluation of Two Trephine Techniques for Removal of Fractured Rotary Nickel-titanium Instruments from Root Canals. *J. Endod.* **2017**, *43*, 116–120. [CrossRef]
2. Panitvisai, P.; Parunnit, P.; Sathorn, C.; Messer, H.H. Impact of a retained instrument on treatment outcome: A systematic review and meta-analysis. *J. Endod.* **2010**, *36*, 775–780. [CrossRef]
3. Al-Fouzan, K.S. Incidence of rotary ProFile instrument fracture and the potential for bypassing in vivo. *Int. Endod. J.* **2003**, *36*, 864–867. [CrossRef] [PubMed]
4. Schäfer, E.; Schulz-Bongert, U.; Tulus, G. Comparison of hand stainless steel and nickel titanium rotary instrumentation: A clinical study. *J. Endod.* **2004**, *30*, 432–435. [CrossRef]
5. Sattapan, B.; Nervo, G.J.; Palamara, J.E.; Messer, H.H. Defects in rotary nickel-titanium files after clinical use. *J. Endod.* **2000**, *26*, 161–165. [CrossRef] [PubMed]
6. Yoldas, O.; Oztunc, H.; Tinaz, C.; Alparslan, N. Perforation risks associated with the use of Masserann endodontic kit drills in mandibular molars. *Oral Surg. Oral Med. Oral Pathol. Oral Radiol. Endod.* **2004**, *97*, 513–517. [CrossRef] [PubMed]
7. Wong, R.; Cho, F. Microscopic management of procedural errors. *Dent. Clin. N. Am.* **1997**, *41*, 455–479.
8. Gettleman, B.H.; Spriggs, K.A.; ElDeeb, M.E.; Messer, H.H. Removal of canal obstructions with the endo extractor. *J. Endod.* **1991**, *17*, 608–611. [CrossRef]
9. Roig-Greene, J. The retrieval of foreign objects from root canals: A simple aid. *J. Endod.* **1983**, *9*, 394–397. [CrossRef]
10. Flanders, D.H. New techniques for removing separated root canal instruments. *N. Y. State Dent. J.* **1996**, *62*, 30–32. [PubMed]
11. Carr, G.B. Microscopes in endodontics. *J. Can. Dent. Assoc.* **1992**, *20*, 55–61.
12. Suter, B. A new method for retrieving silver points and separated instruments from root canals. *J. Endod.* **1998**, *24*, 446–448. [CrossRef]
13. Eleazer, P.D.; O'Connor, R.P. Innovative uses for hypodermic needles in endodontics. *J. Endod.* **1999**, *25*, 190–191. [CrossRef]
14. Machtou, P.; Reit, C. Non-surgical retreatment. In *Endodontology*, 1st ed.; Machtou, P., Reit, C., Eds.; Blackwell Munksgaard: Oxford, UK, 2003; pp. 300–310.
15. Ruddle, C. Nonsurgical retreatment. *J. Endod.* **2004**, *30*, 827–845. [CrossRef] [PubMed]

16. Fu, M.; Zhang, Z.; Hou, B. Removal of broken files from root canals by using ultrasonic techniques combined with dental microscope: A retrospective analysis of treatment outcome. *J. Endod.* **2011**, *37*, 619–622. [CrossRef] [PubMed]
17. Peters, O.A.; Laib, A.; Gohring, T.N.; Barbakow, F. Changes in root canal geometry after preparation assessed by high-resolution computed tomography. *J. Endod.* **2001**, *27*, 1–6. [CrossRef]
18. Paque, F.; Balmer, M.; Attin, T.; Peters, O.A. Preparation of oval-shaped root canals in mandibular molars using nickel-titanium rotary instruments: A micro-computed tomography study. *J. Endod.* **2010**, *36*, 703–707. [CrossRef] [PubMed]
19. Miguéns-Vila, R.; Martín-Biedma, B.; De-Deus, G.; Belladonna, F.G.; Peña-López, A.; Castelo-Baz, P. Micro-computed Tomographic Evaluation of Dentinal Microcracks after Preparation of Curved Root Canals with ProTaper Gold, WaveOne Gold, and ProTaper Next Instruments. *J. Endod.* **2021**, *47*, 309–314. [CrossRef] [PubMed]
20. Madarati, A.A.; Qualtrough, A.J.; Watts, D.C. A microcomputed tomography scanning study of root canal space: Changes after the ultrasonic removal of fractured files. *J. Endod.* **2009**, *35*, 125–128. [CrossRef]
21. Rover, G.; Belladonna, F.G.; Bortoluzzi, E.A.; De-Deus, G.; Silva, E.J.N.L.; Teixeira, C.S. Influence of Access Cavity Design on Root Canal Detection, Instrumentation Efficacy, and Fracture Resistance Assessed in Maxillary Molars. *J. Endod.* **2017**, *43*, 1657–1662. [CrossRef] [PubMed]
22. Terauchi, Y.; O'Leary, L.; Kikuchi, I.; Asanagi, M.; Yoshioka, T.; Kobayashi, C.; Suda, H. Evaluation of the efficiency of a new file removal system in comparison with two conventional systems. *J. Endod.* **2007**, *33*, 585–588. [CrossRef]
23. Faus-Llácer, V.; Luna-Roa, M.; Faus-Matoses, I.; Ruiz-Sánchez, C.; Zubizarreta-Macho, A.; Sauro, S.; Faus-Matoses, V. Comparative Analysis of the Smear Layer Removal Capability between EndoVac and Endoactivator Endodontic Irrigation Systems at the Root Canal System and Isthmus: A Micro-Computed Tomography Analysis. *Appl. Sci.* **2020**, *10*, 7033. [CrossRef]
24. Iqbal, M.K.; Kohli, M.R.; Kim, J.S. A retrospective clinical study of incidence of root canal instrument separation in an endodontics graduate program: A PennEndo database study. *J. Endod.* **2006**, *32*, 1048–1052. [CrossRef]
25. Shen, Y.; Peng, B.; Cheung, G.S. Factors associated with the removal of fractured NiTi instruments from root canal systems. *Oral Surg. Oral Med. Oral Pathol. Oral Radiol. Endod.* **2004**, *98*, 605–610. [CrossRef]
26. Mandel, E.; Adib-Yaszdi, M.; Benhamou, L.M.; Lachkar, T.; Mesgouez, C.; Sobel, M. Rotary Ni-Ti profile systems for preparing curved canals in resin blocks: Influence of operator on instrument breakage. *Int. Endod. J.* **1999**, *32*, 436–443. [CrossRef]
27. Lertchirakarn, V.; Palamara, J.E.A.; Messer, H.H. Patterns of vertical rootfracture: Factors affecting stress distribution in the root canal. *J. Endod.* **2003**, *29*, 523–528. [CrossRef]
28. Souter, N.J.; Messer, H.H. Complications associated with fractured file removal using an ultrasonic technique. *J. Endod.* **2005**, *31*, 450–452. [CrossRef] [PubMed]
29. Nevares, G.; Cunha, R.S.; Zuolo, M.L.; Bueno, C.E. Success rates for removing or bypassing fractured instruments: A prospective clinical study. *J. Endod.* **2012**, *38*, 442–444. [CrossRef]
30. Shiyakov, K.K.; Vasileva, R.I. Effectiveness in the curve of eight types of endodontic tips for broken instruments removal. *J. IMAB* **2014**, *20*, 595–600. [CrossRef]
31. Nagai, O.; Tani, N.; Kayaba, Y.; Kodama, S.; Osada, T. Ultrasonic removal of broken instruments in root. *Int. Endod. J.* **1986**, *19*, 298–304. [CrossRef] [PubMed]

DISCUSIÓN

DIÁMETRO APICAL DEL INSTRUMENTAL ENDODÓNTICO DE Ni-Ti

Los resultados derivados del estudio titulado "**The Effect of Taper and Apical Diameter on the Cyclic Fatigue Resistance of Rotary Endodontic Files Using an Experimental Electronic Device**" mostraron que el aumento del diámetro apical de los instrumentos endodónticos rotatorios de NiTi reducía significativamente ($p < 0.001$) la resistencia a la fractura de los instrumentos endodónticos rotatorios (170).

CONICIDAD DEL INSTRUMENTAL ENDODÓNTICO DE Ni-Ti

Alcalde et al, demostraron que las limas endodónticas reciprocantes de NiTi 25.06 (ProDesigner R, Easy, Belo Horizonte, Brasil) presentaron una mayor resistencia a la fatiga cíclica que las limas endodónticas reciprocantes de NiTi 25.08 (Reciproc, VDW, Munich, Alemania) y 25.07 (WaveOne Gold, Dentsply Sirona, Ballaigues, Suiza) (106). Sin embargo, el diferente diseño de la sección transversal, la microestructura cristalina de las aleaciones de NiTi y las cinemáticas de los movimientos reciprocantes podrían influir sobre los resultados obtenidos en este estudio. Por este motivo, el instrumental endodóntico rotatorio de NiTi utilizado en el estudio titulado "**The Effect of Taper and Apical Diameter on the Cyclic Fatigue Resistance of Rotary Endodontic Files Using an Experimental Electronic Device"** fue seleccionado porque proporcionaba instrumentos endodónticos rotatorios de NiTi con diferentes diámetros apicales manteniendo el diseño de la sección transversal, la estructura cristalina de la aleación de NiTi y la conicidad.

Además, Gambarini reportó una resistencia a la fatiga cíclica significativamente más alta ($p < 0.01$) de los instrumentos endodónticos rotatorios de NiTi 25.04 (ProFile, Maillefer, Baillagues, Suiza) comparadas con los instrumentos endodónticos rotatorios de NiTi 20.06 (ProFile, Maillefer, Baillagues, Suiza) los instrumentos endodónticos rotatorios de NiTi 25.06 NiTi (ProFile, Maillefer, Baillagues, Suiza) (118). Estos resultados están alineados con los obtenidos en

el estudio y destacan la influencia de la forma cónica por encima del diámetro apical.

Capar et al también analizaron la resistencia a la fatiga cíclica de los instrumentos endodónticos rotatorios de NiTi y concluyó que los instrumentos endodónticos rotatorios 15.02 (HyFlex GPF, Coltene-Whaledent, Allstetten, Suiza) mostraron una resistencia a la fatiga cíclica estadísticamente mayor ($p < 0.05$) en comparación con los instrumentos endodónticos rotatorios 12.03 (Pathfinding, G archivos, Micro-Mega, Besançon Cedex, Francia), 16.04 (ProGlider, Dentsply Maillefer, Ballaigues, Suiza), 16.02 (Pathfile, Dentsply Maillefer, Ballaigues, Suiza) y 15.02 (Scout Race, FKG Dentaire, La Chaux-de-Fonds, Suiza) (171). Estos resultados coinciden con los obtenidos en el presente estudio, donde se atribuye más influencia a la conicidad del instrumental endodóntico que al diámetro apical.

Así mismo, Camargo et al observaron que los instrumentos endodónticos reciprocantes de NiTi 25.06 (ProDesigner R, Easy, Belo Horizonte, Brasil) mostraron capacidades similares de centrado y transporte de canales después de la preparación de los segundos canales mesiovestibulares en comparación con los instrumentos endodónticos reciprocantes de NiTi 25.08 (Reciproc, VDW, Munich, Alemania); sin embargo, los instrumentos endodónticos reciprocantes de NiTi 25.06 (ProDesigner R, Easy, Belo Horizonte, Brasil) resultaron más conservadores con la dentina radicular (172,173).

Cabe mencionar que la conicidad ha destacado como un factor significativo en la remoción de dentina radicular durante la conformación del sistema de conductos radiculares. Duque et al evidenciaron que los instrumentos endodónticos reciprocantes de NiTi 35.06 (WaveOne Gold, Dentsply Sirona, Ballaigues, Switzerland) eliminaban significativamente más dentina radicular que los instrumentos endodónticos reciprocantes de NiTi 35.05 (ProDesign R, Easy, Belo Horizonte, Brazil); sin embargo, no mostraron diferencias estadísticamente significativas respecto al transporte apical (174).

Numerosos estudios se han llevado a cabo para analizar la influencia de la sección transversal del instrumental endodóntico rotatorio de NiTi en la resistencia a la fatiga cíclica del instrumental endodóntico. Algunos de ellos se han evaluado mediante el desarrollo de modelos matemáticos basados en elementos finitos para simular el comportamiento mecánico en condiciones de torsión y flexión (38,175,176,177,178,179).

Los resultados derivados del estudio "**Influence of the Geometrical Cross-Section Design on the Dynamic Cyclic Fatigue Resistance of NiTi Endodontic Rotary Files-An In Vitro Study"** reportaron que el sistema de instrumentación endodóntica rotatoria de NiTi Mtwo (VDW, Munich, Germany) con sección transversal en forma de S itálica, mostró una mayor resistencia a la fatiga cíclica dinámica que el sistema de instrumentación endodóntica rotatoria de NiTi T Pro E1 (Perfect Endo, Shenzhen Perfect Medical Instruments, Shanwei City, China) con sección transversal rectangular, el sistema de instrumentación endodóntica rotatoria de NiTI T Pro E2 (Perfect Endo, Shenzhen Perfect Medical Instruments, Shanwei City, China) con sección transversal triangular convexa y el sistema de instrumentación endodóntica rotatoria de NiTi T Pro E4 (Perfect Endo, Shenzhen Perfect Medical Instruments, Shanwei City, China) con sección transversal triangular. Los resultados concluyen que el área de la sección transversal y por ende la masa del instrumental endodóntico rotatorio de NiTi, así como el número de puntos de contacto entre la superficie del instrumento y las paredes de dentina del conducto radicular, disminuyen la resistencia a la fatiga cíclica de los instrumentos endodónticos rotatorios de NiTi (180). Este también puede influir en la flexibilidad de las limas endodónticas rotatorias de NiTi y conducir a los instrumentos endodónticos rotatorios de NiTi a causar una remoción excesiva de dentina en el conducto radicular, transporte apical (181), perforaciones radiculares, y fracturas dentarias (121,182).

Estudios previos han analizado la influencia del diseño de la sección transversal en la mecánica del comportamiento de los instrumentos endodónticos rotatorios de NiTi. Sekar et al analizaron el efecto de la sección

transversal sobre la resistencia a la fatiga cíclica de los instrumentos endodónticos rotatorios y reciprocantes de NiTi y observó que los instrumentos 25.06 del sistema de instrumentación endodóntico rotatorio de NiTi Mtwo son significativamente más resistentes que los instrumentos Revo-S SU y One Shape tanto en movimiento continuo ($p < 0.001$) como alterno ($p < 0.001$) (183). Estos hallazgos son consistentes con los resultados de nuestro estudio, que concluyó que el sistema de instrumentación endodóntico rotatorio de NiTi Mtwo (VDW, Munich, Germany) con sección transversal en S itálica mostró una mayor resistencia a la fatiga cíclica que el sistema de instrumentación endodóntico rotatorio de NiTi T Pro E1 (Perfect Endo, Shenzhen Perfect Medical Instruments, Shanwei City, China) con sección transversal rectangular, el sistema de instrumentación endodóntico rotatorio de NiTi T Pro E2 (Perfect Endo, Shenzhen Perfect Medical Instruments, Shanwei City, China) con sección transversal triangular convexa y el sistema de instrumentación endodóntico rotatorio de NiTi T Pro E4 (Perfect Endo, Shenzhen Perfect Medical Instruments, Shanwei City, China) con sección transversal triangular (181).

Además, de Menezes et al informaron que los instrumentos endodónticos rotatorios de NiTi ProDesign (Easy, Belo Horizonte, Brazil) con sección transversal en forma de S itálica presentó un número de ciclos significativamente mayor ($p < 0.05$) (910.37 ± 472.10) que los instrumentos endodónticos reciprocantes de NiTi Wave One Gold (Dentsply Sirona, Ballaigues, Switzerland) (264.76 ± 305.42) con una sección transversal en forma de paralelogramo en conductos radiculares artificiales con un 60° curvatura y radio de curvatura de 5mm (184,185).

Además, Adiguzel et al mostraron que los instrumentos endodónticos rotatorios de NiTi XP-endo Shaper con sección transversal triangular presentaron una número significativamente mayor ($p < 0.05$) de ciclos hasta la fractura que los instrumentos endodónticos rotatorios de NiTi HyFlex CM (3064.0 ± 248.1) con una sección transversal de diseño variable (de triangular a trapezoidal y cuadrático) 1120.5 ± 106.1) en conductos radiculares artificiales con una curvatura de 60° y 3mm radio de curvatura (186); sin embargo, Uygun et al

mostraron que los instrumentos endodónticos rotatorios de NiTi HyFlex EDM con una sección transversal de diseño variable (de triangular a trapezoidal y cuadrática) presentó un número de ciclos significativamente mayor ($p < 0.05$) (1710.42 ± 114.89) que los instrumentos endodónticos rotatorios de NiTi Vortex Blue con una sección transversal triangular convexa (548.39 ± 77.64), los instrumentos endodónticos rotatorios de NiTi ProTaper Gold (Dentsply Sirona, Ballaigues, Switzerland) (600.83 ± 66.49), con una sección transversal triangular convexa, y los instrumentos endodónticos rotatorios de NiTi One Curve con una sección transversal de diseño variable (de S itálica a triangular) (959.58 ± 61.18) en raíz artificial canales con una curvatura de 60 y un radio de curvatura de 3 mm (187).

Por otra parte, algunos de estos estudios han utilizado archivos digitales originales de sistemas de instrumentación endodóntica rotatoria de NiTi disponibles en el mercado como ProTaper (Dentsply Maillefer, Ballaigues, Suiza), ProFile (Dentsply Maillefer, Ballaigues, Suiza) o Mtwo (VDW, Munich, Germany), lo que dificulta la evaluación independiente de variables geométricas aisladas como la geometría de la sección transversal, el área de la sección transversal o el paso (38,176,177,178,179,). Otros estudios han modelizado instrumentos no basados en instrumentos existentes en el mercado con el objetivo de aislar la variable a analizar. Baek et al analizaron cuatro secciones transversales diferentes y tres pasos valores bajo torsión, pero no proporcionó información detallada sobre el modelo de material para la aleación con memoria de forma de los archivos o sobre la calidad de la malla de elementos finitos (178). En otro estudio, Versluis et al analizaron el efecto del *pitch* y la geometría de la sección transversal sobre la rigidez a la flexión y las tensiones utilizando un modelo representativo; sin embargo, el diseño del instrumento no se adaptaban a la norma ISO 3630-1:2008 (188) y los valores de flexión aplicados resultan bajos respecto a otros utilizados en otros estudios, lo que llevó a tensiones von Mises máximas por debajo de la tensión inicial para la transformación de austenita a martensita y, por lo tanto, el efecto de la superelasticidad de los instrumentos no fue analizado; además, el comportamiento de torsión no se incluyó en el estudio (175). Arbab-Chirani et al analizaron el efecto de la geometría de la sección transversal y el *pitch* en la

tendencia de "atornillado" del instrumental endodóntico de NiTi, pero se utilizó un modelo digital lineal (180). Basheer Ahamed et al evaluaron diferentes opciones geométricas de secciones transversales triangulares (rectos, convexos y cóncavos), así como el uso de limas con combinaciones de estos geometrías a lo largo del instrumento; sin embargo, no se analizó el efecto de pitch (176). El método de elementos finitos ha demostrado ser una herramienta útil, proporcionando información sobre la distribución de las tensiones y el comportamiento mecánico del instrumental antes de su fabricación, eludiendo las limitaciones atribuidas a la variabilidad experimental.

Los resultados del estudio "**Influence of Cross-Section and Pitch on the Mechanical Response of NiTi Endodontic Files under Bending and Torsional Conditions-A Finite Element Analysis**" demostraron que, la sección transversal del instrumental endodóntico rotatorio de NiTi (triangular o cuadrada), tiene un efecto mayor que el *pitch* en condiciones de flexión y rigidez torsional para un mismo diámetro apical y conicidad del instrumento endodóntico rotatorio de NiTi. Cuando del instrumental endodóntico rotatorio de NiTi está sometida a flexión o torsión, según la normativa ISO3630, aparece el comportamiento superelástico del material, lo cual es evidente a partir de una importante disminución de la rigidez del instrumento, como resultado de la progresión de la transformación de la fase austenítica a martensítica en las zonas más tensionadas del instrumento. Los resultados indican que este cambio en la rigidez ocurre cuando la rotación del extremo del vástago es de aproximadamente 20° en flexión o 30° en torsión respecto al extremo de la lima, para una lima con un vástago de 1.2mm de diámetro y una conicidad de 6%. Además, la rigidez del instrumental endodóntico rotatorio de NiTi se reduce por un factor mayor a 2 después de este punto de transformación (189).

DISTANCIA ENTRE LAS ARISTAS DE CORTE DEL INSTRUMENTAL ENDODÓNTICO DE NiTi (PITCH)

Los resultados del estudio "**Influence of Cross-Section and Pitch on the Mechanical Response of NiTi Endodontic Files under Bending and Torsional Conditions-A Finite Element Analysis**" demostraron que el efecto

del *pitch* sobre la rigidez fue sólo apreciable para pasos de rosca inferiores a 3 mm, y fue más importante para secciones transversales triangulares que para secciones transversales cuadradas (189).

La reducción del *pitch* del instrumental endodóntico rotatorio de NiTi provoca una disminución de la rigidez del instrumento en condiciones de flexión; sin embargo, aumenta la rigidez a la torsión. Este efecto es común para secciones transversales triangulares y cuadradas en fase austenítica, pero menos corriente en la fase de transformación, donde la rigidez se muestra menos afectada por el *pitch* (189). Estos resultados coinciden con los obtenidos en estudios previos. Versluis, et al mostraron que la reducción del *pitch* incrementa la eficacia de corte, debido a la mayor rigidez torsional y a la mejor adaptación a la anatomía original del sistema de conductos radiculares, debido a la menor rigidez a la flexión (175). Los resultados obtenidos en este estudio de simulación se refieren a las condiciones establecidas en la ISO 3630; sin embargo, la distribución de las tensiones experimentadas en el interior del instrumental endodóntico rotatorio de NiTi no siempre es comparable con las tensiones sufridas durante su función clínica, ya que la flexión de la lima está condicionada por el contacto con las paredes de dentina radicular, lo que provoca una deformación diferente dependiendo de la curvatura y sección transversal del sistema de conductos radiculares. Roda-Casanova et al mostraron que la tensión máxima generalmente se registra cerca del punto de máxima curvatura del sistema de conductos radiculares y la resistencia a la fatiga depende del radio de curvatura de este; sin embargo, atendiendo a la normativa ISO 3630, el punto de máxima curvatura del instrumental endodóntico rotatorio de NiTi está cerca de la punta de este, por lo que las conclusiones de este estudio son válidas para conductos radiculares con el radio de curvatura ubicado cerca del extremo apical.

PROCESO TERMOMECÁNICO DE FABRICACIÓN DEL INSTRUMENTAL ENDODÓNTICO DE NiTi

Estudios previos han analizado la influencia de la aleación y los procesos termomecánicos de fabricación del instrumental endodóntico rotatorio o

reciprocante de NiTi en la resistencia a la fatiga cíclica. La mayoría de estos estudios coinciden en destacar la microestructura cristalina en fase martensítica como la más resistente a la fatiga por flexión. El estudio **"The Influence of NiTi Alloy on the Cyclic Fatigue Resistance of Endodontic Files"** se comparó la resistencia a la fatiga cíclica de instrumentos endodónticos rotatorios de NiTi convencional (F2 ProTaper Universal, Dentsply Maillefer, Baillagues, Suiza), instrumentos endodónticos rotatorios de NiTi M-Wire (X2, ProTaper Next, Dentsply Maillefer, Baillagues, Suiza), instrumentos endodónticos rotatorios de NiTi CM-Gold Wire (F2, ProTaper Gold, Dentsply Maillefer, Baillagues, Suiza) e instrumentos endodónticos rotatorios de NiTi CM-Blue Wire (ProFile Vortex Blue Dentsply Tulsa Dental, Tulsa, OK, EEUU) y se observó que instrumentos endodónticos rotatorios de NiTi CM-Gold Wire mostró una mayor resistencia a la fatiga cíclica que los instrumentos endodónticos rotatorios sometidos a otros tratamientos termomecánicos (). En este estudio, la resistencia a la fatiga cíclica estática de los instrumentos endodónticos rotatorios ProTaper Universal con aleación de NiTi convencional (1.24 ± 0.21 min) mostró diferencias estadísticamente significativas ($p < 0.001$) respecto a los instrumentos endodónticos rotatorios ProTaper Next con aleación de NiTi M-Wire (2.63 ± 0.58 min). Además, la resistencia a la fatiga cíclica estática de los instrumentos endodónticos rotatorios ProTaper Universal con aleación de NiTi convencional y los instrumentos endodónticos rotatorios ProTaper Gold con aleación de NiTi CM-Gold Wire (3.42 ± 0.85 min) mostró diferencias estadísticamente significativas ($p < 0.001$). Estos sistemas endodónticos rotatorios de NiTi presentan un diseño geométrico similar lo que destaca la influencia de la aleación de NiTi sobre la resistencia a la fatiga cíclica de los instrumentos endodónticos rotatorios de NiTi. Además, la comparación entre la aleación de NiTi CM-Gold Wire y la aleación NiTi CM-Blue Wire (2.86 ± 0.82 min) también mostraron diferencias estadísticamente significativamente ($p < 0.001$). Estos resultados difieren con los resultados de estudios previos que comparan la resistencia a la fatiga cíclica del sistema endodóntico reciprocante Reciproc Blue con la aleación de NiTi CM-Blue Wire con el sistema endodóntico reciprocante Wave One Gold con la aleación de NiTi CM-Gold Wire. La resistencia a la fatiga cíclica del sistema endodóntico reciprocante Reciproc Blue con la aleación de NiTi CM-Blue Wire mostró una

mayor resistencia a la fatiga cíclica que el sistema endodóntico reciprocante Wave One Gold con la aleación de NiTi CM-Gold Wire, probablemente debido al diseño transversal (190, 191). Por otra parte, Arias et al analizaron la influencia del diseño geométrico y cinemática del movimiento reciprocante sobre la resistencia a la fatiga cíclica del sistema endodóntico reciprocante Reciproc con la aleación de NiTi M-Wire con el sistema endodóntico reciprocante Wave One con la aleación de NiTi M-Wire y mostró que el sistema endodóntico reciprocante Reciproc presentaba una resistencia a la fatiga cíclica significativamente mayor ($p < 0.001$) que el sistema endodóntico Wave One (124). Los nuevos tratamientos térmicos aplicados sobre la aleación de NiTi muestran un incremento en la resistencia a la fatiga cíclica en comparación con las aleaciones convencionales de NiTi. Elanghy et al observaron un aumento estadísticamente significativo en la resistencia a la fatiga cíclica ($p < 0.001$) de los instrumentos endodónticos rotatorios ProTaper Next y ProTaper Gold en comparación con las aleaciones de NiTi convencional de TRUShape y ProTaper Universal (192). Así mismo, Uygun et al mostraron resultados similares al comparar ProFile Vortex Blue y ProTaper Next ProTaper Universal (187). Estos resultados concuerdan con los obtenidos en el presente estudio y destacan la relevancia de los elementos aleantes en la transformación de fase de microestructura cristalina de la aleación de NiTi, que a su vez influye en las propiedades físicas y mecánicas del instrumental endodóntico rotatorio (193). Los resultados obtenidos del microanálisis EDX mostraron la presencia de C, O, N y Al en la aleación de NiTi. Además, el peso atómico (%) de los elementos de la aleación mostró una tendencia al alza de la aleación de NiTi convencional de las limas rotatorias de endodoncia ProTaper Universal C (2,17–3,18 % en peso) y O (1,48–1,61 % en peso), a la aleación NiTi M-Wire de las limas rotatorias de endodoncia PTN C (3,31–4,43 % en peso) y Al (0,56–1,39 % en peso), a la aleación NiTi CM-Blue Wire de PVB rotativo endodóntico C (2.26–2.71 wt.%) y O (11.37–13.30 wt.%)), y finalmente a la aleación NiTi CM-Gold Wire de limas rotatorias endodónticas PTG (C (2,11–2,20 % en peso) y O (6,87–7,54 % en peso); lo que conduce a más estructuras cristalinas que son más martensíticas y por lo tanto más flexibles y resistentes a la fractura, lo cual es consistente con el tiempo hasta la fractura observado en el estudio de resistencia a la fatiga cíclica.

TIPO DE MOVIMIENTO (RECIPROCANTE/ROTACIONAL CONTINUO) Y VELOCIDAD DEL INSTRUMENTAL ENDODÓNTICO DE NiTi

El estudio "**Effect of Rotational Speed on the Resistance of NiTi Alloy Endodontic Rotary Files to Cyclic Fatigue—An In Vitro Study**" analizó la velocidad de rotación de los instrumentos endodónticos rotatorios de NiTi sobre su resistencia a la fatiga cíclica dinámica y concluyó que los instrumentos endodónticos reciprocantes de NiTi con movimiento alterno a 350 rpm con 120° en sentido antihorario y 30° en sentido horario (590.38 ± 11.19 seg) muestra una mayor resistencia a la fatiga cíclica dinámica que instrumentos endodónticos reciprocantes de NiTi con movimiento alterno a 400 rpm con 120° en sentido antihorario y 30° en sentido horario (488.44 ± 12.93 seg), los instrumentos endodónticos de NiTi con movimiento rotacional continuo a 200 rpm (364.30 ± 6.71 seg), los instrumentos endodónticos de NiTi con movimiento rotacional continuo a 350 rpm (282.42 ± 7.19 seg) y los instrumentos endodónticos de NiTi con movimiento rotacional continuo a 500 rpm (143.84 ± 5.70 seg); por lo tanto, es aconsejable utilizar movimientos reciprocantes a baja velocidad. (194).

Los resultados derivados del estudio **"Comparative Study of the SEM Evaluation, EDX Assessment, Morphometric Analysis, and Cyclic Fatigue Resistance of Three Novel Brands of NiTi Alloy Endodontic Files"** también demostraron que el emergente sistema de instrumentación endodóntica reciprocante de NiTi "Smarttrack" mostró una resistencia a la fatiga cíclica significativamente superior ($p < 0.001$) a los sistemas de instrumentación endodóntica rotatoria "Endogal" y "Path Max"; sin embargo, estos sistemas de instrumentación endodóntica de NiTi también diferían en su diseño geométrico, así como su composición metalúrgica (195).

Estudios previos han analizado los efectos de la velocidad de rotación sobre la resistencia a la fatiga cíclica del instrumental endodóntico rotatorio y reciprocante de NiTi. Lopes et al sometieron a los instrumentos endodónticos rotatorios de NiTi convencional ProTaper Universal F3 y F4 a 300 y 600 rpm;

sin embargo, los valores de velocidad seleccionados fueron demasiado distantes, se utilizó un tubo cilíndrico como conducto radicular artificial, y la detección del momento de fractura de los instrumentos resultó subjetivo y, por lo tanto, impreciso. Es más, no llevaron a cabo ningún método de medición adicional (196,197). Los resultados derivados del presente estudio indican que la resistencia a la fatiga cíclica del instrumental endodóntico rotatorio de NiTi es inversamente proporcional a la velocidad de rotación. Además, se demostró que los movimientos reciprocantes son más resistentes a la fatiga cíclica en comparación con los movimientos de rotación continuo. Además, los resultados derivados del presente estudio presentan una aplicación directa al entorno clínico, ya que el movimiento reciprocante proporciona una mayor resistencia a la fatiga cíclica, seguida de los valores más bajos de velocidad rotacional continua. Por lo tanto, se recomienda seleccionar sistemas de movimiento reciprocante o reducir la velocidad de rotación continua.

Los hallazgos de este estudio corroboran los hallazgos de Kim et al, quienes observaron que los instrumentos endodónticos reciprocantes de NiTi M-Wire “Reciproc R25” y “WaveOne Primary” fueron más resistentes a la torsión y la fatiga cíclica en comparación con los instrumentos endodónticos rotatorios de NiTi convencional “ProTaper F2” (198). Del mismo modo, De Deus et al observaron que los instrumentos endodónticos rotatorios de NiTi convencional también mostraron una resistencia significativamente mayor a la fatiga cíclica cuando se emplea en movimiento reciprocante en lugar de movimiento rotacional continuo (199). Además, otros estudios han evidenciado un aumento en la vida útil de las limas endodónticas rotatorias de NiTi cuando se usan en movimiento alterno.

Por otro lado, Martín et al relacionaron la incidencia de fractura del instrumental endodóntico de NiTi con la velocidad rotacional, al demostrar que los instrumentos endodónticos rotatorios de NiTi convencional “ProTaper F2” mostraban una menor resistencia a la fractura a 350 rpm que a 250 rpm y a 150 rpm (200). Sin embargo, Gao et al no reportaron diferencias estadísticamente significativas ($p > 0.05$) en las velocidades de rotación (84). Las discrepancias en estos hallazgos pueden deberse a diferencias en el

diseño metodológico de los estudios, diferentes aleaciones de NiTi o diferentes diseños geométricos de los instrumentos. Además, no sólo el movimiento oscilatorio asimétrico en sentido contrario a las agujas del reloj (movimiento alterno), sino también el movimiento oscilatorio asimétrico en el sentido de las agujas del reloj se puede utilizar con cualquier instrumento rotatorio (84).

Ferreira et al demostraron que los movimientos reciprocantes aumentaban la vida útil de los instrumentos endodónticos de NiTi sometidos a fatiga cíclica (201). Olcay et al demostraron que los instrumentos endodónticos reciprocantes de NiTi CM-Gold Wire “Wave One Gold” archivos mostraron diferencias estadísticamente significativas (p = 0.0001) respecto al tiempo a la fractura (239.60 ± 12.84 s) en comparación con los instrumentos endodónticos rotatorios de NiTi M-Wire Protaper Next (161.40 ± 6.68 s) y los instrumentos endodónticos rotatorios de NiTi 2Shape (77.73 ± 2.61 s); sin embargo, se trataba de un análisis de fatiga cíclica estática, con un conducto radicular artificial cilíndrico de 1,5 mm de diámetro y 5 mm de radio de curvatura. Además, los sistemas de instrumentación presentaban diferentes secciones transversales y aleaciones (202). Scott et al analizó la influencia de la aleación metalúrgica en la resistencia a la fatiga cíclica de sistemas reciprocantes, comparando Wave One Primary, Wave One Gold Primary y EdgeFile X1, y concluyó que los instrumentos endodónticos reciprocantes de NiTi fabricados con aleaciones tratadas térmica y mecánicamente mostraron una mejor resistencia a la fatiga cíclica que los instrumentos endodónticos reciprocantes de NiTi fabricados con aleaciones M-Wire; sin embargo, se analizó mediante una prueba estática con un conducto radicular artificial cilíndrico de paredes paralelas y 5 mm de radio de curvatura y diferentes diámetros apicales (203). Al-Obaida et al también compararon la resistencia a la fatiga cíclica de cinco novedosos sistemas endodónticos reciprocantes de NiTi fabricados con tratamiento térmico y mecánico en sistemas de conductos de simple y doble curvatura y demostraron que el sistema de instrumentación reciprocante de NiTi CM-Blue Wire “Reciproc Blue” (421.92 ± 155.09/ 251.25 ± 47.05 s) presentaba una mayor resistencia a la fatiga cíclica ($p < 0.05$), que el sistema de instrumentación reciprocante de NiTi M-Wire “Reciproc” (180.42 ± 35.43/ 160.58 ± 29.98 s), el sistema de instrumentación reciprocante de NiTi CM-Gold

Wire “Wave One Gold” (167.67 ± 26.73/ 122.92 ± 26.54 s) para ambos tipos de conductos radiculares artificiales (204). Alsilani et al declaró que la sección transversal en S “itálica” del sistema de instrumentación endodóntico reciprocante de NiTi “Reciproc” mostró un aumento del tiempo medio hasta la fractura estadísticamente significativa (p < 0.001) tanto en movimiento rotacional continuo como reciprocante (301.13 ± 54.463/ 836.53 ± 67.960 s) en comparación con One Shape (187.73 ± 33.457/ 275.27 ± 58.410 s) y Revo-S SU (116.67 ± 37.663/ 197.60 ± 41.092 s) (205).

Martins et al evaluaron la resistencia a la fatiga cíclica de tres instrumentos endodónticos rotatorios replicados respecto a los originales en rotación continua y reciprocante; concluyendo que los instrumentos endodónticos de NiTi empleados en movimiento alterno muestran una mayor resistencia a la fatiga cíclica que los instrumentos endodónticos de NiTi empleados en rotación continua, y los instrumentos replicados presentan una mayor resistencia a la fatiga cíclica que los instrumentos originales, debido a una temperatura final de transición austenítica más elevada (206).

Siddique et Nivedhitha destacaron que el movimiento reciprocante asociado a los sistemas de lima única ha demostrado aumentar la vida útil de las limas rotatorias endodónticas de NiTi en comparación con el movimiento de rotación continua, lo que aumenta la resistencia a la fatiga cíclica de los instrumentos endodónticos reciprocantes de NiTi (207). El tratamiento termo-mecánico de la aleación de NiTi y el diseño geométrico de estos sistemas de instrumentación podrían contribuir en la flexibilidad y la resistencia a la fatiga cíclica de estos sistemas de instrumentación (208).

Por otro lado, la cinemática del movimiento reciprocante ha sido objeto de desarrollo para incrementar la resistencia a la fatiga cíclica del instrumental endodóntico reciprocante de NiTi, analizando constantemente la resistencia del instrumento en el interior del sistema de conductos y modificando el tipo de giro para permitir su avance y reducir el riesgo de fractura. El estudio “**Influence of the type of reciprocating motion on the cyclic fatigue resistance of reciprocating files in a dynamic model**” analizó la influencia de dos

movimientos reciprocantes novedosos en la resistencia a la fractura del instrumental endodóntico de NiTi, en comparación con un movimiento alterno convencional. Los autores observaron que los movimientos reciprocantes ReFlex Smart y ReFlex Dynamic incrementaron la resistencia a la fatiga cíclica de los instrumentos endodónticos reciprocantes de NiTi convencional (p < 0.001), respecto a un movimiento alterno convencional (209). Esto se debe a la capacidad del micromotor para analizar la resistencia del instrumental endodóntico reciprocante de NiTi en el interior del sistema de conductos radiculares, adaptar su movimiento para reducir la fricción del mismo, aumentando su resistencia a la fractura por fatiga cíclica o torsional. Di Nardo et al compararon la resistencia a la fatiga cíclica de los sistemas de instrumentación endodóntico reciprocante de NiTi “Reziflow” y “Wave One Gold”, y mostró que el instrumental endodóntico reciprocante de NiTi “Reziflow” presentó una resistencia a la fatiga cíclica significativamente mayor (p < 0.05) (50.75 ± 20.06 seg) que el sistema “Wave One Gold” (30.13 ± 9.40 seg); sin embargo, la prueba de fatiga cíclica se llevó a cabo en condiciones estáticas con un conducto radicular artificial de paredes paralelas, un ángulo de curvatura de 90° y un radio de curvatura 5 mm (210).

NÚMERO DE USOS Y CICLOS DE ESTERILIZACIÓN DEL INSTRUMENTAL ENDODÓNTICO DE NiTi

Los instrumentos endodónticos rotatorios de NiTi a menudo se reutilizan en la práctica clínica, a pesar de que los fabricantes desaconsejan esta práctica clínica. El procedimiento de esterilización sigue los pasos de desinfección, limpieza, lavado, secado y envasado (211). Los pasos de desinfección y limpieza reducen la carga bacteriana y eliminan los residuos orgánicos e inorgánicos presentes en el “*flute*” del instrumento. Así mismo, el proceso de esterilización elimina cualquier forma de microorganismo, incluyendo esporas (212). La esterilización por calor constituye el método más utilizado para la esterilización del instrumental odontológico (213) y evitar así la contaminación cruzada entre pacientes (214). Sin embargo, la temperatura alcanzada durante el proceso de esterilización puede afectar a las propiedades físicas y mecánicas del instrumental endodóntico rotatorio de NiTi (215). Valois et al

evidenció un aumento de la rugosidad superficial de los instrumentos endodónticos rotatorios de NiTi tras ser sometidos a ciclos de esterilización, lo que puede conducir a la aparición de fenómenos corrosivos, la reducción de la capacidad de corte y disminuir la resistencia a la fatiga por flexión y por torsión (216). Además, el estudio **"A Novel Digital Technique to Analyze theWear of CM-Wire NiTi Alloy Endodontic Reciprocating Files: An In Vitro Study"** describió una técnica digital basado en la micro-tomografía de haz cónico, para demostrar y cuantificar con precisión de forma repetible (0.00%) y reproducible (0.00%) el desgaste volumétrico del sistema de instrumentación endodóntico reciprocante de NiTi "Reciproc", tras realizar el tratamiento de conductos de diez primeros molares superiores con cuatro conductos radiculares cada uno (217).

Yang et al también observaron un incremento de la rugosidad superficial de los instrumentos endodónticos rotatorios de NiTi "K3XF" tras ser sometidos a procesos de esterilización; sin embargo, no afectó a la resistencia a la fatiga cíclica tras 30 ciclos de esterilización (218). Además, Pedulla et al informaron que los ciclos repetidos de esterilización no influían en la resistencia a la fatiga cíclica del instrumental endodóntico rotatorio de NiTi, salvo para los instrumentos "Twisted File", que mostraron una reducción estadísticamente significativa ($p < 0.05$) de la resistencia a la fatiga cíclica tras someterse a tres ciclos de esterilización (219).

Por otra parte, algunos autores han especulado que la reutilización y la subsiguiente aplicación de ciclos de esterilización del instrumental endodóntico rotatorio de NiTi pueden disminuir la temperatura final de transformación de fase austenítica hasta producirse una transformación de fase austenítica durante el uso clínico (26,41). Sin embargo, otros autores sugieren que el proceso de autoclavado podría implementar las propiedades mecánicas de los instrumentos endodónticos rotatorios de NiTi como un procedimiento térmico adicional. Si embargo, la aleación de NiTi se muestra muy sensible a las tensiones térmicas y mecánicas generadas durante la fabricación del instrumental endodóntico rotatorio de NiTi, las propiedades superelásticas de los instrumentos requieren un control preciso de las temperaturas de

transformación (220). Champa et al mostraron que los instrumentos endodónticos rotatorios de NiTi sometidos a numerosos ciclos de esterilización incrementaban la resistencia a la fatiga cíclica de los instrumentos endodónticos reciprocantes “Reciproc”, pero reducía la resistencia a la fatiga cíclica de los instrumentos endodónticos reciprocantes de NiTi “Wave One” (221). Özyürek et al también documentaron que los ciclos de esterilización también incrementaban significativamente ($p < 0.05$) la resistencia a la fatiga cíclica de los instrumentos endodónticos rotatorios “PrpTaper Next” y “ProTaper Gold” (222). Zhao et al también evidenciaron que los instrumentos endodónticos rotatorios pre-esterilizados “HyFlex CM” y “K3XF” aumentaban significativamente ($p < 0.05$) la resistencia a la fatiga cíclica tras someterse a diez ciclos de esterilización (223).

En resumen, se puede concluir que la mayoría de los instrumentos endodónticos rotatorios de NiTi fabricados en base a una microestructura cristalina con predominio de fase martensítica, incrementan su resistencia a la fatiga cíclica tras ser sometidos a ciclos de esterilización por calor; sin embargo, los resultados derivados del estudio **“Novel Electronic Device to Quantify the Cyclic Fatigue Resistance of Endodontic Reciprocating Files after Using and Sterilization”** demostraron que los instrumentos endodónticos rotatorios de NiTi fabricados en base a una microestructura cristalina con predominio de fase austenítica, reducían su resistencia a la fatiga cíclica tras ser sometidos a diez ciclos de esterilización por calor (224).

Por otra parte, Kim et al recomendaron desechar los instrumentos endodónticos reciprocantes tras su uso, debido a que su uso repetido influye sobre sus propiedades mecánicas y metalúrgicas, aumentando el riesgo de fractura (198). Además, Generali et al observaron diferencias estadísticamente significativas ($p <0.05$) respecto a la resistencia a la fatiga cíclica de los sistemas de instrumentación endodóntica reciprocante de NiTi “Reciproc” y “Reciproc Blue” entes y después de su uso continuado. Así mismo, informaron que el uso continuado de los sistemas de instrumentación endodóntica reciprocante de NiTi “Reciproc” y “Reciproc Blue” reducía el porcentaje de

transformación a fase martensítica y fase R y causaba la aparición de microfracturas cercanas al "*tip*" del instrumento (225).

Sin embargo, Arias et al evidenciaron que la aplicación de rayos gamma y los procesos de esterilización empleados en la fabricación de los sistemas de instrumentación endodóntica rotatoria de NiTi "Hyflex EDM" y "TRUShape" podrían aumentar la vida útil, aumentando su resistencia a la fatiga cíclica (226). Además, Dioguardi et al sugirieron que la técnica de esterilización por calor podría inducir cambios en la microestructura cristalina de los instrumentos endodónticos rotatorios de NiTi que afectaran a las propiedades físicas y mecánicas del instrumental frente a la fatiga por torsión (227).

RADIO Y ÁNGULO DE CURVATURA DEL SISTEMA DE CONDUCTOS RADICULARES

La anatomía del sistema de conductos radiculares constituye un factor determinante en la resistencia a la fatiga cíclica del instrumental endodóntico rotatorio de NiTi.

La mayoría de los autores coinciden en destacar el efecto de la longitud de los radios de curvatura en la resistencia a la fatiga cíclica, así como el efecto de los ángulos de curvatura de los sistemas de conductos radiculares. El estudio de elementos finitos **"Fatigue Analysis of NiTi Rotary Endodontic Files through Finite Element Simulation: Effect of Root Canal Geometry on Fatigue Life**" evaluó la influencia de la geometría del sistema de conductos radiculares en la vida útil de los instrumentos endodónticos rotatorios de NiTi y destacan la importancia del radio de curvatura con respecto al ángulo de curvatura del conducto radicular (228). Este estudio se basó en el estudio **"Computerized Generation and Finite Element Stress Analysis of Endodontic Rotary Files"**, donde se describió un método de simulación basado en análisis matemáticos para analizar el comportamiento mecánico y distribución de stress del instrumental endodóntico rotatorio de NiTi en condiciones de flexión y torsión (229).

VELOCIDAD DEL MOVIMIENTO DE PICOTEO DEL INSTRUMENTAL ENDODÓNTICO DE NiTi

La frecuencia del movimiento de picoteo del instrumental endodóntico rotatorio de NiTi en el interior del sistema de conductos radiculares no ha sido analizado con relación a su influencia sobre la resistencia a la fatiga cíclica del instrumental endodóntico de NiTi. El estudio **"Influence of the Pecking Motion Frequency on the Cyclic Fatigue Resistance of Endodontic Rotary Files**" demostró la asociación entre la frecuencia del movimiento de picoteo realizado por el operador y la resistencia a la fractura del instrumental endodóntico rotatorio de NiTI. Concretamente, se observaron diferencias estadísticamente significativas entre 30 y 60 movimientos por minuto y entre 30 y 120 movimientos por minuto; sin embargo, no se observaron diferencias estadísticamente significativas entre 60 y 120 movimientos por minuto (p = 0.298) (230).

CONCLUSIONS

In conclusion, within the limitations of these studies, our results show that:

1. The variables analized influences on the resistance of the NiTi alloy endodontic instruments to cyclic fatigue.

2. The increased apical diameter and taper of NiTi endodontic rotary files decreased their resistance to cyclic fatigue.

3. The use of files with a triangular-shaped cross-section and a small pitch are recommended in order to minimize ledging and maximize fatigue life.

4. The double S-shaped cross-section of NiTi alloy endodontic files shows higher cyclic fatigue resistance than the rectangular cross-section, the convex triangular cross-section, and the triangular cross-section of NiTi alloy endodontic files.

5. The NiTi CM-Gold wire alloy of the ProTaper Gold endodontic rotary files resulted in greater resistance to cyclic fatigue than ProFile Vortex Blue, ProTaper Next, and ProTaper Universal endodontic rotary files

6. A low frequency of pecking motion is recommended to reduce the risk of failure of endodontic rotary files associated with cyclic fatigue.

7. NiTi alloy endodontic rotary files using reciprocating movement at 350 rpm with 120° counterclockwise and 30° clockwise motion exhibit greater resistance to dynamic cyclic fatigue than files used with a reciprocating movement at 400 rpm with 120° counterclockwise and 30° clockwise motion, continuous rotational speed at 200 rpm, continuous rotational speed at 350 rpm, or continuous rotational speed at 500 rpm; it is therefore advisable to use reciprocating movements at a low speed.

8. The ReFlex Smart reciprocating movement increased the cyclic fatigue resistance of endodontic reciprocating files compared with traditional reciprocating movement.

9. The time of use of NiTi endodontic reciprocating files negatively afects dynamic cyclic fatigue resistance; however, dynamic cyclic resistance is not afected by the number of sterilization cycles.

10. Smarttrack NiTi alloy endodontic reciprocating files display greater resistance to cyclic fatigue than Endogal and Path Max Pro NiTi alloy endodontic rotary files, due to the reciprocating movement and metallurgical composition.

11. Significant influence of the root canal geometry on the fatigue life of the NiTi rotary files and reveal the higher importance of the radius of curvature with respect to the angle of curvature of the root canal.

12. The CM-wire NiTi alloy endodontic reciprocating files exhibit a volumen wear after clinical use.

13. Ultrasonic tips enable greater ease of removal of NiTi endodontic rotary files from the root canal system, with similar amounts of dentin removal between the two methods.

BIBLIOGRAFÍA

1 Brown LJ, Nash KD, Johns BA, Warren M. The economics of endodontics. ADA Health Policy Resources Center Dental Health Policy Analysis Series, Chicago, IL: 2003.

2 Alharmoodi R, Al-Salehi S. Assessment of the quality of endodontic re-treatment and changes in periapical status on a postgraduate endodontic clinic. J Dent. 2020 Jan;92:103261. doi: 10.1016/j.jdent.2019.103261.

3 Huang S, Chen NN, Yu VSH, Lim HA, Lui JN. Long-term Success and Survival of Endodontic Microsurgery. J Endod. 2020 Feb;46(2):149-157.e4. doi: 10.1016/j.joen.2019.10.022.

4 Kolenbrander PE, Palmer RJ Jr, Rickard AH, Jakubovics NS, Chalmers NI, Diaz PI. Bacterial interactions and successions during plaque development. Periodontol 2000. 2006;42:47-79. doi: 10.1111/j.1600-0757.2006.00187.x.

5 Peters L.B., Peterson B., Jaramillo D.E., Van Der Sluis L. The Use of Scanning Electron Microscopy (SEM) in Visualizing the Root Canal Biofilm. Volume 9. Springer Science and Business Media LLC; Heidelberg, Germany: 2015. pp. 87–101.

6 Haapasalo M, Shen Y, Wang Z, Gao Y. Irrigation in endodontics. Br Dent J. 2014 Mar;216(6):299-303. doi: 10.1038/sj.bdj.2014.204.

7 Nair PN. On the causes of persistent apical periodontitis: a review. Int Endod J. 2006 Apr;39(4):249-81. doi: 10.1111/j.1365-2591.2006.01099.x.

8 Siqueira JF Jr, Rôças IN. Polymerase chain reaction-based analysis of microorganisms associated with failed endodontic treatment. Oral Surg Oral Med Oral Pathol Oral Radiol Endod. 2004 Jan;97(1):85-94. doi: 10.1016/s1079-2104(03)00353-6.

9 Gonçalves LS, Rodrigues RC, Andrade Junior CV, Soares RG, Vettore MV. The Effect of Sodium Hypochlorite and Chlorhexidine as Irrigant Solutions for Root Canal Disinfection: A Systematic Review of Clinical Trials. J Endod. 2016 Apr;42(4):527-32. doi: 10.1016/j.joen.2015.12.021

10 Prada I, Micó-Muñoz P, Giner-Lluesma T, Micó-Martínez P, Collado-Castellano N, Manzano-Saiz A. Influence of microbiology on endodontic failure. Literature review. Med Oral Patol Oral Cir Bucal. 2019 May 1;24(3):e364-e372. doi: 10.4317/medoral.22907.

11 Bronzato JD, Bomfim RA, Hayasida GZP, Cúri M, Estrela C, Paster BJ, Gomes BPFA. Analysis of microorganisms in periapical lesions: A systematic review and meta-analysis. Arch Oral Biol. 2021 Apr;124:105055. doi: 10.1016/j.archoralbio.2021.

12 Kirsch J, Basche S, Neunzehn J, Dede M, Dannemann M, Hannig C, Weber MT. Is it really penetration? Locomotion of devitalized Enterococcus faecalis cells within dentinal tubules of bovine teeth. Arch Oral Biol. 2017 Nov;83:289-296. doi: 10.1016/j.archoralbio.2017.08.012.

13 Peters LB, Wesselink PR. Periapical healing of endodontically treated teeth in one and two visits obturated in the presence or absence of detectable microorganisms. Int Endod J. 2002 Aug;35(8):660-7. doi: 10.1046/j.1365-2591.2002.00541.x.

14 Sjögren U, Figdor D, Persson S, Sundqvist G. Influence of infection at the time of root filling on the outcome of endodontic treatment of teeth with apical periodontitis. Int Endod J. 1997 Sep;30(5):297-306. doi: 10.1046/j.1365-2591.1997.00092.x.

15 Plotino G, Özyürek T, Grande NM, Gündoğar M. Influence of size and taper of basic root canal preparation on root canal cleanliness: a scanning electron microscopy study. Int Endod J. 2019 Mar;52(3):343-351. doi: 10.1111/iej.13002.

16 de Gregorio C, Arias A, Navarrete N, Del Rio V, Oltra E, Cohenca N. Effect of apical size and taper on volume of irrigant delivered at working length with apical negative pressure at different root curvatures. J Endod. 2013 Jan;39(1):119-24. doi: 10.1016/j.joen.2012.10.008.

17 Adıgüzel M, Capar ID. Comparison of Cyclic Fatigue Resistance of WaveOne and WaveOne Gold Small, Primary, and Large Instruments. J Endod. 2017 Apr;43(4):623-627. doi: 10.1016/j.joen.2016.11.021.

18 Walia HM, Brantley WA, Gerstein H. An initial investigation of the bending and torsional properties of Nitinol root canal files. J Endod. 1988 Jul;14(7):346-51. doi: 10.1016/s0099-2399(88)80196-1.

19 Thompson SA. An overview of nickel-titanium alloys used in dentistry. Int Endod J. 2000 Jul;33(4):297-310. doi: 10.1046/j.1365-2591.2000.00339.x.

20 Shen Y, Zhou HM, Zheng YF, Peng B, Haapasalo M. Current challenges and concepts of the thermomechanical treatment of nickel-titanium instruments. J Endod. 2013 Feb;39(2):163-72. doi: 10.1016/j.joen.2012.11.005.

21 Gutmann JL, Gao Y. Alteration in the inherent metallic and surface properties of nickel-titanium root canal instruments to enhance performance, durability and safety: a focused review. Int Endod J. 2012 Feb;45(2):113-28. doi: 10.1111/j.1365-2591.2011.01957.x.

22 Pirani C, Cirulli PP, Chersoni S, Micele L, Ruggeri O, Prati C. Cyclic fatigue testing and metallographic analysis of nickel-titanium rotary instruments. J Endod. 2011 Jul;37(7):1013-6. doi: 10.1016/j.joen.2011.04.009.

23 Peters OA, Morgental RD, Schulze KA, Paqué F, Kopper PM, Vier-Pelisser FV. Determining cutting efficiency of nickel-titanium coronal flaring instruments used in lateral action. Int Endod J. 2014 Jun;47(6):505-13. doi: 10.1111/iej.12177.

24 Pongione G, Pompa G, Milana V, Di Carlo S, Giansiracusa A, Nicolini E, De Angelis F. Flexibility and resistance to cyclic fatigue of endodontic instruments made with different nickel-titanium alloys: a comparative test. Ann Stomatol (Roma). 2012 Jul;3(3-4):119-22.

25 Pereira ÉS, Viana AC, Buono VT, Peters OA, Bahia MG. Behavior of nickel-titanium instruments manufactured with different thermal treatments. J Endod. 2015 Jan;41(1):67-71. doi: 10.1016/j.joen.2014.06.005.

26 Shen Y, Zhou HM, Zheng YF, Campbell L, Peng B, Haapasalo M. Metallurgical characterization of controlled memory wire nickel-titanium rotary instruments. J Endod. 2011 Nov;37(11):1566-71. doi: 10.1016/j.joen.2011.08.005.

27 Berutti E, Chiandussi G, Gaviglio I, Ibba A. Comparative analysis of torsional and bending stresses in two mathematical models of nickel-titanium rotary instruments: ProTaper versus ProFile. J Endod. 2003 Jan;29(1):15-9. doi: 10.1097/00004770-200301000-00005.

28 Braga LC, Faria Silva AC, Buono VT, de Azevedo Bahia MG. Impact of heat treatments on the fatigue resistance of different rotary nickel-titanium instruments. J Endod. 2014 Sep;40(9):1494-7. doi: 10.1016/j.joen.2014.03.007

29 Hilfer PB, Bergeron BE, Mayerchak MJ, Roberts HW, Jeansonne BG. Multiple autoclave cycle effects on cyclic fatigue of nickel-titanium rotary files produced by new manufacturing methods. J Endod. 2011 Jan;37(1):72-4. doi: 10.1016/j.joen.2010.09.011..

30 Kuhn G, Tavernier B, Jordan L. Influence of structure on nickel-titanium endodontic instruments failure. J Endod. 2001 Aug;27(8):516-20. doi: 10.1097/00004770-200108000-00005.

31 Otsuka K, Wayman C. Shape Memory Materials. 1 st ed. Cambridge. UK: Cambridge University Press;1998.

32 Ammon D (2014) Endodontic instruments and the methods of manufacturing thereof. US Patent Application 8916009 B2.

33 Choi J, Oh S, Kim YC, Jee KK, Kum K, Chang S. Fracture Resistance of K3 Nickel-Titanium Files Made from Different Thermal Treatments. Bioinorg Chem Appl. 2016;2016:6374721. doi: 10.1155/2016/6374721.

34 Saburi T. Ti-Ni Shape Memory Alloys. En: Otsuka K, Wayman C, eds. Shape Memory Materials. 1 st. ed Cambridge. UK: Cambridge University Press;1998:p.49-96.

35 Miyazaki S, Otsuka K (1986) Deformation and transition behaviour associated with the R Phase in Ti-Ni alloys. Metallurgical and Materials Transactions A 17A, 53– 63.

36 Otsuka K, Ren X (2005) Physical metallurgy of Ti-Ni based shape memory alloys. Progress in Materials Science 50, 511– 678.

37 Zinelis S, Eliades T, Eliades G. A metallurgical characterization of ten endodontic Ni-Ti instruments: assessing the clinical relevance of shape memory and superelastic properties of Ni-Ti endodontic instruments. Int Endod J. 2010 Feb;43(2):125-34. doi: 10.1111/j.1365-2591.2009.01651.x.

38 Santos Lde A, Bahia MG, de Las Casas EB, Buono VT. Comparison of the mechanical behavior between controlled memory and superelastic nickel-titanium files via finite element analysis. J Endod. 2013 Nov;39(11):1444-7. doi: 10.1016/j.joen.2013.07.030.

39 Zupanc J, Vahdat-Pajouh N, Schäfer E. New thermomechanically treated NiTi alloys - a review. Int Endod J. 2018 Oct;51(10):1088-1103. doi: 10.1111/iej.12924.

40 Perez- Higueras JJ, Arias A, de la Macorra JC. Análisis de los factores que influyen en la resistencia de los instrumentos de níquel-titanio a la fatiga cíclica flexural (tesis doctoral). Universidad Complutense de Madrid, Madrid, España. 2016.

41 Testarelli L, Plotino G, Al-Sudani D, Vincenzi V, Giansiracusa A, Grande NM, Gambarini G. Bending properties of a new nickel-titanium alloy with a lower percent by weight of nickel. J Endod. 2011 Sep;37(9):1293-5. doi: 10.1016/j.joen.2011.05.023.

42 Yoneyama T, Doi H, Kobayashi E, Hamanaka H. Super-elastic property of Ti-Ni alloy for use in dentistry. Front Med Biol Eng. 2000;10(2):97-103. doi: 10.1163/15685570052061955.

43 Miyai K, Ebihara A, Hayashi Y, Doi H, Suda H, Yoneyama T. Influence of phase transformation on the torsional and bending properties of nickel-titanium rotary endodontic instruments. Int Endod J. 2006 Feb;39(2):119-26. doi: 10.1111/j.1365-2591.2006.01055.x.

44 Yahata Y, Yoneyama T, Hayashi Y, Ebihara A, Doi H, Hanawa T, Suda H. Effect of heat treatment on transformation temperatures and bending properties of nickel-titanium endodontic instruments. Int Endod J. 2009 Jul;42(7):621-6. doi: 10.1111/j.1365-2591.2009.01563.x.

45 Zinelis S, Darabara M, Takase T, Ogane K, Papadimitriou GD. The effect of thermal treatment on the resistance of nickel-titanium rotary files in cyclic fatigue. Oral Surg Oral Med Oral Pathol Oral Radiol Endod. 2007 Jun;103(6):843-7. doi: 10.1016/j.tripleo.2006.12.026.

46 Brantley WA, Svec TA, Iijima M, Powers JM, Grentzer TH. Differential scanning calorimetric studies of nickel titanium rotary endodontic instruments. J Endod. 2002 Aug;28(8):567-72. doi: 10.1097/00004770-200208000-00001.

47 Berendt C (2007). Method of preparing Nitinol for use in manufacturing instruments with improved fatigue resistance. US Patent Application 20070072147 A1.

48 Pereira ES, Peixoto IF, Viana AC, Oliveira II, Gonzalez BM, Buono VT, Bahia MG. Physical and mechanical properties of a thermomechanically treated NiTi wire used in the manufacture of rotary endodontic instruments. Int Endod J. 2012 May;45(5):469-74. doi: 10.1111/j.1365-2591.2011.01998.x.

49 Zhou, H., Peng, B. and Zheng, Y.-F. (2013), An overview of the mechanical properties of nickel–titanium endodontic instruments. Endod Topics, 29: 42-54. https://doi.org/10.1111/etp.12045

50 Bonaccorso A, Tripi TR, Rondelli G, Condorelli GG, Cantatore G, Schäfer E. Pitting corrosion resistance of nickel-titanium rotary instruments with different surface treatments in seventeen percent ethylenediaminetetraacetic Acid and sodium chloride solutions. J Endod. 2008 Feb;34(2):208-11. doi: 10.1016/j.joen.2007.11.012.

51 Lopes HP, Elias CN, Vieira MV, Vieira VT, de Souza LC, Dos Santos AL. Influence of Surface Roughness on the Fatigue Life of Nickel-Titanium Rotary Endodontic Instruments. J Endod. 2016 Jun;42(6):965-8. doi: 10.1016/j.joen.2016.03.001.

52 Silva EJNL, Giraldes JFN, de Lima CO, Vieira VTL, Elias CN, Antunes HS. Influence of heat treatment on torsional resistance and surface roughness of nickel-titanium instruments. Int Endod J. 2019 Nov;52(11):1645-1651. doi: 10.1111/iej.13164.

53 Anderson ME, Price JW, Parashos P. Fracture resistance of electropolished rotary nickel-titanium endodontic instruments. J Endod. 2007 Oct;33(10):1212-6. doi: 10.1016/j.joen.2007.07.007.

54 Condorelli GG, Bonaccorso A, Smecca E, Schäfer E, Cantatore G, Tripi TR. Improvement of the fatigue resistance of NiTi endodontic files by surface and bulk modifications. Int Endod J. 2010 Oct;43(10):866-73. doi: 10.1111/j.1365-2591.2010.01759.x

55 Praisarnti C, Chang JW, Cheung GS. Electropolishing enhances the resistance of nickel-titanium rotary files to corrosion-fatigue failure in hypochlorite. J Endod. 2010 Aug;36(8):1354-7. doi: 10.1016/j.joen.2010.02.025.

56 Gambarini G, Grande NM, Plotino G, Somma F, Garala M, De Luca M, Testarelli L. Fatigue resistance of engine-driven rotary nickel-titanium instruments produced by new manufacturing methods. J Endod. 2008 Aug;34(8):1003-5. doi: 10.1016/j.joen.2008.05.007.

57 Alapati SB, Brantley WA, Iijima M, Clark WA, Kovarik L, Buie C, Liu J, Ben Johnson W. Metallurgical characterization of a new nickel-titanium wire for

rotary endodontic instruments. J Endod. 2009 Nov;35(11):1589-93. doi: 10.1016/j.joen.2009.08.004.

58 Braga LC, Magalhães RR, Nakagawa RK, Puente CG, Buono VT, Bahia MG. Physical and mechanical properties of twisted or ground nickel-titanium instruments. Int Endod J. 2013 May;46(5):458-65. doi: 10.1111/iej.12011.

59 de Vasconcelos RA, Murphy S, Carvalho CA, Govindjee RG, Govindjee S, Peters OA. Evidence for Reduced Fatigue Resistance of Contemporary Rotary Instruments Exposed to Body Temperature. J Endod. 2016 May;42(5):782-7. doi: 10.1016/j.joen.2016.01.025.

60 Hieawy A, Haapasalo M, Zhou H, Wang ZJ, Shen Y. Phase Transformation Behavior and Resistance to Bending and Cyclic Fatigue of ProTaper Gold and ProTaper Universal Instruments. J Endod. 2015 Jul;41(7):1134-8. doi: 10.1016/j.joen.2015.02.030.

61 Johnson E, Lloyd A, Kuttler S, Namerow K. Comparison between a novel nickel-titanium alloy and 508 nitinol on the cyclic fatigue life of ProFile 25/.04 rotary instruments. J Endod. 2008 Nov;34(11):1406-1409. doi: 10.1016/j.joen.2008.07.029.

62 Montalvão D, Alçada FS. Numeric comparison of the static mechanical behavior between ProFile GT and ProFile GT series X rotary nickel-titanium files. J Endod. 2011 Aug;37(8):1158-61. doi: 10.1016/j.joen.2011.05.018.

63 Larsen CM, Watanabe I, Glickman GN, He J. Cyclic fatigue analysis of a new generation of nickel titanium rotary instruments. J Endod. 2009 Mar;35(3):401-3. doi: 10.1016/j.joen.2008.12.010.

64 Hou X, Yahata Y, Hayashi Y, Ebihara A, Hanawa T, Suda H. Phase transformation behaviour and bending property of twisted nickel-titanium endodontic instruments. Int Endod J. 2011 Mar;44(3):253-8. doi: 10.1111/j.1365-2591.2010.01818.x.

65 Wu SK, Lin HC, Chou TS A study of electrical resistivity, internal friction and shear modulus on an aged Ti49Ni51 alloy. Acta Metallurgica et Materialia. 1990; 38(1):95-102. doi.org/10.1016/0956-7151(90)90137-6.

66 Zhou HM, Shen Y, Zheng W, Li L, Zheng YF, Haapasalo M. Mechanical properties of controlled memory and superelastic nickel-titanium wires used in

the manufacture of rotary endodontic instruments. J Endod. 2012 Nov;38(11):1535-40. doi: 10.1016/j.joen.2012.07.006.

67 Iacono F, Pirani C, Generali L, Bolelli G, Sassatelli P, Lusvarghi L, Gandolfi MG, Giorgini L, Prati C. Structural analysis of HyFlex EDM instruments. Int Endod J. 2017 Mar;50(3):303-313. doi: 10.1111/iej.12620.

68 Goo HJ, Kwak SW, Ha JH, Pedullà E, Kim HC. Mechanical Properties of Various Heat-treated Nickel-titanium Rotary Instruments. J Endod. 2017 Nov;43(11):1872-1877. doi: 10.1016/j.joen.2017.05.025.

69 Soares RG, Lopes HP, Elias CN, et al. (2017) Comparative study of the mechanical properties of instruments made of conventional, M-wire, R-phase, and controlled memory nickel-titanium alloys. ENDO – Endodontic Practice Today 11, 271– 7.

70 Morgental RD, Vier-Pelisser FV, Kopper PM, de Figueiredo JA, Peters OA. Cutting efficiency of conventional and martensitic nickel-titanium instruments for coronal flaring. J Endod. 2013 Dec;39(12):1634-8. doi: 10.1016/j.joen.2013.08.016.

71 Shen Y, Qian W, Abtin H, Gao Y, Haapasalo M. Effect of environment on fatigue failure of controlled memory wire nickel-titanium rotary instruments. J Endod. 2012 Mar;38(3):376-80. doi: 10.1016/j.joen.2011.12.002.

72 Shen Y, Qian W, Abtin H, Gao Y, Haapasalo M. Fatigue testing of controlled memory wire nickel-titanium rotary instruments. J Endod. 2011 Jul;37(7):997-1001. doi: 10.1016/j.joen.2011.03.023.

73 Plotino G, Testarelli L, Al-Sudani D, Pongione G, Grande NM, Gambarini G. Fatigue resistance of rotary instruments manufactured using different nickel-titanium alloys: a comparative study. Odontology. 2014 Jan;102(1):31-5. doi: 10.1007/s10266-012-0088-8.

74 Daneshmand, Saeed & Farahmand, Ehsan & Abedi, Esmail & Abdolhosseini, M.. (2013). Influence of Machining Parameters on Electro Discharge Machining of NiTi Shape Memory Alloys. International Journal of Electrochemical Science. 8. 3095-3104.

75 Singh, Shankar & Maheshwari, Sachin & Pandey, P.C.. (2004). Some investigations into the electric discharge machining of hardened tool steel using

different electrode materials. Journal of Materials Processing Technology. 149. 272-277. 10.1016/j.jmatprotec.2003.11.046.

76 Uslu G, Özyürek T, Yılmaz K. Comparison of Alterations in the Surface Topographies of HyFlex CM and HyFlex EDM Nickel-titanium Files after Root Canal Preparation: A Three-dimensional Optical Profilometry Study. J Endod. 2018 Jan;44(1):115-119. doi: 10.1016/j.joen.2017.05.023.

77 Pirani C, Iacono F, Generali L, Sassatelli P, Nucci C, Lusvarghi L, Gandolfi MG, Prati C. HyFlex EDM: superficial features, metallurgical analysis and fatigue resistance of innovative electro discharge machined NiTi rotary instruments. Int Endod J. 2016 May;49(5):483-93. doi: 10.1111/iej.12470.

78 Kaval ME, Capar ID, Ertas H. Evaluation of the Cyclic Fatigue and Torsional Resistance of Novel Nickel-Titanium Rotary Files with Various Alloy Properties. J Endod. 2016 Dec;42(12):1840-1843. doi: 10.1016/j.joen.2016.07.015.

79 Pinheiro SR, Alcalde MP, Vivacqua-Gomes N, Bramante CM, Vivan RR, Duarte MAH, Vasconcelos BC. Evaluation of apical transportation and centring ability of five thermally treated NiTi rotary systems. Int Endod J. 2018 Jun;51(6):705-713. doi: 10.1111/iej.12881.

80 Venino PM, Citterio CL, Pellegatta A, Ciccarelli M, Maddalone M. A Micro-computed Tomography Evaluation of the Shaping Ability of Two Nickel-titanium Instruments, HyFlex EDM and ProTaper Next. J Endod. 2017 Apr;43(4):628-632. doi: 10.1016/j.joen.2016.11.022.

81 Hu W, Whitten B, Sedgley C, Svec T. Effect of three NiTi files on transportation of the apical foramen. Int Endod J. 2014 Nov;47(11):1064-71. doi: 10.1111/iej.12249.

82 Pereira ES, Peixoto IF, Viana AC, Oliveira II, Gonzalez BM, Buono VT, Bahia MG. Physical and mechanical properties of a thermomechanically treated NiTi wire used in the manufacture of rotary endodontic instruments. Int Endod J. 2012 May;45(5):469-74. doi: 10.1111/j.1365-2591.2011.01998.x

83 Nguyen HH, Fong H, Paranjpe A, Flake NM, Johnson JD, Peters OA. Evaluation of the resistance to cyclic fatigue among ProTaper Next, ProTaper Universal, and Vortex Blue rotary instruments. J Endod. 2014 Aug;40(8):1190-3. doi: 10.1016/j.joen.2013.12.033.

84 Gao Y, Shotton V, Wilkinson K, Phillips G, Johnson WB. Effects of raw material and rotational speed on the cyclic fatigue of ProFile Vortex rotary instruments. J Endod. 2010 Jul;36(7):1205-9. doi: 10.1016/j.joen.2010.02.015

85 Duke F, Shen Y, Zhou H, Ruse ND, Wang ZJ, Hieawy A, Haapasalo M. Cyclic Fatigue of ProFile Vortex and Vortex Blue Nickel-Titanium Files in Single and Double Curvatures. J Endod. 2015 Oct;41(10):1686-90. doi: 10.1016/j.joen.2015.06.012.

86 Gündoğar M, Özyürek T. Cyclic Fatigue Resistance of OneShape, HyFlex EDM, WaveOne Gold, and Reciproc Blue Nickel-titanium Instruments. J Endod. 2017 Jul;43(7):1192-1196. doi: 10.1016/j.joen.2017.03.009.

87 Eleftheriadis GI, Lambrianidis TP. Technical quality of root canal treatment and detection of iatrogenic errors in an undergraduate dental clinic. Int Endod J. 2005 Oct;38(10):725-34. doi: 10.1111/j.1365-2591.2005.01008.x.

88 Hendi SS, Karkehabadi H, Eskandarloo A. Iatrogenic Errors during Root Canal Instrumentation Performed by Dental Students. Iran Endod J. 2018 Winter;13(1):126-131. doi: 10.22037/iej.v13i1.18507.

89 Ruddle CJ, Machtou P, West JD. The shaping movement: fifth-generation technology. Dent Today. 2013 Apr;32(4):94, 96-9.

90 Topçuoğlu HS, Topçuoğlu G. Cyclic Fatigue Resistance of Reciproc Blue and Reciproc Files in an S-shaped Canal. J Endod. 2017 Oct;43(10):1679-1682. doi: 10.1016/j.joen.2017.04.009.

91 Silva EJNL, Hecksher F, Antunes HDS, De-Deus G, Elias CN, Vieira VTL. Torsional Fatigue Resistance of Blue-treated Reciprocating Instruments. J Endod. 2018 Jun;44(6):1038-1041. doi: 10.1016/j.joen.2018.03.005.

92 Kabil E, Katić M, Anić I, Bago I. Micro-computed Evaluation of Canal Transportation and Centering Ability of 5 Rotary and Reciprocating Systems with Different Metallurgical Properties and Surface Treatments in Curved Root Canals. J Endod. 2021 Mar;47(3):477-484. doi: 10.1016/j.joen.2020.11.003.

93 Drukteinis S, Peciuliene V, Dummer PMH, Hupp J. Shaping ability of BioRace, ProTaper NEXT and Genius nickel-titanium instruments in curved canals of mandibular molars: a MicroCT study. Int Endod J. 2019 Jan;52(1):86-93. doi: 10.1111/iej.12961.

94 da Silva Limoeiro AG, Dos Santos AH, De Martin AS, Kato AS, Fontana CE, Gavini G, Freire LG, da Silveira Bueno CE. Micro-Computed Tomographic Evaluation of 2 Nickel-Titanium Instrument Systems in Shaping Root Canals. J Endod. 2016 Mar;42(3):496-9. doi: 10.1016/j.joen.2015.12.007.

95 Kyaw Moe MM, Ha JH, Jin MU, Kim YK, Kim SK. Root Canal Shaping Effect of Instruments with Offset Mass of Rotation in the Mandibular First Molar: A Micro-computed Tomographic Study. J Endod. 2018 May;44(5):822-827. doi: 10.1016/j.joen.2017.11.012.

96 Yılmaz F, Eren İ, Eren H, Badi MA, Ocak M, Çelik HH. Evaluation of the Amount of Root Canal Dentin Removed and Apical Transportation Occurrence after Instrumentation with ProTaper Next, OneShape, and EdgeFile Rotary Systems. J Endod. 2020 May;46(5):662-667. doi: 10.1016/j.joen.2020.01.022.

97 Yuan G, Yang G. Comparative evaluation of the shaping ability of single-file system versus multi-file system in severely curved root canals. J Dent Sci. 2018 Mar;13(1):37-42. doi: 10.1016/j.jds.2017.09.005.

98 Ahn SY, Kim HC, Kim E. Kinematic Effects of Nickel-Titanium Instruments with Reciprocating or Continuous Rotation Motion: A Systematic Review of In Vitro Studies. J Endod. 2016 Jul;42(7):1009-17. doi: 10.1016/j.joen.2016.04.002.

99 Wu MK, Fan B, Wesselink PR. Leakage along apical root fillings in curved root canals. Part I: effects of apical transportation on seal of root fillings. J Endod. 2000 Apr;26(4):210-6. doi: 10.1097/00004770-200004000-00003.

100 Parashos P, Messer HH. Rotary NiTi instrument fracture and its consequences. J Endod. 2006 Nov;32(11):1031-43. doi: 10.1016/j.joen.2006.06.008.

101 Iqbal MK, Kohli MR, Kim JS. A retrospective clinical study of incidence of root canal instrument separation in an endodontics graduate program: a PennEndo database study. J Endod. 2006 Nov;32(11):1048-52. doi: 10.1016/j.joen.2006.03.001.

102 Spili P, Parashos P, Messer HH. The impact of instrument fracture on outcome of endodontic treatment. J Endod. 2005 Dec;31(12):845-50. doi: 10.1097/01.don.0000164127.62864.7c.

103 Madarati AA, Watts DC, Qualtrough AJ. Factors contributing to the separation of endodontic files. Br Dent J. 2008 Mar 8;204(5):241-5. doi: 10.1038/bdj.2008.152.

104 Sattapan B, Nervo GJ, Palamara JE, Messer HH. Defects in rotary nickel-titanium files after clinical use. J Endod. 2000 Mar;26(3):161-5. doi: 10.1097/00004770-200003000-00008.

105 McGuigan MB, Louca C, Duncan HF. Endodontic instrument fracture: causes and prevention. Br Dent J. 2013 Apr;214(7):341-8. doi: 10.1038/sj.bdj.2013.324.

106 Alcalde MP, Duarte MAH, Bramante CM, de Vasconselos BC, Tanomaru-Filho M, Guerreiro-Tanomaru JM, Pinto JC, Só MVR, Vivan RR. Cyclic fatigue and torsional strength of three different thermally treated reciprocating nickel-titanium instruments. Clin Oral Investig. 2018 May;22(4):1865-1871. doi: 10.1007/s00784-017-2295-8.

107 Cheung GS, Peng B, Bian Z, Shen Y, Darvell BW. Defects in ProTaper S1 instruments after clinical use: fractographic examination. Int Endod J. 2005 Nov;38(11):802-9. doi: 10.1111/j.1365-2591.2005.01020.x.

108 Hull D. Fractography: Observing, Measuring and Interpreting Fracture Surface Topography. Cambridge, UK: Cambridge University Press; 1999.

109 Bahia MG, Buono VT. Decrease in the fatigue resistance of nickel-titanium rotary instruments after clinical use in curved root canals. Oral Surg Oral Med Oral Pathol Oral Radiol Endod. 2005 Aug;100(2):249-55. doi: 10.1016/j.tripleo.2004.10.013.

110 Chaves Craveiro de Melo M, Guiomar de Azevedo Bahia M, Lopes Buono VT. Fatigue resistance of engine-driven rotary nickel-titanium endodontic instruments. J Endod. 2002 Nov;28(11):765-9. doi: 10.1097/00004770-200211000-00005.

111 Borgula L. Rotary nickel-titanium instrument fracture: an experimental and SEMbased analysis. [D Clin Dent (Endo)]. Melbourne: University of Melbourne, 2005.

112 Yared G, Kulkarni GK, Ghossayn F. An in vitro study of the torsional properties of new and used K3 instruments. Int Endod J. 2003 Nov;36(11):764-9. doi: 10.1046/j.1365-2591.2003.00732.x.

113 Guilford WL, Lemons JE, Eleazer PD. A comparison of torque required to fracture rotary files with tips bound in simulated curved canal. J Endod. 2005 Jun;31(6):468-70. doi: 10.1097/01.don.0000148867.30520.9e.

114 Haïkel Y, Serfaty R, Bateman G, Senger B, Allemann C. Dynamic and cyclic fatigue of engine-driven rotary nickel-titanium endodontic instruments. J Endod. 1999 Jun;25(6):434-40. doi: 10.1016/S0099-2399(99)80274-X.

115 Pruett JP, Clement DJ, Carnes DL Jr. Cyclic fatigue testing of nickel-titanium endodontic instruments. J Endod. 1997 Feb;23(2):77-85. doi: 10.1016/S0099-2399(97)80250-6.

116 Ehrhardt IC, Zuolo ML, Cunha RS, De Martin AS, Kherlakian D, Carvalho MC, Bueno CE. Assessment of the separation incidence of mtwo files used with preflaring: prospective clinical study. J Endod. 2012 Aug;38(8):1078-81. doi: 10.1016/j.joen.2012.05.001.

117 Inan U, Gonulol N. Deformation and fracture of Mtwo rotary nickel-titanium instruments after clinical use. J Endod. 2009 Oct;35(10):1396-9. doi: 10.1016/j.joen.2009.06.014.

118 Gambarini G, Gerosa R, De Luca M, Garala M, Testarelli L. Mechanical properties of a new and improved nickel-titanium alloy for endodontic use: an evaluation of file flexibility. Oral Surg Oral Med Oral Pathol Oral Radiol Endod. 2008 Jun;105(6):798-800. doi: 10.1016/j.tripleo.2008.02.017.

119 Ullmann CJ, Peters OA. Effect of cyclic fatigue on static fracture loads in ProTaper nickel-titanium rotary instruments. J Endod. 2005 Mar;31(3):183-6. doi: 10.1097/01.don.0000137641.87125.8f.

120 Schäfer E, Dzepina A, Danesh G. Bending properties of rotary nickel-titanium instruments. Oral Surg Oral Med Oral Pathol Oral Radiol Endod. 2003 Dec;96(6):757-63. doi: 10.1016/s1079-2104(03)00358-5.

121 Grande NM, Plotino G, Pecci R, Bedini R, Malagnino VA, Somma F. Cyclic fatigue resistance and three-dimensional analysis of instruments from two nickel-titanium rotary systems. Int Endod J. 2006 Oct;39(10):755-63. doi: 10.1111/j.1365-2591.2006.01143.x.

122 Ye J, Gao Y. Metallurgical characterization of M-Wire nickel-titanium shape memory alloy used for endodontic rotary instruments during low-cycle fatigue. J Endod. 2012 Jan;38(1):105-7. doi: 10.1016/j.joen.2011.09.028.

123 Arias A, Perez-Higueras JJ, de la Macorra JC. Influence of clinical usage of GT and GTX files on cyclic fatigue resistance. Int Endod J. 2014 Mar;47(3):257-63. doi: 10.1111/iej.12141.

124 Pérez-Higueras JJ, Arias A, de la Macorra JC, Peters OA. Differences in cyclic fatigue resistance between ProTaper Next and ProTaper Universal instruments at different levels. J Endod. 2014 Sep;40(9):1477-81. doi: 10.1016/j.joen.2014.02.025.

125 Johnson E, Lloyd A, Kuttler S, Namerow K. Comparison between a novel nickel-titanium alloy and 508 nitinol on the cyclic fatigue life of ProFile 25/.04 rotary instruments. J Endod. 2008 Nov;34(11):1406-1409. doi: 10.1016/j.joen.2008.07.029.

126 Ninan E, Berzins DW. Torsion and bending properties of shape memory and superelastic nickel-titanium rotary instruments. J Endod. 2013 Jan;39(1):101-4. doi: 10.1016/j.joen.2012.08.010.

127 Aminsobhani M, Meraji N, Sadri E. Comparison of Cyclic Fatigue Resistance of Five Nickel Titanium Rotary File Systems with Different Manufacturing Techniques. J Dent (Tehran). 2015 Sep;12(9):636-46.

128 Li UM, Lee BS, Shih CT, Lan WH, Lin CP. Cyclic fatigue of endodontic nickel titanium rotary instruments: static and dynamic tests. J Endod. 2002 Jun;28(6):448-51. doi: 10.1097/00004770-200206000-00007.

129 Zelada G, Varela P, Martín B, Bahíllo JG, Magán F, Ahn S. The effect of rotational speed and the curvature of root canals on the breakage of rotary endodontic instruments. J Endod. 2002 Jul;28(7):540-2. doi: 10.1097/00004770-200207000-00014.

130 Poulsen WB, Dove SB, del Rio CE. Effect of nickel-titanium engine-driven instrument rotational speed on root canal morphology. J Endod. 1995 Dec;21(12):609-12. doi: 10.1016/S0099-2399(06)81113-1.

131 Dietz DB, Di Fiore PM, Bahcall JK, Lautenschlager EP. Effect of rotational speed on the breakage of nickel-titanium rotary files. J Endod. 2000 Feb;26(2):68-71. doi: 10.1097/00004770-200002000-00002.

132 Yared GM, Bou Dagher FE, Machtou P. Influence of rotational speed, torque and operator's proficiency on ProFile failures. Int Endod J. 2001 Jan;34(1):47-53. doi: 10.1046/j.1365-2591.2001.00352.x.

133 Fife D, Gambarini G, Britto Lr Lr. Cyclic fatigue testing of ProTaper NiTi rotary instruments after clinical use. Oral Surg Oral Med Oral Pathol Oral Radiol Endod. 2004 Feb;97(2):251-6. doi: 10.1016/j.tripleo.2003.08.010.

134 Gambarini G. Cyclic fatigue of ProFile rotary instruments after prolonged clinical use. Int Endod J. 2001 Jul;34(5):386-9. doi: 10.1046/j.1365-2591.2001.00259.x.

135 Svec TA, Powers JM. The deterioration of rotary nickel-titanium files under controlled conditions. J Endod. 2002 Feb;28(2):105-7. doi: 10.1097/00004770-200202000-00014.

136 Yared GM, Bou Dagher FE, Machtou P. Cyclic fatigue of ProFile rotary instruments after clinical use. Int Endod J. 2000 May;33(3):204-7. doi: 10.1046/j.1365-2591.1999.00296.x.

137 Alexandrou GB, Chrissafis K, Vasiliadis LP, Pavlidou E, Polychroniadis EK. SEM observations and differential scanning calorimetric studies of new and sterilized nickel-titanium rotary endodontic instruments. J Endod. 2006 Jul;32(7):675-9. doi: 10.1016/j.joen.2006.01.003.

138 Zhao D, Shen Y, Peng B, Haapasalo M. Effect of autoclave sterilization on the cyclic fatigue resistance of thermally treated Nickel-Titanium instruments. Int Endod J. 2016 Oct;49(10):990-5. doi: 10.1111/iej.12550.

139 Hayashi Y, Yoneyama T, Yahata Y, Miyai K, Doi H, Hanawa T, et al. Phase transformation behaviour and bending properties of hybrid nickel-titanium rotary endodontic instruments. Int Endod J. 2007;40:247-53.

140 Plotino G, Costanzo A, Grande NM, Petrovic R, Testarelli L, Gambarini G. Experimental evaluation on the influence of autoclave sterilization on the cyclic fatigue of new nickel-titanium rotary instruments. J Endod. 2012 Feb;38(2):222-5. doi: 10.1016/j.joen.2011.10.017.

141 Plotino G, Grande NM, Cordaro M, Testarelli L, Gambarini G. A review of cyclic fatigue testing of nickel-titanium rotary instruments. J Endod. 2009 Nov;35(11):1469-76. doi: 10.1016/j.joen.2009.06.015.

142 Booth JR, Scheetz JP, Lemons JE, Eleazer PD. A comparison of torque required to fracture three different nickel-titanium rotary instruments around curves of the same angle but of different radius when bound at the tip. J Endod. 2003 Jan;29(1):55-7. doi: 10.1097/00004770-200301000-00015.

143 Best S, Watson P, Pilliar R, Kulkarni GG, Yared G. Torsional fatigue and endurance limit of a size 30.06 ProFile rotary instrument. Int Endod J. 2004 Jun;37(6):370-3. doi: 10.1111/j.1365-2591.2004.00814.x.

144 Ferrer-Luque CM, Perez-Heredia M, Baca P, Arias-Moliz MT, González-Rodríguez MP. Decalcifying effects of antimicrobial irrigating solutions on root canal dentin. Med Oral Patol Oral Cir Bucal. 2013 Jan 1;18(1):e158-61. doi: 10.4317/medoral.18207.

145 Retamozo B, Shabahang S, Johnson N, Aprecio RM, Torabinejad M. Minimum contact time and concentration of sodium hypochlorite required to eliminate Enterococcus faecalis. J Endod. 2010 Mar;36(3):520-3. doi: 10.1016/j.joen.2009.12.005.

146 Stokes OW, Fiore PM, Barss JT, Koerber A, Gilbert JL, Lautenschlager EP. Corrosion in stainless-steel and nickel-titanium files. J Endod. 1999 Jan;25(1):17-20. doi: 10.1016/s0099-2399(99)80392-6.

147 Haïkel Y, Serfaty R, Wilson P, Speisser JM, Allemann C. Mechanical properties of nickel-titanium endodontic instruments and the effect of sodium hypochlorite treatment. J Endod. 1998 Nov;24(11):731-5. doi: 10.1016/S0099-2399(98)80163-5.

148 La Rosa GRM, Shumakova V, Isola G, Indelicato F, Bugea C, Pedullà E. Evaluation of the Cyclic Fatigue of Two Single Files at Body and Room Temperature with Different Radii of Curvature. Materials (Basel). 2021 Apr 27;14(9):2256. doi: 10.3390/ma14092256.

149 Plotino G, Grande NM, Mercadé Bellido M, Testarelli L, Gambarini G. Influence of Temperature on Cyclic Fatigue Resistance of ProTaper Gold and ProTaper Universal Rotary Files. J Endod. 2017 Feb;43(2):200-202. doi: 10.1016/j.joen.2016.10.014.

150 Dobrzański, L.A.; Dobrzański, L.B.; Dobrzańska-Danikiewicz, A.D.; Dobrzańska, J. Nitinol Type Alloys General Characteristics and Applications in Endodontics. Processes 2022, 10, 101. https://doi.org/10.3390/pr10010101.

151 Siqueira JF Jr, Rôças IN. Polymerase chain reaction-based analysis of microorganisms associated with failed endodontic treatment. Oral Surg Oral Med Oral Pathol Oral Radiol Endod. 2004 Jan;97(1):85-94. doi: 10.1016/s1079-2104(03)00353-6.

152 Strindberg, Lars Z. The Dependence of the Results of Pulp Therapy on Certain Factors: An Analytic Study Based on Radiographic and Clinical Follow-Up Examinations. [tr. from the Swedish Manuscript]. Stockholm, 1956.

153 Topçuoğlu HS, Topçuoğlu G. Cyclic Fatigue Resistance of Reciproc Blue and Reciproc Files in an S-shaped Canal. J Endod. 2017 Oct;43(10):1679-1682. doi: 10.1016/j.joen.2017.04.009.

154 Strindberg, L. The dependence of the results of pulp therapy on certain factors. Acta Odontol. Scand. 1956, 14, 1–175.

155 Siqueira JF Jr. Aetiology of root canal treatment failure: why well-treated teeth can fail. Int Endod J. 2001 Jan;34(1):1-10. doi: 10.1046/j.1365-2591.2001.00396.x.

156 Yang Q, Shen Y, Huang D, Zhou X, Gao Y, Haapasalo M. Evaluation of Two Trephine Techniques for Removal of Fractured Rotary Nickel-titanium Instruments from Root Canals. J Endod. 2017 Jan;43(1):116-120. doi: 10.1016/j.joen.2016.09.001.

157 Sjögren U, Figdor D, Persson S, Sundqvist G. Influence of infection at the time of root filling on the outcome of endodontic treatment of teeth with apical periodontitis. Int Endod J. 1997 Sep;30(5):297-306. doi: 10.1046/j.1365-2591.1997.00092.x.

158 Madarati AA, Hunter MJ, Dummer PM. Management of intracanal separated instruments. J Endod. 2013 May;39(5):569-81. Doi: 10.1016/j.joen.2012.12.033.

159 Fu M, Zhang Z, Hou B. Removal of broken files from root canals by using ultrasonic techniques combined with dental microscope: a retrospective analysis of treatment outcome. J Endod. 2011 May;37(5):619-22. doi: 10.1016/j.joen.2011.02.016.

160 Yoldas O, Oztunc H, Tinaz C, Alparslan N. Perforation risks associated with the use of Masserann endodontic kit drills in mandibular molars. Oral Surg Oral Med Oral Pathol Oral Radiol Endod. 2004 Apr;97(4):513-7. doi: 10.1016/j.tripleo.2003.09.007.

161 Wong R, Cho F. Microscopic management of procedural errors. Dent Clin North Am. 1997 Jul;41(3):455-79.

162 Gettleman BH, Spriggs KA, ElDeeb ME, Messer HH. Removal of canal obstructions with the Endo Extractor. J Endod. 1991 Dec;17(12):608-11. doi: 10.1016/s0099-2399(06)81834-0.

163 Roig-Greene JL. The retrieval of foreign objects from root canals: a simple aid. J Endod. 1983 Sep;9(9):394-7. doi: 10.1016/S0099-2399(83)80193-9.

164 Flanders DH. New techniques for removing separated root canal instruments. N Y State Dent J. 1996 May;62(5):30-2.

165 Carr GB. Microscopes in endodontics. J Calif Dent Assoc. 1992 Nov;20(11):55-61.

166 Suter B. A new method for retrieving silver points and separated instruments from root canals. J Endod. 1998 Jun;24(6):446-8. doi: 10.1016/S0099-2399(98)80032-0.

167 Eleazer PD, O'Connor RP. Innovative uses for hypodermic needles in endodontics. J Endod. 1999 Mar;25(3):190-1. doi: 10.1016/S0099-2399(99)80140-X.

168 Machtou, P.; Reit, C. Non-surgical retreatment. In Endodontology, 1st ed.; Machtou, P., Reit, C., Eds.; Blackwell Munksgaard: Oxford, UK, 2003; pp. 300–310.

169 Ruddle CJ. Nonsurgical retreatment. J Endod. 2004 Dec;30(12):827-45. doi: 10.1097/01.don.0000145033.15701.2d.

170 Faus-Matoses V, Burgos Ibáñez E, Faus-Llácer V, Ruiz-Sánchez C, Zubizarreta-Macho Á, Faus-Matoses I. Comparative Analysis of Ease of Removal of Fractured NiTi Endodontic Rotary Files from the Root Canal System-An In Vitro Study. Int J Environ Res Public Health. 2022 Jan 10;19(2):718. doi: 10.3390/ijerph19020718.

171 Capar ID, Kaval ME, Ertas H, Sen BH. Comparison of the cyclic fatigue resistance of 5 different rotary pathfinding instruments made of conventional nickel-titanium wire, M-wire, and controlled memory wire. J Endod. 2015 Apr;41(4):535-8. doi: 10.1016/j.joen.2014.11.008.

172 Camargo EJ, Duarte MAH, Marques VAS, Só MVR, Duque JA, Alcalde MP, Vivan RR. The ability of three nickel-titanium mechanized systems to negotiate and shape MB2 canals in extracted maxillary first molars: a micro-computed

tomographic study. Int Endod J. 2019 Jun;52(6):847-856. doi: 10.1111/iej.13056.

173 Faus-Llácer, V.; Kharrat, N.H.; Ruiz-Sánchez, C.; Faus-Matoses, I.; Zubizarreta-Macho, Á.; Faus-Matoses, V. The Effect of Taper and Apical Diameter on the Cyclic Fatigue Resistance of Rotary Endodontic Files Using an Experimental Electronic Device. Appl. Sci. 2021, 11, 863. https://doi.org/10.3390/app11020863.

174 Duque JA, Vivan RR, Duarte MAH, Alcalde MP, Cruz VM, Borges MMB, Bramante CM. Effect of larger apical size on the quality of preparation in curved canals using reciprocating instruments with different heat thermal treatments. Int Endod J. 2019 Nov;52(11):1652-1659. doi: 10.1111/iej.13165.

175 Versluis, A.; Kim, H.C.; Lee, W.; Kim, B.M.; Lee, C.J. Flexural stiffness and stresses in nickel-titanium rotary files for various pitch and cross-sectional geometries. J. Endod. 2012, 38, 1399–1403. https://doi.org/10.1016/j.joen.2012.06.008.

176 Basheer Ahamed, S.; Vanajassun, P.; Rajkumar, K.; Mahalaxmi, S. Comparative Evaluation of Stress Distribution in Experimentally Designed Nickel-titanium Rotary Files with Varying Cross Sections: A Finite Element Analysis. J. Endod. 2018, 44, 654–658. https://doi.org/10.1016/j.joen.2017.12.013.

177 Kim, H.; Kim, H.; Lee, C.; Kim, B.; Park, J.; Versluis, A. Mechanical response of nickel-titanium instruments with different crosssectional designs during shaping of simulated curved canals. Int. Endod. J. 2009, 42, 593–602. https://doi.org/10.1111/j.1365- 2591.2009.01553.x.

178 Baek, S.H.; Lee, C.J.; Versluis, A.; Kim, B.M.; Lee,W.; Kim, H.C. Comparison of torsional stiffness of nickel-titanium rotary files with different geometric characteristics. J. Endod. 2011, 37, 1283–1286. https://doi.org/10.1016/j.joen.2011.05.032.

179 Xu, X.; Eng, M.; Zheng, Y.; Eng, D. Comparative study of torsional and bending properties for six models of nickel-titanium root canal instruments with different cross-sections. J. Endod. 2006, 32, 372–375. https://doi.org/10.1016/j.joen.2005.08.012.

180 Arbab-Chirani R, Chevalier V, Arbab-Chirani S, Calloch S. Comparative analysis of torsional and bending behavior through finite-element models of 5 Ni-Ti endodontic instruments. Oral Surg Oral Med Oral Pathol Oral Radiol Endod. 2011 Jan;111(1):115-21. doi: 10.1016/j.tripleo.2010.07.017.

181 Faus-Llácer V, Hamoud-Kharrat N, Marhuenda Ramos MT, Faus-Matoses I, Zubizarreta-Macho Á, Ruiz Sánchez C, Faus-Matoses V. Influence of the Geometrical Cross-Section Design on the Dynamic Cyclic Fatigue Resistance of NiTi Endodontic Rotary Files-An In Vitro Study. J Clin Med. 2021 Oct 14;10(20):4713. doi: 10.3390/jcm10204713.

182 Grande NM, Plotino G, Pecci R, Bedini R, Malagnino VA, Somma F. Cyclic fatigue resistance and three-dimensional analysis of instruments from two nickel-titanium rotary systems. Int Endod J. 2006 Oct;39(10):755-63. doi: 10.1111/j.1365-2591.2006.01143.x.

183 Sekar V, Kumar R, Nandini S, Ballal S, Velmurugan N. Assessment of the role of cross section on fatigue resistance of rotary files when used in reciprocation. Eur J Dent. 2016 Oct-Dec;10(4):541-545. doi: 10.4103/1305-7456.195171.

184 de Menezes SEAC, Batista SM, Lira JOP, de Melo Monteiro GQ. Cyclic Fatigue Resistance of WaveOne Gold, ProDesign R and ProDesign Logic Files in Curved Canals In Vitro. Iran Endod J. 2017 Fall;12(4):468-473. doi: 10.22037/iej.v12i4.17494.

185 Ounsi HF, Salameh Z, Al-Shalan T, Ferrari M, Grandini S, Pashley DH, Tay FR. Effect of clinical use on the cyclic fatigue resistance of ProTaper nickel-titanium rotary instruments. J Endod. 2007 Jun;33(6):737-41. doi: 10.1016/j.joen.2007.03.006.

186 Adiguzel M, Isken I, Pamukcu II. Comparison of cyclic fatigue resistance of XP-endo Shaper, HyFlex CM, FlexMaster and Race instruments. J Dent Res Dent Clin Dent Prospects. 2018 Summer;12(3):208-212. doi: 10.15171/joddd.2018.032.

187 Uygun AD, Unal M, Falakaloglu S, Guven Y. Comparison of the cyclic fatigue resistance of hyflex EDM, vortex blue, protaper gold, and onecurve nickel-Titanium instruments. Niger J Clin Pract. 2020 Jan;23(1):41-45. doi: 10.4103/njcp.njcp_343_19.

188 ISO 3630-1:2008; Dentistry—Root-Canal Instruments—Part 1: General Requirements and Test Methods. International Organization for Standardization: Geneva, Switzerland, 2008.

189 Roda-Casanova V, Pérez-González A, Zubizarreta-Macho A, Faus-Matoses V. Influence of Cross-Section and Pitch on the Mechanical Response of NiTi Endodontic Files under Bending and Torsional Conditions-A Finite Element Analysis. J Clin Med. 2022 May 8;11(9):2642. doi: 10.3390/jcm11092642.

190 Ruiz-Sánchez C, Faus-Llácer V, Faus-Matoses I, Zubizarreta-Macho Á, Sauro S, Faus-Matoses V. The Influence of NiTi Alloy on the Cyclic Fatigue Resistance of Endodontic Files. J Clin Med. 2020 Nov 21;9(11):3755. doi: 10.3390/jcm9113755.

191 Gündoğar M, Özyürek T. Cyclic Fatigue Resistance of OneShape, HyFlex EDM, WaveOne Gold, and Reciproc Blue Nickel-titanium Instruments. J Endod. 2017 Jul;43(7):1192-1196. doi: 10.1016/j.joen.2017.03.009.

192 Elnaghy AM, Elsaka SE. Laboratory comparison of the mechanical properties of TRUShape with several nickel-titanium rotary instruments. Int Endod J. 2017 Aug;50(8):805-812. doi: 10.1111/iej.12700.

193 Zafar MS. Impact of Endodontic Instrumentation on Surface Roughness of Various Nickel-Titanium Rotary Files. Eur J Dent. 2021 May;15(2):273-280. doi: 10.1055/s-0040-1718469.

194 Faus-Matoses V, Faus-Llácer V, Ruiz-Sánchez C, Jaramillo-Vásconez S, Faus-Matoses I, Martín-Biedma B, Zubizarreta-Macho Á. Effect of Rotational Speed on the Resistance of NiTi Alloy Endodontic Rotary Files to Cyclic Fatigue-An In Vitro Study. J Clin Med. 2022 May 31;11(11):3143. doi: 10.3390/jcm11113143.

195 Faus-Matoses V, Pérez García R, Faus-Llácer V, Faus-Matoses I, Alonso Ezpeleta Ó, Albaladejo Martínez A, Zubizarreta-Macho Á. Comparative Study of the SEM Evaluation, EDX Assessment, Morphometric Analysis, and Cyclic Fatigue Resistance of Three Novel Brands of NiTi Alloy Endodontic Files. Int J Environ Res Public Health. 2022 Apr 6;19(7):4414. doi: 10.3390/ijerph19074414.

196 Lopes, H.P.; Ferreira, A.A.; Elias, C.N.; Moreira, E.J.; de Oliveira, J.C.; Siqueira, J.F., Jr. Influence of rotational speed on the cyclic fatigue of rotary nickel-titanium endodontic instruments. J. Endod. 2009, 35, 1013–1016. https://doi.org/10.1016/j.joen.2009.04.003.

197 Varela-Patiño, P.; Ibañez-Párraga, A.; Rivas-Mundiña, B.; Cantatore, G.; Otero, X.L.; Martin-Biedma, B. Alternating versus continuous rotation: A comparative study of the effect on instrument life. J. Endod. 2010, 36, 157–159. https://doi.org/10.1016/j.joen.2009.09.023.

198 Kim JW, Ha JH, Cheung GS, Versluis A, Kwak SW, Kim HC. Safety of the factory preset rotation angle of reciprocating instruments. J Endod. 2014 Oct;40(10):1671-5. doi: 10.1016/j.joen.2014.06.002.

199 De-Deus G, Moreira EJ, Lopes HP, Elias CN. Extended cyclic fatigue life of F2 ProTaper instruments used in reciprocating movement. Int Endod J. 2010 Dec;43(12):1063-8. doi: 10.1111/j.1365-2591.2010.01756.x.

200 Martín, B.; Zelada, G.; Varela, P.; Bahillo, J.G.; Magán, F.; Ahn, S.; Rodríguez, C. Factors influencing the fracture of nickeltitanium rotary instruments. Int. Endod. J. 2003, 36, 262–266. https://doi.org/10.1046/j.1365-2591.2003.00630.x.

201 Ferreira F, Adeodato C, Barbosa I, Aboud L, Scelza P, Zaccaro SM. Movement kinematics and cyclic fatigue of NiTi rotary instruments: a systematic review. Int Endod. 2017;50(2):143–52. https:// doi. org/ 10. 1111/ iej. 12613.

202 Olcay K, Eyuboglu TF, Erkan E. Cyclic fatigue resistance of wave one gold, protaper next and 2shape nickel titanium rotary instruments using a reliable method for measuring temperature. Niger J Clin Pract. 2019;22(10):1335–40. https:// doi. org/ 10. 4103/ njcp. njcp_ 655_ 18.

203 Scott R, Arias A, Macorra JC, Govindjee S, Peters OA. Resistance to cyclic fatigue of reciprocating instruments determined at body temperatura and phase transformation analysis. Aust Endod J. 2019;45(3):400–6. https:// doi. org/ 10. 1111/ aej. 12374.

204 Al-Obaida MI, Merdad K, Alanazi MS, Altwaijry H, AlFaraj M, Alkhamis AA, Al-Madi EM. Comparison of Cyclic Fatigue Resistance of 5 Heat-treated Nickel-titanium Reciprocating Systems in Canals with Single and Double Curvatures. J Endod. 2019 Oct;45(10):1237-1241. doi: 10.1016/j.joen.2019.06.011.

205 Alsilani R, Jadu F, Bogari DF, Jan AM, Alhazzazi TY. Single file reciprocating systems: a systematic review and meta-analysis of the literature: comparison of reciproc and WaveOne. J Int Soc Prev Community Dent. 2016;6(5):402–9. https:// doi. org/ 10. 4103/ 2231-0762. 192945.

206 Martins, J.N.R.; Nogueira Leal Silva, E.J.; Marques, D.; Ginjeira, A.; Braz Fernandes, F.M.; De Deus, G.; Versiani, M.A. Influence of Kinematics on the Cyclic Fatigue Resistance of Replicalike and Original Brand Rotary Instruments. J. Endod. 2020, 46, 1136– 1143. https://doi.org/10.1016/j.joen.2020.05.001.

207 Siddique R, Nivedhitha MS. Effectiveness of rotary and reciprocating systems on microbial reduction: A systematic review. J Conserv Dent. 2019 Mar-Apr;22(2):114-122. doi: 10.4103/JCD.JCD_523_18.

208 Klymus ME, Alcalde MP, Vivan RR, Só MVR, de Vasconselos BC, Duarte MAH. Effect of temperature on the cyclic fatigue resistance of thermally treated reciprocating instruments. Clin Oral Investig. 2019 Jul;23(7):3047-3052. doi: 10.1007/s00784-018-2718-1.

209 Zubizarreta-Macho Á, Albaladejo Martínez A, Falcão Costa C, Quispe-López N, Agustín-Panadero R, Mena-Álvarez J. Influence of the type of reciprocating motion on the cyclic fatigue resistance of reciprocating files in a dynamic model. BMC Oral Health. 2021 Apr 7;21(1):179. doi: 10.1186/s12903-021-01538-8.

210 Di Nardo D, Galli M, Morese A, Seracchiani M, Ferri V, Miccoli G, Gambarini G, Testarelli L. A comparative study of mechanical resistance of two reciprocatingfiles. J Clin Exp Dent. 2019;11(3):e231–5. https:// doi. org/ 10. 4317/jced. 55487.

211 Laneve E, Raddato B, Dioguardi M, Di Gioia G, Troiano G, Lo Muzio L. Sterilisation in Dentistry: A Review of the Literature. Int J Dent. 2019 Jan 15;2019:6507286. doi: 10.1155/2019/6507286.

212 Sheth NC, Rathod YV, Shenoi PR, Shori DD, Khode RT, Khadse AP. Evaluation of new technique of sterilization using biological indicator. J Conserv Dent. 2017 Sep-Oct;20(5):346-350. doi: 10.4103/JCD.JCD_253_16.

213 Raju TB, Garapati S, Agrawal R, Reddy S, Razdan A, Kumar SK. Sterilizing Endodontic Files by four different sterilization methods to prevent cross-infection - An In-vitro Study. J Int Oral Health. 2013 Dec;5(6):108-12.

214 Spagnuolo G, Ametrano G, D'Antò V, Rengo C, Simeone M, Riccitiello F, Amato M. Effect of autoclaving on the surfaces of TiN -coated and conventional nickel-titanium rotary instruments. Int Endod J. 2012 Dec;45(12):1148-55. doi: 10.1111/j.1365-2591.2012.02088.x.

215 Grassi FR, Pappalettere C, Di Comite M, Corsalini M, Mori G, Ballini A, Crincoli V, Pettini F, Rapone B, Boccaccio A. Effect of different irrigating solutions and endodontic sealers on bond strength of the dentin-post interface with and without defects. Int J Med Sci. 2012;9(8):642-54. doi: 10.7150/ijms.4998.

216 Valois CR, Silva LP, Azevedo RB. Multiple autoclave cycles affect the surface of rotary nickel-titanium files: an atomic force microscopy study. J Endod. 2008 Jul;34(7):859-62. doi: 10.1016/j.joen.2008.02.028.

217 Faus-Matoses V, Faus-Llácer V, Aldeguer Muñoz Á, Alonso Pérez-Barquero J, Faus-Matoses I, Ruiz-Sánchez C, Zubizarreta-Macho Á. A Novel Digital Technique to Analyze the Wear of CM-Wire NiTi Alloy Endodontic Reciprocating Files: An In Vitro Study. Int J Environ Res Public Health. 2022 Mar 9;19(6):3203. doi: 10.3390/ijerph19063203.

218 Yang YJ, Hou BX, Hou XM. [Effect of autoclave on surface microstructure and cyclic fatigue resistance of R-phase rotary instruments]. Beijing Da Xue Xue Bao Yi Xue Ban. 2018 Oct 18;50(5):882-886.

219 Pedullà E, Benites A, La Rosa GM, Plotino G, Grande NM, Rapisarda E, Generali L. Cyclic Fatigue Resistance of Heat-treated Nickel-titanium Instruments after Immersion in Sodium Hypochlorite and/or Sterilization. J Endod. 2018 Apr;44(4):648-653. doi: 10.1016/j.joen.2017.12.011.

220 Seago ST, Bergeron BE, Kirkpatrick TC, Roberts MD, Roberts HW, Himel VT, Sabey KA. Effect of repeated simulated clinical use and sterilization on the cutting efficiency and flexibility of Hyflex CM nickel-titanium rotary files. J Endod. 2015 May;41(5):725-8. doi: 10.1016/j.joen.2015.01.011.

221 Champa C, Divya V, Srirekha A, Karale R, Shetty A, Sadashiva P. An analysis of cyclic fatigue resistance of reciprocating instruments in different canal curvatures after immersion in sodium hypochlorite and autoclaving: An in vitro study. J Conserv Dent. 2017 May-Jun;20(3):194-198. doi: 10.4103/0972-0707.218307.

222 Özyürek T, Yılmaz K, Uslu G. The effects of autoclave sterilization on the cyclic fatigue resistance of ProTaper Universal, ProTaper Next, and ProTaper Gold nickel-titanium instruments. Restor Dent Endod. 2017 Nov;42(4):301-308. doi: 10.5395/rde.2017.42.4.301.

223 Zhao D, Shen Y, Peng B, Haapasalo M. Effect of autoclave sterilization on the cyclic fatigue resistance of thermally treated Nickel-Titanium instruments. Int Endod J. 2016 Oct;49(10):990-5. doi: 10.1111/iej.12550.

224 Zubizarreta-Macho, Á.; Alonso-Ezpeleta, Ó.; Albaladejo Martínez, A.; Faus Matoses, V.; Caviedes Brucheli, J.; Agustín-Panadero, R.; Mena Álvarez, J.; Vizmanos Martínez-Berganza, F. Novel Electronic Device to Quantify the Cyclic Fatigue Resistance of Endodontic Reciprocating Files after Using and Sterilization. Appl. Sci.. 2020, 10, 4962. https://doi.org/10.3390/app10144962.

225 Generali L, Puddu P, Borghi A, Brancolini S, Lusvarghi L, Bolelli G, Consolo U, Pedullà E. Mechanical properties and metallurgical features of new and ex vivo used Reciproc Blue and Reciproc. Int Endod J. 2020 Feb;53(2):250-264. doi: 10.1111/iej.13214.

226 Arias A, Macorra JC, Govindjee S, Peters OA. Effect of gamma-ray sterilization on phase transformation behavior and fatigue resistance of contemporary nickel-titanium instruments. Clin Oral Investig. 2020 Sep;24(9):3113-3120. doi: 10.1007/s00784-019-03185-4.

227 Dioguardi M, Sovereto D, Aiuto R, Laino L, Illuzzi G, Laneve E, Raddato B, Caponio VCA, Dioguardi A, Zhurakivska K, Troiano G, Lo Muzio L. Effects of Hot Sterilization on Torsional Properties of Endodontic Instruments: Systematic Review with Meta-Analysis. Materials (Basel). 2019 Jul 8;12(13):2190. doi: 10.3390/ma12132190.

228 Roda-Casanova V, Pérez-González A, Zubizarreta-Macho Á, Faus-Matoses V. Fatigue Analysis of NiTi Rotary Endodontic Files through Finite Element Simulation: Effect of Root Canal Geometry on Fatigue Life. J Clin Med. 2021 Dec 3;10(23):5692. doi: 10.3390/jcm10235692.

229 Roda-Casanova, V.; Zubizarreta-Macho, Á.; Sanchez-Marin, F.; Alonso Ezpeleta, Ó.; Albaladejo Martínez, A.; Galparsoro Catalán, A. Computerized Generation and Finite Element Stress Analysis of Endodontic Rotary Files. Appl. Sci. 2021, 11, 4329. https://doi.org/10.3390/app11104329

230 Zubizarreta-Macho Á, Mena Álvarez J, Albaladejo Martínez A, Segura-Egea JJ, Caviedes Brucheli J, Agustín-Panadero R, López Píriz R, Alonso-Ezpeleta Ó. Influence of the Pecking Motion Frequency on the Cyclic Fatigue Resistance of Endodontic Rotary Files. J Clin Med. 2019 Dec 24;9(1):45. doi: 10.3390/jcm9010045.

ANEXOS

MINISTERIO
DE ENERGÍA, TURISMO
Y AGENDA DIGITAL

Oficina Española
de Patentes y Marcas

Nº SOLICITUD: **U201831396**
Nº PUBLICACIÓN: **ES1219520**
TITULAR/ES:
ZUBIZARRETA MACHO ,Álvaro
RICO ROMANO ,Cristina
GUTIÉRREZ GONZÁLEZ ,Roberto
ORTEGA UFANO ,Daniel
LOBO GALINDO ,Ana Belén

FECHA EXPEDICIÓN: 09/01/2019

TÍTULO
DE
MODELO DE UTILIDAD

Cumplidos los requisitos previstos en la vigente Ley 24/2015, de 24 de julio, de Patentes, se expide el presente TÍTULO, acreditativo de la concesión del Modelo de Utilidad.

Se otorga al titular un derecho de exclusiva en todo el territorio nacional, bajo las condiciones y con las limitaciones en la Ley de Patentes. La duración del modelo de utilidad será de **diez años** contados a partir de la fecha de presentación de la solicitud (13/10/2017).

El modelo de utilidad se concede sin perjuicio de tercero y sin garantía del Estado en cuanto a la validez y a la utilidad del objeto sobre el que recae.

Para mantener en vigor el modelo de utilidad concedido, deberán abonarse las tasas anuales establecidas, a partir de la tercera anualidad. Asimismo, deberá explotarse el objeto de la invención, bien por su titular o por medio de persona autorizada de acuerdo con el sistema de licencias previsto legalmente, dentro del plazo de cuatro años a partir de la fecha de presentación de la solicitud del modelo de utilidad, o de tres años desde la publicación de la concesión en el Boletín Oficial de la Propiedad Industrial, aplicándose el plazo que expire más tarde.

OFICINA ESPAÑOLA DE PATENTES Y MARCAS

Ana María Redondo Mínguez
Jefe/a de Servicio de Actuaciones Administrativas
(P.D. del Director/a del Departamento de Patentes e I.T., Resolución 18 de Julio 2017)

(19) OFICINA ESPAÑOLA DE PATENTES Y MARCAS

ESPAÑA

(11) Número de publicación: **1 219 520**

(21) Número de solicitud: 201831396

(51) Int. CI.:

A61C 5/42 (2007.01)
B23Q 17/09 (2006.01)
G01N 3/32 (2006.01)

(12) SOLICITUD DE MODELO DE UTILIDAD U

(22) Fecha de presentación:

13.10.2017

(43) Fecha de publicación de la solicitud:

24.10.2018

(71) Solicitantes:

ZUBIZARRETA MACHO, Álvaro (20.0%)
Pinos, 6
37184 Villares de la Reina (Salamanca) ES;
RICO ROMANO, Cristina (20.0%);
GUTIÉRREZ GONZÁLEZ, Roberto (20.0%);
ORTEGA UFANO, Daniel (20.0%) y
LOBO GALINDO, Ana Belén (20.0%)

(72) Inventor/es:

ZUBIZARRETA MACHO, Álvaro;
RICO ROMANO, Cristina;
GUTIÉRREZ GONZÁLEZ, Roberto;
ORTEGA UFANO, Daniel;
LOBO GALINDO, Ana Belén;
MENA ÁLVAREZ, Jesús;
ALONSO EZPELETA, Luis Óscar;
DURÁN SINDREU, Fernando;
ABELLA SANS, Francesc;
LÓPEZ PÍRIZ, Roberto;
FERNÁNDEZ DOMÍNGUEZ, Manuel;
SEGURA EGEA, Juan José;
DEL CAMPO MORENO, Rosa María;
LÓPEZ SUÁREZ, Carlos;
LÓPEZ-MALLA MATUTE, Joaquín;
AGUSTÍN PANADERO, Rubén;
GARRIDO MARTÍNEZ, Pablo;
PUEBLA GONZÁLEZ, Manuel;
BERRENDERO DÁVILA, Santiago;
QUISPE LÓPEZ, Norberto;
CENTENERA CENTENERA, María Belén;
PELÁEZ RICO, Jesús;
MORENO ALONSO, Iván;
CAVIEDES BRUCHELI, Javier Fernando;
TOBAR ARRIBAS, Celia;
CARRILLO SÁNCHEZ, Alberto José;
FERREIROA NAVARRO, Alberto;
GONZALO IÑIGO, Esther;
GIL VILLAGRÁ, Luis Javier;
MACIAS GARCIA, Antonio;
PLATA REGUERA, Enrique;
MARTÍN MUÑOZ, Cristina y
ALFARO DOMINGUEZ, Manuel

(74) Agente/Representante:

BAÑOS TRECEÑO, Valentin

(54) Título: **MÁQUINA PARA TESTAR INSTRUMENTAL ENDODÓNTICO**

ES 1 219 520 U

MÁQUINA PARA TESTAR INSTRUMENTAL ENDODÓNTICO

DESCRIPCIÓN

Máquina para testar instrumental endodóntico.

OBJETO DE LA INVENCION

La presente invención se refiere a una máquina destinada a estudiar y testar la influencia de distintas variables sobre la fatiga cíclica de instrumental endodóntico, preferentemente limas, y por ende sobre la resistencia a la fractura de dicho instrumental testado, y es una máquina constituida por un cuerpo que permite fijar en ella el instrumento endodóntico, que alberga un mecanismo que interactúa con el instrumental testado, y un conjunto de sensores y un procesador que analiza y muestra los resultados obtenidos.

El objetivo de la invención es conseguir una solución con la que se puede estudiar y testar de una manera fiable y objetiva diferentes instrumentos endodónticos que posteriormente van a ser utilizados en los pacientes, y conseguir obtener resultados de una correcta resistencia a la fractura para desechar aquellos instrumentos potencialmente peligrosos para la práctica médica y el paciente, y tener una certeza de que dicho instrumental médico es fiable para ejercer la práctica por parte de los profesionales.

El campo de aplicación de la presente invención se engloba dentro del sector médico, en especial está dirigido al campo de la odontología, y más concretamente a las máquinas, dispositivos, sistemas o metodologías de pruebas y ensayos de instrumental endodóntico.

ANTECEDENTES.

El conseguir resultados fiables a la hora de probar y testar instrumental médico dentro del campo de la odontología es un problema conocido dentro de este sector. Esta problemática es especialmente relevante a la hora de probar instrumental

sometido a acciones y tensiones provenientes tanto de una constante manipulación del instrumento por parte del especialista, como de las tensiones y resistencias que se producen por el íntimo contacto entre el tejido dentario y la superficie del instrumento.

Dentro de los diferentes elementos o instrumentos de práctica más comunes y utilizados se destacan las limas endodónticas y los implantes; no obstante, la presente invención va destinada a todo instrumental con configuración tubular en el que su extremo dispone de una configuración que permite sean introducidos en conductos radiculares de los dientes, siendo de común conocimiento que estos conductos pueden ser rectos, curvos, con dobles curvaturas, dilaceraciones, conductos fusionados o bifurcados, conductos calcificados o estrechos.

Es también ampliamente conocido que el empleo del instrumental en dichas zonas de difícil acceso hace que la posible fractura de dichos extremos sea relativamente alta, y ello conlleva una serie de problemas indeseables. Es cierto, que si bien es preferible no dejar fragmentos en el interior de los conductos, hay estudios que indican que la incidencia de éxito o fracaso de un tratamiento no está afectada por dicho accidente, dado que el material es un metal previamente esterilizado, de acero inoxidable quirúrgico o Niquel-Titanio, tal como está divulgado por ejemplo en el documento EP1086659, y que el inconveniente no es el fragmento en sí, que es inerte, sino la falta de limpieza del conducto al momento de producirse el accidente. No obstante, es altamente probable que por la falta de desinfección de la raíz y el taponamiento del conducto con el instrumento fracturado se produzca un fracaso de la endodoncia y eso implique realizar una apicectomía, una amputación radicular, una hemisección dentaria o la extracción de la pieza dentaria completa.

Como conclusión, la rotura de dicho instrumental es un accidente que trae más complicaciones que una endodoncia convencional debido al taponamiento del conducto, el futuro de la pieza dentaria depende del grado de limpieza del conducto previo al momento de fracturarse el instrumento, y por norma general, para solucionar esta problemática se requiere de una cirugía endodóntica o la extracción de la pieza dentaria.

Cara al estudio y control de la calidad de este tipo de instrumental, hasta la fecha se han realizado prototipos estáticos. Destaca la existencia o desarrollo de ciertos dispositivos constituidos por cilindros metálicos huecos que impedían determinar el momento de la fractura, no reproducían la anatomía del sistema de conductos radiculares, ni los movimientos del operador. Posteriormente, estos cilindros fueron sustituidos por otros abiertos que facilitaban la detección de la fractura del instrumental endodóntico, pero persistían las limitaciones mencionadas anteriormente. En este sentido, la forma más generalizada de realizar estos ensayos era el testar un ejemplar de un lote cualquiera, de tal manera que se le sometía a un esfuerzo con material de laboratorio hasta la fractura y se extrapolaba ese resultado a todo el lote de ejemplares comunes. De estas maneras y técnicas solo se puede constatar que si un lote es apto o no; solo se tiene en cuenta el punto de fractura de un instrumento, por tanto, no hay un criterio objetivo a otras variables como la deformación admisible y en ningún momento se pueden obtener datos objetivos que permitan una optimización del proceso de producción de estos instrumentales; no se testa el instrumento de acuerdo a las solicitaciones o fatiga real que al que se va a someter; y además este tipo de ensayos solo pueden realizarse en laboratorios especializados con una maquinaria genérica para cualquier tipo de instrumento o material, y no estando por tanto sometido a unas condiciones similares o simuladas a las que se encuentra en los canales radiculares.

En este sentido, se destaca el documento EP0722300 que divulga un instrumento endodóntico cuya composición interna permite tener una mayor flexibilidad y por tanto minimizar posibles fracturas; no obstante, el problema de la comprobación de manera objetiva y el asegurarse que no va a fracturar el instrumento durante la práctica del especialista no se puede ni asegurar ni augurar.

Teniendo en cuenta todos estos aspectos previos, y la problemática que existe cuando el producto se fractura o quiebra cuando está siendo utilizado en un paciente, y lo problemático, subjetivo y aleatorio que son los procesos y mecanismos de testeo de este tipo de instrumentales, surge la necesidad de desarrollar una máquina que solvente y supere esta problemática.

Por esta razón, la máquina descrita en el presente documento permite estudiar y testar la influencia de distintas variables sobre la fatiga cíclica y la resistencia a la

fractura de dicho instrumental testado según criterios objetivos y en una situación similar a la real; permite ser instalada o utilizada en cualquier lugar; y permite conseguir datos y valores que permitan una optimización en el proceso de fabricación del instrumental y previo a su uso, aumentando por tanto la fiabilidad final de dicho instrumental.

DESCRIPCIÓN DEL INVENTO

Tal como se ha definido con anterioridad, la prognosis del tratamiento de conductos dentales, y por ende la supervivencia del propio diente tratado, depende de la asepsia y limpieza alcanzada en el interior del sistema de conductos radiculares por el instrumental endodóntico previo a la obturación del canal radicular. La posible fractura del instrumental en el interior del sistema de conductos radiculares por la acción rotatoria de la manipulación por parte del especialista y de las tensiones producidas dentro del propio conducto, impiden la desinfección de los mismos, y predisponen a la formación de infecciones endodónticas y tratamientos secundarios posteriores.

La máquina que se describe en la presente memoria descriptiva permite el estudio descriptivo in vitro del instrumental, en el que se analizan las variables que influyen sobre la fatiga cíclica, así como el comportamiento del instrumental sometido a estas variables, y permite obtener valores objetivos que permitan una correcta fabricación de posteriores instrumentos, o bien considerar la idoneidad o no de uno ya que ya está siendo utilizado.

En este sentido, el uso de la máquina de la presente invención es precisamente el de testar instrumental endodóntico, preferentemente limas o implantes, y dicha máquina está constituida por una estructura o carcasa, que hace que el conjunto sea transportable e instalable en cualquier lugar de una manera cómoda, y que comprende:

- un soporte de sustentación sobre la carcasa de la máquina para la sustentación de un micromotor endodóntico, en el que el instrumental a testar está colocado en el interior de un contraángulo reductor, y provoca que gire sobre su propio eje a una velocidad regulada por el operador. La

posición del micromotor endodóntico sobre el soporte de sustentación, influye sobre la inserción del instrumental endodóntico en el interior de una proforma metálica, que posteriormente se define;

- el soporte dispone internamente de un micromotor, de una abertura a modo de abrazadera con un juego de guiado por rodamientos accionados por el micromotor, que hacen que cuando el instrumento es introducido en dicha abertura, este rote respecto de su eje longitudinal, pero se mantenga en una posición fija. En este sentido el instrumental, como una lima, un implante u otros instrumentales son cuerpos de configuración tubular. La razón por la que el soporte hace rotar al mango es simular la acción manual de un especialista cuando está utilizando dicho instrumental en el paciente. El soporte de sustentación se ubica preferentemente en la parte superior de la estructura o carcasa de la máquina;

- un motor eléctrico de engranajes interno en la carcasa, controlado y gestionado por un procesador, preferentemente tipo Arduino, y un módulo de control de motores, conectado a una pluralidad de botones de calibración y en el que el procesador y los botones de calibración hacen llegar información a una pantalla, preferentemente LCD;

- un mecanismo interno consistente en una leva en conexión y accionada por el motor eléctrico de engranajes, estando la leva sujeta al motor por un pasador en cuya parte exterior dispone de un tornillo prisionero y una pieza de latón. En la zona de contacto del pasador entre la leva y el motor se dispone de unos rodamientos preferentemente de bolas, que permite la rotación y movimiento giratorio de la leva;

- una montura que sostiene una preforma metálica, y que comprende:

  - un canal inferior que alberga en su interior unos rodamientos y que está en contacto con la leva;

  - unas guías lineales de rodamientos que permiten al soporte tener un movimiento ascendente o descendente, dependiendo del movimiento de la leva;

- una preforma metálica con un ranurado superficial a modo de conducto que puede o no incorporar un ángulo, y que simula el conducto dental del paciente;

- al menos un sensor LED que emite luz, ubicado preferentemente en el extremo apical del conducto simulado;

- al menos un sensor fotoeléctrico, preferentemente de LDR y ubicado también el extremo apical del conducto y enfrentado con el sensor LED para la detección y cuantificación de la luz emitida por el sensor LED.

Con esta máquina se consigue:

- simular el movimiento rotatorio que un especialista manual imprime al instrumento endodóntico;

- simular el recorrido que el instrumental endodóntico hace dentro del conducto radicular del diente del paciente mediante un movimiento ascendente/descendente de la preforma metálica, estando a su vez el instrumental sometido al movimiento rotatorio previamente dicho; y

- se obtienen resultados objetivos de diferentes variables estudiadas que permiten analizar el comportamiento del instrumental sometido a una simulación real de su uso.

Dentro de los componentes electrónicos previamente destacados, la electrónica se divide en tres partes diferenciadas: un acondicionamiento de las señales necesarias para la detección del instrumental, para lo que se utiliza el procesador, preferentemente tipo Arduino; un módulo controlador de control de velocidad del movimiento manual del operador; y una interface de usuario que comunica el procesador y la pantalla LCD donde se muestra información.

En añadidura, la detección tanto de la presencia del instrumento a testar en el interior del conducto, al igual que identificar el momento de su fractura, es una de las claves de la invención. Por ello se destaca la existencia de un conducto en la preforma metálica, a modo de ranurado, siendo la preforma metálica preferentemente de acero inoxidable. Este ranurado o conducto es un conducto

simulado en el cuerpo de la preforma ejecutado por electroerosión por hilo. Las dimensiones del conducto guardan similitud con las dimensiones del instrumental a testar, a fin de favorecer un íntimo contacto entre el instrumental y el conducto simulado. Con el objetivo de eliminar imperfecciones micro-estructurales superficiales, mejorar la resistencia y prolongar la vida útil de la preforma metálica, la preforma dispone de una película de cromo sobre el cuerpo de acero inoxidable, siendo dicha película preferentemente dentro del rango de 15-25 μm. También a modo de ejemplo, el conducto simulado tiene una longitud de entre 10 y 20 mm, un diámetro de entre 200 y 300 μm en su extremo apical, y una conicidad regular de entre 4 y 10º. Por otro lado, en el extremo apical de uno de los lados del conducto simulado se ubica un sensor LED, preferentemente blanco de alta luminosidad y de 5 mm, y en el extremo opuesto se coloca un sensor fotoeléctrico LDR para cuantificar la luz que penetra a través del extremo apical del conducto simulado. Las lecturas obtenidas por el sensor fotoeléctrico LDR permiten identificar la presencia/ausencia del instrumental en el interior del conducto.

Cara a resolver posibles problemas con dicha detección lumínica, se puede realizar un acondicionamiento de la señal recibida por el sensor fotoeléctrico con un amplificador, cuya función es la de amplificar la diferencia de los valores de tensión obtenidos en el divisor resistivo utilizado para mediar las variaciones de luz en el conducto. Para realizar el acondicionamiento se efectúa una primera fase, en la que se disminuye el valor mínimo de tensión a un valor próximo a 0V, lo que facilita la realización de las medidas. En este sentido se utiliza un Amplificador Operacional AO con una configuración de restador, para que, a la salida del AO, la tensión obtenida sea la resta de su entrada positiva (+) y su entrada negativa (-), siendo su entrada positiva (+) la tensión obtenida de la LDR que mide las variaciones de luz en función de la posición del instrumental en el interior del conducto, y la entrada negativa (-) la tensión configurable a través de un potenciómetro. A continuación, se amplifican las lecturas mediante un segundo AO con configuración de amplificador, de modo que la ganancia es configurable mediante un segundo potenciómetro. Ajustando la ganancia del segundo AO a un valor próximo a 10, los valores de señal de detección obtenidos varían entre 0 y 4 V, valores suficientemente separados como para permitir su identificación.

Los sensores que identifican la presencia/ausencia del instrumental en el interior del conducto de la proforma quedan conectados a la placa del procesador, de forma que esos datos obtenidos son tratados en el procesador y, por tanto, los resultados tratados finales permiten ser observados en la pantalla LCD.

Por otro lado, definimos los elementos encargados del movimiento de los mecanismos de la máquina. La velocidad y dirección del movimiento del motor eléctrico de engranajes que mueve la leva, y en consecuencia la preforma metálica con el conducto simulado, se regula mediante el procesador con un módulo controlador de motores que incorpora un circuito o estructura electrónica en forma de puente H que permite controlar la dirección del movimiento del motor y su velocidad, mediante una pluralidad de interruptores modulados con transistores, en el que en función de la posición de los interruptores se regula la dirección del movimiento del motor eléctrico. Estos interruptores son accionados desde el exterior por el operario por medio de los botones de calibración.

Para controlar la velocidad y dirección del movimiento del motor eléctrico, se genera una interface en el módulo controlador que se comunica con la pantalla LED para la muestra de resultados.

Cara a la alimentación de la máquina, se dispone de un puerto conector de corriente eléctrica desde un módulo de alimentación externa. Por otro lado, también se dispone de un puerto de cable USB para la conexión de la máquina a un ordenador externo que implemente las prestaciones del procesador, aumente el flujo de información, facilite la conexión y gestión inalámbrica tanto del tratamiento de los datos obtenidos como del funcionamiento de los diferentes componentes.

También es preciso destacar que el soporte de sustentación del instrumental endodóntico comprende internamente de un micromotor, alimentado eléctricamente desde el módulo de alimentación externo, dispone de un contra ángulo reductor, no requiere de funciones de cambio de sentido y tiene un funcionamiento independiente al motor interno que mueve la leva. Tal como se ha adelantado también, el instrumental endodóntico se ubica en el interior del contraángulo reductor del micromotor endodóntico, que provoca que el instrumental gire sobre su propio eje para estudiar la acción y resistencia de dicho instrumental ante

movimientos rotatorios. El contraángulo reductor se ubica en el extremo del micromotor endodóntico, que está posicionado sobre el soporte de sustentación de la máquina; preferentemente constituido por una abertura o abrazadera.

Para acabar, las variables a estudiar introducidas en el procesador para obtener una regla objetiva para la gestión tanto de los movimientos como de las lecturas de los sensores se fundamentan en el haber testado previamente juegos de instrumentos similares analizando las variables ángulo de curvatura, radio de curvatura, número de esterilizaciones, torsión mecánica o torque, revoluciones por minuto (r.p.m.) y agente lubricante. Cada una de estas variables tienen el propósito de evaluar el efecto individual y colectivo sobre la fatiga cíclica del instrumental testado, y mediante índices de la tendencia central y de la dispersión de las variables cuantitativas obtenidos de las distribuciones muestrales, y el empleo de medias aritméticas y de desviaciones, se consigue obtener una regla general objetiva para el correcto examen y testeo del instrumental endodóntico. Estos valores obtenidos se adecuan y extrapolan en la placa o el módulo de programación del procesador a tiempos de exposición del sensor fotoeléctrico y las diferentes variables del control de movimiento del motor, de tal manera que tiempos estimados de presencia o ausencia del instrumental en el interior del conducto indican la fractura o problemas en la fatiga del instrumento testado.

Para completar la descripción que se está realizando y con objeto de ayudar a una mejor comprensión de las características del invento, se acompaña como parte integrante de la misma un juego de dibujos en donde con carácter ilustrativo y no limitativo se ha representado lo siguiente:

La Figura 1 es una representación en perspectiva de la máquina objeto de la presente invención.

La Figura 2 muestra una vista del alzado de acuerdo con la figura anterior.

La Figura 3 muestra una vista del perfil izquierdo de acuerdo con las figuras anteriores.

La Figura 4 muestra una vista del perfil derecho de acuerdo con las figuras anteriores.

La Figura 5 muestra una vista de la planta de acuerdo con las figuras anteriores.

La Figura 6 es una representación de un detalle de la preforma metálica.

La Figura 7 es una representación esquemática de la conexión entre los diferentes componentes de la máquina.

Descripción detallada de los dibujos

En las Figuras 1 a 5 se puede observar una realización preferente de la máquina para testar instrumental endodóntico, en el que dicha máquina está constituida por una estructura o carcasa (1) que permite su ubicación en cualquier lugar, y en un lateral cualquiera de dicha carcasa (1) se ubica una pantalla (52) LCD de donde se pueden visualizan los datos y resultados obtenidos.

Por un lado, se puede observar que en su parte superior se ubica el soporte de sustentación (2) del micromotor endodóntico (3), donde se ubica el instrumental endodóntico a testar. El contraángulo reductor (31) del micromotor endodóntico (3), provoca que el instrumental endodóntico gire respecto a su propio eje. El micromotor endodóntico (3) está fijado al soporte de sustentación por una abertura o abrazadera (21).

Por otro lado, se puede ver que en la parte interna de la carcasa (1) la máquina está constituida por un motor eléctrico de engranajes (4), controlado por un procesador (5), el cual controla y gestiona la máquina, y tal como se puede observar en la Figura 7, comprende al menos de un módulo de control (51) del motor (4) y una pluralidad de interruptores (54) conectados a unos de botones de calibración (6) exteriores en la carcasa (1) y ubicados en una de sus laterales, y una placa o módulo de programación (53).

Tal como se puede observar en estas figuras, la máquina tiene un mecanismo interno consistente en una leva (7) en conexión y accionada por el motor eléctrico de engranajes (4), estando la leva (7) sujeta a dicho motor (4) por un pasador, y en el que en la zona de contacto entre la leva (7) y el motor (4) se dispone de unos rodamientos que permiten el movimiento giratorio de la leva (7), y en el que el pasador es cerrado por una pieza de latón con un tornillo prisionero (41) a fin de evitar la rotación del eje del motor sobre la pieza. Sobre estos elementos se ubica

una montura (8) vertical que dispone de un canal inferior que alberga en su interior unos rodamientos y que está en contacto con la leva (7) de tal manera que la montura recibe la acción de la leva, y la montura dispone de unas guías lineales de rodamientos que permiten a la montura (8) tener un movimiento ascendente o descendente, dependiendo del movimiento giratorio de la leva (7). En la parte superior de la montura (8) sustenta una preforma metálica (9) en su parte superior que sobresale de la carcasa (1) y que dispone en su cuerpo de un ranurado superficial a modo de conducto (91) que simula el conducto radicular de un diente, tal como puede observarse en la Figura 6. En la parte superior de la montura (8) se dispone de al menos un sensor LED (81) que emite luz ubicado en el extremo apical del conducto simulado (91); y al menos un sensor fotoeléctrico (82) LDR ubicado en la cara opuesta de la proforma metálica (9), en el mismo extremo del conducto (91) simulado y enfrentado con el sensor LED (81) que detecta y cuantifica de la luz emitida por el sensor LED (81), estando ambos sensores en conexión con el procesador (5), tal como también se advierte en la Figura 7.

También se observa en las figuras 4, 5 y 7, que la máquina dispone en una de las caras de la carcasa (1), preferentemente en la cara opuesta a donde se ubica la pantalla, de al menos un puerto conector (12) de corriente eléctrica desde un módulo de alimentación externa (120), y también dispone de al menos un puerto de cable USB (11) para la conexión de la máquina a un ordenador externo (110) o dispositivo electrónico similar que implemente las prestaciones del procesador (5) aumente el flujo de información, facilite la conexión y gestión inalámbrica tanto del tratamiento de los datos obtenidos como del funcionamiento de los diferentes componentes.

REIVINDICACIONES

1.- Máquina para testar instrumental endodóntico, en el que dicha máquina está constituida por una estructura o carcasa (1) que permite su ubicación en cualquier lugar, que dispone en una de las caras de la carcasa (1) de una pantalla (52) donde se visualizan los datos obtenidos, estando la máquina alimentada eléctricamente, y que comprende:

- un soporte de sustentación (2) sobre la carcasa (1) que comprende un micromotor endodóntico (3) en cuyo extremo dispone de un contraángulo reductor (31) en el que se inserta el instrumental endodóntico a testar y que hace que el instrumental endodóntico gire respecto a su propio eje;
- un motor eléctrico de engranajes (4) en el interior de la carcasa (1) que mueve un mecanismo interno que comprende de al menos una leva (7) que desplaza verticalmente una montura (8);
- una montura (8) que comprende una preforma metálica (9) que sobresale de la carcasa (1) y que dispone en su cuerpo de un ranurado a modo de conducto (91) que simula un conducto radicular y donde se introduce el material endodóntico a testar;

y que se caracteriza por que adicionalmente comprende

- un procesador (5) interno que comprende al menos un módulo de control (51) de un motor eléctrico de engranajes (4); una pluralidad de interruptores (54) conectados a unos de botones de calibración (6) exteriores en la carcasa (1); un módulo de programación (53) o placa; y estando la pantalla (52) en conexión con dicho procesador (5);
- el motor eléctrico de engranajes (4) que está controlado por el procesador (5);
- y donde la montura (8) adicionalmente comprende:
    - o al menos un sensor LED (81) que emite luz ubicado en un extremo del conducto (91); y
    - o al menos un sensor fotoeléctrico (82) ubicado en la cara opuesta de la proforma metálica (9), en el mismo extremo del conducto (91) y enfrentado con el sensor LED (81) que detecta y cuantifica de la luz emitida por el sensor LED (81), estando ambos sensores en conexión con el módulo de programación (53) del procesador (5).

2.- Máquina para testar instrumental endodóntico, según la reivindicación 1, que se caracteriza porque la leva (7) sujeta al motor (4) por un pasador, habiendo en su zona de contacto unos rodamientos (41) que permiten el movimiento giratorio de la leva (7).

3.- Máquina para testar instrumental endodóntico, según la reivindicación 1 y 2, que se caracteriza porque la montura (8) dispone de un canal inferior donde contacta con la leva (7) y donde alberga unos rodamientos en su interior.

4.- Máquina para testar instrumental endodóntico, según las reivindicaciones 1-3, que se caracteriza porque la montura (8) dispone de unas guías lineales de rodamientos que permiten a la montura (8) desplazarse verticalmente tras la acción giratoria de la leva (7).

5.- Máquina para testar instrumental endodóntico, según la reivindicación 1, que se caracteriza porque el módulo de control (51) del motor incorpora un circuito o estructura electrónica en forma de puente H.

6.- Máquina para testar instrumental endodóntico, según la reivindicación 1, que se caracteriza por que los interruptores (54) están modulados con transistores.

7.- Máquina para testar instrumental endodóntico, según la reivindicación 1, que se caracteriza porque el sensor LED (81) y el sensor fotoeléctrico (82) se ubican en el extremo apical del conducto (91).

8.- Máquina para testar instrumental endodóntico, según la reivindicación 1 o 7, que se caracteriza porque el sensor fotoeléctrico (82) es LDR.

9.- Máquina para testar instrumental endodóntico, según la reivindicación 1, que se caracteriza porque el cuerpo de la preforma (9) es de acero inoxidable y está recubierto de una película de cromo.

10.- Máquina para testar instrumental endodóntico, según la reivindicación 1, que se caracteriza porque el soporte de sustentación (2) dispone de una abrazadera (21) donde se fija el micromotor endodóntico (3).

11.- Máquina para testar instrumental endodóntico, según cualquiera de las reivindicaciones anteriores, que se caracteriza porque la máquina dispone de al menos un puerto de cable USB (11) para la conexión del procesador (5) de la máquina a un ordenador externo (110) o dispositivo electrónico similar.

Fig.1

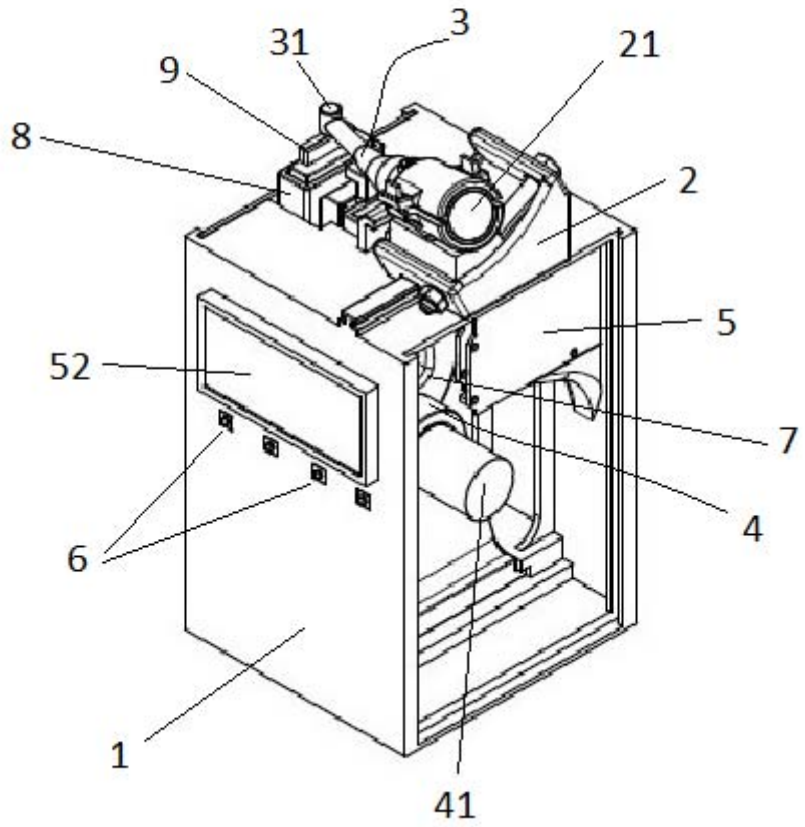

Fig.2

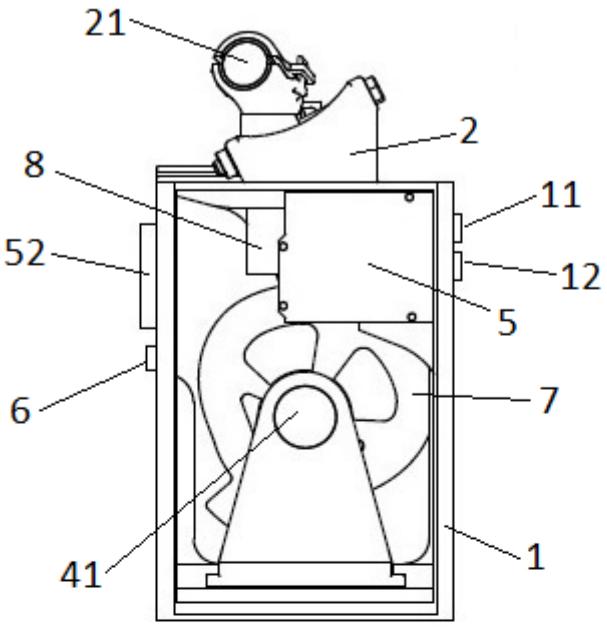

Fig.3

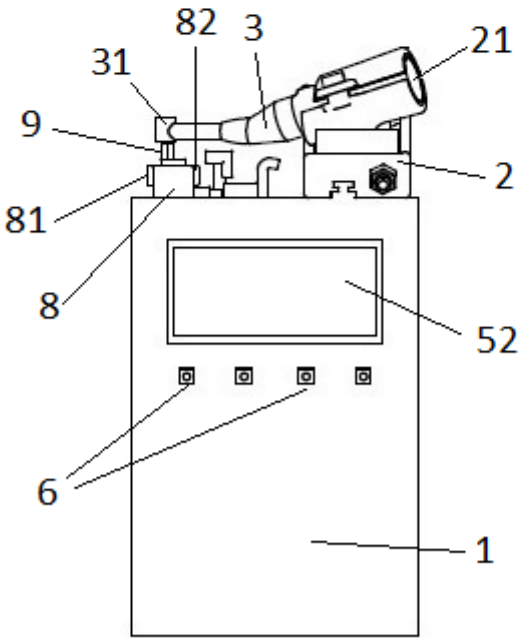

Fig.4

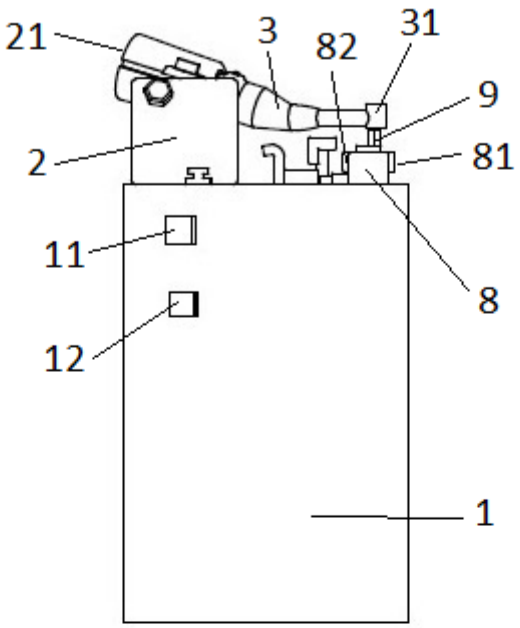

Fig.5

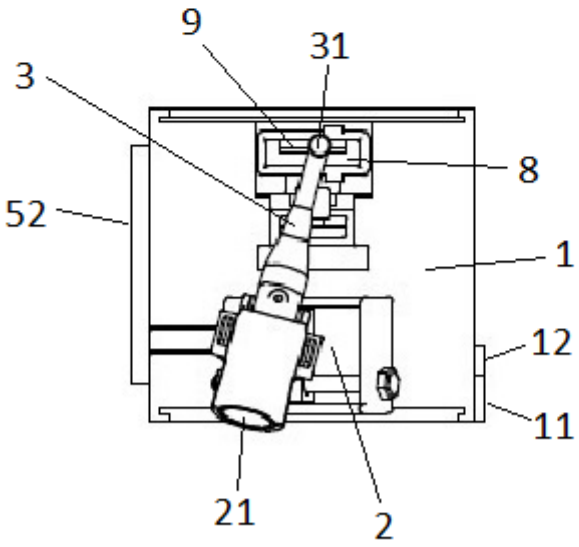

Fig.6

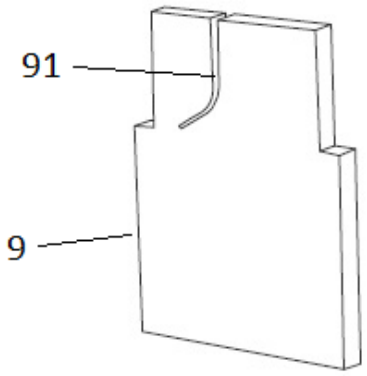

Fig.7

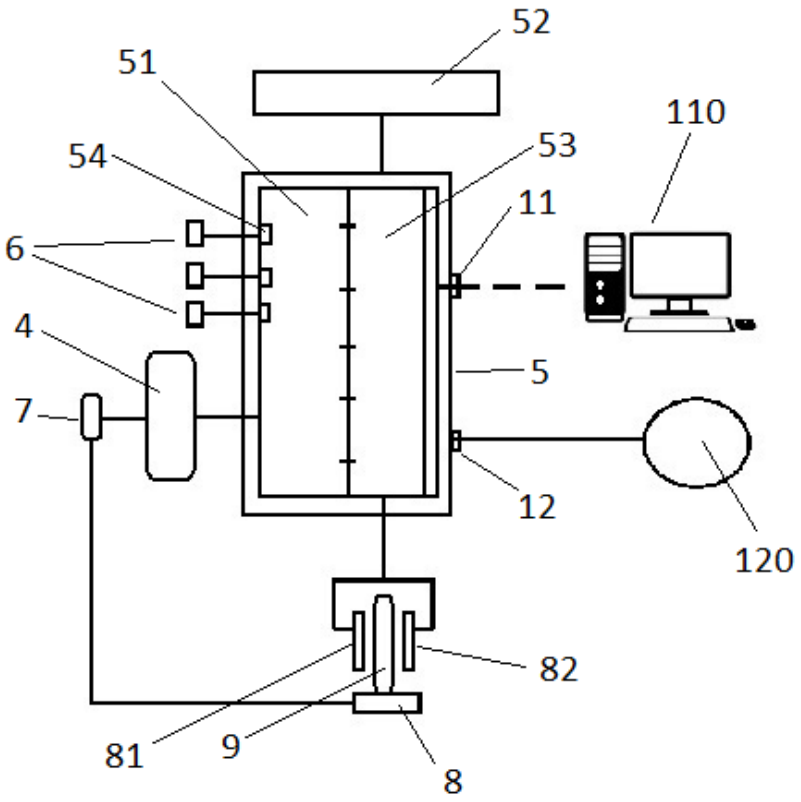

Carlos Falcão Costa
Professor Auxiliar da Faculdade Ciências da Saúde
Universidade Fernando Pessoa

Ex.mo Sr. Dr Alvaro Zubizarreta Macho
Aluno de Doutoramento
Universidade de Salamanca - Espanha

Porto, 16 de Março de 2019

Assunto: Carta de aceitação de Estância como Investigador

Venho por este meio comunicar formalmente a aceitação na nossa Instituição para que prossiga com o seu projeto de Doutoramento intitulado "***Análisis de las variables que influyen sobre la fatiga cíclica del instrumental endodóntico***.", com uma estância de investigação Científica na nossa Universidade Fernando Pessoa, Porto, Portugal, durante o período compreendido entre 11 de Novembro de 2019 a 16 de Março de 2020.

Com os meus melhores cumprimentos,

(Prof. Auxiliar da Universidade Fernando Pessoa)

SEOC

Certifica que el Póster de Investigación Endodoncia con título:

Influencia de la velocidad en la fatiga cíclica de las limas NiTi

Que tiene por autores a **Jaramillo-Vásconez S., Faus-Matoses V., Hamoud-Kharrat N., Faus-Matoses I., Martín-Biedma B., Zubizarreta-Macho A., and Faus-Llácer V.**

ha sido presentado en el XXIV Congreso Nacional y XI Internacional de la Sociedad Española de Odontología Conservadora y Estética, celebrado en Pamplona los días 12, 13 y 14 de mayo de 2022

Y para que así conste, se expide certificado en:

Pamplona, 14 de mayo de 2022

• *Isabel Giráldez de Luis* •
Presidenta SEOC

• *Juan José Gaite García* •
Presidente Congreso

SEOC

Certifica que el Póster de Investigación Endodoncia con título:

Estudio comparativo: resistencia a la fatiga cíclica de limas rotatorias endodónticas de NiTi

Que tiene por autores a **Pérez García, R, Zubizarreta-Macho, A, Marhuenda Ramos, M.T, Faus-Matoses, I, Faus-Matoses, V y Faus-Llácer, V.**

ha sido presentado en el XXIV Congreso Nacional y XI Internacional de la Sociedad Española de Odontología Conservadora y Estética, celebrado en Pamplona los días 12, 13 y 14 de mayo de 2022

Y para que así conste, se expide certificado en:

Pamplona, 14 de mayo de 2022

• *Isabel Giráldez de Luis*•
Presidenta SEOC

• *Juan José Gaite García* •
Presidente Congreso

CONGRESO VIRTUAL 2021

AEDE

AEDE
Asociación Española de
ENDODONCIA

JORNADAS DE INVESTIGACIÓN

DIPLOMA DE PONENTE

Nombre y Apellido

NIRMINE HAMOUD KHARRAT

Ha presentado la Comunicación de Investigación:

Influencia de la sección transversal en la resistencia a la fatiga cíclica de las limas endodónticas rotatorias de NiTi

en representación a los autores:

HAMOUD KHARRAT, NIRMINE ; FAUS LLACER, VICENTE ; HAMOUD KHARRAT, NIRMINE; FAUS MATOSES, IGNACIO ; ZUBIZARRETA MACHO, ÁLVARO ; FAUS MATOSES, VICENTE

Durante las Jornadas de Investigación organizadas por la Asociación Española de Endodoncia (AEDE) los días 22 y 23 de octubre de 2021, en formato online

Presidente del Congreso AEDE

Juan José Segura

CONGRESO VIRTUAL 2021

AEDE

AEDE
Asociación Española de
ENDODONCIA

JORNADAS DE INVESTIGACIÓN

DIPLOMA DE PÓSTER

Nombre y Apellido

Marhuenda Raamos, María Teresa (1); Faus Llácer, Vicente (1); Faus Matoses, Ignacio (1); Zubizarreta Macho, Álvaro (2); Faus Matoses, Vicente (1); Sauro, Salvatore (4); Sánchez Marín, Francisco (3); Roda Casanova, Victor (3)

Ha presentado el póster

¿INFLUYE LA SECCIÓN TRANSVERSAL Y EL PITCH EN EL COMPORTAMIENTO MECÁNICO DE LAS LIMAS ENDODÓNTICAS ROTATORIAS?

en las Jornadas de Investigación organizadas por AEDE en los días 22 y 23 de noviembre

Presidente del Congreso AEDE

Juan José Segura

Dear Alvaro Zubizarreta Macho,

This is certify that below e-posters are displayed during 10th Conseuro Congress which has been held virtually on 22 – 24 April 2021.

Title: EP – 048 Efficacy of XP-Endo Retreatment System In Removing Thermafil and Guttacore Using Micro-CT

Corresponding / Presenting author: Rubén Linero Pérez

Authors: Rubén Linero Pérez[1], Vicente Faus LLácer[1], Ignacio Faus Mastoses[1], Celia Ruiz Sánchez[1], Álvaro Zubizarreta Macho[2], Salvatore Sauro[3], Vicente Faus Mastoses[1]

Type of presentation: Eposter

Institution:

[1]University of Valencia, Faculty of Medicine and Dentistry, Department of Stomatology, Valencia, Spain
[2]Alfonso X El Sabio University, Faculty of Health Sciences, Department of Endodontics, Madrid, Spain
[3]CEU Cardenal Herrera University, Faculty of Health Sciences, Department of Dentistry, Valencia, Spain

---

Title: EP – 107 Functional, Esthetic and Conservative Rehabilitation of a Class III Malocclussion: An Interdisciplinary Ortho-Restorative Approach

Corresponding / Presenting author: Dalia Pulido-Ouardi

Authors: Vicente Faus-Matoses[1], Ignacio Faus-Matoses[2], Dalia Pulido-Ouardi[1], Alvaro Zubizarreta-Macho[1], Celia Ruiz-Sanchez[1], Vicente Jose Faus-Llacer[1]

Type of presentation: Eposter

Institution:

[1]University of Valencia, Faculty of Medicine and Dentistry, Department of PTD II, Valencia, Spain
[2]University of Valencia, Faculty of Medicine and Dentistry, Department of Orthodontics, Valencia, Spain

Title: EP – 108 Non-Generalized Dental Erosion Treatment: A Conservative Ortho-Resto Approach Applying Dahl´s Principle

Corresponding / Presenting author: Raúl Pérez García

Authors: Vicente Faus Matoses[1], Ignacio Faus Matoses[2], Raúl Pérez García[1], Alvaro Zubizarreta Macho[1], Celia Ruiz Sanchez[1], Vicente José Faus Llacer[1]

Type of presentation: Eposter

Institution:

[1]University Of Valencia, Faculty of Medicine and Dentistry, Department of PTD II., Valencia, Spain
[2]University of Valencia, Faculty of Medicine and Dentistry, Department of Orthodontics, Valencia, Spain

---

Title: EP – 109 Pre-Orthodontic Long-Term Mock-Up in a Patient Affected by Attrition: A Conservative Approach

Corresponding / Presenting author: Tannaz Moradian

Authors: Vicente Faus-Matoses[1], Ignacio Faus-Matoses[2], Tannaz Moradian[1], Alvaro Zubizarreta-Macho[1], Celia Ruiz-Sanchez[1], Vicente José Faus-Llacer[1]

Type of presentation: Eposter

Institution:

[1]University of Valencia, Faculty of Medicine and Dentistry, Department of PTD II., Valencia, Spain
[2]University of Valencia, Faculty of Medicine and Dentistry, Department of Orthodontics, Valencia, Spain

Title: EP – 110 Aesthetic Correction of Gingival Display, Overbite and Overjet: An Interdisciplinary Restorative Approach

Corresponding / Presenting author: Pablo Reid-Beros

Authors: Vicente Faus-Matoses[1], Ignacio Faus-Matoses[2], Pablo Reid-Beros[1], Alvaro Zubizarreta-Macho[1], Celia Ruiz-Sánchez[1], Vicente José Faus-Llácer[1]

Type of presentation: Eposter

Institution:

[1]University of Valencia, Faculty of Medicine and Dentistry, Department of PTD II., Valencia, Spain
[2]University of Valencia, Faculty of Medicine and Dentistry, Department of Orthodontics, Valencia, Spain

---

Title: EP – 123 Do Cross Section and Pitch Affect the Mechanical Behavior of Endodontic Rotary Files?

Corresponding / Presenting author: María Teresa Marhuenda Ramos

Authors: María Teresa Marhuenda Ramos[1], Álvaro Zubizarreta Macho[2], Vicente Faus Matoses[1], Vicente Faus Llácer[1], Victor Roda Casanova[3], Francisco Sánchez Marín[3]

Type of presentation: Eposter

Institution:

[1]University of Valencia, Spain
[2]Alfonso X el Sabio University, Faculty of Health Sciences, Department of Implant Surgery, Madrid, Spain
[3]Jaume I University

Title: EP – 146 Interdisciplinary Orthodontic and Restorative Minimally Invasive Approach to Treat the Anterior Dental Attrition

Corresponding / Presenting author: Nirmine Hamoud-Kharrat

Authors: Vicente Faus-Matoses[1], Ignacio Faus-Matoses[2], Nirmine Hamoud-Kharrat[1], Alvaro Zubizarreta- Macho[1], Celia Ruiz-Sanchez[1], Vicente Jose Faus-Llacer[1]

Type of presentation: Eposter

Institution:
[1]University of Valencia, Faculty of Medicine and Dentistry, Department of PTD II, Valencia, Spain
[2]University of Valencia, Faculty of Medicine and Dentistry, Department of Orthodontics, Valencia, Spain

---

Title: EP - 154 Interdisciplinary Management of the Midline Due to a Concrescence

Corresponding / Presenting author: Alvaro Aldeguer-Muñoz

Authors: Vicente Faus-Matoses[1], Ignacio Faus-Matoses[2], Alvaro Aldeguer-Muñoz[1], Alvaro Zubizarreta-Macho[1], Celia Ruiz-Sanchez[1], Vicente Jose Faus-Llacer[1]

Type of presentation: Eposter

Institution:
[1]University of Valencia, Faculty of Medicine and Dentistry, Department of PTD II., Valencia, Spain
[2]University of Valencia, Faculty of Medicine and Dentistry, Department of Orthodontics, Valencia Spain

Sincerely yours,

Prof. Dr. Şebnem Türkün

President of EFCD

EFCD
EUROPEAN FEDERATION
OF CONSERVATIVE DENTISTRY

RESTORATİF DİŞHEKİMLİĞİ DERNEĞİ
RDD
1990
Turkish Society of
Restorative Dentistry

10th CONSEURO
22-24 April 2021

· E-POSTER CERTIFICATE ·

ÁLVARO ZUBIZARRETA MACHO

Alfonso X el Sabio University, Faculty of Health Sciences,
Department of Implant Surgery, Madrid, Spain

has attended the 10th Conseuro Congress on 22-24 April, 2021 with the e-poster:

EP – 006
Comparative Analysis of Stress Distribution of Experimentally Designed Endodontic Rotary Files

Prof. Dr. L. Şebnem Türkün
President of EFCD

Prof. Dr. Esra Can
President of RDD

16 CE Point

AEDE
Asociación Española de
ENDODONCIA

AEDE
Palexco. A Coruña
2017

El Comité Organizador certifica que

D./Dª. **Álvaro Zubizarrieta Macho Cristina Rico Romano Roberto Gutierrez González Daniel Gutierrez Ufano Jesús Mena Álvarez**

han presentado una comunicación Comunicación oral investigación (COI) que ha sido seleccionada como finalista en el

38º CONGRESO NACIONAL DE ENDODONCIA

celebrado del 1 al 3 de noviembre de 2017 en A Coruña, con el título

File Breaker. Un nuevo dispositivo de análisis de fatiga cíclica

Y para que así conste, se expide el siguiente certificado en
A Coruña, a 3 de noviembre de 2017

Presidente
José María Malfaz

Secretario
Roberto Carlos Aza